15 February 2013 | $10

Science

Gordon Research Conferences

AAAS

RESEARCH FROM ANYWHERE

START WITH ENDNOTE®

Finally a research tool that is readily available whenever and wherever you need it. Access and manage your *EndNote* library from anywhere, even your iPad, with *EndNoteSync*.

- Find full text for your references in one click.
- Search hundreds of online resources for references and PDFs.
- Watch your references appear as you write with patented *Cite While You Write*® technology.

START AT ENDNOTE.COM

Use Coupon Code: **science13** for exclusive pricing

Available for Windows® and Macintosh®

THOMSON REUTERS™

MiSeq®. Next-generation sequencing for all you seek.

You want amazing accuracy and performance on your benchtop. Illumina delivers—yet again. The MiSeq personal sequencer is the only fully integrated, truly end-to-end benchtop solution around. It's just one more example of why Illumina solutions generate a remarkable 90% of all the world's sequencing data. Discover what's possible.

www.illumina.com/miseq

illumina®

NEW ENGLAND BioLabs® Inc.
enabling technologies in the life sciences

Make ends meet.

Gibson Assembly™ Cloning Kit

New England Biolabs has revolutionized your laboratory's standard cloning methodology. The Gibson Assembly Cloning Kit combines the power of the Gibson Assembly Master Mix with NEB 5-alpha Competent *E. coli*, enabling fragment assembly and transformation in just under two hours. Save time, without sacrificing efficiency.

Making ends meet is now quicker and easier than ever before, with the Gibson Assembly Cloning Kit from NEB.

NEBuilder™ for Gibson Assembly

Visit **NEBGibson.com** to view the latest tutorials and to try our primer design tool.

Gibson Assembly Cloning Kit provides robust transformation efficiencies

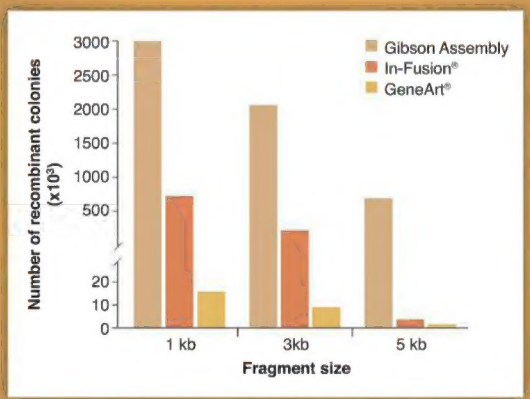

Assembly reactions containing 25 ng of linear pUC19 vector and 0.04 pmol of each fragment were performed following individual suppliers' recommended protocols and using the competent cells provided with the kit. The total number of recombinant colonies was calculated per 25 ng of linear pUC19 vector added to the assembly reaction.

SYNTHETIC GENOMICS®

Some components of this product are manufactured by New England Biolabs, Inc. under license from Synthetic Genomics, Inc.

CONTENTS continued >>

page 750

page 759

COVER

Victoria Harbor in Hong Kong. Gordon Research Conferences has established a venue in Hong Kong where investigators from around the globe can discuss their work and challenges in an informal, interactive format; improve collaborations between the East and West; and advance the frontiers of science. See page 834 for the 2013 conference schedule and preliminary programs.

Photo: Hong Kong Tourism Board

DEPARTMENTS

WE'RE BRINGING A NEW PERSPECTIVE TO

cancer metabolism research

FIRST WE MADE IT POSSIBLE – NOW WE'VE MADE IT EASY.

XF technology provides the easiest and most comprehensive assessment of cancer cell metabolism, measuring glucose and glutamine metabolism, and fatty acid oxidation of cancer cells in a microplate, in real-time!

— David Ferrick, PhD,
CSO, Seahorse Bioscience

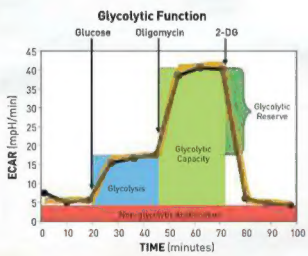

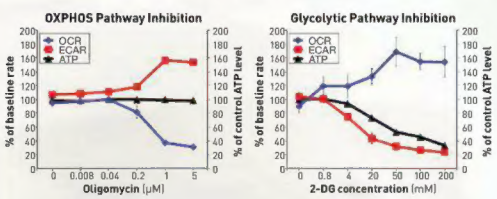

The Seahorse XF^e Extracellular Flux Analyzer

Measurements of cellular glycolysis are essential to understanding cancer, immune response, stem cell differentiation, aging, and cardiovascular and neurodegenerative diseases. The XF^e Analyzer and XF Glycolysis Stress Test Kit make it easy to measure the three key parameters of cellular glycolysis in a microplate: glycolysis, glycolytic capacity, and glycolytic reserve, revealing critical information not evident in mitochondrial respiration measurements alone.

See what's possible.

Scan this QR code to view videos and see what the XF Analyzer can achieve. Visit **www.seahorsebio.com/science** for more information!

Seahorse *Bioscience*

RESEARCH ARTICLES

REPORTS

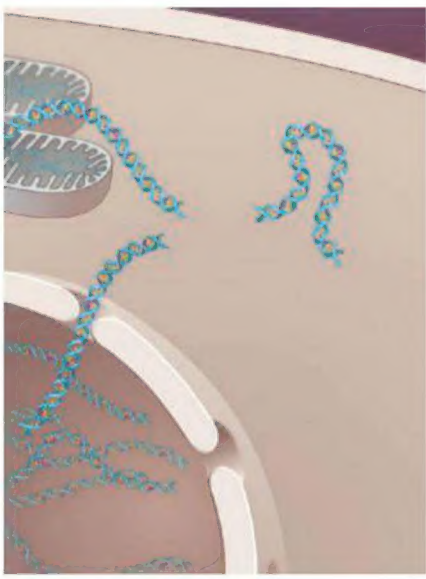

pages 763, 786, & 826

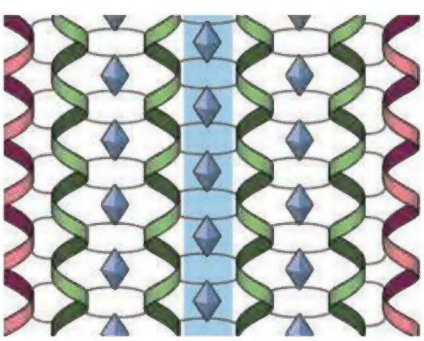

page 811

SCIENCE (ISSN 0036-8075) is published weekly on Friday, except the last week in December, by the American Association for the Advancement of Science, 1200 New York Avenue, NW, Washington, DC 20005. Periodicals Mail postage (publication No. 484460) paid at Washington, DC, and additional mailing offices. Domestic individual membership and subscription (51 issues): $149 ($74 allocated to subscription). Domestic institutional subscription (51 issues): $990; Foreign postage extra: Mexico, Caribbean (surface mail) $55; other countries (air assist delivery) $85. First class, airmail, student, and emeritus rates on request. Canadian rates with GST available upon request, GST #1254 88122. Publications Mail Agreement Number 1069624. **Printed in the U.S.A.**

Change of address: Allow 4 weeks, giving old and new addresses and 8-digit account number. **Postmaster:** Send change of address to AAAS, P.O. Box 96178, Washington, DC 20090–6178. **Single-copy sales:** $10.00 current issue, $15.00 back issue prepaid includes surface postage; bulk rates on request. **Authorization to photocopy** material for internal or personal use under circumstances not falling within the fair use provisions of the Copyright Act is granted by AAAS to libraries and other users registered with the Copyright Clearance Center (CCC) Transactional Reporting Service, provided that $30.00 per article is paid directly to CCC, 222 Rosewood Drive, Danvers, MA 01923. The identification code for *Science* is 0036-8075. *Science* is indexed in the *Reader's Guide to Periodical Literature* and in several specialized indexes.

EDITED BY STELLA HURTLEY

The Building Blocks of Life

Biological organisms are often limited in the resources that they can use to make structural materials. Primary building blocks may be weak or brittle materials, such as minerals and biopolymers, and processing conditions by default have to be mild. Despite this, a wide range of strong and tough structures exist, including shells, bones, quills, and fibers. **Meyers *et al.*** (p. 773) review a wide range of materials and architectures used in nature to make strong and tough materials and show how many of the design principles have also been used or are being considered for manmade materials and structures.

Allostery Across DNA

Proteins, such as transcription factors and RNA polymerase, bind close to each other on DNA and their function is coordinated. **Kim *et al.*** (p. 816; see the Perspective by **Crothers**) report single-molecule experiments that show that the DNA binding affinity of a protein is significantly altered by a second protein bound nearby. The effect oscillates between stabilizing and destabilizing the binding with a periodicity equal to the helical pitch of DNA. Allosteric coupling between a transcriptional repressor and RNA polymerase modulated gene expression in living bacteria.

DNA Sensing Is a (c)GAS

DNA is normally localized to the nucleus, and so its cytoplasmic localization sends off alarm bells to the immune system because it indicates that a virus may have entered. But how does the immune system actually detect the DNA (see the Perspective by **O'Neill**)? **Sun *et al.*** (p. 786, published online 20 December) identify cyclic GMP-AMP (cGAMP) cyclase (cGAS), which can bind to cytoplasmic DNA directly and catalyze the production of cGAMP. cGAMP then acts as a second messenger to activate downstream signaling events that trigger antiviral immunity. **Wu *et al.*** (p. 826, published online 20 December) show that cGAMP, produced in response to cytoplasmic DNA, binds to and activates the signaling adaptor protein STING.

Macroscopic Uncertainty

According to the Heisenberg uncertainty principle, it is impossible to know both the position and the momentum of a microscopic particle with absolute certainty; pinpointing the location introduces an uncertainty in the velocity, which translates into position uncertainty at later times. Now, **Purdy *et al.*** (p. 801; see the Perspective by **Milburn**) have measured the position of a macroscopic object (a small, but visible-to-the-naked-eye membrane suspended in an optical cavity) at cryogenic temperatures and observed the uncertainty in its position caused by the recoiling photons used for the measurement.

Genome Editing >>

Clustered regularly interspaced short palindromic repeats (CRISPR) function as part of an adaptive immune system in a range of prokaryotes: Invading phage and plasmid DNA is targeted for cleavage by complementary CRISPR RNAs (crRNAs) bound to a CRISPR-associated endonuclease (see the Perspective by **van der Oost**). **Cong *et al.*** (p. 819, published online 3 January) and **Mali *et al.*** (p. 823, published online 3 January) adapted this defense system to function as a genome editing tool in eukaryotic cells.

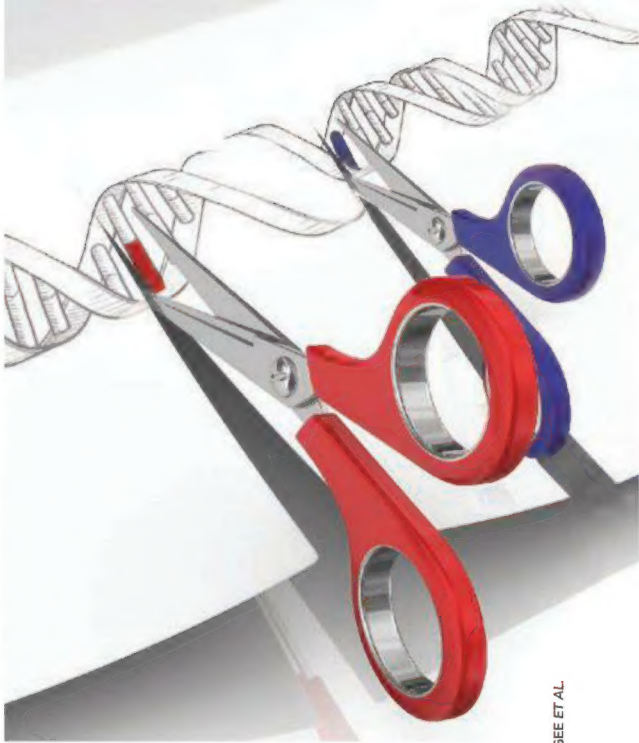

CREDIT (TOP TO BOTTOM): IMAGE BY LAUREN SOLOMON, COURTESY OF BROAD INSTITUTE. COMPONENTS COURTESY OF WWW.ISTOCKPHOTO.COM AND WWW.CANPHOTO.COM; AGEE *ET AL.*

So Different and So Similar

Most known meteorites from Mars fit into one class. **Agee *et al.*** (p. 780, published online 3 January; see the Perspective by **Humayun**) describe a meteorite, NWA 7034, which shares some characteristics with other martian meteorites but does not fit within the usual classification. NWA 7034 matches the composition of Mars' surface but is also richer in water than other martian meteorites, and has different oxygen isotope composition, which suggests the existence of multiple oxygen isotopic reservoirs within Mars. Its radiometric age of 2.1 billion years makes it a unique sample of the Amazonian period on Mars.

Crystalline Pores Writ Large

Porous inorganic materials are often made by using molecular templates that help to maintain internal channels during synthesis. The success with small molecules for creating microporous zeolites and related materials with angstrom-scale channels has been extended with molecular assemblies such as vesicles being used to create mesoporous materials with nanometer-scale channels. However, the walls of these materials are usually amorphous. **Lin *et al.*** (p. 811, published online 24 January) now report that crystalline mesoporous gallium zincophosphites can be made with very large channels (up to 72-membered rings spanning 3.5 nanometers) by using long-chain amine templates. The materials have limited thermal stability that hinders template removal, but when appropriately doped and loaded with chromophores, the materials exhibit broadband photoluminescence.

Unintended Recipients of Antidepressants

Pharmaceuticals are used to treat a wide variety of ailments and conditions in humans. However, many animal species share physiologies, receptors, and pathways that may be acted upon by pharmaceutical compounds. Increasingly, pharmaceuticals are being found in natural aquatic systems. Such pharmaceutical pollution can cause mortality and alter development and reproduction of aquatic animals. **Brodin *et al.*** (p. 814) report that excreted drugs may also have far more subtle, yet eventually significant, impacts in natural systems. Benzodiazepines, which reduce anxiety in humans, alter social and foraging behavior in fish. European perch exposed to oxazepam were bolder, more active, less social and fed more rapidly.

Bruce Alberts is Editor-in-Chief of *Science*.

Designing Scientific Meetings

THIS ISSUE OF *SCIENCE* CONTAINS ANNOUNCEMENTS FOR MORE THAN 100 DIFFERENT GORDON Research Conferences, on topics that range from atomic physics to developmental biology. The brainchild of Neil Gordon of Johns Hopkins University, these week-long meetings are designed to promote intimate, informal discussions of frontier science. Often confined to fewer than 125 attendees, they have traditionally been held in remote places with minimal distractions. Beginning in the early 1960s, I attended the summer Nucleic Acids Gordon Conference in rural New Hampshire, sharing austere dorm facilities in a private boys' school with randomly assigned roommates. As a beginning scientist, I found the question period after each talk especially fascinating, providing valuable insights into the personalities and ways of thinking of many senior scientists whom I had not encountered previously. Back then, there were no cellphones and no Internet, and all of the speakers seemed to stay for the entire week. During the long, session-free afternoons, graduate students mingled freely with professors. Many lifelong friendships were begun, and—as Gordon intended—new scientific collaborations began. Leap forward to today, and every scientist can gain immediate access to a vast store of scientific thought and to millions of other scientists via the Internet. Why, nevertheless, do in-person scientific meetings remain so valuable for a life in science?

Part of the answer is that science works best when there is a deep mutual trust and understanding between the collaborators, which is hard to develop from a distance. But most important is the critical role that face-to-face scientific meetings play in stimulating a random collision of ideas and approaches. The best new science occurs when someone combines the knowledge gained by other scientists in non-obvious ways to create a new understanding of how the world works. A successful scientist needs to deeply believe, whatever the problem being tackled, that there is always a better way to approach that problem than the path currently being taken. The scientist is then constantly on the alert for new paths to take in his or her work, which is essential for making breakthroughs. Thus, as much as possible, scientific meetings should be designed to expose the attendees to ways of thinking and techniques that are different from the ones that they already know.

There is a danger of scientific meetings becoming overly specialized as the amount of scientific knowledge expands. There is no longer a Gordon Conference called Nucleic Acids; understandably, it was replaced long ago by a whole set of meetings on related subspecialties. But I would argue that one should try to avoid producing a scientific meeting where all of the attendees use the same approaches and read the same scientific literature. In fact, the most stimulating scientific meetings that I have attended have taken the extreme opposite approach, intentionally mixing scientists with very different backgrounds and interests, convening them to produce a set of new ideas for attacking a challenging scientific puzzle.

One example of such a meeting was an intensive 2-day 1995 workshop on schizophrenia that involved 18 carefully selected scientists, most of whom knew almost nothing about the disease. The meeting began with a few invited experts presenting what was known about schizophrenia to the non-experts, answering their many questions in informal discussions around a large square table. All of the remaining time was spent in brainstorming about possible new approaches to understanding the cellular basis for the disease and discovering better treatments. In the process, we all learned a great deal of new science, and we produced a report with valuable new ideas.* This simply could not have happened via e-mail or Skype. A second, larger example is the Keck Futures Initiative, convened annually by the U.S. National Academies.† Could more meetings of this type play a powerful role in accelerating the scientific innovation needed to address the world's many new challenges?

– Bruce Alberts

10.1126/science.1236324

*S. H. Barondes *et al.*, *Proc. Natl. Acad. Sci. U.S.A.* **94**, 1612 (1997). †See www.keckfutures.org/about/index.html.

EDITED BY KRISTEN MUELLER AND MARIA CRUZ

ANIMAL COGNITION

Give Her What She Wants

Most humans have excellent state-attribution skills; that is, we regularly attribute states we experience ourselves (e.g. hopes, desires, beliefs) to others. Such skills are essential for day-to-day human interactions and are particularly important in bonded relationships. The ability to understand another's perspective and wants has generally been considered to be specific to humans, but the benefits of such skills could confer an adaptive advantage for many species. Thus, these skills may be present in nonhuman animals but just difficult to demonstrate. Ostojić *et al.* use a suite of controlled experiments in Eurasian jays and find evidence that state attribution is present in these monogamous birds. Specifically, consumption of one preferred food by females reduced their desire for it later, when compared with another preferred food. They showed that males were attuned to this "specific satiety" and flexibly offered females the preferred food that they had not been offered previously. The authors ruled out several alternative explanations, such as the potential that the female was giving behavioral cues during the feeding: Males had to be able to observe the initial feeding in order to best judge what the female would most want next. Besides demonstrating that male Eurasian jays make thoughtful and observant mates, these results suggest that state attribution may not be ours alone. — SNV

Proc. Natl. Acad. Sci. U.S.A. **110**, 10.1073/pnas.1209926110 (2013).

PHYSICS

Remote Sensing with a Twist

Our eyes sense light that has bounced off objects, with our brain then making sense of the input flowing through the optic nerve. In this case, the photons that hit our eyes must interact with the object. However, it is possible to get information about an object using photons that have not actually hit the object. This counterintuitive process of "ghost imaging" follows from the quantum-mechanical properties of photons and the ability to find correlations between specially generated pairs of photons. Uribe-Patarroyo *et al.* use such correlations between beams of light that have been imprinted with specific values of optical angular momentum: The light beam is effectively twisted, with the photons mapping out a spiral as they propagate. Using correlated photons produced by parametric downconversion, whereby a high-energy photon is converted into a pair of correlated photons of lower energy, they send one of the photons to the object and hold on to the other. When the photon hits the object, the process of that interaction changes its degree of twist and in turn affects the correlation between the pair. The object can then be determined by looking at changes in the correlations between the two photons. With a modification of the experimental setup, it should be possible to remotely sense reflective targets at large distances, with the target unaware that it is being watched. — ISO

Phys. Rev. Lett. **110**, 043601 (2013).

MICROBIOLOGY

All Together Now

Among communities of microorganisms, interspecies gene transfer is rife, but as a microbial community consumes local resources and develops in time and space, it is becoming increasingly apparent that the products of diverse metabolic activities can also be publicly shared. Otteson *et al.* set adrift a buoy with a robotic sampler off the coast of northern California to collect, every 4 hours over 2 days and about 50 km of distance, wild picoplankton for community RNA sequencing. Analyses of transcriptional dynamics revealed that the photosynthetic eukaryote *Ostreococcus* and the bacterium *Synechococcus* co-expressed large numbers of genes diurnally. The proteorhodopsin-expressing heterotroph *Pelagibacter* did not show diel gene expression but did show well-orchestrated regulatory patterns and a high degree of covariance between some major metabolic pathways, indicating immediate responses to changing growth conditions. Whether this apparent coordination stems from species-to-species communication and signaling cascades or is the product of individual responses remains to be determined. — CA

Proc. Natl. Acad. Sci. U.S.A. **110**, 10.1073/pnas.1222099110 (2013).

ASTRONOMY

A Celestial X-ray Mirror

Bok globules, named after astronomer Bart Bok, are dense clouds of cold gas and dust that are usually condensing to form one or more stars. They are so dense that they can be totally opaque to visible light, often appearing in optical images as dark patches against the bright stellar background. McCollough *et al.* report a Bok globule that scatters the x-ray light emitted by a nearby binary system and thus appears as an x-ray emission feature in data taken with NASA's Chandra x-ray Observatory. The binary system, Cygnus X-3, is a powerful x-ray source located in the plane of our galaxy, where a massive, evolved star and either a black hole or neutron star orbit around their common center of mass. The x-ray data show an extended emission region associated with Cygnus X-3 that varies in flux

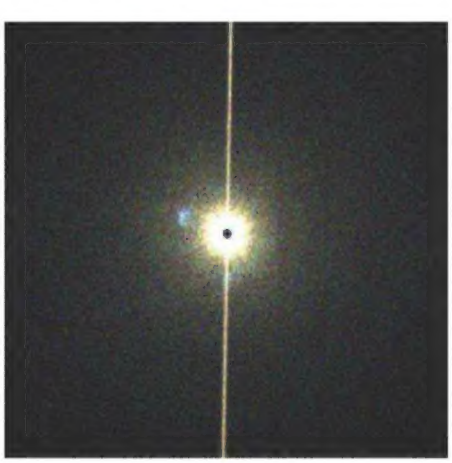

and orbital phase with the binary. This behavior is best explained as the result of scattering from a cloud located between Cygnus X-3 and the observer, which acts as an x-ray mirror to Cygnus X-3. The cloud's size, density, and mass, derived from the x-ray data, are consistent with those of a Bok globule. — MJC

Astrophys. J. **762**, 2 (2013).

BIOMEDICINE

Protecting Pregnancies

Preeclampsia is a dangerous complication of up to 5% of human pregnancies. The only treatment is removal of the fetoplacental unit by surgery or delivery. To better understand this condition, Doridot *et al.* generated a preeclampsia mouse model by overexpressing the transcription factor STOX1, which has previously been associated with preeclampsia. When control females were mated to transgenic males, the pregnant female mice showed characteristic features of preeclampsia, such as hypertension and protein in the urine. In addition, an elevated plasma level of soluble antiangiogenic factors was seen. When aspirin was administered early in the pregnancy via the drinking water, hypertension was prevented, as were elevated protein levels in the urine. An effect was also seen in the litter size: Control mice had slightly larger litters than their transgenic counterparts; however, with administration of aspirin, litter size was normalized. These results indicate that providing low doses of aspirin to preeclamptic mice early in gestation prevents disease development and suggests a potential means of human therapeutic intervention for this life-threatening condition. — BAP

Hypertension 10.1161/HYPERTENSIONAHA.111.202994 (2013).

CHEMISTRY

Customizing Polymer Brushes

One way to modify a surface and control or improve its properties is to grow polymer chains off the surface to form a "brush." One method for growing polymer brushes from surfaces—atom-transfer radical polymerization—can be controlled electrochemically, in that the process can be catalyzed by Cu^{+} ions but not by Cu^{2+}. Li *et al.* used this method to create gradients in the length of polymer brushes grown on a substrate modified with a suitable initiator. They polymerized 3-sulfopropyl-methacrylate with Cu^{+}-bipyridyl catalysts generated from Cu^{2+} in a mixed water-methanol solvent. The substrate was placed opposite a working electrode in an electrochemical cell. Because the Cu^{+} catalyst diffused toward the substrate, a concentration gradient was established along the cell. If the substrate was placed parallel to the working electrode, uniform brushes were grown, but if it was placed at an angle, a gradient in polymer brush length (measured with ellipsometry) was created, corresponding to the gradient in catalyst concentration. Prepatterning of the initiator on the substrates—which included gold, silicon, and silicone rubber—allowed the brush to form a "staircase" structure. — PDS

J. Am. Chem. Soc. 10.1021/ja3116197 (2013).

PSYCHOLOGY

Sound Judgment

A centuries-old line of thinking by moral philosophers has linked judgments about moral character to emotions. Contemporary psychological research has provided an experimental basis for these ideas, although the precise mapping of emotions

onto morality has not always been established. Seidel and Prinz have been able to demonstrate this by using auditory stimuli that selectively activate the distinct emotional channels of anger—via harshly dissonant music—and disgust—via the sounds of a person vomiting. After a short listening session, people were then presented with scenarios describing violations of autonomy—in which a person was harmed, as in a robbery—or violations of purity—in which cultural norms rendered some actions unnatural. They observed that evoking anger increased the severity with which people judged violations of autonomy but not those of purity, whereas eliciting disgust yielded higher ratings for the latter and not the former kind of moral transgression. — GJC

Cognition **127**, 1 (2013).

CREDIT: WIKIMEDIA COMMONS

www.sciencemag.org

Science

1200 New York Avenue, NW
Washington, DC 20005
Editorial: 202-326-6550, FAX 202-289-7562
News: 202-326-6591, FAX 202-371-9227
Bateman House, 82-88 Hills Road
Cambridge, UK CB2 1LQ
+44 (0) 1223 326500, FAX +44 (0) 1223 326501

Subscription Services For change of address, missing issues, new orders and renewals, and payment questions: 866-434-AAAS (2227) or 202-326-6417, FAX 202-842-1065. Mailing addresses: AAAS, P.O. Box 96178, Washington, DC 20090-6178 or AAAS Member Services, 1200 New York Avenue, NW, Washington, DC 20005

Institutional Site Licenses please call 202-326-6755 for any questions or information

Reprints: Author Inquiries 800-635-7181
Commercial Inquiries 803-359-4578

Permissions 202-326-7074, FAX 202-682-0816

Member Benefits AAAS Travels: Betchart Expeditions 800-252-4910; Apple Store www.store.apple.com/us/go/eppstore/aaas; NASA Federal, 1-888-NASA-FCU (1-888-627-2328) or www.nasafcu.com; Cold Spring Harbor Laboratory Press Publications www.cshlpress.com/affiliates/aaas.htm; GEICO Auto Insurance www.geico.com/landingpage/go51.htm?logo=17624; Hertz 800-654-2200 CDP#343457; Office Depot https://bsd.officedepot.com/portalLogin.do; Seabury & Smith Life Insurance 800-424-9883; Subaru VIP Program 202-326-6417; VIP Moving Services www.vipmayflower.com/domestic/index.html; Other Benefits: AAAS Member Services 202-326-6417 or www.aaasmember.org.

science_editors@aaas.org	(for general editorial queries)
science_letters@aaas.org	(for queries about letters)
science_reviews@aaas.org	(for returning manuscript reviews)
science_bookrevs@aaas.org	(for book review queries)

Published by the American Association for the Advancement of Science (AAAS), *Science* serves its readers as a forum for the presentation and discussion of important issues related to the advancement of science, including the presentation of minority or conflicting points of view, rather than by publishing only material on which a consensus has been reached. Accordingly, all articles published in *Science*—including editorials, news and comment, and book reviews—are signed and reflect the individual views of the authors and not official points of view adopted by AAAS or the institutions with which the authors are affiliated.

AAAS was founded in 1848 and incorporated in 1874. Its mission is to advance science, engineering, and innovation throughout the world for the benefit of all people. The goals of the association are to: enhance communication among scientists, engineers, and the public; promote and defend the integrity of science and its use; strengthen support for the science and technology enterprise; provide a voice for science on societal issues; promote the responsible use of science in public policy; strengthen and diversify the science and technology workforce; foster education in science and technology for everyone; increase public engagement with science and technology; and advance international cooperation in science.

Information for Authors
See pages 716 and 717 of the 8 February 2013 issue or access www.sciencemag.org/about/authors

EDITOR-IN-CHIEF **Bruce Alberts**
EXECUTIVE EDITOR **Monica M. Bradford** NEWS EDITOR **Colin Norman**
MANAGING EDITOR, RESEARCH JOURNALS **Katrina L. Kelner**
DEPUTY EDITORS **R. Brooks Hanson, Barbara R. Jasny, Andrew M. Sugden, Valda J. Vinson**

Editorial senior editors/commentary Lisa D. Chong, Brad Wible; **senior editors** Gilbert J. Chin, Pamela J. Hines, Paula A. Kiberstis (Boston), Marc S. Lavine (Toronto), Beverly A. Purnell, L. Bryan Ray, Guy Riddihough, H. Jesse Smith, Phillip D. Szuromi (Tennessee), Jake S. Yeston, Laura M. Zahn (San Diego); **associate editors** Melissa R. McCartney (Education Projects), Kristen L. Mueller, Jelena Stajic, Sacha Vignieri (Oregon), Nicholas S. Wigginton; **book review editor** Sherman J. Suter; **associate letters editor** Jennifer Sills; **editorial manager** Cara Tate; **senior copy editors** Jeffrey E. Cook, Cynthia Howe, Harry Jach, Lauren Kmec, Barbara P. Ordway, Trista Wagoner; **copy editor** Chris Filiatreau; **senior editorial coordinators** Carolyn Kyle, Beverly Shields; **editorial coordinators** Joi S. Granger, Anita Wynn; **publications assistants** Ramatoulaye Diop, Aneera Dobbins, Jeffrey Hearn, Lisa Johnson, Dona Mathieu, Le-Toya Mayne Flood, Shannon McMahon, Scott Miller, Jerry Richardson, Teresa R. Sakon, Brian White; **editorial assistant** Patricia M. Moore; **executive editorial assistant** Yolanda O'Bannon (San Francisco); **executive assistant** Alison Crawford; **administrative support** Maryrose Madrid

Editorial director, web and new media Stewart Wills; **senior web editor** Sarah Crespi; **web editor** Kerry Klein; **web development manager** Martyn Green; **web developer** Corinna Cohn

News deputy news editors Robert Coontz, Elizabeth Culotta, David Grimm (Online), Eliot Marshall, Jeffrey Mervis, Leslie Roberts, Richard Stone, John Travis; **contributing editor** Polly Shulman; **news writers** Yudhijit Bhattacharjee, Adrian Cho, Jennifer Couzin-Frankel, Carolyn Gramling, Jocelyn Kaiser, Richard A. Kerr, David Malakoff, Elizabeth Pennisi, Robert F. Service (Pacific NW), Erik Stokstad, Emily Underwood; **web developer** Daniel Berger; **social media strategist** Meghna Sachdev; **intern** Lizzie Wade; **contributing correspondents** John Bohannon, Jon Cohen (San Diego, CA), Ann Gibbons, Sam Kean, Eli Kintisch, Andrew Lawler, Mitch Leslie, Charles C. Mann, Virginia Morell, Gary Taubes; **copy editors** Melissa Raimondi, Kara Estelle; **administrative support** Scherraine Mack; **bureaus** San Diego, CA: 760-942-3252, FAX 760-942-4979; Pacific Northwest: 503-963-1940

Production director Wendy K. Shank; **assistant manager** Rebecca Doshi; **senior specialists** Steve Forrester, Christopher Redwood, Anthony Rosen; **Preflight director** David M. Tompkins; **manager** Marcus Spiegler; **specialists** Jason Hillman, Tara Kelly

Art director Yael Fitzpatrick; **associate art director** Laura Creveling; **senior illustrators** Chris Bickel, Katharine Sutliff; **illustrator** Yana Hammond; **senior art associates** Holly Bishop, Preston Huey; **art associates** Kay Engman, Garvin Grutlón, Chrystal Smith; **photo editor** Leslie Blizard

***Science* International**

Europe (science@science-int.co.uk) **editorial: international managing editor** Andrew M. Sugden; **senior editor/commentary** Julia Fahrenkamp-Uppenbrink; **senior editors** Caroline Ash, Stella M. Hurtley, Ian S. Osborne, Peter Stern; **associate editor** Maria Cruz; **contributing editor** Helen Pickersgill; **editorial support** Rachel Roberts, Alice Whaley; **administrative support** Janet Clements, Jenny Hinson, John Wood; **news: deputy news editor, u.k.** Daniel Clery; **contributing editor, europe** Martin Enserink; **contributing correspondents** Michael Balter (Paris), Kai Kupferschmidt (Berlin), Gretchen Vogel (Berlin)

Asia Japan Office: Asca Corporation, Tomoko Furusawa, Rustic Bldg. 7F, 77 Tenjin-cho, Shinjuku-ku, Tokyo 162-0808, Japan; +81 3 6802 4616, FAX +81 3 6802 4615, inquiry@sciencemag.jp; **contributing editor, asia** Mara Hvistendahl [China: mhvisten@aaas.org]; **contributing correspondents** Dennis Normile [Japan: +81 (0) 3 3391 0630, FAX +81 (0) 3 5936 3531; dnormile@gol.com]; Hao Xin [China: cindyhao@gmail.com]; Pallava Bagla [South Asia: +91 (0) 11 2271 2896; pbagla@vsnl.com]

EXECUTIVE PUBLISHER **Alan I. Leshner**
PUBLISHER **Beth Rosner**

Fulfillment Systems and Operations (membership@aaas.org); **customer service supervisor** Pat Butler; **specialists** LaToya Casteel, Michelle Ofordire, April Marshall; **manager, data entry** Mickie Napoleoni; **data entry specialists** JJ Regan, Jaimee Wise, Fiona Gildin

Business Operations and Administration director Deborah Rivera-Wienhold; **business systems and financial analysis director** Randy Yi; **manager, fulfillment systems** Frits Buningh; **systems analyst** Nicole Mehmedovich; **manager, business analysis** Eric Knott; **manager, business operations** Jessica Tierney; **business analysts** Cory Lipman, Celeste Troxler; Christine Wehrli; **financial analyst** Jeremy Clay; **rights and permissions: administrator** Emilie David; **associate** Elizabeth Sandler; **marketing director** Ian King; **marketing managers** Alison Chandler, Julianne Wielga, Justin Sawyers; **marketing associates** Mary Ellen Crowley, Elizabeth Sattler, Rebecca Riffkin; **senior marketing executive** Jennifer Reeves; **director, site licensing** Tom Ryan; **director, corporate relations** Eileen Bernadette Moran; **senior publisher relations specialist** Kiki Forsythe; **publisher relations manager** Catherine Holland; **publisher relations, eastern region** Keith Layson; **publisher relations, western region** Ryan Rexroth; **customer relations manager** Iquo Edim; **marketing manager** Christina Schlecht; **marketing associates** Paulina Curto, Mitchell Edmund; **customer relations analysts** Simon Chong, Lana Guz; **electronic media: director** Lizabeth Harman; **assistant manager** Lisa Stanford; **production specialists** Antoinette Hodal, Nichele Johnston, Lori Murphy, Kimberly Oster; **web and new media: senior project manager** Trista Smith, **project leader** Luke Johnson **computer specialists** Walter Jones, Kai Zhang, **web developer** Chris Coleman; **program director, aaas member central** Peggy Mihelich

director, global collaboration, custom publications, advertising Bill Moran
editor, custom publishing Sean Sanders: 202-326-6430
assistant editor, custom publishing Tianna Hicklin 202-326-6463
associate director, collaboration, custom publications/china/taiwan/korea/singapore Ruolei Wu +86-1367-101-5294

Product (science_advertising@aaas.org); **midwest** Rick Bongiovanni: 330-405-7080, FAX 330-405-7081; **east coast/e. canada** Laurie Faraday: 508-747-9395, FAX 617-507-8189; **west coast/w. canada** Lynne Stickrod: 415-931-9782, FAX 415-520-6940; **uk europe/asia** Roger Goncalves: TEL/FAX +41 43 243 1358; **japan,** Makiko Hara: +81 (0) 3 6802 4616, FAX +81 (0) 3 6802 4615; ads@sciencemag.jp; **china/taiwan** Ruolei Wu: +86 1367 1015 294 rwu@aaas.org

worldwide associate director of *Science* Careers Tracy Holmes: +44 (0) 1223 326525, FAX +44 (0) 1223 326532

Classified (advertise@sciencecareers.org); **u.s.: east coast/west coast/south central/south america** Tina Burks: 202-326-6577; **midwest/canada/industry** Allyson Rosen: 202-326-6578; **sales administrator** Marci Gallun; **europe/row sales** Lucy Nelson; **sales assistant** Kelly Grace; **japan** Yuri Kobayashi +81 (0)90-9110-1719; careerads@sciencemag.jp; **china/taiwan** Ruolei Wu: +86 1367 1015 294 rwu@aaas.org; **advertising support manager** Karen Foote: 202-326-6740; **advertising production operations manager** Deborah Tompkins; **senior production specialist/graphic designer** Amy Hardcastle; **production specialist** Yuse Lajiminmuhip; **senior traffic associate** Christine Hall; **sales coordinator** Shirley Young; **marketing manager** Allison Pritchard; **marketing associate** Aimee Aponte

AAAS Board of Directors retiring president, chair Nina V. Fedoroff; **president** William H. Press; **president-elect** Phillip A. Sharp; **treasurer** David E. Shaw; **chief executive officer** Alan I. Leshner; **board** May R. Berenbaum, Bonnie L. Bassler, Stephen L. Mayo, Raymond Orbach, Julia M. Phillips, Sue V. Rosser, David D. Sabatini, Inder M. Verma

AAAS
ADVANCING SCIENCE, SERVING SOCIETY

The Clinical Aspirations of Microarrays

Although most microarray applications are currently research-use-only, this technology appears poised to move to the clinic for genomics-based applications. In fact, some products can already be used in medical diagnostics and many more are in development. For example, microarrays can be customized to detect small, specific genetic changes that indicate a particular disease. In the future, this technology will likely remain a useful tool for both research and clinical applications

See full story on page 858.

Upcoming Features

Proteomics—March 1
Fluorescence Multiplexing—April 12
Proteomics: Maldi Imaging—May 31

AROUND THE WORLD

Tokyo **1**

High Cost of Scientific Whaling

Japan's scientific whaling effort is in the red, costing taxpayers $378 million since 1987, even as demand for whale meat has shrunk and the research has proven of little value, according to a 5 February report by the International Fund for Animal Welfare. Under the International Whaling Commission convention, scientific whaling is allowed despite a moratorium on commercial whaling since 1986. The meat can be sold to cover the cost of research.

Backers of the scientific whaling program insist that it has value, stating that the numbers of scientific whales taken actually fall far short of official targets, which limits the usefulness of the data for studying the size and health of stocks. But critics disagree. "It is well established in the scientific literature that there are many ways to study whale diet and condition without killing them," says Leah Gerber, a marine conservation biologist at Arizona State University, Tempe.
http://scim.ag/Japwhal

Geneva, Switzerland **2**

LHC Intermezzo

Physicists have shut down the world's biggest atom smasher, the Large Hadron Collider (LHC) at the European particle physics laboratory, CERN, for 2 years of repairs. The work should allow the LHC to run at full energy from 2015 onward. The collider had been cantering at about half energy since it broke down in September 2008—just 9 days after starting up—and sidelined itself for 14 months.

It may be an anxious wait. The LHC triumphed last summer when physicists discovered a particle that appears to be the Higgs boson, the last piece of their standard model of the known particles. But if the LHC produces nothing else, it could be the last collider physics gets.

"If the standard model Higgs is all that emerges from the LHC then, yes, justifying the expense of a major future facility is not obvious," says CERN spokesperson James Gillies. Still, he says, "we have every chance of making a discovery with this machine when it comes back on again or—who knows?—with the data we already have."

Lompoc, California **3**

Landsat's Lucky Number Is Eight

The world's oldest Earth-observing satellite system is still alive and off death row—at least for a while. Landsat 8, the latest in a line of U.S. orbiters first launched in 1972, was carried into space on 11 February by an Atlas V rocket launched from Vandenberg Air Force Base in California (pictured). The spacecraft is expected to reach its final orbit 705 kilometers above Earth by mid-April, and begin transmitting data by early summer. Researchers have long relied on Landsat data to monitor environmental and climate changes, but the program has faced several near-death budget crises. Landsat 8, which is expected to operate for at least 5 years, cost nearly $900 million. It will ultimately replace two existing orbiters: Landsat 5, which was launched in 1984 and decommissioned late last year after a record 28 years and 10 months of service, and Landsat 7, which was launched in 1999 but has struggled with technical glitches since 2003. It is uncertain whether Congress and the White House will be willing to find money for a Landsat 9.

Kano, Nigeria **4**

Health Clinics Attacked

Nine polio coworkers were killed on 8 February when gunmen stormed two health clinics in Kano state in northern Nigeria. Details remain murky, but the attacks occurred at the tail end of a polio immunization campaign. The shootings sparked fears that the assailants were targeting the polio eradication program in Nigeria, in an unsettling echo of recent events in Pakistan, where nine polio workers were shot and killed in December. As a precaution, the government of Kano halted polio vaccination activities, and U.N.

THEY SAID IT

"Funds currently spent by the government on social science, including on politics, of all things, would be better spent helping find cures to diseases."

—House of Representatives Majority Leader Eric Cantor (R–VA), renewing his attack on National Science Foundation funding of the social sciences in a speech on 5 February at the American Enterprise Institute in Washington, D.C.

CREDITS (TOP TO BOTTOM): NASA; KYODO VIA AP IMAGES

agencies pulled their polio staff members from the field.

No one has claimed responsibility for the attacks. In a statement, Nigerian Health Minister Muhammad Ali Pate promised an aggressive investigation, describing the "heinous" attacks as part of a "long standing cycle of violence that has engulfed [the northern states] in recent months."

Nigeria is one of three countries, with Pakistan and Afghanistan, where polio remains endemic. Cases are concentrated in the north, which is largely Muslim. Efforts to wipe out the virus there have been hobbled by rumors that the vaccine is part of a Western plot to sterilize Muslim children.

Strasbourg, France 5

Inching Toward E.U. Fisheries Reform

The European Parliament approved a plan on 6 February to reform the European Union's Common Fisheries Policy by a 502-to-137 vote. The plan aims to improve the much-criticized policy, last reviewed in 2002, by capping catches at sustainable levels, banning discards of unwanted species, and making better use of scientific data for long-term planning. According to the European

Commission, 68% of the European Union's stocks are overfished.

Under the revamped rules, starting in 2015 regulators would set catch limits using a data-driven standard known as maximum sustainable yield that is commonly used in fisheries regulation in the United States. If fully adopted, the rules will allow fish stocks to "recover by 2020, enabling us to take 15 million tons more fish and create 37,000 new jobs," predicted Ulrike Rodust, a German member of the Parliament who was responsible for revising and offering a legislative proposal originally developed by the European Commission in July 2011.

The reform plan still has to be discussed with governments from the European Union's 27 member states. If they reach an agreement by the end of June, the plan could come into force next year.
http://scim.ag/EUfish

NEWSMAKERS

'Arab Nobels' Honor Genetics Of Obesity, Superfast Physics

Score a "twoonie" for Canada. **Paul Corkum**, a Canadian physicist at the University of Ottawa, and **Ferenc Krausz**, a Hungarian-Austrian physicist of both the Max Planck Institute of Quantum Optics in Garching, Germany, and Ludwig Maximilians University in Munich, Germany, have won the 2013 King Faisal International Prize for Science for their independent work on ultrashort pulses of laser light. Such work has enabled scientists to track the motion of electrons within atoms and molecules. The two will share the roughly $200,000 prize, which is awarded annually and is sometimes called an "Arab Nobel Prize."

Meanwhile, American **Jeffrey Michael Friedman**, a geneticist with Rockefeller University and the Howard Hughes Medical Institute in New York City, and Canadian-born **Douglas Coleman**, retired from Jackson Laboratory in Bar Harbor, Maine, share the 2013 King Faisal International Prize for Medicine for their pioneering work together on the hormone leptin and the genetics of obesity. Friedman and Coleman have racked up several prizes in recent years.

David Evans to Lead U.S. Science Teachers Group

David Evans has never taught science at the precollege level. Nor has he carried out research on how to improve science teaching and learning. But the new executive director of the National Science Teachers Association says he sees value in bringing a fresh eye to the rapidly changing field.

"Information is much more accessible, and people can get it in a variety of new ways," says Evans, who last week took the helm at the 60,000-member society, based in Arlington, Virginia. He says two important changes for teachers—whom he calls "classroom teachers of science rather than science teachers, because not all of them have a background in the subject"—are the proliferation of free online courses and the arrival later this year of the Next Generation Science Standards, a national effort to get states to voluntarily adopt improvements in teaching science in elementary and secondary schools.

Trained as a physical oceanographer, the 66-year-old Evans spent 2 decades with the federal government, including a stint as undersecretary for science at the Smithsonian Institution. **http://scim.ag/EvansNSTA**

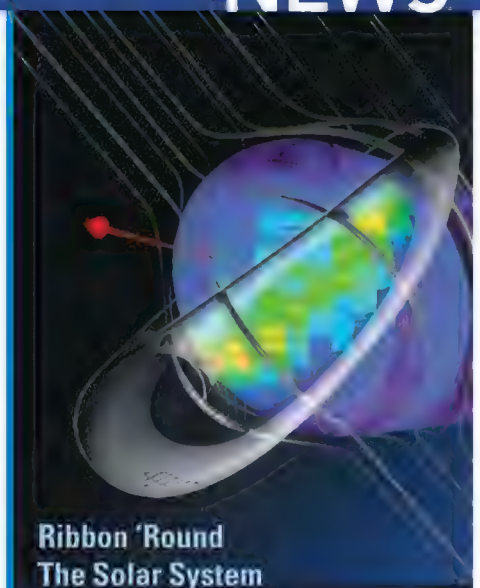

Ribbon 'Round The Solar System

More than 3 years ago, stunned space physicists reported the discovery of a narrow band of sky lit up in the cameras of NASA's Interstellar Boundary Explorer (IBEX). The spacecraft's cameras, trained toward the outer edge of the heliosphere where the sun's wind of charged particles encounters the oncoming magnetic field that courses between the stars, were observing a mysterious ribbon of high-powered hydrogen atoms streaming inward from that boundary. A dozen theories later, a pair of IBEX researchers reports this week in *The Astrophysical Journal* that the interstellar magnetic field (thin gray lines wrapping around the region filled by solar wind in the image) may be temporarily trapping and concentrating outbound particles. The trapping would be most effective where the solar wind squarely crosses interstellar magnetic field lines (gray "life preserver"). IBEX "sees" those particles that escape the trap as the ribbon, here rendered in reds, yellows, and greens.

CREDITS (TOP TO BOTTOM): EOS/UNIVERSITY OF NEW HAMPSHIRE; DAVE WEATHERALL/UNIVERSITY OF OTTAWA; JOM/WIKIPEDIA; 2012 © EVA GRIFFETH, COURTESY OF NSTA

FINDINGS

Sweaty Human Evolution, Through a Mouse Lens

Mice are helping scientists learn about the evolution of some humans' sweat glands. In 2007, computational analyses revealed that some Asians carry a particular version of a gene called *EDAR*. To learn the effects of that version, called 370A, Harvard Medical School's Yana Kamberov and her colleagues developed a strain of mice that carried 370A instead of the usual *EDAR* gene. Those mice have thicker hair, more sweat glands (blue tubes in the mouse footpad, above), denser mammary glands, and smaller fat pads around those mammary glands, the researchers report this week in *Cell*. The team also evaluated sweat gland density in Han Chinese carrying one or two copies of 370A and found that those with two copies had more sweat glands.

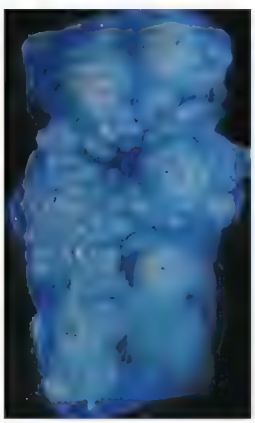

"It's one of the first papers that clearly shows that a change that was important in recent human evolution can be modeled in the mouse," says Wolfgang Enard, an evolutionary geneticist at the Max Planck Institute for Evolutionary Anthropology in Leipzig, Germany. The analysis suggests 370A arose in Central China 30,000 years ago and may have been favored as an adaptation to the humid environment. **http://scim.ag/sweatyev**

First Evidence of Life Under Antarctic Ice

Researchers have gotten the first glimpse of life lurking beneath Antarctic ice. Last month, a U.S. team drilled through 1000 meters of ice to reach subglacial Lake Whillans, part of a complex hydrological system in West Antarctica—and on 7 February the team announced that they now have obtained the first evidence of microbial life in a subglacial Antarctic lake.

Last month, a team of Russian scientists announced that they had successfully sampled another subglacial lake located thousands of kilometers away on the East Antarctic Ice Sheet; what microbes might exist in those waters are still unknown. But the two systems are very different:

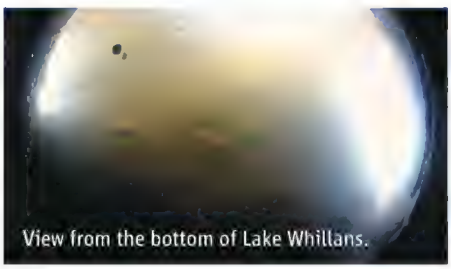

View from the bottom of Lake Whillans.

Unlike Lake Vostok, the Whillans system has been in periodic contact with surface waters, rather than isolated from the rest of the planet for millions of years. The team, which is seeking clues not only to glacial microbiology but also to ice sheet dynamics and the impact of climate change on the continent, hopes the Lake Whillans microbial community can shed light on organisms that can exist in the extreme dark and cold, and how such microbes might affect the chemistry of the ice.

Proto-RNA: Clues to Origin of Life

Origin of life researchers have long thought that RNA, the molecular cousin of the DNA that encodes our genes, may have played a starring role in the initial evolution of life from a soup of organic molecules.

But there are problems with this "RNA World" hypothesis. For starters, in water, the four chemical components of RNA, the nucleotides abbreviated A, G, C, and U, don't spontaneously assemble to create sizable molecules. So it remains a mystery how the first long gene-length chains of RNA would have ever taken shape in Earth's ancient environment.

Now, researchers led by Nicholas Hud, a chemist at the Georgia Institute of Technology in Atlanta, report in the *Journal of the American Chemical Society* that they have created a pair of RNA-like molecules that can spontaneously assemble into gene-length chains in water. Although it's likely to be difficult to determine whether these proto-RNAs or others like them were present at the dawn of life, the researchers are now working to see if the proto-RNAs can indeed faithfully encode information and evolve toward RNA. **http://scim.ag/RNAlife**

Science LIVE

This week, *Science* is reporting from the AAAS Annual Meeting in Boston. Visit **http://scim.ag/aaas_2013** for full coverage.

Random Sample

Diamonds Are a Sperm's Best Friend

It's hard out here for a sperm—even the petri dishes researchers use to store and culture the cells might actually harm their delicate cargo. Researchers in Germany suspect that exposing your standard polystyrene petri dish to water can cause its surface to soften into a layer of toxic goo made of chemicals called reactive oxygen species, or ROS. ROS have been wreaking havoc on sperm and egg cells during in vitro fertilization (IVF) procedures for decades, but until now, nobody thought to blame the petri dish.

So the researchers, led by materials scientist Andrei Sommer of Ulm University in Germany, came up with a solution that could bring back the sparkle: Make a petri dish out of quartz, and then coat it with a nanolayer of diamond. About 20% more sperm survived for 42 hours in diamond-coated petri dishes than in the polystyrene containers usually used for IVF, the researchers report in the *Online Proceedings Library* of the Materials Research Society.

"It's an interesting preliminary study," says Pravin Rao, a urologist at Johns Hopkins' James Buchanan Brady Urological Institute in Baltimore, Maryland, who was not involved in the study. "The most important thing to see is whether [the diamond-coated dishes] would improve IVF success rates"—particularly in cases complicated by low sperm counts, he says. "If you just have 10 sperm, it's great if even one extra sperm survives." **http://scim.ag/diamsperm**

Up in the air. After a budget cut, can Europe's GMES program afford enough Sentinel satellites?

CREDIT: P. CARRIL/ESA

SCIENCE FUNDING

European Budget Fight Moves to Parliament

BERLIN—After last week's marathon negotiating session in Brussels, which sought to set the European Union's budget for the next 7 years, science policy chiefs are breathing a sigh of relief, but also vowing to push for a better deal for research. In the face of an unprecedented 3.4% overall cut, the news that the budget's "competitiveness" section, which includes research spending, had won a 37% increase was welcome. But there's still disappointment that the main science funding program, Horizon 2020, is slated to get €70.96 billion—a significant hit compared with the €80 billion researchers had wanted.

European science leaders are making a pitch for a major correction. "Our feeling is that €80 billion is required to deliver on the ambitious and exciting proposal that the [European] commission presented [for Horizon 2020]. Anything other than that is disappointing news from Science Europe's perspective," says Paul Boyle, president of Science Europe, which lobbies for national science funding organizations. In a statement, Máire Geoghegan-Quinn, E.U. commissioner for research, innovation, and science, said that in upcoming negotiations she "will continue to fight for increased funding for the research, innovation and science sectors." Researchers' hopes now rest with the European Parliament, which must approve the final budget.

During the lengthy budget-setting process, the European Commission, the European Union's executive branch, initially proposed €80 billion for Horizon 2020 (a 60% increase over its predecessor program, Framework 7). That got batted back and forth between the commission, the Parliament, and the European Council, which represents the 27 member states (*Science*, 9 December 2011, p. 1331). Parliament was even more generous toward Horizon 2020, calling for €100 billion, but the council, which ultimately controls the purse strings, wanted considerably less in this time of austerity.

The exact figure for Horizon 2020 isn't spelled out in the summit conclusions, but it does say the program's funding "will represent a real growth compared to 2013 level." Over the weekend, Brussels' number crunchers calculated an "indicative" budget of €70.96 billion, says Michael Jennings, spokesperson for Geoghegan-Quinn.

A coalition of grassroots scientists, research organizations, and industry groups has been arguing for months that €80 billion is needed to make Horizon 2020 work the way it is designed. Even if it receives a slight rise over 2013 funding levels for Framework 7, the money will be spread more thinly, Boyle notes, because Horizon 2020 includes industrial research programs and the European Institute of Innovation and Technology, which Framework 7 doesn't fund.

Others see a silver lining. "I am getting signals from the community that we can live with [these numbers]," says Marja Makarow, vice president for research at the Academy of Finland and former head of the European Science Foundation. One closely watched part of Horizon 2020 is the European Research Council (ERC), which funds investigator-driven research and is widely regarded as one of the European Union's most successful grant programs. It looks likely to see its yearly budget grow from the €1.7 billion it has in 2013, says Tim Hunt, a member of ERC's Scientific Council.

The "competitiveness" budget also includes money for three large infrastructure projects that will be funded outside the Horizon 2020 program. The ITER fusion reactor will receive €2.7 billion, matching the commission's proposal. The Galileo global positioning satellite system will receive €6.3 billion, or €0.7 billion less than requested. But the Global Monitoring for Environment and Security (GMES) Earth-observing program gets just €3.79 billion, €2 billion less than proposed. The program is an ambitious effort to build an environmental monitoring system. Such a cut would force program managers to play a "risky game" with GMES's priorities, says Volker Liebig, head of Earth observation for the European Space Agency, because they may have to delay construction of duplicate satellites and hope that the ones soon to be in space will last many years beyond their specified lifetime.

The budget numbers could shift in the coming weeks during negotiations between the council, Parliament, and the commission before Parliament votes. The leaders of several of the largest parties in the Parliament issued a statement on Friday saying they "cannot accept today's deal in the European Council as it is." They listed four points they would "not abandon," including "strengthening European competitiveness and research."

But Maria Da Graça Carvalho, a member of Parliament from Portugal who is on the parliamentary committee in charge of Horizon 2020, tells *Science* that she doesn't expect major changes during negotiations, given the difficulty the council had reaching an agreement. If Parliament rejects the budget, the European Union would roll over its 2013 budget into 2014, with a slight increase for inflation. It is "not a very convenient or practical situation," she says, and would mean new programs couldn't start on time. "We have to see what's best for Europe," she says. **–GRETCHEN VOGEL**

With reporting by Daniel Clery.

U.S. SCIENCE POLICY

NSF Opening Adds to Concerns About Obama's Second-Term Science Team

Who will be the key scientific performers in Act II of the Obama administration? U.S. researchers are waiting anxiously for news after Subra Suresh, the director of the National Science Foundation (NSF), announced last week that he was leaving to become president of Carnegie Mellon University (CMU) in Pittsburgh, Pennsylvania.

His departure next month rings down the curtain on the so-called "dream team," a group of prominent academic scientists drawn to Washington because of a president who repeatedly emphasizes the importance of research in solving societal problems. The group includes three appointees returning home to the West Coast in the next few weeks: Department of Energy (DOE) Secretary Steven Chu (*Science*, 8 February, p. 635); Jane Lubchenco, head of the National Oceanic and Atmospheric Administration (NOAA); and U.S. Geological Survey (USGS) Director Marcia McNutt.

Hello, goodbye. John Holdren, shown swearing in Subra Suresh as NSF director in 2010, is expected to play a key role in finding his successor.

Other jobs are also open. At DOE, interim officeholders are running the Advanced Research Projects Agency-Energy and hold all three undersecretary slots, for energy, science, and nuclear security. The Census Bureau has had an acting director since Robert Groves left in August to become provost of Georgetown University. In addition, only one of the four divisions within the White House Office of Science and Technology Policy (OSTP) is led by someone confirmed by the Senate.

To be sure, some of the original cast is still on stage. John Holdren remains the president's science adviser and director of OSTP. The two presidential appointees at the National Institutes of Health—director Francis Collins and National Cancer Institute head Harold Varmus—give every indication that they are staying. ("I have no other plans than to continue what I am enjoying doing," Varmus says.) NASA Administrator Charles Bolden remains despite persistent rumors of his departure, and William Brinkman, who leads DOE's Office of Science, has just asked the community to update the office's 20-year facilities plan, confounding those who expected him to bow out after last fall's election.

Suresh, a former dean of engineering at the Massachusetts Institute of Technology, has earned high marks from the White House and congressional leaders for trying to expand NSF's international activities, foster interdisciplinary collaborations, promote entrepreneurship, and increase opportunities for young scientists. So his decision to leave before reaching the halfway point of his 6-year term surprised many observers.

His brief tenure highlights a curious phenomenon at NSF: Its directors either leave relatively early or remain on board for the full ride. The first group, to which Suresh belongs, consists of scientists in their late 40s and early 50s who leave to lead major research universities. In addition to Suresh, the list includes Richard Atkinson, who left in 1980, after 3 years (plus 9 months as acting director) to become chancellor of the University of California (UC), San Diego; John Slaughter, who left in 1982, after 2 years, to be chancellor of the University of Maryland; and Walter Massey, who left in 1993, after 2 years, to be the second in command at UC and later president of Morehouse College.

The second group—older, more senior scientists who have already made their marks—tend to complete their term or at least remain until the end is in sight. That roster includes Erich Bloch, Neal Lane (who moved to the White House to become science adviser to President Bill Clinton), Rita Colwell, and Arden Bement, Suresh's immediate predecessor.

Suresh, who arrived at NSF in October 2010, says he wasn't looking for a new job. "My reasons for leaving are very simple," he explains. "This was a wonderful opportunity, and Carnegie Mellon is an institution that I had long admired. It would have been nice to have stayed another year or two, but opportunities come when they come."

Dan Arvizu, chair of the National Science Board, NSF's oversight body, notes that Suresh and other NSF directors who left prematurely "are in the prime years of their earning power." Given their highly visible perch at NSF, he says, most have many opportunities to maximize that potential.

Slaughter, a Carter appointee, spent a tumultuous 2 years in office fighting attempts by President Ronald Reagan to eliminate the foundation's education directorate and its social and behavioral science programs. But "the main reason I left was economic," he says. "I had two children in college, and $57,500 was well below the private sector. I was offered a 40% increase in salary, and that was way too hard to turn down."

Suresh's move will be even more lucrative. Outgoing CMU President Jared Cohon received $860,982 in total compensation in 2010, more than four times Suresh's $179,700 salary at NSF.

If form holds, former NSF directors say, Holdren will play a key role in identifying a replacement for Suresh. NSF is often a bellwether for how a president and his administration view academic research, a topic that falls squarely in the purview of the science adviser. Having the backing of the science adviser is also essential for a successful tenure at NSF. "The president wouldn't nominate anyone who the science adviser doesn't support," Massey says. "And if he does, that person shouldn't take the job."

The reason, Massey says, is access. "The science adviser is the person who works directly with OMB [the Office of Management and Budget within the executive office] and who provides you with access to important meetings," he says. "Without his support, you run the risk of being marginalized."

The science adviser appears to play a smaller role in filling other top science jobs. At USGS, for example, the U.S. National Academy of Sciences has historically helped

CREDIT: CHRISTY BOWE/IMAGE CATCHER NEWS

vet potential nominees, who are almost always earth scientists. "If you want the job, it helps to have your name on that list," says former USGS head Charles "Chip" Groat, who led the agency from 1998 to 2005. But rounding up political support helps, too: Groat says that when he was under consideration for the job, he "called around" to members of Congress and senior administration officials, "just to make it clear I was very interested."

Science groups have traditionally played a lesser role in nominating potential DOE and NOAA chiefs, in part because those agencies have responsibilities that go far beyond research. DOE, for instance, oversees nuclear weapons programs and energy development issues; NOAA's tasks include building satellites and regulating fisheries. As a result, potential nominees can come from an array of nonresearch fields.

The next 4 years promise to be a challenging time for whoever gets these high-profile jobs, given the polarized politics and dire budget forecasts. "You are going to need someone who is very tolerant of pain, because you may be managing a decline in your program," Groat says. Still, he and others expect there will be plenty of scientists who want to come to Washington, seeing it as a chance to serve a president whose policies they admire and to advance their careers. As Groat notes, "these jobs just don't come open that often."

–JEFFREY MERVIS AND DAVID MALAKOFF

GERMANY

Plagiarism Hunters Take Down Research Minister

BERLIN—When Annette Schavan, Germany's minister for science and education, resigned on 9 February, even politicians from opposition parties called the move "tragic." She is the latest in a string of officials here who have stepped down amid plagiarism allegations. But Schavan's case, centering on her 1980 dissertation in education studies, was less clear-cut than others, and it has opened up a debate in German academia.

Questions about Schavan's title were first raised last May by an anonymous accuser who posted an analysis of her 351-page dissertation on a Web site called schavanplag. Schavan asked the University of Düsseldorf to investigate. An initial report leaked to the press last October found that roughly 60 passages in the 351-page treatise were paraphrased without adequate citation. On 5 February, a university committee revoked Schavan's doctorate degree; 4 days later, she announced her resignation.

Some high-profile academics have argued that Schavan's wrongdoing was too trivial to warrant stripping her of her degree, and that relaxed citation standards were common practice in education studies at that time. The University of Düsseldorf has been criticized for allowing the report to be leaked, for not inviting Schavan's thesis adviser to testify, and for not asking external experts to evaluate the dissertation. Her defenders also argue that other German politicians felled by plagiarism scandals had engaged in far more egregious conduct: cutting and pasting whole newspaper articles into their dissertations.

In a statement to *Science*, Peter Gruss, president of the Max Planck Society, said that he understood Schavan's decision to step down. "The circumstances that led to her resignation, however," he wrote, "leave many questions open—especially with regard to the way we deal with people who receive particular public attention based on their office." Last month, Max Planck and other German science organizations outlined procedures for plagiarism investigations, and in doing so leveled indirect criticism at University of Düsseldorf. Among other things, their statement argued for using more than one person to investigate such allegations—a single professor authored Düsseldorf's report—and called for considering the context of when a dissertation was written.

Others contend that in plagiarism, there are no mitigating circumstances. No external evaluation is necessary and context has no role to play in establishing plagiarism, asserts Volker Rieble, a law professor at Ludwig Maximilians University Munich in Germany, who has written a book on plagiarism. To Rieble, Schavan's case involves "all the usual hallmarks of intent."

Schavan has conceded having made mistakes in her thesis, but she denies any intent to mislead and has said she will challenge the university's decision in court. At the press conference, she said that her legal battle would have made it awkward for her to lead the ministry. She could not be reached for further comment.

After 7 years at the helm, Schavan will be succeeded by Johanna Wanka, education and research minister of Lower Saxony. Jürgen Mlynek, president of the Helmholtz Association, which runs many of Germany's largest research facilities, praised the appointment. "She does not avoid conflict, she takes clear positions, but at the same time she's free of any ideology," he said in a statement. Wanka earned a mathematics doctorate in 1980 for her dissertation, "Solution of contact and steering problems with potential-theoretical methods." Martin Heidingsfelder, a co-founder of VroniPlag, a plagiarism Web site that targets politicians, told *Hamburger Morgenpost* that he and others would "of course" check Wanka's dissertation. (He just created a new Web site, PolitPlag, which accepts donations from individuals who want to see a particular politician's doctorate scrutinized.) Heidingsfelder admitted that the topic would make it "a bit more difficult" than the political science and humanities dissertations they have scoured to date—and he welcomed help from sympathetic mathematicians.

–KAI KUPFERSCHMIDT AND GRETCHEN VOGEL

Last stand. Chancellor Angela Merkel and science minister Annette Schavan face the press to announce the minister's resignation. Merkel accepted the resignation with a "very heavy heart."

CREDIT: JOHN MACDOUGALL/AFP/GETTY IMAGES/NEWSCOM

SPACE ASTRONOMY

Cash-Strapped NASA Gets Many Ideas for 'Free' Telescopes

Astronomers and planetary scientists are used to dreaming up missions from scratch. But last week they gathered in Huntsville, Alabama, to discuss building a mission around existing hardware—to be precise, two telescopes that fell into NASA's lap 2 years ago.

The ideas flowed freely, from an exoplanet-hunting spacecraft to a Hubble-like observatory to study the deep universe. But it's not certain any will ever fly. Although the telescopes are paid for, the money to design and build an accompanying suite of instruments, and then launch the entire mission, is in short supply.

The two 2.4-meter telescopes were built by the National Reconnaissance Office (NRO) for use on intelligence-gathering satellites. But early last year, NRO decided that the telescopes, each worth an estimated $250 million, would not suit future intelligence missions. NRO offered them to NASA with one condition: They could not be used to look down on Earth.

Facing a declining budget that has crippled its ability to plan new missions, NASA gratefully accepted the gift. Officials hoped the telescopes could be the starting point for two NASA missions, working in concert with cameras and spectrographs, to explore specific pressing questions. The telescopes are in storage while NASA figures out how best to use them.

The agency's initial thought was to use one of the telescopes as a centerpiece of the Wide-Field Infrared Survey Telescope (WFIRST)—a $1.5 billion dark energy mission that received top billing among space-based astronomy projects in the last astronomy and astrophysics decadal survey. But after scientists complained about being shut out of the decision-making process, NASA put out a call for concepts in November. Last week, 33 of the resulting proposals were discussed at NASA's Marshall Space Flight Center.

One popular suggestion would use one of the telescopes as part of a successor to the Hubble observatory, which is likely to be turned off within 5 years. Hubble has several specialized instruments that allow it to see in the infrared, visible, and ultraviolet spectra, and when Hubble shuts down, the United States will have no space observatories studying the universe at ultraviolet wavelengths. (The $8.8 billion James Webb telescope, scheduled for launch late in the decade, would observe primarily in the infrared.)

Another idea was a mission dedicated to following up on distant gamma ray bursts—flashes of energetic radiation resulting from the collapse of a star into a black hole. Gamma ray bursts provide astronomers with a unique tool to study the early universe. But scientists now have only a limited ability to take spectra from gamma ray bursts detected in deep space.

"Our proposal is to have this be a spectroscopic telescope that would for the first time systematically identify and take spectra from high red-shift gamma ray bursts," says astronomer Jonathan Grindlay of Harvard University. Such a telescope could follow up on the hundreds of distant bursts that the Large Synoptic Survey Telescope, a ground-based facility now in the works, is expected to spot every night. Not being able to study some of those in detail would be a shame, Grindlay says.

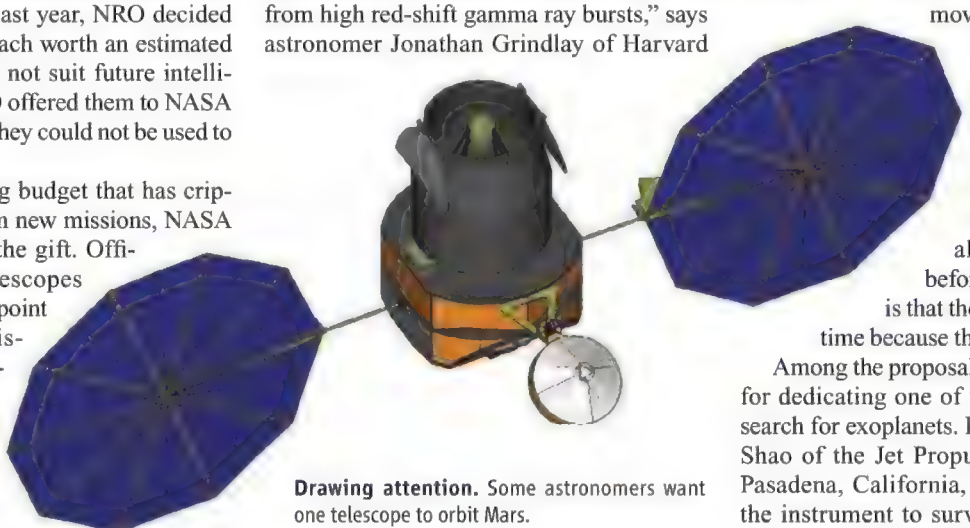

Drawing attention. Some astronomers want one telescope to orbit Mars.

CREDIT: LOCKHEED MARTIN

Some astronomers want to put one of the telescopes in orbit around Mars. One proposal, the Mars Observing Space Telescope (MOST), would deploy the hardware for a high-resolution survey of the martian surface. Its instruments would seek clues to habitability, such as ancient water flows. The telescope would serve double duty: When pointed away from Mars, it could take ultraviolet observations of nearby and faraway stars.

The observatory, proposed by Alfred McEwen, a planetary astronomer at the University of Arizona in Tucson, and others, would travel to Mars using solar electric propulsion, a possible technology for future deep space exploration. "NASA has a strong desire for a new Mars orbiter to support surface exploration beyond 2020 and a replacement space telescope with UV-visible capability to replace the Hubble Space Telescope," McEwen notes. "MOST could be attractive to NASA as a single mission to accomplish both high-priority objectives, and it would be less expensive than two separate missions."

Bundling multiple NASA priorities into one proposal would make them more affordable, an important consideration given that any space mission deploying the gifted hardware would cost in the neighborhood of $1 billion. But there is no money available to move forward on any of these proposals right now. In the words of a former NASA science official who did not wish to be named: "One reason they can go through all of these concepts before deciding what to do is that there's time. And there's time because there's no money."

Among the proposals were a host of ideas for dedicating one of the telescopes to the search for exoplanets. For example, Michael Shao of the Jet Propulsion Laboratory in Pasadena, California, proposed deploying the instrument to survey 200 nearby stars in search of Earth-like planets. Timothy Livengood and his colleagues from NASA's Goddard Space Flight Center in Greenbelt, Maryland, want to go beyond direct detection of planets around nearby stars to characterizing the atmosphere of newly found planets. That would require a near-infrared imaging instrument.

One of the more unusual proposals, from Goddard's Avi Mandell, involves flying one of the telescopes on a long-duration balloon flight. The arrangement would allow the instruments on the telescope to be serviced without having to send astronauts into space.

NASA officials plan to pick six of the concepts presented last week for further study this spring, says NASA's W. George Fletcher in Huntsville, who helped organize the workshop. Meanwhile, a panel of astrophysicists is conducting a study of how the hardware would fit into plans for WFIRST.

–YUDHIJIT BHATTACHARJEE

REPRODUCTIVE BIOLOGY

Faulty DNA Repair Linked to Ovarian Aging in Mice and Humans

A woman's cache of eggs drops precipitously right around her 37th birthday, but the reasons have always been puzzling. Researchers are converging on one new and eminently logical answer: The ovary's ability to repair damaged DNA may decline over time, and with it, the survival of its eggs.

A new study of mice and humans whose natural ability to fix DNA is impaired, published this week in *Science Translational Medicine*, bolsters this theory. Years ago Kutluk Oktay, a reproductive endocrinologist at the New York Medical College's Institute for Fertility Preservation in Rye, began helping young women with breast cancer freeze their eggs and embryos before chemotherapy, which often affects fertility. To Oktay's surprise, those with mutations in the *BRCA1* gene, which predispose people to breast and ovarian cancer, didn't respond as well to fertility drugs as he'd expected. In late 2009, he and his colleagues reported in the *Journal of Clinical Oncology* that among 47 women with breast cancer seeking egg preservation, more than one-third of those with *BRCA1* mutations responded poorly to drugs that stimulate the ovaries. Among those who didn't carry a *BRCA* mutation, 3%, or one out of 33, were poor responders.

BRCA1, Oktay knew, is a gene that keeps cells genomically intact. What if *BRCA1* mutations were causing egg DNA to go haywire and killing the cells?

In the new work, Oktay and his group found that so-called "double-strand breaks"—a measure of DNA damage—were more likely in the eggs of older mice than in younger ones. About 33% of ovarian follicles from 1-month-old mice had evidence of damage, compared with 59% from their 11-month-old counterparts. Furthermore, expression of genes that repair these double-strand breaks, including *BRCA1*, faded with age. (One exception was the gene *BRCA2*, which when mutated also predisposes people to cancer, although later in life than *BRCA1*.)

In eggs from 24 healthy women of different ages, several DNA repair genes like *BRCA1* also lost expression over time. This suggested that the ability of eggs to repair their DNA worsened with age, although it didn't prove that faulty DNA repair was a reason for the die-off of older eggs.

Oktay's group then examined mice and women with abnormal *BRCA1* function. Animals whose *BRCA1* gene was silenced had more follicles with DNA damage, and more follicles dying—about 70%, compared with 35% of a control group. Silencing other DNA repair genes correlated with similarly abnormal eggs. Finally, women with *BRCA1* mutations had lower levels of anti-Müllerian hormone (AMH), which is often used to assess a woman's egg reserve. Their levels were about half of those without *BRCA1* mutations; those with *BRCA2* mutations fell somewhere in between.

The study tells us that, "Guess what? Ooctyes aren't unique" when it comes to maintenance, says David Albertini, a reproductive biologist at the University of Kansas Medical Center in Kansas City. Like other cells, eggs "need to repair their DNA … one way or another."

While Oktay's work focuses on *BRCA1*, several recent studies have pointed to DNA repair generally as something that falters with ovarian age. Last year, a Dutch study that scanned the genomes of nearly 40,000 women linked several DNA repair genes to natural menopause (although *BRCA1* was not among them). "The ovary could be an interesting sensor of how well you age," says Aleksandar Rajkovic, a reproductive geneticist at the University of Pittsburgh in Pennsylvania. Women with premature menopause are also at risk of cardiovascular disease and, more generally, an earlier death, for reasons that are not well understood.

Still, many details of DNA repair and ovarian aging remain poorly understood. "We need to look at the mechanisms before we say it's of huge significance," says Karen Berkowitz, a reproductive endocrinologist and biologist at Drexel University College of Medicine in Philadelphia, Pennsylvania.

Indeed, although Oktay's experiments hint that women with *BRCA1* mutations are more likely to struggle with infertility, other studies haven't borne this out. Steven Narod, who studies familial breast cancer at the Women's College Research Institute at the University of Toronto in Canada, followed up on Oktay's 2009 paper by looking at hundreds of women with *BRCA* mutations. The women with *BRCA1* experienced menopause at about age 49 (women with *BRCA2* were several months later), rather than the average of 51. But they reported no more fertility issues than the control group. "It didn't seem to be recognized as a problem by the women," sways Narod, whose paper is in press at the journal *Fertility and Sterility*. He thinks that's because a slightly earlier menopause doesn't necessarily have anything to do with fertility in your 30s.

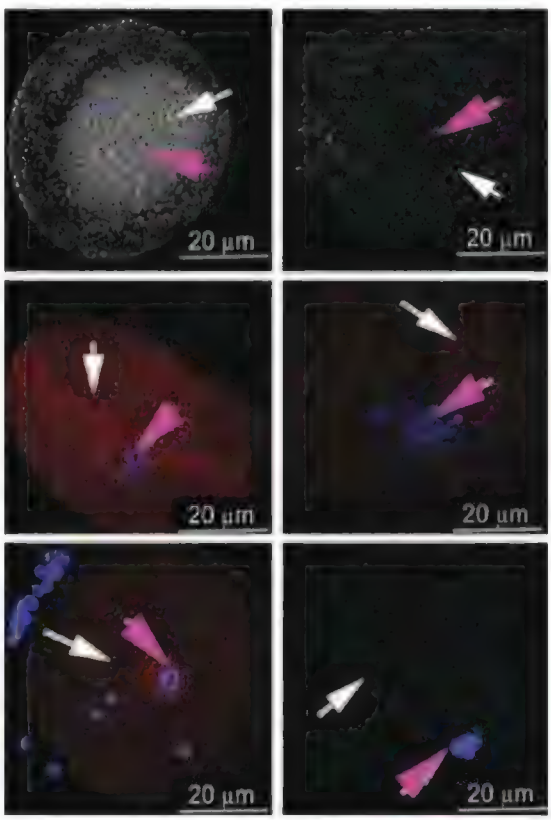

Dwindling. The expression of DNA repair proteins—including BRCA1 (*top panel*), RAD51 (*middle*), and Mre11 (*bottom*)—is vivid in younger eggs on the left but not in older ones. White arrows indicate cytoplasm and pink arrows point to the nucleus.

If faltering DNA repair helps explain why eggs die generally, and not just in *BRCA1* carriers, one big question is, "How can you foster DNA repair?" says Joshua Johnson, a reproductive biologist at Yale University School of Medicine. Here, things get tricky. It's widely known that in addition to dying off, older eggs also accumulate chromosomal abnormalities at a much higher rate than younger ones. Even if the dying eggs can be saved, should they be? Rajkovic asks. "Maybe these ooctyes should be eliminated," he says, because if they survive they might be unhealthy.

–JENNIFER COUZIN-FRANKEL

CREDIT: TITUS *ET AL.*, *SCIENCE TRANSLATIONAL MEDICINE* **5**, 172 (13 FEBRUARY)

The Many Ways of Making Academic Research Pay Off

Universities are learning that commercialization means more than patents, licensing fees, and startups

THREE YEARS AGO, AHMED ELLAITHY LEFT A HIGH-TECH STARTUP in Dubai to help his alma mater, the prestigious American University in Cairo, launch one of the first offices in Egypt dedicated to turning academic research into commercial products. "I faced some very existential questions," recalls the 31-year-old engineer. "What's the point of commercialization? What are we trying to accomplish? How will we know if it's working?"

A lot of academic administrators around the world have similar questions about a suite of activities that goes by the name "technology transfer." Research universities are under growing pressure to play a more active, entrepreneurial role in commercial innovation. Intent on fueling economic growth—and dazzled by the ability of research-intensive campuses such as Stanford University in Palo Alto, California, to spawn multibillion-dollar businesses—governments are trying to encourage academic researchers to transform their discoveries into products. University leaders, in turn, increasingly regard tech transfer as a prerequisite for luring top faculty members and students, raising research funds, and potentially cashing in on lucrative inventions. "There's this growing sentiment that you can't be a strong university without having a serious plan for research commercialization," says Steven Price of Oklahoma State University (OSU), Stillwater, who helps mentor aspiring tech transfer administrators like Ellaithy.

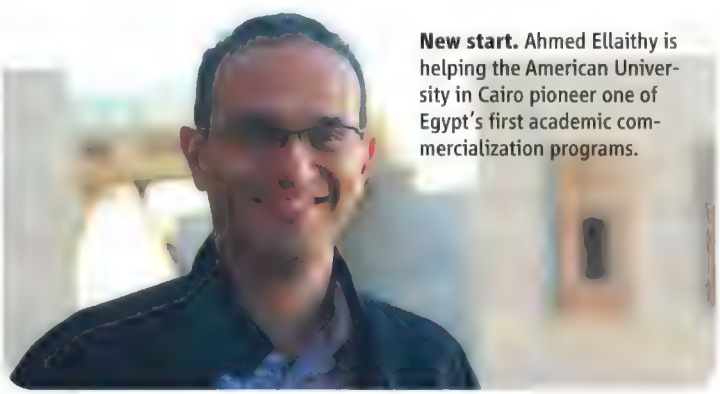

New start. Ahmed Ellaithy is helping the American University in Cairo pioneer one of Egypt's first academic commercialization programs.

But efforts to turn universities into commercial hothouses often don't succeed: Tech transfer is a net money-loser at most universities, studies suggest, with legal and administrative costs often exceeding revenues. Indeed, a growing number of scholars warn that government and university officials too often create unrealistic expectations by overstating the potential benefits of commercialization and underestimating how hard it is to do and what it will cost. Many advise schools to focus instead on "knowledge transfer"—helping society benefit from the discoveries and skills of faculty members and students without focusing just on finances. That's the broader approach Ellaithy is taking at the American University in Cairo, at least initially.

"You are seeing a lot of reassessing, a lot of experiments," says Phyl Speser, CEO of Foresight Science & Technology, a consulting firm in Providence, and a vice president of the U.S. Association of University Technology Managers (AUTM). "People are trying to figure out the best way to do this."

Universities have a big stake in getting it right. A well-tailored tech transfer effort can bolster a school's bottom line, enhance its contribution to society, and please politicians. A flawed program, however, can become a financial drain, raise potential conflicts of interest, and interfere with an institution's mission to teach and carry out research.

CREDITS (TOP TO BOTTOM): SUMMER AZMI; G. GRULLÓN/*SCIENCE*; ADAPTED FROM: "MANAGING UNIVERSITY INTELLECTUAL PROPERTY IN THE PUBLIC INTEREST," NATIONAL ACADEMIES PRESS, 2010

"Technology transfer has become a focus of innovation policy in many places, and there are some high expectations," says economic sociologist Martin Kenney of the University of California, Davis. The challenge, he says, is "to get the incentives aligned right, so that everyone benefits: the inventor, the university, society. And there are plenty of ways you can get them wrong."

Singles and home runs

Although the idea of commercialization seems straightforward, its implementation is not. Legal and institutional arrangements vary by nation, by university, and even by academic department and discipline, and so do strategies. "There's really no such thing as 'typical' tech transfer," says Foresight's Speser.

Some schools try to commercialize as many discoveries as possible in hopes that a few will hit it big. Others are pickier, choosing quality over quantity. Some put their own money into spinoff companies; others don't want to run the financial risk, or are prohibited from doing so. Given the vastly different budgets, cultures, and goals of modern research universities, "there cannot be a single template for technology transfer," concluded a 2010 report from the National Research Council (NRC) of the U.S. National Academies entitled *Managing University Intellectual Property in the Public Interest*.

In general, however, Egypt and most other nations are following a path blazed by the United States. In 1980, federal legislators responded to concerns that government red tape was trapping many inventions in the lab by passing the Bayh-Dole Act. The law gave U.S. universities an unambiguous right to claim ownership of promising discoveries, such as cancer-fighting molecules or better computer algorithms, even if the research was conducted with public funds. Since then, dozens of countries have adopted similar policies.

Generating good ideas is just the first step. If an invention appears to have commercial value, a university can create intellectual property (IP) by applying for a patent, copyright, or some other form of ownership that it can legally enforce. The university can then sell or license the right to use the invention to one or more companies—or assume the risks of launching its own startup. Any payments or profits are typically divided equally among the inventor, the inventor's academic department, and the university's general fund.

The Bayh-Dole system has opened the door to some eye-popping payouts. In 2005, for example, Stanford earned $336 million from selling its stake in Google, and New York University and its researchers have earned more than $650 million since the mid-2000s from the science underpinning Remicade, an arthritis drug. In 2011 alone, Northwestern University in Evanston, Illinois, earned $192 million from its tech transfer operation, topping the most recent annual chart assembled by AUTM. And a federal jury recently awarded a whopping $1.2 billion to Carnegie Mellon University in Pittsburgh, Pennsylvania, after it found that a semiconductor company had used the university's inventions without permission. (The company is appealing the verdict.)

The problem facing would-be copycats is that such windfalls are the exceptions, not the rule. "The great majority of [university] inventions generate modest revenues and many generate none," the NRC report found. "A handful of universities and a small fraction of all inventions are responsible for a large fraction of the revenues received."

In recent years, for example, analysts estimate that fewer than 15 of the roughly 100 major U.S. universities have reaped more than 50% of all commercialization revenues, which totaled $2.5 billion in 2011. And less than 1% of the thousands of academic licenses granted in the last few decades have generated more than $1 million in royalty income. (That low batting average is true even at Stanford.) Indeed, many U.S. schools earn much more from television contracts to broadcast athletic events than they do from tech transfer. Universities in Europe and Asia fare even worse, on average, using similar financial metrics.

The bottom line, the NRC report says, is that tech transfer pro-

GLOBAL RESEARCH UNIVERSITIES

WWW.SCIENCEMAG.ORG/EXTRA/GLOBAL

This is the fifth is a series of articles on global research universities. Previous stories have examined how mobility shapes an institution (7 September 2012, p. 1162), the growth of satellite laboratories (28 September, p. 1600), how France and Germany hope to strengthen a handful of elite universities (2 November, p. 596), and the problems facing the fledgling King Abdullah University of Science and Technology (7 December, p. 1276).

CREDITS (TOP TO BOTTOM): ISTOCKPHOTO.COM; G. GRUILLON/SCIENCE; ADAPTED FROM: "MANAGING UNIVERSITY INTELLECTUAL PROPERTY IN THE PUBLIC INTEREST," NATIONAL ACADEMIES PRESS, 2010

grams "should not be predicated on the goal of raising significant revenue for the institution. The likelihood of success is small and the probability of disappointed expectations high."

A USTAR is born

Those fiscal realities haven't prevented technology transfer from becoming a powerful tool for some research universities in attracting star scientists, obtaining more funding, and moving up in the academic rankings. In Utah, for example, the state's two major public universities—the University of Utah (UU) and Utah State University—have used a high-profile commitment to commercialization to help persuade state officials to spend nearly $100 million since 2007 on the Utah Science Technology and Research Initiative (USTAR).

Incubator. A new research laboratory at the University of Utah is part of a state-funded effort to attract star scientists.

The program has helped the two universities build state-of-the-art laboratories, strengthen their tech transfer offices, and offer hefty startup packages to new faculty members working in a handful of fields. Those areas, including biomedicine, nanotechnology, and energy, were deemed most promising by a USTAR governing board made up of business and education leaders. In return, the universities have promised to generate new patents, licenses, and spinoff companies that would create good jobs and plenty of tax revenue (and potentially revenue for the inventor and the school).

The link between commercialization and academic quality makes sense, outsiders say. "A good commercialization record is an outcome of having a good university, not the other way around," says economist Jerry Thursby of the Georgia Institute of Technology (Georgia Tech) in Atlanta. It didn't hurt, however, that UU already had a solid record of commercializing research and ranks among the top 20 U.S. institutions in creating startup companies and earning commercialization revenue.

So far, USTAR seems to be paying off for the two schools. The money has helped them hire about 50 scientists, who in turn have won more than $190 million in government research grants. That's definitely punching above their weight, university officials say: Although USTAR researchers represent just 1% of the total faculty at both schools, their presence has boosted extramural funding at the two schools by 5%. "USTAR was designed to allow us to aggressively recruit very productive scientists, and it is working," says USTAR chief Ted McAleer.

UU chemist Shelley Minteer is one of those scientists. "I was intrigued and impressed by how well tech transfer was integrated into the effort—the process is really valued by the university," says Minteer, who was recruited last year from Saint Louis University in Missouri. She has two technologies, including one involved in producing solar power, under review for their commercial potential, and says that tech transfer officials "make it very easy to get help with developing your ideas."

Overall, USTAR researchers have so far filed about 340 such invention disclosures that have generated more than 200 patents. Those numbers top the performance of the average faculty member, as well as USTAR's own projections.

Turning USTAR into cash and jobs, however, has proven difficult. The patents have so far produced less licensing revenue than originally forecast, and although the program has spun off nine companies, many are struggling to thrive, McAleer says. However, he cautions that it often takes 7 years for ventures to start to pay off.

The program has also experienced growing pains. The recession led to a cut in state funding, one of the new state-funded buildings has higher than expected operating costs, and officials are still tinkering with the best way to organize the USTAR teams.

Still, university officials see many advantages from USTAR. The program has created a buzz in the business community and solidified the standings of both universities in world rankings of science departments. UU, for instance, has jumped 11 slots since 2007, to 82nd in 2012, in a world ranking of research universities developed by China's Shanghai Jiao Tong University.

State politicians appear happy with the results. The governor has asked for $20 million to keep USTAR rolling in 2013, and $25 million for 2014. University administrators don't know how long that political support will hold up, however, if USTAR fails to generate long-term jobs or licensing revenue.

Going with the flow

Although many university and government officials point to USTAR as a promising commercialization model, some question the wisdom of using patenting and licensing metrics to prove its worth. Those statistics, although relatively easy to collect and present, can overshadow an array of factors that are harder to quantify, including other ways that knowledge flows from academia into the private sector. Too often, those pathways are overlooked because public discussion is "skewed by the abundance of data regarding licensing" and other financial metrics, the NRC report concluded.

In recent years, scholars have identified at least eight major pathways for "knowledge transfer" from universities—of which licensing intellectual property is just one (see graphic). The others include informal contacts between researchers and industry, private consulting contracts between university scientists and firms, and research collaborations that allow students to take jobs in industry and government. The use of a broader array of metrics would bolster the rankings of some universities that are now seen as tech transfer weaklings, researchers argue, especially in Europe, where universities often lag behind comparable U.S. campuses in traditional commercialization measures.

To capture a more complete picture, many academics and university groups are now trying to devise new metrics. The Association of Public and Land-grant Universities, a collection of 218 U.S. institutions, for example, is in the midst of a multiyear effort to quantify knowledge transfer with such metrics as the number of times local businesses seek advice from a professor or the number of student interns that a company hires.

Such interactions were very much on the mind of engineer C. Daniel Mote Jr., incoming president of the U.S. National Academy of Engineering, during his 12 years as president of the University of Maryland (UMD), College Park. When he began his tenure, in 1998, he recalls, many universities were ramping up their tech transfer offices, with some making "pretty unrealistic claims about how much money they could make." Mote preferred a knowledge transfer approach that placed less emphasis on the bottom line.

"I was much more inclined to build relationships [with industry] rather than build revenues," he says. "I wanted to create an entrepreneurial culture with lots of opportunities for interactions between

CREDIT: IMAGE COURTESY OF THE UNIVERSITY OF UTAH

faculty, students, and companies." Students, he adds, "are basically your principal tech transfer asset; they transfer skills and enterprise to the community."

That philosophy has helped shape an array of institutional arrangements at UMD, including events intended to maximize interactions with potential industry partners. Along with a traditional patenting and licensing operation and "incubators" where entrepreneurial faculty members and students can nurture their startups, there's also a growing undergraduate entrepreneurship program and informal mixers with business leaders and local venture capitalists. The school's Maryland Technology Enterprise Institute (Mtech) also hosts regular entrepreneur hours where anyone can get advice from experts on commercializing their ideas regardless of their relationship to the university.

At one gathering last year, for instance, two UMD geneticists wondered if they could sell information about equine DNA to racehorse breeders, while a local businessman described trying to commercialize a patented recipe for converting discarded crab shells into a valuable biochemical. "We're interested in creating connections in the broader community, not just on campus," says Dean Chang, a former computer science entrepreneur who now helps lead UMD's innovation programs. Those connections are in line with the university's mission to help develop the local and national economy, Chang and other college officials say.

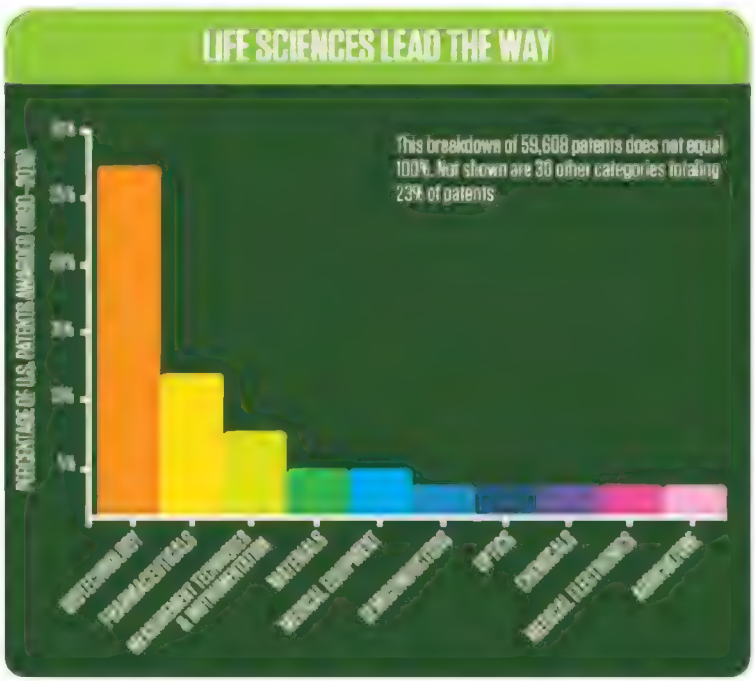

Intellectual property. Academic discoveries related to biotechnology and new drugs have been the top sources of patents won by U.S. universities in recent years.

CREDIT: NATIONAL SCIENCE FOUNDATION, SCIENCE AND ENGINEERING INDICATORS 2012

UMD's approach is consistent with research showing that "innovation requires an ecosystem and experience, not just an office," says Lesa Mitchell, a vice president of the Ewing Marion Kauffman Foundation in Kansas City, Missouri, which has funded extensive studies of commercialization. "You want a rich mixing bowl where people are running into each other in all kinds of settings." Large urban campuses with diverse, well-developed economies often have an edge, she adds, because cities can provide a critical mix of skilled talent, influential contacts, and investment capital.

Many universities are also experimenting with ways to cut the red tape surrounding IP. One approach is to offer potential partners standardized online legal agreements executed with the click of a mouse. Other institutions are going further, allowing professors and students to found startups without a license from the university. Todd Sherer, the president of AUTM and head of the technology transfer office at Emory University in Atlanta, says schools taking that approach are essentially saying: "Don't worry too much about charging for this technology now; we'll get it back in donations later if the company succeeds."

Economist Marie Thursby of Georgia Tech, who has spent decades studying tech transfer, likes those approaches. "Inventions shouldn't get tied up just so the university can get its cut," she asserts.

Making an impact

In Egypt, Ellaithy has tried to draw on such advice as he builds a tech transfer office at his nearly century-old university. Although relatively small, AUC is known as one of the country's best. Roughly one-third of its approximately 5500 undergraduates and 1500 graduate students study science and engineering, and the university recently launched its first doctoral programs, starting with technical fields.

But research spending is sparse by U.S. and European standards, representing only 5% of the university's $180 million operating budget. And AUC professors often aren't eligible for government funding because of national policies favoring public institutions. "We're used to being creative and fending for ourselves," he says.

That creativity got a new outlet in 2002 when the Egyptian government rewrote intellectual property laws to make it easier for universities to take ownership of ideas developed by their scholars. In 2009, AUC and three other Egyptian universities won a grant from the European Union to set up academic commercialization offices and hired Ellaithy to lead the effort. He says he spent much of his first year "looking for approaches that might work for us."

In the end, AUC leaders opted for a version of what some call an "impact first, income later" strategy. They hope tech transfer will become a platform for building relationships with industry that might lead to collaborative research funding, jobs for graduates, and other, more personal forms of transferring technology. In the short run, new companies and licensing revenue would be icing on the cake, Ellaithy says.

One of Ellaithy's first jobs was to persuade faculty members to reveal their discoveries so his office can vet them for possible IP protection. Faculty members around the world are often reluctant to make such "disclosures," and Ellaithy notes that entrepreneurial academics in Egypt have traditionally felt entitled to own and commercialize their work.

At AUC, however, he has been pleasantly surprised by the faculty's response. Since the 2.5-person office formally opened in 2010, it has prepared a dozen patent applications and is in the process of standing up its first startup company, which is developing a quick diagnostic tool for hepatitis C invented by AUC chemist Hassan Azzazy. Ellaithy is also drafting new conflict of interest rules in a bid to head off problems. "We're sort of swamped," he admits.

Despite these early achievements, Ellaithy knows that tech transfer is a marathon—and that success isn't measured solely by monetary gains. "We might shoot ourselves in the foot if we do really well with licensing one year," he says. "People could come to expect that's the way it is always going to be."

–DAVID MALAKOFF

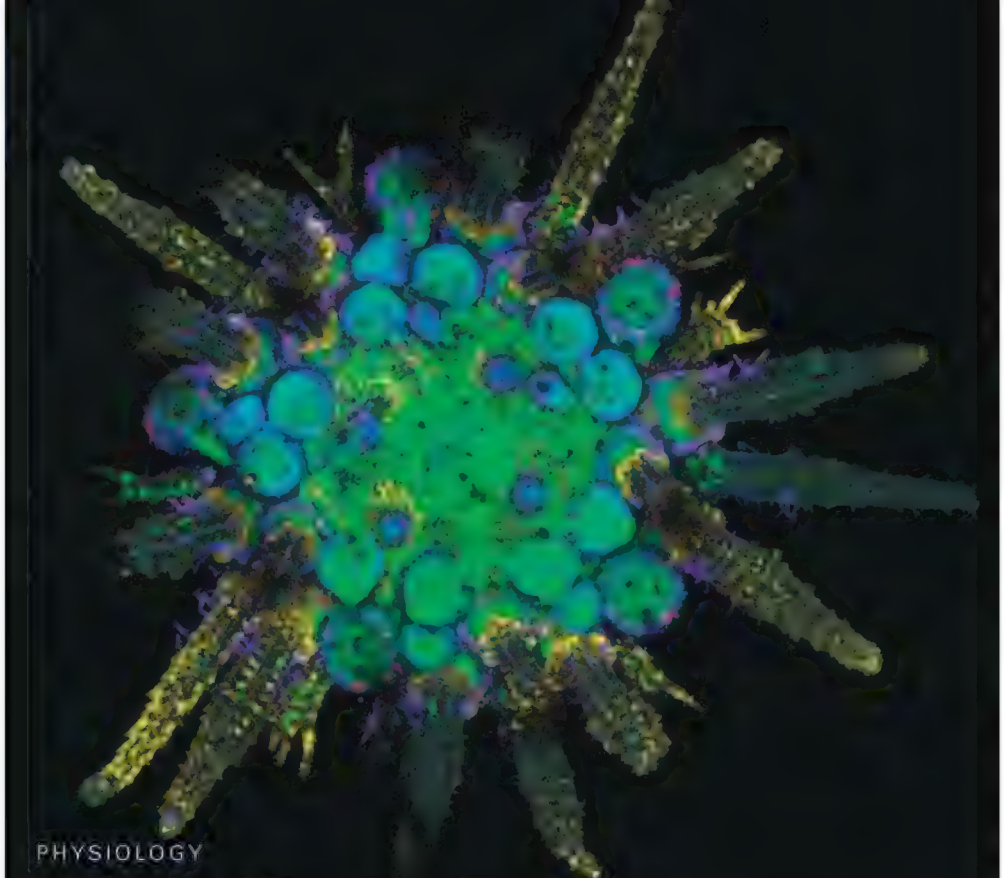

Light sensors. Opsin-laden photoreceptor cells (green, red) provide juvenile sea urchins a means to detect light.

PHYSIOLOGY

Opsins: Not Just for Eyes

Studies in invertebrates are enriching our sense of how versatile and ancient these light-sensitive proteins are

When researchers got their first glimpse of the sea urchin genome in 2006, they were surprised to find genes for opsins, light-sensitive proteins without which vision as we know it today would be impossible. Living in the subtidal zones, sea urchins are not only eyeless, but also headless, and, ostensibly brainless. They seemed to lack the specialized photoreceptor cells that house opsins in the eyes of other animals. "Nobody knew what [the opsins] were for," recalls Maria Ina Arnone, a developmental biologist who has long studied sea urchins at the Stazione Zoologica Anton Dohrn in Naples, Italy, one of the world's oldest marine labs.

Arnone's preliminary analyses suggested an opsin gene was active at the base of the tube feet, the tiny projections located in and around urchin spines. And in 2011, her group showed that these tube feet were loaded with photoreceptor cells that had been missed because they lack pigment typically associated with opsins.

That work and other recent studies have driven home the fact that a wide variety of organisms don't need traditional eyes to make use of opsins, and that opsins can likely sense more than light. Last month, at the annual meeting of the Society for Integrative and Comparative Biology (SICB) in San Francisco, Arnone and other researchers revealed the rich history and unexpectedly broad utility of these proteins. In fruit flies, for example, they may be involved in hearing. "Opsins can be expressed in many more tissues than the simple eye," Arnone says.

Beyond eyes

Hints that opsins existed outside the eye started dribbling in almost 25 years ago, with suggestions that fish skin and dove brains contained the molecules. Among the first to pin down an extraocular opsin protein were Ignacio Provencio and Mark Rollag at the Uniformed Services University of the Health Sciences in Bethesda, Maryland, and their colleagues. They knew that pigment cells in amphibian skin reacted to light and eventually isolated an opsin in frog skin that they named melanopsin in 1998. Until then, researchers thought there was one kind of opsin in vertebrates, called ciliary opsin, and another, more ancient kind, rhabdomeric opsin, in invertebrates. But though melanopsin was found in a frog, it looked more like the invertebrate opsin.

Provencio and Rollag also found melanopsin in the frog eye and brain and over the next few years, a flurry of papers teased out which other vertebrates possess the protein and provided clues to melanopsin's function. Researchers have found it in mouse and human neural tissue, for example, and in some animals, it helps establish circadian rhythms (*Science*, 20 December 2002, p. 2297).

Melanopsin hinted at an underappreciated complexity of opsins. And a 2003 survey of opsins throughout the animal kingdom by Detlev Arendt from the European Molecular Biology Laboratory in Heidelberg, Germany, drove home that both rhabdomeric and ciliary opsins are ancient and that the invertebrate/vertebrate divide for these types doesn't hold up. But the search for opsins in animals other than vertebrates and insects and in places other than eyes didn't really take off until recent advances in DNA sequencing made it possible to probe the genomes of a wide variety of organisms, such as the sea urchin.

Arnone has slowly homed in on how opsins help this simple creature use light and "see." These spiny echinoderms tend to avoid direct sunshine. Some will cover themselves with debris; others move under rocks in search of shadow. Researchers have shown some that sea urchins can even distinguish different shaped objects. Last month at the SICB meeting, Arnone proposed that the opsin photoreceptor cells in the sea urchin are positioned at the base of the tube feet such that they lie partially in the shadow of its calcite skeleton, allowing the skeleton to serve the same purpose as pigment in typical eyes—most opsins co-occur with pigment, which shields part of a photoreceptor cell so it can register the direction of incoming light. She has also shown that the photoreceptor cells connect to the five radial nerves in the brainless urchin, which may enable the input from the different photoreceptor cells to be compiled, much like an insect's compound eye does.

In echinoderms, the opsin story is complex. The opsin at the base of the tube feet

Online
sciencemag.org
Podcast interview with author Elizabeth Pennisi (http://scim.ag/pod_6121).

CREDIT: MARIA INA ARNONE/STAZIONE ZOOLOGICA ANTON DOHRN

is the rhabdomeric type, and Arnone has also found this version in microscopic light-sensitive "eyes" located at the tips of starfish arms. At the meeting, she described a second, ciliary opsin in the tips of urchin tube feet, in urchin skin, and possibly in its muscles. It's also present in their larvae, she said. Arnone is not sure what this ciliary opsin does. But because echinoderms, which include starfish and sea urchins, sit at the base of the deuterostomes, the animal group that includes vertebrates, both types of opsins were likely already present in the earliest deuterostomes. How the different opsins later became specialized for use in vision remains a mystery, she notes.

Opsins everywhere

After opsins were found in sea urchins, evolutionary biologist Todd Oakley from the University of California (UC), Santa Barbara, wondered where else they might be. He and his colleagues started looking even closer to the base of the animal tree of life for these proteins. In 2007, Oakley recalls, "that led us to Cnidaria," the group of animals, including hydra and jellyfish, characterized by specialized cells that fire venom-equipped barbs that sting prey or deter predators. His group found opsins in cells associated with cnidarian stinging cells, and in the 5 March 2012 issue of *BMC Biology* they reported that stinging cells were less likely to fire in bright light. "Even though [stinging cells] had been studied for decades, there were very few hints that light was involved in firing," Oakley says. The prevailing wisdom was that chemicals in the water influenced firing. But here was a light-sensing role for opsins that did not involve image generation or true vision.

His team has now found that opsins have a similar sway over the firing of stinging cells in several distant cnidarian relatives—two anemone species and moon jelly polyps—suggesting that this nonvisual role for opsins is ancient. "It may be that [a] role in vision came later," suggests Craig Montell, a neurobiologist who recently moved to UC Santa Barbara.

At the San Francisco meeting, David Plachetzki from UC Davis reported that the hydra's opsin-laden cells near the stinging cells also contain taste receptors. That leads Plachetzki to propose that the ancestor to specialized photoreceptor cells was a cell that responded to several types of stimuli.

Supporting evidence for that scenario comes from other work. Desmond Ramirez in Oakley's lab reported finding opsins in the cilia of octopus skin, which are already known to be sensitive to mechanical stimuli. "So it's potentially another case where there is multimodal sensation," Oakley says. And his postdoc Daniel Speiser found opsins in small sensory tentacles extending from the shell plates of mollusks called chitons. Whether these proteins are involved in mechanosensing or light-sensing is still to be determined.

Probing even deeper down the animal tree of life, Christine Schnitzler from the National Human Genome Research Institute in Bethesda has found three strange-looking opsin genes in the recently completed genome of the comb jelly *Mnemiopsis leidyi*. Comb jellies are considered by many to be among the first multicellular animals to arise. Two comb jelly opsins loosely resemble the rhabdomeric and ciliary opsins, while a third looks like neither, Schnitzler reported at SICB. The proteins show up in two parts of the animal's gelatinous body—in a sensory organ opposite the comb jelly's mouth that helps the creature stay oriented in the water and in the cells that generate bioluminescence. Because the opsins in those cells are sensitive to the same wavelength as the light given off, they may be used by the animal to sense and control how much it's glowing, Schnitzler proposed at the meeting.

Opsins galore. Opsins have been discovered in eyeless chitons, comb jellies and hydra, and in the skin of octopus (*clockwise from top*).

Other roles

Even in animals with eyes, researchers are finding they have more to learn about opsins. These proteins have been long studied in eyes of the fruit fly *Drosophila melanogaster*, but Martin Göpfert from the University of Göttingen in Germany has now come across them in the insect's antennal ear. His team had been screening for insect ear genes to try to find genes that might be involved in human hearing loss. They looked for genes that were more active in normal fruit flies than in mutant fruit flies lacking the antennal ear. Among the 275 upregulated genes identified were four genes for opsins previously found expressed only in the fly's eyes.

These four genes are also expressed in the mechanosensory cells of the ear and are required for hearing, the Göpfert team reported in the 31 August 2012 issue of *Cell*. "Finding that these cells use opsins for mechanosensation suggests that these proteins may have already served sensory roles before photoreceptors have evolved," Göpfert says. "In the ear, opsin function seems light-independent."

Montell's group has identified what may be another nonvisual role for opsins: temperature sensation. *Drosophila* larvae prefer 18°C, seeking it out over subtly different temperatures, such as 19° to 24°C. In trying to find the temperature sensor, "we weren't expecting opsin to be important," Montell recalls. But in 2011, Montell and his colleagues discovered that mutant flies lacking the visual opsin ninaE no longer showed this preference. When the researchers put a mouse melanopsin gene into the mutant fruit flies, the larvae oriented to 18°C (*Science*, 11 March 2011, p. 1333). Fruit flies have seven opsins, and Montell says that still unpublished work from his lab establishes nonlight-sensing roles for five of them.

Montell predicts that researchers are just beginning to appreciate all that opsins can do. Arnone agrees. When she first looked at opsins 6 years ago, the project was very much a sideline effort. But, aided by a new grant to study the proteins, she expects that opsin research will grow to take up half her lab. In the next year, Montell says, "there will be a lot more to talk about."

–ELIZABETH PENNISI

CREDITS (CLOCKWISE FROM TOP LEFT): DANIEL SPEISER/UNIVERSITY OF CALIFORNIA, SANTA BARBARA; WILLIAM BROWNE/UNIVERSITY OF MIAMI; DAVID PLACHETZKI/UNIVERSITY OF CALIFORNIA, DAVIS; MARKOS A. ALEXANDROU/UNIVERSITY OF CALIFORNIA, SANTA BARBARA

LETTERS

edited by Jennifer Sills

AAAS Position on GM Foods Could Backfire

WE ARE WRITING TO URGE AAAS TO RECONSIDER ITS POLICY AGAINST MANDATED LABELING OF so-called genetically modified (GM) foods (*1*). We do not, as a group, have any position on GM foods, for or against, but we are concerned that AAAS's position represents a poorly informed approach to communicating science.

Successful communication requires mutual trust and a perception of shared values. Appearing to withhold information that people want (whether they want it for reasons we agree with or not) about the food that they eat stands an excellent chance of eroding both of these. Decades of social science research on science communication processes have demonstrated that these elements are almost certainly more important than science literacy in determining public attitudes and opinions. And science itself is built on an ethos of transparency and open dialogue that appears inconsistent with AAAS's position in this situation.

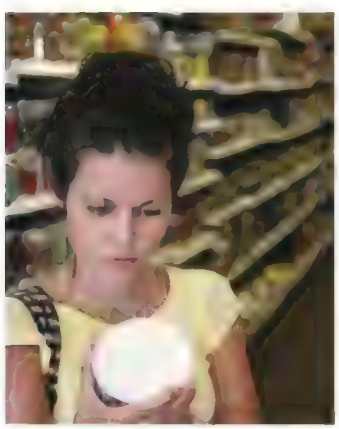

The recent California vote defeating an attempt to require GM labeling was immediately followed by a pledge from its supporters to pursue this issue at the national level (*2*). The debate is clearly not over yet. AAAS should let citizens decide this question, which is not a matter of science per se but of public preferences, values, and concerns.

Strategically, appearing to be less than transparent is a really bad idea for the scientific community. Ethically, we believe that people, both as citizens and as consumers, have a right to information that they feel is relevant to their decisions. The most constructive way to address many people's lingering concerns about GM foods is to provide them with the information that they consistently deem relevant, even if this requires new regulation.

SUSANNA HORNIG PRIEST,[1] JOANN M. VALENTI,[2]* ROBERT A. LOGAN,[3] CAROL L. ROGERS,[4] SHARON DUNWOODY,[5] ROBERT J. GRIFFIN,[6] MARILEE LONG,[7] SHARON M. FRIEDMAN,[8] S. HOLLY STOCKING,[9] KATHERINE E. ROWAN,[10] JOCELYN STEINKE[11]

[1]Associate Professor Emeritus, Department of Journalism, Texas A&M University, Olympia, WA 98502, USA. [2]Professor Emeritus, College of Fine Arts and Communications, Brigham Young University, Provo, UT 84602, USA; Tampa, FL 33606, USA. [3]Professor Emeritus, School of Journalism, University of Missouri–Columbia, Columbia, MO 65205, USA; Bethesda, MD 20852, USA. [4]Philip Merrill College of Journalism, University of Maryland, College Park, MD 20742–7111, USA. [5]School of Journalism and Mass Communication, University of Wisconsin–Madison, Madison, WI 53706, USA. [6]Diederich College of Communication, Marquette University, Milwaukee, WI 53201–1881, USA. [7]Department of Journalism and Technical Communication, Colorado State University, Fort Collins, CO 80523, USA. [8]Department of Journalism and Communication, Lehigh University, Bethlehem, PA 18015, USA. [9]Associate Professor Emeritus, School of Journalism, Indiana University, Bloomington, IN 47405, USA. [10]Department of Communication, George Mason University, Fairfax, VA 22030–4444, USA. [11]School of Communication, Western Michigan University, Kalamazoo, MI 49008, USA.

*To whom correspondence should be addressed. E-mail: valentijm@yahoo.com

References and Notes

1. AAAS, "Statement by the AAAS board of directors on labeling of genetically modified foods, 20 October 2012" (www.aaas.org/news/releases/2012/media/AAAS_GM_statement.pdf).
2. "California fails to pass genetically modified foods labeling initiative" *Time*, 7 November 2012 (http://healthland.time.com/2012/11/07/california-fails-to-pass-gm-foods-labeling-initiative/).
3. The authors are members of, but do not write on behalf of, AAAS Fellows, Section Y (General Interest in Science and Engineering).

In Defense of Physician-Investor Collaboration

IN HIS NEWS FOCUS STORY "EXPERT FIRMS play a hidden role in connecting science and finance" (11 January, p. 137), J. Mervis reports on the inner workings of expert networks and how universities are navigating potential conflicts of interest. However, Mervis does not address the apparent disconnect in how users of expert networks are perceived by the university officials setting conflict-of-interest policy and the physician researchers providing advice.

Based on the story, physicians seem to prefer advising investors in private companies that are developing medical technology with a long investment horizon. They are more skeptical of advising Wall Street analysts who plan to use the information for short-term stock trading. Yet, academic centers such as the Cleveland Clinic do not make this distinction or consider the varying risks; they only distinguish between using expert networks and consulting directly for companies that are conducting new research or trying to improve products.

As a venture capitalist at a fund that has invested $600 million into start-ups developing new medicines, I find it unfortunate that academic centers are discouraging participation in expert networks altogether. Many users of expert networks are venture capital investors who are hoping to finance new research to develop medicines, rather than hedge funds that seek to swap stock on public markets and profit. Although venture capitalists attend symposiums and conferences, we rely on expert networks for timely access to physicians to provide information into treatment paradigms, patient epidemiology, and their unmet medical needs.

Academic centers should not assume that all users of expert networks are financial firms, nor should they generalize the motivations of financial firms. Financial firms such as ven-

CREDIT: DAVID H. LEWIS/ISTOCKPHOTO.COM

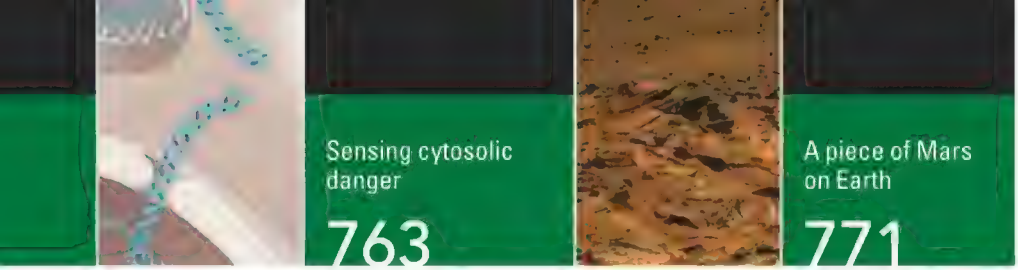

ture capitalists have very little motivation to benefit from insider information, because of multiyear investment horizons. Simply put, learning about trial data a week before a press release is not going to influence a venture capitalist to make a 5-year commitment to a new drug. Academic policy on expert networks should therefore focus on discouraging interaction with public investors such as hedge funds, not venture capitalists seeking to finance the next breakthrough medicine.

JUSTIN CHAKMA

Thomas, McNerney & Partners, La Jolla, CA 92037, USA. E-mail: jchakma@tm-partners.com

Give Shark Sanctuaries a Chance

SEVERAL DEVELOPING NATIONS HAVE ESTABlished shark sanctuaries, most commonly in the form of a moratorium on both commercial shark fishing and the export of shark products in Exclusive Economic Zones (*1*). In her Letter "Shark sanctuaries: Substance or spin?" (21 December 2012, p. 1538), L. N. K. Davidson raises concerns that this ambitious strategy might be doomed to exist only on paper and could discourage investments in other types of shark fisheries management. We agree that enforcement will determine whether these shark sanctuaries live up to their promise, as is true of any new management regime. We disagree, however, with the argument that shark sanctuaries are more challenging to enforce or are less likely to be successful than typical fisheries management strategies, especially considering that even basic information such as fishery catch is often unknown and underestimated in developing countries (*2*).

Shark fisheries management is notoriously difficult and resource intensive, owing to the extreme vulnerability of sharks to overexploitation (*1*). The countries that have successfully managed shark fisheries all possess substantial research, assessment, monitoring, and enforcement capacity devoted to fisheries management (*1*). Developing nations typically have much smaller fisheries management capacity; what they do have is national capacity to detect illicit trade of contraband items (i.e., police, maritime authority, port authority, and customs). By making all shark products illegal, national authorities can work with their fisheries agencies to enforce the moratorium. Enforcing catch or size limits on shark fisheries is more complicated and will generally fall almost entirely under the purview of the fisheries agency on its own.

There is cause for optimism about the conservation potential of well-enforced shark sanctuaries nested within broader international management efforts. Smaller-scale marine protected areas have been shown to benefit certain inshore shark species, while other species tend to return to certain areas on a regular basis (*3*–*6*). These studies suggest that large protected areas may benefit these populations and match biological and governance scales. Well-enforced shark sanctuaries clearly have great potential for shark conservation, and we suggest that the international community and funding agencies should help those developing nations that pursue this approach to ensure that this promise is realized.

DEMIAN D. CHAPMAN,[1,2]* MICHAEL J. FRISK,[1] DEBRA L. ABERCROMBIE,[2] CARL SAFINA,[1,3] SAMUEL H. GRUBER,[4] ELIZABETH A. BABCOCK,[4] KEVIN A. FELDHEIM,[5] ELLEN K. PIKITCH,[1,2] CHRISTINE WARD-PAIGE,[6] BRENDAL DAVIS,[6] STEVEN KESSEL,[7] MICHAEL HEITHAUS,[8] BORIS WORM[6]

[1]School of Marine and Atmospheric Science, Stony Brook University, Stony Brook, NY 11794, USA. [2]Institute for Ocean Conservation Science at Stony Brook University, Stony Brook, NY 11794, USA. [3]Center for Communicating Science, Stony Brook University, Stony Brook, NY 11794, USA. [4]Rosenstiel School of Marine and Atmospheric Science, University of Miami, Miami, FL 33149, USA. [5]Pritzker Laboratory for Molecular Systematics and Evolution, Field Museum of Natural History, Chicago, IL 60605, USA. [6]Department of Biology, Dalhousie University, Halifax, NS, B3H 4R2, Canada. [7]University of Windsor, Windsor, ON, N9B 3P4, Canada. [8]Florida International University, North Miami, FL 33181, USA.

*To whom correspondence should be addressed. E-mail: demian.chapman@stonybrook.edu

Letters to the Editor

Letters (~300 words) discuss material published in *Science* in the past 3 months or matters of general interest. Letters are not acknowledged upon receipt. Whether published in full or in part, Letters are subject to editing for clarity and space. Letters submitted, published, or posted elsewhere, in print or online, will be disqualified. To submit a Letter, go to www.submit2science.org.

References

1. C. A. Ward-Paige *et al.*, *J. Fish. Biol.* **80**, 5 (2012).
2. K. Kelleher, "Discards in the world's marine fisheries: An update" (FAO Fisheries Technical Paper 470, Rome, 2005); www.fao.org/docrep/008/y5936e/y5936e00.htm.
3. M. E. Bond *et al.*, *PLoS One* **7**, 3 (2012).
4. W. D. Robbins *et al.*, *Curr. Biol.* **16**, 23(2006).
5. R. E. Hueter *et al.*, *J. Northw. Atl. Fish. Sci.* **35**, 239 (2005).
6. C. A. Ward-Paige *et al.*, *PLoS One* **5**, 8 (2010).

CORRECTIONS AND CLARIFICATIONS

News Focus: "The Tale of the TALEs" by E. Pennisi (14 December 2012, p. 1408). A fungus, not *Xanthomonas* bacteria, caused the black rot in the apple shown on page 1411.

Reports: "Cryo-EM model of the bullet-shaped vesicular stomatitis virus" by P. Ge *et al.* (5 February 2010, p. 689). On page 690, second complete paragraph, the second sentence incorrectly transposed the ends of the RNA molecule. The sentence should read, "The docked crystal structure shows that the 3′ end is at the conical tip of the bullet and the 5′ end is at the base of the trunk." The HTML and PDF versions online have been corrected.

Reports: "Relating three-dimensional structures to protein networks provides evolutionary insights" by P. M. Kim *et al.* (22 December 2006, p. 1938). The column headings for Table 1 should be transposed.

TECHNICAL COMMENT ABSTRACTS

Comment on "Evolutionary Trade-Offs, Pareto Optimality, and the Geometry of Phenotype Space"

Pim Edelaar

Shoval *et al.* (Reports, 1 June 2012, p. 1157) showed how configurations of phenotypes may identify tasks that trade off with each other, using randomizations assuming independence of data points. I argue that this assumption may not be correct for most and possibly all examples and led to pseudoreplication and inflated significance levels. Improved statistical testing is necessary to assess how the theory applies to empirical data.

Full text at http://dx.doi.org/10.1126/science.1228281

Response to Comment on "Evolutionary Trade-Offs, Pareto Optimality, and the Geometry of Phenotype Space"

Oren Shoval, Hila Sheftel, Guy Shinar, Yuval Hart, Omer Ramote, Avi Mayo, Erez Dekel, Kathryn Kavanagh, Uri Alon

Edelaar raises concerns about the way we tested our theory. Our mathematical theorem predicts that despite the high dimensionality of trait space, trade-offs between tasks lead to phenotypes in low-dimensional regions in trait space, such as lines and triangles. We address Edelaar's questions with statistical tests that eliminate pseudoreplication concerns, finding that our predictions remain convincingly supported.

Full text at http://dx.doi.org/10.1126/science.1228921

STATISTICS

Mr. Bayes Goes to Washington

Sam Wang[1] and Benjamin C. Campbell[2]

One day before the 2012 U.S. presidential election, former Reagan speechwriter Peggy Noonan wrote that "nobody knows anything" about who would win, asserting that Republican candidate Mitt Romney's supporters had the greater passion and enthusiasm (*1*). From a similarly data-free remove, columnist George Will predicted a Romney electoral landslide. MSNBC's Joe Scarborough said "it could go either way … anybody that thinks that this race is anything but a tossup right now … should be kept away from typewriters, computers, laptops, and microphones, because they're jokes." (*2*)

In the end, these pundits were the ones whose opinions proved dispensable. They were unable to detect a plain fact: based on public opinion polls with collectively excellent track records, President Obama had an advantage of 3 to 4 percentage points for nearly the entire campaign season. However, the world of political punditry measures success not by accuracy but by readership and viewership. And so it came to pass that legions of commentators expressed total confidence—and were wrong.

Beating the pundits has been possible since at least 2004, when one of us was among the first to statistically aggregate polls (*3*). In 2008, Nate Silver emerged as a poster child for aggregation, armed with a degree in economics, a love of numbers, and a professional track record in analyzing baseball performance and financial data. He enlivened a mostly suspenseless presidential race, providing timely quantitative analysis and color commentary on his website FiveThirtyEight, which became highly popular and was snapped up by the New York Times (*4*). His fame rose further in 2012, when he and other aggregators and modelers used hardnosed analysis (*3*–*6*) to silence skeptics.

Now Silver has written *The Signal and the Noise*, a book that addresses predictions not just in politics but in all aspects of modern life, with the eye of a hobbyist and a sense of fun. Freed from the word limits of blog essays, the book is a meandering, nerd's-eye view of what principles, if any, are common to good forecasting in daily life, leisure activity, and science.

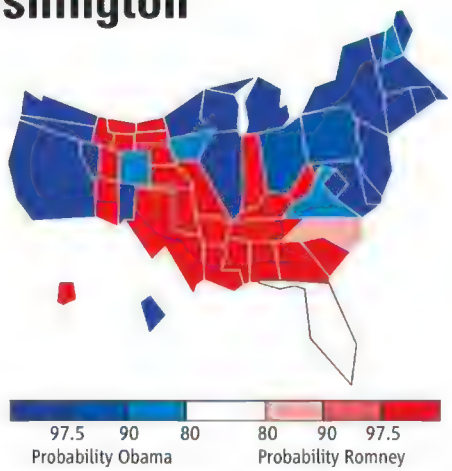

Validated by the outcome. The Princeton Election Consortium's final electoral college predictions for November 2012. (States are sized according to their share of electoral votes.)

The Signal and the Noise
Why So Many Predictions Fail—But Some Don't/ The Art and Science of Prediction
by Nate Silver
Penguin, New York, 2012. 542 pp. $27.95, C$29.50. ISBN 9781594204111.
Allen Lane, London. £25. ISBN 9781846147524.

We use predictions to guide our future actions, from planning weekend outings to taking care of our health, but most people have no idea how scientific predictions are made. This book is for them. Silver introduces some of the concepts behind data modeling, including probability, Bayesian inference, and uncertainty. He takes lengthy looks at topics ranging from flu epidemics to the 1996 chess-playing triumphs of Deep Blue.

A reappearing theme in *The Signal and the Noise* is Bayesian reasoning, an approach that has swept the sciences. Probability had been conventionally interpreted as meaning the true likelihood of an event—for instance, how often the total of two rolled dice will add up to seven. Such a "frequentist" point of view has in many cases given way to an approach pioneered by Reverend Thomas Bayes in the 18th century, which emphasizes that probability can only be interpreted in terms of the hypotheses that preceded the measurement.

Although Silver asserts that Bayesian political forecasting has more in common with poker than with hard sciences such as physics and biology, these topics all use the same mathematical toolkit. Large-scale physics collaborations depend on sensitive models to predict the probabilistic decay rates of particles, looking for outliers that might represent signals in the noise and hence discoveries. In our field, many neuroscientists have begun to view the brain as a prediction machine (*7*). We perceive the world around us by making inferences from noisy and incomplete data. To do so, the brain must form a model of its environment—a set of "priors" learned over a lifetime that is used to interpret incoming data. This Bayesian machine continually updates its priors to correspond to its environment. Through this process, our brains spend many years honing appropriate priors for the complex tasks that we perform effortlessly.

Silver gives a well-known equation for how to take into account the Bayesian prior but doesn't show where it comes from. Readers wanting a deeper explanation of Bayes's rule might consult another source such as BetterExplained.com (*8*), which teaches the subject by using e-mail spam filtering as an example. Silver's chosen anecdotes include the classic example of mammogram interpretation—but also how to interpret that unfamiliar underwear that just showed up in your partner's dresser drawer.

At times Silver writes as if the cure for bad modeling can be reduced to "more Bayes." Such a prescription does not do justice to the historic controversies surrounding interpretations of probability. A beginner might come away from this book believing that an earlier generation of frequentists were simply ignorant. In a cartoonish account, Silver lobs a broadside at a monumental figure in statistics, Ronald A. Fisher, who late in life argued against the idea that smoking causes cancer—and who coined "Bayesian" as a derogatory term. Silver suggests that Fisher's aversion to Bayes caused him to err. In fact, the real problem was that Fisher was a smoker (*9*). Fisher's prior beliefs prevented him from accepting epidemiological and biological evidence, an erroneous prior if ever there was one.

Our biggest criticism of the book is that although statistics and Bayesian inference are powerful ideas, they are not a cure-all. In his enthusiasm for the good Reverend, Silver has stuffed a fair bit into the same Procrustean bed. Silver uses the old fox-hedgehog analogy, saying that foxes (including himself) use many ideas, whereas hedgehogs focus on one subject only. But here he is a hedgehog with one big idea: statistics.

However, Bayesian reasoning works only if the prior is adapted for the task. According to Silver, many of today's "half-baked

[1]Department of Molecular Biology and Neuroscience Institute, Princeton University, Princeton, NJ 08544, USA. E-mail: sswang@princeton.edu [2]Laboratory of Biological Modeling, Rockefeller University, 1230 York Avenue, New York, NY 10065, USA. E-mail: bcampbell@rockefeller.edu

policy ideas" could be rectified by Bayesian thinking, but that is only part of the story. The more difficult task is determining good priors. Silver rejects bad priors effectively in his own field of electoral forecasting by dismissing much of the noise of political punditry. In other fields, he does not always bring the same critical attitude.

Scientific research is often confronted by political and economic forces that are not always appreciated by nontechnical outsiders. For example, Silver somewhat perversely takes climate scientists to task for bringing politics into their work (*10*). If anything, climate scientists have been dragged unwillingly into a dispute with political interest groups such as the Heartland Institute. At this point in history, human-induced global warming is a fact and no longer a matter of disputing probabilities. The book's extended treatment of scientific fringe figures has the inadvertent effect of giving credence to antiscientific views that fly in the face of experimentation and hypothesis-testing on the greenhouse effect dating back to Arrhenius over a century ago. When Silver, now himself a prominent pundit, depicts a "controversy," he highlights the challenge scientists face in convincing people that carbon dioxide is a pollutant. Not all priors are equally defensible.

Silver's quirky personality and eclectic interests come through in his writing. *The Signal and the Noise* is strongest when Silver sticks with subjects he has pursued for a living: political forecasting, baseball, and poker. Poker is a game of clear probabilities, but he points out that understanding the math is not enough. A key step is to identify at least one doomed "fish" at the table. As the joke goes, if you can't identify the fish, it's you. In political prediction, Peggy Noonan and other traditional pundits are the fish.

On the central topic of how to make a good prediction, Silver is right that there is no magic formula. Heuristics are no substitute for careful and rigorous study—in other words, expertise. In political prognostication, Silver found the barrier to entry to be "invitingly low." For areas that require more scientific rigor, his enthusiasm and fame have blazed a trail for other data enthusiasts to follow.

References

1. P. Noonan, http://blogs.wsj.com/peggynoonan/2012/11/05/monday-morning/, 5 November 2012.
2. D. Byers, "Nate Silver: One-term celebrity?" www.politico.com/blogs/media/2012/10/nate-silver-romney-clearly-could-still-win-147618.html, 29 October 2012.
3. S. Wang, Princeton Election Consortium, http://election.princeton.edu.
4. N. Silver, http://fivethirtyeight.blogs.nytimes.com.
5. D. Linzer, http://votamatic.org.
6. S. Jackman, www.huffingtonpost.com/simon-jackman/pollster-predictive-perfo_b_2087862.html, 7 November 2012.
7. K. Doya, S. Ishii, A. Pouget, R. P. N. Rao, Eds., *Bayesian Brain: Probabilistic Approaches to Neural Coding* (MIT Press, Cambridge, MA, 2011).
8. K. Azad, "An intuitive and short explanation of Bayes' theorem," http://betterexplained.com.
9. P. D. Stolley, *Am. J. Epidemiol.* **133**, 416, discussion 426 (1991).
10. M. E. Mann, "FiveThirtyEight: The number of things Nate Silver gets wrong about climate change," www.huffingtonpost.com/michael-e-mann/nate-silver-climate-change_b_1909482.html, 24 September 2012.

10.1126/science.1232290

NEUROBIOLOGY

The End of the Beginning for the Brain

Christof Koch

How to Create a Mind
The Secret of Human Thought Revealed
by Ray Kurzweil
Viking, New York, 2012. 352 pp. $27.95, C$29.50. ISBN 9780670025299
Duckworth, London, £20. ISBN 9780715645376

Science-fiction novels and films have long popularized the notion that machines will, sooner or later, match and ultimately exceed human-level intelligence. On the way they will acquire feelings and consciousness. In the most famous such movie, *Blade Runner*, a replicant exclaims in the face of its imminent demise, "I've seen things you people wouldn't believe. Attack ships on fire off the shoulder of Orion. I watched c-beams glitter in the dark near the Tannhäuser Gate. All those moments will be lost in time, like tears in rain. Time to die."—revealing in its eloquence and poignancy its (simulated) humanity.

A strand of Anglo-American thought fervently believes in the infinite betterment of the human condition through cultural and technological means. The more extreme version is known as transhumanism (h+ for short). Transhumanists argue that biological limitations, including aging and insufficient memory and intelligence, should, and will, be transcended by nanotechnology and artificial intelligence (AI). Their prophet is the engineer, inventor, and futurist Ray Kurzweil, who has just been made a head of engineering at Google. He is best known for his advocacy of the singularity, the point in time when computers—designing and redesigning themselves in a continuously accelerating feedback loop—will become smarter than people, thereby bringing human history to an end. Kurzweil believes that this momentous, eschatological event is a mere decade or two away and will usher in an earthly paradise. Rapture for techies!

In his latest book, Kurzweil takes a romp through the history of AI. He is one of the field's pioneers, having developed and successfully commercialized optical character recognition, advanced music synthesizers, and speech recognition. Kurzweil highlights some notable successes: Deep Blue (the IBM program that beat the reigning chess master in 1997), self-driving Google cars, smart phones that can access the entire repertoire of human knowledge within seconds, the answer engine Wolfram Alpha, and Watson. Another IBM creation, Watson publicly bested humans in the TV quiz show Jeopardy! in 2011. It represents a milestone on the way to true AI, as the program had to learn to parse and understand highly ambiguous sentences by repre-

CREDIT: LADD COMPANY/WARNER BROS./THE KOBAL COLLECTION

Replicant's end. Publicity still from Ridley Scott's *Blade Runner* (1982).

The reviewer is at the Allen Institute for Brain Science, 551 North 34th Street, Seattle, WA 98103, USA. E-mail: koch.christof@gmail.com

senting hundreds of millions of pages such as the full text of Wikipedia. Yet except for these restricted special domains, AI remains a long way from its human variant.

Kurzweil introduces the reader to one of AI's signature mathematical techniques that he himself used to build speech recognition systems: hierarchical, hidden Markov models (HHMMs). These are trainable algorithms well matched to deal with the many levels of human language, from phonemes to words to sentences and beyond. For certain types of simple problems, HHMMs can be trained fairly automatically and are easy to implement in "units" that are connected by ascending and descending links.

It is here that Kurzweil leaves the solid ground of his expertise to wade into the muddier waters of biology and psychology. For he now categorically asserts that HHMMs provide a powerful and universal model of neocortical computation, with 300 million pattern recognizers distributed across the cortical sheet.

Kurzweil introspects into his own mind's capabilities and the nature of perception and memory, without bothering to refer to the massive literature on these topics. One of the most basic lessons of psychology is that we have little idea of what goes on in our minds, as evolution has not given us access to most parts of the brain (explaining why so much philosophy of mind has been barren when all it could rely on was introspecting philosophers). He then moves on to the brain, describing its anatomy in terms of the "new" brain, higher-order regions of the neocortex, and the "old" brain (everything else). According to Kurzweil, the new brain is clever, learns flexibly, and controls the primitive impulses of the old brain relating to food, sex, and aggression. His understanding of neuroanatomy is about as sophisticated as U.S. Secretary of Defense Donald Rumsfeld's understanding of international politics when he articulated his belief of a division of Europe into an Old and a New one during the run-up to the second Gulf War in 2003.

Kurzweil's knowledge of neuroscience is simply inadequate to the task at hand. From the tens of thousands of studies published annually, he selectively cites a handful of papers that buttress his points, without giving any context. He mistakes the striatum for cortex and apical dendrites for axons, belies the cognitive contributions of the basal ganglia, and denies higher mental abilities to insects, cephalopods, and birds that don't have a neocortex. Yet he has the unerring belief of the prophet (or the fool): "I maintain that the model I have presented is the only possible model that satisfies all of the constraints that the research and our thought experiments have established."

Scientists trying to simulate the mind-brain fall along a continuum, ranging from extreme biological chauvinism (the need to consider every ionic channel, action potential, and neuron to fully do justice to the baroque complexity of the brain's circuits) to the austerity of a purely algorithmic approach of replicating the mind in software (the mind is not wet, after all). Mathematicians and engineers naturally belong to the later camp, convinced that one algorithm rules them all. Previous favorites include logical calculus, neural networks, cellular automata, self-referential programs, and, yes, hidden Markov models [as proposed a few years earlier by fellow entrepreneur and inventor of the PalmPilot Jeff Hawkins (*1*)].

Kurzweil correctly points out that the pace at which biologists accumulate data has increased dramatically over the years (although I only wish that his claim that "the spatial resolution of brain scanning … [is] doubling every year" were true). From this he infers that a complete understanding of the brain and the mind can't be far away.

Paradoxically, the endless data fields make it ever more difficult to distinguish the signal from the noise. Indeed, the torrent of data begets the illusion of progress. While data about the brain accumulate exponentially, our understanding increases sublinearly. Basic questions about cortical circuitry posed by future Nobel laureates David Hubel and Torsten Wiesel in a celebrated publication in 1962 (*2*) remain unanswered 50 years later. Functional human brain imaging has yet to affect standard medical practice (the upcoming fifth edition of the *Diagnostic and Statistical Manual of Mental Disorders* does not even mention any functional magnetic resonance imaging diagnostic criteria). And even the lowly roundworm *Caenorhabditis elegans*, a creature no bigger than the letter l and with exactly 302 nerve cells, is for now beyond the ability of computational neuroscience to comprehend. Kurzweil's claim that we will soon figure out how the 100 billion neurons of the human brain function on the basis of designed HHMMs is complete bosh.

One thing is certain. Biology knows nothing of simplicity. Brains are not assembled out of billons of identical LEGO blocks but out of hundreds of distinct nerve cell types. Each cell type has its own idiosyncratic morphology, signaling, and active genes. And they are interconnected with elaborate wiring rules that we only discern darkly. To paraphrase Winston Churchill, neuroscience is (perhaps) at the end of the beginning of the quest to understand our brain and mind.

References

1. J. Hawkins, S Blakeslee, *On Intelligence* (Times Books, New York, 2005).
2. D. H. Hubel, T. N. Wiesel, *J. Physiol.* **160**, 106 (1962).

10.1126/science.1233813

BROWSINGS

Mathematical Excursions to the World's Great Buildings. Alexander J. Hahn. Princeton University Press, Princeton, NJ. 2012. 344 pp. $49.50, £34.95. ISBN 9780691145204.

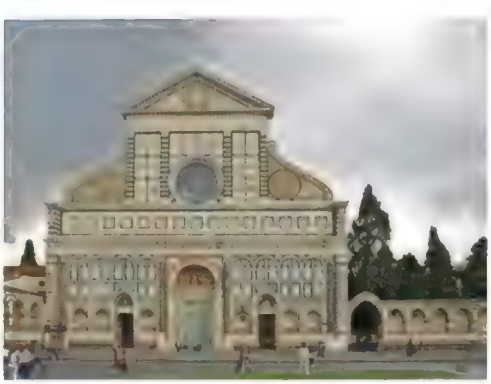

CREDIT: JEBULON/WIKIMEDIA COMMONS

While touring examples of western architecture from the great pyramids of Giza to Frank Gehry's Bilbao Guggenheim Museum, mathematician Hahn intertwines two historical narratives: The architectural focuses on aspects of appearance (shapes, symmetry, and proportion) and mechanics (loads, compressions, tensions, and thrusts). The mathematical progresses from Euclidean geometry and trigonometry to basic calculus. His discussions reveal how mathematics provides insights into the design and construction of the buildings and how the buildings incarnate the math. [Carefully composed using circles and squares, Leon Battista Alberti's 15th-century facade (above) for the medieval church Santa Maria Novella in Florence was a source of inspiration to a number of Renaissance architects.] As Hahn notes, his two strands are linked topically rather than chronologically, because the actual builders generally lacked the mathematics that clarifies understanding of their constructions. Readers wishing to shore up their own understanding of that mathematics can work through the chapter-end problem sets and discussions.

ARMS CONTROL

Beyond Arms-Control Monitoring

Environmental monitoring can become a useful long-term objective of arms-control treaty verification.

Raymond Jeanloz,[1,2]* Inez Fung,[1] Theodore W. Bowyer,[3] Steven C. Wofsy[4]

Arms-control treaties are often considered burdensome, yet they need to be sustained into the indefinite future. In particular, because compliance must be verified, arms-control treaties can be intrusive and may be perceived as a challenge to the sovereignty of nations being monitored.

This condition is unlikely to become easier in the foreseeable future. Treaty monitoring would presumably have to become both more intrusive and more pervasive (i.e., apply more generally to all nations) to the degree that there is progress toward a world free of nuclear weapons, for example. Even without such progress, the advance of technology that empowers individuals for good or ill is likely to require enhanced monitoring of activities everywhere, all the time; as technology becomes more powerful, its misuse could outweigh benefits in new and unexpected ways.

Arms-control treaties are also costly to those engaged in monitoring. This can lead to a "lose-lose" scenario, where (i) success of a treaty regime weakens the ability to sustain monitoring, yet (ii) any violation undermines confidence in the treaty's utility or relevance. For instance, if the Comprehensive Nuclear-Test-Ban Treaty (CTBT) is successful in the sense that there are no nuclear explosions for many years or decades, it becomes difficult to justify the effort and expense associated with the CTBT's International Monitoring System (IMS) (*1*). Even with the best intentions among all interested parties, sustaining technical capability is challenging when there is nothing to be measured. Nevertheless, any nuclear-explosion testing would undermine the CTBT; none would want treaty violation merely for the sake of exercising the IMS.

However, the situation may not be so bad. Although potentially harmful applications of newly developed technologies may require ever more effort in monitoring, advances in technology can also facilitate monitoring and transparency. Still, it is important to identify a future "end state" for treaty monitoring that is realistic, sustainable, and provides credible and effective verification (*2*), whether or not the verification regime is actively applied. Treaty monitoring can also serve as a deterrent: One might consider both the IMS and on-site inspection regimes under the CTBT to discourage nuclear-explosion testing.

Fortunately, given the challenge of sustaining, let alone expanding, arms-control regimes, there is an opportunity to accomplish this "end-state" goal by identifying and implementing nontreaty applications of monitoring. We describe how treaty-monitoring systems can be used for environmental monitoring, as well as how systems intended for monitoring the environment can be used to support arms-control. We focus on technical aspects, one piece of a larger puzzle involving diplomatic, economic, and other concerns.

The HIAPER aircraft approaching Deadhorse, Alaska.

CREDIT: NATIONAL SCIENCE FOUNDATION, NATIONAL CENTER FOR ATMOSPHERIC RESEARCH

Opportunities: CTBT and Open Skies

A major breakthrough in this regard came with the recognition that the CTBT IMS could have helped save many lives during the December 2004 Indian Ocean tsunami disaster (*3*, *4*). As a result, the international array of sensors initially deployed to monitor nuclear explosions is now also being used to enhance tsunami warning in the Indian Ocean. To expand this capability worldwide, more sensors could be deployed and response times further shortened.

More recently, the ability to monitor radionuclides in the atmosphere—including with IMS measurement systems—played a prominent role in tracking the radioactive plume of gas and debris from the 2011 Fukushima accident (*5*). The data provided national health authorities vital information regarding expected dose rates to populations. Atmospheric monitoring has also been key to managing air travel and maintaining safety during volcanic eruptions, aiding hundreds of thousands of individuals (*4*). In these ways, even though the main role of the IMS is currently related to specific treaty objectives, it is clear that the IMS also has great value for nontreaty applications.

The IMS benefits from an infrastructure, including a rapidly growing community of technical experts being established in countries around the world (*6*). This is not only a matter of important capacity building, through enhanced scientific capability in developing nations; it also means that—should there be cause for discussing a violation of the CTBT, let alone for demanding on-site inspections—there is already a vastly expanded population of experts who can reliably assess the technical evidence associated with nuclear explosions. Although any discussions of treaty violations are likely to be highly political, the main point is that it is useful to have more—rather than fewer—who can reliably evaluate the technical monitoring information.

That community of scientific experts has grown by many hundreds in just the past few years, because of implementation of the CTBT monitoring capability, and it is likely to keep growing for many years (*7*). Those experts, in turn, become important resources in enhancing their own countries' abilities to respond to—perhaps even mitigate or avoid—natural catastrophes, pollution, stresses associated with resource depletion, and so on (*8*).

The Open Skies Treaty (OST), first proposed by U.S. President Eisenhower in 1955 and signed in 1992 during President George H. W. Bush's administration, is likewise providing opportunities for significant nontreaty applications of aircraft-based monitoring. With more than 840 successful observational flights (*9*) over the United States, Russia, and partner countries since entry into force in 2002 (*10*), OST provides far more detailed monitoring, via aircraft-borne sensors, than is possible by satellite (*11*).

[1]University of California, Berkeley, Berkeley, CA 94707, USA. [2]Hoover Institution, Stanford University, Stanford, CA 94305, USA. [3]Pacific Northwest National Laboratory, Richland, WA 99354, USA. [4]Harvard University, Cambridge, MA 02138, USA.
*Author for correspondence. E-mail: jeanloz@berkeley.edu

The OST regime has potentially more flexibility than CTBT in supporting nontreaty applications of monitoring. Existing OST monitoring platforms have been successfully used, for example, in support of humanitarian relief after the 2005 hurricanes Katrina and Rita in the United States and the 12 January 2010 earthquake in Haiti (*12*). Moreover, Russia has expressed support for this concept (*13*), so there may be opportunities for fielding new technologies in aircraft-based monitoring (*11*) and for at least bilateral (and ultimately multilateral) engagement through nontreaty monitoring.

A case in point is the characterization and tracking of dust in the atmosphere, which faces challenges similar to those of global radionuclide monitoring. Lofted across continents and oceans, dust has an important influence on climate because it can both absorb and reflect sunlight, and its distribution is a symptom of global atmospheric conditions (*14*–*18*). Microorganisms are also transported along with the dust, so that public health is affected over intercontinental distances (*19*–*21*). Despite its significance for environment and health (from agriculture and climate to pollution and disease), little is known about the nature of dust in the troposphere. Much could be learned from physical collections made possible by complementary surface- and aircraft-based platforms.

More generally, collection of gases and aerosols both at and above ground level can greatly improve atmospheric-transport models, which have applications ranging from medium- and long-term weather forecasting to tracking radioactive plumes caused by human activity. Examples of success include a study using the distribution of krypton-85 to constrain atmospheric transport times between northern and southern hemispheres (*22*). Similarly, the Global Network of Isotopes in Precipitation, operated jointly by the International Atomic Energy Agency and World Meteorological Organization, provides data that have led to improved quantification of sources and transformation of water in the atmosphere, as well as better predictions of precipitation (*23*).

Aircraft can measure vertical profiles of constituents in the atmosphere much better than satellites, providing data crucial for identifying sources and sinks (e.g., for CO_2 and other greenhouse gases). For example, "Civil Aircraft for the Regular Investigation of the Atmosphere Based on an Instrument Container" (www.caraabic-atmospheric.org) uses an instrumented passenger airliner to monitor gases and aerosols and has proven to be invaluable for tracking volcanic clouds, air pollution, and much more.

Similarly, the High-performance Instrumented Airborne Platform for Environmental Research (HIAPER) Pole-to-Pole Observations Project used a Gulfstream V research plane (see the photo) to document concentrations of CO_2, CH_4, and many other gases from sea level up to 47,000 feet, with unique science return from hundreds of profiles along the Pacific (*24*). But only five pole-to-pole transects have been completed to date. This flight design can serve either treaty or environmental monitoring objectives.

Collecting and analyzing gas and particulate data are essential for improving atmospheric transport models and greatly advance the ability to characterize the atmosphere to distances of hundreds and even thousands of kilometers from a flight path or a ground-based station. That is, the information can help in monitoring neighboring countries, as well as the country being overflown (*25*).

Finally, airborne LIDAR (Light Detection and Ranging, the laser-based analog of RADAR) can play an important role in monitoring forest carbon stocks (*26*). This is valuable for such efforts as the United Nations Reducing Emissions from Deforestation and Forest Degradation program, as well as broader applications.

We have touched on a few examples to illustrate rich opportunities for scientific advancement and international cooperation that would be offered by implementing far more extensive aircraft- and ground-based environmental monitoring around the globe.

Recommendations

In some sense, nontreaty applications should be viewed as one of the ultimate long-term objectives of an arms-control monitoring regime. Without such applications, monitoring may not be sustainable. With such applications, however, monitoring can be enhanced through implementation of new technologies, engagement of more participants and—more generally—through improvements in transparency among nations.

Specifically, our recommendations are (i) to acknowledge the opportunities offered by nontreaty applications of monitoring capabilities that originally derive from arms-control regimes; (ii) to develop and implement concrete, realistic plans to pursue those opportunities, requiring input from many disciplines and countries; and (iii) for the United States and willing partners to take leadership in promoting nontreaty applications of monitoring, starting with bilateral projects.

A key aspect to implementation of nontreaty monitoring is to define approaches that are flexible, clear, and mutually acceptable to all parties concerned. There is opportunity not only for applying existing capabilities to new circumstances, but also in developing new technologies for global environmental monitoring that can serve the broader mandate of improving transparency and enhancing confidence. The idea is to create a win-win scenario whereby the monitoring capability is viewed as beneficial to all, perhaps even first and foremost of benefit to the country being studied.

References and Notes

1. Adopted by the UN General Assembly in 1996, the CTBT has not yet entered into force. Of 337 planned IMS facilities, 274 have thus far been certified. See (*3*).
2. U.S. Ambassador Paul Nitze defined "effective verification" in 1988 as: "if the other side moves beyond the limits of the treaty in any militarily significant way, we would be able to detect such violations in time to respond effectively and thereby deny the other side the benefit of the violation."
3. CTBTO Preparatory Commission, www.ctbto.org/verification-regime/.
4. O. Dahlman *et al.*, *Detect and Deter: Can Countries Verify the Nuclear Test Ban?* (Springer, New York, 2011).
5. A. Stohl *et al.*, *Atmos. Chem. Phys. Discuss.* **11**, 28319 (2011).
6. Capacity Development Initiative, www.ctbto.org.
7. There is considerable variability in this growth: see (*4*, *6*).
8. Details on implementation, cost, etc., are complicated by differences among monitoring technologies (e.g., seismic versus radionuclide) and the associated research communities.
9. A small fraction of attempted overflights are not successful due to weather or mechanical problems.
10. Organization for Security and Co-operation in Europe, Open Skies Treaty Observation Flights, From Entry-Into-Force to December 2011 [Open Skies Consultative Commission (OSCC), Vienna, 2012]; www.osce.org/secretariat/68315/.
11. S. D. Drell, C. W. Stubbs, *Arms Control Today* **41**(6), 15 (2011).
12. M. Betts, D. Spence, presentation at 2nd Open Skies Review Conference, Vienna, Austria, 7 to 9 June 2010 (OSCC, Vienna, 2010); www.osce.org/secretariat/68251.
13. S. Federyakov, presentation at 2nd Open Skies Review Conference, Vienna, Austria, 7 to 9 June 2010 (OSCC, Vienna, 2010); www.osce.org/secretariat/68573.
14. J. M. Prospero *et al.*, *Rev. Geophys.* **40**, 1002 (2002).
15. D. M. Cwiertny, M. A. Young, V. H. Grassian, *Annu. Rev. Phys. Chem.* **59**, 27 (2008).
16. K. A. Prather, C. D. Hatch, V. H. Grassian, *Annu. Rev. Anal. Chem.* **1**, 485 (2008).
17. M. Pósfai, P. R. Buseck, *Annu. Rev. Earth Planet. Sci.* **38**, 17 (2010).
18. S. A. Strode, L. E. Ott, S. Pawson, T. W. Bowyer, *J. Geophys. Res.* **117**, (D9), D09302 (2012).
19. D. W. Griffin, *Clin. Microbiol. Rev.* **20**, 459 (2007).
20. S. Ravi *et al.*, *Rev. Geophys.* **49**, RG3001 (2011).
21. C. E. Morris *et al.*, *Biogeosciences* **8**, 17 (2011).
22. D. J. Jacob *et al.*, *J. Geophys. Res.* **92**, (D6), 6614 (1987).
23. Global Network of Isotopes in Precipitation, www-naweb.iaea.org/napc/ih/IHS_resources_gnip.html.
24. S. Wofsy *et al.*, *Philos. Trans. R. Soc. London Ser. A* **369**, 2073 (2011).
25. This can have practical implications in that a friendly neighboring state may more readily authorize overflights.
26. Forest Carbon and Credent form partnership on LiDAR technology, http://forest-carbon.org/media/forest-carbon-credent-lidar-partnership.

Acknowledgments: We thank S. D. Drell, J. E. Goodby, G. P. Shultz, and C. W. Stubbs for helpful discussions. Views presented here are the authors' and do not necessarily reflect those of the U.S. government.

10.1126/science.1228731

IMMUNOLOGY

Sensing the Dark Side of DNA

An enzyme that senses foreign and mislocated DNA in the cell cytoplasm acts as an alarm that triggers host defense responses.

Luke A. J. O'Neill

To immunologists, DNA has always had a dark side. Long before it was shown to be the genetic material, it was known to stimulate immune responses (*1*). When DNA is in the wrong place, it is a sign of danger. The danger can be in the form of infection where microbial DNA is sensed, or cellular damage that leaks DNA into the cytoplasm from the nucleus or mitochondria. In the latter scenario, DNA can cause havoc, provoking autoimmune conditions such as systemic lupus erythematosus. On pages 826 and 786 of this issue, Wu *et al.* (*2*) and Sun *et al.* (*3*), show that an enzyme called cyclic guanosine monophosphate–adenosine monophosphate (cGAMP) synthase (cGAS) detects cytoplasmic DNA and triggers a signaling system never before observed in metazoans, to galvanize host defense, inflammatory, and autoimmune responses.

There are several candidate DNA sensors in mammalian cells [including DNA-dependent activator of interferon regulatory factors (DAI), DEAD box polypeptide 41 (DDX41), and interferon inducible protein 16 (IFI16)] (*4*), all of which activate a cytoplasmic protein called stimulator of interferon genes (STING). STING then turns on two protein kinases called IκB kinase (IKK) and TANK binding kinase 1 (TBK1), which in turn, respectively, activate the transcription factors nuclear factor κB (NF-κB) and interferon regulatory factor 3 (IRF3). Both signaling cascades lead to the production of type I interferons and other cytokines that participate in host immune responses. However, the precise mechanism of STING activation has not been clear, nor the relative importance of the possible DNA sensors.

Wu *et al.* and Sun *et al.* searched for a cytosolic sensor of DNA through an in vitro assay based on two mammalian cell lines—one that was screened for a sensor(s), and one that acted as a reporter cell line to detect the sensor(s). Factors in the cytoplasm of the screened cells gained access to the cytoplasm of reporter cells that were permeabilized. Activation of the transcription factor IRF3 in the reporter cells served as the readout for activation of the STING pathway. In this assay, exposure of the screened cells to multiple types of DNA resulted in cytoplasm that could activate the STING pathway in the reporter cells. Through biochemical purification, a factor that activates STING was identified as the cyclic dinucleotide cGAMP. This is intriguing because two other bacterial molecules, cyclic diadenylate monophosphate (c-di-AMP) and cyclic diguanylate monophosphate (c-di-GMP), also bind to STING and induce the production of type I interferons (*5*, *6*). It is also interesting that cGAMP acts as a signaling molecule in the bacterium *Vibrio cholerae* (to control motility) (*7*). Wu *et al.* report that treating the screened cell line with chemically synthesized cGAMP at concentrations as low as 10 nM stimulated the production of interferon-β—an effect much more potent than that of c-di-GMP or c-di-AMP. Exposure of the screened cells to herpes simplex virus I or vaccinia virus also caused an increase in cytoplasmic cGAMP concentration. Wu *et al.* also show that STING binds to cGAMP directly. Whereas c-di-GMP produced by bacteria [and by the protozoan *Dictyostelium* (*8*)] acts as a pathogen-associated molecular pattern (PAMP) molecule that activates STING, cGAMP could be described as a danger-associated molecular pattern (DAMP), although the term "second messenger" is more biochemically correct given that it resembles the well-known

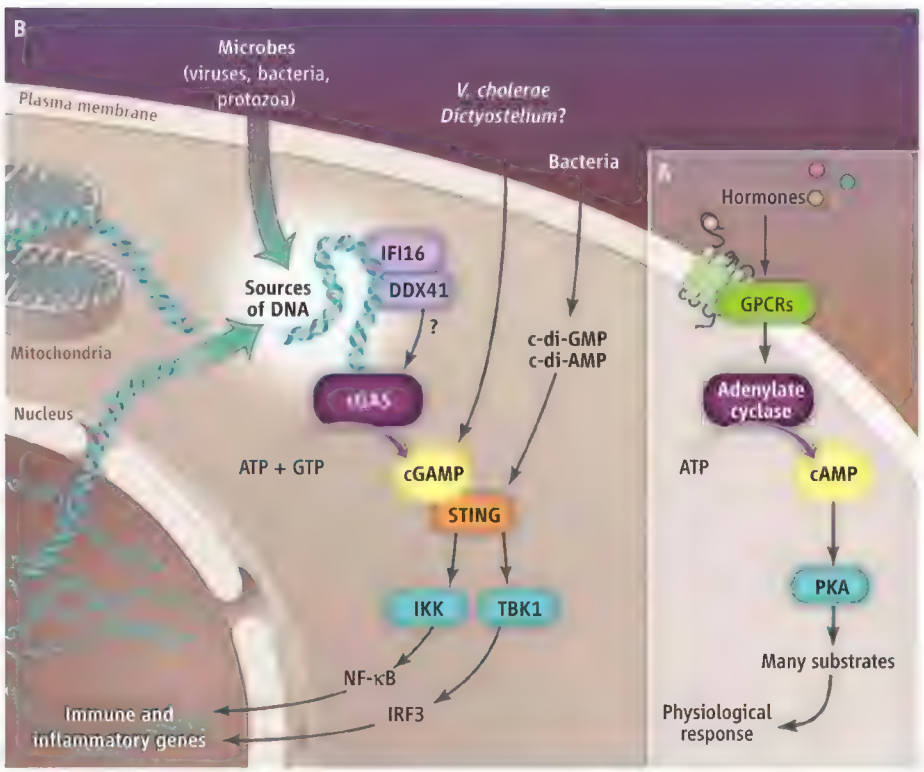

DNA sensor. **(A)** A well-characterized signaling pathway involves adenylate cyclase, which is activated by many hormones via G protein–coupled receptors (GPCRs) at the cell surface. Adenylate cyclase produces the second messenger molecule cAMP, which activates protein kinase A (PKA) and many cellular processes. **(B)** DNA from diverse microbes is sensed in the cytosol of infected cells as a danger signal. The cyclase cGAS binds this DNA, becomes catalytically active, and generates cGAMP as a second messenger. cGAMP binds to STING, which activates two signaling pathways that increase the expression of immune and inflammatory genes, thereby promoting host defense. The same process is likely to sense host DNA that leaks out of mitochondria or the nucleus in damaged cells, acting as a danger signal. Certain microbes make c-di-GMP or c-di-AMP, which activate STING; other microbes (and protozoa) can also synthesize cGAMP. How other DNA sensors fit into this process is unclear.

CREDIT: K. SUTLIFF/*SCIENCE*

School of Biochemistry and Immunology, Trinity Biomedical Sciences Institute, Trinity College, Dublin, Ireland. E-mail: laoneill@tcd.ie

second messenger signaling molecule cyclic adenosine monophosphate (cAMP).

To identify the enzyme generating cGAMP, Wu *et al.* and Sun *et al.* carried out three independent routes of purification of cytoplasm, each consisting of four steps of chromatography. Many proteins copurified with cGAS activity, but only three copurified in all three routes. One of the three is a member of the nucleotidyltransferase family, which includes adenylate cyclase, the enzyme that generates cAMP. This is especially interesting because cGAS would be predicted to be a cyclase on the basis of its amino acid sequence. The expression of endogenous cGAS was high in the screened cell line of the assay and in macrophages (immune cells that are critical for innate immunity) but very low in a cell line that does not contain an endogenous STING pathway. Among the many experiments carried out in both studies, the ectopic expression of cGAS and STING in the latter cell line fully restored responsiveness to DNA—an effect several orders of magnitude greater than that achieved by the ectopic expression of other DNA sensors such as DAI, IFI16, and DDX41. In vitro and in cells, DNA interacted directly with cGAS.

Wu *et al.* and Sun *et al.* provide compelling new insights into how DNA is sensed in the cytoplasm of mammalian cells. DNA binds to the enzyme cGAS, which catalyzes the production of the second messenger molecule cGAMP. This molecule in turn binds to STING, which triggers two different signaling cascades that launch the expression of host defense and inflammatory proteins (see the figure). Moreover, some bacteria appear to bypass cGAS by producing dicyclic nucleotides that bind to STING directly. The discovery of cGAS means that any microbe with DNA that stimulates gene expression by the transcription factors NF-κB and IRF3 will also signal via a cyclic dinucleotide, this time made by the host cell via cGAS. The pathway is also likely to be important for the sensing of self DNA, which can lead to autoimmunity.

What role does cGAS play relative to the other DNA sensors? This is not yet clear, and it is possible that cell type specificity will be found. Because cGAS has catalytic activity, it is possible that a small-molecule inhibitor could have therapeutic potential for autoimmune diseases. Whether that would leave the patient vulnerable to infection would need to be evaluated.

References

1. I. Mechnikov, Nobel Prize acceptance speech, 11 December 1908, www.nobelprize.org/nobelprizes/physics/laureates/2012.
2. J. Wu *et al.*, *Science* **339**, 826 (2013); 10.1126/science.1229963.
3. L. Sun, J. Wu, F. Du, X. Chen, Z. J. Chen, *Science* **339**, 786 (2013); 10.1126/science.1232458.
4. S. E. Keating, M. Baran, A. G. Bowie, *Trends Immunol.* **32**, 574 (2011).
5. J. J. Woodward, A. T. Iavarone, D. A. Portnoy, *Science* **328**, 1703 (2010).
6. D. L. Burdette *et al.*, *Nature* **478**, 515 (2011).
7. B. W. Davies, R. W. Bogard, T. S. Young, J. J. Mekalanos, *Cell* **149**, 358 (2012).
8. Z. H. Chen, P. Schaap, *Nature* **488**, 680 (2012).

10.1126/science.1234724

EVOLUTION

The Animal Tree of Life

A molecular phylogeny of the animal kingdom published 25 years ago was the precursor to today's widely accepted phylogeny of all animal phyla.

Maximilian J. Telford

In a letter to T. H. Huxley written on 26 September 1857, Charles Darwin imagined a time to come "though I shall not live to see it, when we shall have very fairly true genealogical trees of each great kingdom of nature" (*1*). The publication of *On the Origin of Species*, two years later, prompted a century and a half of disagreement among zoologists proposing often wildly contradictory schemes of animal evolution. Clarity began to emerge with Field *et al.*'s landmark publication 25 years ago of an analysis of animal relationships based on ribosomal RNA (rRNA) sequences (*2*). The paper made zoologists realize that molecular biology could and should be applied to traditional zoological questions.

The earlier disagreements derived from varying interpretations of the morphological and embryological characteristics of animals. Many of these characters have evolved repeatedly in unrelated lineages as adaptations to similar selective pressures or have been lost from certain groups through disuse. Today's strengthening consensus is almost entirely thanks to the use of molecular genetic data in reconstructing trees. Heritable changes in nucleotides and amino acids are abundant and generally much less prone to the problems of convergent evolution and loss than are morphological characters (*3*).

Field *et al.*'s sequencing of 18*S* rRNAs from species across the animal kingdom narrowly predates the polymerase chain reaction (PCR) era (*4*). The authors instead produced their sequence data by direct reverse transcriptase sequencing of rRNA (*5*). They sequenced three regions of the 18*S* rRNA molecule from species representing 10 of the ~30 animal phyla. This approach produced ~1000 nucleotides of sequence per taxon, almost an order of magnitude greater than previous work using 5*S* rRNA (*6*).

If we consider a summary of the trees produced from these data (see the figure, panel A), we find some familiar groups (arthropods, chordates, and echinoderms), as well as some surprises. For example, almost all premolecular phylogenies supposed a close link between the brachiopods (lamp shells) and the deuterostomes (chordates and echinoderms). Yet in Field *et al.*'s tree, the brachiopods are placed far from the deuterostomes in the Lophotrochozoa, which include annelids and mollusks. This major rearrangement suggests that certain "deuterostomian" characters of brachiopods may have evolved more than once.

Similarly, premolecular phylogenies agreed on a close relationship of the annelids and arthropods (collectively the Articulata in reference to a body divided into segments that is typical of both groups). Field *et al.*'s tree provided the first hint that the annelids and arthropods are in fact independent groups, each more closely related to unsegmented phyla (see the figure, panel A).

Other surprises in the tree were less welcome. Probably the most striking result, and the one that provoked the strongest reaction at the time, was the conclusion that the multicellular animals evolved on two separate occasions from unicellular relatives (see the figure, panel A). It quickly became clear that this conclusion was incorrect and that it resulted from the cnidarians being

Department of Genetics, Evolution and Environment, University College London, London WC1E 6BT, UK. E-mail: m.telford@ucl.ac.uk

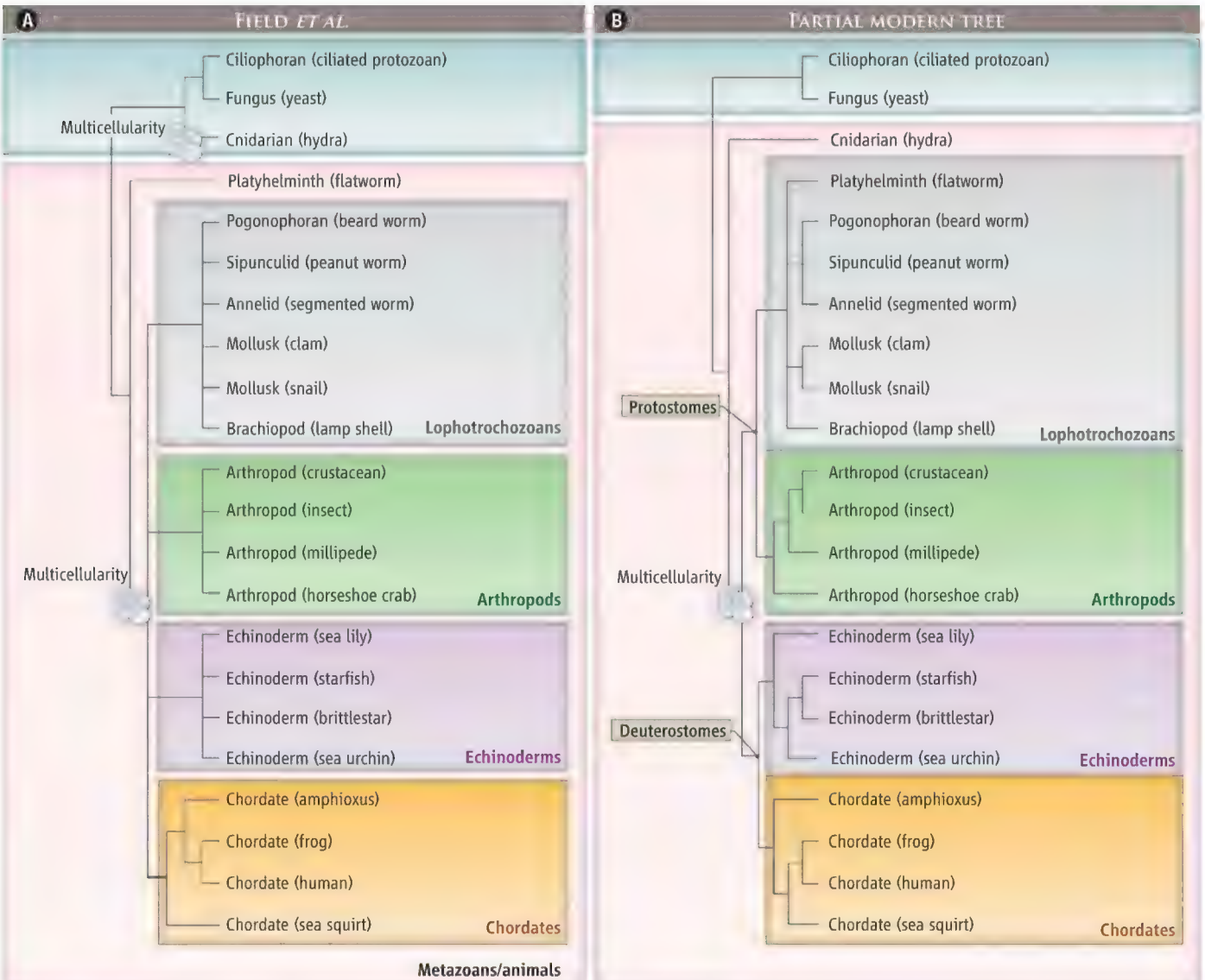

Toward a consensus. **(A)** Summary of the trees presented by Field *et al.* (*2*). This landmark tree began to clarify the evolutionary relationships of the animal phyla but could not resolve all relationships between groups at higher levels of the hierarchy. The tree contained some erroneous placements, the most striking of which was the conclusion that multicellularity evolved twice. **(B)** Modern tree. To facilitate comparison with (A), only those groups also studied by Field *et al.* are shown. Major groups are resolved into Protostomes and Deuterostomes. Today, constituent species of all 30 known animal phyla have been sampled. A more complete tree would, for example, include the pseudocoelomate phyla (including nematodes), which together with the arthropods constitutes the Ecdysozoa. The Deuterostomes contain two phyla (the hemichordates and xenacoelomorphs) that were not studied by Field *et al.* and are not shown.

misplaced in the tree. A second error—the placement of the flatworm *Dugesia* (Platyhelminthes) as a branch outside of the main groups of animals (see the figure, panel A)—took longer to resolve. We know now that its correct place is within the lophotrochozoans (see the figure, panel B) (*7*). Both errors arose because the 18*S* rRNA genes of the misplaced groups evolve at an unusually high rate, resulting in "long branch attraction," whereby rapidly evolving species are incorrectly placed close to the long branch leading to the species used to root the tree (such as yeast and ciliate, as in the trees in the figure) (*8*).

Building on the foundations of Field *et al.*, some of the most important progress has stemmed from the development of probabilistic methods that can accommodate the systematic biases present in real sequences, such as unequal rates of evolution (*9*).

A second important trend has been an enormous expansion in taxonomic coverage. Field *et al.* covered 10 animal phyla; today, species from all 30 known phyla have been sampled (*10*). Broader sampling can help to improve the accuracy of the tree by allowing the experimenter to select among species from a given group to find those least affected by systematic biases and by highlighting systematic errors by providing information on the substitutions that have occurred along problematic branches. Both of these advantages of deeper sampling were instrumental in the identification of the Ecdysozoa, a group of animals that links the arthropods to other ecdysing (cuticle molting) animals such as nematodes (*11*, *12*).

The third important development has been the use of increasingly comprehensive multigene phylogenies. The earliest of these made use of large data sets derived from the first complete animal genomes to test the controversial Ecdysozoa grouping. The burgeoning availability of genome sequences

from many phyla is now making the use of alignments of hundreds or even thousands of genes a standard procedure.

These studies have led to a widely accepted phylogeny of all animal phyla that has radically changed our views of animal evolution (*3*). Premolecular phylogenies generally envisaged a gradual increase in complexity from the earliest animals without a body cavity or coelom (acoelomate flatworms) via pseudocoelomate worms (such as nematodes and rotifers) to coelomate protostomes (annelids, arthropods, and mollusks) and deuterostomes (echinoderms and chordates) with a sophisticated mesoderm-lined coelomic body cavity.

In contrast, today's tree divides bilaterally symmetrical animals into protostomes and deuterostomes (see the figure, panel B). Within the deuterostomes, the simple urochordates (sea squirts) are closer relatives of the vertebrates than the more fishlike cephalochordates (amphioxus) (*13*); a third phylum of deuterostomes, the hemichordates (acorn worms), are the sister group of echinoderms and not of the chordates (*14*).

The acoelomate platyhelminths, as we have seen, are now known to be related to the coelomate annelids, mollusks, and brachiopods within the Lophotrochozoa. A second acoelomate group, the Xenacoelomorphs, although historically linked to the flatworms, have rather controversially been placed close to echinoderms to form a fourth phylum of deuterostome (*15*). Pseudocoelomate phyla, including nematodes and rotifers, are scattered throughout the protostomes.

All these rearrangements suggest that many characters thought to be important—such as the coelomic body cavity—have in fact been gained and lost multiple times.

Although much of the animal tree is now resolved, a number of problems remain. These problems tend to involve relationships either of taxa with extreme systematic biases or among groups that seem to have originated in a rapid radiation, resulting in a lack of signal supporting individual nodes. Future progress will depend on increasing useful signal with larger "phylogenomic" data sets from the widest possible taxonomic sample and on continued improvement in the correspondence between real data and the models used when reconstructing trees.

References and Notes

1. C. R. Darwin, Letter to T. H. Huxley (1857); www.darwinproject.ac.uk, Letter 2143.
2. K. G. Field *et al.*, *Science* **239**, 748 (1988).
3. M. J. Telford, R. R. Copley, *Trends Genet.* **27**, 186 (2011).
4. R. K. Saiki *et al.*, *Science* **239**, 487 (1988).
5. D. J. Lane *et al.*, *Proc. Natl. Acad. Sci. U.S.A.* **82**, 6955 (1985).
6. T. Ohama, T. Kumazaki, H. Hori, S. Osawa, *Nucleic Acids Res.* **12**, 5101 (1984).
7. G. Balavoine, *C.R. Acad. Sci. III* **320**, 83 (1997).
8. J. Felsenstein, *Syst. Zool.* **27**, 401 (1978).
9. N. Lartillot, H. Philippe, *Mol. Biol. Evol.* **21**, 1095 (2004).
10. P. H. Holland, *The Animal Kingdom* (Oxford Univ. Press, Oxford, UK, 2011).
11. A. M. Aguinaldo *et al.*, *Nature* **387**, 489 (1997).
12. H. Philippe, N. Lartillot, H. Brinkmann, *Mol. Biol. Evol.* **22**, 1246 (2005).
13. F. Delsuc, H. Brinkmann, D. Chourrout, H. Philippe, *Nature* **439**, 965 (2006).
14. K. M. Halanych, *Biol. Bull.* **190**, 1 (1996).
15. H. Philippe *et al.*, *Nature* **470**, 255 (2011).

Acknowledgments: M.J.T. is supported by a Royal Society Wolfson Research Merit Award.

10.1126/science.1234378

BIOPHYSICS

Fine Tuning Gene Regulation

An allosteric effect in which distortion of the DNA duplex by one protein modulates the binding of another protein may be important in gene regulation.

Donald M. Crothers

On page 816 of this issue, Kim *et al.* (*1*) report that a DNA-bound protein can influence the properties of an adjacent protein if both are bound to the DNA strand within about 15 base pairs (bp) of each other. The authors attribute their observations to an allosteric effect, in which a distortion of the DNA strand by the first protein modulates the binding of the second protein. The observations have important implications for gene regulation.

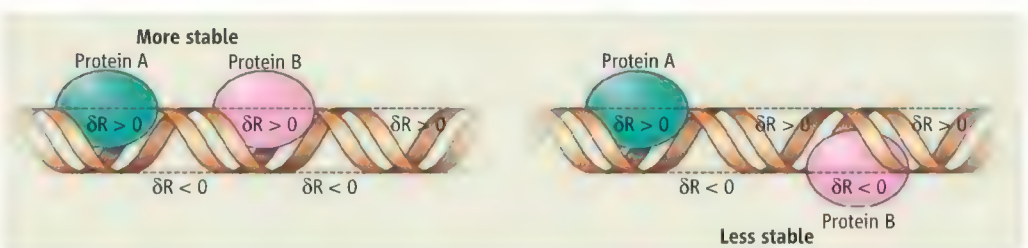

Allosteric coupling. Kim *et al.* show that oscillation of the major groove width $R(L)$ causes variation of the allosteric coupling between two DNA-binding proteins A and B, both of which widen the major groove. Thus, binding of A energetically favors binding of B at positions where R is already widened ($\delta R > 0$, top), but disfavors binding of B where R is narrowed ($\delta R < 0$, bottom). [Adapted from (*1*)]

The authors use single-molecule methods to detect the influence of the first protein (protein A) on the dissociation rate of the second protein (protein B), measured relative to the value without protein A. They show that the effect is strongly phase-dependent, with a periodicity of 10 bp and amplitude of ~4-fold change in the dissociation rate.

Department of Chemistry, Yale University, New Haven, CT 06511, USA. E-mail: donald.crothers@yale.edu

The natural first interpretation of these results would be that the effect is due to protein-protein contacts or through-space electrostatic effects. However, these explanations are rendered unlikely by control experiments, which show that a hairpin loop can replace protein A, the effect is nearly independent of salt concentration, and the rate constant oscillation is much attenuated by a nick or unmatched base pair between the two proteins.

The authors studied various protein pairs, including the T7 RNA polymerase (T7 RNAp)–lac repressor (LacR) combination. In vitro single-molecule kinetic experiments showed that T7 RNAp stabilizes or destabilizes LacR, depending on the distance between them along the DNA strand. In transcription experiments in vivo, LacR was placed upstream of the T7 promoter used to transcribe the lac Z gene. It is a general thermodynamic principle that if one protein stabilizes/destabilizes the binding of another protein, the second must have the same stabilizing/destabilizing effect on the first. Lac Z expression levels, which

depend on the binding strength of the polymerase, were found to oscillate by a factor of three depending on how far upstream the lac repressor was bound. The results correspond to the effects of T7 RNAp on LacR stability, as required by thermodynamics.

The authors propose that the helical phase-dependence of DNA-bound protein stability is due to transmission of allosteric effects through DNA. The concept of allostery was initially proposed to explain how the properties of the active site of an enzyme can be affected by binding an effector at a distant site, but it is useful in a wider context. Monod *et al.* (*2*) have defined allosteric effects broadly as indirect interactions between distinct specific binding sites. In accordance with this definition, Pohl *et al.* (*3*) described the cooperative binding of ethidiuim to a left-handed Z-DNA sample in terms of an allosteric conversion of the structure to B-form, to which ethidium binds tightly. Because B-Z junctions have a large unfavorable free energy, there are not many of them. As a consequence, large blocks of DNA are converted simultaneously. Only a small increase in ethidium concentration is needed to tip the balance, and hence the conversion is cooperative.

More recent studies of allostery in DNA have invoked subtle transmission of structural influence, rather than a switch between canonical structural models. Proposed effects include influence of the detailed sequence of a protein binding site (*4*) and strain induced by DNA bending (*5*, *6*).

Probably the most relevant study to that of Kim *et al.* is the characterization by Wang *et al.* (*7*) of the net repressor binding to a DNA strand containing 256 tandem repeats of the lac operator. In DNA molecules attached to fused silica surfaces or constrained in nanochannels, they found that only about 2.5% of the *lac* operator sites are occupied, at protein concentrations well above the solution-phase dissociation constant. The results imply strong anticooperative effects in repressor binding with a range of ~150 bp (*8*), ascribed to strain induced in the DNA. It would be of interest to see the tandem *lac* operator system analyzed by the kinetic method of Kim *et al.*

The model proposed by Kim *et al.* to explain the allosteric effects invokes correlation and anticorrelation between DNA groove widths, depending on distance between sites. The authors show in a molecular dynamics simulation that such correlations exist. Thermal fluctuations lead to variation in major groove width at position zero; when the groove is wider/narrower at position zero, it is likely to be wider/narrower at a position ~10 bp away. When the sites are half a helical turn apart, the correlation is reversed to narrower/wider (see the figure). These correlated motions reflect low-frequency vibrational modes of DNA. In simple terms, widening the groove by binding a protein at position zero widens the groove at +10 bp, enhancing binding of a protein that favors a wider major groove. This can also be viewed as quenching one or more long-range vibrational modes by binding protein A, an entropic cost that does not have to be paid by binding protein B.

It is now clear that the quantitative aspects of gene regulation are influenced quite substantially by the relative placement of regulatory elements. Distance changes of half a helical turn can alter stability and rates by a factor of three or more. This effect provides evolution with fine-tuning capability for adjusting relative kinetics in regulatory networks and makes our comparative interpretation of genome sequences even more challenging.

References

1. S. Kim, X. S. Xie, *Science* **339**, 816 (2013).
2. J. Monod, J. Wyman, J. P. Changeux, *J. Mol. Biol.* **12**, 88 (1965).
3. F. M. Pohl, T. M. Jovin, W. Baehr, J. J. Holbrook, *Proc. Natl. Acad. Sci. U.S.A.* **69**, 3805 (1972).
4. H. G. Garcia *et al.*, *Cell Rep.* **2**, 150 (2012).
5. B. S. Parekh, G. W. Hatfield, *Proc. Natl. Acad. Sci. U.S.A.* **93**, 1173 (1996).
6. J. Rudnick, R. Bruinsma, *Biophys. J.* **76**, 1725 (1999).
7. Y. M. Wang *et al.*, *Proc. Natl. Acad. Sci. U.S.A.* **102**, 9796 (2005).
8. Y. M. Wang, J. O. Tegenfeldt, J. Sturm, R. H. Austin, *Nanotechnology* **16**, 1993 (2005).

10.1126/science.1232663

PHYSICS

Beating Classical Computing Without a Quantum Computer

Photons performing quantum random walks can be used to calculate matrix properties without actually implementing quantum logic gates.

James D. Franson

Physics Department, University of Maryland Baltimore County, 1000 Hilltop Circle, Baltimore, MD 21250, USA. E-mail: jfranson@umbc.edu

Quantum computers are expected to be able to solve mathematical problems that are not feasible on a classical computer. Although considerable progress has already been made, building a full-scale quantum computer would require controlled interactions between the quantum bits, or qubits, in order to implement the logic operations required for addition, subtraction, and multiplication. On pages 798 and 794 of this issue, Spring *et al.* (*1*) and Broome *et al.* (*2*), as well as Tillmann *et al.* (*3*), have shown that quantum systems—in this case, photons interacting along waveguides—could outperform a classical computer for certain kinds of matrix calculations without the need for logic operations.

This new method for performing calculations is based on the random walk process, as illustrated in the figure. In a classical random walk, one or more particles travel along a channel or path. At each moment in time, there is a probability P_L that a particle will hop over to the channel to its left and a probability P_R that it will hop over to the channel to its right. These probabilities may vary as a function of channel number and time. It is assumed that the particles do not interact with each other, so that the total probability of finding a particle in a given output channel is just a sum of the independent probabilities for the individual particles.

A quantum random walk (*4*) differs from a classical random walk because the particles also have wavelike properties in quantum mechanics. The wavelike properties of a particle are described by its wave function $\Psi(x)$, which depends on its position x. Although a particle propagates as a wave, it will only be detected at a single location. The probability of detection at location x is equal to the square of the magnitude of $\Psi(x)$. As illustrated in panel A of the figure, a particle will spread out as a wave while it propagates through the random walk process, but it will only be detected in a single output channel.

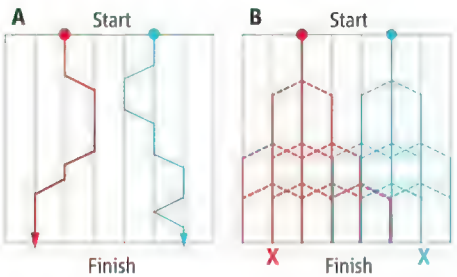

Calculating with quantum random walks. (**A**) A classical random walk process in which *M* particles are initially located in *N* paths or channels. There is some probability that a particle will hop to an adjacent channel at any moment in time. (**B**) A quantum random walk process in which the wavelike nature of each particle spreads out among many channels. Nonetheless, each particle will be found in a single channel when its position is measured at the end of the process, as indicated by the two Xs at the bottom in this example. The probability of detecting the photons is proportional to the output of certain matrix calculations (the permanent) and allows these calculations to be performed much faster than with classical algorithms for large *N*.

The output probability distribution from a quantum random walk process does not simply correspond to a sum of the independent probabilities for the individual particles even if there is no physical interaction between the particles (panel B of the figure). The extra interactions arise because the state of the system must obey the rule that $\Psi(x_1, x_2) = \pm\Psi(x_2, x_1)$ when two indistinguishable particles are swapped or interchanged. The plus sign applies to particles that are known for historical reasons as bosons, whereas the minus sign applies to particles known as fermions. Applying this rule to the wave function produces an effective attraction between identical bosons and an effective repulsion between identical fermions. For example, the probability of finding two identical fermions at the same location $x_1 = x_2$ is zero because that corresponds to $\Psi(x_1, x_1) = -\Psi(x_1, x_1)$. These effects are commonly referred to as exchange forces, even though there is no physical interaction between the particles. Roughly speaking, the exchange forces provide an effective interaction that can be used to perform certain calculations.

Spring *et al.*, Broome *et al.*, and Tillmann *et al.* used indistinguishable particles of light (photons) to implement a quantum random walk of this kind called boson sampling. The photons propagated through a series of conducting channels known as waveguides that were fabricated on the surface of a chip. Neighboring channels were coupled to each other by bringing them sufficiently close together that a photon had some probability of hopping to the adjacent waveguide. The probabilities of detecting the photons in the various output channels were then measured with single-photon detectors. It is possible to fabricate a much larger number of waveguides on the surface of a chip than were used in these examples, so full-scale implementations should be possible in the future.

The probability of detecting a photon (a boson) in each of the output channels is proportional to the so-called permanent of a matrix (*5*). The permanent of an $N \times N$ matrix is defined as the sum of all products of N elements of the matrix chosen in such a way that each row and column appears only once. The permanent is similar to the more familiar determinant aside from the minus signs that appear in the determinant. There are efficient methods for calculating the determinant of a matrix that use classical computers, but the best-known classical algorithm for calculating the permanent requires an exponentially large number of computational steps and is not feasible for large N. The relevant matrices are related to the coupling coefficients between the N input and output channels, which can be controlled experimentally.

Experiments of this kind provide a simple demonstration of the ability of a quantum system to perform a potentially useful computation without the need for the quantum logic operations required for a general-purpose quantum computer. For larger values of N, this approach may eventually provide the first demonstration of an actual calculation that can be done faster using quantum techniques than could be achieved with a classical computer. In addition, Childs *et al.* (*6*) have shown that any calculation can be performed using quantum random walks if quantum logic operations (*7*, *8*) between the photons are also included. The combination of these two techniques may eventually lead to the building of a full-scale quantum computer.

References

1. J. B. Spring *et al.*, *Science* **339**, 798 (2013); 10.1126/science.1231692.
2. M. A. Broome *et al*, *Science* **339**, 794 (2013); 10.1126/science.1231440.
3. M. Tillmann *et al.*, http://arxiv.org/abs/1212.2240 (2012).
4. Y. Aharonov, L. Davidovich, N. Zagury, *Phys. Rev. A* **48**, 1687 (1993).
5. S. Aaronson, A. Arkhipov, in *Proceedings of ACM Symposium on the Theory of Computing, STOC* (Association for Computing Machinery, New York, 2011), pp. 333–342, http://dl.acm.org/citation.cfm?id=1993682.
6. A. M. Childs, D. Gosset, Z. Webb, *Science* **339**, 791 (2013).
7. E. Knill, R. Laflamme, G. J. Milburn, *Nature* **409**, 46 (2001).
8. T. B. Pittman, M. J. Fitch, B. C. Jacobs, J. D. Franson, *Phys. Rev. A* **68**, 032316 (2003).

10.1126/science.1234061

MOLECULAR BIOLOGY

New Tool for Genome Surgery

John van der Oost

A bacterial system that uses RNA to edit DNA is harnessed for engineering mammalian genomes.

Gene therapy is the holy grail of human medicine. Many diseases are caused by a defective gene, sometimes with a mutation as subtle as a single-nucleotide variation. Before restoration of such a mutation in a patient's genome can take place, the target nucleotide sequence has to be cleaved at a single position, out of 3 billion possibilities. This degree of precise surgery requires an enzyme with highly selective target recognition. Successful editing of eukaryotic genomes has been accomplished with DNA nucleases designed to bear a unique site that binds to a specific DNA sequence. A major drawback of these protein-guided systems to "engineer" genomes, however, is that each new target sequence requires laboriously adjusting the specificity of the nuclease's DNA binding site. On pages 819 and 823 of this issue, Cong *et al.* (*1*) and Mali *et al.* (*2*) describe efficient genome editing in human cells based on an RNA-guided system.

Upon identifying the exact genomic target site, an endonuclease will cleave the DNA. Depending on the nature of the consequential DNA damage (single-strand nicks or double-strand breaks) and on the type of DNA repair system that is activated in response to the damage (homologous or nonhomologous recombination), strand religation may either seamlessly revert to

Laboratory of Microbiology, Wageningen University, 6703 HB Wageningen, Netherlands. E-mail: john.vanderoost@wur.nl

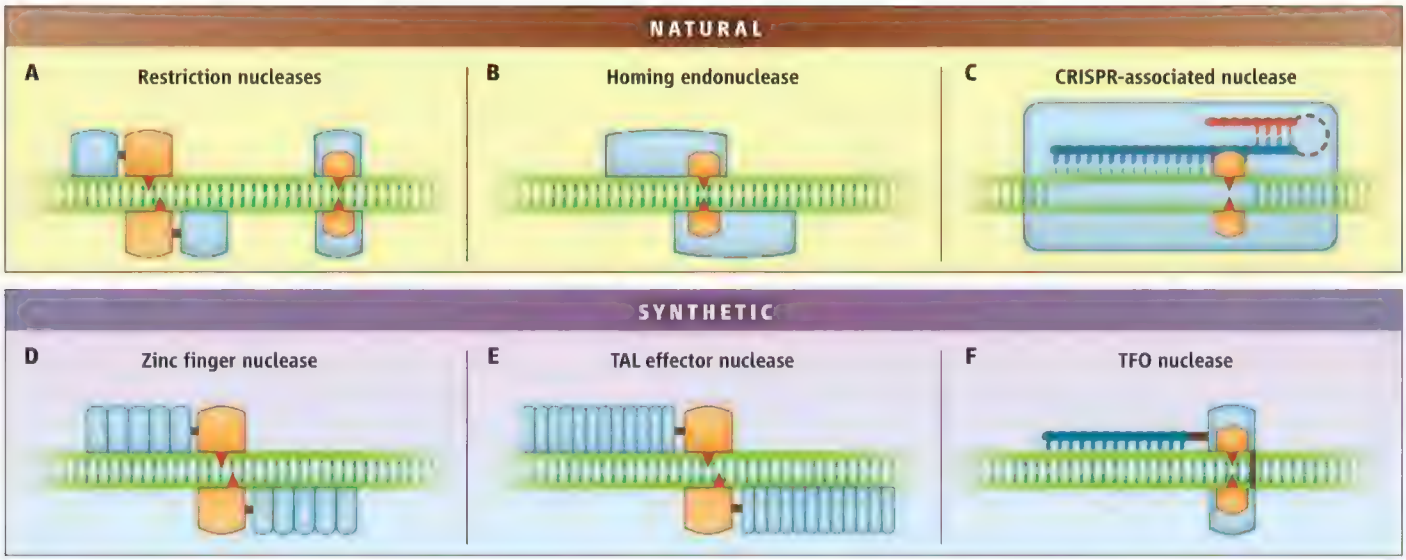

Potential genome editing. Schematic comparison of nucleases with DNA-binding (blue) and DNA-cleaving domains (red). (Top) Natural nuclease classes: (**A**) Restriction enzyme (shown as a dimer), with separate DNA binding and DNA cleavage domains (left) and with a single dual-function domain (right); (**B**) homing endonuclease with an extended DNA binding domain; (**C**) type II CRISPR-associated nuclease with a guiding crRNA (blue) and tracrRNA (red). (Bottom) Synthetic nuclease classes: (**D**) zinc finger nuclease dimer; (**E**) transcription activator-like effector nuclease (TALEN) dimer with nuclease domains; (**F**) triple-helix–forming oligonucleotides with a single-chain nuclease (shown as a dimer).

the original sequence or result in different modifications. The latter changes range from exchange of designed DNA donor fragments by homologous recombination (thus, the editing of an existing gene or integration of a new gene) to small insertions and deletions by nonhomologous end joining of double-strand breaks (disruption of a gene).

Classical restriction endonucleases are not suitable for genome engineering because the sites they recognize are very short [4 to 8 base pairs (bp); see the figure] and occur too frequently in the genome. Homing endonucleases recognize longer targets (20 to 30 bp), but adjusting their specificity requires laborious protein design (*3*). More recently, artificial chimeric proteins have been created by fusing a nuclease domain to a DNA binding protein. One class, zinc finger nucleases, consists of a nuclease that is fused to a set of zinc finger domains that each interacts with three nucleotides; dimeric zinc finger nucleases can target up to 36-bp sequences. Adjusting the specificity of zinc finger nucleases relies on the shuffling of domains with established triplet specificity (*4*). Another class of DNA binding protein, transcription activator-like effector nucleases (TALENs), are composed of a nuclease that is fused to a protein consisting of an array of 12 to 26 domains, each of which specifically interacts with a single base; in dimer designs, this results in at least 24-bp binding sites (*5*). Thus, rational design toward any target DNA sequence can be accomplished by relatively straightforward protein engineering.

An attractive alternative strategy for binding DNA fragments with high specificity may be the use of oligonucleotides as a recognition module. An initial attempt to synthesize such a tunable nuclease was the development of a short triple-helix–forming oligonucleotide conjugated to a restriction endonuclease (*6*). Application of this approach is mainly hampered by the restriction of triple-helix formation to DNA fragments with strands composed of either purines or pyrimidines.

Recently, a natural RNA-guided DNA nuclease system has been discovered in bacteria and archaea. Analysis of clustered regularly interspaced short palindromic repeats (CRISPR) has elucidated a unique system for adaptive immunity by CRISPR-associated (Cas) proteins. The specificity of the CRISPR-Cas system relies on tightly bound CRISPR RNA (crRNA), which efficiently guides a nuclease to its target—a complementary DNA fragment (*7*, *8*). A type II CRISPR-associated nuclease (Cas9) causes specific double-strand breaks in a DNA target. Processing of its crRNA guide involves a second, trans-acting crRNA (tracrRNA) and a ribonuclease (RNase III) (*9*). When loaded with both crRNA and tracrRNA (or an artificial chimera of the two RNAs), the Cas9 nuclease cleaves a DNA fragment that is complementary to the exposed part of the crRNA (*10*, *11*). Dedicated cleavage of plasmids in vitro (*9*) demonstrates the promise of CRISPR-mediated gene targeting as a more generic molecular engineering tool.

Cong *et al.* and Mali *et al.* report different applications of the bacterial Cas9 nuclease for RNA-guided engineering of mammalian genomes. Both groups describe the functional expression of Cas9 in the nucleus of cultured human cells. Cas9 that is loaded with guiding crRNA and assisting tracrRNA can carry out programmed DNA cleavage, which is eventually partly repaired by nonhomologous end joining, an event that frequently results in small insertions and deletions. Whereas the wild-type Cas9 generates double-strand breaks, Cong *et al.* and Mali *et al.* have used a Cas9 mutant in which one of the nuclease active sites is disrupted (*10*, *11*). This variant generates breaks in only one of the DNA strands, which should diminish nonhomologous recombination. Indeed, both groups demonstrate a reduction in off-target mutations due to insertions and deletions. In this context, distinct donor DNA fragments were successfully integrated at the site of cleavage. Moreover, the simultaneous introduction of two adjacent double-strand breaks resulted in efficient deletion of the intervening fragment. Notably, as Cong *et al.* and Mali *et al.* show, this also allows for scaling up by multiplex editing of distinct target loci. Similarly, Jinek *et al.* (*12*) have reported dedicated double-strand DNA breaks based on Cas9-mediated genome editing in human cells. Cas9 cleaving efficiencies depended mainly on the design of the chimeric RNA, suggesting

a means for further optimizing the editing performance of Cas9.

Efficient strategies for directed editing of mammalian genomes will enable sophisticated genetic engineering for both fundamental and applied purposes. Especially in medical applications, high-fidelity target recognition is critical, as off-site nuclease activity will jeopardize the safety of the engineering operation; thus, long stretches of nucleotides should be specifically recognized. In addition, adjusting the system's specificity toward new target sequences should be easy and affordable; this is a major advantage of the Cas9 system, as it merely requires changing the sequence of the guide RNA. Furthermore, the recombination should be fast, efficient, and scalable. Compared to the most promising currently available genome editing systems (zinc finger domains and TALENs), the RNA-guided Cas9 nuclease probably is closest to meeting these requirements. However, efficiency and specificity still can be improved—for instance, by laboratory evolution. Applying these genome surgery techniques to correct human disease-associated genetic mutations, resulting in functional gene therapy and in curing genetic disorders, will therefore take time. The spectacular recent development of dedicated nucleases suggests, however, that we are entering the final stage of this quest.

References

1. L. Cong *et al.*, *Science* **339**, 819 (2013); 10.1126/science.1231143.
2. P. Mali *et al.*, *Science* **339**, 823 (2013); 10.1126/science.1232033.
3. B. L. Stoddard, *Structure* **19**, 7 (2011).
4. F. D. Urnov, E. J. Rebar, M. C. Holmes, H. S. Zhang, P. D. Gregory, *Nat. Rev. Genet.* **11**, 636 (2010).
5. A. J. Bogdanove, D. F. Voytas, *Science* **333**, 1843 (2011).
6. K. Eisenschmidt *et al.*, *Nucleic Acids Res.* **33**, 7039 (2005).
7. B. Wiedenheft, S. H. Sternberg, J. A. Doudna, *Nature* **482**, 331 (2012).
8. E. R. Westra *et al.*, *Annu. Rev. Genet.* **46**, 311 (2012).
9. E. Deltcheva *et al.*, *Nature* **471**, 602 (2011).
10. M. Jinek *et al.*, *Science* **337**, 816 (2012).
11. G. Gasiunas, R. Barrangou, P. Horvath, V. Siksnys, *Proc. Natl. Acad. Sci. U.S.A.* **109**, E2579 (2012).
12. M. Jinek *et al.*, *elife* 2013; 2:300471 (2013).

10.1126/science.1234726

PHYSICS

Demonstrating Uncertainty

Heisenberg's uncertainty principle is demonstrated with a vibrating macroscopic mirror.

Gerard J. Milburn

Anyone using a modern camera is implementing an optical position measurement. In an active autofocus camera, a pulse of infrared light is emitted from the camera, and the time taken for it to be reflected back to the camera is used to compute the distance between the object and the image plane. Imagine how difficult it would be to operate such a system if the object recoiled every time the infrared pulse was reflected from it. Heisenberg suggested that this is precisely what would happen if light were used to determine the position of a quantum object as accurately as his famous uncertainty principle would allow. On page 801 of this issue, Purdy *et al.* (*1*) demonstrate this quantum back-action effect in an optical measurement of the position of a macroscopic mirror.

The mechanical action of light has long been known (*2*). Kepler suggested that the reason comet tails point away from the Sun is due to the mechanical action of light. In the early 1970s, Arthur Ashkin of Bell Laboratories showed that optical intensity gradients could exert a force on micrometer-size particles. This observation eventually led to laser cooling and the field of atom optics.

The history of using optical transducers to monitor the quantized position of an object at the Heisenberg limit goes back to the early proposals for the optical detection of gravitational radiation (*3*). The relative length of the two orthogonal arms in a Michelson-Morley interferometer is changed by the tidal forces exerted by gravitational waves. This length difference leads to changes in the interference of light at the output mirror. Monitoring the output intensity can thus be used to measure the relative position of the end mirrors.

The effect is small, however, and very small changes in the intensity need to be detected. This eventually runs into a problem caused by the essential granular nature of light (light pulses are made up of individual photons). Even the most carefully stabilized laser produces light with intensity fluctuations due to the random arrival of individual photons, called shot noise. We rarely need to account for this as the relative size of the intensity fluctuation falls off as the inverse square root of the intensity, so we can always increase the intensity to improve the signal-to-noise ratio. But there is another problem.

If we take into account the mechanical action of light, we see that a price must be paid for

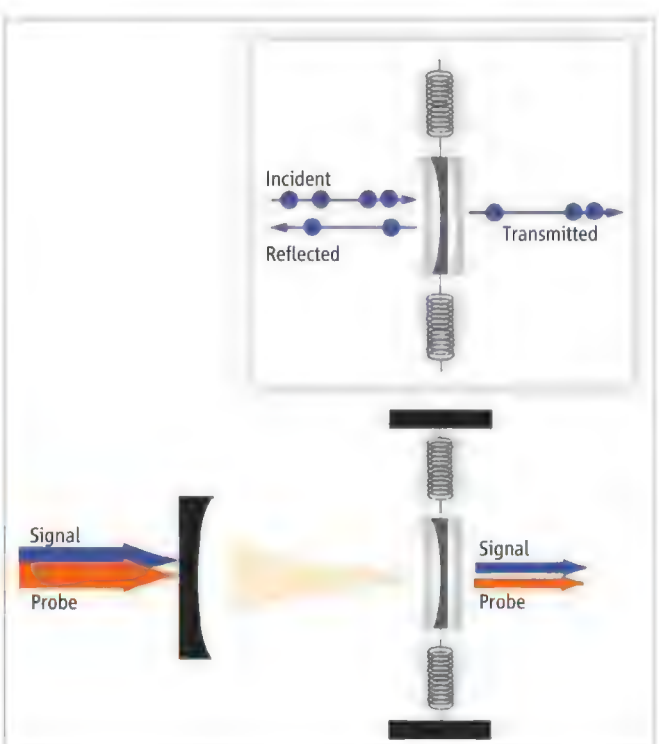

An optical cavity with a vibrating mirror. As this mirror moves, the intensity of the transmitted light can be used to monitor its position. (**Inset**) When the quantum nature of light is included, the random reflection of individual photons shakes the mirror, adding radiation pressure noise to the position measurement.

Centre for Engineered Quantum Systems, The University of Queensland, St Lucia, Brisbane, QLD 4072, Australia. E-mail: milburn@physics.uq.edu.au

increasing the accuracy of the measurement by increasing the intensity. As individual photons are reflected from a movable mirror, it will recoil, and the shot noise of individual photon arrivals will lead to a fluctuating force on the mirror; it will begin to shake ever more violently as the intensity is increased, limiting the gain in accuracy due to increasing intensity. This is the radiation pressure shot noise, and it is the physical mechanism enforcing the Heisenberg uncertainty principle in an optomechanical position transducer.

Balancing the effects of shot noise and radiation pressure noise leads to the standard quantum limit for an optomechanical position transducer. Large interferometers designed to detect gravitation waves are not yet at this limit, which would require more laser power than the optical components could stand, yet it will need to be taken into account in the next generation of detectors.

Purdy *et al.* report the first direct demonstration of the radiation pressure shot noise. Their study is a landmark in the emerging field of quantum optomechanics (*4*), where the objective is to coherently control the quantum motion of a collective vibrational degree of freedom of a mechanical element. In their experiment, the mechanical element is a 7-ng square dielectric membrane placed inside a Fabry-Perot optical interferometer. The bulk mechanical resonance frequency is above 1 MHz with a linewidth less than 1 Hz (see the figure).

As the membrane moves, it modulates the frequency of the optical resonance and consequently modulates the amplitude and phase of the transmitted light. This motion can be detected with high efficiency by means of optical detection. Fluctuations of the membrane due to radiation pressure noise appear in the noise power spectrum of the optical signal. In the experiment, two optical modes were used; one with high power, the signal, is the source of the radiation pressure shot noise, while the other, weaker probe beam monitors the displacement of the membrane to detect the radiation pressure noise. The experiment can also be thought of as a quantum nondemolition measurement of the photon number in the strong signal beam using a coupling to the signal beam mediated by the mechanical element.

The experiment of Purdy *et al.* represents one of the few approaches that demonstrate the physical mechanism responsible for enforcing the Heisenberg uncertainty limit. Can we beat this limit by creating light sources with no intensity fluctuations at all? Such squeezed light sources are indeed under development, yet they will be of no use in trying to beat the Heisenberg limit in optomechanical systems. The reason is that if the intensity of a light source is well defined, its phase becomes increasingly randomized—a quantum optical Heisenberg principle—and an interferometer cannot be operated with a rapidly fluctuating phase. A natural extension of the Purdy *et al.* experiment would demonstrate precisely this trade-off.

References

1. T. P. Purdy, R. W. Peterson, C. A. Regal, *Science* **339**, 801 (2013).
2. P. Meystre, *Atom Optics* (Springer Verlag, New York, 2001).
3. C. M. Caves, K. S. Thorne, R. W. P. Drever, V. D. Sandberg, M. Zimmermann, *Rev. Mod. Phys.* **52**, 341 (1980).
4. M. Aspelmeyer, P. Meystre, K. Schwab, *Phys. Today* **65**, 29 (2012).

10.1126/science.1234109

PLANETARY SCIENCE

A Unique Piece of Mars

A meteorite with a chemical makeup resembling that of rocks from Mars' Gusev Crater has been identified.

Munir Humayun

Following the pioneering Mars Exploration Rovers, NASA's Curiosity rover is actively exploring the crustal rocks of Mars. Despite the exciting results returned by the rovers, there is no substitute for a hand sample of crustal rock. Because such samples will not be returned to Earth anytime soon, geochemists who want a piece of Mars in their labs must satisfy themselves with martian meteorites (*1*). These comprise a group of igneous rocks with telltale signs of martian alteration products (*2*) and have provided ground truth for the information returned by the rovers. Oddly, however, the hundred or so known martian meteorites are chemically unrepresentative of the martian crust determined by missions (*3*). On page 780 of this issue, Agee *et al.* (*4*) put an end to this conundrum with the finding of a new martian meteorite, Northwest Africa (NWA) 7034, a basaltic breccia unique among known martian meteorites with respect to age, oxygen isotopes, and petrology.

Department of Earth, Ocean and Atmospheric Science and National High Magnetic Field Laboratory, Florida State University, Tallahassee, FL 32310, USA. E-mail: humayun@magnet.fsu.edu

One might wonder whether such a rock should even be construed to be of martian origin. Oxygen isotopes are the meteoritic equivalent of DNA fingerprinting, each unique signature implying a different planetary reservoir (*5*). One of the big surprises in NWA 7034 is that its oxygen isotopes are shifted to greater ^{16}O depletion, and to heavier isotopic compositions, than those of the SNC (shergottite, nakhlite, and chassignite) martian meteorites. Had it not been for the alertness of Agee *et al.*, NWA 7034 would likely have been classified as a unique achondrite (an asteroidal sample) on the basis of its distinct oxygen isotope composition. However, they showed that the mineral chemistry of pyroxenes from NWA 7034 plot on the distinct FeO versus MnO trend defined by other martian meteorites. Another distinguishing characteristic of martian meteorites over achondrites is their young radiometric ages [<4 billion years ago (Ga)]; NWA 7034 has been dated about 2 Ga, older than SNC meteorites but younger than ALH 84001 (*6*). What makes NWA 7034 so exciting is that its major element composition is a close fit with the chemical data returned by the Mars rovers, as well as with the global chemical composition of Mars' crust returned by the orbiting gamma-ray spectrometer onboard Mars Odyssey (*4*). NWA 7034 appears to be a chemical analog of rocks from Gusev Crater (*3*).

Given that the other known martian meteorites are a poor match for crust exposed at the martian surface, what can we learn from a meteorite that resembles just about any rock from Mars? The first important discovery is that the new meteorite has a distinctly greater deficiency of the ^{16}O isotope among its oxygen isotopes than the other martian meteorites, which are bunched so close together on an oxygen isotope plot that they can be classified as a group on the basis of a single measurement of their $\Delta^{17}O$ (*5*). That this should be the case was anticipated by pioneering studies that found the martian hydrosphere and atmosphere to have

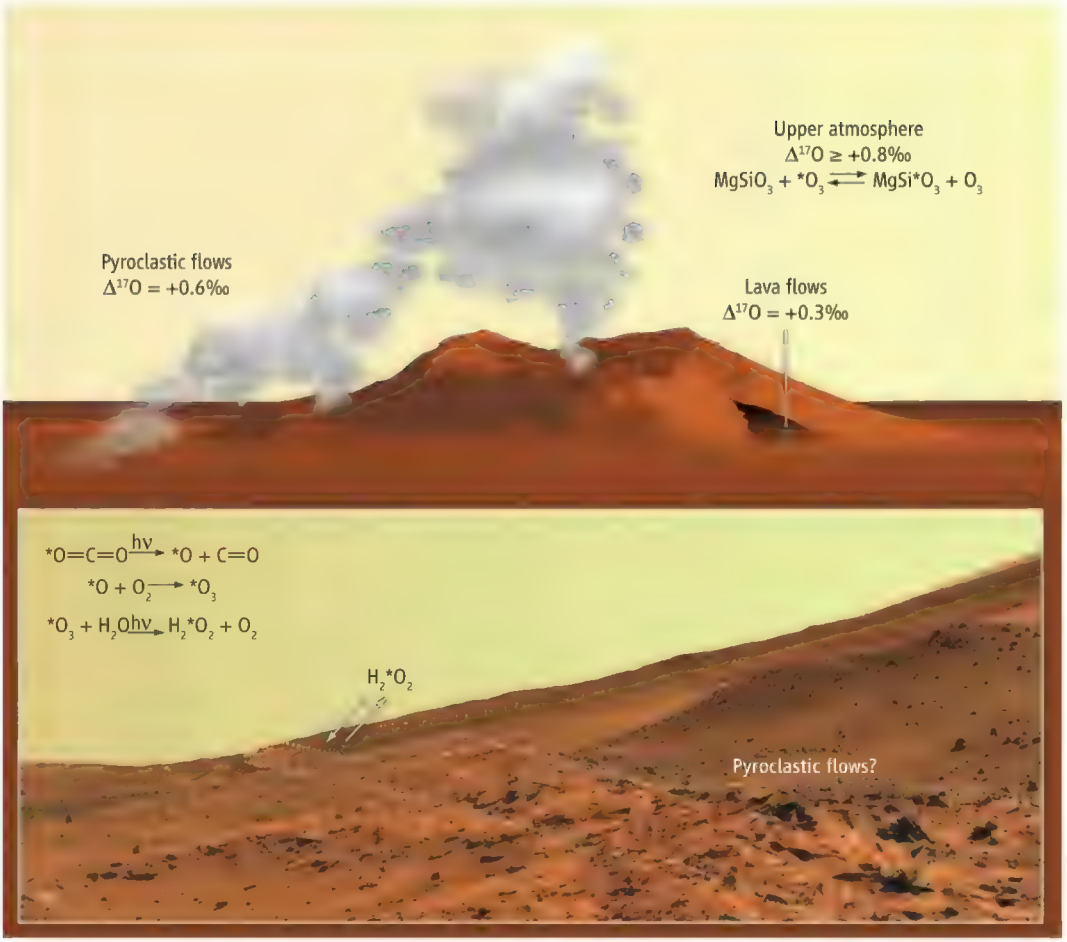

Spirit of exploration. A cartoon of a volcanic pyroclastic flow schematically depicting how NWA 7034 may have formed on Mars (*4*) and how photochemical reactions may imprint isotopic signatures in the newly formed rock. **(Inset)** An image of Gusev Crater viewed by Spirit (PIA02688, 19 February 2006) showing possible pyroclastic deposits.

mass-independent isotope fractionations driven by the penetration of ultraviolet light through the thin atmosphere of Mars (*7*, *8*). Further, on Earth such processes would be wiped out by plate tectonics, but the absence of subduction on Mars resulted in the preservation of mass-independent isotope anomalies (*7*, *8*). Ever since the Viking mission in 1976, it has been known that Mars' atmosphere is escaping the planet's gravitational grasp with attendant mass fractionation, but that carbon and oxygen isotopes did not exhibit the extreme mass-dependent fractionation observed in nitrogen. Therefore, a reservoir on Mars must be buffering the C and O isotopes (*9*). Agee *et al.* now show that the lithosphere may be part of the buffering (at least for oxygen) because the bulk oxygen isotope composition of NWA 7034 has been shifted toward the atmospheric end relative to other martian meteorites (see the figure). Incidentally, this is one of the questions Curiosity is designed to tackle on Mars, but Agee *et al.* may have beaten the rover to the punch line.

Another interesting aspect of NWA 7034 is its clastic nature, whereby numerous fragments of rock and mineral are bound together. It is unknown whether these clasts all originate from a single (pyroclastic) volcanic eruption, or whether multiple clasts are introduced by impact or some other external agent. Experience with lunar rocks revealed a wealth of information in 2- to 4-mm rock fragments; is this an opportunity to repeat that exercise on Mars?

Agee *et al.* measured 0.6 weight percent water in NWA 7034 with a distinct oxygen isotope composition from the bulk rock, effectively a sample of the martian hydrosphere or permafrost trapped within the matrix of NWA 7034. What are the host minerals? As a rock that appears to have originated at the martian surface, NWA 7034 may contain the elusive hydrous minerals that host water on Mars and their mineralogy might now be determined in the laboratory, with important inputs into directing Curiosity or designing the next generation of Mars probes.

And, finally, there is macromolecular organic carbon (MMC) recognized in inclusions within feldspar crystals (*4*). It is tempting to wonder whether the volcanic activity associated with the igneous clasts in NWA 7034 provided a warm haven for martian life. If so, this is the place to start a search. Because NWA 7034 is a desert find and not a fresh fall (even though it appears rather fresh by Saharan meteorite standards), an important question is whether the organic matter in NWA 7034 is actually from Mars. This can be settled by measurement of the D/H (deuterium/hydrogen) ratio for the MMC because the martian hydrogen is characterized by a high D/H ratio relative to terrestrial organics (*10*). If an extraterrestrial origin is indeed confirmed, it may yet prove to be meteoritic organics associated with micrometeorite infall on the martian surface. Anyway, the hunt for life on Mars in another meteorite will then be on.

If one were to wish for a single martian meteorite, it would be NWA 7034, the first known archetypal crustal rock from Mars. When other such rocks are found, they may help to clarify many remaining questions about the martian surface. For example, has hydrothermal activity occurred on Mars? Have ore mineralizations occurred? Is there evidence of soil (aeolian dust) in the breccia? Is trapped ancient atmosphere (nitrogen, noble gases) present in the amorphous material? Stay tuned for more exciting discoveries.

References

1. H. Y. McSween Jr., *Meteorit. Planet. Sci.* **37**, 7 (2002).
2. A. H. Treiman, J. D. Gleason, D. D. Bogard, *Planet. Space Sci.* **48**, 1213 (2000).
3. H. Y. McSween Jr., G. J. Taylor, M. B. Wyatt, *Science* **324**, 736 (2009).
4. C. B. Agee *et al.*, *Science* **339**, 780 (2013); 10.1126/science.1228858.
5. R. N. Clayton, T. K. Mayeda, *Geochim. Cosmochim. Acta* **60**, 1999 (1996).
6. T. J. Lapen *et al.*, *Science* **328**, 347 (2010).
7. H. R. Karlsson, R. N. Clayton, E. K. Gibson Jr., T. K. Mayeda, *Science* **255**, 1409 (1992).
8. J. Farquhar, M. H. Thiemens, T. Jackson, *Science* **280**, 1580 (1998).
9. A. O. Nier, M. B. McElroy, *Science* **194**, 1298 (1976).
10. L. A. Leshin, E. Vicenzi, *Elements* **2**, 157 (2006).

10.1126/science.1232490

Structural Biological Materials: Critical Mechanics-Materials Connections

Marc André Meyers,[1,2]* Joanna McKittrick,[1] Po-Yu Chen[3]

Spider silk is extraordinarily strong, mollusk shells and bone are tough, and porcupine quills and feathers resist buckling. How are these notable properties achieved? The building blocks of the materials listed above are primarily minerals and biopolymers, mostly in combination; the first weak in tension and the second weak in compression. The intricate and ingenious hierarchical structures are responsible for the outstanding performance of each material. Toughness is conferred by the presence of controlled interfacial features (friction, hydrogen bonds, chain straightening and stretching); buckling resistance can be achieved by filling a slender column with a lightweight foam. Here, we present and interpret selected examples of these and other biological materials. Structural bio-inspired materials design makes use of the biological structures by inserting synthetic materials and processes that augment the structures' capability while retaining their essential features. In this Review, we explain this idea through some unusual concepts.

Materials science is a vibrant field of intellectual endeavor and research. This field applies physics and chemistry, melding them in the process, to the interrelationship between structure, properties, and performance of complex materials with technological applications. Thus, materials science extends these rigorous scientific disciplines into complex materials that have structures providing properties and synergies beyond those of pure and simple solids. Initially geared at synthetic materials, materials science has recently extended its reach into biology, especially into the extracellular matrix, whose mechanical properties are of utmost importance in living organisms. Some of the seminal work and important contributions in this field are either presented or reviewed in (*1*–*5*). There are a number of interrelated features that define biological materials and distinguish them from their synthetic counterparts [inspired by Arzt (*6*)]: (i) Self-assembly. In contrast to many synthetic processes to produce materials, the structures are assembled from the bottom up, rather than from the top down. (ii) Multi-functionality. Many components serve more than one purpose. For example, feathers provide flight capability, camouflage, and insulation, whereas bones provide structural framework, promote the growth of red blood cells, and provide protection to the internal organs. (iii) Hierarchy. Different, organized scale levels (nano- to ultrascale) confer distinct and translatable properties from one level to the next. We are starting to develop a systematic and quantitative understanding of this hierarchy by distinguishing the characteristic levels, developing constitutive descriptions of each level, and linking them through appropriate and physically based equations, enabling a full predictive understanding. (iv) Hydration. The properties are highly dependent on the level of water in the structure. There are some exceptions, such as enamel, but this rule applies to most biological materials and is of importance to mechanical properties such as strength (which is decreased by hydration) and toughness (which is increased). (v) Mild synthesis conditions. The majority of biological materials are fabricated at ambient temperature and pressure as well as in an aqueous environment, a notable difference from synthetic materials fabrication. (vi) Evolution and environmental constraints. The limited availability of useful elements dictates the morphology and resultant properties. The structures are not necessarily optimized for all properties but are the result of an evolutionary process leading to satisfactory and robust solutions. (vii) Self-healing capability. Whereas synthetic materials undergo damage and failure in an irreversible manner, biological materials often have the capability, due to the vascularity and cells embedded in the structure, to reverse the effects of damage by healing.

The seven characteristics listed above are present in a vast number of structures. Nevertheless, the structures of biological materials can be divided into two broad classes: (i) non-mineralized ("soft") structures, which are composed of fibrous constituents (collagen, keratin, elastin, chitin, lignin, and other biopolymers) that display widely varying mechanical properties and anisotropies depending on the function, and (ii) mineralized ("hard") structures, consisting of hierarchically assembled composites of minerals (mainly, but not solely, hydroxyapatite, calcium carbonate, and amorphous silica) and organic fibrous components (primarily collagen and chitin).

The mechanical behavior of biological constituents and composites is quite diverse. Biominerals exhibit linear elastic stress-strain plots, whereas the biopolymer constituents are nonlinear, demonstrating either a *J* shape or a curve with an inflection point. Foams are characterized by a compressive response containing a plastic or crushing plateau in which the porosity is eliminated. Many biological materials are composites with many components that are hierarchically structured and can have a broad variety of constitutive responses. Below, we present some of the structures and functionalities of biological materials with examples from current research. Here, we focus on three points: (i) How high tensile strength is achieved (biopolymers), (ii) how high toughness is attained (composite structures), and (iii) how bending resistance is achieved in lightweight structures (shells with an interior foam).

Structures in Tension: Importance of Biopolymers

The ability to sustain tensile forces requires a specific set of molecular and configurational conformations. The initial work performed on extension should be small, to reduce energy expenditure, whereas the material should stiffen close to the breaking point, to resist failure. Thus, biopolymers, such as collagen and viscid (catching spiral) spider silk, have a *J*-shaped stress-strain curve where molecular uncoiling and unkinking occur with considerable deformation under low stress.

This stiffening as the chains unfurl, straighten, stretch, and slide past each other can be represented analytically in one, two, and three dimensions. Examples are constitutive equations initially developed for polymers by Ogden (*7*) and Arruda and Boyce (*8*). An equation specifically proposed for tissues is given by Fung (*3*). A simpler formulation is given here; the slope of the stress-strain (σ-ε) curve increases monotonically with strain. Thus, one considers two regimes: (i) unfurling and straightening of polymer chains

$$\frac{d\sigma}{d\varepsilon} \propto \varepsilon^n (n > 1) \quad (1)$$

and (ii) stretching of the polymer chain backbones

$$\frac{d\sigma}{d\varepsilon} \propto E \quad (2)$$

where E is the elastic modulus of the chains. The combined equation, after integrating Eqs. 1 and 2, is

$$\sigma = k_1 \varepsilon^{n+1} + H(\varepsilon_c) E(\varepsilon - \varepsilon_c) \quad (3)$$

Here k_1 is a parameter, and H is the Heaviside function, which activates the second term at $\varepsilon = \varepsilon_c$, where ε_c is a characteristic strain at which collagen fibers are fully extended. Subsequent strain gradually becomes dominated by chain stretching. The computational results by Gautieri *et al.* (*9*) on collagen fibrils corroborate Eq. 3 for $n = 1$. This corresponds to a quadratic relation between

[1]Department of Mechanical and Aerospace Engineering and Materials Science and Engineering Program, University of California, San Diego, La Jolla, CA 92093, USA. [2]Department of Nanoengineering, University of California, San Diego, La Jolla, CA 92093, USA. [3]Department of Materials Science and Engineering, National Tsing Hua University, Hsinchu 30013, Taiwan, Republic of China.

*To whom correspondence should be addressed. E-mail: mameyers@ucsd.edu

Fig. 1. Tensile stress-strain relationships in biopolymers. (**A**) *J*-shaped curve for hydrated and dry collagen fibrils obtained from molecular dynamics (MD) simulations and AFM and SAXS studies. At low stress levels, considerable stretching occurs due to the uncrimping and unfolding of molecules; at higher stress levels, the polymer backbone stretches. Adapted from (*9*, *12*). (**B**) Stretching of dragline spider silk and molecular schematic of the protein fibroin. At low stress levels, entropic effects dominate (straightening of amorphous strands); at higher levels, the crystalline parts sustain the load. (**C**) Molecular dynamics simulation of silk: (i) short stack and (ii) long stack of β-sheet crystals, showing that a higher pullout force is required in the short stack; for the long stack, bending stresses become important. Hydrogen bonds connect β-sheet crystals. Adapted from (*14*). (**D**) Egg whelk case (bioelastomer) showing three regions: straightening of the α helices, the α helix–to–β sheet transformation, and β-sheet extension. A molecular schematic is shown. Adapted from (*18*).

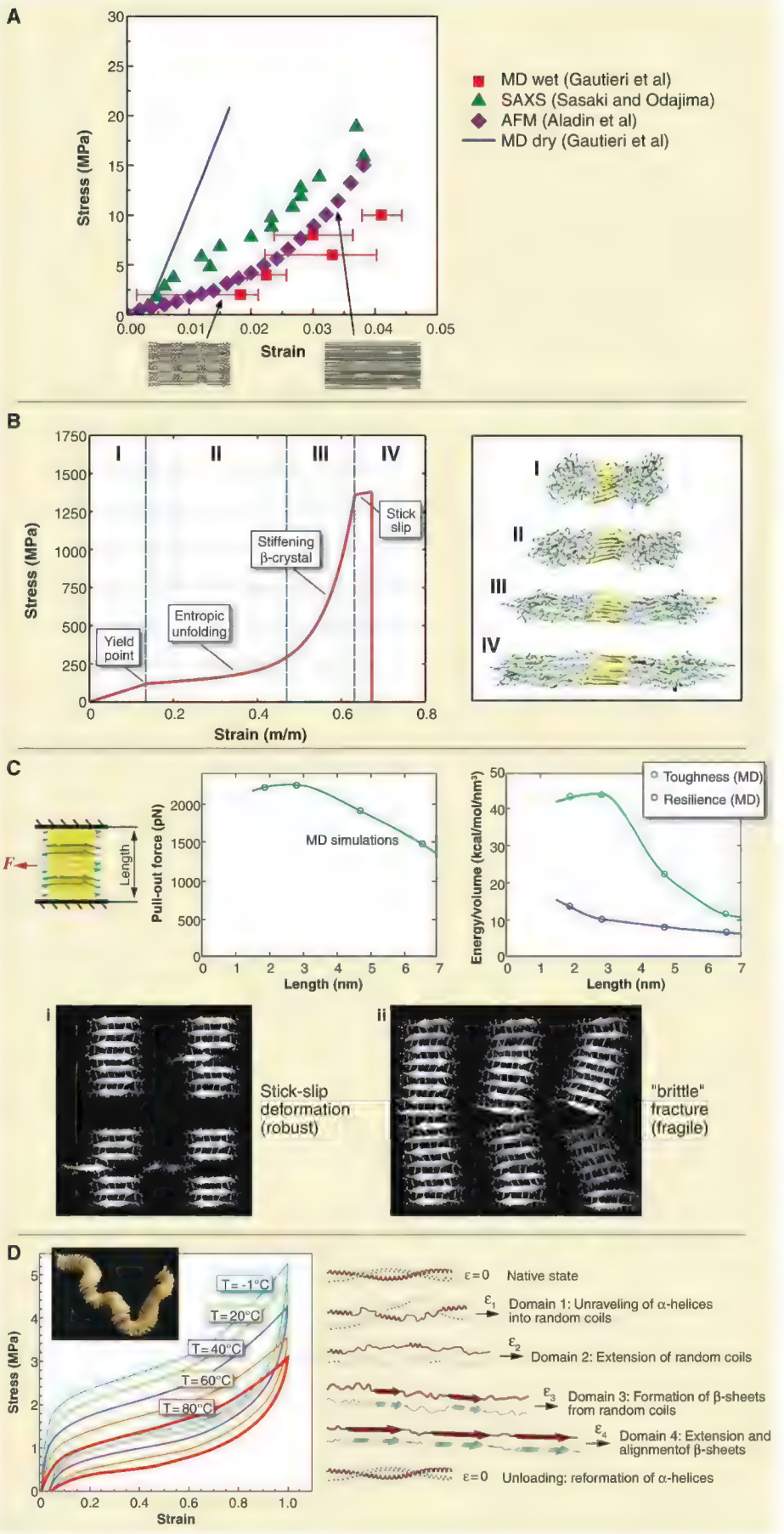

stress and strain ($\sigma \propto \varepsilon^2$), which has the characteristic *J* shape.

Collagen is the most important structural biological polymer, as it is the key component in many tissues (tendon, ligaments, skin, and bone), as well as in the extracellular matrix. The deformation process is intimately connected to the different hierarchical levels, starting with the polypeptides (0.5-nm diameter) to the tropocollagen molecules (1.5-nm diameter), then to the fibrils (~40- to 100-nm diameter), and finally to fibers (~1- to 10-μm diameter) and fascicles (>10-μm diameter). Molecular dynamics computations (*9*) of entire fibrils show the *J*-curve response; these computational predictions are well matched to atomic force microscopy (AFM) (*10*), small-angle x-ray scattering (SAXS) (*11*), and experiments by Fratzl *et al.* (*12*), as shown in Fig. 1A. The effect of hydration is also seen and is of great importance. The calculated density of collagen decreases from 1.34 to 1.19 g/cm^3 with hydration and is accompanied by a decrease in the Young's modulus from 3.26 to 0.6 GPa.

The response of silk and spider thread is fascinating. As one of the toughest known materials, silk also has high tensile strength and extensibility. It is composed of β sheet (10 to 15 volume %) nanocrystals [which consist of highly conserved poly-(Gly-Ala) and poly-Ala domains] embedded in a disordered matrix (*13*). Figure 1B shows the *J*-shape stress-strain curve and molecular configurations for the crystalline domains in silkworm (*Bombyx mori*) silk (*14*). Similar to collagen, the low-stress region corresponds to uncoiling and straightening of the protein strands. This region is followed by entropic unfolding of the amorphous strands and then stiffening due to load transfer to the crystalline β sheets. Despite the high strength, the major molecular interactions in the β sheets are weak hydrogen bonds. Molecular dynamics simulations,

shown in Fig. 1C, illustrate an energy dissipative stick-slip shearing of the hydrogen bonds during failure of the β sheets (*14*). For a stack with a height $L \leq 3$ nm (left-hand side of Fig. 1C), the shear stresses are more substantial than the flexure stresses, and the hydrogen bonds contribute to the high strength obtained (1.5 GPa). However, if the stack of β sheets is too high (right-hand side of Fig. 1C), it undergoes bending with tensile separation between adjacent sheets. The nanoscale dimension of the β sheets allows for a ductile instead of brittle failure, resulting in high toughness values of silk. Thus, size affects the mechanical response considerably, changing the deformation characteristics of the weak hydrogen bonds. This has also been demonstrated in bone (*15*–*17*), where sacrificial hydrogen bonds between mineralized collagen fibrils contribute to the excellent fracture resistance.

Other biological soft materials have more complex responses, marked by discontinuities in $d\sigma/d\varepsilon$. This is the case for wool, whelk eggs, silks, and spider webs. Several mechanisms are responsible for this change in slope; for instance, the transition from α- to β-keratin, entropic changes with strain (such as those prevalent in rubber, where chain stretching and alignment decrease entropy), and others. The example of egg whelk is shown in Fig. 1D (*18*). In this case, there is a specific stress at which α-keratin helices transform to β sheets, with an associated change in length. Upon unloading, the reverse occurs, and the total reversible strain is, therefore, extensive. This stress-induced phase transformation is similar to what occurs in shape-memory alloys. Thus, this material can experience substantial reversible deformation (up to 80%) in a reversible fashion, when the stress is raised from 2 to 5 MPa, ensuring the survival of whelk eggs, which are continually swept by waves.

These examples demonstrate the distinct properties of biopolymers that allow these materials to be strong and highly extensible with distinctive molecular deformation characteristics. However, many interesting biological materials are composites of flexible biopolymers and stiff minerals. The combination of these two constituents leads to the creation of a tough material.

Imparting Toughness: Importance of Interfaces

One hallmark property of most biological composites is that they are tough. Toughness is defined as the amount of energy a material absorbs before it fails, expressed as

$$U = \int_0^{\varepsilon_f} \sigma d\varepsilon \qquad (4)$$

where U is the energy per volume absorbed, σ is the stress, ε is the strain, and ε_f is the failure strain. Tough materials show considerable plastic deformation (or permanent damage) coupled with considerable strength. This maximizes the integral expression in Eq. 4. Biological composite materials (for example, crystalline and noncrystalline components) have a plethora of toughening mechanisms, many of which depend on the presence of interfaces. As a crack impinges on an interface or discontinuity in the material, the crack can be deflected around the interface (requiring more energy to propagate than a straight crack) or can drive through it. The strength of biopolymer fibers in tension impedes crack opening; bridges between microcracks are another mechanism. The toughening mechanisms have been divided into intrinsic (existing in the material ahead of crack) and extrinsic (generated during the progression of failure) categories (*19*). Thus, toughening is accomplished by a wide variety of stratagems. We illustrate this concept for four biological materials, shown in Fig. 2.

All inorganic materials contain flaws and cracks, which reduce the strength from the theoretical value (~E/10 to E/30). The maximum stress (σ_{max}) a material can sustain when a preexisting crack of length a is present is given by the Griffith equation

$$\sigma_{max} = \sqrt{\frac{2\gamma_s E}{\pi a}} = \frac{YK_{Ic}}{\sqrt{\pi a}} \qquad (5)$$

where E is the Young's modulus, γ_s is the surface (or damage) energy, and Y is a geometric parameter. $K_{Ic} = Y^{-1}\sqrt{2\gamma_s E}$ is the fracture toughness, a materials property that expresses the ability to resist crack propagation. Abalone (*Haliotis rufescens*) nacre has a fracture toughness that is vastly superior to that of its major constituent, monolithic calcium carbonate, due to an ordered assembly consisting of mineral tiles with an approximate thickness of 0.5 μm and a diameter of ~10 μm (Fig. 2A). Additionally, this material contains organic mesolayers (separated by ~300 μm) that are thought to be seasonal growth bands. The tiles are connected by mineral bridges with ~50-nm diameter and are separated by organic layers, consisting of a chitin network and acidic proteins, which, when combined, have a similar thickness to the mineral bridge diameters. The Griffith fracture criterion (Eq. 5) can be applied to predict the flaw size (a_{cr}) at which the theoretical strength σ_{th} is achieved. With typical values for the fracture toughness (K_{Ic}), σ_{th}, and E, the critical flaw size is in the range of tens of nanometers. This led Gao *et al.* (*20*) to propose that at sufficiently small dimensions (less than the critical flaw size), materials become insensitive to flaws, and the theoretical strength (~E/30) should be achieved at the nanoscale. However, the strength of the material will be determined by fracture mechanisms operating at all hierarchical levels.

The central micrograph in Fig. 2A shows how failure occurs by tile pullout. The interdigitated structure deflects cracks around the tiles instead of through them, thereby increasing the total length of the crack and the energy needed to fracture (increasing the toughness). Thus, we must determine how effectively the tiles resist pullout. Three contributions have been identified and are believed to operate synergistically (*21*). First, the mineral bridges are thought to approach the theoretical strength (10 GPa), thereby strongly attaching the tiles together (*22*). Second, the tile surfaces have asperities that are produced during growth (*23*) and could produce frictional resistance and strain hardening (*24*). Third, energy is required for viscoelastic deformation (stretching and shearing) of the organic layer (*25*).

One important aspect on the mechanical properties is the effect of alignment of the mineral crystals. The oriented tiles in nacre result in anisotropic properties with the strength and modulus higher in the longitudinal (parallel to the organic layers) than in the transverse direction. For a composite with a dispersed mineral m of volume fraction V_m embedded in a biopolymer (bp) matrix that has a much lower strength and Young's modulus than the mineral, the ratio of the longitudinal (L) and transverse (T) properties P (such as elastic modulus) can be expressed, in simplified form, as

$$\frac{P_L}{P_T} = \frac{P_m}{P_{bp}} V_m(1 - V_m) \qquad (6)$$

Thus, the longitudinal properties are much higher than the transverse properties. This anisotropic response is also observed in other oriented mineralized materials, such as bone and teeth.

Another tough biological material is the exoskeleton of an arthropod. In the case of marine animals [for instance, lobsters (*26*, *27*) and crabs (*28*)], the exoskeleton structure consists of layers of mineralized chitin in a Bouligand arrangement (successive layers at the same angle to each other, resulting in a helicoidal stacking sequence and in-plane isotropy). These layers can be envisaged as being stitched together with ductile tubules that also perform other functions, such as fluid transport and moisture regulation. The cross-ply Bouligand arrangement is effective in crack stopping; the crack cannot follow a straight path, thereby increasing the materials' toughness. Upon being stressed, the mineral components fracture, but the chitin fibers can absorb the strain. Thus, the fractured region does not undergo physical separation with dispersal of fragments, and self-healing can take place (*29*). Figure 2B shows the structure of the lobster (*Homarus americanus*) exoskeleton with the Bouligand arrangement of the fibers.

Bone is another example of a biological material that demonstrates high toughness. Skeletal mammalian bone is a composite of hydroxyapatite-type minerals, collagen and water. On a volumetric basis, bone consists of ~33 to 43 volume % minerals, 32 to 44 volume % organics, and 15 to 25 volume % water. The Young's modulus and strength increase, but the toughness decreases with increasing mineral volume fraction (*30*). Cortical (dense) mammalian bone has blood vessels extending along the long axis of the limbs. In animals larger than rats, the vessel is encased in a circumferentially laminated structure called the osteon. Primary osteons are surrounded by hypermineralized regions, whereas secondary

(remodeled) osteons are surrounded by a cement line (also of high mineral content) (*31*). In mammalian cortical bone, the following intrinsic toughening mechanisms have been identified: molecular uncoiling and intermolecular sliding of collagen, fibrillar sliding of collagen bonds, and microcracking of the mineral matrix (*19*). Extrinsic mechanisms are collagen fibril bridging, uncracked ligament bridging, and crack deflection and twisting (*19*). Rarely does a limb bone snap in two with smooth fracture surfaces; the crack is often deflected orthogonal to the crack front direction. In the case of (rehydrated) elk (*Cervus elaphus*) antler bone (shown in Fig. 2C) (*32*), which has the highest toughness of any bone type by far (*33*), the hypermineralized regions around the primary osteons lead to crack deflection, and the high amount of collagen (~60 volume %) adds mechanisms of crack retardation and creates crack bridges behind the crack front. The toughening effect in antlers has been estimated as: crack deflection, 60%; uncracked ligament bridges, 35%; and collagen as well as fibril bridging, 5% (*33*). A particularly important feature in bone is that the fracture toughness increases as the crack propagates, as shown in the plot. This plot demonstrates the crack extension resistance curve, or *R*-curve, behavior, which is the rate of the total energy dissipated as a function of the crack size. This occurs by the activation of the extrinsic toughening mechanisms. In this manner, it becomes gradually more difficult to advance the crack. In human bone, the cracks are deflected and/or twisted around the cement lines surrounding the secondary osteons and also demonstrate *R*-curve behavior (*34*).

The final example illustrating how the presence of interfaces is used to retard crack propagation is the glass sea sponge (*Euplectella aspergillum*). The entire structure of the Venus' flower basket is shown in Fig. 2D. Biological silica is amorphous and, within the spicules, consists of concentric layers, separated by an organic material, silicatein (*35*, *36*). The flexure strength of the spicule notably exceeds (by approximately fivefold) that of monolithic glass (*37*). The principal reason is the presence of interfaces, which can arrest and/or deflect the crack.

Biological materials use ingenious methods to retard the progression of cracks, thereby

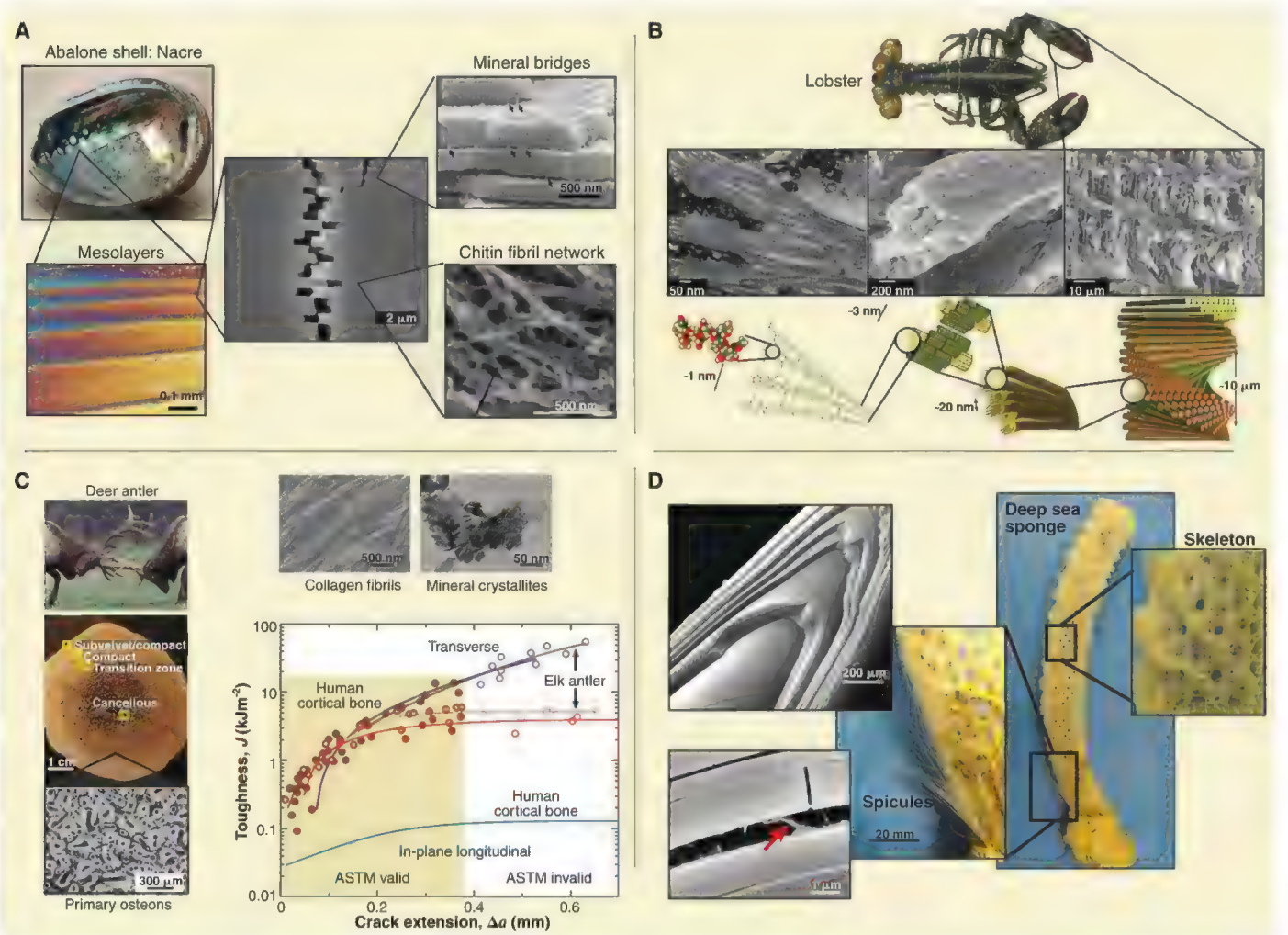

Fig. 2. Hierarchical structures of tough biological materials demonstrating the heterogeneous interfaces that provide crack deflection. (**A**) Abalone nacre showing growth layers (mesolayers), mineral bridges between mineral tiles and asperities on the surface, the fibrous chitin network that forms the backbone of the inorganic layer, and an example of crack tortuosity in which the crack must travel around the tiles instead of through them [adapted from (*4*, *21*)]. (**B**) Lobster exoskeleton showing the twisted plywood structure of the chitin (next to the shell) and the tubules that extend from the chitin layers to the animal [adapted from (*27*)]. (**C**) Antler bone image showing the hard outer sheath (cortical bone) surrounding the porous bone. The collagen fibrils are highly aligned in the growth direction, with nanocrystalline minerals dispersed in and around them. The osteonal structure in a cross section of cortical bone illustrates the boundaries where cracks perpendicular to the osteons can be directed [adapted from (*33*)]. ASTM, American Society for Testing and Materials. (**D**) Silica sponge and the intricate scaffold of spicules. Each spicule is a circumferentially layered rod: The interfaces between the layers assist in arresting crack propagation. Organic silicate in bridging adjacent silica layers is observed at higher magnification (red arrow) (*36*).

increasing toughness. These methods operate at levels ranging from the nanoscale to the structural scale and involve interfaces to deflect cracks, bridging by ductile phases (e.g., collagen or chitin), microcracks forming ahead of the crack, delocalization of damage, and others.

Lightweight Structures Resistant to Bending, Torsion, and Buckling—Shells and Foams

Resistance to flexural and torsional tractions with a prescribed deflection is a major attribute of many biological structures. The fundamental mechanics of elastic (recoverable) deflection, as it relates to the geometrical characteristics of beams and plates, is given by two equations: The first relates the bending moment, M, to the curvature of the beam, d^2y/dx^2 (y is the deflection)

$$\frac{d^2y}{dx^2} = \frac{M}{EI} \quad (7)$$

where I is the area moment of inertia, which depends on the geometry of the cross section ($I = \pi R^4/4$, for circular sections, where R is the radius). Importantly, the curvature of a solid beam, and therefore its deflection, is inversely proportional to the fourth power of the radius. The second equation, commonly referred to as Euler's buckling equation, calculates the compressive load at which global buckling of a column takes place (P_{cr})

$$P_{cr} = \frac{\pi^2 EI}{(kL)^2} \quad (8)$$

where k is a constant dependent on the column-end conditions (pinned, fixed, or free), and L is the length of the column. Resistance to buckling can also be accomplished by increasing I. Both Eqs. 7 and 8 predict the principal design

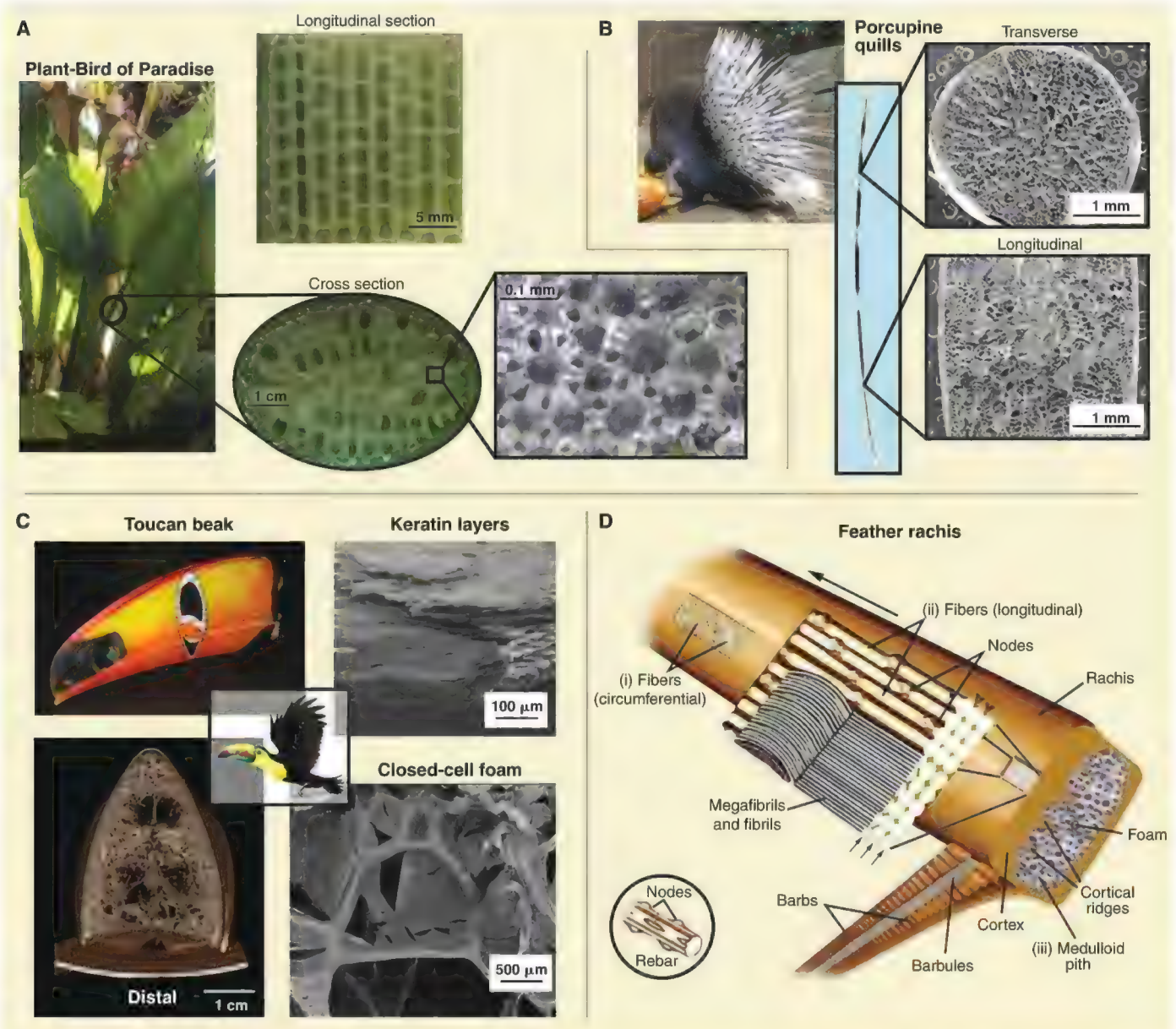

Fig. 3. Low-density and stiff biological materials. The theme is a dense outer layer and a low-density core, which provides a high bending strength–to–weight ratio. **(A)** Giant bird of paradise plant stem showing the cellular core with porous walls. **(B)** Porcupine quill exhibiting the dense outer cortex surrounding a uniform, closed-cell foam. Taken from (*42*). **(C)** Toucan beak showing the porous interior (bone) with a central void region [adapted from (*43*)]. **(D)** Schematic view of the three major structural components of the feather rachis: (i) superficial layers of fibers, wound circumferentially around the rachis; (ii) the majority of the fibers extending parallel to the rachidial axis and through the depth of the cortex; and (iii) foam comprising gas-filled polyhedral structures. Taken from (*45*).

guideline for a lightweight and/or stiff structure: For equal mass, I can be increased by placing the mass farthest from the neutral axis (that passes through the centroid of the cross section). This is readily accomplished by having a hollow tube with radius R and thickness t. For equal mass, $I_{tube}/I_{cylinder} = 1 + x^2$, where $x = 1 - t/R$. Thus, to increase bending resistance, t should be minimized and R maximized. However, the local buckling (crimping) tendency increases with an increase t and a decrease in R (*38*)

$$\sigma_{cr} = \frac{E}{\sqrt{3(1-\nu^2)}}\left(\frac{t}{R}\right) \quad (9)$$

where ν is Poisson's ratio. A compromise must be reached between bending and buckling resistance. The same reasoning can also be extended to torsion.

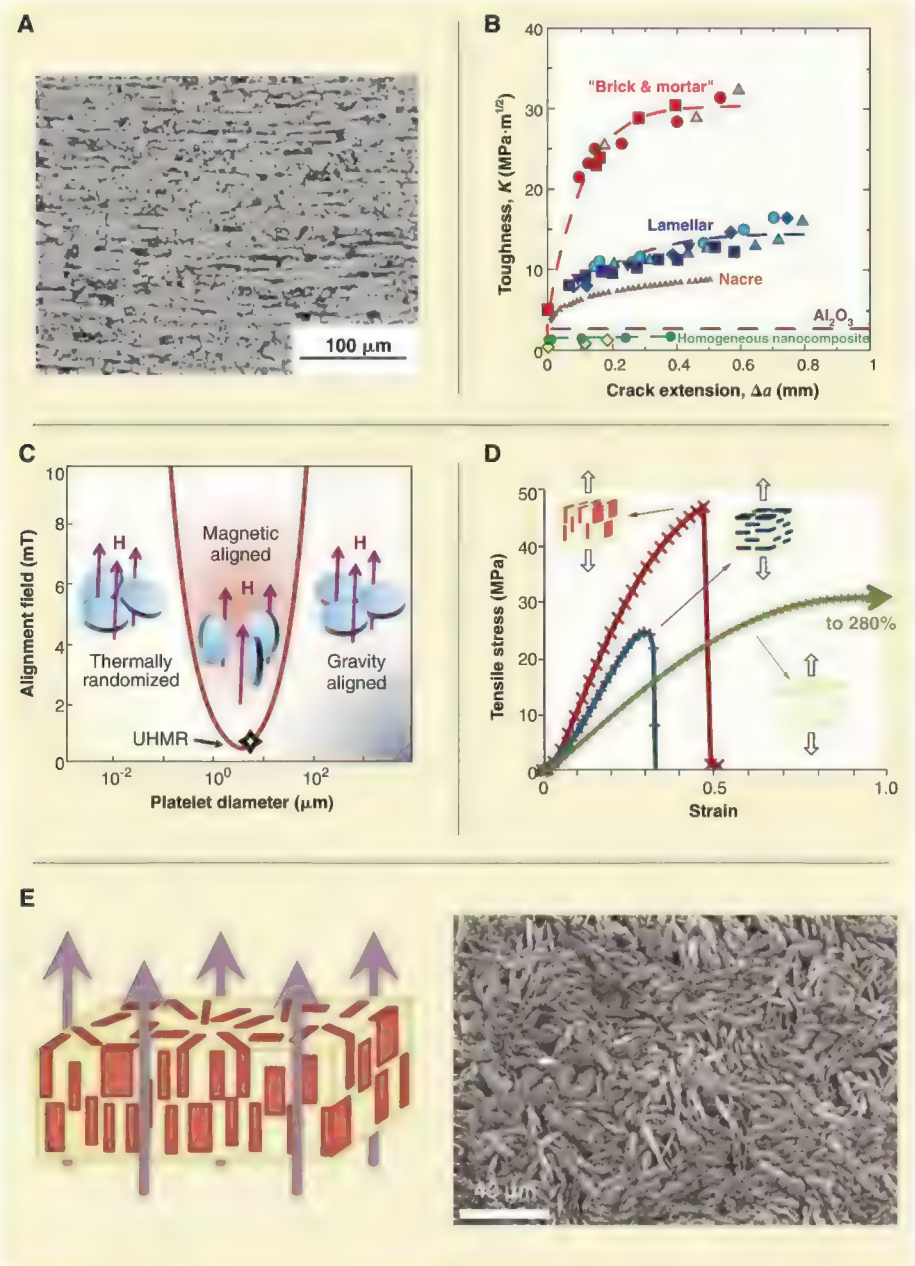

Fig. 4. Examples of bio-inspired designs. (**A**) Synthetic nacre consisting of alumina layers infiltrated with an engineering polymer and (**B**) crack propagation resistance [taken from (*56*)]. (**C**) Schematic diagram of platelet alignment in which magnetic fields are used to create a three-dimensional composite. UMHR, ultrahigh magnetic response; H, direction of magnetic field. (**D**) Stress-strain curves of a 20–volume % Al_2O_3 platelet-reinforced polyurethane with alignment parallel and perpendicular to the loading direction. The green curve shows the behavior of polyurethane. (**E**) Schematic representation (left) and SEM micrograph (right) of the composite. Taken from (*57*).

Nature has addressed this problem with ingenious solutions: creating a thin solid shell and filling the core with lightweight foam (*39*) or adding internal reinforcing struts or disks (*40*). These stratagems provide resistance to local buckling (crimping) with a minimum weight penalty. Primary examples of these design principles are antlers and some skeletal bones that have a cellular core (cancellous bone) and a solid exterior (cortical bone). Bamboo has a hollow tube with periodic disks at prescribed separations. The wing bones of soaring birds use this strategy with internal struts. Gibson and Ashby (*40*) and Gibson *et al.* (*41*) have covered this topic in detail.

To illustrate the ubiquity of this biological design principle, we present in Fig. 3 four additional examples: plants, porcupine quills, bird beaks, and feathers. Plant stalks are composed of cellulose and lignin arranged in cells aligned with the axis of growth. The giant bird of paradise (*Strelitzia*) (Fig. 3A) plant stem exhibits this structure. The longitudinal section shows rectangular cells, whereas the cell walls in the cross section are radially aligned. Thus, the cells have a cylindrical shape. The struts are not fully solid but instead have a pattern of holes, further decreasing the weight. The structure is designed to resist flexure stresses without buckling. Figure 3B shows the porcupine (*Hystrix cristata*) quill, a keratinous structure that has a high flexural strength-to-weight ratio (*42*). The external shell (cortex) surrounds a cellular core that provides stability to the walls under compression. This structure has a larger resistance to buckling than one in which the entire weight is concentrated on the external cortex (*39*).

Bird beaks are yet another example of this design principle. Beaks generally fall into two classes: short and thick or long and thin. The toucan (*Ramphastos toco*) is a notable exception; its beak is one third of its length and needs to be fairly thick for the foraging and fencing activities in the tree canopies. The beak is only $^1/_{30}$ of the bird's overall weight and has an extremely low density of 0.1 g/cm^3. The structure of the beak is fairly elaborate, with an external keratinous shell and an internal bony cellular structure (Fig. 3C) (*43*). The cells are composed of bony struts connected by membranes. An additional distinct feature of the toucan beak is a hollow core inside the foam, resulting in a further decrease in weight. The fundamental mechanics equation connecting the bending stresses in the radial distance, y, measured from the centroid is

$$\sigma_y = \frac{My}{I} \quad (10)$$

Because the stresses increase linearly with y, the central core does not experience substantial stresses and does not contribute to the flexure resistance; thus, nature removes the core.

Another example is the bird feather, which illustrates the extreme design considerations of the stiffness-to-weight ratio (*44*). Bird feathers are composed of a central shaft (rachis), out of which lateral branches (barbs) diverge. These

branches are connected by thin, folded membranes (barbules). We illustrate the structure of the rachis of a domestic chicken (*Gallus gallus*) in Fig. 3D (*45*). The entire feather is made of keratin; the external cortex is solid and is itself a composite, with longitudinal and circumferential layers of fibers. The core is filled with a closed-cell foam (level I). Close observation of the cell walls reveals that they are also made of a foam in a second level of porosity that further decreases density (level II). By applying an equation for a foam and assuming geometrical self-similarity, we have (*40*)

$$\frac{\rho_f}{\rho_s} = C\left(\frac{t}{l}\right)^4 \quad (11)$$

where ρ_f is the density of the foam, ρ_s is the density of the solid, C is a constant, t is the thickness of the cell struts, and l is the length of the struts (either level I or II). This fourth-order dependency demonstrates that the decrease in density accomplished by hierarchical foam of levels I and II is dramatic, as illustrated by the cortex foams of the feather rachis and bird of paradise flower.

The design principles delineated above—internal foams of various types and maximized moments of inertia—are used by biological systems in applications where the stiffness-to-weight ratio is of critical importance. Many engineering applications also use these concepts, but biological systems have distinct aspects (such as the hierarchical foam of the feather rachis) that are only at the conceptual stage at present but that may lead to substantial weight reduction.

Bio-Inspired Materials and Design

Due to the noteworthy physical and mechanical properties exhibited by biological materials, materials science has attracted considerable attention to the new research area of bio-inspiration. Some examples of bio-inspired materials design include Velcro (inspired by plant burrs), surfaces that are self-cleaning (super-hydrophobic surface of a lotus leaf) (*46*), antireflective surfaces of solar panels (insect compound eye) (*47*), fiber-reinforced composites (wood), and surfaces inspired by the structure of shark skin (*48*). Shark skin has small ridges separated by ~50 μm that are aligned in the direction of water flow. Instead of turbulent instabilities arising on the surface, a more laminar flow is achieved, which results in drag reduction (*48*). This concept has been applied to reduce drag in pipelines (*49*) and aircraft (*50*). Additionally, because of the surface roughness, bacterial colonies cannot develop; thus, a commercial product, Sharklet, is used in hospitals (*51*). Recent discoveries in the biomineralization area (*52*) and the gecko foot–inspired sticky tapes (*53*) are prime examples of new bio-inspired fabrication methods. Highly adhesive tapes have been demonstrated with carbon nanotubes and polymer nanopillars that reproduce the gecko foot setae structure (*54*, *55*). Thus, the field of bio-inspiration is generating innovations. However, it is challenging to fabricate bio-inspired materials that have structural function and robustness.

We have described two current efforts at creating structural bio-inspired materials. Mineralized biological materials have aligned mineral crystals that orient to maximize performance for required loading conditions; this concept is observed in bone, teeth, and mollusk shells. The abalone "brick-and-mortar" structure is an example of a tough material and is the subject of considerable research efforts. The most promising results have been obtained by freeze casting, a well-established ceramic processing method, followed by sintering and impregnation with a polymer or metal, as shown in Fig. 4A (*56*). The results are especially important, because the toughness obtained in a 80–volume % alumina, 20–volume % polymethyl methacrylate composite is very high: more than 30 MPa·$m^{1/2}$ (Fig. 4B). In comparison, pure alumina has a toughness of 2 to 3 MPa·$m^{1/2}$. With another method, Erb *et al.* (*57*) demonstrated alignment of alumina particles coated with superparamagnetic nanoparticles in a polyurethane matrix under a magnetic field (during solvent extraction from the polymer). Figure 4, C and D, shows a schematic representation of magnetic alignment of platelets and stress-strain curves of platelets oriented parallel and perpendicular to the loading direction, respectively. Figure 4E shows a scanning electron microscopy (SEM) micrograph and schematic rendition of the aligned particles—platelets orientated along the loading direction increase the yield strength and Young's modulus (Fig. 4, D and E). This concept was recently established by Porter *et al.* (*58*), who showed that the spiraling nature of the narwhal tusk could be reproduced by magnetic alignment of particles under a rotating magnetic field.

In conclusion, the application of the mechanics and materials science methodologies is promoting a new understanding of biological materials and guiding the design of biologically inspired materials and structures. This field is rapidly expanding, and we foresee a continued effort in bio-inspired materials and design, which will extend to sustainable development by employing more energy efficient and "greener" designs.

References and Notes

1. J. F. V. Vincent, *Structural Biomaterials* (Princeton University Press, Princeton, NJ, 1991).
2. A. H. Heuer *et al.*, *Science* **255**, 1098 (1992).
3. Y. C. Fung, *Biomechanics: Mechanical Properties of Living Tissues* (Springer, New York, ed. 2, 1993).
4. M. A. Meyers, P.-Y. Chen, A. Y. M. Lin, Y. Seki, *Prog. Mater. Sci.* **53**, 1 (2008).
5. P.-Y. Chen, J. McKittrick, M. A. Meyers, *Prog. Mater. Sci.* **57**, 1492 (2012).
6. E. Arzt, *Mater. Sci. Eng. C* **26**, 1245 (2006).
7. R. W. Ogden, *Proc. R. Soc. London Ser. A Math. Phys. Sci.* **326**, 565 (1972).
8. E. M. Arruda, M. C. Boyce, *J. Mech. Phys. Solids* **41**, 389 (1993).
9. A. Gautieri, S. Vesentini, A. Redaelli, M. J. Buehler, *Nano Lett.* **11**, 757 (2011).
10. D. M. Aladin *et al.*, *J. Orthop. Res.* **28**, 497 (2010).
11. N. Sasaki, S. Odajima, *J. Biomech.* **29**, 1131 (1996).
12. P. Fratzl *et al.*, *J. Struct. Biol.* **122**, 119 (1998).
13. A. H. Simmons, C. A. Michal, L. W. Jelinski, *Science* **271**, 84 (1996).
14. S. Keten, Z. Xu, B. Ihle, M. J. Buehler, *Nat. Mater.* **9**, 359 (2010).
15. G. E. Fantner *et al.*, *Nat. Mater.* **4**, 612 (2005).
16. J. B. Thompson *et al.*, *Nature* **414**, 773 (2001).
17. J. D. Currey, *Nature* **414**, 699 (2001).
18. A. Miserez, S. S. Wasko, C. F. Carpenter, J. H. Waite, *Nat. Mater.* **8**, 910 (2009).
19. M. E. Launey, M. J. Buehler, R. O. Ritchie, *Annu. Rev. Mater. Res.* **40**, 25 (2010).
20. H. Gao, B. Ji, I. L. Jäger, E. Arzt, P. Fratzl, *Proc. Natl. Acad. Sci. U.S.A.* **100**, 5597 (2003).
21. A. Y. M. Lin, M. A. Meyers, *J. Mech. Behav. Biomed. Mater.* **2**, 607 (2009).
22. F. Song, Y. L. Bai, *Acta Mech. Sin.* **17**, 251 (2001).
23. T. E. Schäffer *et al.*, *Chem. Mater.* **9**, 1731 (1997).
24. A. G. Evans *et al.*, *J. Mater. Res.* **16**, 2475 (2001).
25. A. P. Jackson, J. F. V. Vincent, R. M. Turner, *Proc. R. Soc. London Ser. B Biol. Sci.* **234**, 415 (1988).
26. D. Raabe, C. Sachs, P. Romano, *Acta Mater.* **53**, 4281 (2005).
27. S. Nikolov *et al.*, *Adv. Mater.* **22**, 519 (2010).
28. P.-Y. Chen, A. Y. M. Lin, J. McKittrick, M. A. Meyers, *Acta Biomater.* **4**, 587 (2008).
29. C. A. Melnick, Z. Chen, J. J. Mecholsky Jr., *J. Mater. Res.* **11**, 2903 (1996).
30. J. D. Currey, *Philos. Trans. R. Soc. London Ser. B Biol. Sci.* **304**, 509 (1984).
31. J. D. Currey, *Bone: Structure and Mechanics* (Princeton University Press, Princeton, NJ, 2002).
32. P.-Y. Chen, A. G. Stokes, J. McKittrick, *Acta Biomater.* **5**, 693 (2009).
33. M. E. Launey, P.-Y. Chen, J. McKittrick, R. O. Ritchie, *Acta Biomater.* **6**, 1505 (2010).
34. R. K. Nalla, J. J. Kruzic, J. H. Kinney, R. O. Ritchie, *Biomaterials* **26**, 217 (2005).
35. J. N. Cha *et al.*, *Proc. Natl. Acad. Sci. U.S.A.* **96**, 361 (1999).
36. J. Aizenberg *et al.*, *Science* **309**, 275 (2005).
37. L. Qiao, Q.-L. Feng, X.-H. Wang, Y.-M. Yang, *J. Inorg. Mater.* **23**, 337 (2008).
38. S. Timoshenko, *Theory of Elastic Stability* (McGraw-Hill, New York, 1936).
39. G. N. Karam, L. J. Gibson, *Int. J. Solids Struct.* **32**, 1259 (1995).
40. L. J. Gibson, M. F. Ashby, *Cellular Solids: Structure and Properties* (Cambridge Univ. Press, Cambridge, ed. 2, 1997).
41. L. J. Gibson, M. F. Ashby, B. Harley, *Cellular Materials in Nature and Medicine* (Cambridge Univ. Press, Cambridge, 2010).
42. W. Yang, C. Chao, J. McKittrick, *Acta Biomater.* **9**, 5297 (2013).
43. Y. Seki, M. S. Schneider, M. A. Meyers, *Acta Mater.* **53**, 5281 (2005).
44. P. P. Purslow, J. F. V. Vincent, *J. Exp. Biol.* **72**, 251 (1978).
45. T. Lingham-Soliar, R. H. C. Bonser, J. Wesley-Smith, *Proc. R. Soc. London Ser. B Biol. Sci.* **277**, 1161 (2010).
46. T. Sun, L. Feng, X. Gao, L. Jiang, *Acc. Chem. Res.* **38**, 644 (2005).
47. F. Chiadini, V. Fiumara, A. Scaglione, A. Lakhtakia, *Bioinspir. Biomim.* **5**, 026002 (2010).
48. J. Oeffner, G. V. Lauder, *J. Exp. Biol.* **215**, 785 (2012).
49. S.-J. Lee, H.-C. Lim, M. Han, S. S. Lee, *Fluid Dyn. Res.* **37**, 246 (2005).
50. P. R. Viswanath, *Prog. Aerosp. Sci.* **38**, 571 (2002).
51. www.sharklet.com
52. J. Aizenberg, *MRS Bull.* **35**, 323 (2010).
53. E. P. Chan, C. Greiner, E. Arzt, A. J. Crosby, *MRS Bull.* **32**, 496 (2007).
54. S. Sethi, L. Ge, L. Ci, P. M. Ajayan, A. Dhinojwala, *Nano Lett.* **8**, 822 (2008).
55. K. Jin *et al.*, *Langmuir* **28**, 5737 (2012).
56. E. Munch *et al.*, *Science* **322**, 1516 (2008).
57. R. M. Erb, R. Libanori, N. Rothfuchs, A. R. Studart, *Science* **335**, 199 (2012).
58. M. M. Porter *et al.*, *Mater. Sci. Eng. A* **556**, 741 (2012).

Acknowledgments: We thank W. Yang and C.-H. Lu for help with the figures. This work is funded by the NSF, Ceramics Program grant 1006931 (M.A.M. and J.M.), and the National Science Council, Taiwan, grants NSC-100-2218-E-007-016-MY3 and NSC-101-2628-E-007-017-MY3 (P.-Y.C.).

10.1126/science.1220854

Unique Meteorite from Early Amazonian Mars: Water-Rich Basaltic Breccia Northwest Africa 7034

Carl B. Agee,[1,2]* Nicole V. Wilson,[1,2] Francis M. McCubbin,[1,2] Karen Ziegler,[1] Victor J. Polyak,[2] Zachary D. Sharp,[2] Yemane Asmerom,[2] Morgan H. Nunn,[3] Robina Shaheen,[3] Mark H. Thiemens,[3] Andrew Steele,[4] Marilyn L. Fogel,[4] Roxane Bowden,[4] Mihaela Glamoclija,[4] Zhisheng Zhang,[3,5] Stephen M. Elardo[1,2]

We report data on the martian meteorite Northwest Africa (NWA) 7034, which shares some petrologic and geochemical characteristics with known martian meteorites of the SNC (i.e., shergottite, nakhlite, and chassignite) group, but also has some unique characteristics that would exclude it from that group. NWA 7034 is a geochemically enriched crustal rock compositionally similar to basalts and average martian crust measured by recent Rover and Orbiter missions. It formed 2.089 ± 0.081 billion years ago, during the early Amazonian epoch in Mars' geologic history. NWA 7034 has an order of magnitude more indigenous water than most SNC meteorites, with up to 6000 parts per million extraterrestrial H_2O released during stepped heating. It also has bulk oxygen isotope values of $\Delta^{17}O = 0.58 \pm 0.05$ per mil and a heat-released water oxygen isotope average value of $\Delta^{17}O = 0.330 \pm 0.011$ per mil, suggesting the existence of multiple oxygen reservoirs on Mars.

The only tangible samples of the planet Mars available today for study in Earth-based laboratories are the so-called SNC (shergottite, nakhlite, and chassignite) meteorites (*1*) and a single cumulate orthopyroxenite (Allan Hills 84001). The SNCs currently number 110 named stones and have provided a treasure trove for elucidating the geologic history of Mars (*2*). But, because of their unknown field context and geographic origin on Mars and their fairly narrow range of igneous rock types and formation ages (*3*), it is uncertain to what extent SNC meteorites sample the crustal diversity of Mars. In fact, geochemical data from NASA's orbiter and lander missions suggest that the SNC meteorites are a mismatch for much of the martian crust exposed at the surface (*4*). For example, the basalts analyzed by the Mars Exploration Rover Spirit at Gusev Crater (*5*, *6*) are distinctly different from SNC meteorites, and Odyssey Orbiter gamma-ray spectrometer (GRS) data (*7*) show that the average martian crust composition does not closely resemble SNC.

NWA 7034, on deposit at the Institute of Meteoritics in Albuquerque, was purchased by Jay Piatek from Aziz Habibi, a Moroccan meteorite dealer, in 2011. It is a 319.8-g single stone, porphyritic basaltic monomict breccia, with a few euhedral phenocrysts up to several millimeters and many phenocryst fragments of dominant andesine, low-Ca pyroxene, pigeonite, and augite set in a very fine-grained, clastic to plumose, groundmass with abundant magnetite and maghemite; accessory sanidine, anorthoclase, Cl-rich apatite, ilmenite, rutile, chromite, pyrite, a ferric oxide hydroxide phase, and a calcium carbonate were identified by electron microprobe analyses on eight different sections at the University of New Mexico (UNM). X-ray diffraction (XRD) analyses conducted at UNM on a powdered sample and on a polished surface show that plagioclase feldspar is the most abundant phase (38.0 ± 1.2%), followed by low-Ca pyroxene (25.4 ± 8.1%), clinopyroxenes (18.2 ± 4.0%), iron oxides (9.7 ± 1.3%), alkali feldspars (4.9 ± 1.3%), and apatite (3.7 ± 2.6%). The x-ray data also indicate a minor amount of iron sulfide and chromite. The data are also consistent with magnetite and maghemite making up ~70% and ~30%, respectively, of the iron oxide detected (*8*).

Petrology and geochemistry. Numerous clasts and textural varieties are present in NWA 7034, including gabbros, quenched melts, and iron oxide– and ilmenite-rich reaction spherules (figs. S1 to S4) (*8*). However, the dominant textural type is a fine-grained basaltic porphyry with feldspar and pyroxene phenocrysts. NWA 7034 is a monomict brecciated porphyritic basalt that is texturally unlike any SNC meteorite. Basaltic breccias are common in Apollo samples, lunar meteorites, and HED meteorites but are wholly absent in the world's collection of SNC meteorites (*9*). The absence of shock-produced SNC breccias seems curious at face value, because nearly all of them show evidence of being subjected to high shock pressures, with feldspar commonly converted to maskelynite. Martian volcanic breccias are probably not rare, given the observed widespread occurrence of volcanism on Mars. However, launch and delivery of such materials to Earth as meteorites has not been observed (*9*). Although NWA 7034 is texturally heterogeneous, both in the hand specimen and microscopically (Fig. 1), it can be considered a monomict breccia because it shows a continuous range of feldspar and pyroxene compositions that are consistent with a common petrologic origin (figs. S5 and S6). We find no outlier minerals or compositions that would indicate the existence of multiple lithologies or exotic components. We also see no evidence for polymict lithologies in either the radiogenic or stable isotope ratios of NWA 7034 solids. However, many clasts and some of the fine-grained groundmass have phases that appear to have been affected by secondary processes to form reaction zones. We observed numerous reaction textures, some with a ferric oxide hydroxide phase; this phase and apatite are the main hosts of the water in NWA 7034 (fig. S2). Impact processes are likely to have affected NWA 7034 by virtue of the fact that this meteorite was launched off of Mars, exceeding the escape velocity—presumably by an impact—although the shock pressures did not produce maskelynite. One large (1-cm) quench melt clast that was found could originate from shock processes (fig. S3). On the other hand, the very fine groundmass with the large phenocrystic feldspars and pyroxenes strongly suggests an eruptive volcanic origin for NWA 7034; thus, it is likely that volcanic processes are a source of the brecciation.

It has been shown (*10*) that Fe-Mn systematics of pyroxenes and olivines are an excellent diagnostic for classifying planetary basalts. The Fe-Mn systematics of NWA 7034 pyroxenes, as determined by electron microprobe analyses, most resemble the trend of the SNC meteorites from Mars (Fig. 2); other planetary pyroxenes such as in lunar samples and basalts from Earth are poor matches for NWA 7034. Furthermore, feldspar compositions (fig. S5) (*8*) and compositions of other accessory phases in NWA 7034 are consistent with mineralogies commonly found in SNC meteorites (*11*) but not with any other known achondrite group. However, the average bulk chemical composition of NWA 7034 does not overlap in major element space with SNC; instead, it is remarkably similar to the geochemistry of the rocks and soils at Gusev Crater and the average martian crust composition from the Odyssey Orbiter GRS (Fig. 3 and figs. S7 and S8). NWA 7034, Gusev rocks, and the GRS average martian crust all have higher concentrations of the alkali elements sodium and potassium than do SNC meteorites. Other major and minor element ratios such as Mg/Si, Al/Si, and Ni/Mg have similarly good matches between NWA 7034 and Gusev Crater rocks (figs. S7 and S8). Although some

[1]Institute of Meteoritics, University of New Mexico, Albuquerque, NM 87131, USA. [2]Department of Earth and Planetary Sciences, University of New Mexico, Albuquerque, NM 87131, USA. [3]Department of Chemistry and Biochemistry, University of California, San Diego, La Jolla, CA 92093, USA. [4]Geophysical Lab, Carnegie Institution of Washington, Washington, DC 20005, USA. [5]School of Environmental Science and Engineering, Sun Yat-Sen University, Guangzhou 510275, China.

*To whom correspondence should be addressed. E-mail: agee@unm.edu

experimental work has been conducted to link martian meteorites to surface rocks analyzed by the Mars Exploration Rovers (*12*–*14*), and aside from the exotic "Bounce Rock" (*15*) at Meridiani Planum and a hypothesized martian soil component in Tissint melt pockets (*16*), there has been no direct link between the bulk chemical compositions of martian meteorites and surface rocks to date.

The rare-earth element (REE) abundances of NWA 7034 were determined by multicollector inductively coupled plasma mass spectrometry (Neptune MC-ICP-MS) at UNM. They are enriched relative to chondritic abundances, with a marked negative europium anomaly ($Eu/Eu^* = 0.67$) (fig. S9 and table S2). The REE pattern has a negative slope, and light rare-earth elements (LREE) are elevated relative to the heavy rare-earth elements (HREE) [CI-chondrite normalized lanthanum-ytterbium ratio $(La/Yb)_N = 2.3$]. Bulk SNC meteorites are much less enriched in REE (*17*) than is NWA 7034 (fig. S10); although LREE enrichment relative to HREE and REE patterns with negative slopes are seen in nakhlites, only magmatic inclusions and mesostasis in nakhlites and estimated nakhlite parent magmas have LREE enrichments comparable to those of NWA 7034 (*17*, *18*). We observed ubiquitous, relatively large (up to ~100 μm) Cl-rich apatite grains in NWA 7034 that presumably harbor a substantial fraction of the REEs in this meteorite, as neither merrillite nor whitlockite were identified in any of the investigated thin sections or probe mounts.

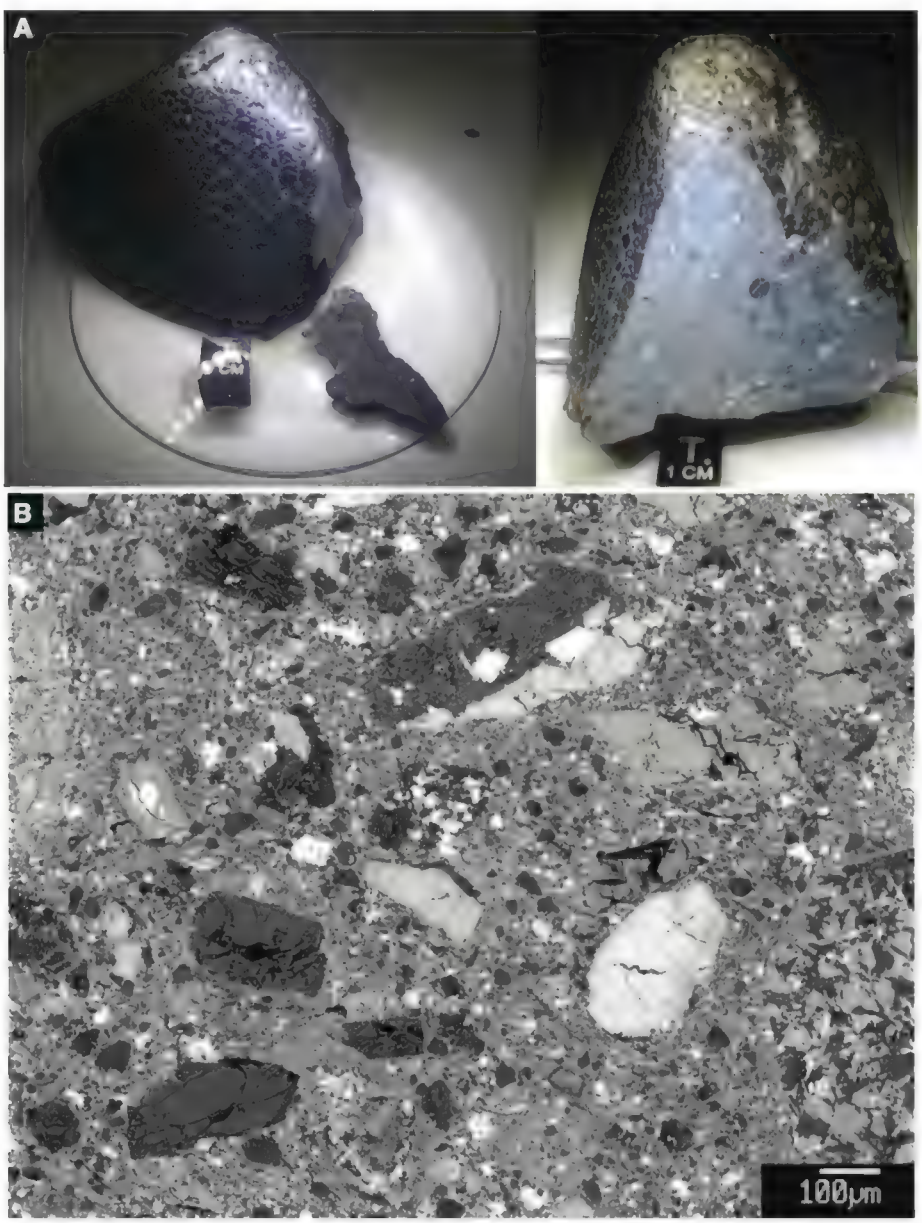

Fig. 1. (**A**) Two views of the NWA 7034 hand specimen. (**B**) Backscatter electron image of porphyritic texture in NWA 7034. Large dark crystals are feldspar; large light-colored crystals are pyroxene. A portion of a gabbroic clast is shown above the scale bar.

Radiometric age. A five-point isochron gives an Rb-Sr age for NWA 7034 of 2.089 ± 0.081 billion years ago (Ga) [2σ; mean square weighted deviation (MSWD) = 6.6], an initial $^{87}Sr/^{86}Sr$ ratio of 0.71359 ± 54 (Fig. 4), and a calculated source $^{87}Rb/^{86}Sr$ ratio of 0.405 ± 0.028 (Fig. 5). The Sm-Nd data for the same samples result in an isochron of 2.19 ± 1.4 Ga (2σ). The high uncertainty in the latter is due to minimal separation between the data points generated from analysis of mineral separates. The small error on the Rb-Sr age may come from the abundance and variety of feldspar compositions in NWA 7034 (fig. S5). Furthermore, we are confident that the Rb-Sr isochron and variations in the $^{87}Sr/^{86}Sr$ values are the result of the time-integrated radiogenic growth from ^{87}Rb and not the results of mixing between end members with different $^{87}Sr/^{86}Sr$ values (figs. S11 to S14). The combined REE and isotopic data show that NWA 7034 is an enriched martian crustal rock (Fig. 5). The whole rock has $^{143}Nd/^{144}Nd = 0.511756$ and $^{147}Sm/^{144}Nd = 0.1664$, giving a calculated initial (source value) $^{143}Nd/^{144}Nd = 0.509467 \pm 0.000192$ (initial $\varepsilon_{Nd} = -9.1 \pm 1.7$, calculated using the Rb-Sr age). This requires that NWA 7034 was derived from an enriched martian reservoir (*19*), with an inferred time-integrated $^{147}Sm/^{144}Nd = 0.1680 \pm 0.0061$, assuming separation from a chondrite-like martian mantle at 4.513 Ga (*18*). Data for each of our analyses are available in table S3. An age of ~2.1 Ga for NWA 7034 would make it the only dated meteorite sample from the early Amazonian (*19*) epoch in Mars' geologic history.

NWA 7034 is derived from the most enriched martian source identified to date; it is even more enriched than the most enriched shergottites (*20*–*23*) (Fig. 5). On the basis of REE enrichment, isotopic values, and match to rover elemental data, NWA 7034 may better represent the composition of Mars' crust than other martian meteorites. Although NWA 7034 may not be representative of a magmatic liquid, the negative europium anomaly and the absence of merrillite or whitlockite (*24*) suggest either that the magma(s) parental to basaltic breccia NWA 7034 underwent plagioclase fractionation before eruption or that feldspar was left in the residuum during partial melting. Because of the instability of plagioclase at high pressure (*25*), these processes would have necessarily occurred in the crust or upper mantle of Mars. Consequently, the geochemically enriched source that produced NWA 7034 could have originated from the martian crust or mantle, much like the geochemically enriched reservoir(s) that are recorded in the shergottites (*26*–*30*).

Carbon. Confocal Raman imaging spectroscopy conducted at the Carnegie Institution Geophysical Laboratory in Washington, DC, identified the presence of macromolecular carbon (MMC) within mineral inclusions in the groundmass minerals of NWA 7034 (*8*). This MMC is spectrally

similar to reduced organic macromolecular carbon that has been identified in several shergottites and a single nakhlite meteorite (fig. S15) (*30*), indicating that the production of organic carbon from abiogenic processes in the martian interior may not be unique to SNC-like source regions in Mars. Steele *et al.* (*31*) also demonstrated that the formation mechanism of MMC requires reducing magmatic conditions consistent with oxygen fugacities below the fayalite-magnetite-quartz (FMQ) buffer. Consequently, much of the ferric iron in the oxides of NWA 7034, as evidenced by electron probe microanalysis and XRD, was likely a product of oxidation subsequent to igneous activity as a result of secondary processes.

Bulk carbon and carbon isotopic measurements on NWA 7034 were also carried out at Carnegie, using combustion in an elemental analyzer (Carlo Erba NC 2500) interfaced through a Conflo III to a Delta V Plus isotope ratio mass spectrometer (ThermoFisher) in the same manner as the data reported by (*31*, *32*) [see (*8*)]. These data indicate that carbon is present within mineral inclusions in NWA 7034 at concentrations of at least 22 ± 10 ppm, and that the $\delta^{13}C$ isotopic value of this carbon is –23.4 ± 0.73‰, which is very similar to previous bulk C and $\delta^{13}C$ analyses of carbon included in shergottite meteorites analyzed in the same manner (*31*, *32*). These data indicate that multiple geochemical reservoirs in the martian interior may have similarly light $\delta^{13}C$ values. The bulk C concentration in the untreated sample performed in these measurements was 2080 ± 80 ppm C, with a corresponding $\delta^{13}C$ value of –3.0 ± 0.16‰. Scattered carbonate veinlets from desert weathering were observed by backscatter electron imaging and element mapping with the electron microprobe, especially in the near-surface material but less frequently in the deeper interior slices of NWA 7034. Although this carbonate is below the detection limits of our XRD analyses of the bulk sample and is thus a minor phase within the meteorite, we believe that this weathering product is sampled in our bulk carbon and carbonate analyses (*8*) (fig. S16).

Oxygen isotopes. Measurements of oxygen isotopic composition were performed by laser fluorination at UNM on acid-washed and non–acid-washed bulk sample and at the University of California, San Diego (UCSD), on vacuum preheated (1000°C) bulk sample (table S4). The triple oxygen isotope precision on San Carlos olivine standard [$\delta^{18}O$ = 5.2‰ versus standard mean ocean water (SMOW); $\Delta^{17}O$ = 0‰] analyzed during sessions at UNM was $\Delta^{17}O$ = ±0.03‰; the precision at UCSD using NBS-28 quartz standard ($\delta^{18}O$ = 9.62‰) was also $\Delta^{17}O$ = ±0.03‰. In total, we carried out 21 analyses of bulk NWA 7034 (Fig. 6). The mean value obtained at UNM was $\Delta^{17}O$ = 0.58 ± 0.05‰ (n = 13) for acid-washed samples and $\Delta^{17}O$ = 0.60 ± 0.02‰ (n = 6) for non–acid-washed samples; at UCSD the mean value was $\Delta^{17}O$ = 0.50 ± 0.03‰ (n = 2) for vacuum preheated samples that were dewatered and decarbonated. The combined data give $\Delta^{17}O$ = 0.58 ± 0.05‰ (n = 21). These interlab values of bulk samples are in good agreement but are significantly higher than literature values for SNC meteorites ($\Delta^{17}O$ range 0.15 to 0.45‰) (*33*–*36*). Figure 6 shows that the $\delta^{18}O$ values (5.5 to 7.0‰ versus SMOW) of NWA 7034 are higher than any determination from the SNC group. The $\Delta^{17}O$ values of the non–acid-washed samples measured at UNM are similar to and within error of the acid-washed samples; this indicates that NWA 7034 has, at most, only minor terrestrial weathering products, which would drive the non–acid-washed values closer to $\Delta^{17}O$ = 0.00. The slope of the best-fit line to the combined UNM acid-washed and non–acid-washed data is 0.517 ± 0.025, which suggests that the oxygen isotopic composition of NWA 7034 is the result of mass-dependent fractionation processes.

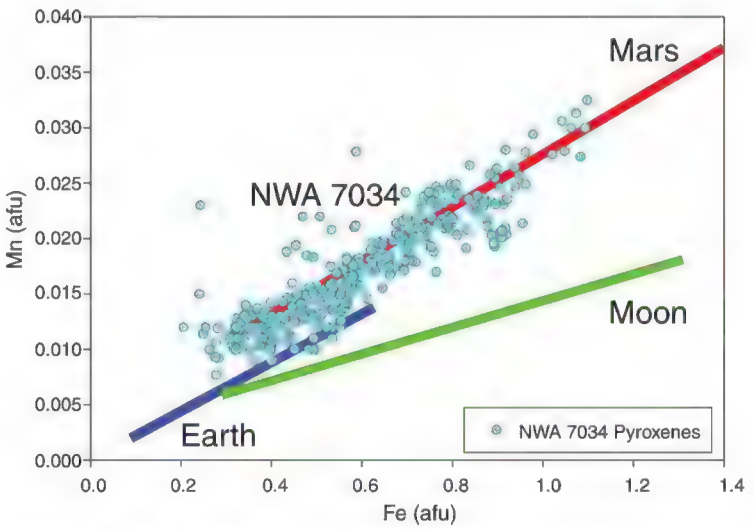

Fig. 2. Fe versus Mn (atomic formula units) showing the trend for all NWA 7034 pyroxenes (cyan dots, 349 microprobe analyses) and, for comparison, pyroxene trends from Mars (red), the Moon (green), and Earth (blue) (*10*).

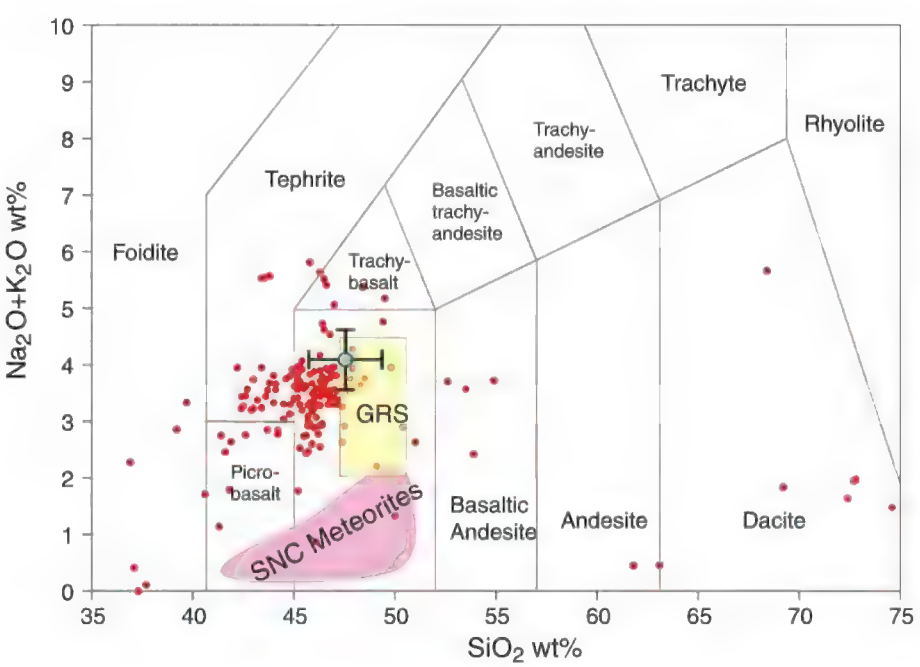

Fig. 3. Volcanic rock classification scheme based on the abundance of alkali elements and SiO_2, modified after McSween *et al.* (*4*). Red dots denote analyses of rocks and soils at Gusev Crater by the Alpha Particle X-ray Spectrometer (APXS) onboard the Spirit rover (*5*, *6*). The yellow rectangle is the average martian crust as measured by the GRS onboard the Mars Odyssey orbiter (*7*). The pink field is the known range of martian meteorite (SNC) compositions. The cyan dot is the mean value of bulk NWA 7034 as determined by 225 electron microprobe analyses of fine-grained groundmass; error bars denote SD.

There are no other known achondrites or planetary samples with bulk oxygen isotope values similar to those of NWA 7034. Most achondrite groups have negative or near-zero $\Delta^{17}O$ values, as do rocks from Earth and the Moon. The oxygen isotope compositions of Venus and Mercury are currently unknown, but NWA 7034 is too oxidized and iron-rich to be derived from Mercury (*37*–*39*), and it seems to be a poor match for Venus because it experienced low-temperature alteration on its parent body and has significant indigenous water, which would not persist with the high surface temperatures on Venus (*40*).

The distinct $\delta^{18}O$ and $\Delta^{17}O$ values relative to other martian meteorites can be explained by multiple reservoirs—either within the martian lithosphere or between the lithosphere and a surficial component (*41*, *42*)—or by incorporation of exotic material. The idea of separate long-lived silicate reservoirs is supported by radiogenic isotope studies (*21*, *23*). The distinct $\Delta^{17}O$ and $\delta^{18}O$ values of the silicate fraction of NWA 7034 relative to all SNC meteorites measured to date further support the idea of distinct lithospheric reservoirs that have remained unmixed throughout martian history. A near-surface component with high $\Delta^{17}O$ values has been proposed on the basis of analysis of low-temperature alteration products (*41*–*43*), and this may in part explain the $\Delta^{17}O$ differences between the bulk and "water-derived" components of NWA 7034. However, the $\Delta^{17}O$ value of 0.58‰ for the bulk silicate is different from the $\Delta^{17}O$ value of 0.3‰ found in all SNC samples measured to date. If materials with a $\Delta^{17}O$ value other than 0.3‰ are attributed to a surficial (atmospheric) component, then the bulk of NWA 7034 would have necessarily undergone extensive exchange with this reservoir. This is a possibility, given the abundance of low-temperature iron oxides. The ramifications of distinct lithospheric reservoirs are very different from those attributed to a different surficial reservoir. The latter could be explained by photochemical-induced isotope fractionation and/or hydrodynamic escape (*44*–*46*), whereas the former is consistent with a lack of initial planet-wide homogenization and an absence of plate tectonics (*41*). Isolated lithospheric oxygen isotope reservoirs are inconsistent with a global magma ocean scenario for early Mars, which would have very efficiently homogenized oxygen isotopes in the planet, as occurred for Earth and the Moon. Instead, Mars' differentiation could have been dominated by basin-forming impacts that left regional or even hemisphere-scale magmatic complexes (*47*, *48*) with distinct and varied isotopic and geochemical characteristics.

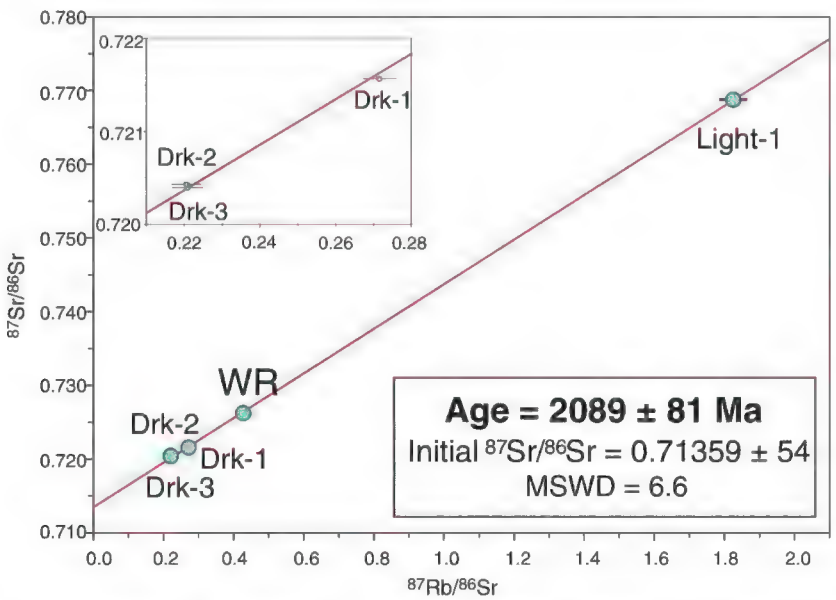

Fig. 4. Rb-Sr whole-rock mineral isochron of NWA 7034. The mineral fractions are labeled as Light-1, Drk-1, Drk-2, and Drk-3 according to abundance of dark magnetic minerals. Light-1, with high $^{87}Rb/^{86}Sr$, was the least magnetic fraction. An MSWD value of 6.6 suggests that the small scatter in the values cannot be explained by analytical errors and may include slight isotopic heterogeneities in the rock. 2σ measurement errors were used for the $^{87}Sr/^{86}Sr$ data; 2% errors for the $^{87}Rb/^{86}Sr$ data were used for age calculation. Larger errors were assigned to the $^{87}Rb/^{86}Sr$ ratios because of the inability to perform internal mass fractionation on Rb isotopic measurements (Rb only has two isotopes). There was not enough Sm and Nd in the mineral fractions to provide a meaningful age.

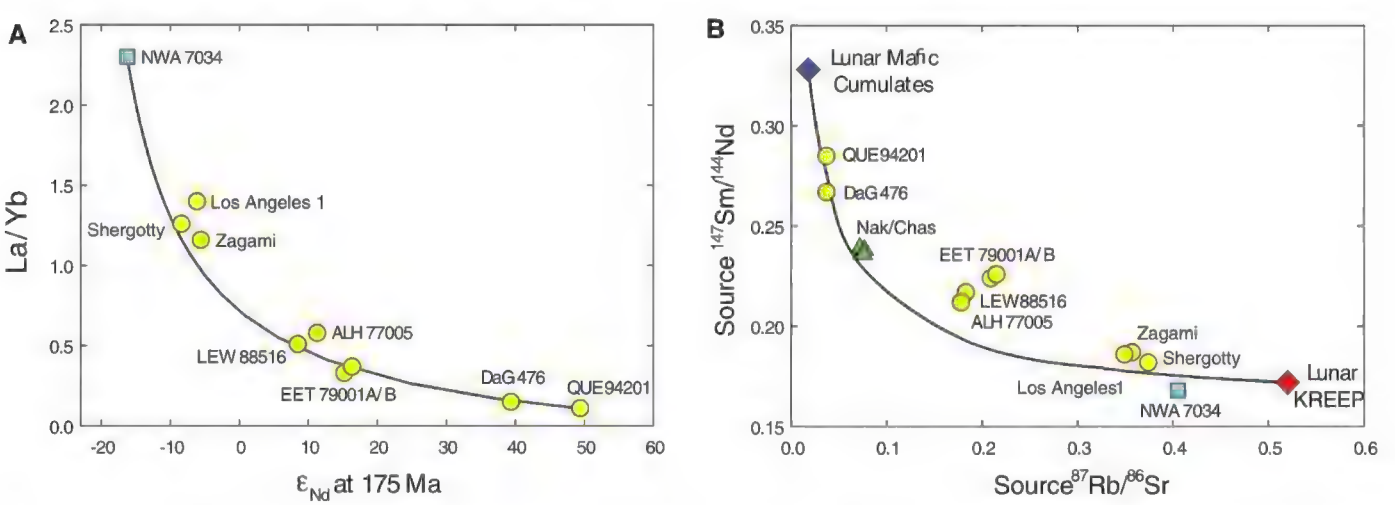

Fig. 5. (**A**) Plot of bulk rock La/Yb ratio versus ε_{Nd} calculated at 175 Ma for NWA 7034 and basaltic shergottites. Solid line represents two-component mixing line between NWA 7034 and QUE 94201. (**B**) Plot of calculated parent/daughter source ratios for NWA 7034, basaltic shergottites, nakhlites including Chassigny (which has values similar to nakhlites) (Nak/Chas), and lunar mantle sources. Solid line represents two-component mixing line between depleted lunar mafic cumulates and lunar potassium, rare-earth elements, and phosphorus (KREEP). Depleted lunar mafic cumulates are estimated by (*54*–*56*). Lunar KREEP is estimated by (*56*). Data for basaltic shergottites, nakhlites, and Chassigny are from (*22*, *23*) and references therein.

Another possibility is that NWA 7034 originally had oxygen isotope values similar to or the same as SNC, but a cometary component with higher $\delta^{18}O$, $\delta^{17}O$, and $\Delta^{17}O$ was mixed with it through impact processes on Mars, thus producing a $\Delta^{17}O$ excess relative to SNC. Until we find clear evidence of such an exotic component in NWA 7034, this scenario seems less likely than the other two.

Water. The oxygen isotope ratio of water released by stepped heating in a vacuum at UCSD (table S5) shows that most, possibly all, of the water in NWA 7034 is extraterrestrial, with $\Delta^{17}O$ values well above the terrestrial fractionation line (Fig. 7). NWA 7034 water falls primarily within the range of values for bulk SNC meteorites, with a weighted mean value of $\Delta^{17}O = +0.33 \pm 0.01$‰; $\delta^{18}O$ and $\delta^{17}O$ values give a slope of 0.52, indicating mass-dependent fractionation. Note that the $\Delta^{17}O$ value for NWA 7034 water is lower than, and outside the range of, the $\Delta^{17}O$ for bulk NWA 7034, offering clear evidence that there are multiple distinct oxygen isotope sources for this sample. The $\Delta^{17}O$ value of the water released at the 500° to 1000°C range (+0.09‰) approaches terrestrial values, possibly because of decomposition of the terrestrial carbonate veins in the meteorite and equilibration of the produced CO_2 with the released water. Karlsson *et al.* (*41*) reported oxygen isotope values of water from several SNC meteorites and also saw that they differed from the $\Delta^{17}O$ of the bulk SNC samples. However, their observed $\Delta^{17}O$ relationship between bulk rock and water is reverse to the one seen in NWA 7034, with waters in general having more positive $\Delta^{17}O$ values than their respective host rocks (Nakhla, Chassigny, and Lafayette). Only two shergottites (Shergotty and EETA-79001A) have waters with $\Delta^{17}O$ values more negative than the host rock, and Nakhla has water similar to its host rock. Romanek (*43*) analyzed iddingsite, an alteration product of olivine and pyroxene, in Lafayette and found the $\Delta^{17}O$ value is 1.37‰ for a 90% iddingsite separate, supporting the positive $\Delta^{17}O$ shift of Lafayette water relative to host rock. Karlsson (*41*) argued that this $\Delta^{17}O$ difference suggested a lack of equilibrium between water and host rock, with the lithosphere and hydrosphere having distinct oxygen isotopic reservoirs. Our data support this conclusion but suggest that the $\Delta^{17}O$ value of the "water" reservoir is not always heavier than the rock reservoir.

We determined the deuterium/hydrogen isotope ratio (δD value versus SMOW) and the water content of whole-rock NWA 7034 at UNM by both bulk combustion and stepped heating in a continuous-flow helium stream with high-temperature carbon reduction (*49*) (Fig. 8 and table S6). Six whole-rock combustion measurements yielded a bulk water content of 6190 ± 620 ppm. The mean δD value for the bulk combustion analyses was +46.3 ± 8.6‰. The maximum δD values in two separate stepwise heating experiments were +319‰ and +327‰, reached at 804°C and 1014°C, respectively (table S6), similar to values seen in the nakhlites (*50*). Figure 8 shows that most of the water in NWA 7034 is released between approximately 150° and 500°C, and that there are two plateaus of δD values, one around −100‰ at 50° to 200°C and a second around +300‰ at 300° to 1000°C. This suggests that there are two distinct δD components in NWA 7034: a low-temperature negative-value component and a high-temperature positive-value component. One possibility is that the low-temperature negative values are from terrestrial water contamination, although the $\Delta^{17}O$ values in water released at even the lowest temperature step of 50°C have a 0.3‰ anomaly (Fig. 7). It is also possible that protium-rich water is released at the lowest steps of dehydration, although such fractionation is not observed on terrestrial samples. Alternatively, the hydrogen but not the oxygen isotope ratios could have been affected by terrestrial alteration. Finally, it is possible that nearly all the released water from NWA 7034 is in fact martian and not terrestrial. In this case, the hydrogen isotope ratios have fractionated as a function of temperature, or there are two distinct hydrogen isotope reservoirs.

Our data show that NWA 7034 has more than an order of magnitude more indigenous water than most SNC meteorites. The amount of water released at high temperature (>320°C) is 3280 ± 720 ppm. Leshin *et al.* (*50*) measured an average of 249 ± 129 ppm H_2O released above 300° to 350°C in seven bulk SNC meteorites, with the exception of the anomalous Lafayette nakhlite (which released 1300 ppm H_2O above 300°C). They (*50*) argued that some of the water released at temperatures as low as 250°C could in fact be from martian alteration products. Given our oxygen water analyses, this could also be the case for NWA 7034 at temperatures as low as 50°C. Hence, the total amount of martian water in NWA 7034 could be in the vicinity of 6000 ppm, possibly supporting hypotheses that aqueous alteration of near-surface materials on Mars occurred during the early Amazonian epoch (2.1 Ga) either by magmatically derived or meteoric aqueous fluids (*51*–*53*).

Conclusions. The young crystallization age of NWA 7034, 2.1 Ga, requires that it is planetary

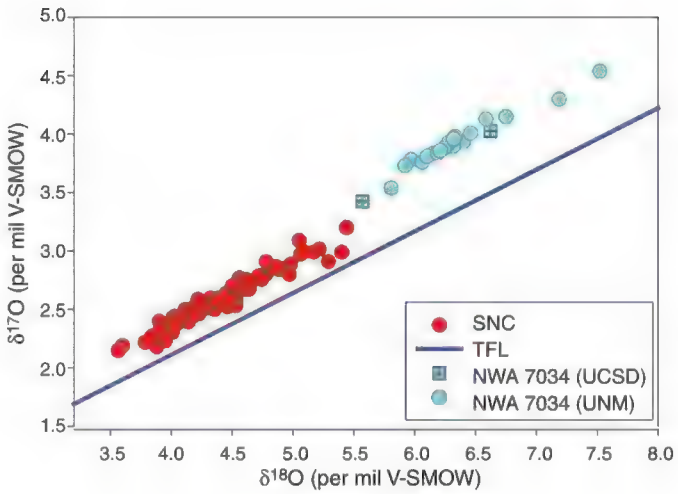

Fig. 6. Oxygen isotope plot showing the values of NWA 7034 from this study. Cyan dots, 13 analyses of acid-washed and six analyses of non–acid-washed bulk samples (UNM); cyan squares, two analyses of dry, decarbonated bulk preheated to 1000°C (UCSD). Red dots are SNC meteorites from the literature (*33*–*36*, *41*). TFL, terrestrial fractionation line (slope 0.528).

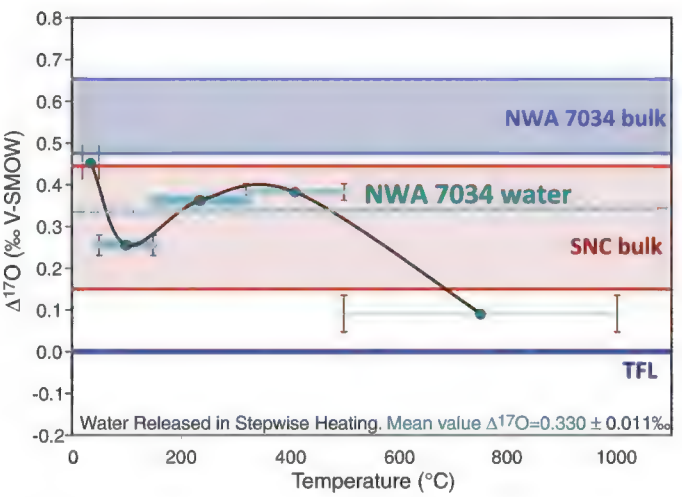

Fig. 7. Plot of $\Delta^{17}O$ versus temperature, showing values for NWA 7034 water released by stepped heating. Vertical error bars are given for each data point; horizontal line segments show the temperature range for each step, and the thickness of the line segment indicates the relative proportion of water released at each step. Dashed line is the mean value of $\Delta^{17}O$ for NWA 7034 water. Also shown are ranges of $\Delta^{17}O$ for bulk NWA 7034 analyses and for bulk SNC values from the literature.

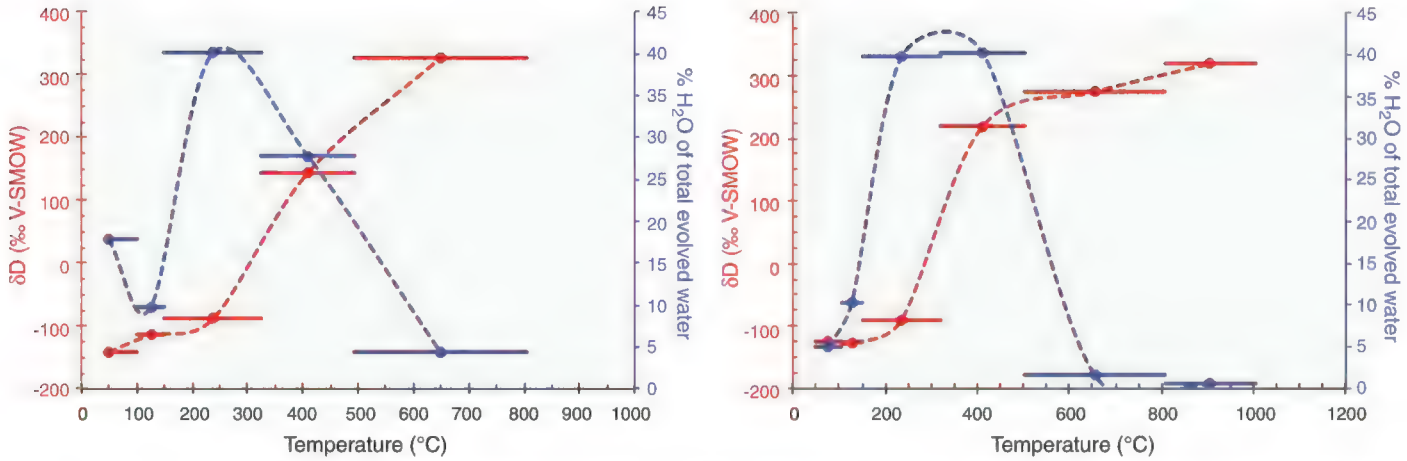

Fig. 8. Plots of δD versus temperature, showing data for the NWA 7034 bulk sample during stepped heating. The horizontal solid lines represent the temperature intervals; circles are mid-interval temperatures. The two plots represent two aliquots of the NWA 7034 sample.

in origin. Its major, minor, trace, and isotopic chemistry is inconsistent with originating from Earth, the Moon, Venus, or Mercury, and it is most similar to rocks from Mars. Nonetheless, NWA 7034 is uniquely different from any other known martian meteorite, as it is the most geochemically enriched rock from Mars found to date. Moreover, the bulk chemistry of NWA 7034 is strikingly similar to recently collected orbital and lander data collected at the martian surface, allowing for a direct link between a martian meteorite and orbital and lander spacecraft data from Mars. NWA 7034 is also distinct from the SNC meteorites because it has higher bulk $\delta^{18}O$ and $\Delta^{17}O$, suggesting the existence of multiple oxygen isotopic reservoirs within the lithologic portion of Mars.

References and Notes

1. A. H. Treiman, J. D. Gleason, D. D. Bogard, *Planet. Space Sci.* **48**, 1213 (2000).
2. H. Y. McSween, T. L. Grove, J. Wyatt, *J. Geophys. Res. Planets* **108**, 5135 (2003).
3. L. E. Nyquist *et al.*, in *Chronology and Evolution of Mars*, R. Kallenbach, J. Geiss, W. K. Hartmann, Eds. (Springer, New York, 2001), p. 105.
4. H. Y. McSween Jr., G. J. Taylor, M. B. Wyatt, *Science* **324**, 736 (2009).
5. R. Gellert *et al.*, *J. Geophys. Res. Planets* **111**, E02S05 (2006).
6. D. W. Ming *et al.*, *J. Geophys. Res. Planets* **113**, E12S39 (2008).
7. W. V. Boynton *et al.*, *J. Geophys. Res. Planets* **112**, E12S99 (2007).
8. See supplementary materials on *Science* Online.
9. S. P. Wright, P. R. Christensen, T. G. Sharp, *J. Geophys. Res. Planets* **116**, E09006 (2011).
10. J. J. Papike, J. M. Karner, C. K. Shearer, P. V. Burger, *Geochim. Cosmochim. Acta* **73**, 7443 (2009).
11. F. M. McCubbin, H. Nekvasil, *Am. Mineral.* **93**, 676 (2008).
12. J. Filiberto, *Geochim. Cosmochim. Acta* **72**, 690 (2008).
13. H. Nekvasil, F. M. McCubbin, A. Harrington, S. Elardo, D. H. Lindsley, *Meteorit. Planet. Sci.* **44**, 853 (2009).
14. F. M. McCubbin, H. Nekvasil, A. D. Harrington, S. M. Elardo, D. H. Lindsley, *J. Geophys. Res. Planets* **113**, E11013 (2008).
15. J. Zipfel *et al.*, *Meteorit. Planet. Sci.* **46**, 1 (2011).
16. H. Chennaoui Aoudjehane *et al.*, *Science* **338**, 785 (2012).
17. M. Wadwa, G. Crozaz, J.-A. Barrat, *Antarct. Meteorite Res.* **17**, 97 (2004).
18. J. M. Day, L. A. Taylor, C. Floss, H. Y. Mcsween Jr., *Meteorit. Planet. Sci.* **41**, 581 (2006).
19. W. K. Hartmann, G. Neukum, in *Chronology and Evolution of Mars*, R. Kallenbach, J. Geiss, W. K. Hartmann, Eds. (Springer, New York, 2001), p. 165–194.
20. L. E. Borg, D. S. Draper, *Meteorit. Planet. Sci.* **38**, 1713 (2003).
21. L. E. Borg, L. E. Nyquist, L. A. Taylor, H. Wiesmann, C.-Y. Shih, *Geochim. Cosmochim. Acta* **61**, 4915 (1997).
22. L. E. Borg, L. E. Nyquist, H. Wiesmann, Y. Reese, *Geochim. Cosmochim. Acta* **66**, 2037 (2002).
23. L. E. Borg, L. E. Nyquist, H. Wiesmann, C.-Y. Shih, Y. Reese, *Geochim. Cosmochim. Acta* **67**, 3519 (2003).
24. C. K. Shearer *et al.*, *Am. Mineral.* **96**, 1418 (2011).
25. C. B. Till, T. L. Grove, M. J. Krawczynski, *J. Geophys. Res.* **117**, B06206 (2012).
26. M. D. Norman, *Meteorit. Planet. Sci.* **34**, 439 (1999).
27. C. D. K. Herd, L. E. Borg, J. H. Jones, J. J. Papike, *Geochim. Cosmochim. Acta* **66**, 2025 (2002).
28. A. B. Sarbadhikari, J. M. D. Day, Y. Liu, D. Rumble III, L. A. Taylor, *Geochim. Cosmochim. Acta* **73**, 2190 (2009).
29. A. B. Sarbadhikari, C. A. Goodrich, Y. Liu, J. M. D. Day, L. A. Taylor, *Geochim. Cosmochim. Acta* **75**, 6803 (2011).
30. C. D. K. Herd, *Meteorit. Planet. Sci.* **38**, 1793 (2003).
31. A. Steele *et al.*, *Science* **337**, 212 (2012).
32. M. M. Grady, A. B. Verchovsky, I. P. Wright, *Int. J. Astrobiol.* **3**, 117 (2004).
33. R. N. Clayton, T. K. Mayeda, *Earth Planet. Sci. Lett.* **62**, 1 (1983).
34. I. A. Franchi, I. P. Wright, A. S. Sexton, C. T. Pillinger, *Meteorit. Planet. Sci.* **34**, 657 (1999).
35. D. W. Mittlefehldt, R. N. Clayton, M. J. Drake, K. Righter, *Rev. Mineral. Geochem.* **68**, 399 (2008).
36. D. Rumble *et al.*, *Proc. 40th Lunar Planet. Sci. Conf.* **40**, 2293 (2009).
37. F. M. McCubbin, M. A. Riner, K. E. Vander Kaaden, L. K. Burkemper, *Geophys. Res. Lett.* **39**, L09202 (2012).
38. M. A. Riner, F. M. McCubbin, P. G. Lucey, G. J. Taylor, J. J. Gillis-Davis, *Icarus* **209**, 301 (2010).
39. L. R. Nittler *et al.*, *Science* **333**, 1847 (2011).
40. K. Lodders, B. Fegley, *The Planetary Scientist's Companion* (Oxford Univ. Press, Oxford, 1998).
41. H. R. Karlsson, R. N. Clayton, E. K. Gibson Jr., T. K. Mayeda, *Science* **255**, 1409 (1992).
42. J. Farquhar, M. H. Thiemens, T. Jackson, *Science* **280**, 1580 (1998).
43. C. S. Romanek *et al.*, *Meteorit. Planet. Sci.* **33**, 775 (1998).
44. E. D. Young, R. D. Ash, P. England, D. Rumble 3rd, *Science* **286**, 1331 (1999).
45. Y. L. Yung, W. B. Demore, *Photochemistry of Planetary Atmospheres* (Oxford Univ. Press, Oxford, 1999).
46. J. Farquhar, M. H. Thiemens, *J. Geophys. Res. Planets* **105**, 11991 (2000).
47. C. C. Reese, V. S. Solomatov, *Icarus* **184**, 102 (2006).
48. F. Nimmo, S. D. Hart, D. G. Korycansky, C. B. Agnor, *Nature* **453**, 1220 (2008).
49. Z. D. Sharp, V. Atudorei, T. Durakiewicz, *Chem. Geol.* **178**, 197 (2001).
50. L. A. Leshin, S. Epstein, E. M. Stolper, *Geochim. Cosmochim. Acta* **60**, 2635 (1996).
51. L. Borg, M. J. Drake, *J. Geophys. Res. Planets* **110**, E12S03 (2005).
52. B. L. Ehlmann *et al.*, *Nature* **479**, 53 (2011).
53. F. M. McCubbin *et al.*, *Earth Planet. Sci. Lett.* **292**, 132 (2010).
54. G. A. Snyder, L. A. Taylor, C. R. Neal, *Geochim. Cosmochim. Acta* **56**, 3809 (1992).
55. G. A. Snyder, D.-C. Lee, L. A. Taylor, A. N. Halliday, E. A. Jerde, *Geochim. Cosmochim. Acta* **58**, 4795 (1994).
56. P. H. Warren, J. T. Wasson, *Rev. Geophys. Space Phys.* **17**, 73 (1979).

Acknowledgments: We thank J. Piatek for acquiring the NWA 7034 specimen and for his generous donation to the UNM Meteorite Museum, which has enabled this research and sample allocations for future research on NWA 7034. We also thank M. Spilde, V. Atudorei, and J. Connolly at the University of New Mexico for assistance with data collection. Supported by NASA Cosmochemistry Program grants NNX11AH16G (C.B.A.) and NNX11AG76G (F.M.M.). S.M.E. acknowledges support from the New Mexico Space Grant Consortium, NASA Earth and Space Science Fellowship NNX12AO15H, and NASA Cosmochemistry grant NNX10AI77G to Charles K. Shearer. M.H.T. and R.S. acknowledge NSF award ATM0960594, which allowed the development of an analytical technique to measure oxygen triple isotopic composition of small (<1 μM) sulfate samples.

Supplementary Materials

www.sciencemag.org/cgi/content/full/science.1228858/DC1
Materials and Methods
Figs. S1 to S16
Tables S1 to S6
References (*57*–*71*)

15 August 2012; accepted 14 December 2012
Published online 3 January 2013;
10.1126/science.1228858

Cyclic GMP-AMP Synthase Is a Cytosolic DNA Sensor That Activates the Type I Interferon Pathway

Lijun Sun,[1,2]* Jiaxi Wu,[1]* Fenghe Du,[1,2] Xiang Chen,[1,2] Zhijian J. Chen[1,2]†

The presence of DNA in the cytoplasm of mammalian cells is a danger signal that triggers host immune responses such as the production of type I interferons. Cytosolic DNA induces interferons through the production of cyclic guanosine monophosphate–adenosine monophosphate (cyclic GMP-AMP, or cGAMP), which binds to and activates the adaptor protein STING. Through biochemical fractionation and quantitative mass spectrometry, we identified a cGAMP synthase (cGAS), which belongs to the nucleotidyltransferase family. Overexpression of cGAS activated the transcription factor IRF3 and induced interferon-β in a STING-dependent manner. Knockdown of cGAS inhibited IRF3 activation and interferon-β induction by DNA transfection or DNA virus infection. cGAS bound to DNA in the cytoplasm and catalyzed cGAMP synthesis. These results indicate that cGAS is a cytosolic DNA sensor that induces interferons by producing the second messenger cGAMP.

DNA was known to stimulate immune responses long before it was shown to be a genetic material, but the mechanism by which DNA functions as an immune stimulant remains poorly understood (*1*). Although DNA can stimulate the production of type I interferons in dendritic cells through binding to Toll-like receptor 9 (TLR9) in the endosome, it is still unclear how DNA in the cytosol induces interferon. In particular, the sensor that detects cytosolic DNA in the interferon pathway remains elusive (*2*). Although several proteins—including DAI, RNA polymerase III, IFI16, DDX41, and several other DNA helicases—have been suggested to function as the potential DNA sensors that induce interferon, no consensus has emerged (*3*).

Purification and identification of cyclic GMP-AMP synthase (cGAS). We showed that delivery of DNA to mammalian cells or cytosolic extracts triggered the production of cyclic GMP-AMP (cGAMP), which bound to and activated STING, leading to the activation of the transcription factor IRF3 and induction of interferon-β (IFN-β) (*4*). To identify the cGAMP synthase (cGAS), we fractionated cytosolic extracts (S100) from the murine fibrosarcoma cell line L929, which contains the cGAMP-synthesizing activity. This activity was assayed by incubating the column fractions with adenosine triphosphate and guanosine triphosphate (ATP and GTP) in the presence of herring testis DNA (HT-DNA). After digestion of the DNA with Benzonase (Novagen) and heating at 95°C to denature proteins, the heat-resistant supernatants that contained cGAMP were incubated with perfringolysin O (PFO)–permeabilized Raw264.7 cells (transformed mouse macrophages). cGAMP-induced IRF3 dimerization in these cells was analyzed by native gel electrophoresis (*4*). Using this assay, we carried out three independent routes of purification, each consisting of four steps of chromatography but differing in the columns or the order of the columns used (fig. S1A). In particular, the third route included an affinity purification step using a biotinylated DNA oligo [a 45–base pair DNA known as immune stimulatory DNA (ISD)].

[1]Department of Molecular Biology, University of Texas Southwestern Medical Center, Dallas, TX 75390, USA. [2]Howard Hughes Medical Institute, University of Texas Southwestern Medical Center, Dallas, TX 75390, USA.

*These authors contributed equally to this work.
†To whom correspondence should be addressed. E-mail: zhijian.chen@utsouthwestern.edu

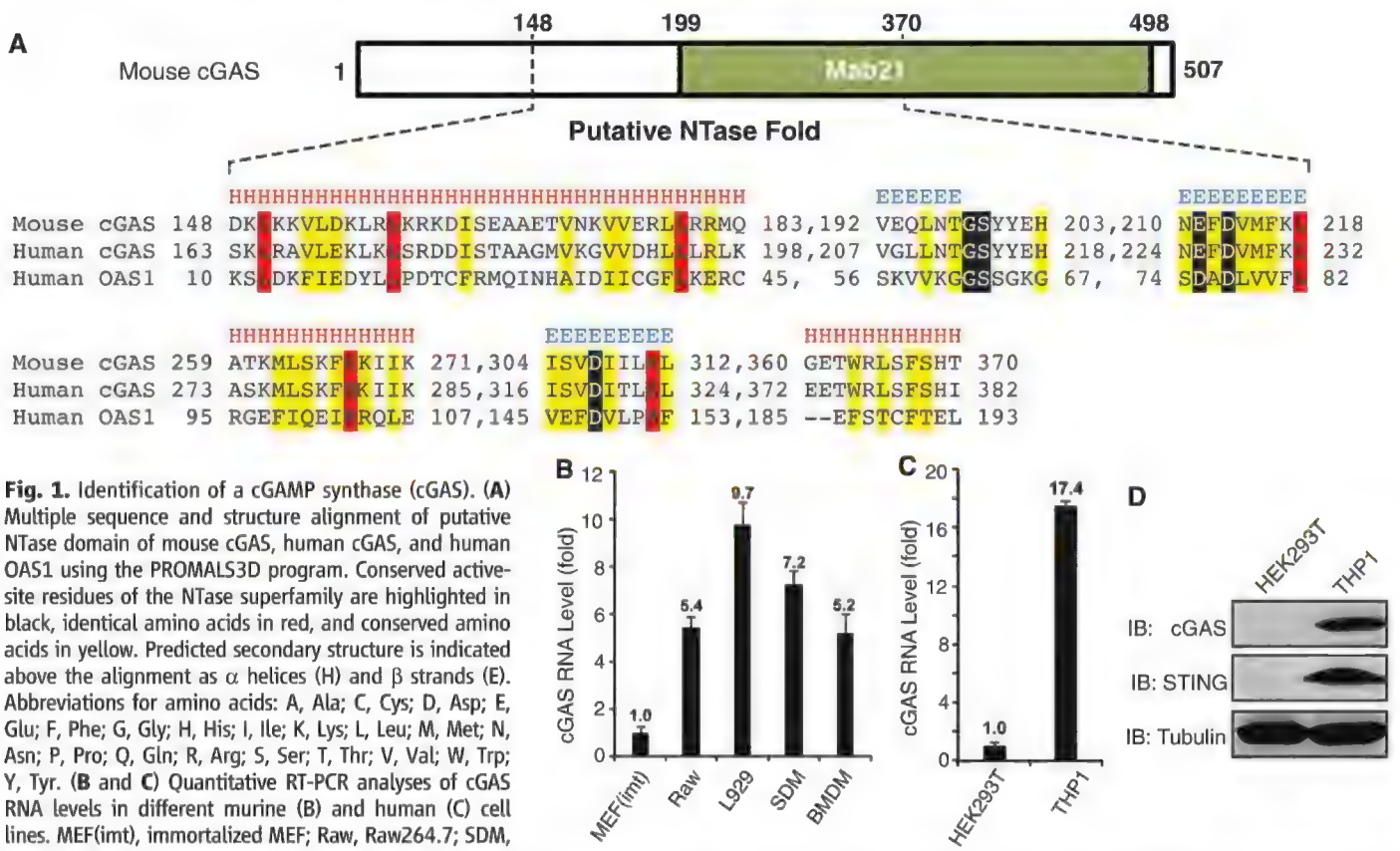

Fig. 1. Identification of a cGAMP synthase (cGAS). (**A**) Multiple sequence and structure alignment of putative NTase domain of mouse cGAS, human cGAS, and human OAS1 using the PROMALS3D program. Conserved active-site residues of the NTase superfamily are highlighted in black, identical amino acids in red, and conserved amino acids in yellow. Predicted secondary structure is indicated above the alignment as α helices (H) and β strands (E). Abbreviations for amino acids: A, Ala; C, Cys; D, Asp; E, Glu; F, Phe; G, Gly; H, His; I, Ile; K, Lys; L, Leu; M, Met; N, Asn; P, Pro; Q, Gln; R, Arg; S, Ser; T, Thr; V, Val; W, Trp; Y, Tyr. (**B** and **C**) Quantitative RT-PCR analyses of cGAS RNA levels in different murine (B) and human (C) cell lines. MEF(imt), immortalized MEF; Raw, Raw264.7; SDM, spleen-derived macrophage; BMDM, bone marrow–derived macrophage. Here and in all other qRT-PCR assays, error bars denote SEM (n = 3). (**D**) Immunoblotting of endogenous human proteins in HEK293T and THP1 cells with the indicated antibodies.

We estimated that we achieved a range of 8000- to 15,000-fold purification and 2 to 5% recovery of the activity from these routes of fractionation. However, in the last step of each of these purification routes, silver staining of the fractions did not reveal clear protein bands that copurified with the cGAS activity, which suggests that the abundance of the putative cGAS protein might be very low in L929 cytosolic extracts.

We developed a quantitative mass spectrometry strategy to identify a list of proteins that copurified with the cGAS activity at the last step of each purification route. We reasoned that the putative cGAS protein must copurify with its activity in all three purification routes, whereas most "contaminating" proteins would not. Thus, from the last step of each purification route, we chose fractions that contained most of the cGAS activity (peak fractions) and adjacent fractions that contained very weak or no activity (fig. S1B). The proteins in each fraction were separated by SDS–polyacrylamide gel electrophoresis (PAGE) and identified by nano–liquid chromatography–mass spectrometry (nano-LC-MS). The data were analyzed by label-free quantification using the MaxQuant software (*5*); the proteins that copurified with the cGAS activity are shown in table S1 and illustrated in a Venn diagram (fig. S1C). Remarkably, although many proteins copurified with the cGAS activity in one or two purification routes, only three proteins copurified in all three routes. All three were putative uncharacterized proteins: E330016A19 (NCBI accession number NP_775562), Arf-GAP with dual PH domain–containing protein 2 (NP_742145), and signal recognition particle 9-kD protein (NP_036188). Among these, more than 24 unique peptides were identified in E330016A19, representing 41% coverage in this protein of 507 amino acids (fig. S2A).

Bioinformatic analysis drew our attention to E330016A19, which exhibited structural and sequence homology to the catalytic domain of human oligoadenylate synthase (OAS1) (Fig. 1A). In particular, E330016A19 contains a conserved Gly[Gly/Ser]x_{9-13}[Glu/Asp]h[Glu/Asp]h motif, where x_{9-13} indicates 9 to 13 flanking residues consisting of any amino acid and h indicates a hydrophobic amino acid. This motif is found in the nucleotidyltransferase (NTase) family (*6*). Besides OAS1, this family includes adenylate cyclase, polyadenylate polymerase, and DNA polymerases. The C terminus of E330016A19 contained a Mab21 (male abnormal 21) domain, which was first identified in the *Caenorhabditis elegans* protein Mab21 (*7*). Sequence alignment revealed that the C-terminal NTase and Mab21 domains are highly conserved from zebrafish to human (fig. S2, B and C), whereas the N-terminal sequences are much less conserved (*8*). The human homolog of E330016A19, C6orf150 (also known as MB21D1), was recently identified as one of several positive hits in a screen for interferon-stimulated genes (ISGs) whose overexpression inhibited viral replication (*9*). For clarity, and on the basis of evidence presented below, we propose to name the mouse protein E330016A19 as m-cGAS and the human homolog C6orf150 as h-cGAS.

Quantitative reverse transcription polymerase chain reaction (qRT-PCR) showed that the expression of m-cGAS was low in immortalized mouse embryo fibroblasts (MEFs) but high in L929 cells, Raw264.7 cells, and bone marrow–derived macrophages (Fig. 1B). Similarly, the

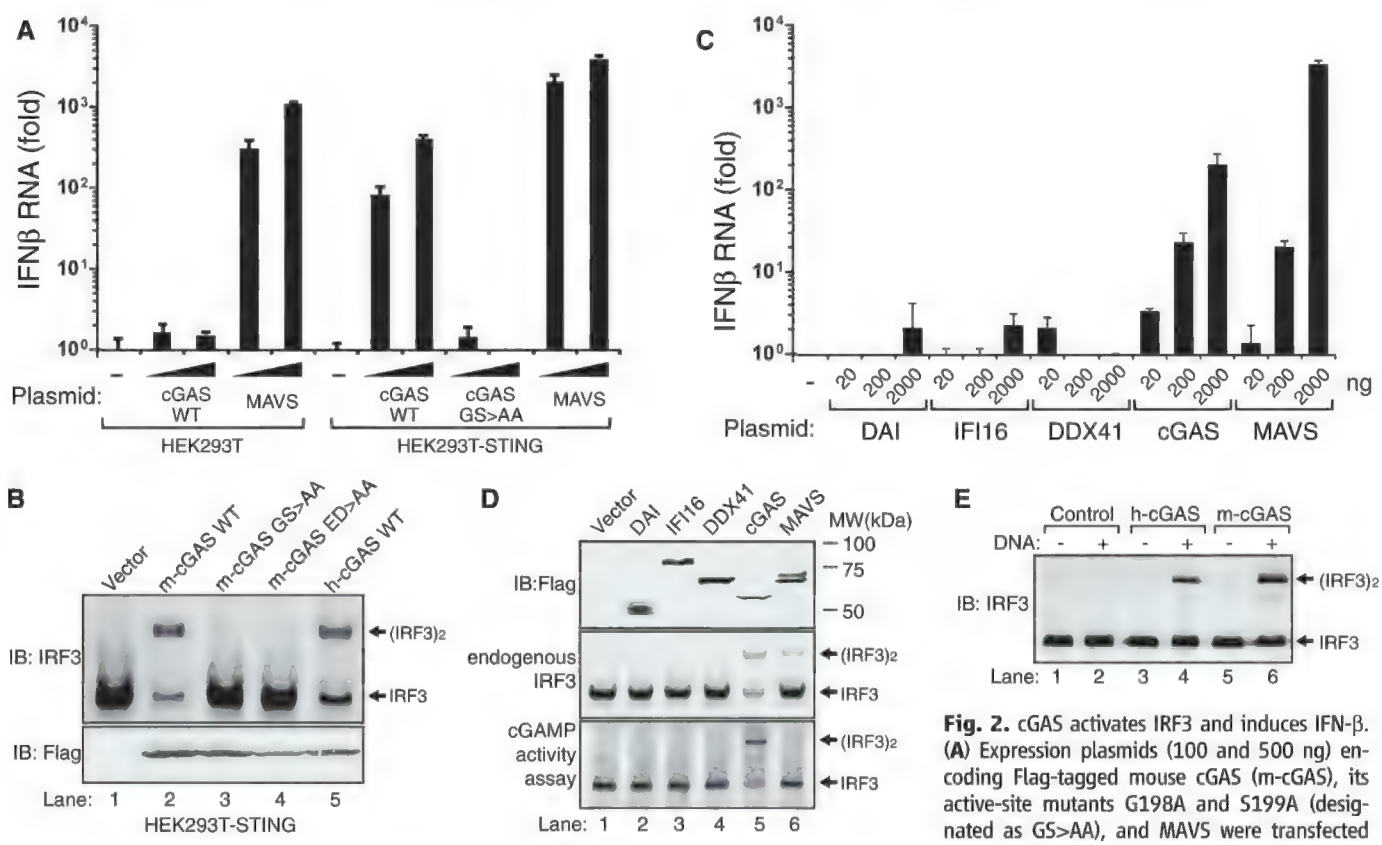

Fig. 2. cGAS activates IRF3 and induces IFN-β. (**A**) Expression plasmids (100 and 500 ng) encoding Flag-tagged mouse cGAS (m-cGAS), its active-site mutants G198A and S199A (designated as GS>AA), and MAVS were transfected into HEK293T cells or the same cell line stably expressing STING (HEK293T-STING). IFN-β RNA was measured by qRT-PCR 24 hours after transfection. (**B**) Similar to (A), except that cell lysates were analyzed for IRF3 dimerization by native gel electrophoresis (top). Expression levels of the transfected genes were monitored by immunoblotting with antibody to Flag (bottom). h-cGAS, human cGAS; ED>AA, E211A and D213A in mouse cGAS. (**C**) Expression vectors for the indicated proteins were transfected into HEK293T-STING cells, followed by measurement of IFN-β by qRT-PCR. (**D**) Cell lysates shown in (C) were immunoblotted with antibodies to Flag and IRF3 after SDS-PAGE and native PAGE, respectively (top two panels). Aliquots of the cell extracts were assayed for the presence of cGAMP activity, which was measured by detecting IRF3 dimerization after delivery into permeabilized Raw264.7 cells (bottom). (**E**) Human and mouse cGAS were expressed in HEK293T cells and affinity-purified with antibody to Flag. The proteins were incubated with ATP and GTP in the presence or absence of HT-DNA, and the synthesis of cGAMP was assessed by its ability to induce IRF3 dimerization in Raw264.7 cells.

expression of h-cGAS RNA was very low in human embryonic kidney (HEK) 293T cells but high in the human monocytic cell line THP1 (Fig. 1C). Immunoblotting further confirmed that h-cGAS protein was expressed in THP1 cells but not HEK293T cells (Fig. 1D; no mouse cGAS antibody is available yet). Thus, the expression levels of m-cGAS and h-cGAS in different cell lines correlated with the ability of these cells to produce cGAMP and induce IFN-β in response to cytosolic DNA (*4*, *10*).

Catalysis by cGAS triggers type I interferon production. Overexpression of m-cGAS in HEK293T, which lacks STING expression (Fig. 1D), did not induce IFN-β, whereas stable expression of STING in HEK293T cells rendered these cells highly competent in IFN-β induction by m-cGAS (Fig. 2A). Point mutations of the putative catalytic residues Gly^{198} and Ser^{199} to alanine abolished the ability of m-cGAS to induce IFN-β. These mutations, as well as mutations of the other putative catalytic residues Glu^{211} and Asp^{213} to alanine, also abrogated the ability of m-cGAS to induce IRF3 dimerization in HEK293T-STING cells (Fig. 2B).

The magnitude of IFN-β induction by c-GAS was comparable to that induced by MAVS (an adaptor protein that functions downstream of the RNA sensor RIG-I) and was higher than that induced by other putative DNA sensors, including DAI, IFI16, and DDX41, by several orders of magnitude (Fig. 2C). To determine whether overexpression of cGAS and other putative DNA sensors led to the production of cGAMP in cells, we incubated supernatants from heat-treated cell extracts with PFO-permeabilized Raw264.7 cells, followed by measurement of IRF3 dimerization (Fig. 2D, bottom). Among all the proteins expressed in HEK293T-STING cells, only cGAS was capable of producing the cGAMP activity in the cells.

To test whether cGAS could synthesize cGAMP in vitro, we purified wild-type and mutant Flag-cGAS proteins from transfected HEK293T cells. Wild-type m-cGAS and h-cGAS, but not the catalytically inactive mutants of cGAS, were able to produce the cGAMP activity, which stimulated IRF3 dimerization in permeabilized Raw264.7 cells (fig. S3A). We found that the in vitro activities of both m-cGAS and h-cGAS were dependent on the presence of HT-DNA (Fig. 2E). To test whether DNA enhances IFN-β induction by cGAS in cells, we transfected different amounts of cGAS expression plasmid, with or without HT-DNA, into HEK293T-STING cells (fig. S3B). HT-DNA markedly enhanced IFN-β induction by low (10 and 50 ng) but not high (200 ng) doses of cGAS plasmid. It is possible that the transfected cGAS plasmid DNA activated the cGAS protein in the cells, resulting in IFN-β induction. In contrast to cGAS, IFI16 and DDX41 did not induce IFN-β even when HT-DNA was cotransfected.

cGAS is required for IFN-β induction by DNA transfection and DNA virus infection. We used two different pairs of small interfering RNA (siRNA) to knock down m-cGAS in L929 cells, and found that both siRNA oligos strongly inhibited IFN-β induction by HT-DNA; moreover, the degree of inhibition correlated with the efficiency of knocking down m-cGAS RNA (fig. S4A). We also established two L929 cell lines stably expressing short hairpin RNA (shRNA) sequences that targeted distinct regions of m-cGAS (fig. S4B). The ability of these cells to induce IFN-β in response to HT-DNA was severely compromised relative to another cell line expressing a control shRNA against green fluorescent protein (shGFP; Fig. 3A).

Expression of cGAS in the L929–sh-cGAS cells restored IFN-β induction (Fig. 3B). Expression of STING or MAVS in these cells (Fig. 3B) or delivery of cGAMP to these cells (Fig. 3C) also induced IFN-β. In contrast, expression of cGAS or delivery of cGAMP failed to induce IFN-β in L929-shSTING cells, whereas expression of STING or MAVS restored IFN-β induction in these cells (Fig. 3, B and C). Quantitative RT-PCR analyses confirmed the specificity and efficiency of knocking down cGAS and STING in the

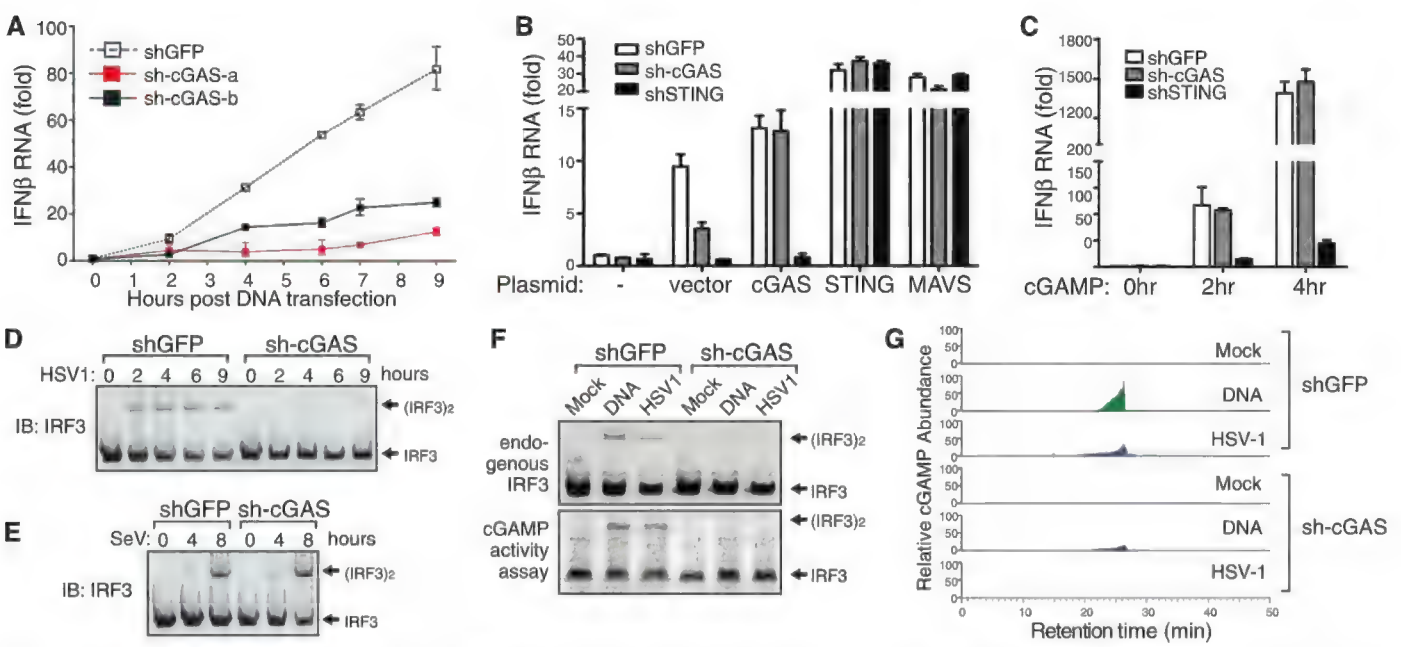

Fig. 3. cGAS is essential for IRF3 activation and IFN-β induction by DNA transfection and DNA virus infection. (**A**) L929 cell lines stably expressing shRNA targeting GFP (control) or two different regions of m-cGAS were transfected with HT-DNA for the indicated times, followed by measurement of IFN-β RNA by qRT-PCR. See fig. S4B for RNA interference (RNAi) efficiency. (**B**) L929 cells stably expressing shRNA against GFP, cGAS, or STING were transfected with pcDNA3 (vector) or the same vector driving the expression of the indicated proteins. IFN-β RNA was measured by qRT-PCR 24 hours after transfection; see fig. S4C for RNAi efficiency. (**C**) cGAMP (100 nM) was delivered to digitonin-permeabilized L929 cells stably expressing shRNA against GFP, cGAS, or STING. IFN-β RNA was measured by qRT-PCR at the indicated times after cGAMP delivery. (**D** and **E**) L929 cells stably expressing shRNA against GFP or cGAS were infected with HSV1 (ΔICP34.5) (D) or Sendai virus (SeV) (E) for the indicated times, followed by measurement of IRF3 dimerization. (**F**) L929 cells stably expressing shRNA against GFP or cGAS were transfected with HT-DNA or infected with HSV1 for 6 hours, followed by measurement of IRF3 dimerization (top). Extracts from these cells were used to prepare heat-resistant supernatants, which were delivered to permeabilized Raw264.7 cells to stimulate IRF3 dimerization (bottom). (**G**) The heat-resistant supernatants in (F) were fractionated by high-performance liquid chromatography using a C18 column; the abundance of cGAMP was quantitated by mass spectrometry using SRM.

L929 cell lines stably expressing the corresponding shRNAs (fig. S4C). These results indicate that cGAS functions upstream of STING and is required for IFN-β induction by cytosolic DNA.

Herpes simplex virus 1 (HSV-1) is a DNA virus known to induce interferons through the activation of STING and IRF3 (*3*). L929 cells expressing shRNA against m-cGAS, but not against GFP, were severely compromised in IRF3 dimerization in response to HSV-1 infection (Fig. 3D). In contrast, knockdown of cGAS did not affect IRF3 activation by Sendai virus, an RNA virus (Fig. 3E). To determine whether cGAS is required for the generation of cGAMP in cells, we transfected HT-DNA into L929-shGFP and L929–sh-cGAS cells or infected these cells with HSV-1, then prepared heat-resistant fractions that contained cGAMP, which was subsequently delivered to permeabilized Raw264.7 cells to measure IRF3 activation. Knockdown of cGAS largely abolished the cGAMP activity generated by DNA transfection or HSV-1 infection (Fig. 3F, bottom). Quantitative mass spectrometry using selective reaction monitoring (SRM) showed that the abundance of cGAMP induced by DNA transfection or HSV-1 infection was markedly reduced in L929 cells depleted of cGAS (Fig. 3G). Taken together, these results demonstrate that cGAS is essential for producing cGAMP and activating IRF3 in response to DNA transfection or HSV-1 infection.

To determine whether cGAS is important in the DNA sensing pathway in human cells, we established a THP1 cell line stably expressing a shRNA targeting h-cGAS (fig. S4D). The knockdown of h-cGAS strongly inhibited IFN-β induction by HT-DNA transfection or infection by vaccinia virus, another DNA virus, but not by Sendai virus (fig. S4D). The knockdown of h-cGAS also inhibited IRF3 dimerization induced by HSV-1 infection in THP1 cells (fig. S4E). This result was further confirmed in another THP1 cell line expressing a shRNA targeting a different region of h-cGAS (fig. S4F). The strong and specific effects of multiple cGAS shRNA sequences in inhibiting DNA-induced IRF3 activation and IFN-β induction in both mouse and human cell lines demonstrate a key role of cGAS in the STING-dependent DNA sensing pathway.

Recombinant cGAS protein catalyzes cGAMP synthesis from ATP and GTP in a DNA-dependent manner. To test whether cGAS is sufficient to catalyze cGAMP synthesis, we expressed Flag-tagged h-cGAS in HEK293T cells and purified it to apparent homogeneity (Fig. 4A). In the presence of HT-DNA, purified c-GAS protein catalyzed the production of cGAMP activity, which stimulated IRF3 dimerization in permeabilized Raw264.7 cells (Fig. 4B). Deoxyribonuclease I (DNase I) treatment abolished this activity. The cGAS activity was also stimulated by other DNAs, including poly(deoxyadenosine-deoxythymidine), poly(deoxyguanosine-deoxycytidine), and ISD, but not by the RNA poly(inosine-cytidine). The synthesis of cGAMP by cGAS required both ATP and GTP but did not require cytidine triphosphate (CTP) or uridine triphosphate (UTP) (Fig. 4C). These results indicate that the cyclase activity of purified cGAS protein was stimulated by DNA but not by RNA.

We also expressed m-cGAS in *Escherichia coli* as a SUMO (small ubiquitin-related modifier protein) fusion protein. After purification, SUMO–m-cGAS generated the cGAMP activity in a DNA-dependent manner (fig. S5, A and C). However, after the SUMO tag was removed by a SUMO protease, the m-cGAS protein catalyzed cGAMP synthesis in a DNA-independent manner (fig. S5, B and C). The reason for this loss of DNA dependency is unclear but could be due to some conformational changes after SUMO removal. Titration experiments showed that recombinant cGAS protein at less than 1 nM led to detectable IRF3 dimerization, whereas the catalytically inactive mutant of cGAS failed to activate IRF3 even at high concentrations (Fig. 4D). To formally prove that cGAS catalyzes the synthesis of cGAMP, we analyzed the reaction products by nano-LC-MS using SRM. cGAMP was detected in a 60-min reaction containing purified cGAS, ATP, and GTP (Fig. 4E). The identity of cGAMP was further confirmed by ion fragmentation using collision-induced dissociation (CID). The fragmentation pattern of cGAMP synthesized by purified cGAS revealed product ions whose mass/charge ratio (*m/z*) values matched those of chemically synthesized cGAMP (fig. S5D). Collectively, these results demonstrate that purified cGAS catalyzes the synthesis of cGAMP from ATP and GTP.

cGAS binds to DNA. The stimulation of cGAS activity by DNA suggests that c-GAS is a DNA sensor (Fig. 4B). Indeed, both GST (glutathione *S*-transferase) fused to the N terminus of m-CGAS (GST–m-cGAS) and GST–h-cGAS, but not GST–RIG-I N terminus [RIG-I(N)], were precipitated by biotinylated ISD (Fig. 5A). In contrast, biotinylated RNA did not bind cGAS (Fig. 5B). Deletion analyses showed that the h-cGAS N-terminal fragment containing residues 1 to 212, but not the

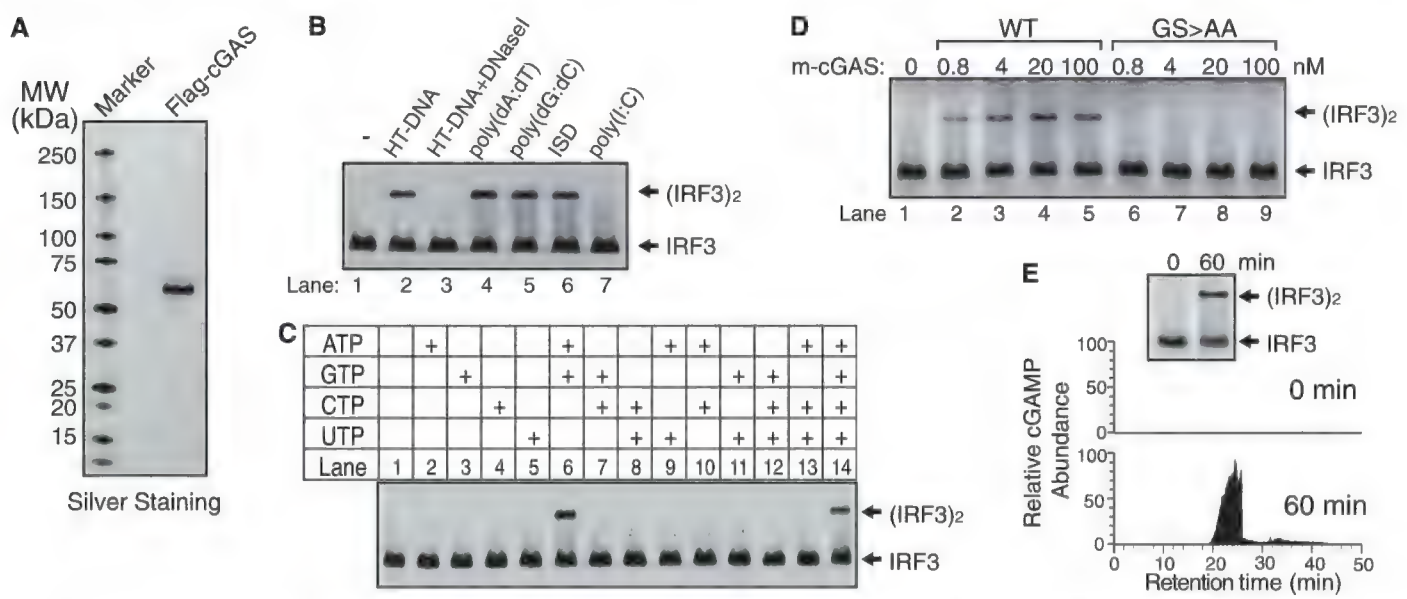

Fig. 4. DNA-dependent synthesis of cGAMP by purified cGAS. (**A**) Silver staining of Flag–h-cGAS expressed and purified from HEK293T cells. (**B**) Purified Flag–h-cGAS as shown in (A) was incubated with ATP and GTP in the presence of different forms of nucleic acids as indicated. Generation of cGAMP was assessed by its ability to induce IRF3 dimerization in Raw264.7 cells. (**C**) Similar to (B), except that reactions contained HT-DNA and different combinations of nucleotide triphosphates as indicated. (**D**) Similar to (B), except that wild-type and mutant cGAS proteins were expressed and purified from *E. coli* and assayed for their activities at the indicated concentrations. (**E**) Purified m-cGAS from *E. coli* was incubated with ATP, GTP, and DNA for 0 or 60 min, and the production of cGAMP was analyzed by IRF3 dimerization assay (top) and mass spectrometry using SRM (bottom).

C-terminal fragment (residues 213 to 522), bound to ISD (Fig. 5C). A longer C-terminal fragment containing residues 161 to 522 did bind to ISD, which suggests that the sequence 161 to 212 may be important for DNA binding. However, deletion of residues 161 to 212 from h-cGAS did not impair ISD binding, which suggests that cGAS contains another DNA binding domain at the N terminus. Indeed, the N-terminal fragment containing residues 1 to 160 also bound ISD (Fig. 5C). Thus, cGAS may contain two separate DNA binding domains at the N terminus. Our attempts to express the cGAS fragment containing residues 161 to 212 in *E. coli* or HEK293T cells have not been successful, so at present we do not know whether this sequence alone is sufficient to bind DNA. Nonetheless, it is clear that the N terminus of h-cGAS containing residues 1 to 212 is both necessary and sufficient to bind DNA.

Different deletion mutants of h-cGAS were overexpressed in HEK293T-STING cells to determine their ability to activate IRF3 and induce IFN-β and the cytokine tumor necrosis factor–α (TNF-α) (Fig. 5C and fig. S6A). The protein fragment containing residues 1 to 382, which lacks the C-terminal 140 residues including much of the Mab21 domain, failed to induce IFN-β (Fig. 5C, right) or TNF-α or to activate IRF3 (fig. S6A), which suggests that an intact Mab21 domain is important for cGAS function. As expected, deletion of the N-terminal 212 residues (residues 213 to 522), which include part of the NTase domain, abolished the cGAS activity (Fig. 5C and fig. S6A). An internal deletion of just four amino acids (Lys^{171}, Leu^{172}, Lys^{173}, and Leu^{174}) within the first helix of the NTase fold preceding the catalytic residues also destroyed the cGAS activity (fig. S6A).

Deletion of the N-terminal 160 residues did not affect IRF3 activation or cytokine induction by cGAS (Fig. 5C and fig. S6A). In vitro assay showed that this protein fragment (residues 161 to 522) still activated the IRF3 pathway in a DNA-dependent manner (fig. S6B). Thus, the N-terminal 160 amino acids of h-cGAS, whose primary sequence is not highly conserved evolutionarily, appear to be largely dispensable for DNA binding and catalysis by cGAS. In contrast, the NTase and Mab21 domains are important for cGAS activity.

cGAS is predominantly localized in the cytosol. To determine whether cGAS is a cytosolic DNA sensor, we prepared cytosolic and nuclear extracts from THP1 cells and analyzed the localization of endogenous h-cGAS by immunoblotting. h-cGAS was detected in the cytosolic extracts but was barely detectable in the nuclear extracts (Fig. 6A). The THP1 extracts were further subjected to differential centrifugation to separate subcellular organelles from one another and from the cytosol (Fig. 6B). Similar amounts of h-cGAS were detected in S100 and in the pellet after 100,000*g* centrifugation, which suggests that this protein is soluble in the cytoplasm but that a substantial fraction of the protein is associated with light vesicles or organelles. The cGAS protein was not detected in the pellet after 5000*g* centrifugation, which contained mitochondria and endoplasmic reticulum (ER) as evidenced by the presence of VDAC and STING, respectively. cGAS was also not detectable in the pellet after 20,000*g* centrifugation, which contained predominantly ER and heavy vesicles (Fig. 6B).

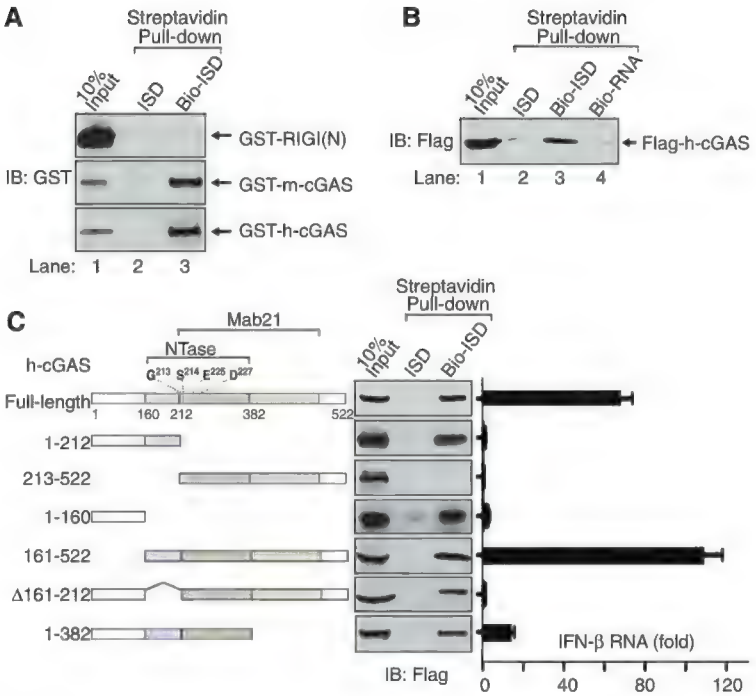

Fig. 5. cGAS is a DNA binding protein. **(A)** The indicated GST fusion proteins were expressed and purified from *E. coli* and then incubated with streptavidin beads in the presence of ISD or biotin-ISD. Bound proteins were eluted with SDS sample buffer and detected by immunoblotting with a GST antibody. **(B)** Flag–h-cGAS was expressed and purified from HEK293T cells and then incubated with streptavidin beads as described in (A), except that a Flag antibody was used in immunoblotting and a biotin-RNA was also tested for binding to cGAS. **(C)** Flag-tagged full-length or truncated human cGAS proteins were expressed in HEK293T cells and affinity-purified. Their ability to bind biotin-ISD was assayed as described in (B). Right panel: Expression plasmids encoding full-length and deletion mutants of h-cGAS were transfected into HEK293T-STING cells, and IFN-β RNA was then measured by qRT-PCR.

We also examined the localization of cGAS by confocal immunofluorescence microscopy of L929 cells stably expressing Flag–m-cGAS (Fig. 6C). The cGAS protein was distributed throughout the cytoplasm but could also be observed in the nuclear or perinuclear region. After the cells were transfected with Cyanine 3 (Cy3)–labeled ISD for 2 or 4 hours, punctate forms of cGAS were observed, and they overlapped with the DNA fluorescence. Such colocalization and apparent aggregation of cGAS and Cy3-ISD was observed in more than 50% of the cells under observation. These results, together with the biochemical evidence of direct binding of cGAS with DNA, suggest that cGAS binds to DNA in the cytoplasm.

Discussion. We have developed a strategy that combines quantitative mass spectrometry with conventional protein purification to identify biologically active proteins partially purified from crude cell extracts. This strategy may be generally applicable to proteins that are difficult to purify to homogeneity because of very low abundance, labile activity, or scarce starting materials. As a proof of principle, we used this strategy to identify the mouse protein E330016A19 as the enzyme that synthesizes cGAMP. This discovery led to the identification of a large family of cGAS that is conserved from fish to human, formally demonstrating that vertebrate animals contain evolutionarily conserved enzymes that synthesize cyclic dinucleotides, which were previously found only in bacteria, archaea, and protozoa (*11*–*13*). *Vibrio cholerae* can synthesize cGAMP through its cyclase DncV (VC0179), which contains an NTase domain but has no obvious primary sequence homology to the mammalian cGAS (*12*).

Our results not only demonstrate that cGAS is a cytosolic DNA sensor that triggers the type I interferon pathway, but also reveal a mechanism of immune signaling in which cGAS generates the second messenger cGAMP, which binds to and activates STING (*4*), thereby triggering type I interferon production. It remains to be determined whether STING evolved first to detect cyclic dinucleotides from bacteria, or to detect endogenous cGAMP in the host as a mechanism of responding to cytosolic DNA. Although STING can directly detect certain cyclic dinucleotides produced by some bacteria, the deployment of cGAS as a cytosolic DNA sensor greatly expands the repertoire of microorganisms detected by the host immune system. In principle, all microorganisms that can carry DNA

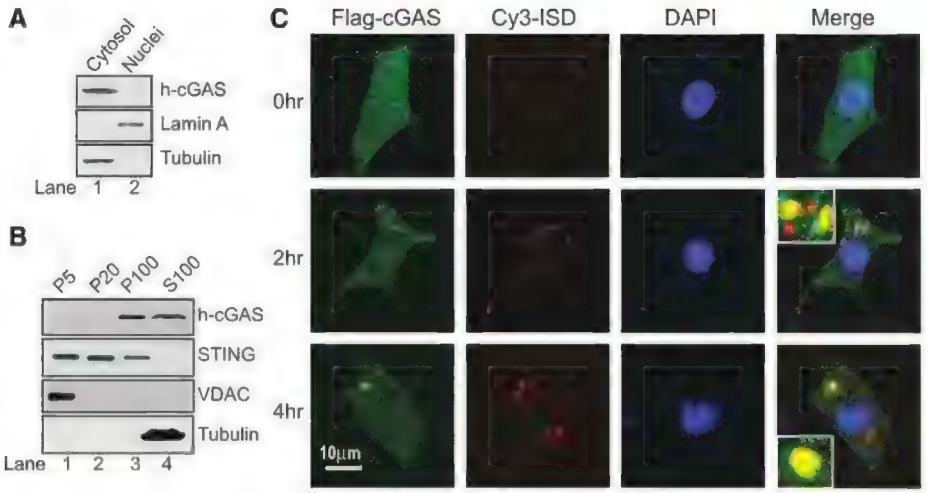

Fig. 6. cGAS binds to DNA in the cytoplasm. **(A)** Nuclear and cytoplasmic fractions were prepared from THP-1 cells and analyzed by immunoblotting with the indicated antibodies. **(B)** THP-1 cells were homogenized in hypotonic buffer and subjected to differential centrifugation. Pellets at different speeds of centrifugation (e.g., P100: pellets after 100,000*g*) and S100 were immunoblotted with the indicated antibodies. **(C)** L929 cells stably expressing Flag-cGAS (green) were transfected with Cy3-ISD (red). At different time points after transfection, cells were fixed, stained with antibody to Flag or with 4′,6-diamidino-2-phenylindole (DAPI), and imaged by confocal fluorescence microscopy. The insets in the merged images are magnifications of the small boxed areas. These images are representative of at least 10 cells at each time point (representing >50% of the cells under examination).

into the host cytoplasm—such as DNA viruses, bacteria, parasites (e.g., malaria), and retroviruses (e.g., HIV)—could potentially trigger the cGAS-STING pathway (*14*, *15*). The enzymatic synthesis of cGAMP by cGAS provides a mechanism of signal amplification for a robust and sensitive immune response. However, the detection of self DNA in the host cytoplasm by cGAS could also lead to autoimmune diseases, such as systemic lupus erythematosus, Sjögren's syndrome, and Aicardi-Goutières syndrome (*16*–*18*).

Several other DNA sensors, such as DAI, IFI16, and DDX41, have been reported to induce type I interferons (*19*–*21*). Overexpression of DAI, IFI16, or DDX41 did not lead to the production of cGAMP. We also found that knockdown of DDX41 and p204 (a mouse homolog of IFI16) by siRNA did not inhibit the generation of cGAMP activity in HT-DNA–transfected L929 cells (fig. S7). Nonetheless, it is possible that distinct DNA sensors exist in different cell types. Unlike other putative DNA sensors and most pattern recognition receptors (e.g., TLRs), cGAS is a cyclase that is likely more amenable to inhibition by small-molecule compounds. These inhibitors may be developed into therapeutic agents for the treatment of human autoimmune diseases.

References and Notes

1. L. A. O'Neill, *Cell* **138**, 428 (2009).
2. G. N. Barber, *Immunol. Rev.* **243**, 99 (2011).
3. S. E. Keating, M. Baran, A. G. Bowie, *Trends Immunol.* **32**, 574 (2011).
4. J. Wu *et al.*, *Science* **339**, 826 (2013).
5. J. Cox, M. Mann, *Nat. Biotechnol.* **26**, 1367 (2008).
6. K. Kuchta, L. Knizewski, L. S. Wyrwicz, L. Rychlewski, K. Ginalski, *Nucleic Acids Res.* **37**, 7701 (2009).
7. K. L. Chow, D. H. Hall, S. W. Emmons, *Development* **121**, 3615 (1995).
8. J. Pei, B. H. Kim, N. V. Grishin, *Nucleic Acids Res.* **36**, 2295 (2008).
9. J. W. Schoggins *et al.*, *Nature* **472**, 481 (2011).
10. Y. H. Chiu, J. B. Macmillan, Z. J. Chen, *Cell* **138**, 576 (2009).
11. C. Pesavento, R. Hengge, *Curr. Opin. Microbiol.* **12**, 170 (2009).
12. B. W. Davies, R. W. Bogard, T. S. Young, J. J. Mekalanos, *Cell* **149**, 358 (2012).
13. Z. H. Chen, P. Schaap, *Nature* **488**, 680 (2012).
14. S. Sharma *et al.*, *Immunity* **35**, 194 (2011).
15. N. Yan, Z. J. Chen, *Nat. Immunol.* **13**, 214 (2012).
16. V. Pascual, L. Farkas, J. Banchereau, *Curr. Opin. Immunol.* **18**, 676 (2006).
17. Y. Yao, Z. Liu, B. Jallal, N. Shen, L. Ronnblom, *Autoimmun. Rev.* 10.1016/j.autrev.2012.10.006 (2012).
18. R. E. Rigby, A. Leitch, A. P. Jackson, *Bioessays* **30**, 833 (2008).
19. A. Takaoka *et al.*, *Nature* **448**, 501 (2007).
20. L. Unterholzner *et al.*, *Nat. Immunol.* **11**, 997 (2010).
21. Z. Zhang *et al.*, *Nat. Immunol.* **12**, 959 (2011).

Acknowledgments: We thank W. Li for helpful discussion on bioinformatics analyses. The GenBank accession numbers for human and mouse cGAS sequences are KC294566 and KC294567, respectively. Supported by NIH grant AI-093967. Z.J.C. is an investigator of Howard Hughes Medical Institute.

Supplementary Materials

www.sciencemag.org/cgi/content/full/science.1232458/DC1
Materials and Methods
Figs. S1 to S7
Table S1
References (*22*, *23*)

7 November 2012; accepted 12 December 2012
Published online 20 December 2012;
10.1126/science.1232458

REPORTS

Universal Computation by Multiparticle Quantum Walk

Andrew M. Childs,[1,2] David Gosset,[1,2]* Zak Webb[2,3]

A quantum walk is a time-homogeneous quantum-mechanical process on a graph defined by analogy to classical random walk. The quantum walker is a particle that moves from a given vertex to adjacent vertices in quantum superposition. We consider a generalization to interacting systems with more than one walker, such as the Bose-Hubbard model and systems of fermions or distinguishable particles with nearest-neighbor interactions, and show that multiparticle quantum walk is capable of universal quantum computation. Our construction could, in principle, be used as an architecture for building a scalable quantum computer with no need for time-dependent control.

Quantum walk is a versatile and intuitive framework for developing quantum algorithms. Applications of continuous- (*1*) and discrete-time (*2*, *3*) models of quantum walk include an example of exponential speed-up over classical computation (*4*) and optimal algorithms for element distinctness (*5*) and formula evaluation (*6*).

Quantum walk is also a powerful computational model capable of performing any quantum computation (*7*). However, the graph used to perform a computation on n qubits is exponentially large as a function of n. Such a quantum walk cannot be efficiently implemented using an architecture where each vertex of the graph occupies a different spatial location. Nevertheless, many nonscalable implementations of quantum walk have been carried out (*8*–*10*) despite substantial

[1]Department of Combinatorics and Optimization, University of Waterloo, Waterloo, Ontario N2L 3G1, Canada. [2]Institute for Quantum Computing, University of Waterloo, Waterloo, Ontario N2L 3G1, Canada. [3]Department of Physics and Astronomy, University of Waterloo, Waterloo, Ontario N2L 3G1, Canada.

*To whom correspondence should be addressed. E-mail: dngosset@gmail.com

overhead that precludes efficient universal quantum computation.

We consider generalizations of quantum walk with many interacting walkers and show that multiparticle quantum walk is universal for quantum computation using a graph of polynomial size. We present efficient universal constructions based on the Bose-Hubbard model, fermions with nearest-neighbor interactions, and distinguishable particles with nearest-neighbor interactions. We also show that almost any interaction gives rise to universality when using indistinguishable particles.

Because our graphs are exponentially smaller than those in reference (*7*), our construction is amenable to experimental implementation using an architecture where vertices of the graph occupy different spatial locations (although we leave issues of fault tolerance for future work). Current two-particle experiments involve only noninteracting bosons (*11*–*14*), but other experiments could realize interactions. Specifically, a Bose-Hubbard model of the type we consider could naturally be realized in a variety of systems, including traditional nonlinear optics (*15*), neutral atoms in optical lattices (*16*, *17*), or photons in arrays of superconducting qubits (*18*).

Multiparticle quantum walk has been considered as an algorithmic tool for solving graph isomorphism (*19*), although this technique has known limitations (*20*). Other previous work has focused on two-particle quantum walk (*11*–*14*, *21*–*25*) and multiparticle quantum walk without interactions (*11*–*14*, *21*, *22*, *26*). Here, we consider multiparticle quantum walks with interactions, which seem to be required to achieve computational universality (*27*, *28*).

It has been shown that systems of interacting particles on a lattice can perform universal computation with a time-dependent Hamiltonian (*29*, *30*). However, because of the time dependence, such a system should not be considered a quantum walk. In our scheme, the Hamiltonian is time-independent and the computation is encoded entirely in the unweighted graph on which the particles interact.

In a multiparticle quantum walk, particles (either distinguishable or indistinguishable) interact in a local manner on a simple graph G with vertex set $V(G)$ and edge set $E(G)$. The Hilbert space for m distinguishable particles on G is spanned by the basis

$$\{|i_1,\ldots,i_m\rangle : i_1,\ldots,i_m \in V(G)\} \qquad (1)$$

where i_w is the location of the wth particle. A continuous-time multiparticle quantum walk of m distinguishable particles on G is generated by a time-independent Hamiltonian

$$H_G^{(m)} = \sum_{w=1}^{m} \sum_{(i,j)\in E(G)} (|i\rangle\langle j|_w + |j\rangle\langle i|_w) + \sum_{i,j\in V(G)} \mathcal{U}_{ij}(\hat{n}_i, \hat{n}_j) \qquad (2)$$

where the subscript w indicates that the operator acts nontrivially only on the location register for the wth particle. Here, the operators $\hat{n}_i$ and $\hat{n}_j$ count the numbers of particles at vertices i and j, respectively (explicitly, $\hat{n}_i = \sum_{w=1}^{m} |i\rangle\langle i|_w$).

The first term of Eq. 2 moves particles between adjacent vertices, and the second term is an interaction between particles. We assume that $\mathcal{U}_{ij}$ is zero whenever one of its arguments evaluates to zero and that $\mathcal{U}_{ii}$ is zero if there is only one particle at vertex i (thus, the Hamiltonian for a single particle reduces to that of a standard quantum walk). We also assume that the interaction $\mathcal{U}_{ij}$ only depends on the distance between i and j and has a constant range. Finally, we assume that the norm of each term $\mathcal{U}_{ij}$ is upper-bounded by a polynomial in m.

Indistinguishable particles can be represented in the basis specified in Eq. 1 as states that are either symmetric (for bosons) or antisymmetric (for fermions) under the interchange of any two particles. The Hamiltonian preserves both the symmetric and antisymmetric subspaces and, restricted to the appropriate subspace, generates a quantum walk of m bosons or m fermions on G.

This framework includes well-known interacting many-body systems defined on graphs. For example, it includes the Bose-Hubbard model, with interaction $\mathcal{U}_{ij}(\hat{n}_i,\hat{n}_j) = (U/2)\delta_{i,j}\hat{n}_i(\hat{n}_i - 1)$. It also includes systems with nearest-neighbor interactions, such as with $\mathcal{U}_{ij}(\hat{n}_i,\hat{n}_j) = U\delta_{(i,j)\in E(G)}\hat{n}_i\hat{n}_j$.

The dynamics of our scheme can be understood by considering scattering events involving only one or two particles and can be analyzed using a discrete version of scattering theory (*31*). We first discuss single-particle scattering.

Consider a single-particle quantum walk on an infinite graph G obtained by attaching a semi-infinite path to each of N chosen vertices of an arbitrary $(N + m)$–vertex graph $\hat{G}$ (Fig. 1A). A particle is initially prepared in a state that moves (under Schrödinger time evolution) toward the subgraph $\hat{G}$ along one of the semi-infinite paths. After scattering through the subgraph, the particle moves away from $\hat{G}$ in superposition along the semi-infinite paths. To understand this process, we discuss the scattering eigenstates of the Hamiltonian $H_G^{(1)}$.

Given the graph $\hat{G}$, for each momentum $k \in (-\pi,0)$ and path $j \in \{1,2\ldots,N\}$, there is a scattering state $|\mathrm{sc}_j(k)\rangle$ with amplitudes

$$\langle x,q|\mathrm{sc}_j(k)\rangle = e^{-ikx}\delta_{qj} + e^{ikx}S_{qj}(k) \qquad (3)$$

on the semi-infinite paths [with the labeling (x,q) of vertices on the paths as in Fig. 1A], where $S(k)$ is an N by N unitary matrix called the S-matrix [see section S1 of (*32*)]. The state $|\mathrm{sc}_j(k)\rangle$ is an eigenstate of $H_G^{(1)}$ with energy $2\cos k$.

A wave packet is a normalized state with most of its amplitude on scattering states with momenta close to some particular value. The scattering state $|\mathrm{sc}_j(k)\rangle$ gives us information about how a wave packet with momenta near k located on path j scatters from $\hat{G}$. The wave packet initially moves toward the graph with speed $|\frac{dE}{dk}| = |2\sin k|$. After scattering, the amplitude associated with finding the wave packet on path q is $S_{qj}(k)$. This picture of the scattering process remains valid when the finite extent of the wave packets is taken into account and when the infinite paths are truncated to be long but finite [section S5 of (*32*)].

We now consider scattering of two indistinguishable particles on an infinite path. Translation symmetry makes this system easier to analyze than more general two-particle quantum walks (*33*). Consider two indistinguishable particles initially prepared in spatially separated wave packets moving toward each other along a path with momenta $k_1 \in (-\pi, 0)$ and $k_2 \in (0, \pi)$. After scattering, the particles move apart with momenta

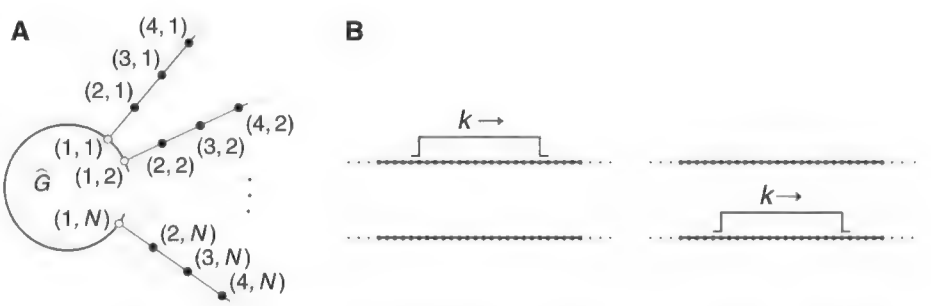

Fig. 1. (**A**) The infinite graph G. The vertices labeled $(1, j)$ belong to $\hat{G}$. (**B**) Encoded $|0\rangle$ (left) and $|1\rangle$ (right).

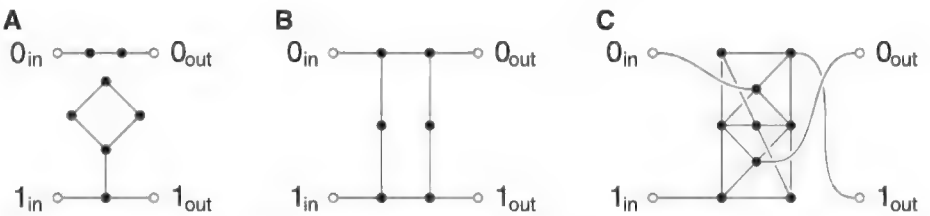

Fig. 2. (**A**) Phase gate at $-\pi/4$. (**B**) Basis-changing gate at $-\pi/4$. (**C**) Hadamard gate at $-\pi/2$.

k_1 and k_2 (by conservation of energy and momentum). The effect of the interaction is to change the global phase of the wave function after scattering (relative to the case with no interaction). This phase can be calculated given the two momenta, the interaction $\mathcal{U}$, and the particle type [section S2 of (*32*)]. In our scheme, we use $k_1 = -\pi/2$ and $k_2 = \pi/4$, and we write $e^{i\theta}$ for the phase acquired at these momenta. This picture of the two-particle scattering process holds even on a long (but finite) path and with finite wave packets [section S5 of (*32*)].

We now describe our scheme for universal computation by multiparticle quantum walk. We encode n logical qubits into the locations of n indistinguishable particles on a graph of size poly(n) [see section S3.2 of (*32*) for a refinement of our scheme using distinguishable particles]. In addition to these n particles, we use another particle to encode an ancilla qubit that facilitates two-qubit gates. We call the original n qubits computational qubits, and we call the ancilla qubit the mediator qubit. Time evolution of a simple initial state with the Hamiltonian corresponding to a suitably chosen graph G implements a quantum circuit on this encoded data.

The quantum circuit to be simulated (on the n computational qubits) is given as a product of gates from a universal set consisting of single-qubit gates along with the two-qubit controlled phase gate CP = diag(1,1,1,$-i$). A controlled phase between computational qubits i and j can be expanded as the following sequence of gates also acting on the mediator qubit m.

$$\begin{aligned}&\mathrm{CP}_{ij}|a_i,b_j,0_\mathrm{m}\rangle\\ &\quad=\mathrm{CNOT}_{im}\mathrm{CP}_{jm}\mathrm{CNOT}_{im}|a_i,b_j,0_\mathrm{m}\rangle\\ &\quad=\mathrm{H_m CP}^2_{im}\mathrm{H_m CP}_{jm}\mathrm{H_m CP}^2_{im}\mathrm{H_m}|a_i,b_j,0_\mathrm{m}\rangle\end{aligned}$$

Writing the controlled phase gate in this way, we transform the given n-qubit circuit into an $(n+1)$–qubit circuit with only single-qubit gates on computational qubits, Hadamard gates H on the mediator qubit, and controlled phase gates between the mediator qubit and arbitrary computational qubits.

We represent each of the $n+1$ qubits using a dual-rail encoding with two paths that run through the graph (Fig. 1B). The encoded state $|0\rangle$ has a particle moving along the top path, whereas the encoded state $|1\rangle$ has a particle moving along the bottom path. The particle moves as a wave packet with momentum near k. For the n computational qubits we choose $k = -\pi/4$, and for the mediator qubit we choose $k = -\pi/2$ (for concreteness).

To implement single-qubit unitaries, we design the graph so that the particles scatter through a series of small subgraphs while remaining far apart. When the particles are all far from each other, the interaction term in the Hamiltonian is negligible and the $n+1$ wave packets propagate independently [our analysis in section S4 of (*32*) accounts for the error in this approximation]. In this case, the multiparticle quantum walk can be viewed as a single-particle quantum walk for each of the particles.

To apply a one-qubit unitary U to an encoded qubit, we insert an associated graph $\hat{G}$ into the paths representing the qubit as follows. We attach two long "input" paths and two long "output" paths to four suitably chosen vertices of $\hat{G}$ so that the S-matrix at the relevant momentum has the form

$$S = \begin{pmatrix} 0 & U' \\ U & 0 \end{pmatrix} \qquad (4)$$

A particle incident on the input paths with the relevant momentum transmits perfectly to the output paths, with amplitudes determined by the 2 by 2 unitary matrix U.

Graphs $\hat{G}$ that implement a phase gate and a basis-changing gate at momentum $-\pi/4$ are shown in Fig. 2, A and B, respectively (*7*). The input and output paths are attached to the vertices denoted by open circles. The S-matrices at momentum $-\pi/4$ for these graphs are of the form given in Eq. 4, with lower-left 2 by 2 submatrices.

$$U_{\mathrm{phase}} = \begin{pmatrix} e^{-i\pi/4} & 0 \\ 0 & 1 \end{pmatrix}$$

$$U_{\mathrm{basis}} = -\frac{i}{\sqrt{2}}\begin{pmatrix} 1 & -i \\ -i & 1 \end{pmatrix}$$

These two gates allow us to approximate arbitrary single-qubit unitaries on each of the n computational qubits.

The Hadamard gate is the only single-qubit gate we apply to the mediator qubit. We implement this gate using the graph in Fig. 2C, which has S-matrix at momentum $k = -\pi/2$ of the form in Eq. 4, with lower-left submatrix

$$U_{\mathrm{H}} = -\frac{e^{i\pi/4}}{\sqrt{2}}\begin{pmatrix} 1 & 1 \\ 1 & -1 \end{pmatrix}$$

which is the Hadamard gate up to an irrelevant global phase (*34*).

To implement a controlled phase gate between the mediator qubit and a computational qubit, we use a subgraph that routes two particles toward each other and causes them to interact on a long path for a short time. After scattering, the system returns to a state where the particles are all far apart. We route a computational particle and the mediator particle toward each other along a long path only when the two associated qubits are in state $|11\rangle$. This allows us to implement the two-qubit gate Cθ = diag(1,1,1,$e^{i\theta}$), where $e^{i\theta}$ is the two-particle scattering phase. For some models, such as the Bose-Hubbard model with $U = 2 + \sqrt{2}$, we have Cθ = CP because $e^{i\theta} = -i$ [section S2 of (*31*)]. For nearest-neighbor interactions with fermions, the choice $U = -2 - \sqrt{2}$ gives $e^{i\theta} = i$, so CP = $(\mathrm{C}\theta)^3$. Although tuning the interaction strength makes the CP gate easier to implement, almost any interaction between indistinguishable particles allows for universal computation. We can approximate the required CP gate by repeating the Cθ gate a times, where $e^{ia\theta} \approx -i$ (which is possible for most values of θ, assuming θ is known).

We route particles using a subgraph we call the momentum switch (Fig. 3A). The S-

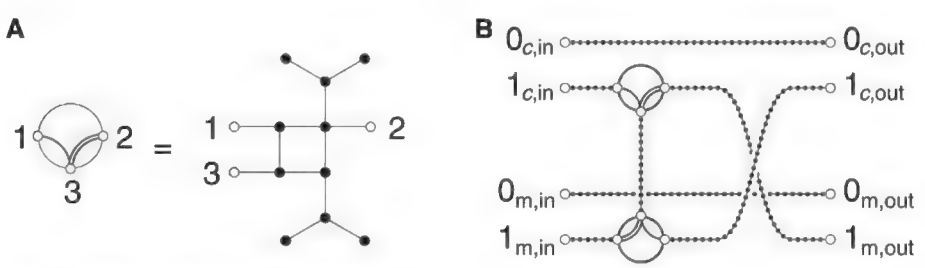

Fig. 3. (**A**) Momentum switch. (**B**) Cθ gate.

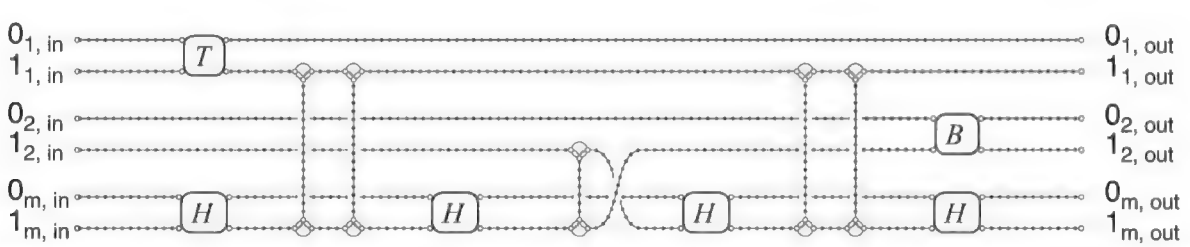

Fig. 4. Schematic depiction of a graph simulating $B_2CP_{1,2}T_1$ on two qubits for the Bose-Hubbard model with interaction strength $U = 2 + \sqrt{2}$. The dotted lines represent paths, and the single-qubit unitary gates represent their corresponding subgraphs.

matrices for this graph at momenta $-\pi/4$ and $-\pi/2$ are

$$S_{\text{switch}}(-\pi/4) = \begin{pmatrix} 0 & 0 & e^{-i\pi/4} \\ 0 & -1 & 0 \\ e^{-i\pi/4} & 0 & 0 \end{pmatrix}$$

$$S_{\text{switch}}(-\pi/2) = \begin{pmatrix} 1 & 0 & 0 \\ 0 & 0 & -1 \\ 0 & -1 & 0 \end{pmatrix} \quad (5)$$

The momentum switch has perfect transmission between vertices 1 and 3 at momentum $-\pi/4$ and perfect transmission between vertices 2 and 3 at momentum $-\pi/2$. Thus, the path a particle follows through the switch depends on its momentum: A particle with momentum $-\pi/2$ follows the double line in Fig. 3A, whereas a particle with momentum $-\pi/4$ follows the single line.

The graph used to implement the CΘ gate is shown in Fig. 3B [see section S4 of (*32*) for the numbers of vertices on each of the paths]. To see why this graph implements a CΘ gate, consider the movement of two particles as they pass through the graph. If either particle begins in the state $|0_{\text{in}}\rangle$, it travels along a path to the output without interacting with the second particle. When either particle begins in the state $|1_{\text{in}}\rangle$, it is routed onto the vertical path as it passes through the first momentum switch and is routed to the right as it passes through the second switch. If both particles begin in the state $|1_{\text{in}}\rangle$, they interact on the vertical path and the wave function acquires a phase $e^{i\Theta}$.

To implement a circuit, the subgraphs representing circuit elements are connected by paths. Figure 4 depicts a graph corresponding to a simple two-qubit computation. Timing is important: Wave packets must meet on the vertical paths for interactions to occur. We achieve this by choosing the numbers of vertices on each of the segments in the graph appropriately, taking into account the different propagation speeds of the two wave packets [see section S4 of (*32*)]. In section S3.1 of (*32*), we present a refinement of our scheme using planar graphs with maximum degree four.

By analyzing the full $(n + 1)$–particle interacting many-body system, we prove that our algorithm performs the desired quantum computation up to an error term that can be made arbitrarily small (*32*). Our analysis goes beyond the scattering theory discussion presented above; we take into account the fact that both the wave packets and the graphs are finite. Specifically, we prove that by choosing the size of the wave packets, the number of vertices in the graph, and the total evolution time to be polynomial functions of both n and g, the error in simulating an n-qubit, g-gate quantum circuit is bounded above by an arbitrarily small constant [section S5 of (*32*)]. For example, for the Bose-Hubbard model and for the nearest-neighbor interaction model, we prove that the error can be made arbitrarily small by choosing the size of the wave packets to be $O(n^{12}g^4)$, the total number of vertices in the graph to be $O(n^{13}g^5)$, and the total evolution time to be $O(n^{12}g^5)$. The bounds we prove, although almost certainly not optimal, are sufficient to establish universality with only polynomial overhead. Because it is also possible to efficiently simulate a multiparticle quantum walk of the type we consider using a universal quantum computer, this model exactly captures the power of quantum computation.

References and Notes

1. E. Farhi, S. Gutmann, *Phys. Rev. A* **58**, 915 (1998).
2. D. Aharonov, A. Ambainis, J. Kempe, U. Vazirani, "Quantum walks on graphs," *Proceedings of the 33rd ACM Symposium on Theory of Computing* (2001), pp. 50–59.
3. A. Ambainis, E. Bach, A. Nayak, A. Vishwanath, J. Watrous, "One-dimensional quantum walks," *Proceedings of the 33rd ACM Symposium on Theory of Computing* (2001), pp. 37–49.
4. A. M. Childs *et al.*, "Exponential algorithmic speedup by quantum walk," *Proceedings of the 35th ACM Symposium on Theory of Computing* (2003), pp. 59–68.
5. A. Ambainis, *SIAM J. Comput.* **37**, 210 (2007).
6. E. Farhi, J. Goldstone, S. Gutmann, *Theory of Computing* **4**, 169 (2008).
7. A. M. Childs, *Phys. Rev. Lett.* **102**, 180501 (2009).
8. B. Do *et al.*, *J. Opt. Soc. Am. B* **22**, 499 (2005).
9. M. Karski *et al.*, *Science* **325**, 174 (2009).
10. H. B. Perets *et al.*, *Phys. Rev. Lett.* **100**, 170506 (2008).
11. Y. Bromberg, Y. Lahini, R. Morandotti, Y. Silberberg, *Phys. Rev. Lett.* **102**, 253904 (2009).
12. A. Peruzzo *et al.*, *Science* **329**, 1500 (2010).
13. J. O. Owens *et al.*, *New J. Phys.* **13**, 075003 (2011).
14. L. Sansoni *et al.*, *Phys. Rev. Lett.* **108**, 010502 (2012).
15. I. L. Chuang, Y. Yamamoto, *Phys. Rev. A* **52**, 3489 (1995).
16. G. K. Brennen, C. M. Caves, P. S. Jessen, I. H. Deutsch, *Phys. Rev. Lett.* **82**, 1060 (1999).
17. W. S. Bakr, J. I. Gillen, A. Peng, S. Fölling, M. Greiner, *Nature* **462**, 74 (2009).
18. A. J. Hoffman *et al.*, *Phys. Rev. Lett.* **107**, 053602 (2011).
19. J. K. Gamble, M. Friesen, D. Zhou, R. Joynt, S. N. Coppersmith, *Phys. Rev. A* **81**, 052313 (2010).
20. J. Smith, *Electron. Notes Discrete Math.* **38**, 795 (2011).
21. Y. Omar, N. Paunković, *Phys. Rev. A* **74**, 042304 (2006).
22. P. K. Pathak, G. S. Agarwal, *Phys. Rev. A* **75**, 032351 (2007).
23. Y. Lahini *et al.*, *Phys. Rev. A* **86**, 011603 (2012).
24. A. Schreiber *et al.*, *Science* **336**, 55 (2012).
25. A. Ahlbrecht *et al.*, *New J. Phys.* **14**, 073050 (2012).
26. P. P. Rohde, A. Schreiber, M. Štefaňák, I. Jex, C. Silberhorn, *New J. Phys.* **13**, 013001 (2011).
27. B. M. Terhal, D. P. DiVincenzo, *Phys. Rev. A* **65**, 032325 (2002).
28. S. Aaronson, A. Arkhipov, "The computational complexity of linear optics," *Proceedings of the 43rd ACM Symposium on Theory of Computing* (2011), pp. 333–342.
29. R. Ionicioiu, P. Zanardi, *Phys. Rev. A* **66**, 050301 (2002).
30. A. Mizel, D. A. Lidar, M. Mitchell, *Phys. Rev. Lett.* **99**, 070502 (2007).
31. A. M. Childs, D Gosset, *J. Math. Phys.* **53**, 102207 (2012).
32. Materials and methods are available as supplementary materials on *Science* Online.
33. M. Valiente, *Phys. Rev. A* **81**, 042102 (2010).
34. B. A. Blumer, M. S. Underwood, D. L. Feder, *Phys. Rev. A* **84**, 062302 (2011).

Acknowledgments: This work was supported in part by MITACS; Natural Sciences and Engineering Research Council of Canada; the Ontario Ministry of Research and Innovation; the Ontario Ministry of Training, Colleges, and Universities; and the U.S. Army Research Office.

Supplementary Materials

www.sciencemag.org/cgi/content/full/339/6121/791/DC1
Materials and Methods
Supplementary Text
Figs. S1 to S10
References

10 September 2012; accepted 17 December 2012
10.1126/science.1229957

Photonic Boson Sampling in a Tunable Circuit

Matthew A. Broome,[1,2]* Alessandro Fedrizzi,[1,2] Saleh Rahimi-Keshari,[2] Justin Dove,[3] Scott Aaronson,[3] Timothy C. Ralph,[2] Andrew G. White[1,2]

Quantum computers are unnecessary for exponentially efficient computation or simulation if the Extended Church-Turing thesis is correct. The thesis would be strongly contradicted by physical devices that efficiently perform tasks believed to be intractable for classical computers. Such a task is boson sampling: sampling the output distributions of n bosons scattered by some passive, linear unitary process. We tested the central premise of boson sampling, experimentally verifying that three-photon scattering amplitudes are given by the permanents of submatrices generated from a unitary describing a six-mode integrated optical circuit. We find the protocol to be robust, working even with the unavoidable effects of photon loss, non-ideal sources, and imperfect detection. Scaling this to large numbers of photons should be a much simpler task than building a universal quantum computer.

A major motivation for scalable quantum computing is Shor's algorithm (*1*), which enables the efficient factoring of large composite numbers into their constituent primes. The presumed difficulty of this task is the basis of the majority of today's public-key encryption schemes. It may be that scalable quantum computers are not realistic if, for example, quantum mechanics breaks down for large numbers of qubits (*2*). If, however, quantum computers are realistic physical devices, then the Extended Church-Turing (ECT) thesis—that any function efficiently computed on a realistic physical device can be efficiently computed on a probabilistic Turing machine—means that a classical efficient factoring algorithm exists. Such an algorithm, long sought after, would enable us to break public-key cryptosystems such as RSA. A third possibility is that the ECT thesis itself is wrong.

How do we answer this trilemma? As yet there is no evidence that large-scale quantum computers are inherently impossible (that will need to be tested directly via experiment), and there is no efficient classical factoring algorithm or mathematical proof of its impossibility. This leaves examining the validity of the ECT thesis, which would be contradicted, for example, by building a physical device that efficiently performs a task thought to be intractable for classical computers.

One such task is boson sampling: sampling from the probability distribution of n identical bosons scattered by some linear unitary process, U. The probabilities are defined in terms of permanents of $n \times n$ submatrices of U [in general, calculating these is exponentially difficult, because calculating the permanent is a so-called "#P-complete" problem (*3*); a class above even "NP-complete" in complexity] and is therefore strongly believed to be intractable. This does not mean that boson sampling is itself #P-complete: The ability to sample from a distribution need not imply the ability to calculate the permanents that gave rise to it. However, by using the fact that the permanent is #P-complete, (*4*) recently showed that the existence of a fast classical algorithm for this "easier" sampling task leads to drastic consequences in classical computational complexity theory, notably collapse of the polynomial hierarchy.

We tested the central premise of boson sampling, experimentally verifying that the amplitudes of $n = 2$ and $n = 3$ photon scattering events are given by the permanents of $n \times n$ submatrices of the operator U describing the physical device. We find the protocol to be robust, working even with imperfect sources, optics, and detectors.

Consider a race between two participants: Alice, who only possesses classical resources, and Bob, who in addition possesses quantum resources. They are given some physical operation, described by an evolution operator, U, and agree on a specific n-boson input configuration. Alice calculates an output sample distribution with a classical computer; Bob either builds or programs an existing linear photonic network, sending n single photons through it and obtaining his sample by measuring the output distribution (Fig. 1A). The race ends when both return samples from the distribution: The winner is whoever returns a sample fastest. As n becomes large, it is conjectured that Bob will always win, because Alice's computation runtime increases exponentially, whereas Bob's experimental runtime does not. It becomes intractable to verify Bob's output against Alice's, and, unlike for Shor's algorithm, there is no known efficient algorithm to verify the result (*4*). However, one can take a large instance—large enough for verification via a classical computer—and show that Bob's quantum computer solves the problem much faster, thereby strongly suggesting that the same behavior will continue for larger systems, casting serious doubt on the ECT thesis. In a fair race, Bob must verify that his device actually implements the target unitary; an alternative fair version is to give both Alice and Bob the same physical device instead of a mathematical description and have Alice characterize it before she predicts output samples via classical computation. Alice can use a characterization method that neither requires nonclassical resources nor adds to the complexity of the task (*5*).

We tested boson sampling using an optical network with $m = 6$ input and output modes and $n = 2$ and $n = 3$ photon inputs. We implemented a randomly chosen operator so that the permanents could not be efficiently calculated (*6*); that is, the elements are complex-valued and the operator U is fully connected, with every input distributed to every output. The 6-input × 6-output modes of U are represented by two orthogonal polarizations in 3 × 3 spatial modes of a fused-fiber beamsplitter (FBS), an intrinsically stable and low-loss device. The mode mapping is $\{1,...,6\} = \{|H\rangle_1,|V\rangle_1,|H\rangle_2,|V\rangle_2,|H\rangle_3,|V\rangle_3\}$, where $|H\rangle_1$ is the horizontally polarized mode for spatial mode 1. We can use polarization controllers at the inputs and outputs of the central 3 × 3 FBS to modify the evolution (see the equivalent circuit diagram in Fig. 1B).

Alice calculates the probability of bosonic scattering events in the following way (*4*, *7*). Having characterized the evolution U using the method detailed in supplementary materials section S1 (*8*), and given the input and output configurations $S = (s_1,...,s_m)$ and $T = (t_1,...,t_m)$ with boson occupation numbers s_i and t_j respectively, she produces an $n \times m$ submatrix U_T by taking t_j copies of the j^{th} column of U. Then, she forms the $n \times n$ submatrix U_{ST} by taking s_i copies of the i^{th} row of U_T. The probability for the scattering event T, for indistinguishable input photons S, is given by $P_T^Q = |\mathrm{Per}(U_{ST}|^2$. Conversely, the classical scattering probabilities when the input photons are distinguishable are given by $P_T^C = \mathrm{Per}(\tilde{U}_{ST})$, where $\tilde{U}_{ST_{ij}} = |U_{ST_{ij}}|^2$.

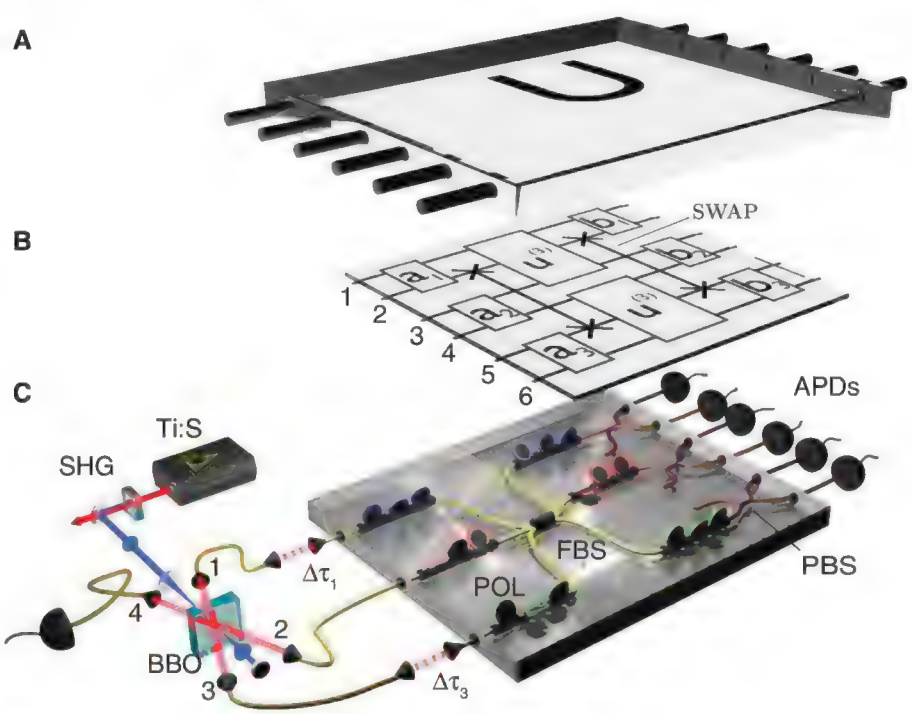

Fig. 1. Experimental scheme for boson sampling. (**A**) Both Alice and Bob (possessing classical and quantum resources, respectively) must sample the output distribution from some unitary, U. (**B**) Equivalent circuit. The orthogonal polarizations in each input spatial mode can be arbitrarily combined by the unitaries $a_1 \ldots a_3$. A multiport, $u^{(3)}$, interferes all modes of the same polarization; orthogonal polarizations are recombined by $b_1 \ldots b_3$. (**C**) Experiment. Photons are produced via downconversion in a nonlinear crystal (BBO) pumped by a frequency-doubled (SHG) laser (Ti:S) (*8*). Photon 4 acts as a trigger and photons 1 to 3 are inputs; 1 and 3 can be delayed or advanced with respect to photon 2 by $\Delta\tau_1$, $\Delta\tau_3$, respectively. Local unitaries $a_1 \ldots b_3$ are implemented with polarization controllers (POL); $u^{(3)}$ is implemented by a 3 × 3 nonpolarizing FBS; three polarizing fiber beam-splitters (PBS) output six spatial modes to single-photon avalanche diodes (APDs). The fiber beam-splitters work by evanescent coupling between multiple input fibers in close proximity.

[1]Centre for Engineered Quantum Systems, School of Mathematics and Physics, University of Queensland, Brisbane, Queensland 4072, Australia. [2]Centre for Quantum Computation and Communication Technology, School of Mathematics and Physics, University of Queensland, Brisbane, Queensland 4072, Australia. [3]Computer Science and Artificial Intelligence Laboratory, Massachusetts Institute of Technology, Cambridge, MA 02139, USA.

*To whom correspondence should be addressed. E-mail: m.a.broome@googlemail.com

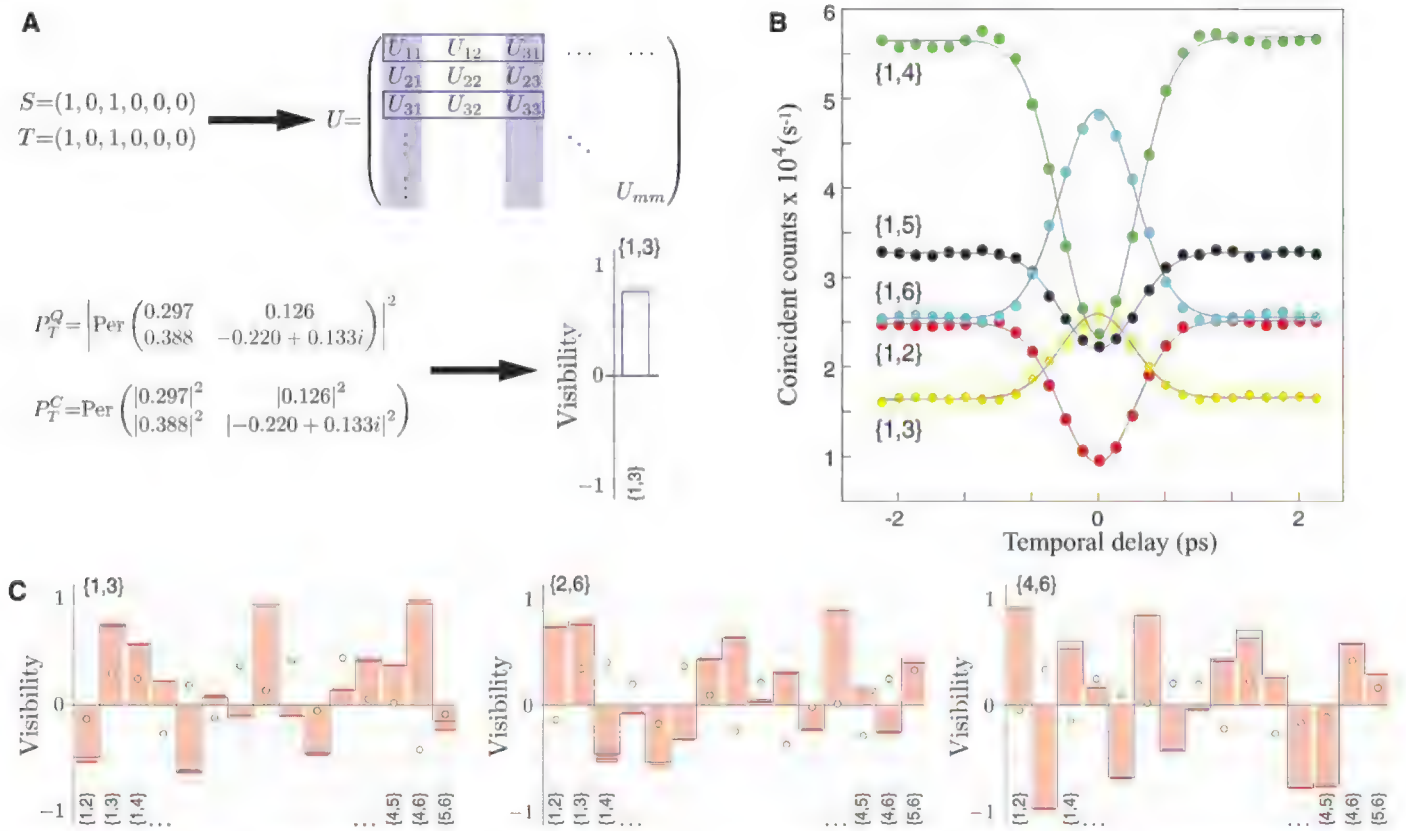

Fig. 2. Two-photon boson sampling. **(A)** Outline of Alice's technique to predict visibilities from the unitary evolution U (*8*). For photons input and output in modes 1 and 3, her prediction is given by the bar at bottom right; its uncertainty, obtained by 10 separate characterizations of the unitary, is represented by the shaded box on top of the bar. **(B)** Two-photon quantum interferences: the five output combinations {1,*m*} for the input configuration of {1,5}. Errors are smaller than marker size, and the solid blue lines are Gaussian fits used to calculate the visibility from Eq. 1. **(C)** Alice's predictions (blue line envelope) and Bob's measurements (orange bars) of two-photon visibilities. Input configurations are shown at the top left of each panel; output modes are labeled at the plot bottom. Errors are given by light blue and dark red boxes at the extremes of each data set. Yellow circles are the visibility predictions, given coherent input states.

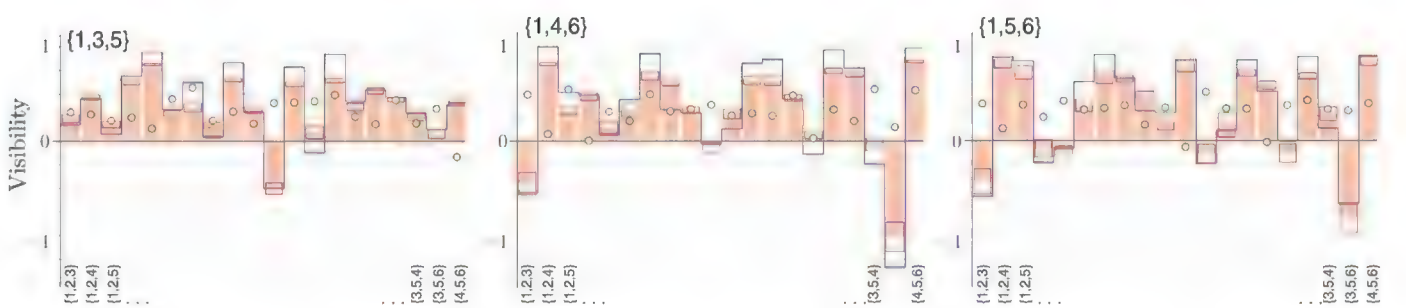

Fig. 3. Three-photon boson sampling. Alice's predictions (blue line envelope) and Bob's measurements (orange bars) for three-photon visibilities are shown. Labels, errors, and symbols are as defined in Fig. 2C).

Bob, on the other hand, experimentally prepares the n-photon Fock state $|t_1,...,t_m\rangle$. After injecting the desired input to the circuit, he determines the probability of the scattering event T by projecting onto its corresponding state using single-photon detectors connected to a coincidence-counting logic. We prepared near–single-photon Fock states via spontaneous parametric downconversion in a nonlinear crystal [Fig. 1C, and for further details, see section S2 (*8*)]. Once the photons pass through the network, they are detected by single-photon avalanche diodes. The boson sampling protocol measures the frequency of output events; i.e., raw coincident photon counts. These, however, are strongly affected by differences in efficiency between photon counters, an effect that can be removed by measuring nonclassical interference visibility instead

$$V_T = \frac{P_T^C - P_T^Q}{P_T^C} \quad (1)$$

where P_T^Q and P_T^C are the quantum and classical probabilities for the output configuration T measured for completely indistinguishable and distinguishable photons, respectively. Distinguishable statistics are obtained by introducing a temporal delay, $\Delta\tau$, between the input photons. When all photons are delayed by significantly more than their respective coherence lengths, L, true two-photon quantum interference cannot occur. Figure 2A outlines the technique Alice uses to predict the visibility from the unitary evolution U. For $n = 2$, high count rates mean that 27 samples of the output T were taken as the temporal delay was changed between the two input photons

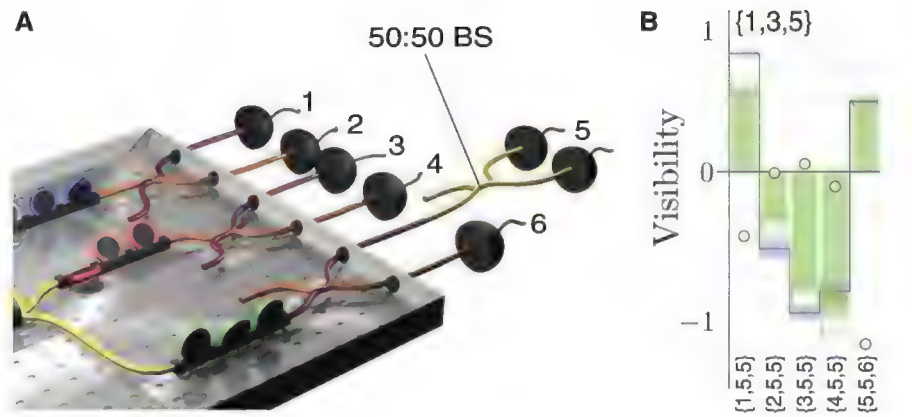

Fig. 4. Three-photon boson sampling with colliding outputs. **(A)** Number resolution was achieved with a 50:50 FBS in mode 5 and an additional detector. An imperfect splitting ratio for this FBS impedes only the effective efficiency of our number-resolving scheme (*10*, *11*). **(B)** For an input configuration {1,3,5}, and measuring two photons in output 5, the solid blue-line envelope shows Alice's predictions; the green bars are Bob's measured visibilities. Labels, errors, and symbols are as defined in Fig. 2C.

(*9*). For $n = 3$, where we used three of the photons from a four-photon state, low count rates mean that only three measurements were taken to avoid optical misalignment and the signal drift that occurs over necessarily long experimental runtimes. Therefore, for $n = 2$, the visibilities are calculated from the fitted Gaussian curves (Fig. 2B); for $n = 3$, the probabilities P_T^C are obtained from just two measurement settings: (i) $P_T^C = \{-\Delta\tau_\infty, 0, \Delta\tau_\infty\}$ and (ii) $P_T^C = \{\Delta\tau_\infty, 0, -\Delta\tau_\infty\}$, where $\{\tau_1, \tau_2, \tau_3\}$ are the temporal delays of photons 1, 2, and 3 with respect to photon 2, and $\Delta\tau_\infty >> L/c$. P_T^C is calculated as the average of these two probabilities to account for optical misalignment. Accordingly, P_T^Q is obtained with a single measurement of the output frequencies for completely indistinguishable photons, given by the delays {0,0,0}.

Figure 2C shows Alice's predictions and Bob's measurements for $n = 2$. We compare their results using the average L_1-norm distance per output configuration, $\mathcal{L}_1 = \frac{1}{C(m,n)} \sum_T |V_T^A - V_T^B|$, where $C(m,n)$ is the binomial coefficient [section S3 (*8*)]. We find excellent agreement between Alice and Bob, with the average across these three configurations being $\overline{\mathcal{L}}_1 = 0.021 \pm 0.001$. Next we show that if Alice uses her classically powerful resources, such as coherent states from a laser [section S4 (*8*)], to perform an analogous experiment to Bob's, she will not obtain the same results. Her classical predictions, given by the yellow circles in Fig. 2C, are markedly different from Bob's quantum measurements, with $\mathcal{L}_1 = 0.548 \pm 0.006$. This large, statistically significant disagreement highlights the fact that Bob is accurately sampling from a highly nonclassical distribution.

Figure 3 shows the results for $n = 3$: There is a larger average distance between Alice and Bob's distributions, $\overline{\mathcal{L}}_1 = 0.122 \pm 0.025$, and consequently a smaller distance between Alice's classical predictions and Bob's measurements, $\overline{\mathcal{L}}_1 = 0.358 \pm 0.086$. We attribute these changes chiefly to the increased ratio of higher-order photon emissions in the three-photon input as compared with the two-photon case [section S5 (*8*)]. Having tested all possible noncolliding output configurations (that is, one photon per output-mode), we also tested colliding configurations, with two photons per output-mode. This requires photon-number resolution (*10*, *11*), using the method shown in Fig. 4A. The results in Fig. 4B show agreement between Alice's predictions and Bob's measurements similar to the noncolliding case, $\mathcal{L}_1 = 0.153 \pm 0.012$, and a much larger distance between Alice's classical predictions and Bob's measurements, $\mathcal{L}_1 = 0.995 \pm 0.045$. The latter is expected because two-photon outputs are correspondingly rarer in the classical distribution.

These results confirm that the $n = 2$ and $n = 3$ photon scattering amplitudes are indeed given by the permanents of submatrices generated from U. The small differences, larger for $n = 3$ than $n = 2$, between Alice's Fock-state predictions and Bob's measurement results are expected, because Alice's calculations are for indistinguishable Fock-state inputs, and Bob does not actually have these. The conditioned outputs from downconversion are known to have higher-order terms; that is, a small probability of producing more than one photon per mode [section S5 and fig. S1 (*8*)], and are also spectrally entangled, leading to further distinguishability. Spectrally mismatched detector responses can alter the observed signals because of contributions from the immanent (*12*), of which the determinant and permanent are special cases. Because of flat spectral responses, we can rule this out in our experiment.

Strong evidence against the ECT thesis will come from demonstrating boson sampling with a larger-sized system, in which Bob's experimental sampling is far faster than Alice's calculation and classical verification is still barely possible; according to (*4*), this regime is on the order of $n = 20$ to $n = 30$ photons in a network with $m >> n$ modes. This is beyond current technologies, but rapid improvements in efficient photon detection (*13*, *14*), low-loss (*15*, *16*) and reconfigurable (*17*, *18*) integrated circuits, and improved photon sources (*19*) are highly promising. Boson sampling has also been proposed using the phononic modes of an ion trap (*20*).

An important open question remains as to the practical robustness of large implementations. Unlike the case of universal quantum computation, there are no known error correction protocols for boson sampling, or indeed for any of the models of intermediate quantum computation, such as deterministic quantum computing with one qubit (DQC1) (*21*, *22*), temporally unstructured quantum computation (IQP) (*23*), or permutational quantum computing (PQC) (*24*). These intermediate models have garnered much attention in recent years, both because of the inherent questions they raise about quantum advantage in computing and because some of them can efficiently solve problems believed to be classically intractable; for example, DQC1 has been applied in fields that range from knot theory (*25*) to quantum metrology (*26*). A recent theoretical study posits that photonic boson sampling retains its computational advantage even in the presence of loss (*27*). Our experimental results are highly promising in regard to the robustness of boson sampling, finding good agreement even with clearly imperfect experimental resources.

References and Notes

1. P. Shor, in *Proceedings of the 35th Annual Symposium on Foundations of Computer Science* (IEEE Computer Society Press, Los Alamitos, CA, 1994), pp. 124–134.
2. P. C. W. Davies, *Fluct. Noise Lett.* **7**, C37 (2007).
3. L. Valiant, *Theor. Comput. Sci.* **8**, 189 (1979).
4. S. Aaronson, A. Arkhipov, in *Proceedings of the ACM Symposium on Theory of Computing* (ACM, New York, 2011), pp. 333–342.
5. S. Rahimi-Keshari *et al.*, http://arxiv.org/abs/1210.6463 (2012).
6. M. Jerrum, A. Sinclair, E. Vigoda, *J. ACM* **51**, 671 (2004).
7. S. Scheel, http://arxiv.org/pdf/quant-ph/0406127.pdf (2004).
8. Materials and methods are available as supplementary materials on *Science* Online.
9. C. K. Hong, Z. Y. Ou, L. Mandel, *Phys. Rev. Lett.* **59**, 2044 (1987).
10. H. Paul, P. Törmä, T. Kiss, I. Jex, *Phys. Rev. Lett.* **76**, 2464 (1996).
11. P. Kok, S. L. Braunstein, *Phys. Rev. A* **63**, 033812 (2001).
12. S. Tan, Y. Gao, H. de Guise, B. Sanders, http://arxiv.org/abs/1208.5677 (2012).
13. A. E. Lita, A. J. Miller, S. W. Nam, *Opt. Express* **16**, 3032 (2008).
14. D. H. Smith *et al.*, *Nat. Commun.* **3**, 625 (2012).
15. J. O. Owens *et al.*, *New J. Phys.* **13**, 075003 (2011).
16. A. Peruzzo *et al.*, *Science* **329**, 1500 (2010).
17. P. Shadbolt *et al.*, *Nat. Photonics* **6**, 45 (2012).
18. B. Metcalf *et al.*, *Nat. Commun.* **4**, 1365 (2013).
19. A. Dousse *et al.*, *Nature* **466**, 217 (2010).
20. H.-K. Lau, D. F. V. James, *Phys. Rev. A* **85**, 062329 (2012).

21. A. Datta, A. Shaji, C. M. Caves, *Phys. Rev. Lett.* **100**, 050502 (2008).
22. B. P. Lanyon, M. Barbieri, M. P. Almeida, A. G. White, *Phys. Rev. Lett.* **101**, 200501 (2008).
23. M. J. Bremner, R. Jozsa, D. J. Shepherd, *Proc. R. Soc. London Ser. A* **467**, 459 (2011).
24. S. Jordan, *Quantum Inf. Comput.* **10**, 470 (2010).
25. P. Shor, S. Jordan, *Quantum Inf. Comput.* **8**, 681 (2008).
26. S. Boixo, R. D. Somma, *Phys. Rev. A* **77**, 052320 (2008).
27. P. P. Rohde, T. C. Ralph, *Phys. Rev. A* **85**, 022332 (2012).

Acknowledgments: We thank R. Fickler for help with characterization; M. de Almeida, D. Biggerstaff, and G. Gillett for experimental assistance; and A. Arkhipov, M. Bremner, and T. Rudolph for discussions. This work was supported in part by the Australian Research Council's Federation Fellow program (grant FF0668810), the Centre for Engineered Quantum Systems (grant CE110001013), and the Centre for Quantum Computation and Communication Technology (grant CE110001027); the University of Queensland Vice-Chancellor's Senior Research Fellowship program; NSF grant no. 0844626 and a Science and Technology Centre grant; a Defense Advanced Research Projects Agency Young Faculty Award grant; a TIBCO Chair; and a Sloan Fellowship.

Supplementary Materials

www.sciencemag.org/cgi/content/full/science.1231440/DC1
Supplementary Text
Fig. S1
Eqs. S1 to S12
References (*28*–*33*)

12 October 2012; accepted 3 December 2012
Published online 20 December 2012;
10.1126/science.1231440

Boson Sampling on a Photonic Chip

Justin B. Spring,[1]* Benjamin J. Metcalf,[1] Peter C. Humphreys,[1] W. Steven Kolthammer,[1] Xian-Min Jin,[1,2] Marco Barbieri,[1] Animesh Datta,[1] Nicholas Thomas-Peter,[1] Nathan K. Langford,[1,3] Dmytro Kundys,[4] James C. Gates,[4] Brian J. Smith,[1] Peter G. R. Smith,[4] Ian A. Walmsley[1]*

Although universal quantum computers ideally solve problems such as factoring integers exponentially more efficiently than classical machines, the formidable challenges in building such devices motivate the demonstration of simpler, problem-specific algorithms that still promise a quantum speedup. We constructed a quantum boson-sampling machine (QBSM) to sample the output distribution resulting from the nonclassical interference of photons in an integrated photonic circuit, a problem thought to be exponentially hard to solve classically. Unlike universal quantum computation, boson sampling merely requires indistinguishable photons, linear state evolution, and detectors. We benchmarked our QBSM with three and four photons and analyzed sources of sampling inaccuracy. Scaling up to larger devices could offer the first definitive quantum-enhanced computation.

Universal quantum computers require physical systems that are well isolated from the decohering effects of their environment, while at the same time allowing precise manipulation during computation. They also require qubit-specific state initialization, measurement, and generation of quantum correlations across the system (*1*–*4*). Although there has been substantial progress in proof-of-principle demonstrations of quantum computation (*5*–*8*), simultaneously meeting these demands has proven difficult. This motivates the search for schemes that can demonstrate quantum-enhanced computation under more favorable experimental conditions. Investigating the space between classical and universal quantum computers has attracted broad interest (*9*–*11*).

Boson sampling has recently been proposed as a specific quantum computation that is more efficient than its classical counterpart but only requires indistinguishable bosons, low decoherence linear evolution, and measurement (*12*). The distribution of bosons that have undergone a unitary transformation U is thought to be exponentially hard to sample from classically (*12*). The probability amplitude of obtaining a certain output is directly proportional to the permanent of a corresponding submatrix of U (*13*). The permanent expresses the wave function of identical bosons, which are symmetric under exchange (*14*, *15*); in contrast, the Slater determinant expresses the wave function of identical fermions, which are antisymmetric under exchange. Whereas determinants can be evaluated efficiently, permanents have long been believed to be hard to compute (*16*); the best-known algorithm scales exponentially with the size of the matrix.

One can envision a race between a classical and a quantum machine to sample the boson distribution given an input state and U. The classical machine would evaluate at least part of the probability distribution, which requires the analysis of matrix permanents. An ideal quantum boson-sampling machine (QBSM) instead creates indistinguishable bosons, physically implements U, and records the outputs. Although the QBSM is not believed to efficiently estimate any individual matrix permanent, for a sufficiently large system it is expected to beat the classical computer in sampling over the entire distribution (*12*).

Photonics is a natural platform to implement boson sampling because sources of indistinguishable photons are well developed (*17*), and integrated optics offers a scalable route to low decoherence linear transformations over many modes (*18*). Such circuits can be rapidly reconfigured to sample from a user-defined operation (*19*, *20*). Importantly, boson sampling requires neither nonlinearities nor on-demand entanglement, which are substantial challenges in photonic universal quantum computation (*21*). This clears the way for experimental boson sampling with existing photonic technology, building on the extensively studied two-photon Hong-Ou-Mandel interference effect (*22*).

A QBSM (Fig. 1) samples the output distribution of a multiparticle bosonic quantum state $|\Psi_{out}\rangle$, prepared from a specified initial state $|\mathbf{T}\rangle$ and linear transformation Λ. Unavoidable losses in the system imply Λ will not be unitary, although lossy QBSMs can still surpass classical computation (*12*, *23*). A trial begins with the input state $|\mathbf{T}\rangle = |T_1 \ldots T_M\rangle \propto \Pi_{i=1}^{M} (\hat{a}_i^\dagger)^{T_i} |0\rangle$, which describes $N = \sum_{i=1}^{M} T_i$ particles distributed in M input modes in the occupation-number representation. The output state $|\Psi_{out}\rangle$ is generated according to the linear map between input and output mode creation operators $\hat{a}_i^\dagger = \sum_{j=1}^{M} \mathbf{\Lambda}_{ij} \hat{b}_j^\dagger$, where $\mathbf{\Lambda}$ is an $M \times M$ matrix. Lastly, the particles in each of the M output modes are counted. The

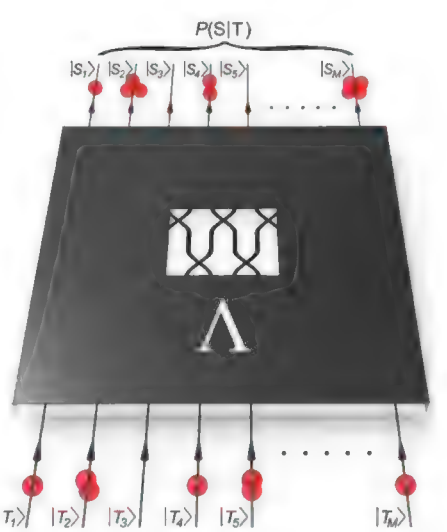

Fig. 1. Model of quantum boson sampling. Given a specified initial number state $|\mathbf{T}\rangle = |T_1 \ldots T_M\rangle$ and linear transformation $\mathbf{\Lambda}$, a QBSM efficiently samples from the distribution $P(\mathbf{S}|\mathbf{T})$ of possible outcomes $|\mathbf{S}\rangle = |S_1 \ldots S_M\rangle$.

[1]Clarendon Laboratory, Department of Physics, University of Oxford, Oxford OX1 3PU, UK. [2]Department of Physics, Shanghai Jiao Tong University, Shanghai 200240, PR China. [3]Department of Physics, Royal Holloway, University of London, London TW20 0EX, UK. [4]Optoelectronics Research Centre, University of Southampton, Southampton SO17 1BJ, UK.

*To whom correspondence should be addressed. E-mail: j.spring1@physics.ox.ac.uk (J.B.S.); i.walmsley1@physics.ox.ac.uk (I.A.W.)

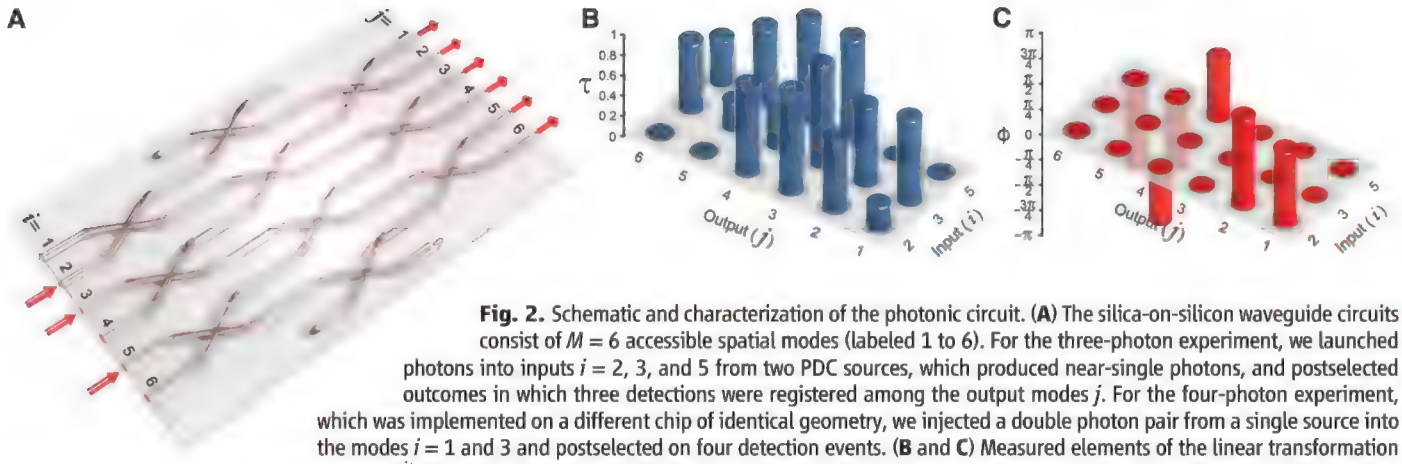

Fig. 2. Schematic and characterization of the photonic circuit. (**A**) The silica-on-silicon waveguide circuits consist of $M = 6$ accessible spatial modes (labeled 1 to 6). For the three-photon experiment, we launched photons into inputs $i = 2$, 3, and 5 from two PDC sources, which produced near-single photons, and postselected outcomes in which three detections were registered among the output modes j. For the four-photon experiment, which was implemented on a different chip of identical geometry, we injected a double photon pair from a single source into the modes $i = 1$ and 3 and postselected on four detection events. (**B** and **C**) Measured elements of the linear transformation $\Lambda_{ij} = \tau_{ij}e^{i\phi_{ij}}$ linking the input mode i to the output mode j of our three-photon apparatus. The circuit geometry dictates that several τ_{ij} are zero, and our phase-insensitive input states and detection methods imply only six nonzero ϕ_{ij}. Only relative values were needed because of postselection, so we rescaled each row of τ so that its maximum value is unity.

probability of a particular measurement outcome $|\mathbf{S}\rangle = |S_1 \ldots S_M\rangle$ is given by

$$P(\mathbf{S}|\mathbf{T}) = |\langle \mathbf{S}|\Psi_{out}\rangle|^2 = \frac{|\mathrm{Per}(\mathbf{\Lambda}^{(\mathbf{S},\mathbf{T})})|^2}{\prod_{j=1}^{M} S_j! \prod_{i=1}^{M} T_i!} \quad (1)$$

where the $N \times N$ submatrix $\mathbf{\Lambda}^{(\mathbf{S},\mathbf{T})}$ is obtained by keeping S_j copies of the j^{th} column (and T_i copies of the i^{th} row) of $\mathbf{\Lambda}$ (*13*).

Our QBSM consists of sources of indistinguishable single photons, a multiport linear optical circuit, and single-photon counting detectors. Two parametric down-conversion (PDC) pair sources (*24*) were used to inject up to four photons into a silica-on-silicon integrated photonic circuit, fabricated by ultraviolet laser writing (*19*, *25*). The circuit (Fig. 2A) consists of $M = 6$ input and output spatial modes coupled by a network of 10 beam splitters (*18*). The output state was measured with single-photon avalanche photodiodes on each mode. We only considered outcomes in which the number of detections equals the intended number of input photons (*13*).

Our central result of three- and four-boson sampling is shown in Fig. 3. In the first case, we repeatedly injected three photons in the input state $|\mathbf{T}\rangle = |011010\rangle$, monitored all outputs, and collected all threefold coincident events. In the four-photon experiment, we used the input $|\mathbf{T}\rangle = |202000\rangle$ and recorded all fourfold events (*26*). For each experiment, the measured relative frequencies P_S^{exp} for every allowed outcome $|\mathbf{S}\rangle$ are shown along with their observed statistical variation. The corresponding theoretical P_S^{th} values, calculated by using the right-hand side of Eq. 1, are shown along with their uncertainties arising from the characterization of $\mathbf{\Lambda}$, described below.

We reconstructed $\mathbf{\Lambda}$ with a series of one- and two-photon transmission measurements to determine its complex-valued elements $\Lambda_{ij} = \tau_{ij}e^{i\phi_{ij}}$ (*27*). The characterization results for the circuit used in the three-photon experiment are shown in Fig. 2, B and C. To obtain the magnitude τ_{ij}, single photons were injected in mode i. The probability of a subsequent detection in mode j is given by $P_1(j,i) = |\Lambda_{ij}|^2 = \tau_{ij}^2$. The phases ϕ_{ij} were determined from two-photon quantum interference measurements. The probability that a photon is detected in each of modes j_1 and j_2

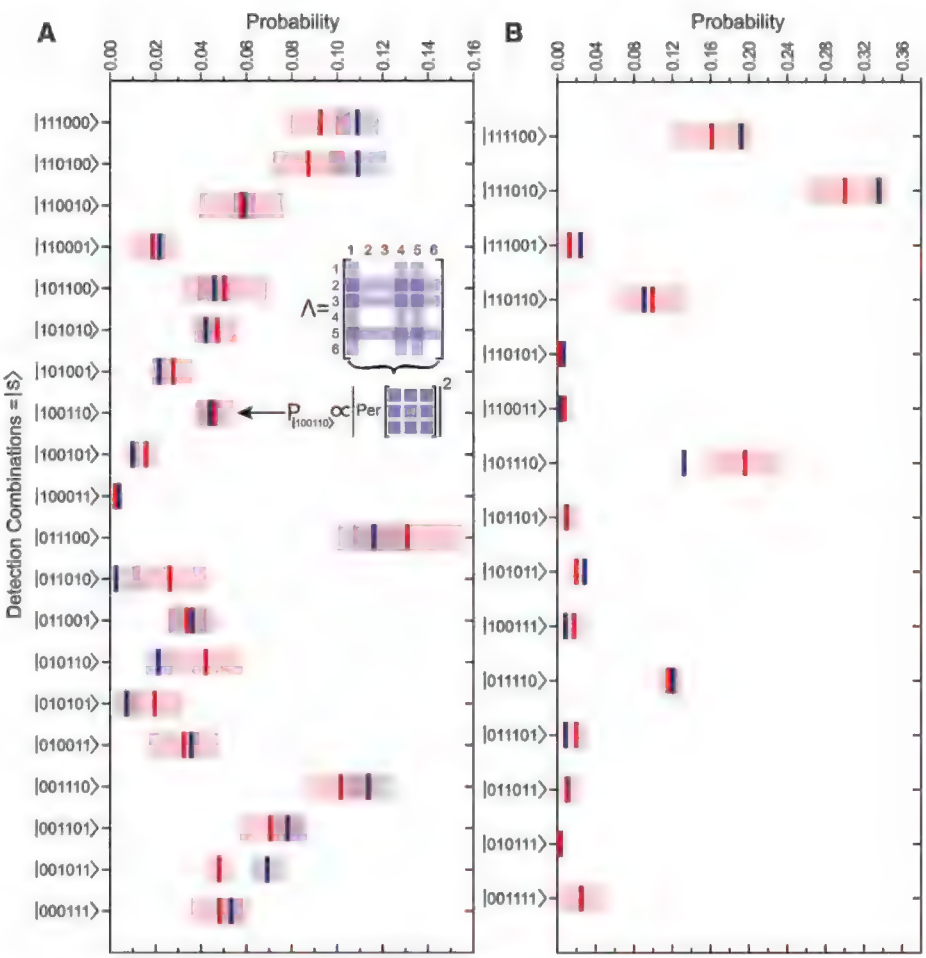

Fig. 3. Boson-sampling results. The measured relative frequencies $\mathbf{P}^{exp}$ of outcomes in which the photons were detected in distinct modes are shown in red for (**A**) three- and (**B**) four-photon experiments. Each data set was collected over 160 hours, and statistical variations in counts are shown by the red shaded bars. The theoretical distributions $\mathbf{P}^{th}$ (blue) are obtained from the permanents of submatrices constructed from the full transformation $\mathbf{\Lambda}$, as depicted in the inset. The blue error bars arise from uncertainties in the characterization of $\mathbf{\Lambda}$.

when they are injected in modes i_1 and i_2 is given by $P_2(j_1,j_2,i_1,i_2) = |\Lambda_{i_1 j_1}\Lambda_{i_2 j_2} + \Lambda_{i_2 j_1}\Lambda_{i_1 j_2}|^2$. This expression was used to find the relevant phases ϕ_{ij} given the previously determined magnitudes τ_{ij} (*13*).

To analyze the performance of our QBSM, we compared our results to an ideal machine. We quantified the match of two sets of relative frequencies $\mathbf{P}^{(1)}$ and $\mathbf{P}^{(2)}$ by calculating the L_1 distance $d^{(N)}(\mathbf{P}^{(1)},\mathbf{P}^{(2)}) = \frac{1}{2}\sum_S |P_S^{(1)} - P_S^{(2)}|$, where N denotes the number of photons in a sample (*28*). Identical and maximally dissimilar distributions correspond to $d = 0$ and $d = 1$, respectively. For our experiments, we calculated $d^{(N)}(\mathbf{P}^{exp},\mathbf{P}^{th})$ to give $d^{(3)} = 0.094 \pm 0.014$ and $d^{(4)} = 0.097 \pm 0.004$, where errors arise solely from the experimental uncertainty represented by the red shaded bars in Fig. 3. Even in an ideal QBSM with perfect state preparation and detection, the statistical variations result in nonzero d. When we substituted for our experimental data a Monte Carlo sampling of $\mathbf{P}^{th}$ with sample size equivalent to our experiments, we instead calculated $d^{(3)} = 0.043 \pm 0.012$ and $d^{(4)} = 0.059 \pm 0.022$. This suggests that there are appreciable contributions to $d(\mathbf{P}^{exp},\mathbf{P}^{th})$ beyond statistical deviation.

Because of experimental limitations, our QBSM occasionally samples distributions other than $\mathbf{P}^{th}$. The dominant sources of this sampling inaccuracy in our experiment are multiphoton emission and partial distinguishability among the photons. In practice, all single-photon sources produce multiple photons with a finite probability (*17*). For our PDC sources, the output state is about $|00\rangle + \lambda|11\rangle + \lambda^2|22\rangle$, with $\lambda << 1$. Both single-photon and undesired multiphoton terms increase with λ. In our three-photon experiments, for example, multiphoton emission from the two PDC sources can lead to input states $|\mathbf{T}\rangle = |021010\rangle$ or $|012020\rangle$, which contribute to threefold coincident events if photons are lost or emerge in the same output mode. In addition, partial distinguishability of the photons contaminates the distribution sampled by the QBSM by mixing in one- and two-photon interference effects (*29*).

We formed a new distribution $\mathbf{P}^{mod}$ that accounts for the effects of multiphoton emission and photon distinguishability (*13*). The distance $d(\mathbf{P}^{exp},\mathbf{P}^{mod})$ shown by the green point (Fig. 4, A and B insets) was found to be consistent with the statistical variation resulting from a finite sample size, for both the three- and four-photon experiments. This suggests we have correctly identified and modeled the sources of inaccuracy. To investigate how the performance of our QBSM depends on λ and photon distinguishability, we calculated $d(\mathbf{P}^{mod},\mathbf{P}^{th})$ for a range of operating parameters (Fig. 4, C and D). In terms of λ, a clear trade-off is presented between data rate and inaccuracy because of multiphoton emission, which is an intrinsic consequence of using PDC sources. Improvement in photon indistinguishability increases the fidelity to the ideal machine and additionally is thought to enhance the computational power of a QBSM (*29*).

Our results demonstrate that boson sampling is related to the computation of matrix permanents, a problem believed to be classically hard. Our successful diagnosis of the source and magnitude of the principal sampling errors, as validated by a reduction in $d(\mathbf{P}^{exp},\mathbf{P}^{mod})$ to within the statistical variation of a perfect QBSM, will inform the design of next-generation devices. Although investigations into quantum-enhanced

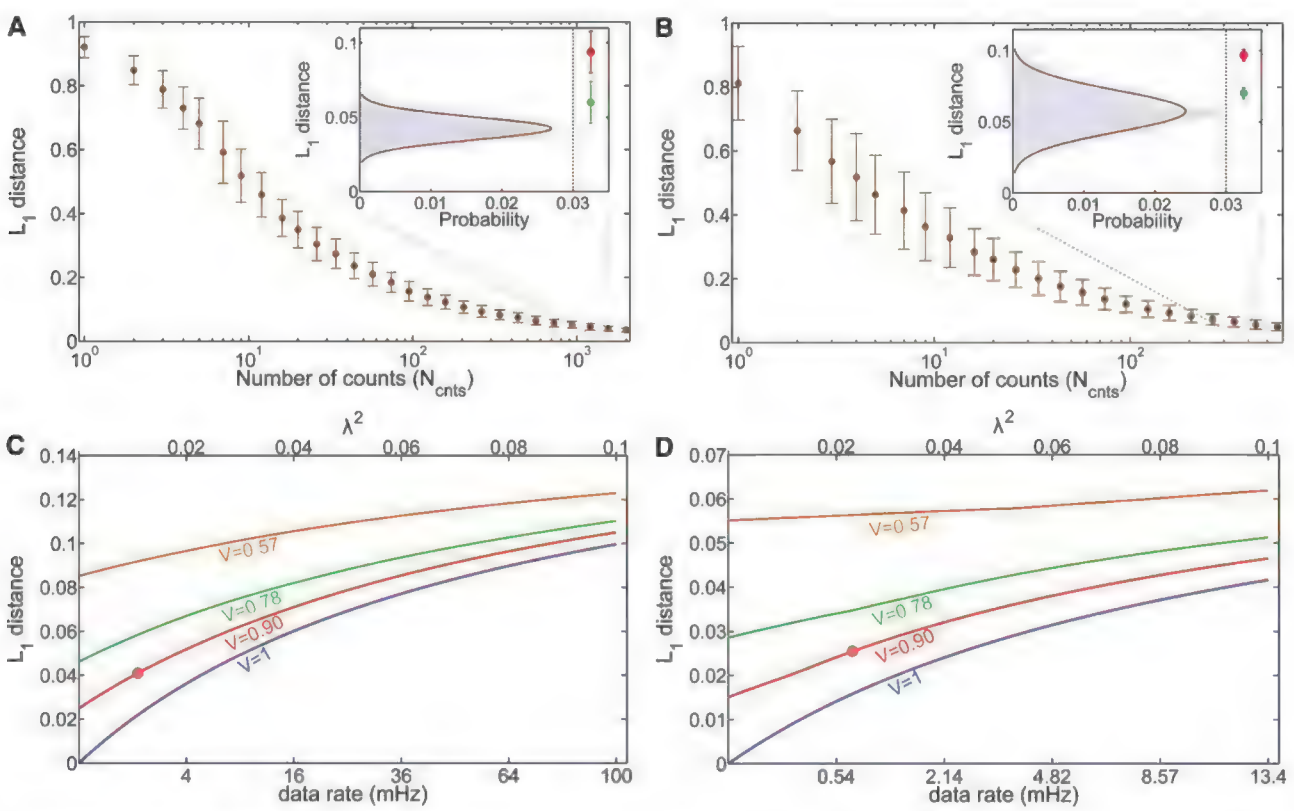

Fig. 4. Sampling accuracy. We consider several boson distributions: the experimental samples $\mathbf{P}^{exp}$, the ideal predictions of the matrix permanent $\mathbf{P}^{th}$, and the predictions of the full model $\mathbf{P}^{mod}$ that includes higher-order emission and photon distinguishability. The L_1 distance d between $\mathbf{P}^{th}$ and a Monte Carlo simulation of an ideal machine that samples $\mathbf{P}^{th}$ a finite number of times for our (**A**) three- and (**B**) four-photon cases. The errors in this case are solely a result of the finite number of samples collected by the ideal machine. (Insets) Histograms show the variation in d expected for a sample size corresponding to the 1421 and 405 counts collected in our three- and four-photon experiments. The distance $d(\mathbf{P}^{exp},\mathbf{P}^{th})$ (red) suggests an underlying systematic inaccuracy because it falls outside the range of outputs of an ideal machine indicated in the histogram. Our full model is validated by the distance $d(\mathbf{P}^{exp},\mathbf{P}^{mod})$ (green), which is consistent with statistical variation. The red and green dot positions correspond to the L_1 axis only. The predicted variation in $d(\mathbf{P}^{th},\mathbf{P}^{mod})$ is shown as a function of λ and the photon distinguishabilites, represented by the reduction in two-photon interference visibility V, for the (**C**) three- and (**D**) four-photon cases. Our experimental conditions are marked (red dot).

computation in the presence of errors is ongoing, it already appears that the boson-sampling model makes less stringent demands on device performance than universal photonic quantum computers (*12*, *23*, *29*). There is thus reason for optimism that ongoing advances in integrated photonics, such as reduced transmission loss, efficient number-resolving detectors (*30*), and multiplexed (*31*, *32*) or single-emitter (*17*) photon sources, will enable larger QBSMs that outperform classical computers. Beyond the specific boson-sampling problem, such a device would provide evidence for the computational power of quantum mechanics.

References and Notes

1. D. P. DiVincenzo, *Fortschr. Phys.* **48**, 771 (2000).
2. R. Raussendorf, H. J. Briegel, *Phys. Rev. Lett.* **86**, 5188 (2001).
3. M. A. Nielsen, *Phys. Lett. A* **308**, 96 (2003).
4. A. M. Childs, *Phys. Rev. Lett.* **102**, 180501 (2009).
5. P. Walther *et al.*, *Nature* **434**, 169 (2005).
6. C.-Y. Lu, D. E. Browne, T. Yang, J.-W. Pan, *Phys. Rev. Lett.* **99**, 250504 (2007).
7. B. P. Lanyon *et al.*, *Science* **334**, 57 (2011).
8. E. Lucero *et al.*, *Nat. Phys.* **8**, 719 (2012).
9. E. Knill, R. Laflamme, *Phys. Rev. Lett.* **81**, 5672 (1998).
10. S. P. Jordan, *Quant. Inf. Comput.* **10**, 470 (2010).
11. D. Shepherd, M. J. Bremner, *Proc. R. Soc. London Ser. A* **465**, 1413 (2009).
12. S. Aaronson, A. Arkhipov, "The computation complexity of linear optics," in *Proceedings of the 43rd Annual ACM Symposium on the Theory of Computing* (STOC'11), San Jose, CA, 6 to 8 June 2011 (Association for Computing Machinery, New York, 2011), pp. 333–342.
13. Materials and methods are available as supplementary materials on *Science* Online.
14. E. Caianiello, *Nuovo Cim.* **10**, 1634 (1953).
15. L. Troyansky, N. Tishby, "Permanent uncertainty: on the quantum evaluation of the determinant and the permanent of a matrix," in *Proceedings of Physics and Computation* (PhysComp 96), Boston, MA, 22 to 24 Nov 1996 (New England Complex Systems Institute, Cambridge, MA, 1996), pp. 314–318.
16. L. G. Valiant, *Theor. Comput. Sci.* **8**, 189 (1979).
17. M. D. Eisaman, J. Fan, A. Migdall, S. V. Polyakov, *Rev. Sci. Instrum.* **82**, 071101 (2011).
18. B. J. Metcalf *et al.*, *Nat. Commun.* **4**, 1356 (2012).
19. B. J. Smith, D. Kundys, N. Thomas-Peter, P. G. R. Smith, I. A. Walmsley, *Opt. Express* **17**, 264 (2009).
20. P. J. Shadbolt *et al.*, *Nat. Photonics* **6**, 45 (2011).
21. E. Knill, R. Laflamme, G. J. Milburn, *Nature* **409**, 46 (2001).
22. C. K. Hong, Z. Y. Ou, L. Mandel, *Phys. Rev. Lett.* **59**, 2044 (1987).
23. P. P. Rohde, T. C. Ralph, *Phys. Rev. A* **85**, 022332 (2012).
24. P. J. Mosley *et al.*, *Phys. Rev. Lett.* **100**, 133601 (2008).
25. D. O. Kundys, J. C. Gates, S. Dasgupta, C. Gawith, P. G. R. Smith, *IEEE Photon. Technol. Lett.* **21**, 947 (2009).
26. Eq. 1 is expected to hold for any $|S\rangle$ and $|T\rangle$; however, the classical hardness of sampling $P(S|T)$ is maximized when $S_i, T_i \in \{0,1\}$ for a given N and Λ.
27. A. Laing, J. L. O'Brien (2012), http://arxiv.org/abs/1208.2868v1.
28. A. Gilchrist, N. K. Langford, M. A. Nielsen, *Phys. Rev. A* **71**, 062310 (2005).
29. P. P. Rohde, *Phys. Rev. A* **86**, 052321 (2012).
30. T. Gerrits *et al.*, *Phys. Rev. A* **84**, 060301 (2011).
31. A. L. Migdall, D. Branning, S. Castelletto, *Phys. Rev. A* **66**, 053805 (2002).
32. J. Nunn *et al.* (2012), http://arxiv.org/abs/1208.1534v1.

Acknowledgments: We thank J. Nunn for valuable insights. This work was supported by the Engineering and Physical Sciences Research Council (EP/C013840/1, EP/H03031X/1, and EP/J000051/1), the European Commission project Q-ESSENCE (248095), the Royal Society, and the Air Force Office of Scientific Research (European Office of Aerospace Research and Development). X.M.J. and N.K.L. are supported by European Union Marie-Curie fellowships (PIIF-GA-2011-300820 and PIEF-GA-2010-275103). J.B.S. acknowledges support from the U.S. Air Force Institute of Technology. The views expressed in this article are those of the authors and do not reflect the official policy or position of the U.S. Air Force, Department of Defense, or the U.S. Government.

Supplementary Materials

www.sciencemag.org/cgi/content/full/science.1231692/DC1
Materials and Methods
Supplementary Text
References (*33*–*37*)

18 October 2012; accepted 3 December 2012
Published online 20 December 2012;
10.1126/science.1231692

Observation of Radiation Pressure Shot Noise on a Macroscopic Object

T. P. Purdy,[1,2]* R. W. Peterson,[1,2] C. A. Regal[1,2]

The quantum mechanics of position measurement of a macroscopic object is typically inaccessible because of strong coupling to the environment and classical noise. In this work, we monitor a mechanical resonator subject to an increasingly strong continuous position measurement and observe a quantum mechanical back-action force that rises in accordance with the Heisenberg uncertainty limit. For our optically based position measurements, the back-action takes the form of a fluctuating radiation pressure from the Poisson-distributed photons in the coherent measurement field, termed radiation pressure shot noise. We demonstrate a back-action force that is comparable in magnitude to the thermal forces in our system. Additionally, we observe a temporal correlation between fluctuations in the radiation force and in the position of the resonator.

In measuring the trajectory of an object at the scale of our everyday experience, we rarely consider the fundamental limitations imposed by quantum mechanics. Yet quantum mechanical effects are present even when monitoring the position of macroscopic objects, and these effects are expected to soon limit, for example, the precision of gravitational wave observatories (*1*). Imagine measuring the position of an object to an accuracy Δx. A momentum uncertainty of at least $\Delta p = \hbar/2\Delta x$ must then be present, where $\hbar$ is the reduced Planck's constant that appears in the Heisenberg uncertainty relation. This requisite momentum (or equivalently velocity) uncertainty adds position uncertainty at a later time. Thus, an observer must weigh pinpointing the location of the object against introducing quantum measurement back-action that obscures the subsequent motion.

For an optical position measurement, this quantum back-action is termed radiation pressure shot noise (RPSN) (*2*, *3*). A fluctuating force arises from, for instance, the recoil momentum transfer of randomly arriving photons (shot noise) reflecting off of an object. In the next-generation advanced gravitational wave observatories—such as the Laser Interferometer Gravitational Wave Observatory (LIGO) (*1*), Virgo, and the Kamioka Gravitational Wave Detector (KAGRA) (*4*)—RPSN is predicted to limit sensitivity, even with test masses of tens of kilograms. Ideas developed to circumvent quantum limits imposed by back-action include quadrature-squeezed light (*5*) and back-action evasion techniques (*4*, *6*). However, for typical objects, the scale of quantum back-action is small compared with thermal motion or classical probing noise. In this Report, we observe RPSN on a solid macroscopic (visible to the naked eye) mechanical resonator by using an optical interferometric measurement of its vibrational motion.

Figure 1A shows the canonical picture of a Heisenberg-limited continuous position measurement. The point at which the sum of the shot noise measurement imprecision (dashed line) and RSPN-induced displacement fluctuations (solid black line) are minimized is termed the standard quantum limit (SQL) (*7*, *8*). Here, the displacement spectral density from RPSN at the mechanical resonance frequency, ω_m, is $S_z^{SQL}(\omega_m) = \hbar/m\omega_m\Gamma_m$, where m and Γ_m are the resonator's mass and damping rate, respectively. This fundamental scale is equivalent to one-half of the resonator's quantum mechanical zero point motion, Z_{zp}. We also define P^{SQL}, the power required for a shot noise–limited measurement imprecision of $S_z^{SQL}(\omega_m)$. Even with other mechanical noise sources present [e.g., thermal motion (solid brown line in Fig. 1A)], quantum back-action may still play an important role if the optical power, P, is sufficiently larger than P^{SQL}.

Whereas shot noise is a ubiquitous measurement limitation, experimental signatures of RPSN

[1]JILA, University of Colorado and National Institute of Standards and Technology, Boulder, CO 80309, USA. [2]Department of Physics, University of Colorado, Boulder, CO 80309, USA.

*To whom correspondence should be addressed. E-mail: tpp@jila.colorado.edu

on solid objects have remained elusive. Mechanical effects of photon recoil are routinely studied in atomic physics [(*9*) and references therein], and a RPSN observation analogous to ours has been made using a dilute gas of ultracold atoms (*10*). A promising route to studying RPSN in solid objects involves experiments that achieve high optomechanical coupling to high-frequency, small (nanometer- to centimeter-scale) mechanical resonators. Using such resonators, groups have initiated searches for RPSN (*11*, *12*), observed classical analogs of RPSN (*13*), and predicted experimental signatures of RPSN (*14*–*16*). Back-action on a nanomechanical resonator has also been observed with the use of other measurement devices, such as single-electron transistors (*17*). Resonators have even been cooled with electromagnetic radiation to near their motional ground state, illustrating the capacity for dominant coherent optical forces (*18*–*20*). In these experiments, quantum back-action has thus far been limited to the scale of Z_{zp}, whereas in this Report, we demonstrate a strong back-action heating effect from RPSN. Additionally, in near–ground-state cooling experiments, correlations between shot noise and RPSN-driven mechanical motion are an important component of the observed optical spectra (*21*) and are responsible for the sideband asymmetry observed in (*22*).

Our optomechanical system consists of a silicon nitride membrane resonator inside of a Fabry-Perot optical cavity that is specially designed to operate at cryogenic temperatures (Fig. 1C) (*23*). Thompson *et al.* have shown that membrane motion can be coupled to a cavity through a dispersive interaction, where the cavity resonance frequency shifts as the membrane moves along the optical standing wave (*24*). This interaction imprints phase and amplitude modulation on transmitted laser light, allowing for readout of the membrane motion. In conjunction, the laser applies an optical gradient force to the membrane, pushing it toward higher optical intensity. Our membrane is a highly tensioned square plate with a 0.5-mm side length, 40-nm thickness, and an effective mass of ~7 ng. We operate in a helium flow cryostat with the resonator at a base temperature of 4.9 K, where intrinsic mechanical linewidths, $\Gamma_0/2\pi$, are typically less than 1 Hz. For the (2,2) mode oscillating at $\omega_m/2\pi = 1.55$ MHz, we achieve a maximum single-photon optomechanical coupling rate $g/2\pi = 16$ Hz.

We use two laser beams derived from the same 1064-nm source, both coupled to the same spatial mode of the cavity, but with orthogonal polarizations (Fig. 1C) (*13*, *14*). The half-planar, 5.1-mm-long cavity has a full linewidth $\kappa/2\pi \sim 1$ MHz, which varies slightly with the membrane position. The high-intensity "signal" beam is actively stabilized to the optical resonance. This beam provides the RPSN, and its transmitted intensity fluctuations constitute a record, which is partially obscured by optical loss, of the optical force on the resonator. The corresponding sensitive position measurement is wholly imprinted in the unrecorded phase quadrature. Additional phase noise from fluctuations in the cavity-laser detuning precludes shot noise–limited phase-quadrature detection (*23*). The much weaker "meter" beam is tuned to the red of the optical resonance imprinting the resonator's displacement spectrum on its transmitted intensity. Although its shot noise drive is much smaller, the meter beam provides optical Raman sideband cooling of the mechanical mode (*25*) to 1.7 mK. The optical damping

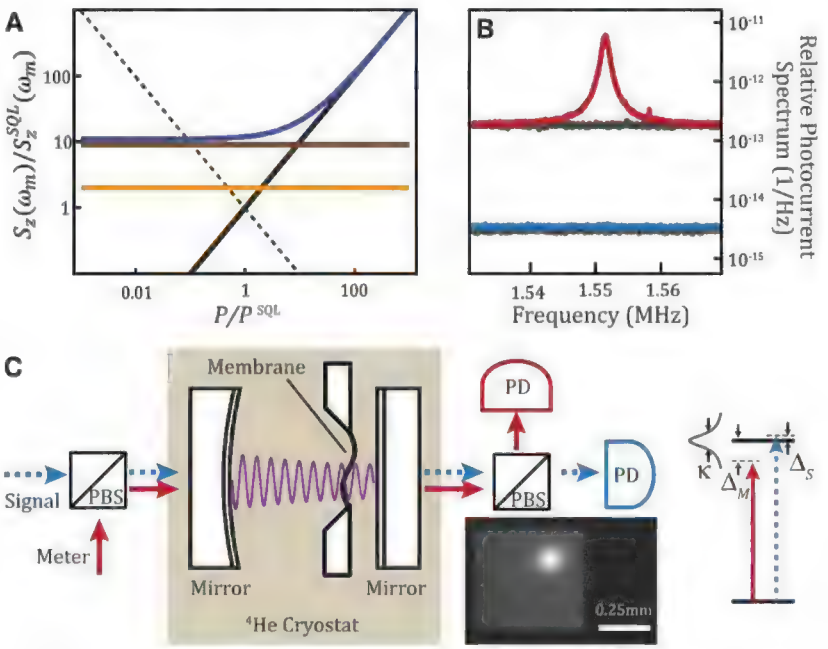

Fig. 1. **(A)** Canonical picture of continuous position measurement. RPSN (black), thermal motion (brown), and zero point motion (orange) combine to give the expected measurement result (blue). The dashed line represents the effective displacement noise from the shot noise–limited imprecision of an optical measurement. **(B)** Photocurrent spectra. The photocurrent spectral densities $S_{I_S}(\omega)/\bar{I}_S^2$ (blue) and $S_{I_M}(\omega)/\bar{I}_M^2$ (red), as well as the noise floors, including detector noise and the dominant shot noise (gray), are shown. **(C)** Experimental setup. Beams are combined and separated with polarizing beam splitters (PBS) and detected directly on photodetectors (PD). The inset photograph shows an in situ image of the square membrane and optical mode spot, with blue dashed lines indicating the nodes of the (2,2) mechanical mode. The inset diagram at right shows laser-cavity detunings.

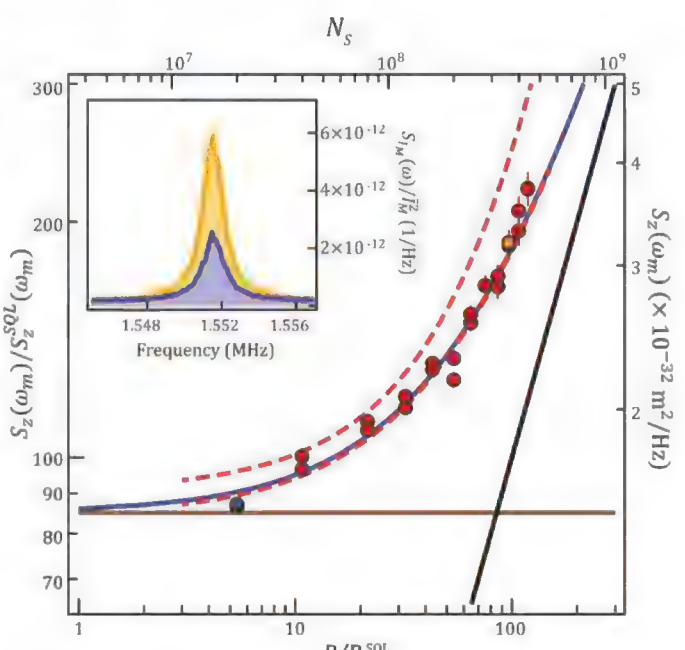

Fig. 2. Displacement spectrum measurements. Measured peak displacement spectral density (circles), thermal contribution (brown line), and expected RPSN contribution (black line) are shown. The blue curve represents the theoretical prediction for the sum of thermal motion and RPSN, and the dashed red curves are bounds on theoretical estimates, including systematic uncertainty in device parameters and the classical noise contribution. Device parameters: $g/2\pi = 16.1 \pm 0.3$ Hz, $\kappa/2\pi = 0.89$ MHz, $\Delta_S/2\pi = 2.0 \pm 0.5$ kHz, $\Delta_M/2\pi = 0.7$ MHz, $N_M = 7.0 \pm 0.3 \times 10^6$, $\omega_m/2\pi = 1.551$ MHz, $\Gamma_0/2\pi = 0.47$ Hz, and $\Gamma_m/2\pi = 1.43$ kHz. **(Inset)** Transmission spectra for $R_S = 0.056$ (blue) and $R_S = 1.0$ (orange), with corresponding points in the main plot highlighted in blue and orange.

greatly eases the requirements on the signal-beam-cavity detuning due to both parametric instabilities at positive detuning and the contamination of cross-correlation by thermal motion (*12*, *15*, *26*), but it does not change the sensitivity of the resonator to RPSN relative to thermal forces.

The effect of the optomechanical coupling on the resonator from a single laser (*25*, *27*) or multiple beams (*15*) has been well studied. The resonator's mechanical susceptibility is modified to include optomechanical damping and frequency shifts from each laser. Additionally, the effective phonon occupation, n_m, is modified. The optomechanical damping cools the resonator; RPSN increases the amplitude of motion. In equilibrium, a simple rate equation gives $n_m = (n_{th}\Gamma_0 + n_S\Gamma_S + n_M\Gamma_M)/\Gamma_m$. Here, n_{th} is the thermal phonon occupation; n_S and Γ_S (or n_M and Γ_M) are the effective bath temperature and optomechanical damping rate of the signal (or meter) laser. The total mechanical damping rate is $\Gamma_m = \Gamma_0 + \Gamma_S + \Gamma_M$. In our experiments $\Gamma_M >> \Gamma_0$ and Γ_S, whereas $\Delta_S \sim 0$ and $N_S >> N_M$, where Δ_S and N_S (or Δ_M and N_M) are the laser-cavity detuning and intracavity photon occupation of the signal (or meter) beam. RPSN dominates over thermal noise when the ratio of radiation to thermal forces $R_S = (C_S/n_{th})[1 + (2\omega_m/\kappa)^2]^{-1} > 1$, where $C_S = 4N_S g^2/\kappa\Gamma_0$ is the multiphoton cooperativity. We are able to reach this high-cooperativity regime ($C_S \sim 10^6$) due to the small mass, weak intrinsic damping, and cryogenic environment of our resonator.

The increase in phonon occupation resulting from RPSN is shown in Fig. 2. The meter beam transmission spectrum, $S_{I_M}(\omega)$ (Fig. 2, inset), shows a marked increase in spectral area, or equivalently, n_m as the measurement strength is increased to where $R_S \sim 1$. Here, the employed $N_S = 3.6 \times 10^8$ is equivalent to ~200 μW of detected optical power. The device shows good agreement with a theory of measurement back-action (Fig. 2, blue curve) based on independently measured device parameters. Because a separate meter beam is used to read out the mechanical motion, the measurement noise floor associated with these data are independent of the shot noise level of the signal beam, as depicted by the dashed line in Fig. 1A. The increased spectral density also includes a small contribution from classical radiation pressure noise. Taking into account the thermal motion and classical laser intensity noise, we can attribute at least 40% of the total displacement spectrum to RPSN at the maximum signal beam strength. We have also measured similar back-action heating on another device with smaller Γ_0 and lower classical intensity noise (fig. S5). The dashed curves of Fig. 2 represent bounds on the expected spectral densities accounting for systematic uncertainties in the device parameters and classical noise level (*26*). Another effect that might mimic RPSN is physical heating. To test for physical heating, we monitor the temperature of a higher-frequency, weakly optomechanically coupled mechanical mode where RSPN is negligible. We do not observe a large response from this mode, which indicates that the absorbed laser light causes a <10% increase in the bath temperature (fig. S4).

We next examine the temporal correlations between the signal and meter beam photocurrents (*14*, *15*). We compute the spectrum of the two-time cross-correlation function $S_{I_{SM}}(\omega) = \langle I_S^*(\omega) I_M(\omega)\rangle$, where $I(\omega)$ is the complex Fourier transform of the photocurrent $I(t)$, and the angle brackets represent an average over many realizations of the experiment. Thermal and other ambient motion, as well as measurement noise uncorrelated to the radiation pressure drive, are rejected by this technique, making it a powerful tool in understanding RPSN. In the limit $\Gamma_m << \kappa$, the correlation should reflect the Lorentzian response function of the optically damped resonator, driven by the locally white shot noise. In Fig. 3A, we show a cross-correlation measurement and, for reference, the product spectrum, $S_{I_S}(\omega) \times S_{I_M}(\omega)$. $S_{I_S}(\omega)$ and $S_{I_M}(\omega)$ for these data are shown in Fig. 1B. If the two beams are perfectly correlated, the cross-correlation and product spectra should coincide. However, an uncorrelated measurement background, dominated by the meter's shot noise and thermal motion, appears only on the product spectrum. Additionally, the imperfect detection efficiency leads to a loss of correlation. We measure a peak normalized correlation (the ratio of the red to black curve peaks in Fig. 3A) of $C(\omega_m) = |S_{I_{SM}}(\omega_m)|^2/S_{I_S}(\omega_m)S_{I_M}(\omega_m) = 0.14$. An estimate, ignoring classical noise and assuming $\Delta_S = 0$, is given by $C(\omega_m) = R_S/(1 + R_S) \times \kappa_R/\kappa \times \varepsilon_S = 0.15 \pm 0.02$, where $R_S/(1 + R_S) = 0.40 \pm 0.03$ is the fraction of $S_z(\omega_m)$ due to RPSN, $\kappa_R/\kappa = 0.59$ is the fraction of the light through the output port, and $\varepsilon_S = 0.63 \pm 0.03$ is the postcavity detection efficiency. By intentionally adding classical intensity noise that is much larger than shot noise to the signal laser, we demonstrate a (classical) normalized cross-correlation that approaches unity (Fig. 3B).

Figure 3C shows the phase of the correlation both with and without large classical intensity noise on the signal beam. Both show the 180° phase shift expected from the mechanical response. Importantly, we also expect a phase offset of $\arctan(2\omega_m/\kappa)$ between the classical noise–dominated drive and the shot noise–dominated drive (*15*, *26*). Measurements of this phase offset imply that 75% of the radiation pressure drive is from shot noise, in agreement with the directly measured classical noise range in $S_{I_S}(\omega)$.

If Δ_S is not zero, the cross-correlation will be distorted. Mechanical motion transduced directly onto I_S may constructively or destructively add to the RPSN correlation, depending on the sign of Δ_S. By fitting the correlation data to the expected line shape (*26*), we estimate $\Delta_S = 0.0003\kappa$, implying only a 3% contribution to $S_{I_{SM}}(\omega_m)$ from thermal motion. We have also performed an experimental test to demonstrate the rejection of ambient motion from the cross-correlation spectrum (Fig. 3B). Here, we mechanically excite

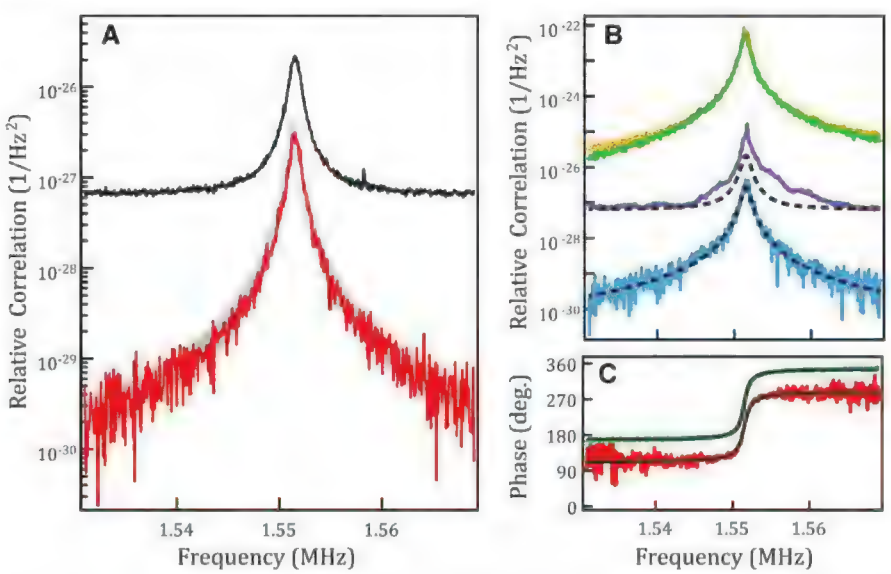

Fig. 3. Cross-correlation measurements. **(A)** $|S_{I_{SM}}(\omega)/\bar{I}_S\bar{I}_M|^2$ measured (red) and expected, including systematic uncertainty (gray), and $S_{I_S}(\omega)/\bar{I}_S^2 \times S_{I_M}(\omega)/\bar{I}_M^2$ (black). Parameters are as listed in the Fig. 2 caption, except $\Delta_S/2\pi = 300 \pm 100$ Hz, $g/2\pi = 14.8 \pm 0.4$ Hz, and $N_S = 3.2 \times 10^8$. The resolution bandwidth is 50 Hz. **(B)** $|S_{I_{SM}}(\omega)/\bar{I}_S\bar{I}_M|^2$ (green) and $S_{I_S}(\omega)/\bar{I}_S^2 \times S_{I_M}(\omega)/\bar{I}_M^2$ (orange), where classical intensity noise at the level of ~40 times the shot noise is added to the signal beam, raising the overall signal levels by the same factor. $|S_{I_{SM}}(\omega)/\bar{I}_S\bar{I}_M|^2$ (blue) and $S_{I_S}(\omega)/\bar{I}_S^2 \times S_{I_M}(\omega)/\bar{I}_M^2$ (purple), where the membrane is driven with excess mechanical noise. Fits to the data from (A) are displayed for reference (dashed black curves), showing that despite increased mechanical motion (purple curve above the top dashed curve), the correlation remains unchanged (blue curve coinciding with the lower dashed curve). **(C)** Phase of the cross-correlation, with classical intensity noise on signal beam (green) and without added noise (red). Black curves are fits to the data.

the membrane with a white noise–driven piezoelectric actuator (purple trace exceeds dashed curve in Fig. 3B), which also drives mechanical modes of the mirrors and supports, leading to extra modulation. However, the cross-correlation spectrum (blue trace) remains unchanged, equal to the unperturbed spectrum (dashed curve), implying that very little of the ambient motion is transduced.

The cross-correlation can also be viewed as evidence that we have made a quantum nondemolition (QND) measurement of the intracavity photon fluctuations of the signal beam (*14*, *28*). Here, the membrane acts as the measurement device, with its state of motion recording the photon fluctuations over the band of the mechanical resonance. The correlation C is equivalent to a state preparation fidelity for a nonideal QND measurement (*29*). Further, it has been shown that frequency-dependent ponderomotive squeezing of the signal beam quantum noise is possible (*30*) and has recently been demonstrated in an atomic gas cavity optomechanical system (*31*). For our current laser configuration ($\Delta_S = 0$), we do not expect to see squeezing in the detected amplitude quadrature. However, our device parameters are sufficient to realize much stronger squeezing than has previously been demonstrated, limited mainly by optical loss. Our observations open the door to realizing position measurement near the SQL if residual thermal noise and excess cavity-laser phase noise can be eliminated with improved devices or a colder base temperature.

References and Notes

1. G. M. Harry, *Class. Quantum Gravity* **27**, 084006 (2010).
2. V. Braginsky, S. Vyatchanin, *Sov. Phys. JETP* **47**, 433 (1978).
3. C. M. Caves, *Phys. Rev. D Part. Fields* **23**, 1693 (1981).
4. K. Somiya, *Class. Quantum Gravity* **29**, 124007 (2012).
5. H. J. Kimble, Y. Levin, A. B. Matsko, K. S. Thorne, S. P. Vyatchanin, *Phys. Rev. D Part. Fields* **65**, 022002 (2001).
6. V. B. Braginsky, Y. I. Vorontsov, K. S. Thorne, *Science* **209**, 547 (1980).
7. J. D. Teufel, T. Donner, M. A. Castellanos-Beltran, J. W. Harlow, K. W. Lehnert, *Nat. Nanotechnol.* **4**, 820 (2009).
8. G. Anetsberger *et al.*, *Phys. Rev. A* **82**, 061804 (2010).
9. D. M. Stamper-Kurn, in *Cavity Optomechanics*, M. Aspelmeyer, T. Kippenberg, F. Marquardt, Eds. (Springer, New York); preprint available at http://arxiv.org/abs/1204.4351.
10. K. W. Murch, K. L. Moore, S. Gupta, D. M. Stamper-Kurn, *Nat. Phys.* **4**, 561 (2008).
11. I. Tittonen *et al.*, *Phys. Rev. A* **59**, 1038 (1999).
12. P. Verlot *et al.*, *C. R. Phys.* **12**, 826 (2011).
13. P. Verlot, A. Tavernarakis, T. Briant, P.-F. Cohadon, A. Heidmann, *Phys. Rev. Lett.* **102**, 103601 (2009).
14. A. Heidmann, Y. Hadjar, M. Pinard, *Appl. Phys. B* **64**, 173 (1997).
15. K. Børkje *et al.*, *Phys. Rev. A* **82**, 013818 (2010).
16. K. Yamamoto *et al.*, *Phys. Rev. A* **81**, 033849 (2010).
17. A. Naik *et al.*, *Nature* **443**, 193 (2006).
18. J. D. Teufel *et al.*, *Nature* **475**, 359 (2011).
19. J. Chan *et al.*, *Nature* **478**, 89 (2011).
20. E. Verhagen, S. Deléglise, S. Weis, A. Schliesser, T. J. Kippenberg, *Nature* **482**, 63 (2012).
21. F. Y. Khalili *et al.*, *Phys. Rev. A* **86**, 033840 (2012).
22. A. H. Safavi-Naeini *et al.*, *Phys. Rev. Lett.* **108**, 033602 (2012).
23. T. P. Purdy, R. W. Peterson, P.-L. Yu, C. A. Regal, *New J. Phys.* **14**, 115021 (2012).
24. J. D. Thompson *et al.*, *Nature* **452**, 72 (2008).
25. F. Marquardt, J. P. Chen, A. A. Clerk, S. M. Girvin, *Phys. Rev. Lett.* **99**, 093902 (2007).
26. Materials and methods are available as supplementary materials on *Science* Online.
27. I. Wilson-Rae, N. Nooshi, W. Zwerger, T. J. Kippenberg, *Phys. Rev. Lett.* **99**, 093901 (2007).
28. K. Jacobs, P. Tombesi, M. J. Collett, D. F. Walls, *Phys. Rev. A* **49**, 1961 (1994).
29. M. J. Holland, M. J. Collett, D. F. Walls, M. D. Levenson, *Phys. Rev. A* **42**, 2995 (1990).
30. C. Fabre *et al.*, *Phys. Rev. A* **49**, 1337 (1994).
31. D. W. C. Brooks *et al.*, *Nature* **488**, 476 (2012).

Acknowledgments: We thank P.-L. Yu for technical assistance and K. Lehnert's group for helpful discussions. This work is supported by: the Defense Advanced Research Projects Agency Quantum-Assisted Sensing and Readout program, the Office of Naval Research Young Investigator Program, and the JILA NSF Physics Frontier Center. T.P.P. thanks the National Research Council for support. C.A.R. thanks the Clare Boothe Luce foundation for support.

Supplementary Materials

www.sciencemag.org/cgi/content/full/339/6121/801/DC1
Materials and Methods
Figs. S1 to S5
References (*32*, *33*)

9 October 2012; accepted 18 December 2012
10.1126/science.1231282

Similarity of Scattering Rates in Metals Showing *T*-Linear Resistivity

J. A. N. Bruin,[1] H. Sakai,[1] R. S. Perry,[2] A. P. Mackenzie[1]

Many exotic compounds, such as cuprate superconductors and heavy fermion materials, exhibit a linear in temperature (T) resistivity, the origin of which is not well understood. We found that the resistivity of the quantum critical metal $Sr_3Ru_2O_7$ is also T-linear at the critical magnetic field of 7.9 T. Using the precise existing data for the Fermi surface topography and quasiparticle velocities of $Sr_3Ru_2O_7$, we show that in the region of the T-linear resistivity, the scattering rate per kelvin is well approximated by the ratio of the Boltzmann constant to the Planck constant divided by 2π. Extending the analysis to a number of other materials reveals similar results in the T-linear region, in spite of large differences in the microscopic origins of the scattering.

When the high-temperature cuprate superconductors were discovered, it quickly became clear that the highest superconducting transition temperatures were seen in materials whose electrical resistivity varied linearly with temperature (T) in certain regions of the temperature-doping phase diagram. Since then, T-linear resistivity has been seen in the pnictide and organic superconductors, as well as in many heavy fermion compounds, both superconducting and non-superconducting. In most of the heavy fermion materials, the T-linear resistivity is seen when they have been tuned by some external parameter to create a low-temperature continuous phase transition known as a quantum critical point (QCP). T-linear resistivity is therefore often associated with quantum criticality. However, other power laws—for example, $T^{1.5}$—are also seen in the resistivity in quantum critical systems (*1*), and the origin of the T-linear term remains the subject of active research and debate. Here, we present an analysis of electrical transport data from 1.5 to 400 K in $Sr_3Ru_2O_7$ and compare our findings to those in a wide variety of other materials, including elemental metals, that exhibit T-linear resistivity.

$Sr_3Ru_2O_7$ is a magnetic-field–tuned quantum critical system (*2*) that can be prepared in single-crystal form with very low levels of disorder (*3*, *4*). For an applied field oriented parallel to the crystallographic c axis, the approach to the quantum critical point at the critical field $\mu_o H_c = 7.9$ T is cut off by the formation of a purity-sensitive nematic phase for 7.8 T $< \mu_o H <$ 8.1 T and $T <$ 1.2 K. Outside this phase, canonical signatures of quantum criticality are seen in a range of physical properties including the spin-lattice relaxation rate, thermal expansion, specific heat, and magnetocaloric effect (*5*–*8*). As the magnetic field is varied at low temperature, both the specific heat and entropy show a strong peak, centered on H_c. Cooling at zero field shows a broad peak in the electronic specific heat coefficient $\gamma = c_{el}/T$, centered at approximately 10 K but extending to $T^* \sim 25$K. As the field is increased, this peak sharpens, and its characteristic temperature is depressed, until at H_c, γ varies as $-\ln T$ for 1.2K $< T <$ 20 K. At all fields, an entropy of $\sim 0.1R\ln 2$ is recovered by T^*, where R is the molar gas constant (*8*). These observations indicate that the ~25K energy scale is associated with a fraction of the states in the Brillouin zone and that these states are responsible for the quantum criticality. Above T^*, they have the entropic characteristics of "classical" fluctuators at all applied fields, with the crossover temperature suppressed on the approach to H_c.

The fact that only some of the states in the Brillouin zone participate thermodynamically in the quantum criticality is consistent with findings from the de Haas-van Alphen (dHvA) effect and angle-resolved photoemission (*9*, *10*). Six distinct dHvA frequencies are identified, each corresponding to quasi–two dimensional (2D) Fermi surface pockets, and the quasiparticle masses are essentially field-independent for five of them (*9*). Thermo-

[1]Scottish Universities Physics Alliance, School of Physics and Astronomy, University of St Andrews, North Haugh, St Andrews KY16 9SS, UK. [2]Scottish Universities Physics Alliance, School of Physics and Astronomy, University of Edinburgh, Mayfield Road, Edinburgh EH9 3JZ, UK.

dynamically, therefore, $Sr_3Ru_2O_7$ can be thought of as two metallic fluids, one which participates directly in the quantum criticality and another, containing a higher density of quasiparticles, which does not.

Given the extensive knowledge of the thermodynamic and quasiparticle properties of $Sr_3Ru_2O_7$, it is natural to investigate its electrical transport properties both below and above T^* (*11*). In Fig. 1, we show the temperature evolution of the data at representative magnetic fields from across the range studied, for $T > T_c$. In zero field, ρ varies approximately quadratically with temperature for $1.2\ K < T < 10\ K$, which is in qualitative agreement with previous reports (*2*, *12*). As the field is increased toward H_c, the temperature range over which the approximately quadratic temperature dependence occurs shrinks, until at the critical field of 7.9 T, the resistivity varies linearly with temperature over the whole range shown, with a gradient of 1.1 microhm·cm/K. For $H > H_c$ (Fig. 1B) there is a small negative magnetoresistance, but the gradient of the resistivity once it has become linear is almost independent of field.

That *T*-linear resistivity is seen in $Sr_3Ru_2O_7$ is surprising. As discussed above, the majority of the quasiparticles do not participate in the mass divergence at H_c. If they were simply an independent Fermi liquid contributing to the conductivity in parallel with the quantum critical fluid, they would be expected to short out the contribution of the small number of carriers that are becoming heavy on the approach to H_c, giving a dominant T^2 contribution to the resistivity. The data of Fig. 1 strongly suggest that as well as inducing a mass divergence in a subset of the carriers, the quantum criticality in $Sr_3Ru_2O_7$ is associated with the onset of efficient scattering, with strength proportional to *T*, which affects all the quasiparticles.

Qualitative support for this basic picture comes from the data presented in Fig. 1C, in which we show the resistivity of $Sr_3Ru_2O_7$ for the same set of fields as in Fig. 1A, but for temperatures extending to 400 K. Above 100 K, ρ is again *T*-linear, in this case at all applied fields, but with a gradient ~30% lower than that seen at H_c for $T < 20$ K. There is an interesting correlation between this observation and previous studies of the specific heat. Measurements to elevated temperatures show that for $T > T^*$, γ is field-independent and ~65% of the low temperature value measured in zero applied field (8). This implies a similar fall in the average effective mass, or equivalently, a 35% rise in the average Fermi velocity. The data in Fig. 1C therefore suggest that there is a similar scattering rate per kelvin below T^* at H_c and well above T^* at all applied fields.

Although attention is typically focused on the power law dependence of the resistivity, the absolute magnitude of the scattering rate is also an important quantity. A phenomenological argument for a *T*-linear scattering rate has been discussed by a number of authors in the context of the cuprates and quantum critical metals and fluids (*13*–*15*). Because quantum criticality is associated with the depression of energy scales toward $T = 0$, temperature becomes the only relevant energy scale. Equipartition of energy then applies, and the characteristic energy of any quantum critical degree of freedom is just k_BT, where k_B is Boltzmann's constant. This in turn implies the existence of a characteristic time, sometimes referred to as the Planck time $\tau_P \sim \hbar/k_BT$, where $\hbar$ is Planck's constant divided by 2π. Although the simplicity of this expression is appealing, it is far from obvious that $(T\tau_P)^{-1} \sim k_B/\hbar$ defines a scattering rate relevant to a measurement of electrical resistivity. Resistive scattering processes must relax

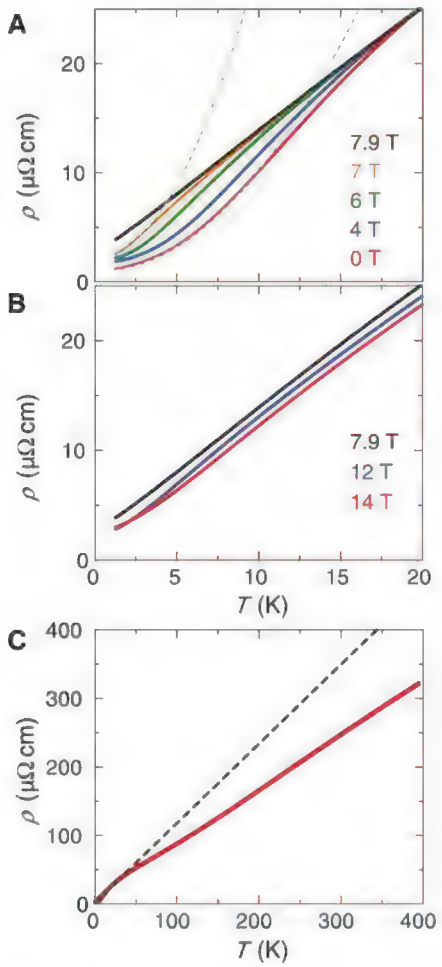

Fig. 1. (**A**) Resistivity (ρ) of high-purity single crystal $Sr_3Ru_2O_7$ at 0 T (red), 4 T (blue), 6 T (green), 7 T (orange), and its critical field $\mu_0H_c = 7.9$ T (black). The gray dashed lines are fits of the type $\rho_0 + AT^2$ to the low-temperature data, which illustrate the suppression of the temperature at which the resistivity crosses over to being quadratic in temperature as *H* is tuned toward H_c. (**B**) ρ at H_c (black), 12 T (blue), and 14 T (red). (**C**) ρ at 0 T, 4 T, 6 T, 7 T, and H_c over an extended temperature range up to 400 K. Above 20 K, there is a negative magnetoresistance, but it is so small that data at all fields overlap when plotted on this scale. The dotted line shows the extrapolation of the low-temperature linear resistivity at 7.9 T.

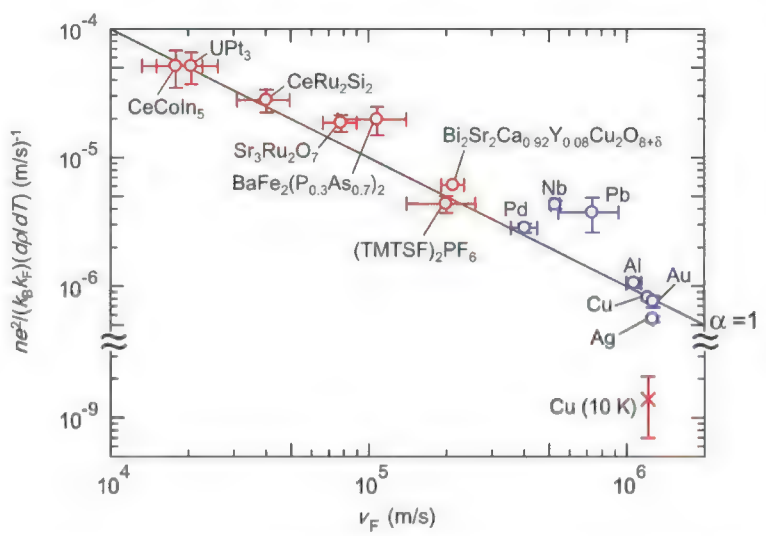

Fig. 2. In spite of two orders of magnitude variations in their Fermi velocities (v_F), a wide range of metals in which the resistivity varies linearly with temperature have similar scattering rates per kelvin. These include heavy fermion, oxide, pnictide, and organic metals for which *T*-linear resistivity can be seen down to low temperatures with appropriate tuning by magnetic field, chemical composition, or hydrostatic pressure, and more conventional metals for which *T*-linear resistivity is seen at high temperatures (blue symbols). At low temperatures, the scattering rate per kelvin of a conventional metal is orders of magnitude lower, as illustrated for the case of Cu at 10 K, shown in the lower right hand corner (*11*). On the graph, the line marked $\alpha = 1$ corresponds to $(\tau T)^{-1} = k_B/\hbar$. The near-universality of the scattering rates is observed in spite of the fact that the scattering mechanisms vary across the range of materials. The point for $Bi_2Sr_2Ca_{0.92}Y_{0.08}Cu_2O_{8+\delta}$ is based on the value $\alpha = 1.3$, which is determined from optical conductivity (*21*), combined with the measured value of v_F for this material (*44*). For all others, the analysis is based on resistivity data combined with knowledge of the Fermi volume and average Fermi velocity. Full details of the determination of the parameters in the axis labels are given in (*11*).

momentum efficiently within the electronic fluid, transfer that momentum to the lattice, and ultimately dissipate energy. In other words, there is no a priori reason to expect the resistive scattering rate τ^{-1} to have either the same temperature dependence or magnitude as τ_P^{-1}. Here, we concentrate on the case in which $\tau(T) \propto \tau_P(T)$, and write $(T\tau)^{-1} \sim \alpha k_B/\hbar$, so that $\tau(T) = \tau_P(T)$ corresponds to phenomenological dimensionless constant $\alpha = 1$. We can measure α in $Sr_3Ru_2O_7$ with some confidence because it has a quasi-2D Fermi surface, and the volume and average Fermi velocity of each Fermi surface sheet have been established empirically, even for fields close to H_c (*9*). Working in a 2D isotropic-relaxation-time approximation that is useful for estimating the average scattering rate (*16*, *17*) we write

$$\frac{1}{\tau} = \frac{e^2\rho}{hd}\sum_i k_{Fi} v_{Fi} \qquad (1)$$

where e is the electronic charge, d is the bilayer-bilayer spacing of 10.35 Å, k_F is the Fermi wave vector, v_F is the Fermi velocity, and index i ensures that the sum is over all pockets, taking into account multiplicities in the Brillouin zone. We then used Eq. 1, in combination with our $\rho(T)$ data, to determine the temperature dependence of τ^{-1}. Performing the calculation using the data for $H = H_c$ and the quasiparticle parameters of (*9*) gives $\alpha = 1.5$ (*11*).

The fact that α is close to 1 in $Sr_3Ru_2O_7$ is intriguing, especially given that similar conclusions have been reached about the cuprates at optimal doping from analysis of high-frequency conductivity data (*13*, *18*–*22*), photoemission spectra (*23*), and transport measurements (*14*). Our observations therefore motivate analysis of the resistivity of other materials in which T-linear resistivity is observed. Converting resistivity data to a scattering rate requires good knowledge of Fermi volumes and Fermi velocities, close to the critical tuning parameter at which the T-linear resistivity is observed. Sufficient information for reliable analysis, usually deduced from the dHvA effect, exists for $BaFe_2(As_{1-x}P_x)_2$ (*24*, *25*), $(TMTSF)_2PF_6$ (*26*, *27*), $CeCoIn_5$ (*28*–*30*), UPt_3 (*31*, *32*), and $CeRu_2Si_2$ (*33*, *34*) (the last two near their metamagnetic transitions). Across this range of strongly correlated materials, we found $0.9 < \alpha < 2.2$, in spite of pronounced differences in both their effective dimensionality [varying from quasi-1D in $(TMTSF)_2PF_6$ to 3D in UPt_3] and the microscopic nature of the interactions. Full details of the calculations, which take the dimensionality of the electronic structure into account, are given in (*11*).

A natural question posed by these observations is whether T-linear scattering at $k_B/\hbar$ per kelvin is exclusive to quantum critical systems. Central to the phenomenological argument that $(\tau T)^{-1} \sim k_B/\hbar$ is the applicability of equipartition of energy to the degree of freedom from which the quasiparticles scatter. In addition to quantum critical systems as $T \to 0$, this condition is well known to apply at high temperatures in a further class of materials in which T-linear resistivity is observed, metals in which the scattering is from phonons rather than excitations of electronic origin. Because the nature of the scattering centers is different, and the high temperature resistivity of metals such as copper, gold, and silver is two orders of magnitude lower than that of the strongly correlated materials discussed above, they are often assumed to be fundamentally different. However, the difference in the absolute value of the resistivity is accounted for by their much higher carrier concentrations and Fermi velocities, and again, $\alpha \sim 1$ [$0.7 < \alpha < 2.7$ for Ag, Au, Pd, Cu, Al, Nb, and Pb, with full analysis described in (*11*)].

The fact that the resistively determined scattering rate per kelvin is approximately $k_B/\hbar$ across such a wide range of materials is our main experimental finding. It is summarized in Fig. 2. Although the main purpose of this paper is to report this empirical fact, we close with a brief discussion of some of the issues that are raised by our observations.

The first concerns the underlying origin for T-linear resistivity in quantum critical systems. Our analysis is based on the assumption that the main effect of quantum criticality on the resistivity is to provide a quasi-classical degree of freedom from which even light, "cold" Fermi liquid quasiparticles scatter rather than to destroy all the quasiparticles. In $Sr_3Ru_2O_7$, this is the only way to understand how T-linear resistivity can be observed. Similar issues of "hot" and cold carriers have been highlighted in the context of cuprates (*35*) and heavy fermion systems (*36*). In fact, most of the other strongly correlated materials shown in Fig. 2 also have cold carriers that, in the simplest models, would short out the T-linear contribution. This seems to be strong evidence that in those materials too, all the carriers are subject to strong scattering. This analysis helps resolve a puzzle about $Sr_3Ru_2O_7$ and some other quantum critical metallic systems: The crossover to T^2 resistivity (Fig. 1) typically occurs at far lower T than the Fermi temperature (T_F) inferred from the average effective mass. If the resistive crossover is related to the characteristic energy of the quantum critical scattering, this might indeed be much lower than T_F for most of the quasiparticles.

In materials in which phonon scattering is thought to dominate, electron-phonon processes in the high temperature limit have a T-linear scattering rate that is conventionally expressed as $(\tau T)^{-1} = 2\pi\lambda k_B/\hbar$, where λ is a dimensionless coupling constant that is not thought to be universal (*37*); in the language of this paper, the phenomenological constant $\alpha = 2\pi\lambda$. The data summarized in Fig. 2, however, suggest that the coupling constant deduced from the electrical resistivity is insensitive to the detail of the scattering processes. This finding also highlights a second key feature of scattering in the strongly correlated materials. Phonon modes at high temperatures are known to have a large wave vector q and hence to be efficient at relaxing electron momentum. The near material-independence of α across electron-phonon and strongly correlated systems implies that whatever their microscopic origin, the low-temperature degrees of freedom in the strongly correlated systems must be equally efficient at high-q scattering, via normal processes, Umklapp processes, or a combination of the two. This is implicit in the data shown in Fig. 1 for $Sr_3Ru_2O_7$; the fact that the linear resistivity is seen at all in this multi-band material implies efficient scattering throughout the Brillouin zone.

A further issue raised is the effect of combining different sources of scattering in the same material. It has always seemed strange that no obvious signatures of electron-phonon scattering are seen in strongly correlated materials such as the cuprates, in which electron-electron processes are thought to dominate. Electron-phonon coupling is also expected to be strong in such materials, so electron-phonon scattering should be visible as an extra contribution to the resistivity, particularly at higher temperatures. There is very little experimental evidence for this additive contribution. One possibility raised by the data shown in Fig. 2 is that there is a universal upper limit to the rate of scattering observable in a measurement of T-linear resistivity, no matter how many sources of scattering are combined.

A final hint toward universal behavior comes from the study of quantum hydrodynamic fluids. In a hydrodynamic fluid, the shear viscosity η is inversely proportional to the scattering rate because all dissipation processes are nonlocal. Experiments have shown that when the scattering rate is T-linear, the ratio of η to entropy density s is very small, with $\eta/s \cong \hbar/2k_B$ for fluids as diverse as the quark-gluon plasma and ultra-cold ^{6}Li (*38*–*40*). Under certain assumptions $\eta/s \cong \tau T$ (*41*), so the measurements correspond to $\alpha \cong 2$, which is quantitatively similar to those reported here for electrons in metals. In the hydrodynamic fluids, calculations based on string theory predict a "minimum viscosity limit" of $\eta/s \geq \hbar/4\pi k_B$ (*42*). Hydrodynamic theory is not directly applicable to most metals (*43*), but if the essence of these calculations is the prediction of a universal bound on a T-linear scattering rate, there may prove to be relevance to the observations that we have reported here. Whatever the final explanation, the data summarized in Fig. 2 provide a novel perspective on a decades-old problem.

References and Notes

1. G. R. Stewart, *Rev. Mod. Phys.* **73**, 797 (2001).
2. S. A. Grigera *et al.*, *Science* **294**, 329 (2001).
3. R. S. Perry *et al.*, *Phys. Rev. Lett.* **92**, 166602 (2004).
4. S. A. Grigera *et al.*, *Science* **306**, 1154 (2004).
5. K. Kitagawa *et al.*, *Phys. Rev. Lett.* **95**, 127001 (2005).
6. P. Gegenwart, F. Weickert, M. Garst, R. S. Perry, Y. Maeno, *Phys. Rev. Lett.* **96**, 136402 (2006).
7. A. W. Rost, R. S. Perry, J. F. Mercure, A. P. Mackenzie, S. A. Grigera, *Science* **325**, 1360 (2009).
8. A. W. Rost *et al.*, *Proc. Natl. Acad. Sci. U.S.A.* **108**, 16549 (2011).
9. J. F. Mercure *et al.*, *Phys. Rev. B* **81**, 235103 (2010).
10. A. Tamai *et al.*, *Phys. Rev. Lett.* **101**, 026407 (2008).
11. Materials and methods are available as supplementary materials on *Science* Online.
12. L. Capogna *et al.*, *Phys. Rev. Lett.* **88**, 076602 (2002).
13. J. Zaanen, *Nature* **430**, 512 (2004).
14. R. A. Cooper *et al.*, *Science* **323**, 603 (2009).
15. T. Schäfer, D. Teaney, *Rep. Prog. Phys.* **72**, 126001 (2009).

16. N. P. Ong, *Phys. Rev. B* **43**, 193 (1991).
17. P. L. Taylor, *Proc. R. Soc. Lond. A Math. Phys. Sci.* **275**, 209 (1963).
18. J. W. Orenstein *et al.*, *Phys. Rev. B* **42**, 6342 (1990).
19. Z. Schlesinger *et al.*, *Phys. Rev. B* **41**, 11237 (1990).
20. H. L. Liu *et al.*, *J. Phys. Condens. Matter* **11**, 239 (1999).
21. D. van der Marel *et al.*, *Nature* **425**, 271 (2003).
22. C. C. Homes *et al.*, *Nature* **430**, 539 (2004).
23. T. Valla *et al.*, *Science* **285**, 2110 (1999).
24. S. Kasahara *et al.*, *Phys. Rev. B* **81**, 184519 (2010).
25. H. Shishido *et al.*, *Phys. Rev. Lett.* **104**, 057008 (2010).
26. N. Doiron-Leyraud *et al.*, *Eur. Phys. J. B* **78**, 23 (2010).
27. J. S. Brooks, *Rep. Prog. Phys.* **71**, 126501 (2008).
28. M. A. Tanatar, J. Paglione, C. Petrovic, L. Taillefer, *Science* **316**, 1320 (2007).
29. R. Settai *et al.*, *J. Phys. Condens. Matter* **13**, L627 (2001).
30. A. McCollam, S. R. Julian, P. M. C. Rourke, D. Aoki, J. Flouquet, *Phys. Rev. Lett.* **94**, 186401 (2005).
31. J. S. Kim, D. Hall, K. Heuser, G. R. Stewart, *Solid State Commun.* **114**, 413 (2000).
32. N. Kimura *et al.*, *Physica B* **281-282**, 710 (2000).
33. R. Daou, C. Bergemann, S. R. Julian, *Phys. Rev. Lett.* **96**, 026401 (2006).
34. M. Takashita *et al.*, *J. Phys. Soc. Jpn.* **65**, 515 (1996).
35. R. Hlubina, T. M. Rice, *Phys. Rev. B* **51**, 9253 (1995).
36. A. Rosch, *Phys. Rev. Lett.* **82**, 4280 (1999).
37. J. M. Ziman, *Electrons and Phonons* (Clarendon Press, Oxford, UK, 1960).
38. S. S. Adler *et al.*; PHENIX Collaboration, *Phys. Rev. Lett.* **91**, 182301 (2003).
39. T. Schäfer, *Phys. Rev. A* **76**, 063618 (2007).
40. C. Cao *et al.*, *Science* **331**, 58 (2011).
41. D. A. Teaney, *arXiv*:0905.2433v1.
42. P. K. Kovtun, D. T. Son, A. O. Starinets, *Phys. Rev. Lett.* **94**, 111601 (2005).
43. A. V. Andreev, S. A. Kivelson, B. Spivak, *Phys. Rev. Lett.* **106**, 256804 (2011).
44. A. Kaminski *et al.*, *Phys. Rev. B* **71**, 014517 (2005).

Acknowledgments: We are pleased to acknowledge the help of M. Baenitz, M. Nicklas, and C. Klausnitzer of the Max Planck Institute for the Chemical Physics of Solids in Dresden, where the high-temperature resistivity measurements on $Sr_3Ru_2O_7$ were performed, and useful discussions with J. Orenstein, S. A. Kivelson, C. A. Hooley, and J. Zaanen. The research was supported by the UK Engineering and Physical Sciences Research Council. H.S. gratefully acknowledges fellowships from the Canon Foundation Europe and Marubun Research Promotion Foundation, and A.P.M. acknowledges the receipt of a Royal Society–Wolfson Merit Award.

Supplementary Materials

www.sciencemag.org/cgi/content/full/339/6121/804/DC1
Materials and Methods
Supplementary Text
Fig. S1
Tables S1 to S10
References (*45*–*65*)

18 July 2012; accepted 27 November 2012
10.1126/science.1227612

Detection of the Characteristic Pion-Decay Signature in Supernova Remnants

M. Ackermann,[1] M. Ajello,[2] A. Allafort,[3] L. Baldini,[4] J. Ballet,[5] G. Barbiellini,[6,7] M. G. Baring,[8] D. Bastieri,[9,10] K. Bechtol,[3] R. Bellazzini,[11] R. D. Blandford,[3] E. D. Bloom,[3] E. Bonamente,[12,13] A. W. Borgland,[3] E. Bottacini,[3] T. J. Brandt,[14] J. Bregeon,[11] M. Brigida,[15,16] P. Bruel,[17] R. Buehler,[3] G. Busetto,[9,10] S. Buson,[9,10] G. A. Caliandro,[18] R. A. Cameron,[3] P. A. Caraveo,[19] J. M. Casandjian,[5] C. Cecchi,[12,13] Ö. Çelik,[14,20,21] E. Charles,[3] S. Chaty,[5] R. C. G. Chaves,[5] A. Chekhtman,[22] C. C. Cheung,[23] J. Chiang,[3] G. Chiaro,[24] A. N. Cillis,[14,25] S. Ciprini,[13,26] R. Claus,[3] J. Cohen-Tanugi,[27] L. R. Cominsky,[28] J. Conrad,[29,30,31] S. Corbel,[5,32] S. Cutini,[33] F. D'Ammando,[12,34,35] A. de Angelis,[36] F. de Palma,[15,16] C. D. Dermer,[37] E. do Couto e Silva,[3] P. S. Drell,[3] A. Drlica-Wagner,[3] L. Falletti,[27] C. Favuzzi,[15,16] E. C. Ferrara,[14] A. Franckowiak,[3] Y. Fukazawa,[38] S. Funk,[3]* P. Fusco,[15,16] F. Gargano,[16] S. Germani,[12,13] N. Giglietto,[15,16] P. Giommi,[33] F. Giordano,[15,16] M. Giroletti,[39] T. Glanzman,[3] G. Godfrey,[3] I. A. Grenier,[5] M.-H. Grondin,[40,41] J. E. Grove,[37] S. Guiriec,[14] D. Hadasch,[18] Y. Hanabata,[38] A. K. Harding,[14] M. Hayashida,[3,42] K. Hayashi,[38] E. Hays,[14] J. W. Hewitt,[14] A. B. Hill,[3,43] R. E. Hughes,[44] M. S. Jackson,[30,45] T. Jogler,[3] G. Jóhannesson,[46] A. S. Johnson,[3] T. Kamae,[3] J. Kataoka,[47] J. Katsuta,[3] J. Knödlseder,[48,49] M. Kuss,[11] J. Lande,[3] S. Larsson,[29,30,50] L. Latronico,[51] M. Lemoine-Goumard,[52,53] F. Longo,[6,7] F. Loparco,[15,16] M. N. Lovellette,[37] P. Lubrano,[12,13] G. M. Madejski,[3] F. Massaro,[3] M. Mayer,[1] M. N. Mazziotta,[16] J. E. McEnery,[14,54] J. Mehault,[27] P. F. Michelson,[3] R. P. Mignani,[55] W. Mitthumsiri,[3] T. Mizuno,[56] A. A. Moiseev,[20,54] M. E. Monzani,[3] A. Morselli,[57] I. V. Moskalenko,[3] S. Murgia,[3] T. Nakamori,[47] R. Nemmen,[14] E. Nuss,[27] M. Ohno,[58] T. Ohsugi,[56] N. Omodei,[3] M. Orienti,[39] E. Orlando,[3] J. F. Ormes,[59] D. Paneque,[3,60] J. S. Perkins,[14,21,20,61] M. Pesce-Rollins,[11] F. Piron,[27] G. Pivato,[10] S. Rainò,[15,16] R. Rando,[9,10] M. Razzano,[11,62] S. Razzaque,[22] A. Reimer,[3,63] O. Reimer,[3,63] S. Ritz,[62] C. Romoli,[10] M. Sánchez-Conde,[3] A. Schulz,[1] C. Sgrò,[11] P. E. Simeon,[3] E. J. Siskind,[64] D. A. Smith,[52] G. Spandre,[11] P. Spinelli,[15,16] F. W. Stecker,[14,65] A. W. Strong,[66] D. J. Suson,[67] H. Tajima,[3,68] H. Takahashi,[38] T. Takahashi,[58] T. Tanaka,[3,69]* J. G. Thayer,[3] J. B. Thayer,[3] D. J. Thompson,[14] S. E. Thorsett,[70] L. Tibaldo,[9,10] O. Tibolla,[71] M. Tinivella,[11] E. Troja,[14,72] Y. Uchiyama,[3]* T. L. Usher,[3] J. Vandenbroucke,[3] V. Vasileiou,[27] G. Vianello,[3,73] V. Vitale,[57,74] A. P. Waite,[3] M. Werner,[63] B. L. Winer,[44] K. S. Wood,[37] M. Wood,[3] R. Yamazaki,[75] Z. Yang,[29,30] S. Zimmer[29,30]

Cosmic rays are particles (mostly protons) accelerated to relativistic speeds. Despite wide agreement that supernova remnants (SNRs) are the sources of galactic cosmic rays, unequivocal evidence for the acceleration of protons in these objects is still lacking. When accelerated protons encounter interstellar material, they produce neutral pions, which in turn decay into gamma rays. This offers a compelling way to detect the acceleration sites of protons. The identification of pion-decay gamma rays has been difficult because high-energy electrons also produce gamma rays via bremsstrahlung and inverse Compton scattering. We detected the characteristic pion-decay feature in the gamma-ray spectra of two SNRs, IC 443 and W44, with the Fermi Large Area Telescope. This detection provides direct evidence that cosmic-ray protons are accelerated in SNRs.

A supernova explosion drives its progenitor material supersonically into interstellar space, forming a collisionless shock wave ahead of the stellar ejecta. The huge amount of kinetic energy released by a supernova, typically 10^{51} ergs, is initially carried by the expanding ejecta and is then transferred to kinetic and thermal energies of shocked interstellar gas and relativistic particles. The shocked gas and relativistic particles produce the thermal and nonthermal emissions of a supernova remnant (SNR). The mechanism of diffusive shock acceleration (DSA) can explain the production of relativistic particles in SNRs (*1*). DSA generally predicts that a substantial fraction of the shock energy is transferred to relativistic protons. Indeed, if SNRs are the main sites of acceleration of the galactic cosmic rays, then 3 to 30% of the supernova kinetic energy must end up transferred to relativistic protons. However, the presence of relativistic protons in SNRs has been mostly inferred from indirect arguments (*2*–*5*).

A direct signature of high-energy protons is provided by gamma rays generated in the decay of neutral pions (π^0); proton-proton (more generally nuclear-nuclear) collisions create π^0 mesons, which usually quickly decay into two gamma rays (*6*–*8*) (schematically written as $p + p \rightarrow \pi^0 +$ other products, followed by $\pi^0 \rightarrow 2\gamma$), each having an energy of $m_{\pi^0}c^2/2 = 67.5$ MeV in the rest frame of the neutral pion (where m_{π^0} is the rest mass of the neutral pion and c is the speed of light). The gamma-ray number spectrum, $F(\varepsilon)$, is thus symmetric about 67.5 MeV in a log-log representation (*9*). The π^0-decay spectrum in the usual $\varepsilon^2 F(\varepsilon)$ representation rises steeply below ~200 MeV and approximately traces the energy distribution of parent protons at energies greater than a few GeV. This characteristic spectral feature (often referred to as the "pion-decay bump") uniquely identifies π^0-decay gamma rays and thereby high-energy protons, allowing a measurement of the source spectrum of cosmic rays.

Massive stars are short-lived and end their lives with core-collapse supernova explosions. These explosions typically occur in the vicinity of molecular clouds with which they interact. When cosmic-ray protons accelerated by SNRs penetrate into high-density clouds, π^0-decay gamma-ray emission is expected to be enhanced because of more frequent *pp* interactions relative to the interstellar medium (*10*). Indeed, SNRs

interacting with molecular clouds are the most luminous SNRs in gamma rays (*11*, *12*). The best examples of SNR-cloud interactions in our galaxy are the SNRs IC 443 and W44 (*13*), which are the two highest-significance SNRs in the second Fermi Large Area Telescope (LAT) catalog (2FGL) (*14*) and are thus particularly suited for a dedicated study of the details of their gamma-ray spectra. The age of each remnant is estimated to be ~10,000 years. IC 443 and W44 are located at distances of 1.5 kpc and 2.9 kpc, respectively.

We report here on 4 years of observations with the Fermi LAT (4 August 2008 to 16 July 2012) of IC 443 and W44, focusing on the sub-GeV part of the gamma-ray spectrum—a crucial spectral window for distinguishing π^0-decay gamma rays from electron bremsstrahlung or inverse Compton scattering produced by relativistic electrons. Previous analyses of IC 443 and W44 used only 1 year of Fermi LAT data (*15*–*17*) and were limited to the energy band above 200 MeV, mainly because of the small and rapidly changing LAT effective area at low energies. A recent update to the event classification and background rejection (so-called Pass 7) provides an increase in LAT effective area at 100 MeV by a factor of ~5 (*18*), enabling the study of bright, steady sources in the galactic plane below 200 MeV with the Fermi LAT. Note that the gamma-ray spectral energy distribution of W44 measured recently by the AGILE satellite falls steeply below 1 GeV, which the authors interpreted as a clear indication for the π^0-decay origin of the gamma-ray emission (*19*). Also, a recent analysis of W44 at high energies (above 2 GeV) has been reported (*20*), revealing large-scale gamma-ray emission attributable to high-energy protons that have escaped from W44. Here, we present analyses of the gamma-ray emission from the compact regions delineated by the radio continuum emission of IC 443 and W44.

The analysis was performed using the Fermi LAT Science Tools (*21*). We used a maximum likelihood technique to determine the significance of a source over the background and to fit spectral parameters (*22*, *23*). For both SNRs, additional sources seen as excesses in the background-subtracted map have been added to the background model (*24*) and are shown as diamonds in Fig. 1—one in the case of IC 443, three in the case of W44. The inclusion of these sources had no influence on the fitted spectrum of the SNRs. Three close-by sources (2FGL J1852.8+0156c, 2FGL J1857.2+0055c, and 2FGL J1858.5+0129c) have been identified with escaping cosmic rays from W44 (*20*). These 2FGL sources have been removed from the background model (see below) in order to measure the full cosmic-ray content of W44.

Figure 2 shows the spectral energy distribution obtained for IC 443 and W44 through maximum likelihood estimation. To derive the flux points, we performed a maximum likelihood fitting in 24 independent logarithmically spaced energy bands from 60 MeV to 100 GeV. The normalization of the fluxes of IC 443 and W44, and those of neighboring sources and of the galactic diffuse model, was left free in the fit for each bin. In both sources, the spectra below ~200 MeV are steeply rising, clearly exhibiting a break at ~200 MeV. To quantify the significances of the spectral breaks, we fit the fluxes of IC 443 and W44 between 60 MeV and 2 GeV—below the high-energy breaks previously found in the 1-year spectra (*15*, *16*)—with both a single power law of the form $F(\varepsilon) = K(\varepsilon/\varepsilon_0)^{-\Gamma_1}$ and a smoothly broken power law of the form $F(\varepsilon) = K(\varepsilon/\varepsilon_0)^{-\Gamma_1}\left[1 + (\varepsilon/\varepsilon_{br})^{(\Gamma_2-\Gamma_1)/\alpha_1}\right]^{-\alpha}$ with $\varepsilon_0 = 200$ MeV. The spectral index changes from Γ_1 to Γ_2 ($>\Gamma_1$) at the break energy ε_{br}. The smoothness of the break is determined by the parameter α, which was fixed at 0.1 (Table 1). We define the test-statistic value (*TS*) as $2\ln(\mathcal{L}_1/\mathcal{L}_0)$, where $\mathcal{L}_{1/0}$ corresponds to the likelihood value for the source/no-source hypothesis (*24*). The detection significance is given by $\sim\sqrt{TS}$. The smoothly broken power law model yields a significantly larger *TS* than a single power law, establishing the existence of a low-energy break. The improvement in log likelihood when comparing the broken power law to a single power law corresponds to a formal statistical significance of 19σ for the

[1]Deutsches Elektronen Synchrotron (DESY), D-15738 Zeuthen, Germany. [2]Space Sciences Laboratory, University of California, Berkeley, CA 94720, USA. [3]W. W. Hansen Experimental Physics Laboratory, Kavli Institute for Particle Astrophysics and Cosmology, Department of Physics, and SLAC National Accelerator Laboratory, Stanford University, Stanford, CA 94305, USA. [4]Università di Pisa and Istituto Nazionale di Fisica Nucleare, Sezione di Pisa, I-56127 Pisa, Italy. [5]Laboratoire AIM, CEA-IRFU/CNRS/Université Paris Diderot, Service d'Astrophysique, CEA Saclay, 91191 Gif-sur-Yvette, France. [6]Istituto Nazionale di Fisica Nucleare, Sezione di Trieste, I-34127 Trieste, Italy. [7]Dipartimento di Fisica, Università di Trieste, I-34127 Trieste, Italy. [8]Rice University, Department of Physics and Astronomy, MS-108, Post Office Box 1892, Houston, TX 77251, USA. [9]Istituto Nazionale di Fisica Nucleare, Sezione di Padova, I-35131 Padova, Italy. [10]Dipartimento di Fisica e Astronomia "G. Galilei," Università di Padova, I-35131 Padova, Italy. [11]Istituto Nazionale di Fisica Nucleare, Sezione di Pisa, I-56127 Pisa, Italy. [12]Istituto Nazionale di Fisica Nucleare, Sezione di Perugia, I-06123 Perugia, Italy. [13]Dipartimento di Fisica, Università degli Studi di Perugia, I-06123 Perugia, Italy. [14]NASA Goddard Space Flight Center, Greenbelt, MD 20771, USA. [15]Dipartimento di Fisica "M. Merlin" dell'Università e del Politecnico di Bari, I-70126 Bari, Italy. [16]Istituto Nazionale di Fisica Nucleare, Sezione di Bari, 70126 Bari, Italy. [17]Laboratoire Leprince-Ringuet, École Polytechnique, CNRS/IN2P3, 91128 Palaiseau, France. [18]Institut de Ciències de l'Espai (IEEE-CSIC), Campus UAB, 08193 Barcelona, Spain. [19]INAF–Istituto di Astrofisica Spaziale e Fisica Cosmica, I-20133 Milano, Italy. [20]Center for Research and Exploration in Space Science and Technology (CRESST) and NASA Goddard Space Flight Center, Greenbelt, MD 20771, USA. [21]Department of Physics and Center for Space Sciences and Technology, University of Maryland Baltimore County, Baltimore, MD 21250, USA. [22]Center for Earth Observing and Space Research, College of Science, George Mason University, Fairfax, VA 22030, resident at Naval Research Laboratory, Washington, DC 20375, USA. [23]National Research Council Research Associate, National Academy of Sciences, Washington, DC 20001, resident at Naval Research Laboratory, Washington, DC 20375, USA. [24]INFN and Dipartimento di Fisica e Astronomia "G. Galilei," Università di Padova, I-35131 Padova, Italy. [25]Instituto de Astronomía y Física del Espacio, Parbellón IAFE, Cdad. Universitaria, C1428ZAA Buenos Aires, Argentina. [26]ASI Science Data Center, I-00044 Frascati (Roma), Italy. [27]Laboratoire Univers et Particules de Montpellier, Université Montpellier 2, CNRS/IN2P3, Montpellier, France. [28]Department of Physics and Astronomy, Sonoma State University, Rohnert Park, CA 94928, USA. [29]Department of Physics, Stockholm University, AlbaNova, SE-106 91 Stockholm, Sweden. [30]Oskar Klein Centre for Cosmoparticle Physics, AlbaNova, SE-106 91 Stockholm, Sweden. [31]Royal Swedish Academy of Sciences Research Fellow, funded by a grant from the K. A. Wallenberg Foundation. [32]Institut Universitaire de France, 75005 Paris, France. [33]Agenzia Spaziale Italiana (ASI) Science Data Center, I-00044 Frascati (Roma), Italy. [34]IASF Palermo, 90146 Palermo, Italy. [35]INAF–Istituto di Astrofisica Spaziale e Fisica Cosmica, I-00133 Roma, Italy. [36]Dipartimento di Fisica, Università di Udine and Istituto Nazionale di Fisica Nucleare, Sezione di Trieste, Gruppo Collegato di Udine, I-33100 Udine, Italy. [37]Space Science Division, Naval Research Laboratory, Washington, DC 20375, USA. [38]Department of Physical Sciences, Hiroshima University, Higashi-Hiroshima, Hiroshima 739-8526, Japan. [39]INAF Istituto di Radioastronomia, 40129 Bologna, Italy. [40]Max-Planck-Institut für Kernphysik, D-69029 Heidelberg, Germany. [41]Landessternwarte, Universität Heidelberg, Königstuhl, D-69117 Heidelberg, Germany. [42]Department of Astronomy, Graduate School of Science, Kyoto University, Sakyo-ku, Kyoto 606-8502, Japan. [43]School of Physics and Astronomy, University of Southampton, Highfield, Southampton SO17 1BJ, UK. [44]Department of Physics, Center for Cosmology and Astro-Particle Physics, Ohio State University, Columbus, OH 43210, USA. [45]Department of Physics, Royal Institute of Technology (KTH), AlbaNova, SE-106 91 Stockholm, Sweden. [46]Science Institute, University of Iceland, IS-107 Reykjavik, Iceland. [47]Research Institute for Science and Engineering, Waseda University, 3-4-1, Okubo, Shinjuku, Tokyo 169-8555, Japan. [48]CNRS, IRAP, F-31028 Toulouse Cedex 4, France. [49]GAHEC, Université de Toulouse, UPS-OMP, IRAP, 31028 Toulouse, France. [50]Department of Astronomy, Stockholm University, SE-106 91 Stockholm, Sweden. [51]Istituto Nazionale di Fisica Nucleare, Sezione di Torino, I-10125 Torino, Italy. [52]Université Bordeaux 1, CNRS/IN2p3, Centre d'Études Nucléaires de Bordeaux Gradignan, 33175 Gradignan, France. [53]Funded by contract ERC-StG-259391 from the European Community. [54]Department of Physics and Department of Astronomy, University of Maryland, College Park, MD 20742, USA. [55]Mullard Space Science Laboratory, University College London, Holmbury St. Mary, Dorking, Surrey RH5 6NT, UK. [56]Hiroshima Astrophysical Science Center, Hiroshima University, Higashi-Hiroshima, Hiroshima 739-8526, Japan. [57]Istituto Nazionale di Fisica Nucleare, Sezione di Roma "Tor Vergata," I-00133 Roma, Italy. [58]Institute of Space and Astronautical Science, JAXA, 3-1-1 Yoshinodai, Chuo-ku, Sagamihara, Kanagawa 252-5210, Japan. [59]Department of Physics and Astronomy, University of Denver, Denver, CO 80208, USA. [60]Max-Planck-Institut für Physik, D-80805 München, Germany. [61]Harvard-Smithsonian Center for Astrophysics, Cambridge, MA 02138, USA. [62]Santa Cruz Institute for Particle Physics, Department of Physics, and Department of Astronomy and Astrophysics, University of California, Santa Cruz, CA 95064, USA. [63]Institut für Astro- und Teilchenphysik and Institut für Theoretische Physik, Leopold-Franzens-Universität Innsbruck, A-6020 Innsbruck, Austria. [64]NYCB Real-Time Computing Inc., Lattingtown, NY 11560, USA. [65]Department of Physics and Astronomy, University of California, Los Angeles, CA 90095, USA. [66]Max-Planck-Institut für Extraterrestrische Physik, 85748 Garching, Germany. [67]Department of Chemistry and Physics, Purdue University Calumet, Hammond, IN 46323, USA. [68]Solar-Terrestrial Environment Laboratory, Nagoya University, Nagoya 464-8601, Japan. [69]Department of Physics, Graduate School of Science, Kyoto University, Sakyo-ku, Kyoto 606-8502, Japan. [70]Department of Physics, Willamette University, Salem, OR 97031, USA. [71]Institut für Theoretische Physik und Astrophysik, Universität Würzburg, D-97074 Würzburg, Germany. [72]NASA Postdoctoral Program Fellow. [73]Consorzio Interuniversitario per la Fisica Spaziale, I-10133 Torino, Italy. [74]Dipartimento di Fisica, Università di Roma "Tor Vergata," I-00133 Roma, Italy. [75]Department of Physics and Mathematics, Aoyama Gakuin University, Sagamihara, Kanagawa 252-5258, Japan.

*To whom correspondence should be addressed. E-mail: funk@slac.stanford.edu (S.F.); ttanaka@cr.scphys.kyoto-u.ac.jp (T.T.); uchiyama@slac.stanford.edu (Y.U.)

low-energy break in IC 443 and 21σ for that in W44, when assuming a nested model with two additional degrees of freedom.

To determine whether the spectral shape could indeed be modeled with accelerated protons, we fit the LAT spectral points with a π^0-decay spectral model, which was numerically calculated from a parameterized energy distribution of relativistic protons. Following previous studies (*15*, *16*), the parent proton spectrum as a function of momentum p was parameterized by a smoothly broken power law in the form of

$$\frac{dN_p}{dp} \propto p^{-s_1}\left[1+\left(\frac{p}{p_{br}}\right)^{\frac{s_2-s_1}{\beta}}\right]^{-\beta} \quad (1)$$

Best-fit parameters were searched using χ^2-fitting to the flux points. The measured gamma-ray spectra, in particular the low-energy parts, matched the π^0-decay model (Fig. 2). Parameters for the underlying proton spectrum are $s_1 = 2.36 \pm 0.02$, $s_2 = 3.1 \pm 0.1$, and $p_{br} = 239 \pm 74$ GeV c^{-1} for IC 443, and $s_1 = 2.36 \pm 0.05$, $s_2 = 3.5 \pm 0.3$, and $p_{br} = 22$ GeV c^{-1} for W44 (statistical errors only). In Fig. 3 we show the energy distributions of the high-energy protons derived from the gamma-ray fits. The break p_{br} is at higher energies and is unrelated to the low-energy pion-decay bump seen in the gamma-ray spectrum. If the interaction between a cosmic-ray precursor (i.e., cosmic rays distributed in the shock upstream on scales smaller than ~0.1R, where R is the SNR radius) and adjacent molecular clouds were responsible for the bulk of the observed GeV gamma rays, one would expect a much harder energy spectrum at low energies (i.e., a smaller value for the index s_1), contrary to the Fermi observations. Presumably, cosmic rays in the shock downstream produce the observed gamma rays; the first index s_1 represents the shock acceleration index with possible effects due to energy-dependent propagation, and p_{br} may indicate the momentum above which protons cannot be effectively confined within the SNR shell. Note that p_{br} results in the high-energy break in the gamma-ray spectra at ~20 GeV and ~2 GeV for IC 443 and W44, respectively.

The π^0-decay gamma rays are likely emitted through interactions between "crushed cloud" gas and relativistic protons, both of which are highly compressed by radiative shocks driven into molecular clouds that are overtaken by the blast wave of the SNR (*25*). Filamentary structures of synchrotron radiation seen in a high-resolution radio continuum map of W44 (*26*) support this picture. High-energy particles in the "crushed cloud" can be explained by reacceleration of the preexisting galactic cosmic rays (*25*) and/or freshly accelerated particles that have entered the dense region (*20*). The mass of the shocked gas

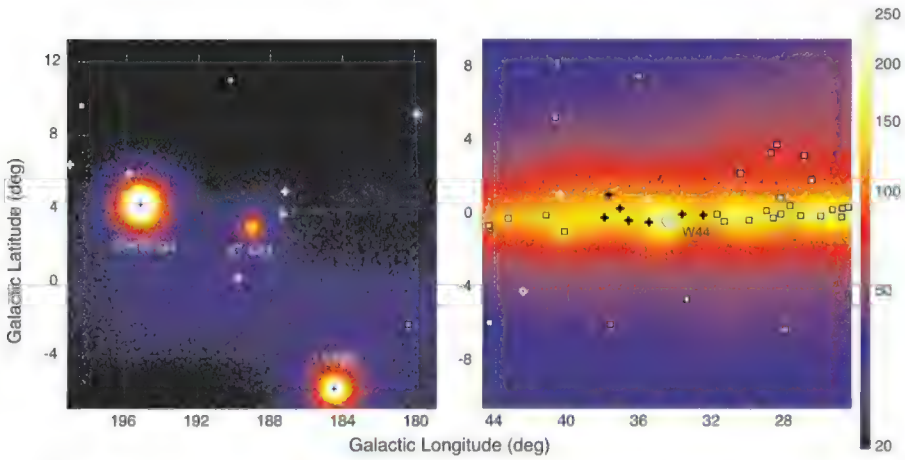

Fig. 1. Gamma-ray count maps of the 20° × 20° fields around IC 443 (**left**) and W44 (**right**) in the energy range 60 MeV to 2 GeV. Nearby gamma-ray sources are marked as crosses and squares. Diamonds denote previously undetected sources. For sources indicated by crosses and diamonds, the fluxes were left as free parameters in the analysis. Events were spatially binned in regions of side length 0.1°, the color scale units represent the square root of count density, and the colors have been clipped at 20 counts per pixel to make the galactic diffuse emission less prominent. Given the spectra of the sources and the effective area of the LAT instrument, the bulk of the photons seen in this plot have energies between 300 and 500 MeV. IC 443 is located in the galactic anti-center region, where the background gamma-ray emission produced by the pool of galactic cosmic rays interacting with interstellar gas is rather weak relative to the region around W44. The two dominant sources in the IC 443 field are the Geminga pulsar (2FGL J0633.9+1746) and the Crab (2FGL J0534.5+2201). For the W44 count map, W44 is the dominant source (subdominant, however, to the galactic diffuse emission).

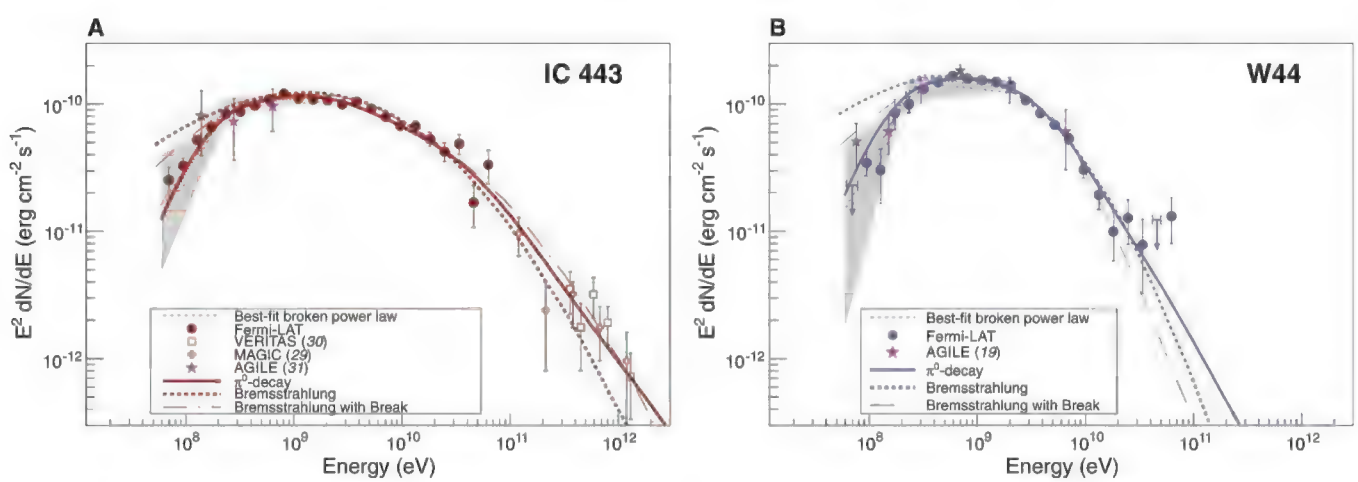

Fig. 2. (**A** and **B**) Gamma-ray spectra of IC 443 (A) and W44 (B) as measured with the Fermi LAT. Color-shaded areas bound by dashed lines denote the best-fit broadband smooth broken power law (60 MeV to 2 GeV); gray-shaded bands show systematic errors below 2 GeV due mainly to imperfect modeling of the galactic diffuse emission. At the high-energy end, TeV spectral data points for IC 443 from MAGIC (*29*) and VERITAS (*30*) are shown. Solid lines denote the best-fit pion-decay gamma-ray spectra, dashed lines denote the best-fit bremsstrahlung spectra, and dash-dotted lines denote the best-fit bremsstrahlung spectra when including an ad hoc low-energy break at 300 MeV c^{-1} in the electron spectrum. These fits were done to the Fermi LAT data alone (not taking the TeV data points into account). Magenta stars denote measurements from the AGILE satellite for these two SNRs, taken from (*31*) and (*19*), respectively.

($\sim 1 \times 10^3\ M_\odot$ and $\sim 5 \times 10^3\ M_\odot$ for IC 443 and W44, respectively, where $M_\odot$ is the mass of the Sun) is large enough to explain the observed gamma-ray luminosity. Because the "crushed cloud" is geometrically thin, multi-GeV particles are prone to escape from the dense gas, which may explain the break p_{br}.

Escaped cosmic rays reaching the unshocked molecular clouds ahead of the SNR shock can also produce π^0-decay gamma rays (*27*, *28*). Indeed, the gamma rays emitted by the escaped cosmic rays in the large molecular complex that surrounds W44 (total extent of 100 pc) have been identified with three close-by sources (*20*), which led us to remove them from the model in the maximum likelihood analysis, as mentioned above. With this treatment, the measured fluxes below 1 GeV contain small contributions from the escaped cosmic rays, but this does not affect our conclusions. The escaped cosmic rays may significantly contribute to the measured TeV fluxes from IC 443 (*29*, *30*). Emission models could be more complicated. For example, the cosmic-ray precursor with a scale of $\sim 0.1R$ at the highest energy could interact with the adjacent unshocked molecular gas, producing hard gamma-ray emission. This effect is expected to become important above the LAT energy range.

We should emphasize that radiation by relativistic electrons cannot account for the gamma-ray spectra of the SNRs as naturally as radiation by relativistic protons can (*23*). An inverse-Compton origin of the emission was not plausible on energetic grounds (*11*). The most important seed photon population for scattering is the infrared radiation produced locally by the SNR itself, with an energy density of ~ 1 eV cm^{-3}, but this is not large enough to explain the observed gamma-ray emission. Unless we introduce in an ad hoc way an additional abrupt break in the electron spectrum at 300 MeV c^{-1} (Fig. 2, dash-dotted lines), the bremsstrahlung models do not fit the observed gamma-ray spectra. If we assume that the same electrons are responsible for the observed synchrotron radiation in the radio band, a low-energy break is not expected to be very strong in the radio spectrum, and thus the existing data do not rule out this scenario. The introduction of the low-energy break introduces additional complexity, and therefore a bremsstrahlung origin is not preferred. Although most of the gamma-ray emission from these SNRs is due to π^0 decay, electron bremsstrahlung may still contribute at a lower level. The Fermi LAT data allow an electron-to-proton ratio K_{ep} of ~ 0.01 or less, where K_{ep} is defined as the ratio of dN_e/dp and dN_p/dp at $p = 1$ GeV c^{-1} (figs. S2 and S3).

Finding evidence for the acceleration of protons has long been a key issue in attempts to elucidate the origin of cosmic rays. Our spectral measurements down to 60 MeV enable identification of the π^0-decay feature, thus providing direct evidence for the acceleration of protons in SNRs. The proton momentum distributions, well constrained by the observed gamma-ray spectra, are yet to be understood in terms of acceleration and escape processes of high-energy particles.

Table 1. Spectral parameters in the energy range of 60 MeV to 2 GeV for power-law (PL) and broken power-law (BPL) models. $TS = 2\ \ln(\mathcal{L}_1/\mathcal{L}_0)$ is the test-statistic value.

Model	K (cm^2 s^{-1} MeV^{-1})	Γ_1	Γ_2	ε_{br} (MeV)	TS
IC 443					
PL	$11.7\ (\pm 0.2) \times 10^{-10}$	1.76 ± 0.02	—	—	21,651
BPL	$11.9\ (\pm 0.6) \times 10^{-10}$	0.57 ± 0.25	$1.95^{+0.02}_{-0.02}$	245^{+16}_{-15}	22,010
W44					
PL	$13.0\ (\pm 0.4) \times 10^{-10}$	1.71 ± 0.03	—	—	6,920
BPL	$15.8\ (\pm 1.0) \times 10^{-10}$	0.07 ± 0.4	$2.08^{+0.03}_{-0.03}$	253^{+11}_{-11}	7,351

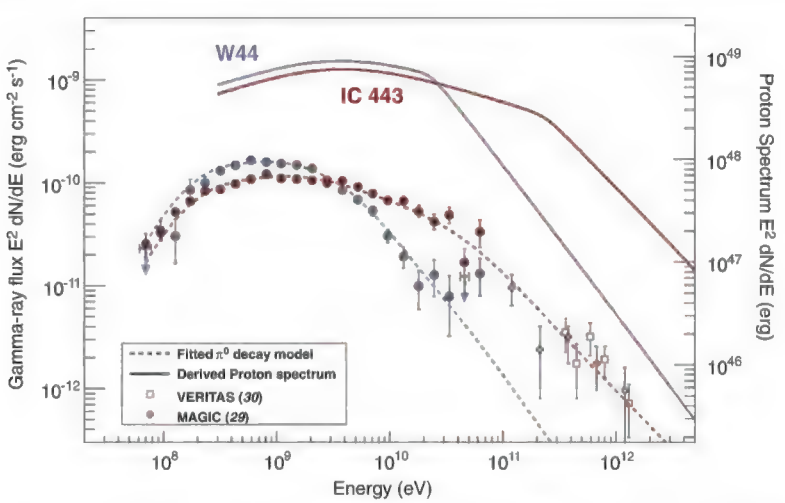

Fig. 3. Proton and gamma-ray spectra determined for IC 443 and W44. Also shown are the broadband spectral flux points derived in this study, along with TeV spectral data points for IC 443 from MAGIC (*29*) and VERITAS (*30*). The curvature evident in the proton distribution at ~2 GeV is a consequence of the display in energy space (rather than momentum space). Gamma-ray spectra from the protons were computed using the energy-dependent cross section parameterized by (*32*). We took into account accelerated nuclei (heavier than protons) as well as nuclei in the target gas by applying an enhancement factor of 1.85 (*33*). Note that models of the gamma-ray production via *pp* interactions have some uncertainty. Relative to the model adopted here, an alternative model of (*6*) predicts ~30% less photon flux near 70 MeV; the two models agree with each other to better than 15% above 200 MeV. The proton spectra assume average gas densities of $n = 20$ cm^{-3} (IC 443) and $n = 100$ cm^{-3} (W44) and distances of 1.5 kpc (IC 443) and 2.9 kpc (W44).

References and Notes

1. M. A. Malkov, L. O'C. Drury, *Rep. Prog. Phys.* **64**, 429 (2001).
2. J. S. Warren *et al.*, *Astrophys. J.* **634**, 376 (2005).
3. Y. Uchiyama, F. A. Aharonian, T. Tanaka, T. Takahashi, Y. Maeda, *Nature* **449**, 576 (2007).
4. E. A. Helder *et al.*, *Science* **325**, 719 (2009).
5. G. Morlino, D. Caprioli, *Astron. Astrophys.* **538**, A81 (2012).
6. C. D. Dermer, *Astron. Astrophys.* **157**, 223 (1986).
7. L. O'C. Drury, F. A. Aharonian, H. J. Völk, *Astron. Astrophys.* **287**, 959 (1994).
8. T. Naito, F. Takahara, *J. Phys. G* **20**, 477 (1994).
9. F. W. Stecker, *NASA Spec. Publ. 249* (1971).
10. F. A. Aharonian, L. O'C. Drury, H. J. Völk, *Astron. Astrophys.* **285**, 645 (1994).
11. A. A. Abdo *et al.*, *Astrophys. J.* **706**, L1 (2009).
12. D. J. Thompson, L. Baldini, Y. Uchiyama, http://arxiv.org/abs/1201.0988 (2012).
13. M. Seta *et al.*, *Astrophys. J.* **505**, 286 (1998).
14. P. L. Nolan *et al.*, *Astrophys. J. Suppl. Ser.* **199**, 31 (2012).
15. A. A. Abdo *et al.*, *Science* **327**, 1103 (2010).
16. A. A. Abdo *et al.*, *Astrophys. J.* **712**, 459 (2010).
17. J. Lande *et al.*, *Astrophys. J.* **756**, 5 (2012).
18. M. Ackermann *et al.*, *Astrophys. J. Suppl. Ser.* **203**, 4 (2012).
19. A. Giuliani *et al.*, *Astrophys. J.* **742**, L30 (2011).
20. Y. Uchiyama *et al.*, *Astrophys. J.* **749**, L35 (2012).
21. http://fermi.gsfc.nasa.gov/ssc/
22. The region model fitted to the data includes the SNR of interest (IC 443 or W44), background point sources from the 2FGL catalog (*14*), the galactic diffuse emission (ring_2year_P76_v0.fits), and a corresponding isotropic component (isotrop_2year_P76_source v0.txt).
23. J. R. Mattox *et al.*, *Astrophys. J.* **461**, 396 (1996).
24. See supplementary materials on *Science* Online.
25. Y. Uchiyama, R. D. Blandford, S. Funk, H. Tajima, T. Tanaka, *Astrophys. J.* **723**, L122 (2010).
26. G. Castelletti, G. Dubner, C. Brogan, N. E. Kassim, *Astron. Astrophys.* **471**, 537 (2007).
27. S. Gabici, F. A. Aharonian, S. Casanova, *Mon. Not. R. Astron. Soc.* **396**, 1629 (2009).
28. Y. Ohira, K. Murase, R. Yamazaki, *Mon. Not. R. Astron. Soc.* **410**, 1577 (2011).
29. J. Albert *et al.*, *Astrophys. J.* **664**, L87 (2007).
30. V. A. Acciari *et al.*, *Astrophys. J.* **698**, L133 (2009).
31. M. Tavani *et al.*, *Astrophys. J.* **710**, L151 (2010).

32. T. Kamae, N. Karlsson, T. Mizuno, T. Abe, T. Koi, *Astrophys. J.* **647**, 692 (2006).
33. M. Mori, *Astropart. Phys.* **31**, 341 (2009).

Acknowledgments: The Fermi LAT Collaboration acknowledges support from a number of agencies and institutes for both development and the operation of the LAT as well as scientific data analysis. These include NASA and the U.S. Department of Energy (United States); CEA/Irfu and IN2P3/CNRS (France); ASI and INFN (Italy); MEXT, KEK, and JAXA (Japan); and the K. A. Wallenberg Foundation, the Swedish Research Council, and the National Space Board (Sweden). Additional support from INAF in Italy and CNES in France for science analysis during the operations phase is also gratefully acknowledged. Fermi LAT data are available from the Fermi Science Support Center (http://fermi.gsfc.nasa.gov/ssc).

Supplementary Materials
www.sciencemag.org/cgi/content/full/339/6121/807/DC1
Materials and Methods
Figs. S1 to S3
References (*34*–*39*)

5 October 2012; accepted 12 December 2012
10.1126/science.1231160

Crystalline Inorganic Frameworks with 56-Ring, 64-Ring, and 72-Ring Channels

Hsin-Yau Lin,[1] Chih-Yuan Chin,[1] Hui-Lin Huang,[1] Wen-Yen Huang,[1] Ming-Jhe Sie,[1] Li-Hsun Huang,[1] Yuan-Han Lee,[1] Chia-Her Lin,[2] Kwang-Hwa Lii,[3] Xianhui Bu,[4] Sue-Lein Wang[1]*

The development of zeolite-like structures with extra-large pores (>12-membered rings, 12R) has been sporadic and is currently at 30R. In general, templating via molecules leads to crystalline frameworks, whereas the use of organized assemblies that permit much larger pores produces noncrystalline frameworks. Synthetic methods that generate crystallinity from both discrete templates and organized assemblies represent a viable design strategy for developing crystalline porous inorganic frameworks spanning the micro and meso regimes. We show that by integrating templating mechanisms for both zeolites and mesoporous silica in a single system, the channel size for gallium zincophosphites can be systematically tuned from 24R and 28R to 40R, 48R, 56R, 64R, and 72R. Although the materials have low thermal stability and retain their templating agents, single-activator doping of Mn^{2+} can create white-light photoluminescence.

Crystalline open-framework materials are of interest because of their rich structural chemistry and their use ranging from conventional catalysis, gas separation, and ion exchange to modern high-tech low-*k* materials, zeolite-dye microlasers, high-capacity H_2 and CO_2 gas storage (*1*–*4*), and potential lanthanide-free phosphor materials for light-emitting diodes (*5*–*7*). Their functions are mainly attributed to properties related to pore size. Therefore, pore engineering goals such as enlarging the channels, changing channel shape and connectivity, or modifying the wall composition are critical for creating new materials.

For many years, various zeolite-like structures have been synthesized using both simple and complex preparative techniques. In 1982, the discovery of $AlPO_4$-based zeolite structures (*8*) inspired the synthesis of open-framework metal phosphates. Soon after, the crystal structure of an iron phosphate mineral known as cacoxenite (*9*) was solved, revealing that the structure contained notably large channels with a free diameter of 1.4 nm and openings encircled by 36 polyhedra (36R). These discoveries led to increasing interest in pure tetrahedral and mixed polyhedral frameworks with extra-large channels (table S1). Later, many landmark structures were synthesized

[1]Department of Chemistry, Frontier Research Center on Fundamental and Applied Sciences of Matters, National Tsing Hua University, Hsinchu 30013, Taiwan. [2]Department of Chemistry, Chung-Yuan Christian University, Chungli 320, Taiwan. [3]Department of Chemistry, National Central University, Chungli 320, Taiwan. [4]Department of Chemistry and Biochemistry, California State University, Long Beach, CA 90840, USA.
*To whom correspondence should be addressed. E-mail: slwang@mx.nthu.edu.tw

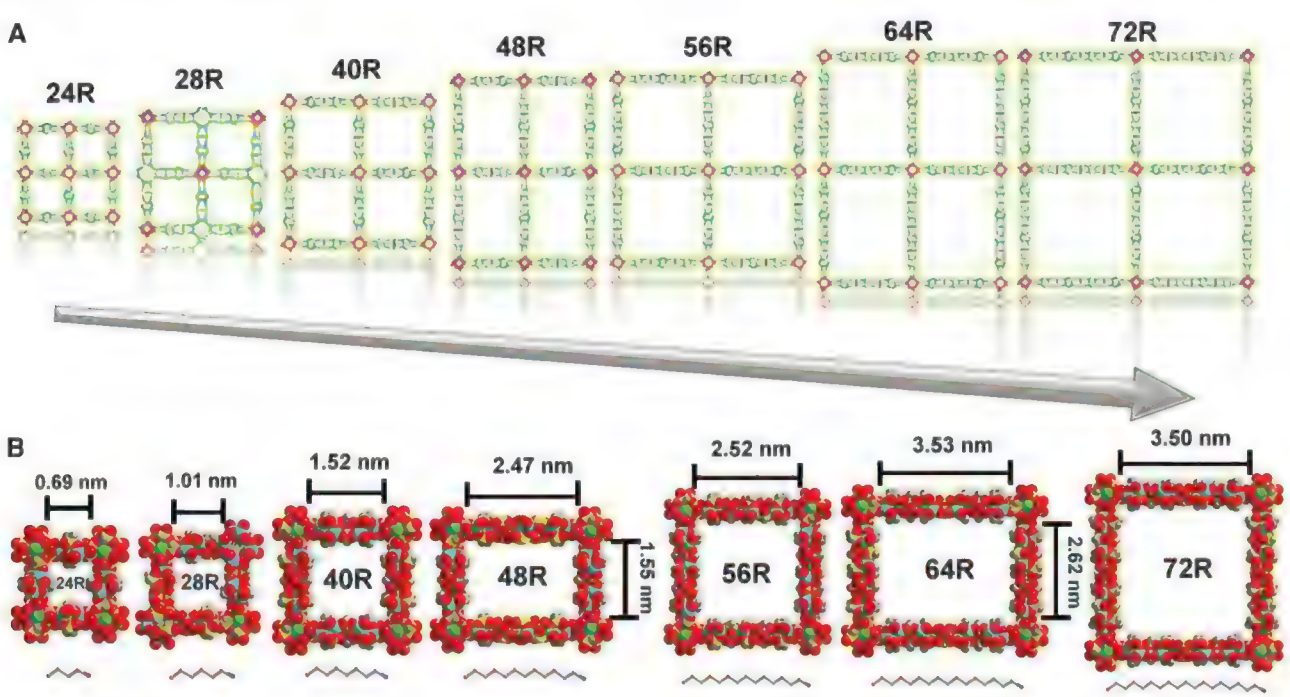

Fig. 1. Systematic expansion of structures with extra-large channels. (**A**) Channel ring size ranging from 24R to 72R. (**B**) Pore diameters spanning the micro and meso regimes. The templates are alkyl monoamines (using a ball-and-stick model) with carbon chain lengths ranging from 4C to 18C.

(*10*–*18*), including SU-M, NTHU-5, and ITQ-37 (*18*), in which the upper limits of the channel sizes were delimited to 14R in aluminosilicates, 24R in phosphates, 26R in phosphites, and 30R in germanium oxides and germanosilicates. Relative to the more recent metal-organic frameworks (MOFs) (*19*, *20*), progress in the expansion of inorganic channels has tended to be slow and accidental, without any way to predict the next channel ring size. This difficulty could be attributed to the lack of tunable spacer units (e.g., organic linkers) and an inability to control the linkages of the inorganic units; although certain germanates have been found to form from modular units (*21*, *22*), neither their presence nor their topologies are predictable prior to the syntheses. In addition, limitations in channel or pore size may result from the fact that organized assemblies such as surfactant-based templates, while capable of creating large pore sizes, generally lead to disordered wall structures as exemplified by the mesoporous silicates. Thus far, the rational design of microporous and mesoporous inorganic frameworks with ordered wall structures has not been reported.

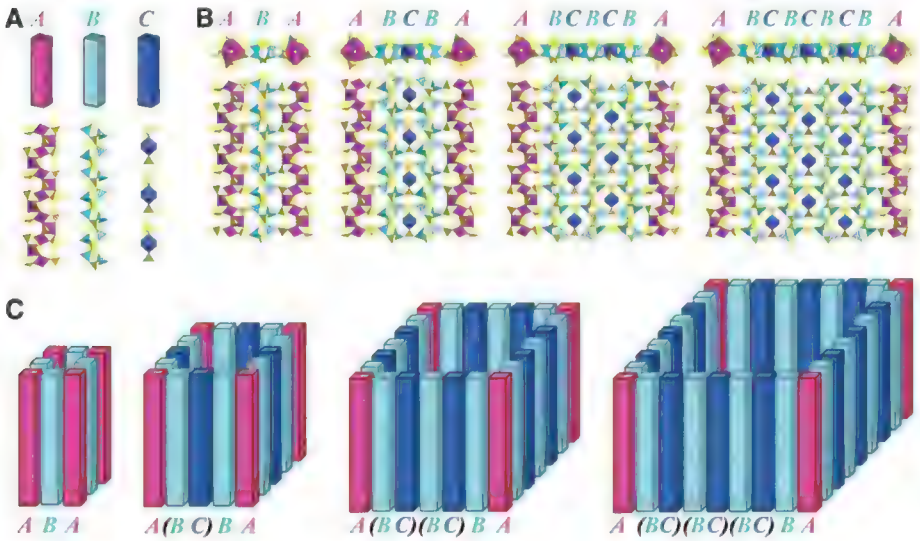

Fig. 2. The structures of the family NTHU-13. (**A**) Three common building blocks. (**B**) Sequential linkages of blocks A, B, and C to yield varied channel edges and wall structures. (**C**) Schematic drawings showing channel expansion from 24R to 40R, 56R, and 72R with the growth of one or more BC pairs as the proliferation unit.

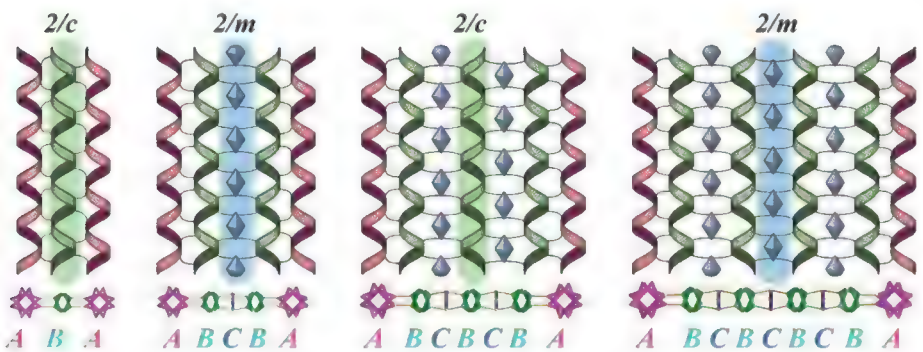

Fig. 3. Periodic variation in symmetry accompanied by channel expansion via the insertion of BC pairs. The formulae for the channel walls, from left to right, are $[A(BC)_nBA]$, n = 0, 1, 2, and 3.

Previously reported microporous structures have been primarily produced via template-directed routes under common hydrothermal or solvothermal conditions; however, the micropores or channels have not been manipulated using any specific type of discrete template molecule. Surfactant-templated reactions provide a rational basis for the synthesis of various mesoporous materials (*23*, *24*) in which long carbon chain surfactants with ammonium head groups aggregate into meso-scale template assemblies surrounded by amorphous inorganic walls (*25*).

We report a systematic synthetic method that allows the production of extra-large channel inorganic frameworks based on gallium zincophosphites and referred to as NTHU-13. A series of aliphatic monoamines with straight carbon chain lengths ranging from four carbons (4C) to 18C were used as templates to enable channel expansion from 24R to 28R and then to 40R, 48R, 56R, 64R, and 72R (Fig. 1). Previous efforts that used monoamines with long straight carbon chains (>8C) in microporous material synthesis often led to lamellar-phased products. We found that we could increase the likelihood of larger channels by using heterometal centers. In single-metal systems, an increase in template size led to dif-

Table 1. Compositions, cell lengths, channel edge connectivity, and pore-related data for the family NTHU-13. The monoamine templates are named according to the number of carbons of the straight-chain amine skeletons. Channel opening refers to the maximum size of a sphere that can fit into the opening (the estimated free diameter); the value in parentheses is the length of the second dimension for a noncircular channel window. SAV [solvent-accessible volume (*28*)] is an estimate of percent unit cell volume not occupied by inorganic frameworks. FD is framework density. D_c is the density of alkyl monoamine templates within channels versus the density (D_a) in a pure liquid state. V_a is the total amount of molecular volume occupied by amine templates in a unit cell.

Code	Template	Framework	a (or b) (Å)	c (Å)	Wall stoichiometry	n	Channel opening (nm)	SAV (%)	FD	D_c/D_a	V_a/SAV
24R*	4C′	$[GaFZn_2(HPO_3)_4]^{2-}$	31.072	10.029	ABA	0	0.69	52.1	11.72	0.78/0.74	0.586
28R	6C′	$[GaFZn_7(H_2O)_4(HPO_3)_{10}]^{4-}$	52.175	10.023	ABCβ	—	1.01	51.7	10.56	0.78/0.77	0.582
40R	8C′	$[Ga_2F_2Zn_9(H_2O)_4(HPO_3)_{14}]^{6-}$	48.393	10.000	A(BC)BA	1	1.52	61.7	8.54	0.72/0.78	0.530
48R	12C′	$[Ga_4F_4Zn_{23}(H_2O)_{12}(HPO_3)_{34}]^{14-}$	48.500	10.054	[A(BC)BA]	1	1.55	66.2	7.55	0.80/0.81	0.592
			66.316 (*b*)		[A(BC)$_2$BA]	2	(2.47)				
56R	14C′	$[GaFZn_7(H_2O)_4(HPO_3)_{10}]^{4-}$	66.310	9.982	A(BC)$_2$BA	2	2.52	70.5	6.56	0.73/0.78	0.540
64R	16C′	$[Ga_4F_4Zn_{33}(H_2O)_{20}(HPO_3)_{46}]^{18-}$	84.043	10.036	[A(BC)$_3$BA]	3	(3.53)	72.3	5.94	0.71/0.78	0.525
			66.298 (*b*)		[A(BC)$_2$BA]	2	2.62				
72R	18C′	$[Ga_2F_2Zn_{19}(H_2O)_{12}(HPO_3)_{26}]^{10-}$	84.115	10.069	[A(BC)$_3$BA]	3	3.50	75.7	5.28	0.66/0.86	0.488

*The structure is a Ga analog of NTHU-5 (*17*).

ferent structures rather than the expansion of ring sizes in the channels. In this study, we used the zinc-gallium bimetallic system and found that increasing the template from 4C-containing (4C′) butylamine to 6C′ hexylamine was sufficient to enlarge the channel sizes from 24R to 28R, creating 28R-NTHU-13 with a channel diameter exceeding 1 nm (Table 1). In subsequent reactions [table S2 (*26*)], the use of longer amine (8C′ octylamine, 10C′ decylamine, or 12C′ dodecylamine) created the larger ring products 40R- and 48R-NTHU-13, respectively. The use of 14C′ tetradecylamine, 16C′ hexadecylamine, and 18C′ octadecylamine led to the synthesis of 56R-NTHU-13, 64R-NTHU-13, and 72R-NTHU-13 in which pore sizes were as large as 3.5 nm (Table 1).

We used single-crystal x-ray diffraction to characterize all six structures in the NTHU-13 family (figs. S1 to S10 and table S3). Four channels were determined in the unit cells for 40R-, 48R-, 56R-, 64R-, and 72R-NTHU-13 (Fig. 1A), and eight channels were found in the orthorhombic cell for 28R-NTHU-13 (fig. S3). Except for the latter, the channel walls were constructed exclusively from the following three building blocks: anionic chains of $_\infty[GaF(HPO_3)_2]^{2-}$ (block A), neutral chains of $_\infty[Zn(HPO_3)]$ (block B), and an anionic trimeric cluster of $[Zn(HPO_3)_2(H_2O)_4]^{2-}$ (block C) (Fig. 2). Block A was located at the four corners of the square-shaped channels (Fig. 2A); both A and C were linked only to B and were never adjacent. A generalized formula of $[A(BC)_nBA]$ describes the stoichiometry and connectivity of the four faces or edges of the inorganic walls: $n = 1$ for each face or edge of the 40R channel, $n = 2$ for the 56R channel, and $n = 3$ for the 72R channel. When $n = 0$, the corresponding channel face is ABA and is observed to form 24R channels. Hence, the 40R, 56R, and 72R square-windowed channels can be viewed as the systematic expansion of the 24R channel by inserting one or more BC pairs as the proliferation unit (Fig. 2B). The rectangular-windowed 48R and 64R channels contain two mixed n values (n and $n + 1$) to describe the shorter and longer window edges (Table 1 and table S4). An increase of one BC pair would add four polyhedra to each channel edge, leading to an expansion by 16 rings for square-windowed channels (24R to 40R; 40R to 56R; 56R to 72R) and 8 rings for rectangular-windowed channels (40R to 48R; 48R to 56R; 56R to 64R; 64R to 72R).

For each 8-ring expansion, there was an approximate 0.8-nm increase in the channel diameter and an ~18 Å increase in the unit cell length (Table 1) in addition to a periodic change in the wall structure symmetry. As illustrated in Fig. 3, the wall structure shows 2/*m* symmetry along *a* (or *b*) when $n = 1$ (or for odd numbers); however, 2/*c* symmetry is observed when $n = 2$ (or for even numbers). These results explain why both 40R- and 72R-NTHU-13 are in the $I4_1/amd$ space group, 56R-NTHU-13 belongs in space group $I4_1/acd$, and the orthorhombic 48R- and 64R-NTHU-13 possess both the *m* and *c* glide planes in their space group symmetry. Notably, each BC pair incorporates additional zinc ions and phosphite groups into the framework at a fixed 5:6 ratio, which causes the Ga concentration to decrease as the channels are expanded. The heterometal centers of Ga^{3+} provide the NTHU-13 family with a key structural component: block A. When $n = \infty$, the NTHU-13 system would reach a maximum M/P value of 5/6 (where M is the total number of Zn and Ga centers, and P is the number of phosphite groups) and would form lamellar structures.

The 56R and 72R channels (with free diameters of 2.52 nm and 3.5 nm, respectively) are in the mesopore regime, which is a mesoporous framework with tetragonal symmetry showing regularly spaced inorganic channels with ordered wall structures at the atomic level (*27*). Among all reported crystalline inorganic frameworks to date, 72R-NTHU-13 possesses the lowest framework density (5.28) and the highest nonframework volume (75.7%) (table S1). The channel space was partially occupied by organized assemblies of monoprotonated amine molecules (~50%) with a density near that of the pure molecular liquid or solid state (Table 1). The templates were distributed quite near the inorganic wall with their ammonium heads pointing primarily toward the negatively charged blocks A and C (and are also likely to contain hydrogen bonds, because the closest N···O distances were observed to fall in the range of 2.83 to 2.90 Å). Their long carbon chain skeletons were disordered and pointed toward the hydrophobic region of the channel centers (fig. S9). Within each of the 56R, 64R, or 72R channels per unit cell, there exist 16, 18, or 20 monoprotonated template-amine molecules. Elemental analysis data (table S5) and solid-state nuclear magnetic resonance studies using ^1H, ^{13}C, and ^{19}F confirmed the content of the organic templates and the presence of fluoride (figs. S11 to S13).

Thermogravimetric analysis (fig. S14) combined with variable-temperature powder x-ray diffraction measurements (fig. S15) were used to determine the thermal stability of 40R-, 48R-, and 56R-NTHU-13, which were thermally stable up to 175°C. When transparent colorless crystals of 40R-NTHU-13 were treated with 0.05 M parafuchsin hydrochloride (in ethanol), the crystals changed to a pink color (fig. S16), which indicates that the dye molecules were adsorbed. Cs^+ ion exchange was performed by treating powder samples of 40R- and 48R-NTHU-13 with a 0.01 M CsCl ethanol solution, and positive results were confirmed by x-ray fluorescence data in combination with powder x-ray diffraction measurements (table S6 and fig. S17). The empty space inside the channels was detected even in the presence of the residual templates, as indicated by preliminary results from gas adsorption measurements performed on 56R-NTHU-13 samples (fig. S18).

Relative to the aluminosilicates, the crystals of NTHU-13 are less robust in nature, and so far have not yet shown impressive conventional pore-related properties such as gas sorption (the maximum CO_2 uptake of 56R-NTHU-13 at 1 atm is 0.32 mmol/g; see figs. S18 and S19). However, very large inorganic channels may display unexpected properties such as pore-related photoluminescence, as we previously reported (*5*–*7*). When the 40R channel framework was successfully doped with Mn^{2+} ions, an unusual broad band of nearly white light emission under ultraviolet excitation was displayed by the resultant Mn@40R-NTHU-13 (fig. S20). Thus, the host lattice of 40R-NTHU-13 revealed the ability to create a white-light phosphor from single-activator doping.

References and Notes

1. A. Corma, *Chem. Rev.* **97**, 2373 (1997).
2. M. E. Davis, *Nature* **417**, 813 (2002).
3. H. Furukawa *et al.*, *Science* **329**, 424 (2010).
4. Y. S. Bae, R. Q. Snurr, *Angew. Chem. Int. Ed.* **50**, 11586 (2011).
5. Y. C. Liao, C. H. Lin, S. L. Wang, *J. Am. Chem. Soc.* **127**, 9986 (2005).
6. Y. C. Yang, S. L. Wang, *J. Am. Chem. Soc.* **130**, 1146 (2008).
7. P. C. Jhang, Y. C. Yang, Y. C. Lai, W. R. Liu, S. L. Wang, *Angew. Chem. Int. Ed.* **48**, 742 (2009).
8. S. T. Wilson, B. M. Lok, C. A. Messina, T. R. Cannan, E. M. Flanigen, *J. Am. Chem. Soc.* **104**, 1146 (1982).
9. P. B. Moore, J. Shen, *Nature* **306**, 356 (1983).
10. M. E. Davis, C. Saldarriaga, C. Montes, J. Garces, C. Crowdert, *Nature* **331**, 698 (1988).
11. M. Estermann, L. B. McCusker, C. Baerlocher, A. Merrouche, H. Kessler, *Nature* **352**, 320 (1991).
12. C. C. Freyhardt, M. Tsapatsis, R. F. Lobo, K. J. Balkus Jr., M. E. Davis, *Nature* **381**, 295 (1996).
13. N. Guillou *et al.*, *Angew. Chem. Int. Ed.* **40**, 2831 (2001).
14. G.-Y. Yang, S. C. Sevov, *J. Am. Chem. Soc.* **121**, 8389 (1999).
15. C. H. Lin, S. L. Wang, K. H. Lii, *J. Am. Chem. Soc.* **123**, 4649 (2001).
16. X. Zou, T. Conradsson, M. Klingstedt, M. S. Dadachov, M. O'Keeffe, *Nature* **437**, 716 (2005).
17. Y. L. Lai, K. H. Lii, S. L. Wang, *J. Am. Chem. Soc.* **129**, 5350 (2007).
18. J. Sun *et al.*, *Nature* **458**, 1154 (2009).
19. N. L. Rosi *et al.*, *Science* **300**, 1127 (2003).
20. H. Deng *et al.*, *Science* **336**, 1018 (2012).
21. M. V. Peskov, X. Zou, *J. Phys. Chem. C* **115**, 7729 (2011).
22. L. Tang *et al.*, *Nat. Mater.* **7**, 381 (2008).
23. C. T. Kresge, M. E. Leonowicz, W. J. Roth, J. C. Vartuli, J. S. Beck, *Nature* **359**, 710 (1992).
24. Q. Huo *et al.*, *Nature* **368**, 317 (1994).
25. Microporous pores and channels have pore diameters (d) < 2.0 nm, whereas mesoporous ones have $2.0 \le d \le 50$ nm.
26. See supplementary materials on *Science* Online.
27. The crystalline inorganic framework will collapse if the organic template is completely removed.
28. A. L. Spek, *Acta Crystallogr. A* **46**, C34 (1990).

Acknowledgments: Supported by National Science Council of Taiwan grants NSC100-2113-M-007-016-MY3, NSC101-2113-M-033-007-MY3, and NSC101-2113-M-008-006-MY3. X.B. was supported by NSF grant DMR-0846958. Crystallographic data for the reported crystal structures have been deposited at the Cambridge Crystallographic Data Centre with codes 892384–892387 and 915187–915191.

Supplementary Materials

www.sciencemag.org/cgi/content/full/339/6121/811/DC1
Materials and Methods
Figs. S1 to S20
Tables S1 to S6
References (*29*–*36*)

29 October 2012; accepted 14 December 2012
10.1126/science.1232097

Dilute Concentrations of a Psychiatric Drug Alter Behavior of Fish from Natural Populations

T. Brodin,[1]* J. Fick,[2] M. Jonsson,[1] J. Klaminder[1]

Environmental pollution by pharmaceuticals is increasingly recognized as a major threat to aquatic ecosystems worldwide. A variety of pharmaceuticals enter waterways by way of treated wastewater effluents and remain biochemically active in aquatic systems. Several ecotoxicological studies have been done, but generally, little is known about the ecological effects of pharmaceuticals. Here we show that a benzodiazepine anxiolytic drug (oxazepam) alters behavior and feeding rate of wild European perch (*Perca fluviatilis*) at concentrations encountered in effluent-influenced surface waters. Individuals exposed to water with dilute drug concentrations (1.8 micrograms liter^{-1}) exhibited increased activity, reduced sociality, and higher feeding rate. As such, our results show that anxiolytic drugs in surface waters alter animal behaviors that are known to have ecological and evolutionary consequences.

Among pharmaceuticals, anxiolytics (pharmaceuticals used to treat anxiety) are a frequently prescribed class of psychotherapeutic drugs of which benzodiazepines are the most commonly used globally (*1*). Benzodiazepines persist in wastewater effluent and can therefore be found at concentrations ranging from 0.01 to several μg liter^{-1} in treated effluent (*1–4*). Further, several benzodiazepines are also quite resistant to photodegradation (*5*), which enables them to persist in aquatic environments, and have been found at concentrations ranging from 0.001 to 0.4 μg liter^{-1} in rivers and streams (*2*, *3*). Because benzodiazepines are designed to alter behavior by binding to γ-aminobutyric acid (GABA) receptors, which are found in a wide range of animal species, it is possible that organisms in aquatic environments receiving treated wastewater effluent are experiencing behavioral modifications (*6*). Behavior is a crucial determinant for important fitness correlates, such as growth, reproduction, and survival (*7*, *8*). Hence, pharmaceuticals such as benzodiazepines, which are designed to alter behavior, could have evolutionary and ecologically important effects through modifications of fish behavior that, over time, influence aquatic community compositions and, consequently, the functioning of aquatic systems. It is therefore surprising that ecotoxicological research thus far has not assessed how psychotherapeutic drugs frequently found in aquatic ecosystems may affect key behaviors of aquatic organisms.

In a screening of Swedish surface waters, we found concentrations of a common benzodiazepine, oxazepam, of 0.73 μg liter^{-1} in treated wastewater effluent and 0.58 μg liter^{-1} in a mid-sized stream (River Fyris) receiving input of treated wastewater (Table 1). These concentrations are comparable to those of benzodiazepines reported in other European and American waters (*1–4*). The concentration of oxazepam in muscle tissue of European perch (*Perca fluviatilis*) from River Fyris was more than six times that in the water, indicating bioaccumulation of this drug in the fish (Table 1). To assess how the presence and subsequent uptake of dissolved oxazepam may affect fish behavior, we exposed naturally spawned juvenile perch to water with two different concentrations of oxazepam: a low, environmentally relevant concentration of 1.8 μg liter^{-1} and a high concentration of 910 μg liter^{-1}. After 7 days of exposure, fish treated with low concentrations had accumulated oxazepam in their muscle tissue at concentrations overlapping with those found in fish from River Fyris (Table 1), indicating that the treatment with low concentrations represents an environmentally relevant oxazepam contamination level. To investigate if oxazepam alters fish behavior, we quantified the behavioral traits boldness, activity, and sociality (*9*) of perch individuals before and after they were exposed to either of the two chosen concentrations. These behavioral traits, sometimes referred to as personality traits (*10*), are known for being both ecologically and evolutionarily important and are used to predict how individuals respond to changed environmental conditions (*11–14*). The studied behavioral traits of untreated and treated fish were quantitatively measured with standardized protocols including video surveillance and subsequent image analysis (*9*). Activity was defined as number of swimming bouts (>2.5 cm) during the observation period (600 s). Boldness was calculated as the inverse of an individual's latency to enter a novel area during the observation period (900 s). Sociality was measured as an individual's spatial use, during 600 s, in relation to a group of conspecifics.

We found strong effects of oxazepam on fish behavior (Fig. 1, A to C). Individuals that were exposed to low concentrations became more active ($F_{1,46}$ = 4.2, P = 0.047) and less social ($F_{1,46}$ = 14.4, P = 0.0001) than fish that were not exposed, whereas boldness was largely unaffected. The reliability of the observed effects at the low concentration was strengthened by similar effects in the high-concentration treatment where all studied behavioral traits showed significant changes; exposed fish became more active ($F_{1,46}$ = 21.8, P = 0.0001), bolder ($F_{1,46}$ = 29.9, P = 0.0005), and more asocial ($F_{1,46}$ = 17.6, P = 0.0001) compared to unexposed individuals.

To assess more direct ecological effects of oxazepam exposure, we measured individual feeding rate, a fundamental fitness correlate (*15–19*). This was done by recording the time it took for each individual to initiate feeding on, and deplete, a resource consisting of 20 zooplankton (*Daphnia pulex*), both before and after pharmaceutical exposure (*9*). There was no significant difference in feeding rate between perch allocated to the three different treatments (control, low, and high) before exposure. However, the drug-induced change in feeding rate of fish

[1]Department of Ecology and Environmental Science, Umeå University, 90187 Umeå, Sweden. [2]Department of Chemistry, Umeå University, 90187 Umeå, Sweden.

*To whom correspondence should be addressed. E-mail: tomas.brodin@emg.umu.se

Table 1. Measured concentrations and relative standard deviations (RSD) of oxazepam in water and muscle-tissue samples and corresponding estimated bioaccumulation factors (BAF).

Sample	Water		Fish muscle tissue			BAF*
	μg liter^{-1}	RSD (%)	μg kg^{-1}	RSD (%)	Range (μg kg^{-1})	
River Fyris	0.58†		3.6‡	121	0.39–13§	6.2
High (1000 μg liter^{-1})	910‖	11	4900¶	33	1500–8500#	5.3
Low (1 μg liter^{-1})	1.8‖	46	18¶	39	6.6–36#	9.7
Control (0 μg liter^{-1})	>LOQ**		>LOQ††			

*Estimated bioaccumulation factors based on average values in water and fish muscle tissue from field and experimental measurements. †Single grab sample. ‡Average value, n = 10. §Range from minimum to maximum in μg liter^{-1}, n = 10. ‖Average value, n = 49. ¶Average value, n = 25. #Range from minimum to maximum in μg liter^{-1}, n = 25. **Below limit of quantification (LOQ), n = 49. ††Below limit of quantification, n = 25. For more details, see supplementary materials.

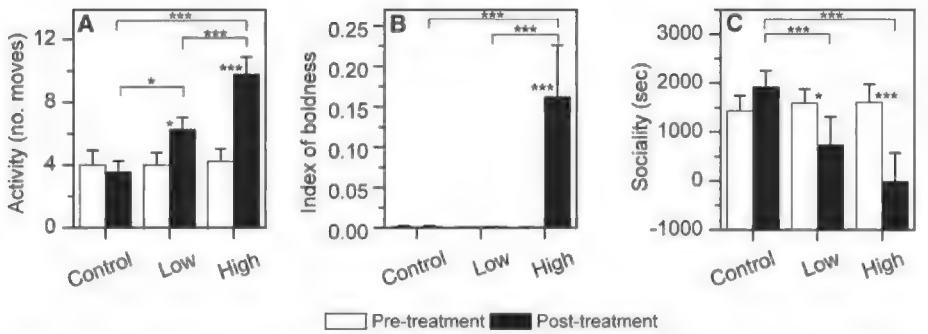

Fig. 1. Fish behavioral response to two concentrations (low: 1.8 μg liter^{-1}; high: 910 μg liter^{-1}) of dissolved oxazepam compared to control treatment (0 μg liter^{-1}). **(A)** Activity, measured as number of swimming bouts (>2.5 cm) during 10 min. **(B)** Boldness, measured as the inverse of latency to enter a novel area during the total trial time (900 s). **(C)** Sociality, measured as the cumulative time (in seconds) spent close to a group of conspecifics. Error bars represent ±1 SE (n = 25 in all treatments); statistically significant differences between the pre- and posttreatments are indicated (*P < 0.05 or ***P < 0.001).

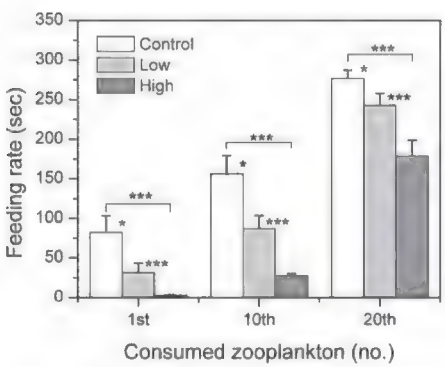

Fig. 2. Feeding rate of perch after oxazepam treatments. Feeding rate is expressed as the latency to capture the first zooplankton, the 10th zooplankton, and the 20th zooplankton. Error bars represent ±1 SE (n = 25 in all treatments); statistically significant differences between the control and treatments are indicated (*P < 0.05 or ***P < 0.001).

was pronounced (Fig. 2). Individuals exposed to the high concentration started feeding earlier and depleted the food resource faster than those exposed to the low concentration ($F_{1,48}$ = 46.3, P = 0.0001 and $F_{1,48}$ = 25.0, P = 0.0001, respectively) and the unexposed individuals ($F_{1,48}$ = 79.6, P = 0.0001 and $F_{1,48}$ = 30.1, P = 0.0001, respectively). This enhanced feeding rate fits well with the observed drug-induced increases in boldness and activity (*7*, *20*). Moreover, also fish exposed to the low concentration initiated feeding earlier ($F_{1,49}$ = 5.9, P = 0.019) and depleted the food resource faster ($F_{1,49}$ = 6.0, P = 0.018) than unexposed fish. That is, fish exposed to oxazepam concentration similar to that found in River Fyris showed altered foraging behavior that resulted in an accelerated depletion of the food resource. Correlations between the different behavioral traits and between the behavioral traits and feeding rate (table S1) suggest that oxazepam exposure induced bolder behavior that, in turn, increased feeding rate. Before exposure, none of the behavioral traits were significantly correlated with each other or with feeding rate, suggesting that oxazepam affects not only individual traits but also how the traits are correlated—relationships referred to as behavioral syndromes (*12*). Considering that the concentrations of oxazepam in muscle tissue of perch exposed to the low concentration are similar to those in wild-caught fish (Table 1), it is likely that behavior and feeding rates are modified also in wild fish exposed to dilute concentrations of anxiolytic drugs.

Changes in fish feeding rate may, over time, have ecosystem-level consequences, as fish are known to influence the structure of aquatic communities (*21*). Given that we found pharmaceutical effects on ecologically important behavioral traits, at environmentally relevant concentrations in water and muscle tissue, ecosystem-level consequences in natural systems seem likely. For example, increased feeding rate, as we observed, may result in top-down effects on primary production (algae) via suppression of primary consumers (zooplankton), especially because some organisms (e.g., zooplankton and algae) lack GABA receptors—a prerequisite for the pharmaceutical effects of benzodiazepines (*6*). However, increased activity and boldness, and reduced sociality (lower prevalence of shoaling), may also increase predation risk (*22*, *23*), making the net outcome of these pharmaceutical effects difficult to predict. Regardless of this uncertainty, it seems likely that fish fitness and food-web structures are altered in oxazepam-contaminated waters.

That environmentally relevant concentrations of a single benzodiazepine affect fish behavior and feeding rate is alarming, considering the cocktail of different pharmaceutical products that are found in waters worldwide (*1*, *4*, *24*). It should also be emphasized that there are several benzodiazepines, and direct additive effects from these compounds on behavior traits cannot be excluded. Further, increasing concentrations of pharmaceutical residues in aquatic systems can be expected, as pharmaceutical use is projected to increase as they become more available for the growing global population (*25*). Our results highlight ecologically important, previously underappreciated effects of psychotherapeutic drugs that enter aquatic ecosystems, and call for new test protocols to examine the full environmental impact of pharmaceutical residues.

References and Notes

1. V. Calisto, V. I. Esteves, *Chemosphere* **77**, 1257 (2009).
2. D. Hummel, D. Löffler, G. Fink, T. A. Ternes, *Environ. Sci. Technol.* **40**, 7321 (2006).
3. T. Kosjek *et al.*, *Water Res.* **46**, 355 (2012).
4. P. Verlicchi, M. Al Aukidy, E. Zambello, *Sci. Total Environ.* **429**, 123 (2012).
5. V. Calisto, M. R. M. Domingues, V. I. Esteves, *Water Res.* **45**, 6097 (2011).
6. L. Gunnarsson, A. Jauhiainen, E. Kristiansson, O. Nerman, D. G. Larsson, *Environ. Sci. Technol.* **42**, 5807 (2008).
7. T. Brodin, F. Johansson, *Ecology* **85**, 2927 (2004).
8. B. R. Smith, D. T. Blumstein, *Behav. Ecol.* **19**, 448 (2008).
9. Materials and methods are available as supplementary materials on *Science* Online.
10. D. Réale, S. M. Reader, D. Sol, P. T. McDougall, N. J. Dingemanse, *Biol. Rev. Camb. Philos. Soc.* **82**, 291 (2007).
11. S. R. X. Dall, A. I. Houston, J. McNamara, *Ecol. Lett.* **7**, 734 (2004).
12. A. Sih, A. Bell, J. C. Johnson, *Trends Ecol. Evol.* **19**, 372 (2004).
13. A. J. Frost, A. Winrow-Giffen, P. J. Ashley, L. U. Sneddon, *Proc. Biol. Sci.* **274**, 333 (2007).
14. J. S. Thomson, P. C. Watts, T. G. Pottinger, L. U. Sneddon, *Horm. Behav.* **61**, 750 (2012).
15. J. M. Elliott, *J. Anim. Ecol.* **45**, 923 (1976).
16. L. Persson, L. A. Greenberg, *Ecology* **71**, 1699 (1990).
17. G. G. Mittelbach, *Ecology* **62**, 1370 (1981).
18. E. E. Werner, D. J. Hall, *J. Ecol.* **69**, 1352 (1988).
19. J. R. Post, D. O. Evans, *Can. J. Fish. Aquat. Sci.* **46**, 1958 (1989).
20. A. J. W. Ward, P. Thomas, P. J. B. Hart, J. Krause, *Behav. Ecol. Sociobiol.* **55**, 561 (2004).
21. F. Johansson, T. Brodin, *J. Freshwat. Ecol.* **18**, 415 (2003).
22. L. A. Dugatkin, *Behav. Ecol.* **3**, 124 (1992).
23. J. Krause, G. D. Ruxton, *Living in Groups* (Oxford Univ. Press, New York, 2002).
24. A. B. A. Boxall *et al.*, *Environ. Health Perspect.* **120**, 1221 (2012).
25. *The World Medicines Situation* (World Health Organization, Geneva, ed. 3, 2011).

Acknowledgments: This study was supported by Umeå University via a Young Researcher Award to T.B., J.F., and J.K. Financial support for M.J. was provided by the Swedish Research Council Vetenskapsrådet and The Swedish Research Council for Environment, Agricultural Sciences and Spatial Planning. Support for this study was also provided by a small starting grant from the strong research environment, "The environment's chemistry—from molecules to the ecosystem." The data reported in this paper are archived at the research database at the Department of Ecology and Environmental Science, Umeå University, and are also included in the online supplementary materials. The authors declare no competing financial interests. All procedures involving handling of fish were permitted by the Ethical Committee on Animal Experiments in Umeå and comply with current Swedish law.

Supplementary Materials

www.sciencemag.org/cgi/content/full/339/6121/814/DC1
Materials and Methods
Table S1
Additional Data
Reference (*26*)

2 July 2012; accepted 3 December 2012
10.1126/science.1226850

Probing Allostery Through DNA

Sangjin Kim,[1*†] Erik Broströmer,[1*] Dong Xing,[2*] Jianshi Jin,[2,3*] Shasha Chong,[1] Hao Ge,[2,4] Siyuan Wang,[1] Chan Gu,[5] Lijiang Yang,[5] Yi Qin Gao,[5] Xiao-dong Su,[2‡] Yujie Sun,[2‡] X. Sunney Xie[1,2‡]

Allostery is well documented for proteins but less recognized for DNA-protein interactions. Here, we report that specific binding of a protein on DNA is substantially stabilized or destabilized by another protein bound nearby. The ternary complex's free energy oscillates as a function of the separation between the two proteins with a periodicity of ~10 base pairs, the helical pitch of B-form DNA, and a decay length of ~15 base pairs. The binding affinity of a protein near a DNA hairpin is similarly dependent on their separation, which—together with molecular dynamics simulations—suggests that deformation of the double-helical structure is the origin of DNA allostery. The physiological relevance of this phenomenon is illustrated by its effect on gene expression in live bacteria and on a transcription factor's affinity near nucleosomes.

Upon binding of a ligand, a macromolecule often undergoes conformational changes that modify the binding affinity of a second ligand at a distant site. This phenomenon, known as "allostery," is responsible for dynamic regulation of biological functions. Although extensive studies have been done on allostery in proteins or enzymes (*1*, *2*), less is known for that through DNA, which is normally considered as a mere template providing binding sites. In fact, multiple proteins, such as transcription factors and RNA or DNA polymerases, bind close to each other on genomic DNA to carry out their cellular functions in concert. Such allostery through DNA has been implicated in previous studies (*3*–*10*) but has not been quantitatively characterized or mechanistically understood.

We performed a single-molecule study of allostery through DNA by measuring the dissociation rate constant (k_{off}) of a DNA-bound protein affected by the binding of another protein nearby. In the assay, DNA duplexes (dsDNA), tethered on the passivated surface of a flow cell, contained two specific protein binding sites separated by a linker sequence of L base pairs (bp) (Fig. 1A and figs. S1 and S2) (*11*). One of the proteins was fluorescently labeled, and many individual protein-DNA complexes were monitored in a large field of view with a total internal reflection fluorescence microscope. Once the labeled protein molecules were bound to DNA, the second protein at a certain concentration was flowed in. Stochastic dissociation times of hundreds of labeled protein molecules were then recorded, the average of which yields the k_{off} (fig. S3) (*12*).

We first present a protein pair that does not substantially bend DNA, namely a Cy3B-labeled DNA binding domain of glucocorticoid receptor (GRDBD), a eukaryotic transcription factor, together with BamHI, a type II endonuclease (Fig. 1A) (*13*, *14*). To prevent the endonuclease activity of BamHI, we used buffer containing Ca^{2+} instead of Mg^{2+}. At a saturating concentration of BamHI, the k_{off} of GRDBD was found to oscillate as a function of L with significant amplitude spanning a factor of 4 and a periodicity of 10 bp, which intriguingly coincides with the helical pitch of B-form DNA (Fig. 1B, red).

When we reversed the DNA sequence of the nonpalindromic GRDBD binding site (GRE) with respect to that of BamHI, the k_{off} of GRDBD oscillated with a phase shift of 4 bp, nearly 180° relative to that of the forward GRE (Fig. 1B). On the other hand, the binding sequence of BamHI is palindromic; therefore, its reversion is not expected to cause any phase shift.

Similar oscillatory modulation in k_{off} was observed with other protein pairs, such as lac repressor (LacR) and EcoRV or LacR and T7 RNA polymerase (T7 RNAp) (figs. S5 and S6). These proteins differ in size, shape, surface

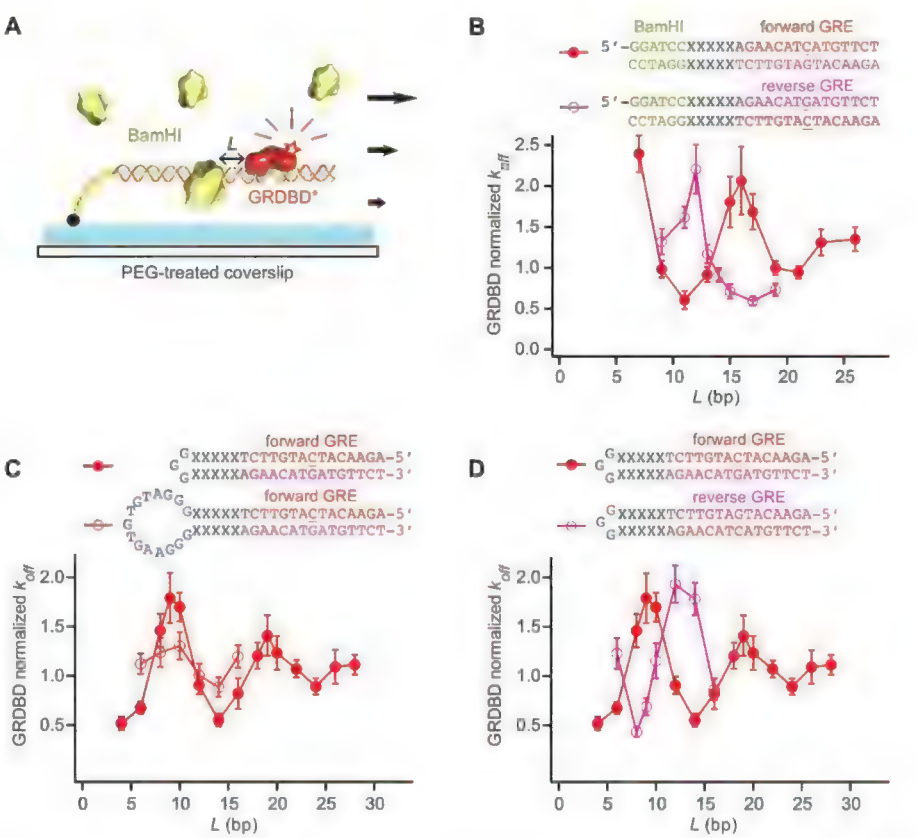

Fig. 1. Allostery through DNA affecting k_{off} of GRDBD near BamHI or near a hairpin loop. **(A)** Schematic for the single-molecule assay in a flow cell. The structural model is for L = 11 with GRDBD from Protein Data Bank (PDB) ID 1R4R (*13*) and BamHI from PDB ID 2BAM (*32*). **(B)** Oscillation in the k_{off} of GRDBD for the forward (red solid circles) and reverse (magenta open circles) GRE sequences, normalized to that measured in the absence of BamHI (±SEM). DNA sequences are shown with the linker DNA (L = 5). The central base of GRE, which makes the sequence nonpalindromic, is underlined. **(C)** Protein binding affinity affected by a nearby DNA hairpin loop, 3 bp and 15 bp (±SEM). **(D)** Effect of 3-bp loop on the forward and reverse GRE (±SEM). The DNA sequence is shown for L = 5. k_{off} is normalized to that measured on DNA without a hairpin loop.

[1]Department of Chemistry and Chemical Biology, Harvard University, Cambridge, MA 02138, USA. [2]Biodynamic Optical Imaging Center (BIOPIC), School of Life Sciences, Peking University, Beijing 100871, China. [3]Academy for Advanced Interdisciplinary Studies, Peking University, Beijing 100871, China. [4]Beijing International Center for Mathematical Research, Peking University, Beijing 100871, China. [5]Institute of Theoretical and Computational Chemistry, College of Chemistry and Molecular Engineering, Peking University, Beijing 100871, China.

*These authors contributed equally to this work.
†Present address: Department of Molecular Cellular and Developmental Biology, Yale University, New Haven, CT 06511, USA.
‡To whom correspondence should be addressed. E-mail: xdsu@pku.edu.cn (X.-D.S.); sun_yujie@pku.edu.cn (Y.S.); xie@chemistry.harvard.edu (X.S.X.)

charge distribution, and DNA binding affinity (*15*–*18*). In fact, the oscillation was independent of ionic strength (fig. S7), suggesting that the electrostatic interaction between the two proteins is not the origin of the allosteric phenomenon. However, the presence of a nick, mismatched bases, or GC-rich sequences in the linker region attenuated the oscillation (figs. S8 to S10), implying that the allostery is largely dependent on the mechanical properties of the linker DNA.

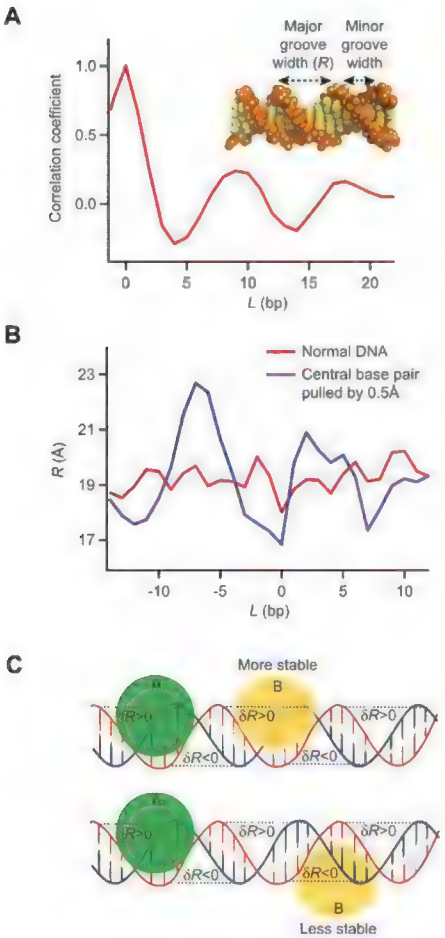

Fig. 2. Allostery through DNA induced by distortion of the major groove. (**A**) MD simulation at room temperature reveals the spatial correlation between the major groove widths (inset, defined as the distance between C3 atoms of the *i*th and *i* + 7th nucleotide sugar-rings) at two positions as a function of their separation *L*, averaged over time *t*, $[\langle \delta R(i;t)\delta R(i+L;t)\rangle_t, i = 5]$. The correlation oscillates with a periodicity of ~10 bp and is attributed to thermally excited low-frequency vibrational modes of dsDNA. (**B**) Upon breaking the symmetry by pulling apart a base pair in the middle of the dsDNA (defined as $L = 0$) by 0.5Å (*12*), the time-averaged *R* (blue) deviates from that of a free DNA (red) and oscillates as a function of the distance (*L*) from the perturbed base pair with a periodicity of ~10 bp. (**C**) Oscillation of $R(L)$ causes the variation of the allosteric coupling between two DNA-binding proteins A and B. If protein B widens *R*, it would energetically favor binding at positions where *R* is already widened ($\delta R > 0$) by protein A (top), but disfavor where *R* is narrowed ($\delta R < 0$) (bottom).

To prove this hypothesis, we replaced the BamHI binding site with a DNA hairpin loop (Fig. 1C), which allows examination of the effect of DNA distortion alone. When the length of linker DNA between the hairpin loop and GRE (*L*) was varied, we observed a similar oscillation in the k_{off} of GRDBD (Fig. 1C). A larger hairpin loop decreased the amplitude of the oscillation, likely because of a smaller distortion induced by the larger hairpin (Fig. 1C). Again when GRE was reversed, the oscillation showed a 4-bp phase shift (Fig. 1D).

The oscillation dampens out with a characteristic decay length of ~15 bp (Fig. 1 and fig. S12) (*12*), which is much shorter than either the bending persistence length (~150 bp) (*19*) or the twisting persistence length (~300 bp) of DNA (*20*). On the other hand, recognizing that proteins primarily interact with the DNA major groove (*21*, *22*), we hypothesized that allostery through DNA results mainly from distortion of the major groove.

We carried out molecular dynamics (MD) simulations first on free dsDNA in aqueous solutions at room temperature (*12*). We evaluated the spatial correlation between the major groove widths (*R*) (Fig. 2A, inset) at two positions (base pairs *i* and $i + L$) as a function of their separation, averaged over time *t*. We observed that the correlation coefficient has a clear oscillation with a periodicity of ~10 bp and dampens within a few helical turns (Fig. 2A). A similar yet slightly weaker oscillation was also observed for the correlation of the minor groove widths. We attribute the oscillation in Fig. 2A to thermally excited low-frequency vibrational modes of dsDNA, which are dictated by the double-helical structure of DNA.

Such spatial correlation as well as the time-averaged *R* (Fig. 2B, red curve) are translationally invariant across a free DNA unless the symmetry is broken, as in the case of hairpin formation or protein binding. We simulated such an effect by applying a harmonic potential to pull a base pair apart in the middle of the strand. Under this condition, we observed that the time-averaged *R* (Fig. 2B, blue curve) deviates from that of a free DNA (Fig. 2B, red curve) and oscillates as a function of the distance (*L*) from the perturbed base pair with a periodicity of ~10 bp. In contrast, no such oscillation was observed for the inter-helical distance.

Such deviation from the free DNA, $\delta R(L)$, is expected to cause variation in the binding of the second DNA-binding protein at a distance *L* bases away. For example, in Fig. 2C, if protein B widens *R*, its binding would be energetically favored at positions where *R* is already widened ($\delta R > 0$) by the hairpin or protein A (Fig. 2C, top) but disfavored where *R* is narrowed ($\delta R < 0$) (Fig. 2C, bottom). Consequently, reversing a non-palindromic binding sequence would invert the binding preference of the protein, explaining the phase shift in Fig. 1. This model is also well supported by the observation that the k_{off} of LacR oscillates with an opposite phase in the presence of BamHI or EcoRV (fig. S6), which is consistent with the fact that BamHI widens whereas EcoRV narrows the major groove (*14*, *15*).

Next, to investigate the effect of DNA allostery on transcription regulation, we studied modulation of RNA polymerase binding affinity when a protein binds near the promoter both in vitro and in vivo. The protein pair we chose is LacR and T7 RNAp, both of which, unlike GRDBD and BamHI, bend DNA (*17*, *23*, *24*) but nevertheless exhibit a similar allosteric effect.

In the in vitro assay, we measured the binding affinity of unlabeled T7 RNAp on its promoter by titrating k_{off} of labeled LacR on *lac* operator O_1 (*lacO1*) with T7 RNAp. k_{off} exhibited hyperbolic T7 RNAp concentration dependence (Michaelis-Menten–like kinetics) (Fig. 3, A and B, and fig. S4), as can be rigorously derived from the kinetic scheme for LacR (protein A) and T7 RNAp (protein B) in Fig. 3C (*12*):

$$k_{off} = \frac{(k_{3\to1} + k_{3\to2})(k_{1\to0} - k_{3\to2})}{[B] \cdot k_{1\to3} + (k_{3\to1} + k_{3\to2})} + k_{3\to2} \quad (1)$$

where $k_{i\to j}$ is the rate constant from state *i* to *j* and [B] is the concentration of T7 RNAp. The plateau value in the titration curve is $k_{3\to2}$. We observed that $k_{3\to2}$ oscillates as a function of *L* with the periodicity and amplitude similar to those of GRDBD and BamHI (Fig. 3D, top).

According to Eq. 1, the dissociation constant of B on the A-bound DNA, $K^{A}_{d,B}(L)$, can be measured from the value of [B] at which k_{off} reaches half of the plateau value in the titration curves (Fig. 3, A and B) (*12*). We found that $K^{A}_{d,B}(L)$ oscillates as a function of *L* (Fig. 3D, middle) in phase with $k_{3\to2}$ [that is, $K^{B}_{d,A}(L) \cdot k_{2\to3}$] (Fig. 3D, top). Therefore, the cooperativity in DNA binding, if present, exhibits either simultaneous stabilization or destabilization between the two proteins. This is a consequence of the fact that free energy is a path-independent thermodynamic state function (Fig. 3C) (*12*):

$$\begin{aligned}\Delta G^{\circ}_{0\to3}(L) &= \Delta G^{\circ}_{1\to3}(L) - \Delta G^{\circ}_{1\to0} \\ &= k_B T \ln[K^{A}_{d,B}(L) \cdot K_{d,A}] \\ &= \Delta G^{\circ}_{2\to3}(L) - \Delta G^{\circ}_{2\to0} \\ &= k_B T \ln[K^{B}_{d,A}(L) \cdot K_{d,B}] \quad (2)\end{aligned}$$

where $K_{d,A}$ and $K_{d,B}$ are the dissociation constant of a protein in the absence of the other, k_B is the Boltzmann constant, and *T* is temperature.

Based on the second line of Eq. 2, the free energy of the ternary complex, $\Delta G^{\circ}_{0\to3}(L)$, was found to oscillate with a periodicity of ~10 bp and an amplitude of ~2 $k_B T$ (Fig. 3D, bottom).

In general, for a ternary complex formed with DNA and proteins A and B, the free energy of the overall system is $\Delta G^\circ_{0\to3}(L) = \Delta G^\circ_A + \Delta G^\circ_B + \Delta\Delta G^\circ_{AB}(L)$, where ΔG°_A and ΔG°_B are the binding free energies of the two individual proteins on DNA, respectively. $\Delta\Delta G^\circ_{AB}(L)$, small relative to ΔG°_A or ΔG°_B, is the energetic coupling involving in the linker DNA, given by the sum of two terms—the variation of protein A binding caused by protein B and the variation of protein B binding caused by protein A:

$$\Delta\Delta G^\circ_{AB}(L) \propto \delta R^A_A \delta R^B_A(L) + \delta R^A_B(L)\delta R^B_B \quad (3)$$

In each δR, or the distortion of the major groove widths, the subscripts indicate where the distortion occurs (binding site of protein A or B), and the superscripts indicate the protein that causes the DNA distortion (*12*). According to our proposed mechanism, $\delta R^B_A(L)$ and $\delta R^A_B(L)$ propagate periodically (Fig. 2B), yielding a damped oscillation in $\Delta\Delta G^\circ_{AB}(L)$. This explains the oscillations of the coupling energy for LacR and T7 RNAp (Fig. 3D, bottom, and fig. S14A) and for GRDBD and BamHI (fig. S14B).

The allosteric coupling between LacR and T7 RNAp is likely to affect transcription in vivo

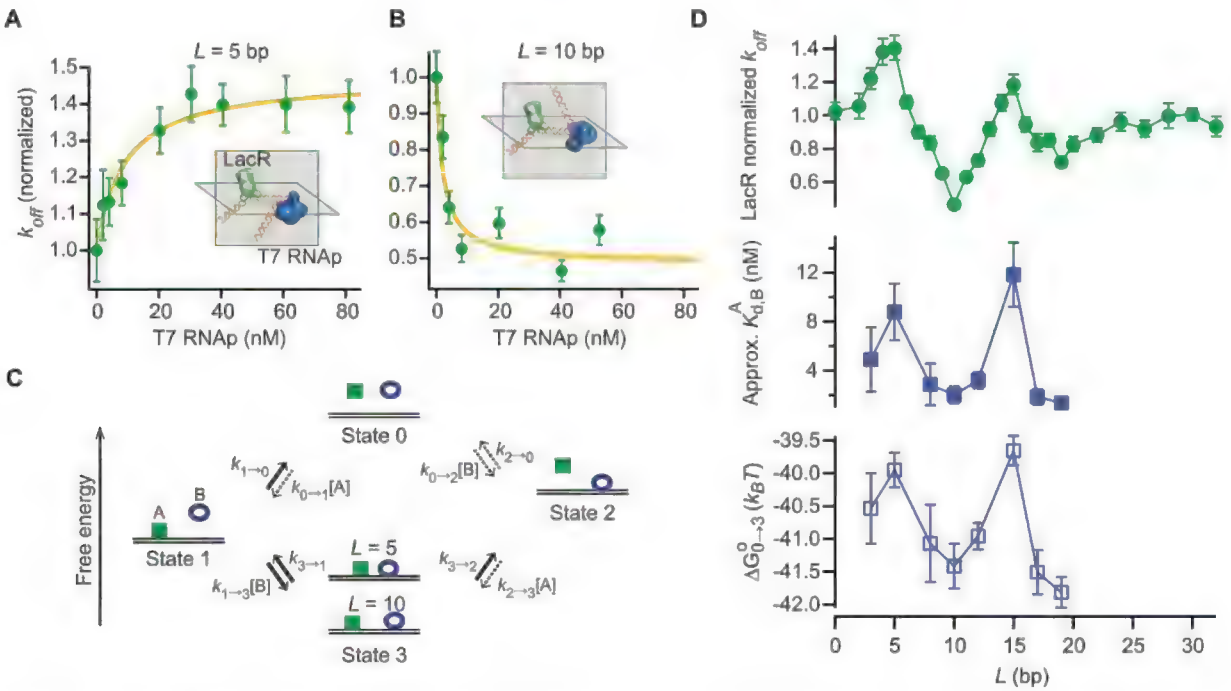

Fig. 3. Allostery through DNA between LacR and T7 RNAp in vitro. (**A** and **B**) Titration curves, where k_{off} values were normalized to those measured in the absence of T7 RNAp on the given template (±SEM). The hyperbolic fit (yellow) is based on Eq. 1. Structural models illustrate the ternary complex of LacR [PDB ID 2PE5 (*33*)] and T7 RNAp [PDB ID 3E2E (*18*)]. (**C**) Kinetic model for the binding of proteins A (LacR) and B (T7 RNAp). Our experiments start with state 1 and proceed to the dissociation of LacR to state 0 or state 2 (via state 3), as shown with solid arrows. Dashed arrows indicate reactions that are not considered in our derivation of Eq. 1. (**D**) The maximum k_{off} of LacR ($k_{3\to2}$), K_d of T7 RNAp in the presence of LacR ($K^A_{d,B}$), and the free energy of the ternary complex ($\Delta G^\circ_{0\to3}$), as function of L, oscillating with a periodicity of 10 bp. Error bars reflect SEM for $k_{3\to2}$ and 1 SD of the χ^2 fit for $K^A_{d,B}$ and $\Delta G^\circ_{0\to3}$ (*12*).

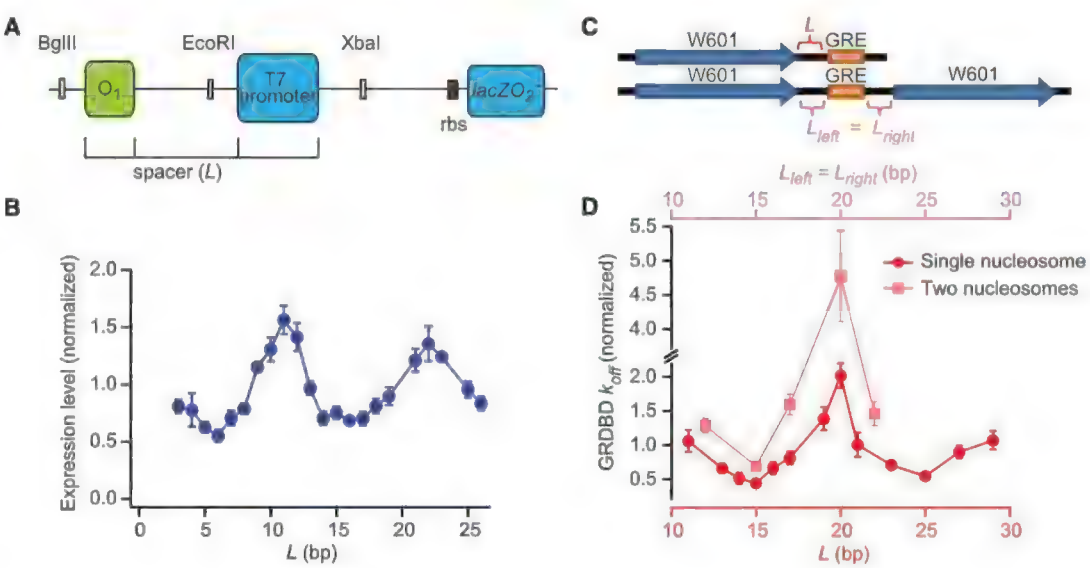

Fig. 4. Physiological relevance of DNA allostery. (**A**) *E. coli* strains constructed to examine cooperativity between LacR and T7 RNAp on the bacterial chromosome. (**B**) The expression level of *lacZ* (normalized to the average expression levels of all *L*s) oscillates as a function of *L* with a periodicity of 10 bp, similar to the corresponding in vitro data (fig. S15). Error bars reflect SEM ($n = 3$ independent experiments). (**C**) Schematic for the DNA sequences used in the GRDBD-nucleosome experiment. W601 is the Widom 601 nucleosome positioning sequence (*34*). (**D**) Oscillation of the k_{off} of GRDBD as a function of *L* (±SEM). Data was normalized to k_{off} of GRDBD in the absence of histone (fig. S17).

because the efficiency of transcription initiation correlates with the binding affinity of T7 RNAp (*25*). We therefore inserted DNA templates used in vitro (fig. S15) into the chromosome of *Escherichia coli* and measured the expression level of *lacZ* using the Miller assay (Fig. 4A) (*26*). Indeed, the gene expression level oscillates as a function of L with a periodicity of ~10 bp (Fig. 4B). Similar oscillations of T7 RNAp activity were observed on plasmids in *E. coli* cells by using a yellow fluorescent protein as a reporter (fig. S16). The oscillation of gene expression levels with a 10-bp periodicity was also seen in a classic experiment on *lac* operon with a DNA loop formed by two operators (*27*). However, our T7 RNAp result illustrates that DNA allostery results in such an oscillatory phenomenon even without a DNA loop, which is consistent with a recent study in which *E. coli* RNA polymerase was used (*10*).

Pertinent to eukaryotic gene expression, DNA allostery may affect the binding affinity of transcription factors near nucleosomes that are closely positioned (*28*, *29*). We placed GRE downstream of a nucleosome (Fig. 4C) and observed a similar DNA allosteric effect in the k_{off} of GRDBD (Fig. 4D and fig. S17). To evaluate DNA allostery in an internucleosomal space, we used two nucleosomes to flank a GRE (Fig. 4C). At the same separation L, GRDBD resides on GRE for a relatively longer time with a single nucleosome nearby than it does with a pair of nucleosomes on both sides of GRE (Fig. 4D). Nonetheless, the fold change between the maximal and minimal k_{off} is larger for GRDBD with two nucleosomes (approximately sevenfold). This indicates moderately large cooperativity between the two flanking nucleosomes in modifying the binding affinity of GRDBD, which is in line with previous in vivo experiments (*30*, *31*). The fact that histones modify a neighboring transcription factor's binding suggests that allostery through DNA might be physiologically important in affecting gene regulation.

References and Notes

1. J. Monod, J. Wyman, J. P. Changeux, *J. Mol. Biol.* **12**, 88 (1965).
2. D. E. Koshland Jr., G. Némethy, D. Filmer, *Biochemistry* **5**, 365 (1966).
3. F. M. Pohl, T. M. Jovin, W. Baehr, J. J. Holbrook, *Proc. Natl. Acad. Sci. U.S.A.* **69**, 3805 (1972).
4. M. Hogan, N. Dattagupta, D. M. Crothers, *Nature* **278**, 521 (1979).
5. B. S. Parekh, G. W. Hatfield, *Proc. Natl. Acad. Sci. U.S.A.* **93**, 1173 (1996).
6. J. Rudnick, R. Bruinsma, *Biophys. J.* **76**, 1725 (1999).
7. D. Panne, T. Maniatis, S. C. Harrison, *Cell* **129**, 1111 (2007).
8. R. Moretti *et al.*, *ACS Chem. Biol.* **3**, 220 (2008).
9. E. F. Koslover, A. J. Spakowitz, *Phys. Rev. Lett.* **102**, 178102 (2009).
10. H. G. Garcia *et al.*, *Cell Reports* **2**, 150 (2012).
11. S. Kim, P. C. Blainey, C. M. Schroeder, X. S. Xie, *Nat. Methods* **4**, 397 (2007).
12. Materials and methods are available as supplementary materials on *Science* Online.
13. B. F. Luisi *et al.*, *Nature* **352**, 497 (1991).
14. M. Newman, T. Strzelecka, L. F. Dorner, I. Schildkraut, A. K. Aggarwal, *Science* **269**, 656 (1995).
15. F. K. Winkler *et al.*, *EMBO J.* **12**, 1781 (1993).
16. M. Lewis *et al.*, *Science* **271**, 1247 (1996).
17. C. G. Kalodimos *et al.*, *EMBO J.* **21**, 2866 (2002).
18. K. J. Durniak, S. Bailey, T. A. Steitz, *Science* **322**, 553 (2008).
19. S. B. Smith, L. Finzi, C. Bustamante, *Science* **258**, 1122 (1992).
20. Z. Bryant *et al.*, *Nature* **424**, 338 (2003).
21. A. A. Travers, *Annu. Rev. Biochem.* **58**, 427 (1989).
22. R. Rohs *et al.*, *Annu. Rev. Biochem.* **79**, 233 (2010).
23. A. Újvári, C. T. Martin, *J. Mol. Biol.* **295**, 1173 (2000).
24. G.-Q. Tang, S. S. Patel, *Biochemistry* **45**, 4936 (2006).
25. Y. Jia, A. Kumar, S. S. Patel, *J. Biol. Chem.* **271**, 30451 (1996).
26. J. H. Miller, *Experiments in Molecular Genetics* (Cold Spring Harbor Laboratory, 1972).
27. J. Müller, S. Oehler, B. Müller-Hill, *J. Mol. Biol.* **257**, 21 (1996).
28. W. Lee *et al.*, *Nat. Genet.* **39**, 1235 (2007).
29. E. Sharon *et al.*, *Nat. Biotechnol.* **30**, 521 (2012).
30. S. John *et al.*, *Nat. Genet.* **43**, 264 (2011).
31. S. H. Meijsing *et al.*, *Science* **324**, 407 (2009).
32. H. Viadiu, A. K. Aggarwal, *Nat. Struct. Biol.* **5**, 910 (1998).
33. R. Daber, S. Stayrook, A. Rosenberg, M. Lewis, *J. Mol. Biol.* **370**, 609 (2007).
34. P. T. Lowary, J. Widom, *J. Mol. Biol.* **276**, 19 (1998).

Acknowledgments: We thank K. Wood for his early involvement and J. Hynes, A. Szabo, C. Bustamante, and J. Gelles for helpful discussions. This work is supported by NIH Director's Pioneer Award to X.S.X., Peking University for BIOPIC, Thousand Youth Talents Program for Y.S., as well as the Major State Basic Research Development Program (2011CB809100), National Natural Science Foundation of China (31170710, 31271423, 21125311).

Supplementary Materials

www.sciencemag.org/cgi/content/full/339/6121/816/DC1
Materials and Methods
Supplementary Text
Figs. S1 to S18
Tables S1 to S11
References (*35*–*75*)

23 August 2012; accepted 7 November 2012
10.1126/science.1229223

Multiplex Genome Engineering Using CRISPR/Cas Systems

Le Cong,[1,2]* F. Ann Ran,[1,4]* David Cox,[1,3] Shuailiang Lin,[1,5] Robert Barretto,[6] Naomi Habib,[1] Patrick D. Hsu,[1,4] Xuebing Wu,[7] Wenyan Jiang,[8] Luciano A. Marraffini,[8] Feng Zhang[1]†

Functional elucidation of causal genetic variants and elements requires precise genome editing technologies. The type II prokaryotic CRISPR (clustered regularly interspaced short palindromic repeats)/Cas adaptive immune system has been shown to facilitate RNA-guided site-specific DNA cleavage. We engineered two different type II CRISPR/Cas systems and demonstrate that Cas9 nucleases can be directed by short RNAs to induce precise cleavage at endogenous genomic loci in human and mouse cells. Cas9 can also be converted into a nicking enzyme to facilitate homology-directed repair with minimal mutagenic activity. Lastly, multiple guide sequences can be encoded into a single CRISPR array to enable simultaneous editing of several sites within the mammalian genome, demonstrating easy programmability and wide applicability of the RNA-guided nuclease technology.

Precise and efficient genome-targeting technologies are needed to enable systematic reverse engineering of causal genetic variations by allowing selective perturbation of individual genetic elements. Although genome-editing technologies such as designer zinc fingers (ZFs) (*1*–*4*), transcription activator–like effectors (TALEs) (*4*–*10*), and homing meganucleases (*11*) have begun to enable targeted genome modifications, there remains a need for new technologies that are scalable, affordable, and easy to engineer. Here, we report the development of a class of precision genome-engineering tools based on the RNA-guided Cas9 nuclease (*12*–*14*) from the type II prokaryotic clustered regularly interspaced short palindromic repeats (CRISPR) adaptive immune system (*15*–*18*).

The *Streptococcus pyogenes* SF370 type II CRISPR locus consists of four genes, including the Cas9 nuclease, as well as two noncoding CRISPR RNAs (crRNAs): trans-activating crRNA (tracrRNA) and a precursor crRNA (pre-crRNA) array containing nuclease guide sequences (spacers) interspaced by identical direct repeats (DRs) (fig. S1) (*19*). We sought to harness this prokaryotic

[1]Broad Institute of MIT and Harvard, 7 Cambridge Center, Cambridge, MA 02142, USA, and McGovern Institute for Brain Research, Department of Brain and Cognitive Sciences, Department of Biological Engineering, Massachusetts Institute of Technology (MIT), Cambridge, MA 02139, USA. [2]Program in Biological and Biomedical Sciences, Harvard Medical School, Boston, MA 02115, USA. [3]Harvard-MIT Health Sciences and Technology, Harvard Medical School, Boston, MA 02115, USA. [4]Department of Molecular and Cellular Biology, Harvard University, Cambridge, MA 02138, USA. [5]School of Life Sciences, Tsinghua University, Beijing 100084, China. [6]Department of Biochemistry and Molecular Biophysics, College of Physicians and Surgeons, Columbia University, New York, NY 10032, USA. [7]Computational and Systems Biology Graduate Program and Koch Institute for Integrative Cancer Research, Massachusetts Institute of Technology, Cambridge, MA 02139, USA. [8]Laboratory of Bacteriology, The Rockefeller University, 1230 York Avenue, New York, NY 10065, USA.

*These authors contributed equally to this work.
†To whom correspondence should be addressed. E-mail: zhang@broadinstitute.org

RNA-programmable nuclease system to introduce targeted double-stranded breaks (DSBs) in mammalian chromosomes through heterologous expression of the key components. It has been previously shown that expression of tracrRNA, pre-crRNA, host factor ribonuclease (RNase) III, and Cas9 nuclease is necessary and sufficient for cleavage of DNA in vitro (*12*, *13*) and in prokaryotic cells (*20*, *21*). We codon-optimized the *S. pyogenes Cas9* (*SpCas9*) and *RNase III* (*SpRNase III*) genes and attached nuclear localization signals (NLSs) to ensure nuclear compartmentalization in mammalian cells. Expression of these constructs in human 293FT cells revealed that two NLSs are most efficient at targeting SpCas9 to the nucleus (Fig. 1A). To reconstitute the noncoding RNA components of the *S. pyogenes* type II CRISPR/Cas system, we expressed an 89-nucleotide (nt) tracrRNA (fig. S2) under the RNA polymerase III U6 promoter (Fig. 1B). Similarly, we used the U6 promoter to drive the expression of a pre-crRNA array comprising a single guide spacer flanked by DRs (Fig. 1B). We designed our initial spacer to target a 30–base pair (bp) site (protospacer) in the human *EMX1* locus that precedes an NGG trinucleotide, the requisite protospacer-adjacent motif (PAM) (Fig. 1C and fig. S1) (*22*, *23*).

To test whether heterologous expression of the CRISPR system (SpCas9, SpRNase III, tracrRNA, and pre-crRNA) can achieve targeted cleavage of mammalian chromosomes, we transfected 293FT cells with different combinations of CRISPR/Cas components. Because DSBs in mammalian DNA are partially repaired by the indel-forming nonhomologous end joining (NHEJ) pathway, we used the SURVEYOR assay (fig. S3) to detect endogenous target cleavage (Fig. 1D and fig. S2B). Cotransfection of all four required CRISPR components resulted in efficient cleavage of the protospacer (Fig. 1D and fig. S2B), which was subsequently verified by Sanger sequencing (Fig. 1E). SpRNase III was not necessary for cleavage of the protospacer (Fig. 1D), and the 89-nt tracrRNA is processed in its absence (fig. S2C). Similarly, maturation of pre-crRNA does not require RNase III (Fig. 1D and fig. S4), suggesting that there may be endogenous mammalian RNases that assist in pre-crRNA maturation (*24*–*26*). Removing any of the remaining RNA or Cas9 components abolished the genome cleavage activity of the CRISPR/Cas system (Fig. 1D). These results define a minimal three-component system for efficient RNA-guided genome modification in mammalian cells.

Next, we explored the generalizability of RNA-guided genome editing in eukaryotic cells by targeting additional protospacers within the *EMX1* locus (Fig. 2A). To improve codelivery, we designed an expression vector to drive both pre-crRNA and SpCas9 (fig. S5). In parallel, we adapted a chimeric crRNA-tracrRNA hybrid (Fig. 2B, top) design recently validated in vitro (*12*), where a mature crRNA is fused to a partial tracrRNA via a synthetic stem loop to mimic the natural crRNA:tracrRNA duplex (Fig. 2B, bottom). We observed cleavage of all protospacer targets when SpCas9 is coexpressed with pre-crRNA (DR-spacer-DR) and tracrRNA. However, not all chimeric RNA designs could facilitate cleavage of their genomic targets (Fig. 2C and table S1). We then tested targeting of additional genomic loci in both human and mouse cells by designing pre-crRNAs and chimeric RNAs targeting the human *PVALB* and the mouse *Th* loci (fig. S6). We achieved efficient modification at all three mouse *Th* and one *PVALB* targets by using the crRNA:tracrRNA duplex, thus demonstrating the broad applicability of the CRISPR/Cas system in modifying different loci across multiple organisms (table S1). For the same protospacer targets, cleavage efficiencies of chimeric RNAs were either lower than those of crRNA:tracrRNA duplexes or undetectable. This may be due to differences in the expression and stability of RNAs, degradation by endogenous RNA interference machinery, or secondary structures leading to inefficient Cas9 loading or target recognition.

Effective genome editing requires that nucleases target specific genomic loci with both high

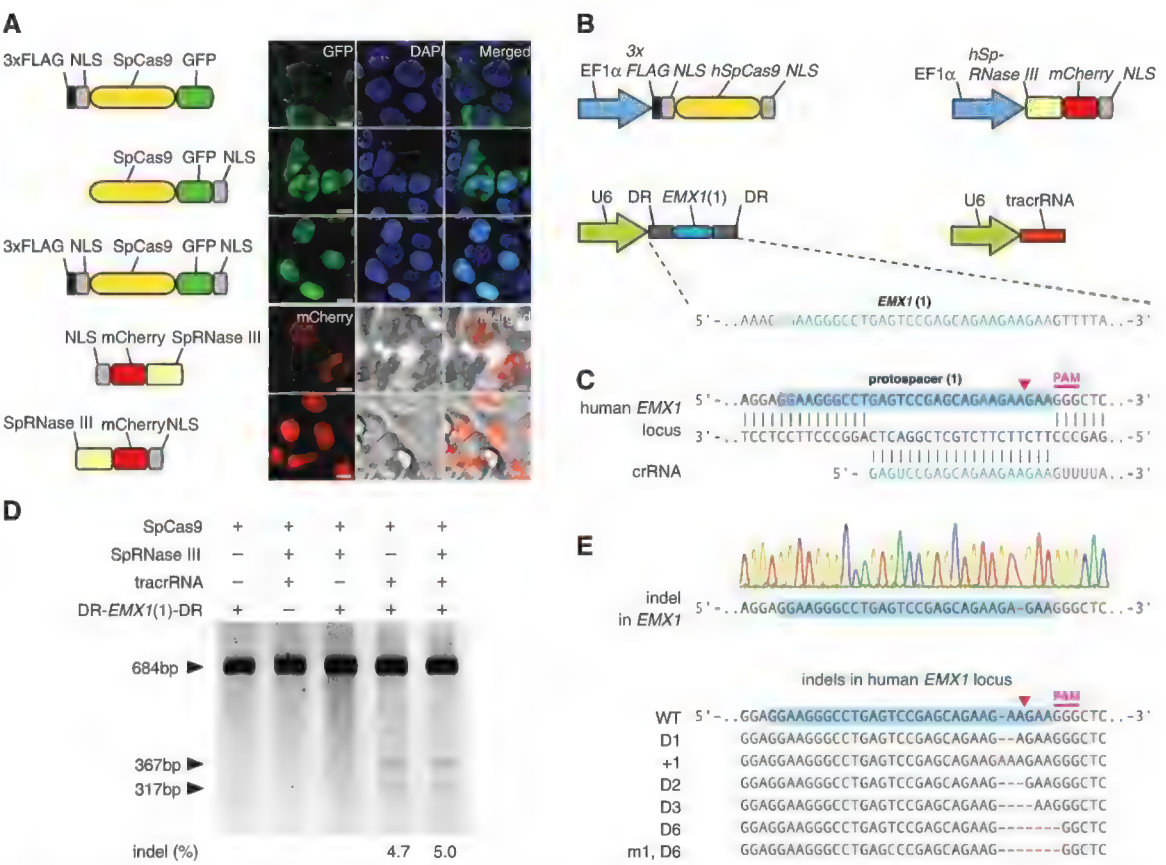

Fig. 1. The type II CRISPR locus from *S. pyogenes* SF370 can be reconstituted in mammalian cells to facilitate targeted DSBs of DNA. (**A**) Engineering of SpCas9 and SpRNase III with NLSs enables import into the mammalian nucleus. GFP indicates green fluorescent protein; scale bars, 10 μm. (**B**) Mammalian expression of human codon–optimized SpCas9 (hSpCas9) and SpRNase III (hSpRNase III) genes were driven by the elongation factor 1α (EF1α) promoter, whereas tracrRNA and pre-crRNA array (DR-Spacer-DR) were driven by the U6 promoter. A protospacer (blue highlight) from the human *EMX1* locus with PAM was used as template for the spacer in the pre-crRNA array. (**C**) Schematic representation of base pairing between target locus and *EMX1*-targeting crRNA. Red arrow indicates putative cleavage site. (**D**) SURVEYOR assay for SpCas9-mediated indels. (**E**) An example chromatogram showing a microdeletion, as well as representative sequences of mutated alleles identified from 187 clonal amplicons. Red dashes, deleted bases; red bases, insertions or mutations.

precision and efficiency. To investigate the specificity of RNA-guided genome modification, we analyzed single-nucleotide mismatches between the spacer and its mammalian protospacer target (Fig. 3A). We observed that single-base mismatch up to 11 bp 5′ of the PAM completely abolished genomic cleavage by SpCas9, whereas spacers with mutations farther upstream retained activity against the protospacer target (Fig. 3B). This is consistent with previous bacterial and in vitro studies of Cas9 specificity (*12*, *20*). Furthermore, SpCas9 is able to mediate genomic cleavage as efficiently as a pair of TALE nucleases (TALENs) targeting the same *EMX1* protospacer (Fig. 3, C and D).

Targeted modification of genomes ideally avoids mutations arising from the error-prone NHEJ mechanism. The wild-type SpCas9 is able to mediate site-specific DSBs, which can be repaired through either NHEJ or homology-directed repair (HDR). We engineered an aspartate-to-alanine substitution (D10A) in the RuvC I domain of SpCas9 to convert the nuclease into a DNA nickase (SpCas9n, Fig. 4A) (*12*, *13*, *20*), because nicked genomic DNA is typically repaired either seamlessly or through high-fidelity HDR. SURVEYOR (Fig. 4B) and sequencing of

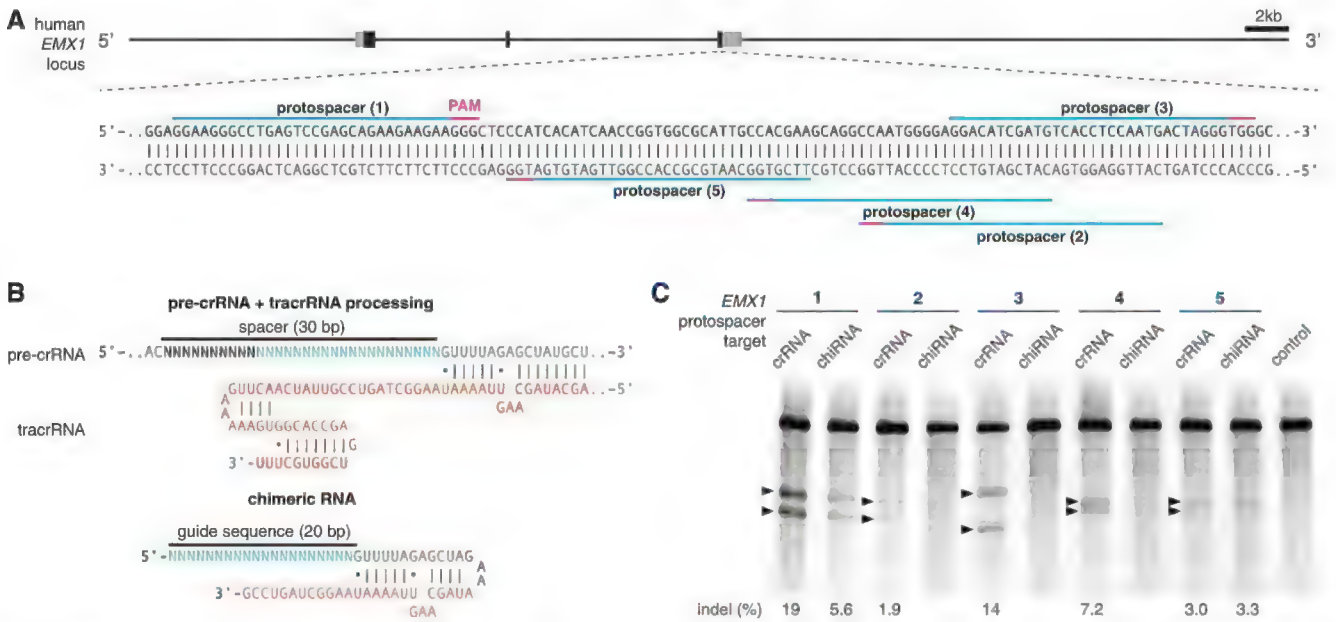

Fig. 2. SpCas9 can be reprogrammed to target multiple genomic loci in mammalian cells. (**A**) Schematic of the human *EMX1* locus showing the location of five protospacers indicated by blue lines with corresponding PAM in magenta. (**B**) Schematic of the pre-crRNA:tracrRNA complex (top) showing hybridization between the direct repeat (gray) region of the pre-crRNA and tracrRNA. Schematic of a chimeric RNA design (*12*) (bottom). tracrRNA sequence is shown in red and the 20-bp spacer sequence in blue. (**C**) SURVEYOR assay comparing the efficacy of Cas9-mediated cleavage at five protospacers in the human *EMX1* locus. Each protospacer was targeted by using either processed pre-crRNA:tracrRNA complex (crRNA) or chimeric RNA (chiRNA). Arrowheads indicate cleavage products for each protospacer target.

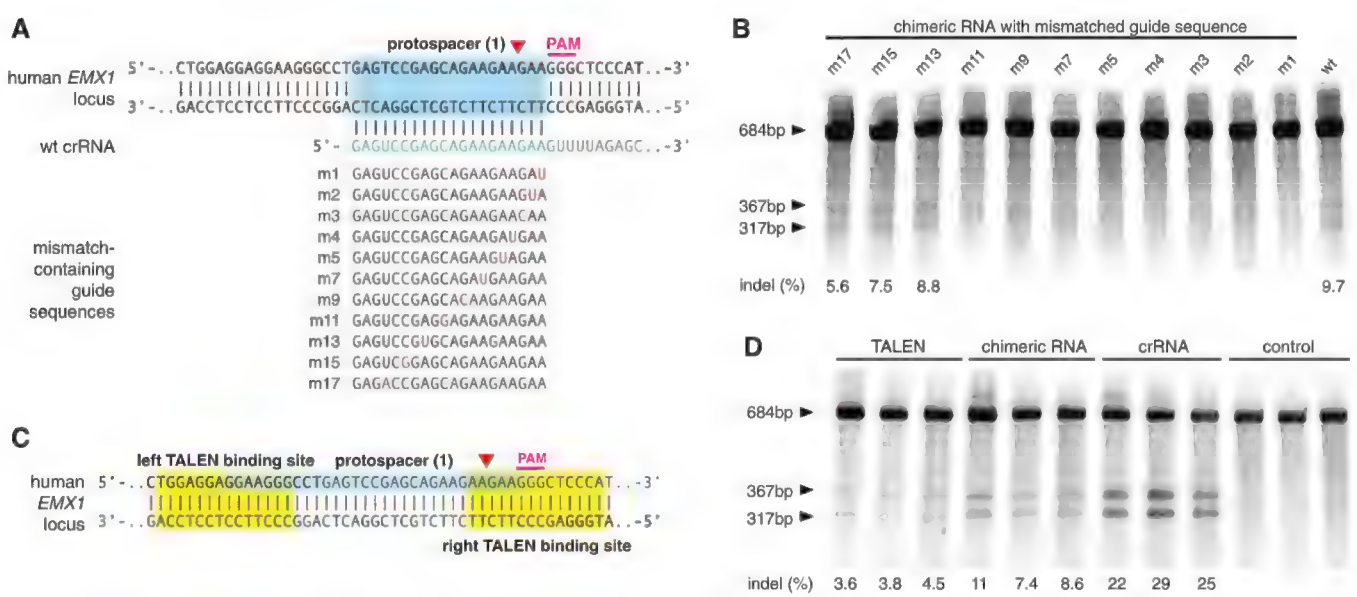

Fig. 3. Evaluation of the SpCas9 specificity and comparison of efficiency with TALENs. (**A**) *EMX1*-targeting chimeric crRNAs with single point mutations were generated to evaluate the effects of spacer-protospacer mismatches. (**B**) SURVEYOR assay comparing the cleavage efficiency of different mutant chimeric RNAs. (**C**) Schematic showing the design of TALENs that target *EMX1*. (**D**) SURVEYOR gel comparing the efficiency of TALEN and SpCas9 ($N = 3$).

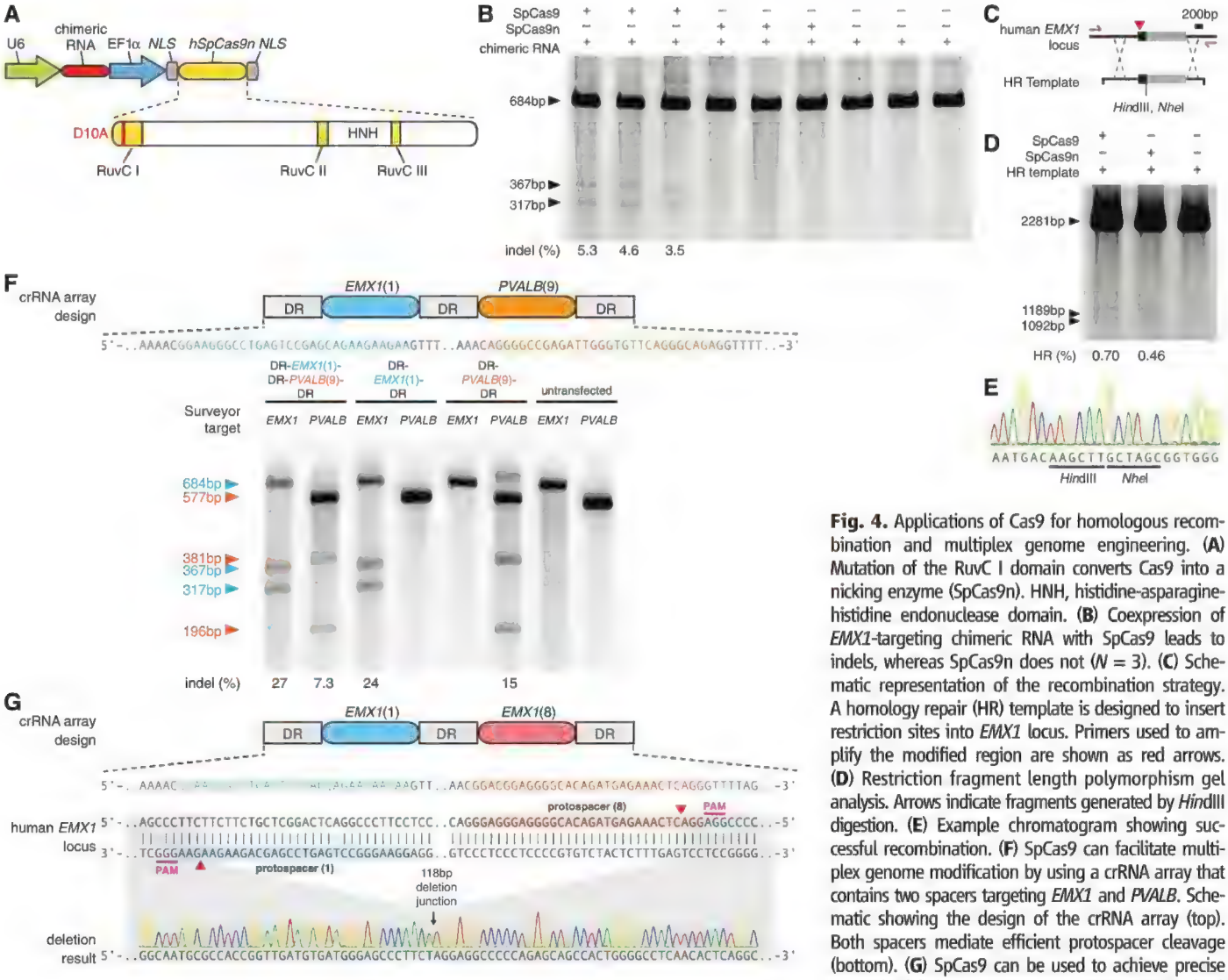

Fig. 4. Applications of Cas9 for homologous recombination and multiplex genome engineering. **(A)** Mutation of the RuvC I domain converts Cas9 into a nicking enzyme (SpCas9n). HNH, histidine-asparagine-histidine endonuclease domain. **(B)** Coexpression of *EMX1*-targeting chimeric RNA with SpCas9 leads to indels, whereas SpCas9n does not ($N = 3$). **(C)** Schematic representation of the recombination strategy. A homology repair (HR) template is designed to insert restriction sites into *EMX1* locus. Primers used to amplify the modified region are shown as red arrows. **(D)** Restriction fragment length polymorphism gel analysis. Arrows indicate fragments generated by *Hin*dIII digestion. **(E)** Example chromatogram showing successful recombination. **(F)** SpCas9 can facilitate multiplex genome modification by using a crRNA array that contains two spacers targeting *EMX1* and *PVALB*. Schematic showing the design of the crRNA array (top). Both spacers mediate efficient protospacer cleavage (bottom). **(G)** SpCas9 can be used to achieve precise genomic deletion. Two spacers targeting *EMX1* (top) mediated a 118-bp genomic deletion (bottom).

327 amplicons did not detect any indels induced by SpCas9n. However, nicked DNA can in rare cases be processed via a DSB intermediate and result in a NHEJ event (*27*). We then tested Cas9-mediated HDR at the same *EMX1* locus with a homology repair template to introduce a pair of restriction sites near the protospacer (Fig. 4C). SpCas9 and SpCas9n catalyzed integration of the repair template into *EMX1* locus at similar levels (Fig. 4D), which we further verified via Sanger sequencing (Fig. 4E). These results demonstrate the utility of CRISPR for facilitating targeted genomic insertions. Given the 14-bp (12 bp from the seed sequence and 2 bp from PAM) target specificity (Fig. 3B) of the wild-type SpCas9, the use of a nickase may reduce off-target mutations.

Lastly, the natural architecture of CRISPR loci with arrayed spacers (fig. S1) suggests the possibility of multiplexed genome engineering. By using a single CRISPR array encoding a pair of *EMX1*- and *PVALB*-targeting spacers, we detected efficient cleavage at both loci (Fig. 4F). We further tested targeted deletion of larger genomic regions through concurrent DSBs by using spacers against two targets within *EMX1* spaced by 119 bp and observed a 1.6% deletion efficacy (3 out of 182 amplicons, Fig. 4G), thus demonstrating the CRISPR/Cas system can mediate multiplexed editing within a single genome.

The ability to use RNA to program sequence-specific DNA cleavage defines a new class of genome engineering tools. Here, we have shown that the *S. pyogenes* CRISPR system can be heterologously reconstituted in mammalian cells to facilitate efficient genome editing; an accompanying study has independently confirmed high-efficiency RNA-guided genome targeting in several human cell lines (*28*). However, several aspects of the CRISPR/Cas system can be further improved to increase its efficiency and versatility. The requirement for an NGG PAM restricts the target space of SpCas9 to every 8 bp on average in the human genome (fig. S7), not accounting for potential constraints posed by crRNA secondary structure or genomic accessibility resulting from chromatin and DNA methylation states. Some of these restrictions may be overcome by exploiting the family of Cas9 enzymes and its differing PAM requirements (*22*, *23*) across the microbial diversity (*17*). Indeed, other CRISPR loci are likely to be transplantable into mammalian cells; for example, the *Streptococcus thermophilus* LMD-9 CRISPR1 system can also mediate mammalian genome cleavage (fig. S8). Lastly, the ability to carry out multiplex genome editing in mammalian cells enables powerful applications across basic science, biotechnology, and medicine (*29*).

References and Notes

1. M. H. Porteus, D. Baltimore, *Science* **300**, 763 (2003).
2. J. C. Miller *et al.*, *Nat. Biotechnol.* **25**, 778 (2007).
3. J. D. Sander *et al.*, *Nat. Methods* **8**, 67 (2011).

4. A. J. Wood *et al.*, *Science* **333**, 307 (2011).
5. M. Christian *et al.*, *Genetics* **186**, 757 (2010).
6. F. Zhang *et al.*, *Nat. Biotechnol.* **29**, 149 (2011).
7. J. C. Miller *et al.*, *Nat. Biotechnol.* **29**, 143 (2011).
8. D. Reyon *et al.*, *Nat. Biotechnol.* **30**, 460 (2012).
9. J. Boch *et al.*, *Science* **326**, 1509 (2009).
10. M. J. Moscou, A. J. Bogdanove, *Science* **326**, 1501 (2009).
11. B. L. Stoddard, *Q. Rev. Biophys.* **38**, 49 (2005).
12. M. Jinek *et al.*, *Science* **337**, 816 (2012).
13. G. Gasiunas, R. Barrangou, P. Horvath, V. Siksnys, *Proc. Natl. Acad. Sci. U.S.A.* **109**, E2579 (2012).
14. J. E. Garneau *et al.*, *Nature* **468**, 67 (2010).
15. H. Deveau, J. E. Garneau, S. Moineau, *Annu. Rev. Microbiol.* **64**, 475 (2010).
16. P. Horvath, R. Barrangou, *Science* **327**, 167 (2010).
17. K. S. Makarova *et al.*, *Nat. Rev. Microbiol.* **9**, 467 (2011).
18. D. Bhaya, M. Davison, R. Barrangou, *Annu. Rev. Genet.* **45**, 273 (2011).
19. E. Deltcheva *et al.*, *Nature* **471**, 602 (2011).
20. R. Sapranauskas *et al.*, *Nucleic Acids Res.* **39**, 9275 (2011).
21. A. H. Magadán, M. E. Dupuis, M. Villion, S. Moineau, *PLoS ONE* **7**, e40913 (2012).
22. H. Deveau *et al.*, *J. Bacteriol.* **190**, 1390 (2008).
23. F. J. Mojica, C. Díez-Villaseñor, J. García-Martínez, C. Almendros, *Microbiology* **155**, 733 (2009).
24. M. Jinek, J. A. Doudna, *Nature* **457**, 405 (2009).
25. C. D. Malone, G. J. Hannon, *Cell* **136**, 656 (2009).
26. G. Meister, T. Tuschl, *Nature* **431**, 343 (2004).
27. M. T. Certo *et al.*, *Nat. Methods* **8**, 671 (2011).
28. P. Mali *et al.*, *Science* **339**, 823 (2013).
29. P. A. Carr, G. M. Church, *Nat. Biotechnol.* **27**, 1151 (2009).

Acknowledgments: We thank the entire Zhang lab for their support and advice; P. A. Sharp for generous help with Northern blot analysis; C. Jennings, R. Desimone, and M. Kowalczyk for helpful comments; and X. Ye for help with confocal imaging. L.C. and X.W. are Howard Hughes Medical Institute International Student Research Fellows. D.C. is supported by the Medical Scientist Training Program. P.D.H. is a James Mills Pierce Fellow. X.W. is supported by NIH grants R01-GM34277 and R01-CA133404 to P. A. Sharp, X.W.'s thesis adviser. L.A.M. is supported by Searle Scholars, R. Allen, an Irma T. Hirschl Award, and a NIH Director's New Innovator Award (DP2AI104556). F.Z. is supported by a NIH Director's Pioneer Award (DP1MH100706); the Keck, McKnight, Gates, Damon Runyon, Searle Scholars, Klingenstein, and Simons foundations; R. Metcalfe; M. Boylan; and J. Pauley. The authors have no conflicting financial interests. A patent application has been filed relating to this work, and the authors plan on making the reagents widely available to the academic community through Addgene and to provide software tools via the Zhang lab Web site (www.genome-engineering.org).

Supplementary Materials

www.sciencemag.org/cgi/content/full/science.1231143/DC1
Materials and Methods
Figs. S1 to S8
Tables S1 and S2
References (*30*–*32*)

5 October 2012; accepted 12 December 2012
Published online 3 January 2013;
10.1126/science.1231143

RNA-Guided Human Genome Engineering via Cas9

Prashant Mali,[1]* Luhan Yang,[1,3]* Kevin M. Esvelt,[2] John Aach,[1] Marc Guell,[1] James E. DiCarlo,[4] Julie E. Norville,[1] George M. Church[1,2]†

Bacteria and archaea have evolved adaptive immune defenses, termed clustered regularly interspaced short palindromic repeats (CRISPR)/CRISPR-associated (Cas) systems, that use short RNA to direct degradation of foreign nucleic acids. Here, we engineer the type II bacterial CRISPR system to function with custom guide RNA (gRNA) in human cells. For the endogenous AAVS1 locus, we obtained targeting rates of 10 to 25% in 293T cells, 13 to 8% in K562 cells, and 2 to 4% in induced pluripotent stem cells. We show that this process relies on CRISPR components; is sequence-specific; and, upon simultaneous introduction of multiple gRNAs, can effect multiplex editing of target loci. We also compute a genome-wide resource of ~190 K unique gRNAs targeting ~40.5% of human exons. Our results establish an RNA-guided editing tool for facile, robust, and multiplexable human genome engineering.

Bacterial and archaeal clustered regularly interspaced short palindromic repeats (CRISPR) systems rely on CRISPR RNAs (crRNAs) in complex with CRISPR-associated (Cas) proteins to direct degradation of complementary sequences present within invading viral and plasmid DNA (*1*–*3*). A recent in vitro reconstitution of the *Streptococcus pyogenes* type II CRISPR system demonstrated that crRNA fused to a normally trans-encoded tracrRNA is sufficient to direct Cas9 protein to sequence-specifically cleave target DNA sequences matching the crRNA (*4*). The fully defined nature of this two-component system suggested that it might function in the cells of eukaryotic organisms such as yeast, plants, and even mammals. By cleaving genomic sequences targeted by RNA sequences (*4*–*6*), such a system could greatly enhance the ease of genome engineering.

Here, we engineer the protein and RNA components of this bacterial type II CRISPR system in human cells. We began by synthesizing a human codon–optimized version of the Cas9 protein bearing a C-terminal SV40 nuclear localization signal and cloning it into a mammalian expression system (Fig. 1A and fig. S1A). To direct Cas9 to cleave sequences of interest, we expressed crRNA-tracrRNA fusion transcripts, hereafter referred to as guide RNAs (gRNAs), from the human U6 polymerase III promoter. Directly transcribing gRNAs allowed us to avoid reconstituting the RNA-processing machinery used by bacterial CRISPR systems (Fig. 1A and fig. S1B) (*4*, *7*–*9*). Constrained only by U6 transcription initiating with G and the requirement for the PAM (protospacer-adjacent motif) sequence -NGG following the 20–base pair (bp) crRNA target, our highly versatile approach can, in principle, target any genomic site of the form $GN_{20}GG$ (fig. S1C; see supplementary text S1 for a detailed discussion).

To test the functionality of our implementation for genome engineering, we developed a green fluorescent protein (GFP) reporter assay (Fig. 1B) in human embryonic kidney HEK 293T cells similar to one previously described (*10*). Specifically, we established a stable cell line bearing a genomically integrated GFP coding sequence disrupted by the insertion of a stop codon and a 68-bp genomic fragment from the AAVS1 locus that renders the expressed protein fragment nonfluorescent. Homologous recombination (HR) using an appropriate repair donor can restore the normal GFP sequence, which enabled us to quantify the resulting GFP^+ cells by flow-activated cell sorting (FACS).

To test the efficiency of our system at stimulating HR, we constructed two gRNAs, T1 and T2, that target the intervening AAVS1 fragment (Fig. 1B) and compared their activity to that of a previously described TAL effector nuclease heterodimer (TALEN) targeting the same region (*11*). We observed successful HR events using all three targeting reagents, with gene correction rates using the T1 and T2 gRNAs approaching 3% and 8%, respectively (Fig. 1C). This RNA-mediated editing process was notably rapid, with the first detectable GFP^+ cells appearing ~20 hours post transfection compared with ~40 hours for the AAVS1 TALENs. We observed HR only upon simultaneous introduction of the repair donor, Cas9 protein, and gRNA, which confirmed that all components are required for genome editing (fig. S2). Although we noted no apparent toxicity associated with Cas9/gRNA expression, work with zinc finger nucleases (ZFNs) and TALENs has shown that nicking only one strand further reduces toxicity. Accordingly, we also tested a Cas9D10A mutant that is known to function as a nickase in vitro, which yielded similar HR but lower nonhomologous end joining (NHEJ) rates (fig. S3) (*4*, *5*). Consistent with (*4*), in which a related Cas9 protein is shown to cut both strands

[1]Department of Genetics, Harvard Medical School, Boston, MA 02115, USA. [2]Wyss Institute for Biologically Inspired Engineering, Harvard University, Cambridge, MA 02138, USA. [3]Biological and Biomedical Sciences Program, Harvard Medical School, Boston, MA 02115, USA. [4]Department of Biomedical Engineering, Boston University, Boston, MA 02215, USA.

*These authors contributed equally to this work.
†To whom correspondence should be addressed. E-mail: gchurch@genetics.med.harvard.edu

3 bp upstream of the PAM, our NHEJ data confirmed that most deletions or insertions occurred at the 3′ end of the target sequence (fig. S3B). We also confirmed that mutating the target genomic site prevents the gRNA from effecting HR at that locus, which demonstrates that CRISPR-mediated genome editing is sequence-specific (fig. S4). Finally, we showed that two gRNAs targeting sites in the GFP gene, and also three additional gRNAs targeting fragments from homologous regions of the DNA methyl transferase 3a (DNMT3a) and DNMT3b genes could sequence-specifically induce significant HR in the engineered reporter cell lines (figs. S5 and S6). Together, these results confirm that RNA-guided genome targeting in human cells is simple to execute and induces robust HR across multiple target sites.

Having successfully targeted an integrated reporter, we next turned to modifying a native locus. We used the gRNAs described above to target the AAVS1 locus located in the PPP1R12C gene on chromosome 19, which is ubiquitously expressed across most tissues (Fig. 2A). We targeted 293Ts, human chronic myelogenous leukemia K562 cells, and PGP1 human induced pluripotent stem (iPS) cells (*12*) and analyzed the results by next-generation sequencing of the targeted locus. Consistent with our results for the GFP reporter assay, we observed high numbers of NHEJ events at the endogenous locus for all three cell types. The two gRNAs T1 and T2 achieved NHEJ rates of 10 and 25% in 293Ts, 13 and 38% in K562s, and 2 and 4% in PGP1-iPS cells, respectively (Fig. 2B). We observed no overt toxicity from the Cas9 and gRNA expression required to induce NHEJ in any of these cell types. As expected, NHEJ-mediated deletions for T1 and T2 were centered around the target site positions, which further validated the sequence-specificity of this targeting process (figs. S7 to S9). Simultaneous introduction of both T1 and T2 gRNAs resulted in high-efficiency deletion of the intervening 19-bp fragment (fig. S8), which demonstrated that multiplexed editing of genomic loci is feasible using this approach.

Last, we attempted to use HR to integrate either a double-stranded DNA donor construct (*13*) or an oligo donor into the native AAVS1 locus (Fig. 2C and fig. S10). We confirmed HR-mediated integration, using both approaches, by polymerase chain reaction (PCR) (Fig. 2D and fig. S10) and Sanger sequencing (Fig. 2E). We also readily derived 293T or iPS clones from the pool of modified cells using puromycin selection over 2 weeks (Fig. 2F and fig. S10). These results demonstrate that this approach enables efficient integration of foreign DNA at endogenous loci in human cells.

Our versatile RNA-guided genome-editing system can be readily adapted to modify other genomic sites by simply modifying the sequence of our gRNA expression vector to match a compatible sequence in the locus of interest. To facilitate this process, we bioinformatically generated ~190,000 specific gRNA-targetable sequences

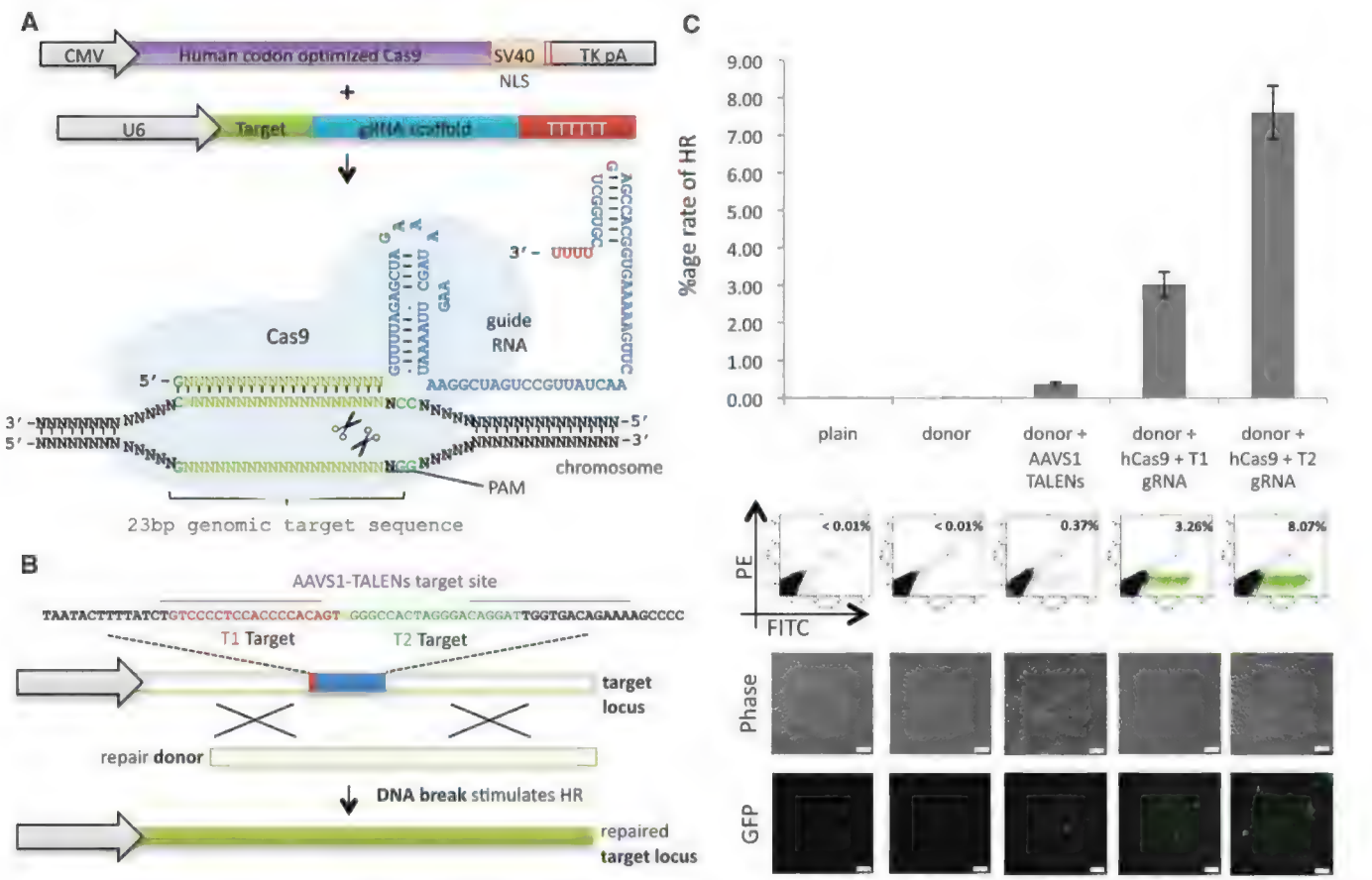

Fig. 1. Genome editing in human cells using an engineered type II CRISPR system. (**A**) RNA-guided gene targeting in human cells involves coexpression of the Cas9 protein bearing a C-terminal SV40 nuclear localization signal (NLS) with one or more gRNAs expressed from the human U6 polymerase III promoter. Cas9 unwinds the DNA duplex and cleaves both strands upon recognition of a target sequence by the gRNA, but only if the correct PAM is present at the 3′ end. Any genomic sequence of the form $GN_{20}GG$ can, in principle, be targeted. CMV, cytomegalovirus promoter; TK, thymidine kinase; pA, polyadenylation signal. (**B**) A genomically integrated GFP coding sequence is disrupted by the insertion of a stop codon and a 68-bp genomic fragment from the AAVS1 locus. Restoration of the GFP sequence by HR with an appropriate donor sequence results in GFP^+ cells that can be quantified by FACS. T1 and T2 gRNAs target sequences within the AAVS1 fragment. Binding sites for the two halves of the TALEN are underlined. (**C**) Bar graph depicting HR efficiencies induced by T1, T2, and TALEN-mediated nuclease activity at the target locus, as measured by FACS. Representative FACS plots and microscopy images of the targeted cells are depicted below. (Scale bar, 100 μm.) Data are shown as means ± SEM ($N = 3$).

targeting ~40.5% exons of genes in the human genome (refer to methods and table S1). We also incorporated these target sequences into a 200-bp format compatible with multiplex synthesis on DNA arrays (*14*) (fig. S11 and tables S2 and S3). This resource provides a ready genome-wide reference of potential target sites in the human genome and a methodology for multiplex gRNA synthesis.

Our results demonstrate the promise of CRISPR-mediated gene targeting for RNA-guided, robust, and multiplexable mammalian genome engineering. The ease of retargeting our system to modify genomic sequences greatly exceeds that of comparable ZFNs and TALENs, while offering similar or greater efficiencies (*4*). Existing studies of type II CRISPR specificity (*4*) suggest that target sites must perfectly match the PAM sequence NGG and the 8- to 12-base "seed sequence" at the 3′ end of the gRNA. The importance of the remaining 8 to 12 bases is less well understood and may depend on the binding strength of the matching gRNAs or on the inherent tolerance of Cas9 itself. Indeed, Cas9 will tolerate single mismatches at the 5′ end in bacteria and in vitro, which suggests that the 5′ G is not required. Moreover, it is likely that the target locus's underlying chromatin structure and epigenetic state will also affect the efficiency of genome editing in eukaryotic cells (*13*), although we suspect that Cas9's helicase activity may render it more robust to these factors, but this remains to be evaluated. Elucidating the frequency and underlying causes of off-target nuclease activity (*15*, *16*) induced by CRISPR, ZFN (*17*, *18*), and TALEN (*19*, *20*) genome-engineering

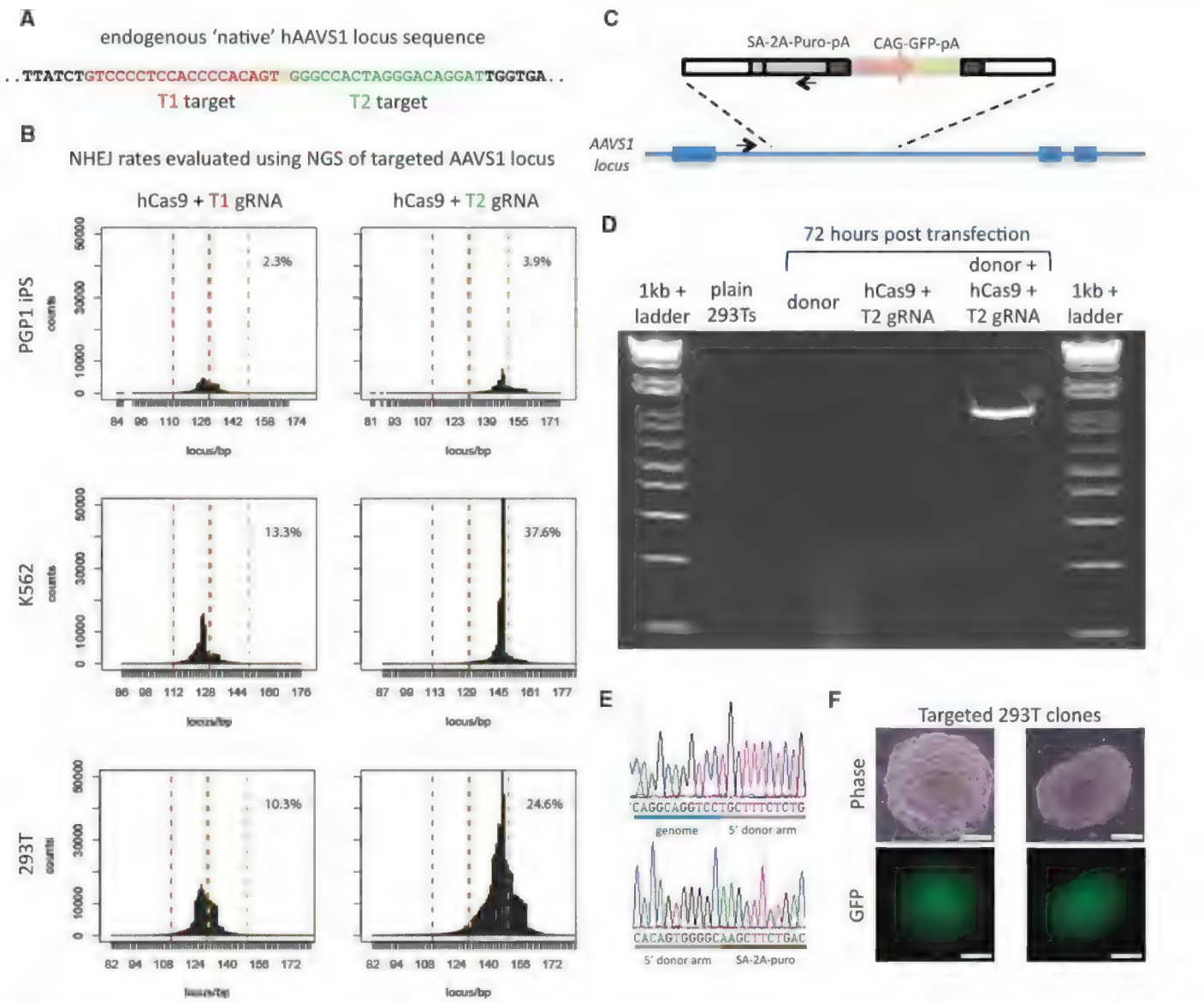

Fig. 2. RNA-guided genome editing of the native AAVS1 locus in multiple cell types. (**A**) T1 (red) and T2 (green) gRNAs target sequences in an intron of the PPP1R12C gene within the chromosome 19 AAVS1 locus. (**B**) Total count and location of deletions caused by NHEJ in 293Ts, K562s, and PGP1 iPS cells after expression of Cas9 and either T1 or T2 gRNAs as quantified by next-generation sequencing. Red and green dashed lines demarcate the boundaries of the T1 and T2 gRNA targeting sites. NHEJ frequencies for T1 and T2 gRNAs were 10% and 25% in 293T, 13% and 38% in K562, and 2% and 4% in PGP1 iPS cells, respectively. (**C**) DNA donor architecture for HR at the AAVS1 locus, and the locations of sequencing primers (arrows) for detecting successful targeted events, are depicted. (**D**) PCR assay 3 days after transfection demonstrates that only cells expressing the donor, Cas9 and T2 gRNA exhibit successful HR events. (**E**) Successful HR was confirmed by Sanger sequencing of the PCR amplicon, which showed that the expected DNA bases at both the genome-donor and donor-insert boundaries are present. (**F**) Successfully targeted clones of 293T cells were selected with puromycin for 2 weeks. Microscope images of two representative GFP+ clones is shown. (Scale bar, 100 μm.)

tools will be of utmost importance for safe genome modification and perhaps for gene therapy. Potential avenues for improving CRISPR specificity include evaluating Cas9 homologs identified through bioinformatics and directed evolution of these nucleases toward higher specificity. Similarly, the range of CRISPR-targetable sequences could be expanded through the use of homologs with different PAM requirements (*9*) or by directed evolution. Finally, inactivating one of the Cas9 nuclease domains increases the ratio of HR to NHEJ and may reduce toxicity (figs. S1A and fig. S3) (*4*, *5*), whereas inactivating both domains may enable Cas9 to function as a retargetable DNA binding protein. As we explore these areas, we note that another parallel study (*21*) has independently confirmed the high efficiency of CRISPR-mediated gene targeting in mammalian cell lines. We expect that RNA-guided genome targeting will have broad implications for synthetic biology (*22*, *23*), the direct and multiplexed perturbation of gene networks (*13*, *24*), and targeted ex vivo (*25*–*27*) and in vivo gene therapy (*28*).

References and Notes

1. B. Wiedenheft, S. H. Sternberg, J. A. Doudna, *Nature* **482**, 331 (2012).
2. D. Bhaya, M. Davison, R. Barrangou, *Annu. Rev. Genet.* **45**, 273 (2011).
3. M. P. Terns, R. M. Terns, *Curr. Opin. Microbiol.* **14**, 321 (2011).
4. M. Jinek *et al.*, *Science* **337**, 816 (2012).
5. G. Gasiunas, R. Barrangou, P. Horvath, V. Siksnys, *Proc. Natl. Acad. Sci. U.S.A.* **109**, E2579 (2012).
6. R. Sapranauskas *et al.*, *Nucleic Acids Res.* **39**, 9275 (2011).
7. T. R. Brummelkamp, R. Bernards, R. Agami, *Science* **296**, 550 (2002).
8. M. Miyagishi, K. Taira, *Nat. Biotechnol.* **20**, 497 (2002).
9. E. Deltcheva *et al.*, *Nature* **471**, 602 (2011).
10. J. Zou, P. Mali, X. Huang, S. N. Dowey, L. Cheng, *Blood* **118**, 4599 (2011).
11. N. E. Sanjana *et al.*, *Nat. Protoc.* **7**, 171 (2012).
12. J. H. Lee *et al.*, *PLoS Genet.* **5**, e1000718 (2009).
13. D. Hockemeyer *et al.*, *Nat. Biotechnol.* **27**, 851 (2009).
14. S. Kosuri *et al.*, *Nat. Biotechnol.* **28**, 1295 (2010).
15. V. Pattanayak, C. L. Ramirez, J. K. Joung, D. R. Liu, *Nat. Methods* **8**, 765 (2011).
16. N. M. King, O. Cohen-Haguenauer, *Mol. Ther.* **16**, 432 (2008).
17. Y. G. Kim, J. Cha, S. Chandrasegaran, *Proc. Natl. Acad. Sci. U.S.A.* **93**, 1156 (1996).
18. E. J. Rebar, C. O. Pabo, *Science* **263**, 671 (1994).
19. J. Boch *et al.*, *Science* **326**, 1509 (2009).
20. M. J. Moscou, A. J. Bogdanove, *Science* **326**, 1501 (2009).
21. L. Cong *et al.*, *Science* **339**, 819 (2013).
22. A. S. Khalil, J. J. Collins, *Nat. Rev. Genet.* **11**, 367 (2010).
23. P. E. Purnick, R. Weiss, *Nat. Rev. Mol. Cell Biol.* **10**, 410 (2009).
24. J. Zou *et al.*, *Cell Stem Cell* **5**, 97 (2009).
25. N. Holt *et al.*, *Nat. Biotechnol.* **28**, 839 (2010).
26. F. D. Urnov *et al.*, *Nature* **435**, 646 (2005).
27. A. Lombardo *et al.*, *Nat. Biotechnol.* **25**, 1298 (2007).
28. H. Li *et al.*, *Nature* **475**, 217 (2011).

Acknowledgments: This work was supported by NIH grant P50 HG005550. We thank S. Kosuri for advice on the oligonucleotide pool designs and synthesis. G.M.C. and P.M. have filed a patent based on the findings of this study.

Supplementary Materials

www.sciencemag.org/cgi/content/full/science.1232033/DC1
Materials and Methods
Supplementary Text
Figs. S1 to S11
Tables S1 to S3
References (*29*–*46*)

26 October 2012; accepted 12 December 2012
Published online 3 January 2013;
10.1126/science.1232033

Cyclic GMP-AMP Is an Endogenous Second Messenger in Innate Immune Signaling by Cytosolic DNA

Jiaxi Wu,[1]* Lijun Sun,[1,2]* Xiang Chen,[1] Fenghe Du,[1] Heping Shi,[3] Chuo Chen,[3] Zhijian J. Chen[1,2]†

Cytosolic DNA induces type I interferons and other cytokines that are important for antimicrobial defense but can also result in autoimmunity. This DNA signaling pathway requires the adaptor protein STING and the transcription factor IRF3, but the mechanism of DNA sensing is unclear. We found that mammalian cytosolic extracts synthesized cyclic guanosine monophosphate–adenosine monophosphate (cyclic GMP-AMP, or cGAMP) in vitro from adenosine triphosphate and guanosine triphosphate in the presence of DNA but not RNA. DNA transfection or DNA virus infection of mammalian cells also triggered cGAMP production. cGAMP bound to STING, leading to the activation of IRF3 and induction of interferon-β. Thus, cGAMP in metazoans and functions as an endogenous second messenger that triggers interferon production in response to cytosolic DNA.

Host defense against foreign genetic elements is one of the most fundamental functions of a living organism. The presence of self or foreign DNA in the cytoplasm is sensed by eukaryotic cells as a danger signal or a sign of foreign invasion (*1*). DNA can be introduced into the cytoplasm by bacterial or viral infection, transfection, or "leakage" from the nucleus or mitochondria under some pathological conditions that cause autoimmune diseases such as lupus. In mammalian cells, cytosolic DNA triggers the production of type I interferons and other cytokines through the endoplasmic reticulum protein STING (also known as MITA, MPYS, or ERIS) (*2*). STING recruits and activates the cytosolic kinases IKK and TBK1, which activate the transcription factors NF-κB and IRF3, respectively. NF-κB and IRF3 then enter the nucleus and function together to induce interferons and other cytokines. DNA-dependent RNA polymerase III has been shown to be a sensor that detects and transcribes AT-rich DNAs such as poly(deoxyadenosine-deoxythymidine) [poly(dA:dT)] into an RNA ligand capable of stimulating the RIG-I pathway to induce interferons (*3*, *4*). However, most DNA sequences do not activate the RNA polymerase III–RIG-I pathway. Instead, cytosolic DNA activates the STING-dependent pathway in a sequence-independent manner. How cytosolic DNA activates the STING pathway remains elusive.

We hypothesized that DNA binds to and activates a putative cytosolic DNA sensor, which then directly or indirectly activates STING, leading to the activation of IRF3 and NF-κB (fig. S1A). To test this model, we developed an in vitro complementation assay using the murine fibrosarcoma cell line L929, which is known to induce interferon-β (IFN-β) in a STING-dependent manner (*5*) (Fig. 1A). We used an L929 cell line stably expressing a short hairpin RNA (shRNA) against STING such that DNA transfection would only activate factors upstream of STING, including the putative DNA sensor (fig. S1, A and B). The L929-shSTING cells were transfected with different types of DNA, and then cytoplasmic extracts from these cells were mixed with the human monocytic cell line THP1 or murine macrophage cell line Raw264.7, which was permeabilized with perfringolysin O (PFO; Fig. 1A). PFO treatment pokes holes in the plasma membrane (*6*), allowing the cytoplasm to diffuse in and out of cells, while retaining organelles including the endoplasmic reticulum (which contains STING) and the Golgi apparatus inside the cells (*7*). If an upstream activator of STING is generated in the DNA-transfected cells, the cytoplasm containing such an activator is expected to activate STING in the PFO-permeabilized cells, leading to the phosphorylation and dimerization of IRF3.

Cytoplasmic extracts from L929-shSTING cells transfected with a DNA sequence known as interferon-stimulatory DNA (ISD; Fig. 1B, lane 2), poly(dA:dT), a GC-rich 50–base pair

[1]Department of Molecular Biology, University of Texas Southwestern Medical Center, Dallas, TX 75390, USA. [2]Howard Hughes Medical Institute, University of Texas Southwestern Medical Center, Dallas, TX 75390, USA. [3]Department of Biochemistry, University of Texas Southwestern Medical Center, Dallas, TX 75390, USA.

*These authors contributed equally to this work.
†To whom correspondence should be addressed. E-mail: zhijian.chen@utsouthwestern.edu

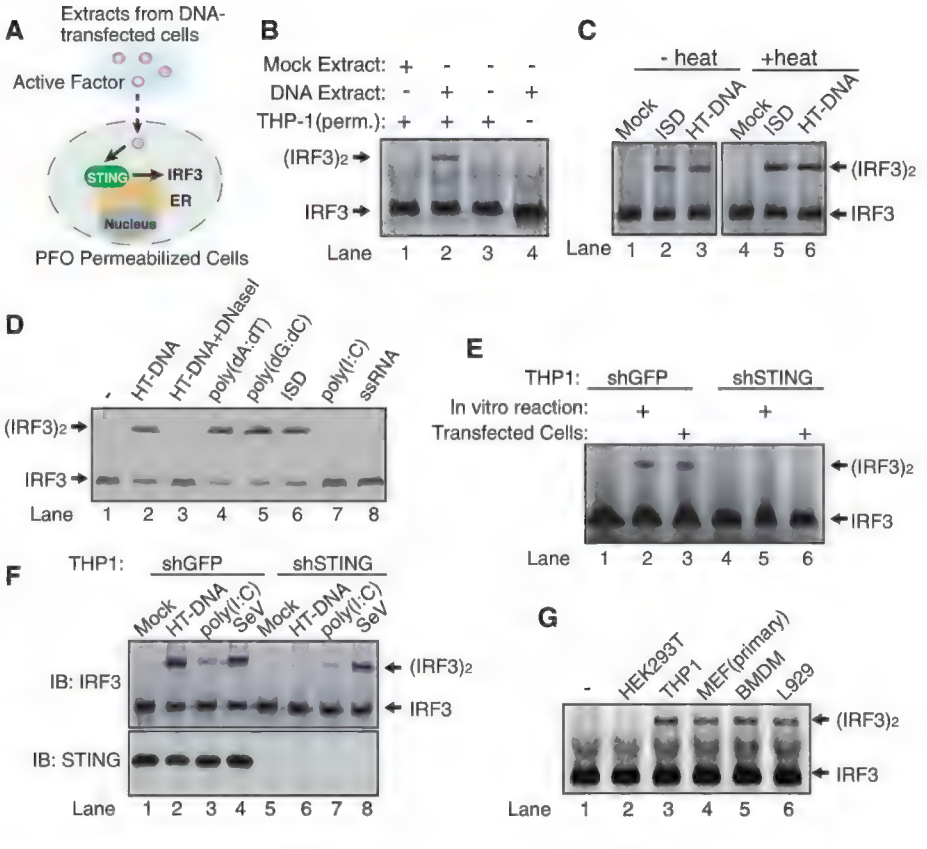

Fig. 1. DNA-dependent generation of a heat-resistant small molecule activates the STING pathway. (**A**) Illustration of an activity assay for cellular factors that activate the STING pathway. (**B**) Cytosolic extracts from mock or ISD-transfected L929-shSTING cells were incubated with PFO-permeabilized THP1 cells together with ^{35}S-labeled IRF3. Dimerization of IRF3 was analyzed by native gel electrophoresis followed by autoradiography. (**C**) Similar to (B), except that in lanes 4 to 6, cytosolic extracts were heated at 95°C for 5 min to denature proteins and then the heat-resistant supernatant was incubated with PFO-permeabilized THP1 cells. (**D**) L929-shSTING cytosolic extracts were incubated with the indicated nucleic acids in the presence of ATP, and then the heat-resistant supernatant was assayed for its ability to stimulate IRF3 dimerization in permeabilized Raw264.7 cells. (**E**) THP1 cells stably expressing shRNA against GFP (control) or STING were permeabilized with PFO and then incubated with the heat-resistant supernatant from the reaction mixture containing DNA-supplemented L929 cytosolic extracts (lanes 2 and 5) or from DNA-transfected L929 cells (lanes 3 and 6). IRF3 activation was analyzed by native gel electrophoresis. (**F**) THP1 cells described in (E) were transfected with HT-DNA or poly(I:C) or infected with Sendai virus (SeV), followed by measurement of IRF3 dimerization. (**G**) Cytosolic extracts from the indicated cell lines were incubated with HT-DNA, and then heat-resistant supernatants were assayed for their ability to stimulate IRF3 dimerization in permeabilized Raw264.7 cells. Unless noted otherwise, all results in this and other figures were representative of at least two independent experiments.

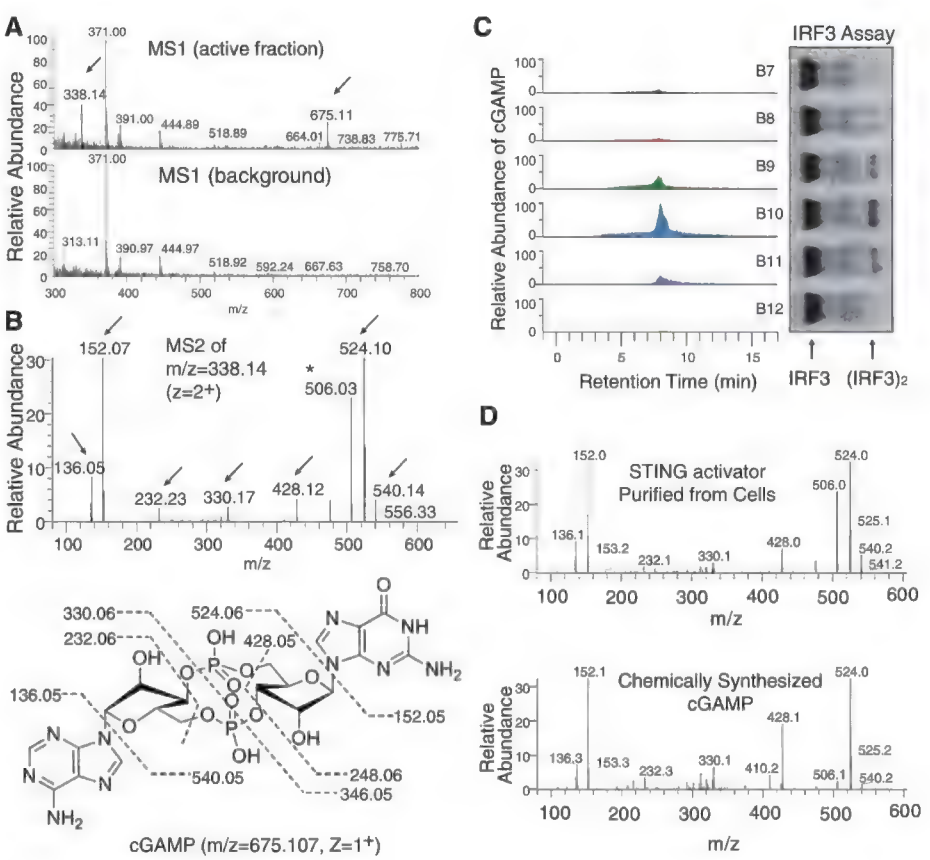

Fig. 2. Purification and identification of the heat-resistant STING activator. (**A**) Full scan nano-LC-MS spectra of active and inactive fractions from the C18 column. Arrows indicate an ion at +1 (675.11) and +2 (338.14) charge states present only in the active fraction. (**B**) Tandem mass (MS2) spectra after CID fragmentation of the ion with m/z = 338.14 (z = 2) from the MS1 scan shown in (A). Arrows indicate the m/z values of the expected fragmentation patterns of cyclic GMP-AMP (cGAMP, bottom). Asterisk indicates an ion (m/z = 506) that resulted from a neutral loss of a water molecule (18) from the ion with m/z = 524. (**C**) Fractions (B7 to B12) from the C18 column were analyzed for the presence of cGAMP by selective reaction monitoring of the expected ions and for their ability to stimulate IRF3 dimerization. (**D**) Comparison of the CID MS2 spectra of the purified STING activator and chemically synthesized cGAMP.

double-stranded DNA (G:C50), poly(deoxyinosine-deoxycytidine) [poly(dI:dC)], or herring testis DNA (HT-DNA; fig. S1C) activated IRF3 in permeabilized THP1 cells, indicating that this activity was independent of DNA sequence. To determine whether the STING activator is a protein, we incubated the cytoplasmic extracts at 95°C to denature most proteins and then incubated the "heat supernatant" with permeabilized THP1 cells. Surprisingly, the heat supernatant from the ISD-transfected or HT-DNA–transfected cells caused IRF3 dimerization (Fig. 1C). This activity was resistant to treatment with Benzonase (Novagen, fig. S1D), which degrades both DNA and RNA, or proteinase K (fig. S1D). Thus, the STING activator is probably not a protein, DNA, or RNA.

To test whether DNA could stimulate the generation of the heat-resistant STING activator in vitro, we incubated HT-DNA with L929-shSTING cytoplasmic extracts (S100) in the presence of ATP (fig. S1E). The reaction mixture was heated at 95°C to denature proteins. Remarkably, incubation of the supernatant with permeabilized Raw264.7 cells led to IRF3 dimerization (Fig. 1D, lane 2). This activity depended on the addition of DNA to the cytoplasmic extracts. Other DNAs, including poly(dA:dT), poly(deoxyguanosine-deoxycytidine), and ISD, also stimulated the generation of the STING activator in L929-shSTING cytoplasmic extracts, whereas poly(inosine-cytidine) [poly(I:C)] and single-stranded RNA had no activity (Fig. 1D). Similar results were obtained with permeabilized THP1 cells (fig. S1F). Knockdown of STING in the permeabilized THP1 cells abolished IRF3 activation by the heat-resistant factor generated by DNA transfected into L929 cells or DNA added to L929 cytosolic extracts (Fig. 1E). Control experiments showed that the knockdown of STING inhibited the activation of IRF3 and induction of IFN-β and tumor necrosis factor–α in THP1 cells by HT-DNA transfection (fig. S1, G and H), but IRF3 activation by poly(I:C) transfection or Sendai virus infection, which is known to activate the RIG-I pathway, was unaffected by the STING knockdown (Fig. 1F). We also tested cytoplasmic extracts from several cell lines for their ability to produce the heat-resistant STING activator (Fig. 1G). Incubation of HT-DNA with extracts from primary mouse embryo fibroblasts (MEFs), mouse bone marrow–derived macrophages (BMDMs), and L929 cells led to generation of the heat-resistant factor that activated IRF3. Human cell extracts from THP1, but not human embryonic kidney (HEK) 293T cells, were also able to produce this STING activator. These results are in agreement with our previous finding that primary MEFs, BMDMs, and L929 and THP1 cells, but not HEK293T cells, possessed the STING-dependent, RNA polymerase III–independent, pathway to induce type I interferons (*3*).

We next used several chromatographic steps, including a STING-Flag affinity purification step, to purify the heat-resistant STING activator from L929 cell extracts (fig. S2, A and B). Previous research has shown that the bacterial molecules cyclic diadenylate monophosphate (c-di-AMP) and cyclic diguanylate monophosphate (c-di-GMP) bind to STING and induce type I interferons (*8*, *9*). However, using nano–liquid chromatography–mass spectrometry (nano-LC-MS), we did not detect MS or MS/MS spectra consistent with those expected of c-di-GMP ($[M+H]^+ = 691$) or c-di-AMP ($[M+H]^+ = 659$). In-depth examination

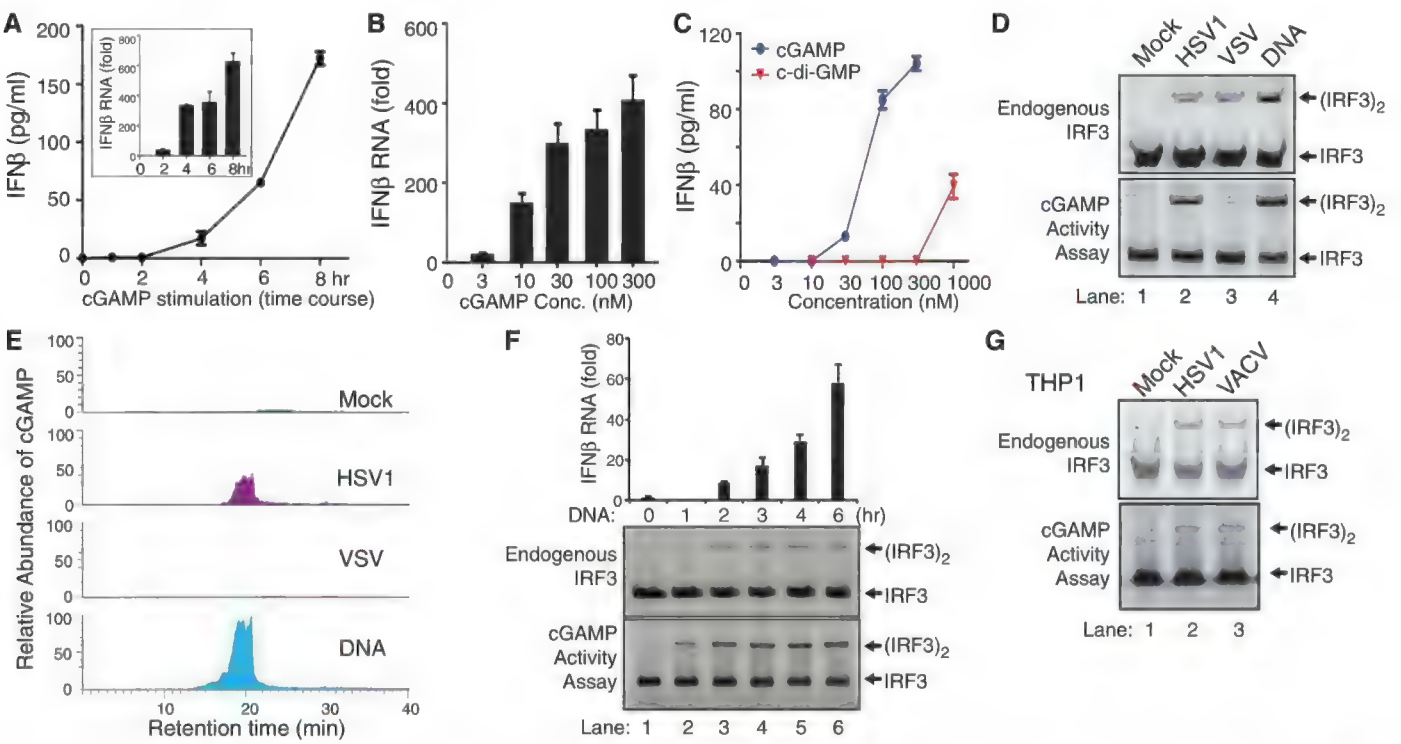

Fig. 3. DNA transfection and DNA virus infection induce IFN-β through cGAMP. (**A**) Chemically synthesized cGAMP (100 nM) was delivered to digitonin-permeabilized L929 cells for the indicated times, then IFN-β RNA and secreted protein were measured by qRT-PCR (inset) and ELISA, respectively. Unless noted otherwise, the error bars in this and all other panels denote SEM ($n = 3$). (**B**) Similar to (A), except that different concentrations of cGAMP were delivered into L929 cells for 8 hours, followed by qRT-PCR analyses of IFN-β RNA. (**C**) Similar to (B), except that different concentrations of cGAMP and c-di-GMP were delivered into L929 cells, followed by ELISA assays for IFN-β. (**D**) L929 cells were infected with HSV-1Δ34.5 or VSV-ΔM51-GFP, transfected with HT-DNA, or mock-treated. An aliquot of the cell extracts was directly analyzed for IRF3 dimerization (top), whereas another aliquot was heated to denature proteins and the heat-resistant supernatant was assayed for its ability to stimulate IRF3 dimerization in permeabilized Raw264.7 cells (bottom). (**E**) The heat-resistant supernatant from (D) was fractionated by HPLC using a C18 column, and the presence of cGAMP in the fractions was measured by mass spectrometry using SRM. (**F**) L929 cells were transfected with HT-DNA (4 μg/ml) for the indicated time, then IFN-β RNA was measured by qRT-PCR and IRF3 dimerization was analyzed by native polyacrylamide gel electrophoresis (PAGE). Aliquots of the cell extracts were tested for the presence of cGAMP on the basis of its ability to induce IRF3 dimerization after delivery into Raw264.7 cells. (**G**) THP1 cells were infected with HSV-1Δ34.5 and vaccinia virus (VACV) for 6 hours, then the activation of endogenous IRF3 and generation of cGAMP activity were measured as described in (F).

of the MS spectra revealed two ions with mass-to-charge ratios (*m/z*) of 675.1 ($z = 1^+$) and 338.1 ($z = 2^+$), which were present in the active fractions but absent in the background spectra (Fig. 2A). These *m/z* values, despite the low mass accuracy of the mass spectrometer (LTQ, Thermo), were equivalent to the average calculated *m/z* values of c-di-GMP and c-di-AMP [675 = (691 + 659)/2]. This observation suggested that the detected ion was a hybrid of c-di-GMP and c-di-AMP—that is, cyclic GMP-AMP, or cGAMP (*m/z* = 675.107, $z = 1^+$; *m/z* = 338.057, $z = 2^+$). Collision-induced dissociation (CID) fragmentation of this ion (*m/z* = 338.1, $z = 2^+$) revealed several prominent ions with *m/z* values expected of the product ions of cGAMP (Fig. 2B). Quantitative mass spectrometry using selective reaction monitoring (SRM) showed that the abundance of the ions representing cGAMP in the fractions from a C18 column correlated very well with their IRF3-stimulatory activities (Fig. 2C and fig. S2C). cGAMP has recently been identified in the bacterium *Vibrio cholerae* and shown to play a role in bacterial chemotaxis and colonization (*10*). However, cGAMP has not been reported to exist or function in eukaryotic cells.

To verify the identity of the heat-resistant STING activator, we used a high-resolution high-accuracy mass spectrometer (Q Exactive, Thermo) to perform nano-LC-MS analysis. The cell-derived STING activator had *m/z* values of 675.107 ($z = 1^+$) and 338.057 ($z = 2^+$), which exactly matched the theoretical values of cGAMP (fig. S2D). To further characterize the structure and function of cGAMP, we developed a 10-step single-flask protocol to chemically synthesize cGAMP (fig. S3). The MS/MS spectra of the cell-derived STING activator were identical to those of the chemically synthesized cGAMP (Fig. 2D). These results demonstrate that L929 cells produced cGAMP.

Quantitative reverse transcription polymerase chain reaction (qRT-PCR) and enzyme-linked immunosorbent assay (ELISA) showed that chemically synthesized cGAMP induced IFN-β RNA and protein in L929 cells after introduction into the cells (Fig. 3A). Titration experiments showed that cGAMP induced IFN-β RNA robustly even at concentrations as low as 10 nM (Fig. 3B). Indeed, ELISA indicated that cGAMP was much more potent than c-di-GMP in inducing IFN-β (Fig. 3C). cGAMP was also more potent than c-di-GMP and c-di-AMP in activating IRF3 (fig. S4A). To determine whether L929 extracts contained enzymes that could synthesize other types of dinucleotides or oligonucleotides capable of activating IRF3, we tested all four ribonucleotides in various combinations (fig. S4B). ATP and GTP were both necessary and sufficient to support the synthesis of an activator of IRF3, further supporting the idea that L929 cells contain an enzyme that synthesizes cGAMP from ATP and GTP.

To determine whether DNA virus infection leads to the production of cGAMP in cells, we infected L929 cells with HSV-1 lacking ICP34.5, a viral protein known to antagonize interferon production in the infected cells (*11*). Like DNA transfection, HSV-1ΔICP34.5 infection led to IRF3 activation in L929 cells (Fig. 3D, upper). Cell extracts from the DNA-transfected or virus-infected cells contained a heat-resistant factor that could activate IRF3 in permeabilized Raw264.7 cells (Fig. 3D, lower panel). As a control, we infected L929 cells with a vesicular stomatitis virus strain, VSV = ΔM51 [fused to green fluorescent protein (VSV-ΔM51-GFP)], an RNA virus known to trigger strong interferon production through the RIG-I pathway (*12*, *13*). In contrast to HSV-1, VSV-infected cells did not contain the heat-resistant IRF3 activator in the same in vitro assay, although VSV infection did induce IRF3 activation in L929 cells (Fig. 3D). The heat-resistant factor in HSV-1–infected cells was enriched by reversed-phase high-performance liquid chromatography (HPLC) and quantified by nano-LC-MS using SRM. DNA-transfected or HSV-1–infected cells, but not mock-treated or VSV-infected cells, produced elevated levels of cGAMP (Fig. 3E). Kinetic experiments showed that after DNA was transfected into L929 cells, cGAMP was produced before IRF3 dimerization and IFN-β induction could be detected (Fig. 3F). To test whether DNA viruses could induce cGAMP production in human cells, we infected THP1 cells with HSV1 or vaccinia virus (VACV; Fig. 3G). Both viruses induced IRF3 dimerization

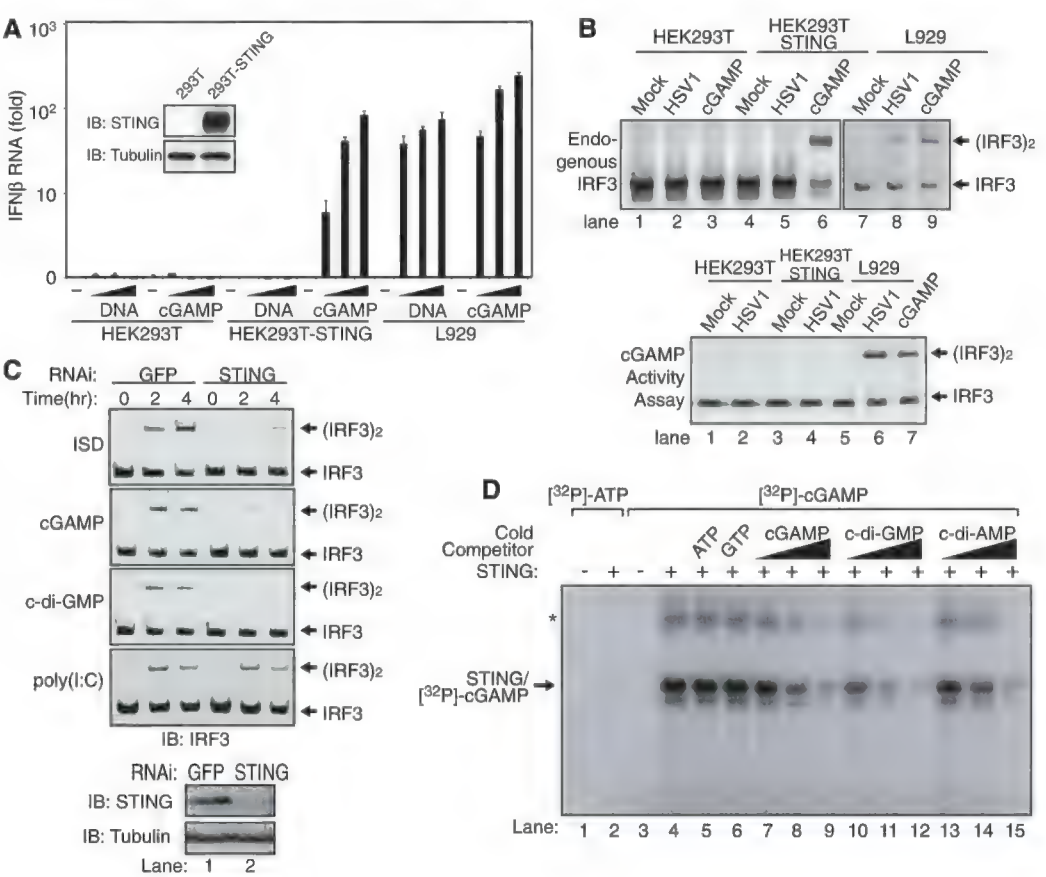

Fig. 4. cGAMP binds to STING and activates IRF3 in a STING-dependent manner. **(A)** Increasing concentrations of HT-DNA or cGAMP were delivered to indicated cells, and the induction of IFN-β was measured by qRT-PCR. Inset shows immunoblots of STING and β-tubulin in the cell lines. **(B)** Indicated cell lines were infected with HSV1Δ34.5 or permeabilized with digitonin and then incubated with cGAMP. Activation of endogenous IRF3 was analyzed by native gel electrophoresis (top). Aliquots of the cytosolic extracts were heated to denature proteins, and the supernatant was assayed for its ability to stimulate IRF3 in permeabilized Raw264.7 cells (bottom). **(C)** cGAMP, c-di-GMP, ISD, or poly(I:C) was delivered into L929 cells stably expressing a shRNA against GFP or STING for the indicated time, followed by analysis of IRF3 dimerization. **(D)** Recombinant STING protein was incubated with [^{32}P]ATP or [^{32}P]cGAMP in the presence or absence of the cold competitors as indicated. After UV cross-linking, the mixtures were resolved by SDS-PAGE followed by autoradiography.

in the cells, and both viruses also triggered the production of cGAMP that activated IRF3 (Fig. 3G, lower panel). Collectively, these results indicate that DNA transfection and DNA virus infections in human and mouse cells produced cGAMP, which led to IRF3 activation.

To determine whether cGAMP activates IRF3 through STING, we carried out three sets of experiments. First, we established a HEK293T cell line stably expressing STING, stimulated these cells with cGAMP, and then measured IFN-β induction by quantitative RT-PCR (Fig. 4A). HEK293T cells did not respond to cGAMP, likely because of absent or very low STING expression in these cells. The expression of STING in HEK293T cells rendered a high level of IFN-β induction by cGAMP. However, DNA did not stimulate HEK293T-STING cells to induce IFN-β, consistent with a defect of HEK293T cells in producing cGAMP in response to DNA stimulation. In contrast, L929 cells induced IFN-β in response to stimulation by either cGAMP or DNA. HSV-1 infection induced IRF3 dimerization in L929 cells but not in HEK293T or HEK293T-STING cells (Fig. 4B, upper panel), which suggests that the production of cGAMP is important for HSV-1 to activate IRF3 in cells. Indeed, extracts from HSV1-infected L929 cells, but not from HEK293T or HEK293T-STING cells, contained the cGAMP activity that led to IRF3 dimerization in permeabilized Raw264.7 cells (Fig. 4B, lower panel). These results indicate that the expression of STING in HEK293T cells installed the ability of the cells to activate IRF3 and induce IFN-β in response to cGAMP, but was insufficient to install the response to DNA or DNA viruses because of a defect of HEK293T cells in synthesizing cGAMP.

Second, we tested the response of L929 and L929-shSTING cells to cGAMP (Fig. 4C). Similar to ISD and c-di-GMP, cGAMP-induced IRF3 dimerization was dependent on STING. In contrast, poly(I:C) still induced IRF3 dimerization in the absence of STING. These results demonstrate that STING is necessary for cGAMP to activate IRF3.

Finally, we examined whether STING binds to cGAMP directly. Recombinant STING protein containing residues 139 to 379, which has been shown to bind c-di-GMP (*14*), was expressed and purified from *Escherichia coli* and then incubated with [^{32}P]cGAMP followed by ultraviolet (UV)–induced cross-linking (Fig. 4D). A radiolabeled band corresponding to a cross-linked STING-cGAMP complex was detected when both STING and [^{32}P]cGAMP were present. High concentrations of ATP or GTP did not compete with the formation of the STING-cGAMP complex. By contrast, the intensity of this band decreased as the concentrations of competing cold cGAMP, c-di-GMP, or c-di-AMP increased; this finding suggests that the cGAMP binding sites on STING might overlap with those that interact with c-di-GMP and c-di-AMP. Indeed, mutations of several residues that were recently shown to participate in the binding of STING to c-di-GMP (*14*), including Ser^{161} → Tyr, Tyr^{240} → Ser, and Asn^{242} → Ala, also impaired the binding of STING to cGAMP (fig. S5). Collectively, these results demonstrate that cGAMP is a ligand that binds to and activates STING.

Cyclic dinucleotides have been shown to function as bacterial second messengers that regulate a variety of physiological processes, including bacterial motility and biofilm formation (*15*). A recent report showed that c-di-GMP is produced in the protozoan *Dictyostelium* and functions as a morphogen to induce stalk cell differentiation (*16*). Our results identify cGAMP as a first cyclic dinucleotide in metazoa and show that cGAMP is a potent inducer of type I interferons. The role of cGAMP is similar to that of cyclic adenosine monophosphate (cAMP), the best-studied second messenger (*17*). Like cAMP, which is synthesized by adenylate cyclase upon its activation by upstream ligands, cGAMP is synthesized by a cyclase in response to stimulation by a DNA ligand (*18*). cAMP binds to and activates protein kinase A and other effector molecules. Similarly, cGAMP binds to and activates STING to trigger the downstream signaling cascades. As an endogenous molecule in mammalian cells, cGAMP may be used in immune therapy or as a vaccine adjuvant.

References and Notes

1. R. Barbalat, S. E. Ewald, M. L. Mouchess, G. M. Barton, *Annu. Rev. Immunol.* **29**, 185 (2011).
2. G. N. Barber, *Immunol. Rev.* **243**, 99 (2011).
3. Y. H. Chiu, J. B. Macmillan, Z. J. Chen, *Cell* **138**, 576 (2009).
4. A. Ablasser *et al.*, *Nat. Immunol.* **10**, 1065 (2009).
5. Y. Tanaka, Z. J. Chen, *Sci. Signal.* **5**, ra20 (2012).
6. J. Rossjohn *et al.*, *J. Mol. Biol.* **367**, 1227 (2007).
7. T. Saitoh *et al.*, *Proc. Natl. Acad. Sci. U.S.A.* **106**, 20842 (2009).
8. J. J. Woodward, A. T. Iavarone, D. A. Portnoy, *Science* **328**, 1703 (2010).
9. D. L. Burdette *et al.*, *Nature* **478**, 515 (2011).
10. B. W. Davies, R. W. Bogard, T. S. Young, J. J. Mekalanos, *Cell* **149**, 358 (2012).
11. K. L. Mossman, J. R. Smiley, *J. Virol.* **76**, 1995 (2002).
12. D. F. Stojdl *et al.*, *Cancer Cell* **4**, 263 (2003).
13. Q. Sun *et al.*, *Immunity* **24**, 633 (2006).
14. Q. Yin *et al.*, *Mol. Cell* **46**, 735 (2012).
15. C. Pesavento, R. Hengge, *Curr. Opin. Microbiol.* **12**, 170 (2009).
16. Z. H. Chen, P. Schaap, *Nature* **488**, 680 (2012).
17. S. A. Blumenthal, *Perspect. Biol. Med.* **55**, 236 (2012).
18. L. Sun, J. Wu, F. Du, X. Chen, Z. J. Chen, *Science* 10.1126/science.1232458 (2012).

Acknowledgments: We thank Y. Tanaka for generating HEK293T-STING and L929-shSTING cell lines; J. Bell, B. Levine, and L. Deng for VSV, HSV-1, and VACV, respectively; R. Debose-Boyd for the PFO plasmid; and V. Sperandio for *V. cholerae* strain C6709. Supported by NIH grants AI-093967 (Z.J.C.) and GM-079554 (C.C.). Z.J.C. is an investigator of Howard Hughes Medical Institute.

Supplementary Materials

www.sciencemag.org/cgi/content/full/science.1229963/DC1
Materials and Methods
Table S1
Figs. S1 to S5
References (*19*, *20*)

10 September 2012; accepted 11 December 2012
Published online 20 December 2012;
10.1126/science.1229963

Prediction Error Governs Pharmacologically Induced Amnesia for Learned Fear

Dieuwke Sevenster,[1,2] Tom Beckers,[1,2,3] Merel Kindt[1,2]*

Although reconsolidation opens up new avenues to erase excessive fear memory, subtle boundary conditions put constraints on retrieval-induced plasticity. Reconsolidation may only take place when memory reactivation involves an experience that engages new learning (prediction error). Thus far, it has not been possible to determine the optimal degree of novelty required for destabilizing the memory. The occurrence of prediction error could only be inferred from the observation of a reconsolidation process itself. Here, we provide a noninvasive index of memory destabilization that is independent from the occurrence of reconsolidation. Using this index, we show in humans that prediction error is (i) a necessary condition for reconsolidation of associative fear memory and (ii) determined by the interaction between original learning and retrieval. Insight into the process of memory updating is crucial for understanding the optimal and boundary conditions on reconsolidation and provides a clear guide for the development of reconsolidation-based treatments.

A consolidated fear memory can enter a transient labile phase upon its reactivation. Pharmacological blockade of the subsequent protein synthesis–dependent restabilization (reconsolidation) produces a memory deficit in both animals (*1*) and humans (*2*). However, an independent measure for memory destabilization other than the occurrence of reconsolidation itself is not yet available. The functional role of reconsolidation might be to keep

memories up to date with new learning. Indeed, reconsolidation is triggered only when there is opportunity for new learning to take place during reactivation (*3*–*5*). Because associative learning requires prediction error (PE) (a discrepancy between actual and expected events) (*6*), reconsolidation might also be a PE-driven process. Even though it has frequently been suggested, there is no experimental evidence that PE is a necessary condition for reconsolidation. So far, PE could only be inferred from effective reconsolidation without an independent assessment of PE-driven relearning (*3*–*5*). Unveiling a crucial role for PE in reconsolidation of fear memory—which may serve as an index for memory destabilization independent from the process of reconsolidation itself—will provide a clear guide for developing treatments to permanently reduce unwanted and excessive fears (such as posttraumatic stress disorder).

General associative learning models (*6*) argue that PE is not determined by the mere co-occurrence of the conditioned stimulus (CS) and unconditioned stimulus (US), but by the discrepancy between what has already been learned (learning history) and what can be learned on a given trial. If memory retrieval follows a fully reinforced asymptotic learning episode, omission of a predicted reinforcement during reactivation (negative PE) (*7*) may destabilize a consolidated memory during its reactivation, whereas a reinforced reactivation trial would leave the memory intact given that PE would then be absent. In contrast, if memory retrieval follows a partially reinforced, non-asymptotic learning episode, a similar reinforced reminder trial (positive PE) (*7*) should generate additional learning and consequently be capable of inducing postretrieval plasticity because memory-strengthening through further learning also requires reconsolidation mechanisms (*8*).

The noradrenergic β-blocker propranolol administered either before or after memory retrieval eliminates affective responding (fear-potentiated startle) in human participants but leaves the predominantly cognitive component of fear (US-expectancy ratings or skin conductance response) intact (*5*, *9*, *10*). Given that propranolol does not affect declarative memory when reactivated with a single trial, online US-expectancy ratings during acquisition, retrieval, and test could serve as an independent measure to test whether PE-driven relearning during reactivation is essential for reconsolidation of affective fear memory. The current study had a threefold aim: (i) to examine the role of PE in reconsolidation of fear memory, (ii) to examine whether PE depends on the interaction between the available information during reactivation and the learning history, and (iii) to provide a measure for memory destabilization that is independent from the occurrence of reconsolidation itself.

In a human differential fear conditioning paradigm, we tested two groups in which fear acquisition was fully reinforced (100% of the trials) (Fig. 1, A and B). To ensure that asymptotic learning was indeed realized, the participants received explicit instructions regarding the contingencies between the CS and the US. On day 2, the memory was reactivated through either an unreinforced (negative PE group; $n = 15$ participants) or a reinforced (no PE group; $n = 15$ participants) reactivation trial, followed by administration of propranolol (40 mg) (Fig. 1, A and B). PE-driven cognitive relearning and corresponding reconsolidation should occur in the negative PE group but not in the no PE group. We tested a third group to examine whether PE depends on the interaction between the information presented during reactivation and the learning history. In this group, acquisition was partially reinforced (33% of the trials), and the memory was reactivated with a reinforced reminder trial (positive PE group; $n = 15$ participants), followed by administration of propranolol (40 mg) (Fig. 1, A and B). In contrast to the full-reinforcement condition, here the reinforced reminder trial should induce PE-driven additional learning given that a partial reinforcement schedule will not induce asymptotic learning. As such, a reinforced reactivation trial might also induce reconsolidation. Noradrenergic blockade after memory retrieval should disrupt reconsolidation—operationalized as a reduction in conditioned startle fear responding—in both the negative PE and positive PE group but not in the no PE group. On day 3, all groups underwent an extinction session followed by a reinstatement procedure to test to what extent the original fear memory trace was weakened (Fig. 1, A and B).

All three groups showed fear learning and memory reactivation on days 1 and 2, respectively, for the startle fear response and online US-expectancy ratings (data available in the supplementary materials).

Analyses of differential US-expectancy ratings (CS1 versus CS2) from the last trial of acquisition (day 1) to the first trial of extinction (day 3) revealed differences between the three groups [stimulus × trial × group, analysis of variance (ANOVA) $F_{2,42} = 25.44$, $P < 0.001$, $\eta^2_p = 0.55$]. Follow-up analyses of the differential US-expectancy ratings from the last trial of acquisition (day 1) to the first trial of extinction (day 3) revealed a decrease in the negative PE group (stimulus × trial × group, $F_{1,28} = 8.18$, $P < 0.008$, $\eta^2_p = 0.23$) and an increase in the positive PE group (stimulus × trial × group, $F_{1,28} = 42.98$, $P < 0.001$, $\eta^2_p = 0.61$) relative to the no PE group (Fig. 2). A non-reinforced reactivation trial resulted in a decrease in differential US-expectancy ratings from the last trial of acquisition (day 1) to the first trial of extinction (day 3), when acquisition was fully reinforced (negative PE) (stimulus × trial, $F_{1,14} = 18.46$, $P < 0.001$, $\eta^2_p = 0.57$) (Fig. 2A). Reinforcement of reactivation left the US-expectancy ratings unaffected in the no PE group (stimulus × trial, $F_{1,14} < 2.47$) (Fig. 2B). However, when acquisition had been partially reinforced, a similar reactivation trial resulted in an increase in US-expectancy ratings (positive PE group; stimulus × trial, $F_{1,14} = 31.72$, $P < 0.001$, $\eta^2_p = 0.69$) (Fig. 2C).

The three groups differed in startle responding on the first retention trial of extinction on day 3 (stimulus × group, $F_{2,42} = 6.49$, $P < 0.003$, $\eta^2_p = 0.24$). Propranolol reduced the differential startle response (CS1 versus CS2) on the first extinction

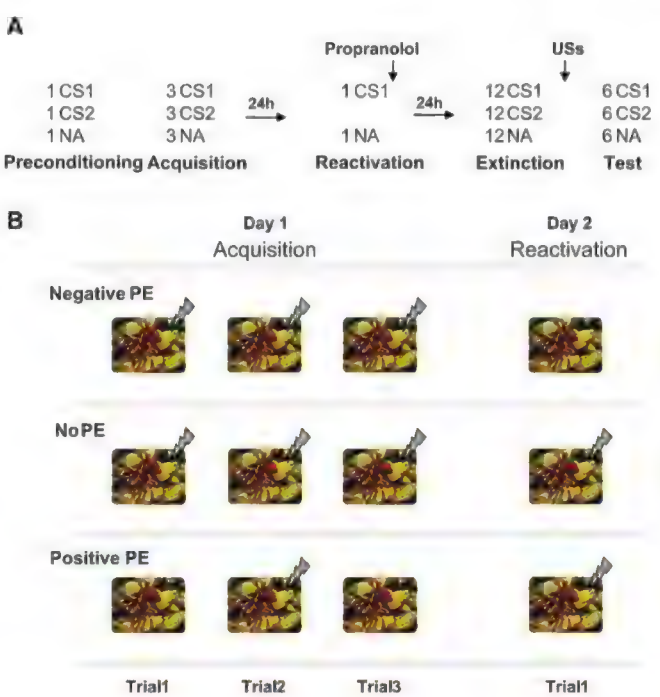

Fig. 1. (**A**) Schematic representation of the experimental design. (**B**) Reinforcement schedule of the CS1 during the acquisition and reactivation phase for the experimental groups. CS1 is depicted as one of the two images used as CSs. US (electrical stimulus) is depicted as a lightning bolt.

[1]Department of Clinical Psychology, University of Amsterdam, Weesperplein 4, 1018 XA, Amsterdam, Netherlands. [2]Cognitive Science Center Amsterdam, 1018 WS, Amsterdam, Netherlands. [3]Department of Psychology, University of Leuven, KU Leuven, Tiensestraat 102, 3712 B-3000, Leuven, Belgium.

*To whom correspondence should be addressed. E-mail: m.kindt@uva.nl

trial in both the negative PE (stimulus × group, $F_{1,28} = 10.76$, $P < 0.003$, $\eta^2_p = 0.28$) and positive PE group (stimulus × group, $F_{1,28} = 7.89$, $P < 0.009$, $\eta^2_p = 0.22$) as compared with the no PE group. Indeed, propranolol completely erased differential responding on the first extinction trial in the negative PE (main effect stimulus, $F_{1,14} < 1$) (Fig. 3A) and positive PE group (main effect stimulus, $F_{1,14} < 1$) (Fig. 3C). In contrast, this propranolol-induced amnesia was not observed when reactivation was devoid of new learning, as indicated by the differential startle response that was still present on the first extinction trial in the no PE group (main effect stimulus, $F_{1,14} = 13.47$, $P < 0.003$, $\eta^2_p = 0.49$) (Fig. 3B). Given that propranolol eliminated differential responding in the reactivation conditions under which new learning occurred, the three groups differed over the course of extinction learning (trial 1 versus trial 12) (stimulus × trial × group, $F_{2,42} = 5.23$, $P < 0.009$, $\eta^2_p = 0.20$) (follow-up analyses are available in the supplementary materials). Thus, propranolol affected startle fear responding only in those groups (negative PE and positive PE) in which the reactivation trial resulted in changes in cognitive learning, be it incremental or decremental.

Differences in startle fear responding (CS1 versus CS2) between the three groups on the reinstatement test trial approached significance (stimulus × group, $F_{2,42} = 2.25$, $P < 0.118$, $\eta^2_p = 0.10$). This small effect can be attributed to a general increase in startle responding from the end of extinction (trial 12) to the test trial in the no PE group (main effect trial, $F_{1,14} = 10.20$, $P < 0.006$, $\eta^2_p = 0.42$), which is typically observed after unpredictable shocks following fear extinction (*2*). Reanalyzing the differential startle response to the test trial with the noise alone (NA) trial as the control stimulus (CS1 versus NA) revealed, however, a significant difference between the three groups (stimulus × group, $F_{2,42} = 5.57$, $P < 0.007$, $\eta^2_p = 0.21$). Follow-up analyses revealed significantly more differential responding in the no PE group as compared with both the negative PE (stimulus × group, $F_{1,28} = 13.25$, $P < 0.001$, $\eta^2_p = 0.32$) and positive PE group (stimulus × group, $F_{1,28} = 7.38$, $P < 0.011$, $\eta^2_p = 0.21$). The startle response indeed recovered in the no PE group as indicated by stronger conditioned responding to the CS1 as compared with the NA (main effect stimulus, $F_{1,14} = 24.01$, $P < 0.001$, $\eta^2_p = 0.63$) (Fig. 3B), whereas no return of fear was observed in either the negative PE (main effect stimulus, $F_{1,14} < 1.44$) (Fig. 3A) or the positive PE group (main effect stimulus, $F_{1,14} < 1$) (Fig. 3C). Affective fear memory was only disrupted when actual learning took place during memory retrieval, showing that postretrieval plasticity depends on PE-driven relearning. Fear memory destabilization was not necessarily triggered by the absence of US-reinforcement (an extinction trial) but was also induced by a reinforced retrieval trial when fear learning on the previous day involved a partial reinforcement schedule. PE was determined by the interaction between the learning history and the retrieval session. PE-driven learning—operationalized by a change in US-expectancy from the end of acquisition (day 1) to the beginning of memory testing (day 3)—may be used as a noninvasive index for memory destabilization.

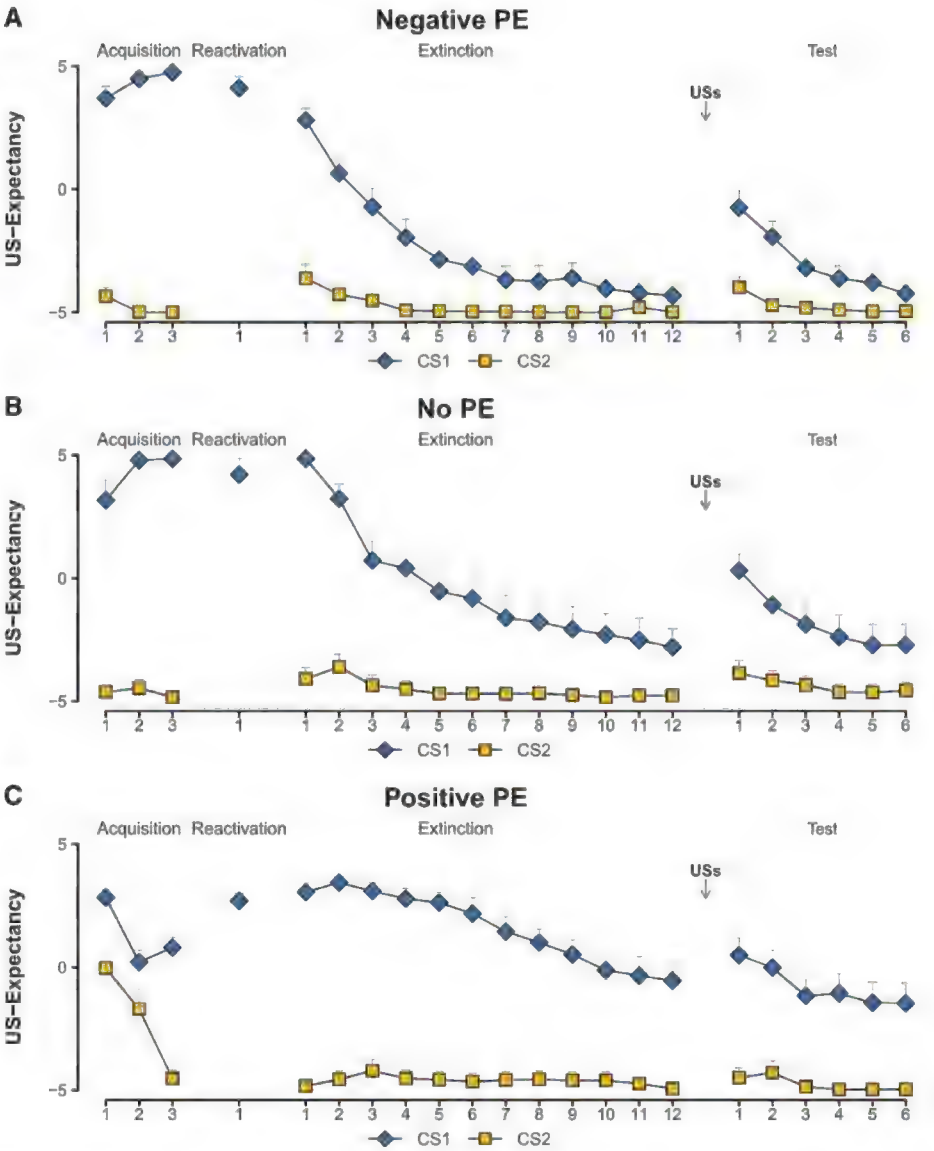

Fig. 2. Online US-expectancy ratings provide a measure of PE-driven learning. (**A** to **C**) Mean US-expectancy ratings to the CS1 and CS2 trials during acquisition, reactivation, extinction, and reinstatement test. US-expectancy ratings (A) decreased from the end of acquisition to the beginning of extinction in the negative PE group (n = 15 participants), (B) remained similar in the no PE group (n = 15 participants), and (C) increased in the positive PE group (n = 15 participants). Error bars represent SEM.

The application of postretrieval amnesic agents is considered to be a highly promising procedure to target excessive emotional memories typically observed in patients suffering from psychiatric disorders (such as posttraumatic stress disorder or addiction). However, the feasibility of disrupting reconsolidation may also be criticized given the subtle boundary conditions under which the amnesic agents do not affect memory (*11*). Reconsolidation is supposed to occur when the retrieval experience is similar but not identical (*12*) to the original learning. Yet, a retrieval session that is too different from the original learning procedure might not cause destabilization of the original memory trace (*13*) but instead initiate the formation of a new memory trace, such as in extinction learning (*14*). Without an independent index of memory destabilization other than the memory-enhancing or amnesic effects of the manipulations themselves, determining the degree of similarity (or dissimilarity) between learning and retrieval presents a problem for empirical falsifiability (*15*).

Criteria for optimal similarity (or dissimilarity) cannot be inferred from the expression of the target memory itself during memory retrieval because the mechanisms that mediate memory destabilization are independent from the behavioral

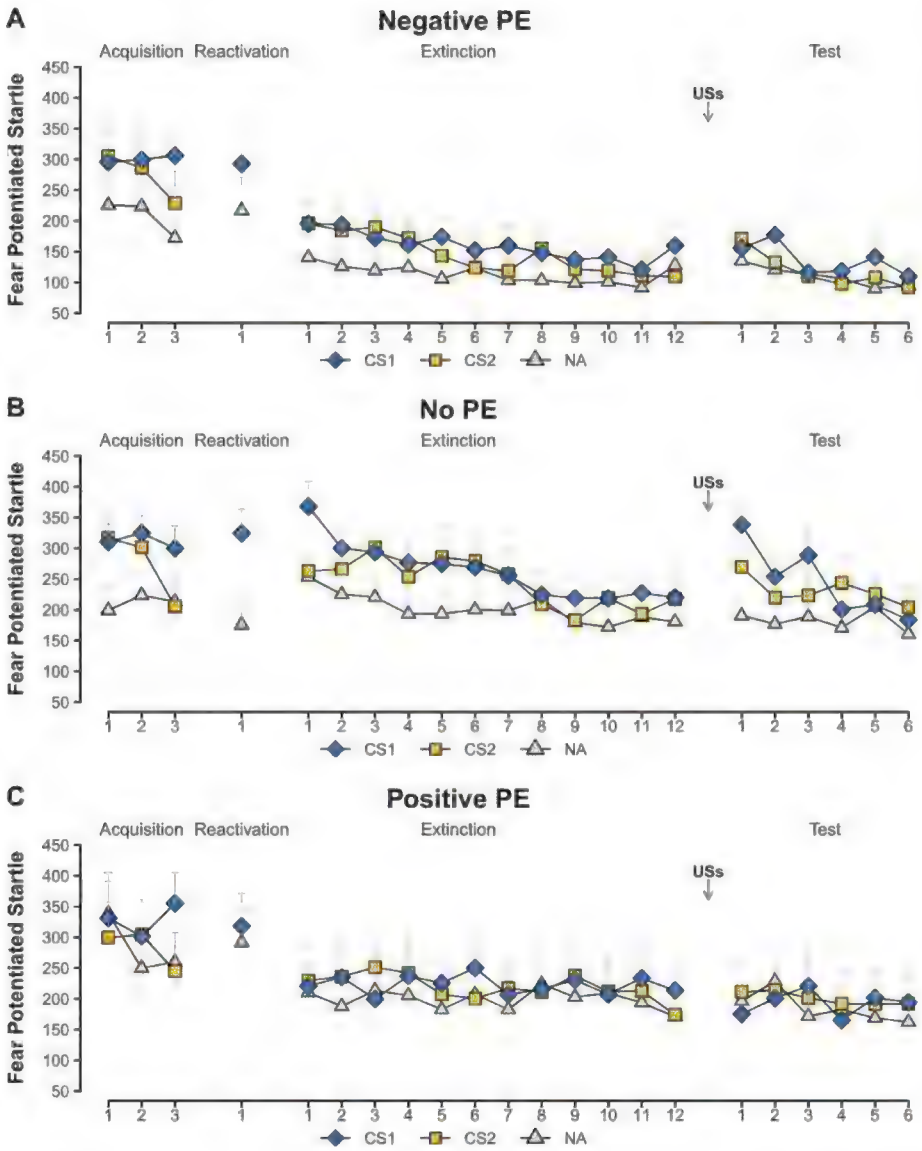

Fig. 3. PE is a necessary condition for reconsolidation. (**A** to **C**) Mean startle responses to the CS1 and CS2 trials during acquisition, reactivation, extinction, and reinstatement test. Propranolol affected the startle response in both (A) the negative PE group (n = 15 participants) and (C) the positive PE group (n = 15 participants) but not in (B) the no PE group (n = 15 participants). Error bars represent SEM.

fear expression (*5*, *16*). In addition, a certain reactivation procedure may induce plasticity after one but not another learning procedure. We have demonstrated that PE can be used as an independent measure of memory destabilization. When there was no modification of CS-US expectancies from acquisition to test, the memory trace was not updated. We believe that at least in the current protocol, it would be difficult to assess PE-driven learning at the moment of reactivation given that a small decrease in CS-US expectancies during the memory retrieval session itself would already induce extinction learning. Then, updating may no longer affect the original memory trace but—as a result of the small degree of similarity between acquisition and retrieval—instate the formation of a new extinction memory. Because reconsolidation of memory traces corresponding to different response systems (amygdala-dependent startle potentiation and hippocampal-dependent declarative memory) calls for different reactivation conditions (*9*, *10*), we are now capable of independently assessing the prerequisite for fear memory destabilization in humans in a noninvasive manner. Conditions that were previously regarded as constraints on reconsolidation (such as too little or too much similarity) may be resolved by taking into account PE during memory retrieval. The assessment of PE provides a feasible tool to develop and optimize reconsolidation-based treatments for patients suffering from chronic relapsing disorders such as anxiety disorders and substance-abuse disorders.

References and Notes

1. K. Nader, G. E. Schafe, J. E. Le Doux, *Nature* **406**, 722 (2000).
2. M. Kindt, M. Soeter, B. Vervliet, *Nat. Neurosci.* **12**, 256 (2009).
3. R. G. Morris *et al.*, *Neuron* **50**, 479 (2006).
4. M. E. Pedreira, L. M. Pérez-Cuesta, H. Maldonado, *Learn. Mem.* **11**, 579 (2004).
5. D. Sevenster, T. Beckers, M. Kindt, *Neurobiol. Learn. Mem.* **97**, 338 (2012).
6. R. A. Rescorla, A. R. Wagner, in *Classical Conditioning II: Current Research and Theory*, A. H. Black, W. F. Prokasy, Eds. (Appleton-Century-Crofts, New York, 1972), pp. 64–99.
7. P. Waelti, A. Dickinson, W. Schultz, *Nature* **412**, 43 (2001).
8. J. L. Lee, *Nat. Neurosci.* **11**, 1264 (2008).
9. M. Soeter, M. Kindt, *Neurobiol. Learn. Mem.* **30**, 4990 (2010).
10. M. Soeter, M. Kindt, *Neuropsychopharmacology* **37**, 1204 (2012).
11. K. Nader, O. Hardt, *Nat. Rev.* **10**, 224 (2009).
12. J. C. Biedenkapp, J. W. Rudy, *Behav. Neurosci.* **118**, 956 (2004).
13. A. Hupbach, O. Hardt, R. Gomez, L. Nadel, *Learn. Mem.* **15**, 574 (2008).
14. M. Bos, T. Beckers, M. Kindt, *Biol. Psychol.* **89**, 598 (2012).
15. P. S. Finnie, K. Nader, *Neurosci. Biobehav. Rev.* **36**, 1667 (2012).
16. C. Ben Mamou, K. Gamache, K. Nader, *Nat. Neurosci.* **9**, 1237 (2006).

Acknowledgments: The authors thank B. Molenkamp for his technical assistance. This study was funded by a Vici grant (M.K.) from the Netherlands Organization for Scientific Research. T.B. is supported by a Vidi grant from the Netherlands Organization for Scientific Research. D.S. collected and analyzed the data. D.S. and M.K. wrote the manuscript.

Supplementary Materials

www.sciencemag.org/cgi/content/full/339/6121/830/DC1
Materials and Methods
Tables S1 and S2
References

10 October 2012; accepted 13 December 2012
10.1126/science.1231357

Gordon Research Conferences

frontiers of science

2013 "Session II" Meetings will be held between June and August in New England in the United States, and internationally in Italy, Switzerland and Hong Kong, China. A list of preliminary programs appears on the following 22 pages. For detailed programs, fees, site/travel information and online application, visit our web site at **www.grc.org**.

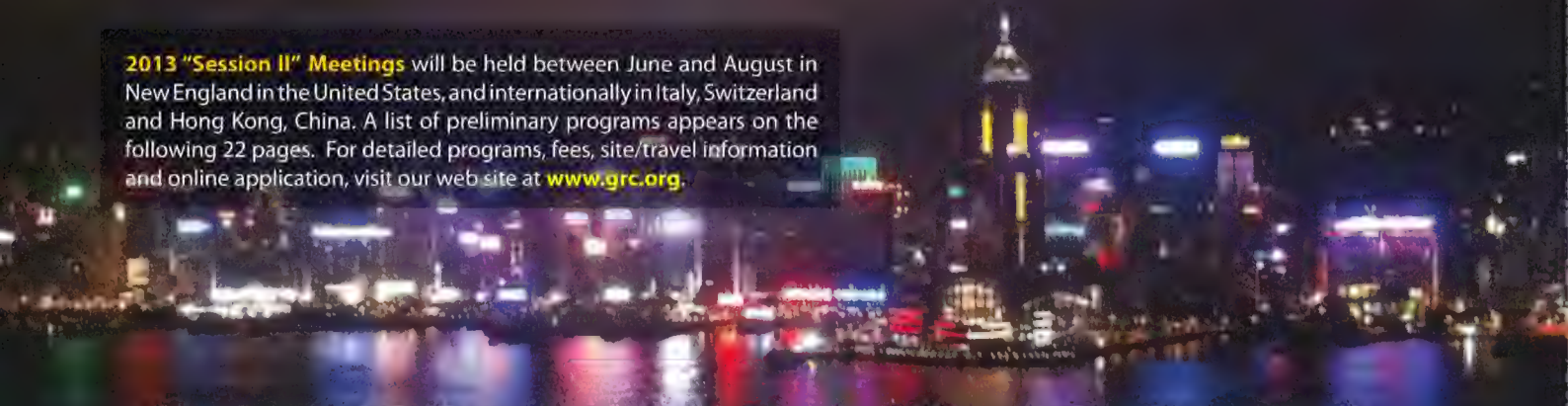

Gordon Research Conferences is proud to announce the establishment of a registered charitable organization in Hong Kong:

Gordon Research Conferences (Hong Kong) Limited

戈登研究會議(香港)有限公司

The GRC expansion in Hong Kong aims to improve scientific collaborations around the world, increase networking opportunities and facilitate advancements in new scientific fields.

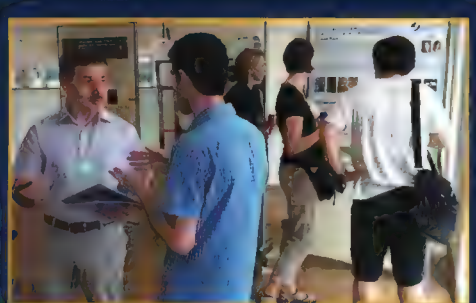

These 7 NEW meetings are scheduled to take place in Hong Kong in 2013. More details are available in the program listings on the following pages.

Germinal Stem Cell Biology
July 14-19, 2013
The Chinese University of Hong Kong
Hong Kong, China
Chair: Wai-Yee Chan

Infections of the Nervous System
Pathogenesis and Worldwide Impact
July 7-12, 2013
The Chinese University of Hong Kong
Hong Kong, China
Chair: Roberto Bruzzone

Marine Molecular Ecology
August 11-16, 2013
Hong Kong University of Science and Technology
Hong Kong, China
Chairs: Pei-Yuan Qian & Roberto G. Kolter

Nano-Mechanical Interfaces
Multiphysics Theory and Experiments
August 4-9, 2013
Hong Kong University of Science and Technology
Hong Kong, China
Chair: Alfonso Ngan

Posttranslational Modification Networks
Phosphosignaling
July 28 - August 2, 2013
Hong Kong University of Science and Technology
Hong Kong, China
Chair: Ning Li

Spin Dynamics in Nanostructures
August 18-23, 2013
Hong Kong University of Science and Technology
Hong Kong, China
Chair: Xiang Rong Wang

T Follicular Helper Cells
Basic Discoveries and Clinical Applications
July 21-26, 2013
The Chinese University of Hong Kong
Hong Kong, China
Chair: Chen Dong

Gordon Research Conferences: 2013 "Session II" Meeting Schedule and Preliminary Programs

The list of meetings, topics and speakers begins below (discussion leaders, where known, are noted in italics).

*Note: **Gordon Research Seminars (GRS)** are listed in boxes below their associated GRC, where applicable. Gordon Research Seminars are 2-day meetings that precede an associated GRC, designed for graduate students, post-docs, and other young scientists to present and exchange new data and cutting edge ideas.*

ADHESION, SCIENCE OF

Interfacial Chemistry and Mechanics in Hard and Soft Material Systems
Jul 14-19, 2013
Mount Holyoke College, South Hadley, MA
Chair: Kenneth Shull
Vice Chair: Anand Jagota

- **Adhesive Bonding**
  (Dick Bossi)
- **Novel Chemistry**
  (*Costantino Creton* / Chris Campbell / Tim Long / Chuanbing Tang)
- **Sustainability**
  (*Chris White* / Megan Robertson / Robert Moon)
- **Hard/Soft Material Interfaces**
  (*Bruce Lee* / Derk Joester / Diethelm Johannsmann / Xuanhe Zhao)
- **Gels**
  (*Joe Lenhart* / Hugh Brown / Frédéric Restagno)
- **Adhesion at the Nanoscale**
  (*Scott Bunch* / Andrey Dobrynin / Kevin Turner / Raymond Friddle)
- **Biomimetics**
  (*Ali Dhinojwala* / Stas Gorb / Russell Stewart)
- **Biomaterials**
  (*Rong Long* / Ana Bedran-Russo / Chris Bowman / Michael Rubinstein)
- **Soft Interfaces in Art and Nature**
  (*Anand Jagota* / David Quéré / Piero Baglioni)

Adhesion, Science of
Jul 13-14, 2013
Chair: Elizabeth Martin

AGING, BIOLOGY OF

Aug 11-16, 2013
Renaissance Tuscany Il Ciocco Resort, Lucca (Barga), Italy
Chairs: Pankaj Kapahi & Nektarios Tavernarakis
Vice Chairs: John M. Sedivy & Yousin Suh

- **Cellular Senescence, Aging and Age-related Diseases**
  (*Pankaj Kapahi, Nektarios Tavernarakis* / Judy Campisi / James Kirkland / Felipe Sierra)
- **Gut Function and Aging**
  (David Walker / Peter Hunt / David Gems / Bruno Lemaitre)
- **Muscle / Exercise**
  (*Simon Melov* / Mark Tarnapolsky / Bente Pedersen / Bill Evans)
- **Circadian Clocks**
  (*Jaga Giebultowicz* / Amita Sehgal / Paolo Sassone-Corsi / Salvador Aznar Benitah / Lenny Guarente)
- **Neuronal & Endocrine Signaling & Aging**
  (*Matt Gill* / Coleen Murphy / Adam Antebi)
- **Proteostasis / Autophagy**
  (*Thomas Nystrom* / Andy Dillin / Ana Maria Cuervo / Thorsten Hoppe / Shu Bing Qian)
- **Stem Cells**
  (*Leanne Jones* / Tom Rando / Anne Brunet)
- **Mitochondria & Fat Metabolism**
  (*Sylvia Lee* / Eric Verdin / Sean Curran / Michael Ristow / Rolf Bodmer)
- **Systems Biology**
  (*John Sedivy, Yousin Suh* / Jan Vijg / Jing-Dong Jackie Han / Rafael deCabo / Shin-Ichiro Imai)

Aging, Biology of
Aug 10-11, 2013
Chair: Amit Khanna
Associate Chair: Vassiliki [illegible]

AMYGDALA IN HEALTH & DISEASE

Jul 28 - Aug 2, 2013
Stonehill College, Easton, MA
Chair: Sumantra Chattarji
Vice Chair: Sheena Josselyn

- **The Amygdala and Emotion: Looking Back to Look Ahead**
  (*Kerry Ressler* / Joseph Ledoux / James McGaugh / Michael Fanselow)
- **Amygdala Function & Connectivity in Humans & Non-human Primates**
  (*John O'Doherty* / Daniel Salzman / Angela Roberts / Sonia Bishop / Rony Paz / Elizabeth Phelps / Christian Büchel)
- **Development of the Amygdala and Fear Regulation**
  (*Sheena Josselyn* / Regina Sullivan / Shubha Tole / Joshua Corbin)
- **Formation and Extinction of Aversive Memories**
  (*Elizabeth Phelps* / Cornelius Gross / Andrew Holmes / Gregory Quirk / Stephen Maren)
- **Inhibitory Circuits in the Amygdala: Structure and Function**
  (*Andreas Luthi* / Hans-Christian Pape / Francesco Ferraguti / Marco Capogna)
- **Role of the Extended Amygdala in Fear and Anxiety**
  (*Elizabeth Bauer* / Denis Pare / Ron Stoop / Bo Li)
- **Reward Learning, Appetitive Behavior and Addiction**
  (*Kay Tye* / Barry Everitt / Sheena Josselyn / Patricia Janak / Geoff Schoenbaum / Bernard Balleine / John O'Doherty)
- **Physiological and Molecular Regulation of Amygdala Circuits**
  (*Denis Pare* / Kerry Ressler / Yann Humeau / Donald Rainnie / Elizabeth Bauer / Robert Pawlak)
- **Modulation of Fear: Cellular and Network Interactions**
  (*Gregory Quirk* / Kay Tye / Alexei Morozov / Pankaj Sah / Joshua Johansen / Andreas Luthi)

Amygdala in Health & Disease
Jul 27-28, 2013
Chair: Susana S. Correia
Associate Chair: Caitlin A. Orsini

ANGIOGENESIS

Aug 4-9, 2013
Salve Regina University, Newport, RI
Chair: Raghu Kalluri
Vice Chair: Holger Gerhardt

- **Keynote Presentations: Hypoxia, Angiogenesis and Anti-Angiogenesis Therapy**
  (William G. Kaelin / Gregg Semenza / Joseph Schlessinger / James D. Watson)
- **Targeting Angiogenesis**
  (Donald M. McDonald / Peter Carmeliet / Kari Alitalo / Douglas Hanahan / Napoleone Ferrara / Rakesh Jain / David Cheresh)
- **Developmental Angiogenesis**
  (Christer Betsholtz / Holger Gerhardt / Shahin Rafii / Michael Simons)
- **Mechanics of Angiogenesis**
  (Valerie Weaver / Elisabetta Dejana)
- **Endothelial Signaling**
  (Lena Claesson-Welsh / Bjorn Olsen / Gabriele Bergers)

Angiogenesis
Aug 3-4, 2013
Chair: [illegible]

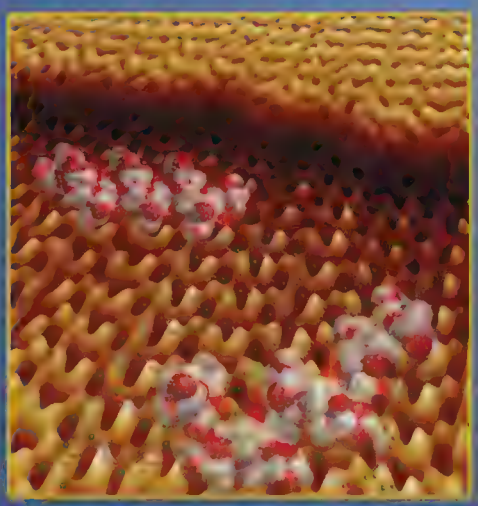

Biomolecules adhered to an in[illegible] surface. Court[illegible] Friddle (Sandia National Laboratories). Submitted by Kenn[illegible] Chair, Science of Adhesion GRC.

APOPTOTIC CELL RECOGNITION & CLEARANCE

Jun 23-28, 2013
University of New England, Biddeford, ME
Chairs: Nathalie Franc & Patrizia Rovere-Querini
Vice Chairs: David S. Ucker & Dror Mevorach

- **Keynote Presentations: Phagocytosis, and Tumor Immunology**
  (*Dror Mevorach* / Sergio Grinstein / Guido Kroemer)
- **Cell Killing, Extrusion, Competition in Tissue Homeostasis and Regeneration**
  (*Lynda Stuart* / Jody Rosenblatt / Laura Johnston / Richard Lang / Zsuzsanna Szondy)
- **Apoptotic Cell Lipids-Associated Molecular Patterns and Signaling**
  (*Kodi Ravichandran* / Xiaochen Wang / Shigekazu Nagata / Donna Bratton)
- **Molecular Mechanisms of Recognition, Engulfment and Degradation of Apoptotic Corpses**
  (*Donna Bratton* / Kodi Ravichandran / Chonglin Yang / Michael Hengartner / Zheng Zhou)
- **Apoptotic Cell Recognition Receptor Signaling**
  (*John Savill* / Estee Kurant / Kim McCall / Ray Birge)
- **Inflammatory Consequences of Apoptotic Cell Clearance**
  (*Doug Green* / Akiko Shiratsuchi / Dmitri Krysko / David Ucker / Lynda Stuart / Ian Dransfield)
- **Tissue Homeostasis in Inflammation and Self-Tolerance**
  (*Peter Henson* / Flavius Martin / Steven Bensinger / William Janssen)
- **Apoptotic Cell Clearance in Neurogenesis and Neurodegeneration**
  (*Martin Herrmann* / Mary Logan / Francesca Peri / Silvia Finnemann / Jonathan Kipnis)
- **Necroptosis, Oncogenesis and Tumor Immunology**
  (*Luciana Dini* / Peter Vandenabeele / Christopher Gregory / Martin Herrmann)

Apoptotic Cell Recognition & Clearance
Jun 22-23, 2013
Chair: Lucia Cottone
Associate Chair: Hui Xiao

APPLIED & ENVIRONMENTAL MICROBIOLOGY

Exploring and Exploiting the Depths of the Microbial Biosphere

Jul 7-12, 2013
Mount Holyoke College, South Hadley, MA
Chair: Janet Jansson
Vice Chair: J. Colin Murrell

- **Is Everything Everywhere or Does the Environment Select?**
  (Rob Knight / Tim Vogel / Curtis Huttenhower)
- **The Human Microbiome - Putting Knowledge into Practice**
  (Barry Fine / Michael Sadowsky / Jeroen Raes / Julen Marchesi)
- **The Deep Biosphere - How Deep Can We Go?**
  (*Nicole Dubilier* / Jennifer Macalady / Olivia Mason)
- **Back to the Future - New Insights from Culturing and Genomics**
  (*Colin Murrell* / Steve Giovanonni / Nikos Krypides / Max Häggblom)
- **Microbes and Host / Environment Interactions**
  (*Lance Price* / Guatam Dantas / Kornelia Smalla)
- **Microbes as Fuel and Energy Sources**
  (*Ken Nealson* / Steve Singer / Filipa Godoy-Vitorino / Gregg Whited)
- **Social Microbes and Interactions**
  (*Beth Shank* / George Salmond / Phil Poole)
- **The Wet Biosphere - Microbes in Aquatic Environments**
  (*Jed Fuhrman* / David Scanlan / Matt Sullivan / Andy Johnston)
- **Close to Home: the Built Environment**
  (*Kerry Kinney* / James Meadow / Jack Gilbert)

Uzon caldera in Kamchatka, Russia. These hot springs are a source of archaea. Submitted by Zvi Kelman & Sonja-Verena Albers, Chairs Archaea: Ecology, Metabolism & Molecular Biology GRC.

ARCHAEA: ECOLOGY, METABOLISM & MOLECULAR BIOLOGY

Jul 28 - Aug 2, 2013
Renaissance Tuscany Il Ciocco Resort, Lucca (Barga), Italy
Chairs: Zvi Kelman & Sonja-Verena Albers
Vice Chairs: Todd Lowe & Ruth A. Schmitz-Streit

- **The Rise of the Archaea**
  (*John Reeve* / Rudolf Thauer / Eugene Koonin)
- **Replication, Recombination and Repair**
  (*Patrick Forterre* / Nick Robinson / Isaac Cann / Stuart MacNeill / Steve Bell)
- **Transcription**
  (*Michael Thomm* / Tom Santangelo / Finn Werner)
- **CRISPR and Viruses**
  (*Ken Stedman* / Anita Marchfelder / Michael Terns / Malcolm White)
- **Small RNAs**
  (Ruth Schmitz-Streit / Todd Lowe)
- **Cell Envelope**
  (*Karl O. Stetter* / Kenneth Jarrell / Mecky Pohlschröder / David Prangishvili / Robert Gunsalus)
- **Posttranslational Modifications**
  (*Fran Porter* / Li Huang / Jerry Eichler / Julie Maupin-Furlow)
- **Ecology and Evolution**
  (*Uri Gophna* / Tim Unch / Graeme Nicol / Rachel Whitaker / Thijs Ettema)
- **Metabolism**
  (*Haruyuki Atomi* / Bettina Siebers / Mike Adams / Bill Metcalf)

ASSISTED CIRCULATION

Reducing Adverse Events, Improving Circulatory Support Systems and Outcomes

Jun 23-28, 2013
Renaissance Tuscany Il Ciocco Resort, Lucca (Barga), Italy
Chairs: Victor L. Poirier & Emma J. Birks
Vice Chairs: Joseph G. Rogers & Heinrich Schima

- **The Quest for Biocompatibility; Factors Effecting Thrombosis and Other Adverse Events**
  (*John Watson, Bartley Griffith* / Marvin Slepian / Geert Schmid-Schonbein / Thomas Webster)
- **Basic Bioengineering Aspects to Reduce Severe Adverse Events Associated with Bleeding and Stroke**
  (*George Wieselthaler, Walt Dembitsky* / Scott Diamond / Egemen Tuzun / Robert Padera)
- **LVAD Utilization and Associated Cost**
  (*Tim Baldwin, Robin Bostic* / Keith Aaronson / Joe Rogers / Mark McClellan)
- **Right Heart Function and Failure in Long Term Mechanical Circulatory Support: Getting Back to Basics**
  (*Eduardo Rame, Frank Pagani* / Michael Bristow / J. Eduardo Rame / James Kirkpatrick / Martin Strueber)
- **Assisted Circulation for Evolving Patient Groups**
  (*Peter Wearden, Patti Massicotte* / David Morales / Christina VanderPluym / Amy Throckmorton / Charles Fraser)
- **Clinical Considerations for Increase Use of LVADS**
  (*Joseph Rogers, Meredith Brisco* / Lynne Stevenson / Matthew Hillebrenner / David Naftel / Mark Slaughter / Todd Dardas)
- **Clinical Trial Design**
  (*Jim Young, Jim Long* / Clyde Yancey / Michael Acker / Ileana Pina)
- **Advancements in Sensor Technology, Power Transmission and the Understanding of LVAD Limitations**
  (*Henrich Schima, Tim Kaufmann* / Thorsten Siess / Pramod Bonde / Uwe Tegtbur)
- **The Future of MCS, Rotary Blood Pumps and the Clinical Considerations**
  (*Donna Mancini* / Richard Wampler / Bud Frazier / Robert Kormos)

Assisted Circulation
Jun 22-23, 2013
Chair: Meredith A. Brisco
Associate Chair: Tim Kaufmann

ATHEROSCLEROSIS

Translating the Biology of Atherosclerosis

Jun 16-21, 2013
Stoweflake Resort and Conference Center, Stowe, VT
Chairs: Elaine W. Raines & Daniel Rader
Vice Chair: Klaus Ley

- **Endothelial Activation and Dysfunction**
  (*Myron Cybulsky* / Mark Feinberg / Cynthia Reinhart-King)
- **Myeloid Cell Trafficking and Innate Immunity in Atherosclerosis**
  (*Gwen Randolph* / Christoph J. Binder / Alma Zernecke / Myron Cybulsky / Gwen Randolph)
- **Adaptive Immunity in Atherosclerosis**
  (*Klaus Ley* / Elena Galkina / Andrew Lichtman / Klaus Ley)
- **Macrophage Phenotypes and Plasticity**
  (*Catherine Hedrick* / Inna Udalova / Catherine Hedrick)
- **Linking Lipoprotein Metabolism and Atherosclerosis**
  (*Sekar Kathiresan* / Kathryn J. Moore / Marlys Koshchinsky / John Danesh)
- **Epigenetics and Atherosclerosis**
  (*Gary K. Owens* / Silvio Zaina / Tapan Chatterjee / Andriana Margariti / Gary K. Owens)
- **Stem Cells and Cardiovascular Disease**
  (*Stefanie Dimmeler* / Matthias Nahrendorf / Mark Majesky)
- **Lesion Dynamics**
  (*Ira Tabas* / Athan Kuliopulos / Ed Plow / Stefanie Dimmeler / Ira Tabas)
- **Thrombosis, Microparticles and Cardiovascular Disease**
  (*Chantal Boulanger* / Nigel Mackman / Chantal Boulanger)

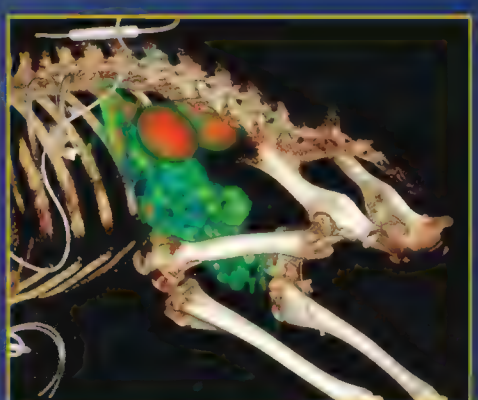

Abdominal perfusion PET/CT of a sheep model implanted with a continuous flow ventricular assist device, fused and volume rendered in 3D. Study shows high perfusion kidney and upper GI areas with skeletal structure overlaid for reference. Courtesy of Egemen Tuzun (Texas A&M University). Submitted by Victor L. Poirier & Emma J. Birks, Chairs Assisted Circulation GRC.

ATMOSPHERIC CHEMISTRY

Jul 28 - Aug 2, 2013
Mount Snow Resort, West Dover, VT
Chairs: Steven S. Brown & Yinon Rudich
Vice Chair: Paul B. Shepson

- **Atmospheric Chemistry and Climate**
  (*Jean-Francois Lamarque* / Daniel Jacob / Ted Parsons / Tami Bond / David Fowler)
- **Energy and Emissions**
  (*Paul Shepson* / Mark Jacobson / Gaby Petron / Chip Miller)
- **Nucleation**
  (*Urs Baltensperger* / Joachim Curtius / Peter McMurray / Henryk Svensmark)
- **Atmosphere Ocean Interactions**
  (*Kim Prather* / Patricia Quinn / Rainer Volkamer / Cristina Facchini)
- **Aerosol Chemistry and Consequences**
  (*Allen Robinson* / Alex Laskin / Daniel Lack / Jamie Schauer / Christian George)
- **New Directions in Atmospheric Oxidation**
  (*Jim Crawford* / Dan Jaffe / Becky Alexander / Maria Kanakidou)
- **Anthropogenic-Biogenic Interactions**
  (*Astrid Kiendler-Schaar* / Ann Marie Carleton / Allen Goldstein)

ATOMIC PHYSICS

Jun 23-28, 2013
Salve Regina University, Newport, RI
Chair: Debbie Jin
Vice Chair: Vladan Vuletic

- **Quantum Information and Quantum Optics**
  (*Ivan Deutsch* / Jian-Wei Pan / Arno Rauschenbeutel)
- **Bose and Fermi Gases**
  (*Dan Stamper-Kurn* / Martin Zwierlein / Gretchen Campbell / Eugene Demler)
- **Dipolar Gases and Cold Molecules**
  (*Luis Santos* / Shin Inouye / Tanya Zelevinsky)
- **Few-Body Systems**
  (*Chris Greene* / Johannes Hecker-Denschlag / Selim Jochim)
- **Mesoscopics and Devices**
  (*Jeff Kimble* / Philipp Treutlein / Michal Lipson)
- **Pulsed Light Spectroscopy**
  (*Margaret Murnane* / Andrea Cavalleri / Tamar Seideman)
- **Quantum Simulation and Optical Lattices**
  (*Immanuel Bloch* / Giovanna Morigi / Ian Spielman)
- **Precision Measurements**
  (*Jun Ye* / John Doyle / James Thompson / Marianna Safronova)
- **Rydberg Atoms**
  (*Mark Saffman* / Philippe Grangier / Alex Kuzmich)

BARRIER FUNCTION OF MAMMALIAN SKIN

Aug 18-23, 2013
Waterville Valley Resort, Waterville Valley, NH
Chairs: Theodora M. Mauro & Philip W. Wertz
Vice Chairs: Dennis R. Roop & Reinhard H H. Neubert

- **Defining Mammalian Barrier Function**
  (*Kenneth Feingold* / Steven Hoath / Peter Elias)
- **New Approaches for Investigating Barrier Function**
  (*Joachim Fluhr* / Konrad Sandhoff / Roger Wepf)
- ***In Vitro* and Animal Models of Barrier Function**
  (*Dennis Roop* / Gopinathan Menon)
- **Atopic Dermatitis as a Model Barrier Disease**
  (*Seung Hun Lee* / Ehrhardt Proksch / Joke Bouwstra)
- **Epidermal Barrier, Antimicrobial Peptides and the Microbiome**
  (Richard Gallo / Heidi Kong)
- **Surmounting the Barrier to Administer Therapy**
  (*Philip Wertz* / Michael Roberts / Richard Guy / Maureen Donovan)
- **Emerging Barrier Functions and Technologies: Late-Breaking Topics & Young Investigator Presentations**
  (*Reinhard Neubert*)
- **Response to Barrier Perturbation: Epidermis and Beyond**
  (*Walter Holleran* / Michael Rosenblum / Eung Ho Choi / Yoshikazu Uchida)
- **Debate: Nature vs. Nurture - Genetics are the Most Important Factor in Determining Barrier Function and Response**

BIOENERGETICS

Molecular Mechanisms and Fundamental Principles to Cellular Energetics in Health and Disease
Jun 23-28, 2013
Proctor Academy, Andover, NH
Chair: Ulrich Brandt
Vice Chair: Karlett J. Parra

- **Diversity of Bioenergetic Systems**
  (*Manuela Pereira* / Rolf Thauer / Pia Ädelroth / Anthony Moore)
- **Structure and Function of Complex I**
  (*Thorsten Friedrich* / Volker Zickermann / Leonid Sazanov / Hideto Miyoshi)
- **Respiratory Complexes in Health and Disease**
  (*Gary Cecchini* / Peter R. Rich / Artur Osyczka)
- **Mechanisms and Energetics of ATP-Synthesis**
  (*Wayne Frasch* / John Walker / David Mueller)
- **Mechanisms and Functions of V-type and A-type ATPases**
  (*Volker Müller* / Patricia Kane / Gerhard Grüber / Dennis Brown)
- **Supramolecular Organization of Bioenergetic Complexes**
  (*Rosemary Stuart* / Karen Davies / Cristina Ugalde / Charles L. Hoppel)
- **Emerging Techniques**
  (*Les Dutton* / Petra Fromme / Manuela Zoonens / Michael Börsch)
- **Talks Selected from Posters**
  (*Karlett Parra, Susanne Arnold*)
- **Systems Biology and Mitochondrial Diseases**
  (*Jan Smeitink* / Salvatore DiMauro / Massimo Zeviani / Antonio Enriquez)

BIOLOGICAL MECHANISMS IN EVOLUTION NEW!

Biological Mechanisms in Evolution in Basic Biology, Cancer, Infectious Disease and Medicine
Jun 2-7, 2013
Stonehill College, Easton, MA
Chair: Susan M. Rosenberg
Vice Chair: Christine Queitsch

- **Keynote Presentations: Pioneers in Stress-Inducible Evolution**
  (*Susan Rosenberg* / Susan Lindquist / Miroslav Radman)
- **Stress-Inducible Genetic Change Mechanisms**
  (*Ivan Matic* / Ivan Matic / Peter Glazer / Philip Hastings)
- **Stress and Evolution**
  (*Marlene Belfort* / Lilach Hadany / Amar Al Mamun)
- **Non-Random Mutagenesis in Genomes**
  (*John W. Drake, Lynn Caporale* / Laura Landweber / Ben Lehner / Anna Malkova)
- **Non-Genetic Inheritance**
  (*Christine Queitsch* / Christine Queitsch / Leah Cowen / Joanna Masel)
- **Stochastic Non-Genetic Inheritance and Adaptation**
  (*David Dubnau, Herbert Levine* / David Dubnau / Stanislas Leibler / Christophe Herman / Arjun Raj)
- **Cancer As Evolution**
  (*Lawrence A. Loeb* / Thea Tlsty / Carlo Maley / Franziska Michor)
- **Evolution of Antibiotic Resistance**
  (*Yousif Shamoo* / Kim Lewis / Robert Austin / Erika Shor)
- **Transmissable Genomic Instability Mechanisms**
  (*Barbara Hohn* / Carmel Mothersill / Yuri Dubrova)

BIOLOGICAL MOLECULES IN THE GAS PHASE & IN SOLUTION

Jul 21-26, 2013
Holderness School, Holderness, NH
Chairs: David Clemmer & Robert J. Woods
Vice Chair: Richard W. Vachet

- **Biomolecule-solvent Interactions**
  (David Russell / Andrea Markelz)
- **Aggregation**
  (*Perdita Baran* / Alison Ashcroft / Michael Przybylski / Lars Konermann / Michael Bowers)
- **Reactivity of Biological Ions**
  (Kathrin Breuker / Graham Cooks / Scott McLuckey / Sarah Trimpin)
- **Large Biomolecular Assemblies**
  (Martin Jarrold / Albert Heck / Vicki Wysocki / Michal Sharon)
- **Glycans and Glycoproteins**
  (Verin Reinhold / James Reilly / Cathy Costello)
- **Protein Structure, Folding, and Dynamics**
  (*Michael Gross* / Brian Chait / Jennifer Brodbelt / Ryan Julian / David Weiss)
- **Computation and Simulations**
  (*Theresa Head-Gordon* / Igor Tvaroska / David van der Spoel / Lachele Foley)
- **Biomolecule Dissociation**
  (Peter Armentrout / Nick Polfer / Kristina Hakansson / Yury Tsybin)
- **Spectroscopy of Isolated Biomolecules**
  (*Evan Williams* / Jos Oomens / Thomas Rizzo / Rebecca Jockusch)

BIOMATERIALS & TISSUE ENGINEERING

Inductive Signals for Tissue Regeneration and Clinical Challenges
Jul 28 - Aug 2, 2013
Holderness School, Holderness, NH
Chair: Shelly E. Sakiyama-Elbert
Vice Chair: Edward A. Botchwey

- **Acellular Tissue Constructs: Inductive Signals and Clinical Challenges**
  (*Shelly Sakiyama-Elbert* / Jennifer Elisseeff / Karen Christman)
- **Tissue Engineering Approaches and Materials for Directing Neural Regeneration**
  (*Erin Lavik* / Sarah Heilshorn / Lonnie Shea / Raj Midha)
- **Immunoresponsive Materials**
  (*Julie Babensee* / Jeffrey Hubbell / Darrell Irvine)
- **Materials for Engineering Vascular Tissues**
  (*Debra Auguste* / Guillermo Ameer / Tatiana Segura / Kristyn Masters)
- **Engineering the Stem Cell Niche**
  (*Edward Botchwey* / Claudia Fischbach / Matthias Lutolf)
- **Drug Delivery Platforms for Tissue Engineering**
  (*Manu Platt* / Horst Von Recum / Tejal Desai / Carsten Werner)
- **Mechanics of Materials and Mechanisms of Directing Cell Response**
  (*Kevin Healy* / Jane Grande-Allen / George Duda)
- **Lessons in Tissue Engineering and Biomaterials: What Industry Wishes Academia Knew**
  (*Andres Garcia* / Amar Sawhney / Paul Drumheller / Elle Nugent)
- **Talks Selected from Posters**
  (*Randolph Ashton*)

Biomaterials & Tissue Engineering
Jul 27-28, 2013
Chair: Carrie E. Brubaker
Associate Chair: Matthew J. Webber

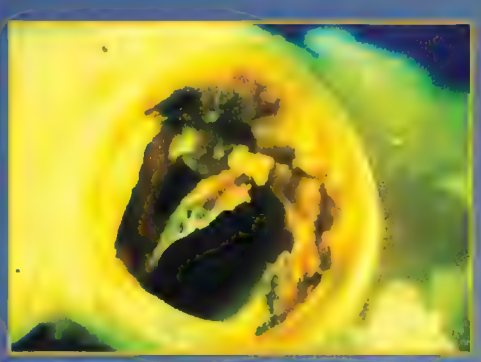

BIOORGANIC CHEMISTRY
Jun 9-14, 2013
Proctor Academy, Andover, NH
Chairs: Jumi Shin & Grant K. Walkup
Vice Chairs: Michael D. Burkart & Stacie Canan

- **Finding Cures for Diseases - From Screening to Patient**
  (Michael Arkin / David Chenoweth / Jeff Kelly)
- **Studying Nucleic Acids Processes with Mimetics & Design**
  (Gabriele Varani / Bruce Armitage / Sara Walker)
- **Novel Peptides for New Biological Impacts**
  (Chana Kelley / Tamaki Suga / Neil Marsh)
- **Chemical Approaches for Fighting Bacteria Disease**
  (Scott Blanchard / John Vederas / Jeff Cirillo)
- **Building Imaging Methods to Understand Biology**
  (Young-Tae Chang / Kai Johnsson)
- **Understanding Enzymes & Putting Them to Work**
  (Dan Herschlag / Joelle Pelletier / Tom Moody)
- **Open Forum: Competition & Pre-competitive Sharing**
  (David Drewry / Zhi-Fu Tao / Gretchen Schroeder)
- **Chemical & Systems Biology: Tools, Insights, & Discoveries**
  (Lara Mahal / Angela Koehler / Gitte Neubauer)
- **Imaging, Designing, & Understanding Biomolecules**
  (Bob Copeland / Steve Benner)

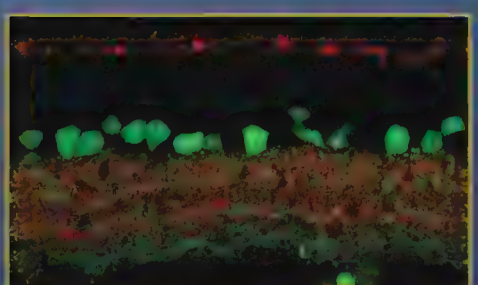

DGL-α in mouse retina. Courtesy of Alex Straiker (Indiana University). Submitted by Andrea G. Hohmann & David Lovinger, Chairs, Cannabinoid Function in the CNS GRC

CAG TRIPLET REPEAT DISORDERS
Basic Science to Therapeutics
Jun 23-28, 2013
Waterville Valley Resort, Waterville Valley, NH
Chair: Leslie M. Thompson

- **Early Clinical Signs, Biomarkers and Systemic Effects**
  (*Beverly Davidson* / Anne B. Young / Kenneth Fischbeck)
- **Proteostasis**
  (*Ai Yamamoto* / Steven Finkbeiner / Jason Gestwicki / Judith Frydman)
- **Epigenetics and Transcription**
  (Ernest Fraenkel / Christopher Gomez)
- **Cell Metabolism**
  (*Al La Spada* / Jeffrey Carroll / Andrew Dillin / J. Lawrence Marsh / Frederic Saudou)
- **Emerging Insights**
  (*Harry Orr* / Elena Cattaneo / Laura Ranum)
- **Metabolic and Immune Contributions to Neurodegeneration**
  (*Sarah Tabrizi* / Asa Petersen / Sarkis Mazmanian / Flaviano Giorgini)
- **Endophenotypes and Associated Disease Mechanisms**
  (*Tim Ebner* / Anthony Hannan / Michael Levine / Bernhard Landwehrmeyer)
- **Therapeutic Approaches**
  (*Dimitri Krainc* / Clive Svendsen / Matthew Wood)
- **Moving Forward**
  (Jang Ho Cha / Gen Sobue)

CAG Triplet Repeat Disorders
Jun 22-23, 2013
Chair: Edward W. Green

CALCIUM SIGNALLING
Jun 16-21, 2013
Renaissance Tuscany Il Ciocco Resort, Lucca (Barga), Italy
Chair: Rosario Rizzuto
Vice Chair: David I. Yule

- **20 Years of Calcium Signalling GRC: Where We Were and How Far We Have Come**
  (Michael Berridge / Tullio Pozzan)
- **Calcium and Cell Function**
  (*Ole Petersen* / Guy Rutter / Tobias Meyer / Yun Zhang)
- **Calcium Entry**
  (*Indu Ambudkar* / Richard Lewis / Donald Gill / Shmuel Muallem)
- **Role of Calcium Entry in Disease**
  (*James Putney* / Mohammed Trebak / Stefan Feske / Annette Dolphin)
- **Intracellular Ca^{2+} Release Channels**
  (*Andrew Thomas* / Colin Taylor / Llewellyn Roderick / Jon Lederer / Antony Galione)
- **Intracellular Calcium Release Channels and Disease**
  (*Martin Bootman* / Marc Montminy / Susan Hamilton / Muthu Periasamy)
- **Mitochondria**
  (*Michael Duchen* / Luca Scorrano / Mei-ling A. Joiner / Jau-nian Chen / Anna Raffaello)
- **Calcium in Inflammatory Diseases**
  (*Barbara Ehrlich* / Daniella Riccardi / Alexey Tepikin / Anant Parekh)
- **Calcium and Neurodegeneration**
  (*Katsuhiko Mikoshiba* / Kevin Foskett / Ilya Bezprozvanny / Grace Stutzmann)
- **Keynote Presentation: The Stim/Orai System for Calcium Entry**
  (*Michael Berridge* / Anjana Rao)

Calcium Signalling
Jun 15-16, 2013
Chair: Johanna T. Lanner

CANCER NANOTECHNOLOGY
NEW!
Jul 14-19, 2013
Mount Snow Resort, West Dover, VT
Chair: James R. Baker
Vice Chair: Leaf Huang

- **Why is Nanotechnology Important for Cancer?**
  (*David Walt* / Bengt Fadeel / Ruth Duncan / Ralph Weissleder)
- **Synthetic Therapeutic Platforms**
  (*Robert Langer* / Omid Farokhzad / Youqing Shen / Kazunori Takaoka / Shyh-Dar Li)
- **Stealth Nanoparticles**
  (*Sonke Svenson* / Sonke Svenson / Rainer Jordan / Rafael T. M. de Rosales)
- **Nanotech Imaging**
  (*Jeff Bulte* / Dan Hammer / Xiangyang Shi / Greg Lanza / Chun Li)
- **Nanotechnology for Cancer Vaccines**
  (*Jim Mule* / Tarek Fahmy / Darrell Irvine / David Mooney)
- **Bio-inspired Therapeutic Platforms**
  (*Erkki Ruoslahti* / Mark Grinstaff / Ashutosh Chilkoti / Nicole F. Steinmetz / Andrew Wang)
- **New Approaches to Applying Nanotechnology**
- **Early Diagnosis of Cancer using Nanotechnology**
  (*Chad Mirkin* / Sanjiv Gambhir / Mehmet Toner / Dan Hayes)
- **Complex Theranostics for Cancer**
  (*Piotr Grodzinski* / George M. Church / M.A. El-Sayed / D.G. Anderson)

CANNABINOID FUNCTION IN THE CNS
Cannabinoids in Synapses, Circuits and the Human Brain
Aug 4-9, 2013
Waterville Valley Resort, Waterville Valley, NH
Chairs: Andrea Hohmann & David Lovinger
Vice Chairs: Tibor Harkany & Mauro Maccarrone

- **Keynote Presentation: Imaging and Controlling Neural Circuits with Light**
  (*Pablo Castillo* / Bernardo Sabatini)
- **Endocannabinoids and Neuronal Circuitry: Learning and Memory**
  (*Beat Lutz* / Rui Costa / Qing-Song Liu / Yasumasa Ueda / Aron Lichtman)
- **Cannabinoid Receptor Trafficking and Signaling**
  (*Heather Bradshaw* / Michelle Glass / Istvan Katona / Jeremy Henley / Guillermo Yudowski / Ken Mackie)
- **Endocannabinoids, Endovanilloids and the Endocannabinoid Metabolome**
  (*Vincenzo Di Marzo* / Andres Chavez / Sachin Patel / Julian Romero / Daniele Piomelli)
- **The Endocannabinoid System and Pain: From the Bench to the Bedside**
  (*Victoria Chapman* / Volker Neugebauer / David Finn / Lih-Chu Chiou / Mark Ware)
- **Endocannabinoid-Dependent Synaptic Plasticity: New Developments**
  (*Raffaella Tonini* / Thomas Nevian / Catherine Wooley / Nagore Puente / Guoping Feng)
- **Endocannabinoids and Neurological/ Neuropsychiatric Diseases and Disease Models**
  (*Daniela Parolaro* / Nicole Calakos / Cecilia Hillard / Tarek Samad / Wim Vandenberghe)
- **Endocannabinoids and Neuronal Circuitry: Substances of Abuse, Reward and Addiction**
  (*Miriam Melis* / Joseph Cheer / Peter Laviolette / Therese Jay / Loren Parsons / Jussi Hirvonen)
- **Endocannabinoids, Inhibitory Synaptic Transmission and Epilepsy**
  (*F. Edward Dudek* / Ivan Soltesz / Karolien Goffin)

Cannabinoid Function in the CNS
Aug 3-4, 2013
Chair: Josee Guindon
Associate Chair: Christina M. Gremel

CARBOHYDRATES
Jun 16-21, 2013
Mount Snow Resort, West Dover, VT
Chairs: Joseph J. Barchi & George O'Doherty
Vice Chairs: Jeffery C. Gildersleeve & Alexei V. Demchenko

- **Sugar Processing Enzymes / Glycosyltransferases**
  (Jon Thorson / Kelley Moreman / Hung-Wen (Ben) Liu / Xi Chen)
- **Glycosylation and Stereochemistry**
  (Scott Rychnovsky / Keith Woerpel / Toshiki Nokami)
- **Lessons from the CFG (Consortium for Functional Glycomics)**
  (James Paulson / Richard Cummings / Anne Dell / Ram Sasisekaran)
- **Carbohydrate Immunology / Immunotherapy**
  (Kate Rittenhouse-Olson / Peter Andreana / Yvette van Kooyk)
- **Sugars and Natural Products**
  (Rodrigo Andrade / Jurgen Rohr / David Jakeman)
- **Chemical Glycobiology**
  (Linda Hsieh-Wilson / David Vocaldo / Dev Arya)
- **Sugar Synthesis and Therapeutics**
  (Horst Kunz / Chang-Chun Ling / Jackie Gervay-Hague)

- **Materials, Particles and Sensors**
  (Theresa Reineke / Xuewei Liu / Nicola Pohl)
- **"All Things Carbohydrate"**
  (Peter Seeberger / Chi Huey Wong / Robert Lindhardt)

CATCHMENT SCIENCE: INTERACTIONS OF HYDROLOGY, BIOLOGY & GEOCHEMISTRY

Catchments Through the Looking Glass: From Microscopes to Telescopes
Jun 16-21, 2013
Proctor Academy, Andover, NH
Chairs: Thomas D. Bullen & Carmen De Jong
Vice Chair: Kathleen C. Weathers

- **Implications of Climate Change: Clear or Cloudy**
  (*Thomas Bullen, Carmen deJong* / Paul Mayewski)
- **Doors of Perception: How the Scale of Our Scientific Lens Shapes Our Understanding of Catchments**
  (*Michael Gooseff, Laurent Pfister* / Eric Masson / Robyn Hannigan / Marcus Weiler / Peter Nico / Antonio Parodi)
- **Changes in Latitudes, Changes in Attitudes: Latitudinal Gradients from Polar to Tropical**
  (*Kevin Bishop, Sherry Schiff* / Berry Lyons / Jennifer Harden / Nancy Dise / Celine Dessert / Howard Wheater)
- **Tools You Can Use: Novel Analytical Techniques and Conceptual Approaches**
  (*Jeff McDonnell, Christine Alewell* / Henry Lin / Sophie Opfergelt / Kamini Singha / Jan Seibert / John Matthews)
- **Animal, Vegetable, Mineral: Linkages Between Biota and the Earth's Surface**
  (*Jeff McDonnell, Christine Alewell* / Jakub Hruska / Suzanne Anderson / Mary Power / Lars Tranvik)
- **Looking Outward: Watersheds on Mars and Beyond**
  (*Thomas Bullen, Carmen deJong* / Vic Baker)

Catchment Science: Interactions of Hydrology, Biology & Geochemistry
Jun 15-16, 2013
Chair: Kate A. Brauman
Associate Chair: Jakob Schelker

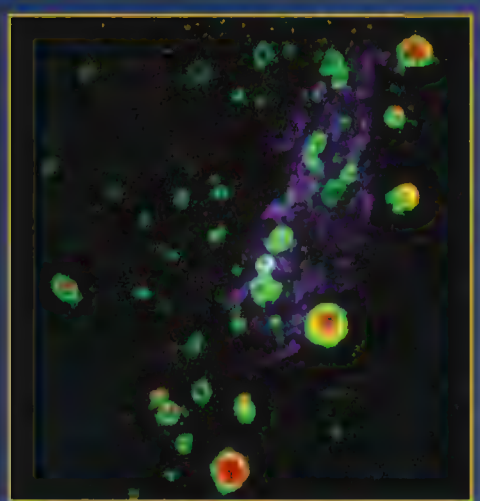

Manganese sensor GPP130 (red) translocating from the Golgi apparatus (purple) to endosomes (green) in response to Golgi manganese. Micrograph: Somshuvra Mukhopadyay and Adam D. Linstedt (Carnegie Mellon University). Submitted by David J. Eide & Caroline C. Philpott, Chairs, Cell Biology of Metals GRC.

CATECHOLAMINES

Aug 11-16, 2013
Mount Snow Resort, West Dover, VT
Chair: Antonello Bonci
Vice Chair: Paul E. Phillips

- **Keynote Presentation: Behavioral Influences of Catecholamines**
  (Roy Wise)
- **Catecholamines and Stress**
  (Marisela Morales / Steven A. Thomas / R. Mark Wightman / Rita Valentino)
- **Catecholamines in Neurological Disorders**
  (D. James Surmeier / Anatol C. Kreitzer / Marie-Françoise Chesselet)
- **Catecholamines and Substance Abuse**
  (Jacqueline F. McGinty / Jill B. Becker / Yolanda Mateo / Terry E. Robinson / Linda J. Porrino / Nora D. Volkow)
- **Synaptic Regulation of Catecholamine Transmission**
  (Veronica A. Alvarez / Stephanie J. Cragg / John T. Williams / Robert C. Malenka)
- **Catecholamine Receptors**
  (Amy H. Newman / David Weinshenker / Virginia M. Pickel / Marc G. Caron / Chris Hague)
- **Circuit-Level Regulation of Catecholamine Function**
  (*Garret D. Stuber* / Richard D. Palmiter / Naoshige Uchida / Susan M. Ferguson / Kay M. Tye)
- **Economic Decision Making**
  (Regina M. Carelli / Kate M. Wassum / Xiaoxi Zhuang)
- **Catecolamines and Cognition**
  (*Patricio O'Donnell* / Anthony A. Grace / Jeremy K. Seamans / Ann M. Graybiel)
- **Catecolamines Transporters**
  (Nancy R. Zahniser / Randy D. Blakely)
- **Keynote Presentation: Functional Implications of Catecholaminergic Circuitry**
  (Susan R. Sesack)

Catecholamines
Aug 10-11, 2013
Chair: Gwendolyn G. Calhoon
Associate Chair: James A. Hardaway

CELL BIOLOGY OF METALS

Jul 28 - Aug 2, 2013
Salve Regina University, Newport, RI
Chairs: David J. Eide & Caroline C. Philpott
Vice Chairs: Dennis J. Thiele & Amy E. Palmer

- **Keynote Session: Genetics and Genomics of Metal Metabolism**
  (*Timothy Stemmler* / Ashley Bush / Sabeeha Merchant)
- **Metalloproteomics and Metallogenomics**
  (*Valeria Culotta* / Chris Dupont / John Tainer / Vadim Gladyshev / David Mendoza-Cozatl)
- **Metals and Microbial Pathogenesis**
  (*Thomas O'Halloran* / Manuella Rafatellu / Mick Petris / Susan Buchanan)
- **Intracellular Metal Trafficking and Utilization**
  (*Mary Lou Guerinot* / Amy Medlock / Iqbal Hamza / Patricia Jennings / Amy Palmer)
- **Metal Cofactor Assembly**
  (*Dennis Winge* / Florian Bittner / David Barondeau / Roland Lill)
- **Metals in Physiology and Disease**
  (*Karin Finberg* / De-liang Zhang / Robert Cousins / Jerry Kaplan / Byung-Eun Kim)
- **Metallosensors as Regulators of Homeostasis**
  (*Ralf Mendel* / David Giedroc / Simon Labbe / Caryn Outten)
- **Metal Homeostasis in Higher Eukaryotes**
  (*Caroline Enns* / Kerry Kornfeld / Terri Long / Jodie Babitt / Dennis Thiele)
- **Keynote Session: Emerging New Areas in the Cell Biology of Metals**
  (*Jose Arguello* / Nigel Robinson / Adam Linstedt)

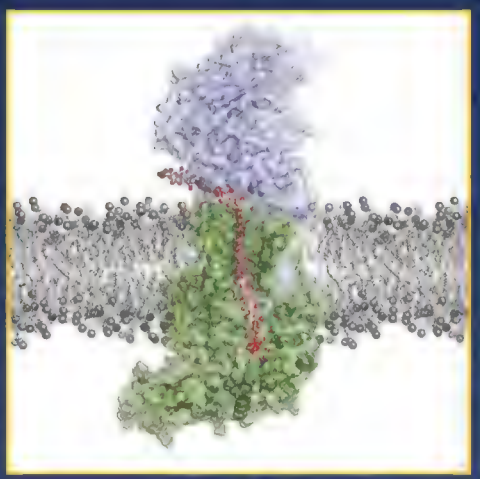

The biological synthesis and degradation of cellulose constitutes a significant portion of the global carbon cycle, and underpins diverse agricultural and industrial products, ranging from biofuels to biomaterials such as paper, textiles, and timber. The seminal crystal structure of a membrane-integrated bacterial cellulose synthase complex provides unique molecular insight into the biosynthesis and translocation of this important polysaccharide. Courtesy of Jochen Zimmer (University of Virginia). Submitted by Harry Brumer, Chair, Cellulosomes, Cellulases & Other Carbohydrate Modifying Enzymes GRC.

CELL CONTACT & ADHESION

Jun 2-7, 2013
Renaissance Tuscany Il Ciocco Resort, Lucca (Barga), Italy
Chair: Andrew P. Kowalczyk
Vice Chair: Cara J. Gottardi

- **Keynote Session: Cell Contact in Perspective**
  (Pamela Cowin / Kathleen Green / John Wallingford)
- **Going with the Flow: Adhesion in Vascular Biology**
  (Elisabetta Dejana / Martin Schwartz / Dietmar Vestweber / Johan de Rooji / Mario Delmar)
- **Cell Adhesion and Signaling in Morphogenesis**
  (Jennifer Zallen / Mark Peifer / Pierre McCrea)
- **Epithelia: Staying in Touch While on the Move**
  (Gregory Longmore / Sandrine Etienne-Manneville / Rachel Hazan / Albert Reynolds / Dorit Hanein)
- **Carrying the Load: Adhesion Receptors and Mechanotransduction**
  (Andrés J. Garcia / Sanjeevi Sivasankar / Jean-Paul Thiery)
- **Cell Contact Regulation and Diversity**
  (Sergey Troyanovsky / Barry Gumbiner / Larry Sha[illegible] / Roberto Cattaneo / Eduard Batlle)
- **Making Connections and Forming Barriers**
  (Carien Niessen / David Kelsell / Terry Lechler)
- **Internal Affairs of Adhesion Receptors**
  (Cara Gottardi / Helen McNeill / Jeff Hardin / William Weis / Alan Fanning)
- **Dynamics of Adhesion Receptors at the Cell Cortex**
  (Masatoshi Takeichi / Andrew McClatchey / Agnes Noy)

Cell Contact & Adhesion
Jun 1-2, 2013
Chair: Benjamin A. Hoon
Associate Chair: Christine M. Disbrow Mercurio

CELL GROWTH & PROLIFERATION
Jun 23-28, 2013
Mount Snow Resort, West Dover, VT
Chair: David Pellman
Vice Chair: Anindya Dutta

- **Keynote Presentation: Oncogene Signaling and the Microenvironment**
  (*David Pellman, Anindya Dutta* / Joan Brugge)
- **Cell Growth and Metabolism**
  (*Gustavo Leone* / David Sabatini / Bruce Edgar /Jan Skotheim / Celeste Simone / Danny Lew)
- **G1 Progression and Cell Cycle Engines**
  (*Bruce Edgar* / Gustavo Leone / Jackie Lees / Peter Sicinski)
- **Chromosome Duplication**
  (*Karen Oegema* / Genevieve Almouzni / Steve Bell / John Diffley / Nick Dyson / Bob Deronio)
- **Getting in and Out of Mitosis**
  (Karen Oegema / Brian Dynlat / Hongtao Yu)
- **The DNA Damage Response and Checkpoints**
  (*Don Cleveland* / Tanya Paull / Michael Yaffe / Steve Elledge / Maria Jasin / Jim Haber)
- **Chromosome Stability**
  (*Maria Jasin* / Don Cleveland / Jan van Deursen / Rong Li)
- **Oncogenes, Tumor Suppressors and Therapeutics**
  (*Celeste Simon* / Franziska Michor / Peter Jackson / Tak Mak / Sally Kornbluth / Alan D'Andrea)
- **Keynote Presentation: New Insights into Tumor Metabolism and Cancer**
  (*David Pellman, Anindya Dutta* / Craig Thompson)

Cell Growth & Proliferation
Jun 22-23, 2013
Chair: Jean M. Davidson
Associate Chair: Gabriel E. Neurohr

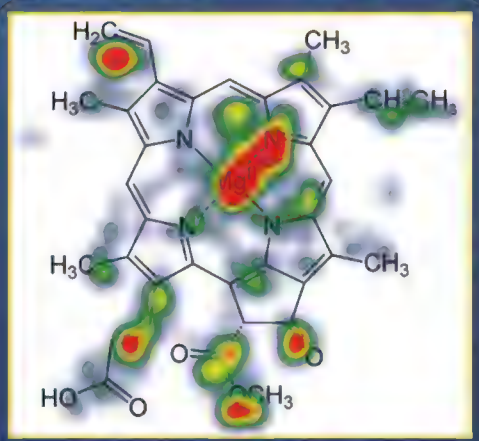

Heatmap of a pre-service teacher searching for functional groups in the given structure. Picture taken from an eyetracking study contrasting chemistry experts and pre-service teachers interpreting chemical structures. Courtesy of Sascha Bernholt and Ilka Parchmann (Leibniz Institute for Science and Mathematics Education). Submitted by Maria Oliver-Hoyo, Chair, Chemistry Education Research & Practice GRC.

CELLULAR & MOLECULAR MECHANISMS OF TOXICITY
NEW!
Aug 11-16, 2013
Proctor Academy, Andover, NH
Chair: Jose E. Manautou
Vice Chair: Dana C. Dolinoy

- **Keynote Presentation: The Nanoness of Nanotechnology: What Makes Nano Toxic?**
  (*Charlene McQueen* / Martin Philbert)
- **New Horizons in Toxicology**
  (*John Richburg* / Tom Van de Wiele / Shawn Bratton)
- **Epigenomics at the Intersection of Toxicity & Disease**
  (*Dana Dolinoy* / Jay Goodman / Trevor Archer / Rebecca Fry)
- **Advances in Stem Cell: Applicability in Drug Discovery and Safety Assessment**
  (*Theodore Rasmussen* / Hu Guang / Mark Mercola)
- **Mitochondria Diseases**
  (*Alvaro Puga* / Gary Fiskum / Patrick Chinnery / Ruben Dagda)
- **miRNA as Circulating and Mechanism-based Biomarkers of Disease**
  (*Jim Stevens* / Kevin Park / Gerald W. Dorn)
- **Genetic Susceptibility in Toxicology: Am I the 1 in 1,000?**
  (*Ruth Roberts* / Hans Ketelslegers / Ann Daley / Judit Marsillach)
- **Nuclear Factor (Erythroid-derived 2) - Like 2 (Nrf2): Is it all Good?**
  (*Bhagavatula Moorthy* / Anil K. Jaiswal / Thomas W. Kensler / David A. Tuveson)
- **Epigenetic Mechanisms of Transcriptional and Translational Regulation of Gene Expression by Xenobiotic Receptors**
  (*Yanan Tian* / Ronald Hines / Ann-Bin Shyu / Nahum Sonenberg)
- **Keynote Presentation: Inter-individual Variations in DNA Repair**
  (*Ivan Rusyn* / Leona Samson)

Cellular & Molecular Mechanisms of Toxicity
Aug 10-11, 2013
Chair: Enrique Fuentes-Mattei

CELLULOSOMES, CELLULASES & OTHER CARBOHYDRATE MODIFYING ENZYMES
Aug 4-9, 2013
Proctor Academy, Andover, NH
Chair: Harry Brumer
Vice Chair: Kiyohiko Igarashi

- **Keynote Session: Biosynthesis and Biodegradation of Terrestrial Biomass**
  (Jochen Zimmer / Bernard Henrissat)
- **Building Walls - Discovery and Functional Analysis of Glycosyltransferases in Plant Genomes**
  (Will York / Henrik Scheller)
- **(Functional) Genomics of Biomass Deconstruction by Microbial Systems**
  (Mark Morrison / Dan Cullen / Paul Harris / Eric Martens)
- **Carbohydrate Recognition by Non-Catalytic Proteins and Modules**
  (David Bolam / Alisdair Boraston)
- **Evolving Methods to Visualize Carbohydrate-Active Enzyme Activity *in situ***
  (Bernd Nidetzky / Emma Master / Shi-you Ding)
- **Cellulosomics**
  (Ed Bayer / Carlos Fontes)
- **Oxidative Polysaccharide Degradation**
  (Gideon Davies / Vincent Eijsink / Roland Ludwig)
- **Structure and Function of Carbohydrate-Active Enzymes**
  (Stephen Withers / Shinya Fushinobu / Harry Gilbert / Henrik Hansson)
- **Marine Biomass Saccharification and Conversion**
  (Jan-Hendrik Hehemann / Yasuo Yoshikuni)
- **Endogenous Glycosidases in the Plant Apoplast**
  (Jens Eklöf / Javier Sampedro / Markus Pauly)
- **Inspired Applications and Future Directions**
  (Markus Linder / Mike Himmel)

Cellulosomes, Cellulases & Other Carbohydrate Modifying Enzymes
Aug 3-4, 2013
Chair: Michael Resch

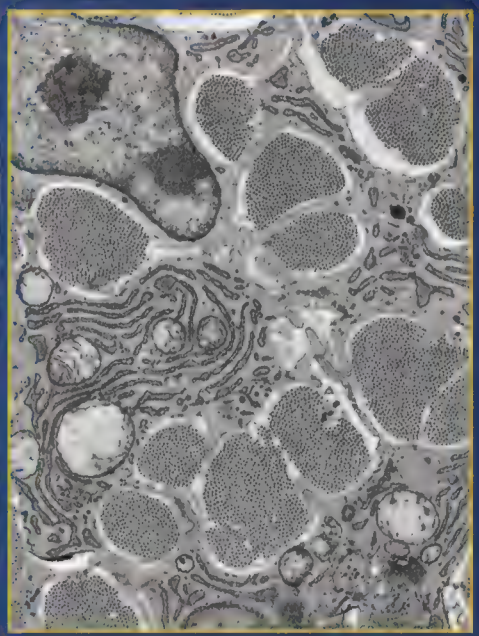

Collagen fibril network in embryonic tendon revealed by electron microscopy. Submitted by Karl Kadler, Chair, Collagen GRC.

CEREBELLUM
NEW!
Aug 11-16, 2013
Colby-Sawyer College, New London, NH
Chair: Indira M. Raman
Vice Chair: Michael D. Mauk

- **Keynote Presentation: What Can Cerebellum Development Tell us About Circuit Organization?**
  (Alexandra Joyner)
- **Human Cerebellar Function**
  (*Reza Shadmehr* / Amy Bastian / Jörn Diedrichsen / Dagmar Timmann)
- **Inputs and Outputs: Inferior Olive and Basal Ganglia**
  (*Dieter Jaeger* / Chris de Zeeuw / Kamran Khodakhah)
- **Sensorimotor Integration**
  (*John Simpson* / Detlef Heck / Megan Carey / Tim Ebner / Germund Hesslow)
- **Emerging Technologies for Studying the Cerebellum**
  (*Michael Häusser* / Hiroshi Nishiyama / Thomas Knöpfel)
- **Synaptic Mechanisms**
  (*Wade Regehr* / Clément Léna / Jacques Wadiche / Stuart Cull-Candy)
- **Cerebellar Anatomy**
  (*Georgia Bishop* / Izumi Sugihara / Abigail Person / Zoltan Nusser)
- **Cerebellar Development**
  (*Roy Sillitoe* / Michisuke Yuzaki / Kathleen Millen / Ferdinando Rossi)
- **Animal Models of Dystonia / Ataxia / Autism**
  (*Kamran Khodakhah* / Vikram Shakkottai / Christopher Gomez / Christian Hansel)

CHEMICAL OCEANOGRAPHY
Chemical Geography of the Sea
Aug 4-9, 2013
University of New England, Biddeford, ME
Chair: James W. Moffett
Vice Chair: Kathleen C. Ruttenberg

- **Overview of the US GEOTRACES North Atlantic Section**
  (*Bob Anderson* / William Jenkins / Ed Boyle)
- **Results from US GEOTRACES North Atlantic Section**
  (*Lauri Juranek* / Chris Measures / Kristen Buck / Phoebe Lam / Bob Anderson)
- **Benthic and Nearshore Processes**
  (*Lelia Hawkins* / Willard Moore / Wilf Gardner)

- **Carbon, Oxygen and the Biological Pump**
  (*Mak Saito* / Steve Emerson / Laurie Juranek / Scott Doney)
- **Towards a Definition of Ocean Biogeochemical Provinces**
  (*Ben Van Mooy* / Jorge Sarmiento / Mick Follows)
- **Biogeography of Organic Compounds in Seawater**
  (*Helen White* / Sergio Sanudo-Wilhelmy / Thorsten Dittmar / Craig Carlson)
- **Time Series in Redox-Active Regimes**
  (*Craig Carlson* / Wajih Naqvi / Mary Scranton)
- **Regional Seas and Boundary Processes**
  (*Bill Jenkins* / Min Han Dai / Maeve Lohan / Burke Hales / Will Berelson)
- **Paleochemical Geography**
  (*Ed Boyle* / Katharina Pahnke / David McGee)

CHEMISTRY EDUCATION RESEARCH & PRACTICE

Strengthening the Pillars of Scholarly Work in Chemistry Education
Jun 9-14, 2013
Salve Regina University, Newport, RI
Chair: Maria Oliver-Hoyo
Vice Chair: Hannah M. Sevian

- **Characterizing Learning Pathways via Learning Progressions**
  (*Gabriela Weaver* / Marianne Wiser / Vicente Talanquer)
- **Interpreting Representations to Measure Cognitive and Affective Achievements**
  (*Kristen Murphy* / Stacey Lowery Bretz / Ilka Parchmann / Len Annetta)
- **Developing Tools for Assessing and Improving Written Explanations of Science**
  (*Daniel King* / Mark Urban-Lurain / Christian Schunn)
- **Translating Chemistry Education Research to Impact Practice**
  (*Debbie Herrington* / Marilyne Stains / Kim Chwee Daniel Tan / MaryKay Orgill)
- **Structures of Pedagogical Content Knowledge in Theory and in Practice**
  (*Sally Hunnicutt* / Gabriel Pinto / Marissa Rollnick)
- **Views on What is Fundamental in Learning Chemistry**
  (*Michael Sanger* / Ingo Eilks / Michelene Chi / Avi Hofstein)
- **Keynote Presentation: Dealing with Non-significant Research Results**
  (*Charles Atwood* / Diane Bunce)
- **Chemistry in Mind: Philosophy, Archeology and Metacognition**
  (*David Salter* / Jose Chamizo / Marcos Martinon-Torres / Santiago Sandi-Urena)
- **Raising Outreach to Scholarly Activity**
  (*Hannah Sevian* / Holly Walter Kerby / Kent Kirshenbaum)

CHRONOBIOLOGY

Circadian Rhythms: From Molecule to Man
Jul 14-19, 2013
Salve Regina University, Newport, RI
Chair: Michael Rosbash
Vice Chair: Achim Kramer

- **Circadian Control of Output, DNA Repair (Cancer) and Physiology**
  (*Michael Brunner, Garret Fitzgerald* / Michael Brunner / Garret Fitzgerald / Aziz Sancar / Mukesh Jain)
- **Systems vs. Autonomous Control of the Clock**
  (*Ravi Allada, Erik Herzog* / Ravi Allada / Erik Herzog / Sato Honma / Maria Ceriani / Michael Hastings)
- **Entrainment: Light, Temperature, Food and Other Entraining Molecules**
  (*Ueli Schibler, Samer Hattar* / Ueli Schibler / Samer Hattar / Joke Meijer / Charlotte Helfrich-Förster)
- **Clock Mechanisms: Transcription, Protein Turnover, Structure, Post-transcriptional Mechanisms**
  (*Joseph Takahashi, Charles Weitz* / Joseph Takahashi / Charles Weitz / Jay Dunlap / Felix Naef / Achim Kramer)
- **Non-transcriptional-translational Oscillator Mechanism**
  (*Akhilesh Reddy, Susan Golden* / Akhilesh Reddy / Susan Golden / Erin O'Shea / John O'Neill)
- **Epigenetics and Chromatin with an Emphasis on Aging**
  (*Steve Brown, Paolo Sassone-Corsi* / Steve Brown / Paolo Sassone-Corsi / Jürgen Ripperger / Leonard Guarente / Satchidananda Panda / Paloma Mas)
- **Plants Including Agriculturally or Industrially Interesting Organisms**
  (*Andrew Millar, Steve Kay* / Andrew Millar / Steve Kay / Takeshi Izawa / Alison Smith / Daniel Forger)
- **Metabolic Diseases: Metabolic Syndrome, Diabetes and Aging**
  (*Joe Bass, Carla Green* / Joe Bass / Carla Green / Katja Lamia / Gad Asher)
- **Sleep**
  (*Mehdi Tafti, Amita Sehgal* / Mehdi Tafti / Amita Sehgal / Luis de Lecea / Paul Shaw / Leslie Griffith / Masashi Yanagisawa)

Chronobiology
Jul 13-14, 2013
Chair: Jerome S. Menet
Associate Chair: Jennifer Mohawk

CLUSTERS, NANOCRYSTALS & NANOSTRUCTURES

From Fundamental Chemical and Physical Processes to Applications
Aug 4-9, 2013
Mount Holyoke College, South Hadley, MA
Chairs: Todd D. Krauss & Simon A. Brown
Vice Chairs: Wolfgang Harbich & Emily A. Weiss

- **Keynote Presentations: Artificial Atoms, Nanostructures and Government Policy**
  (*Emily Weiss* / Chad Mirkin / Kristen Kulinowski)
- **Novel Syntheses**
  (*Louis Brus* / David Norris / Lincoln Lauhon / William Buhro)
- **Fundamentals/Spectroscopy**
  (*Vitaly V. Kresin* / Cherie Kagan / Michael Moseler / Margriet Van Bael)
- **Catalysis/Chemical Reactions**
  (*Beatriz Roldán Cuenya* / Tianquan (Tim) Lian / Riccardo Ferrando / Ueli Heiz / Uri Banin)
- **Applications: Devices I**
  (*Amy Prieto* / Richard Palmer / Paolo Milani / Tobias Hanrath)
- **Applications: Magnetism**
  (*Bernd von Issendorff* / Daniel Gamelin / Tobias Lau / Daniela Rupp)
- **Multiple Exciton Generation and Energy Redux**
  (*Alexander Efros* / Matthew Beard / Christophe Delarue / Laurens D.A. Siebbeles)
- **Fundamentals/Spectroscopy: Interactions with Light**
  (*Patanjali Kambhampati* / Xiaoyang Zhu / Philippe Dugourd / Jennifer S. Martinez / Paul Mulvaney)
- **Nanocrystals to Graphene**
  (*Wolfgang Harbich* / Uzi Landman / Paul McEuen / Jillian Buriak)

Clusters, Nanocrystals & Nanostructures
Aug 3-4, 2013
Chair: Michael Odoi
Associate Chair: Xingchen Ye

COASTAL OCEAN CIRCULATION

Jun 9-14, 2013
University of New England, Biddeford, ME
Chair: Mark Stacey
Vice Chair: Jack Barth

- **Interannual and Long-Term Changes in the Coastal Ocean**
  (*Ruoying He* / Allan Clarke / Art Miller)
- **Submesoscale Dynamics**
  (*Chris Edwards* / Leif Thomas / Amala Mahadevan / Raffaele Ferrari)
- **High-Latitude Coastal Circulation**
  (*Glen Gawarkiewicz* / Ursula Schauer / Dave Sutherland / Rebecca Woodgate)
- **Internal Waves, Solitons and Bores**
  (*Mark Inall* / Jonathan Nash / Matthew Alford / Oliver Fringer)
- **Fjords and Exchanges**
  (*Parker MacCready* / Carlos Moffat / Anders Stigebrandt / Finlo Cottier)
- **Atmospheric Forcing, Air-Sea Interaction**
  (*Melanie Fewings* / Eric Skyllingstad / Greg Gerbi)
- **Particle Tracking and Transport in Coastal Oceans and Estuaries**
  (*Erika McPhee-Shaw* / Alex Horner-Devine / Ann Gargett)
- **Carbon Fluxes and Exchange on Continental Margins**
  (*Neil Banas* / Zouhair Lachkar / Katja Fennel)
- **Scientific Progress from HF Radar**
  (*Libe Washburn* / Jeff Paduan / Nick Shay)

Coastal Ocean Circulation
Jun 8-9, 2013
Chair: Ata S. Suanda
Associate Chair: Rachel Horwitz

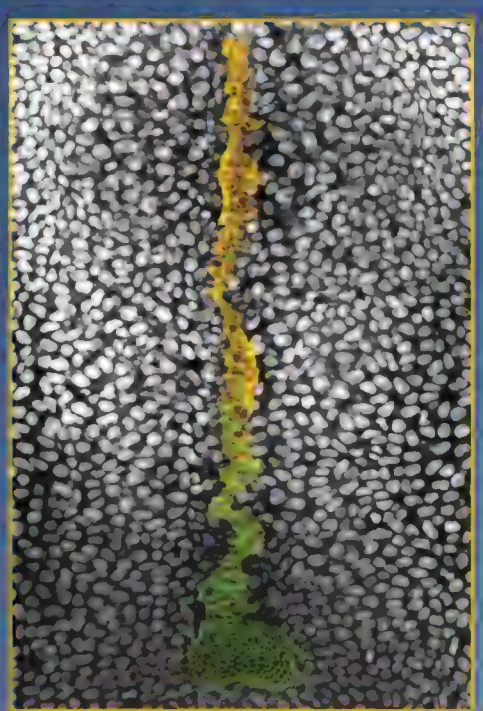

COLLAGEN
In the Context of Matrix, Cells and Regenerative Medicine
Jul 14-19, 2013
Colby-Sawyer College, New London, NH
Chair: Karl Kadler
Vice Chair: Collin M. Stultz

- **Emerging Technologies in Cell-Matrix Research**
  (*John Bateman* / Qing-Jun Meng)
- **Collagen Biosynthesis, Structure and Assembly**
  (*David Hulmes* / David Eyre / Michael Rape / Tak Mak / Antonella de Matteis)
- **Collagen-Protein Interactions and Signaling**
  (*Hilary Ashe* / Amy Bradshaw / Johanna Myllyharju)
- **Developmental Biology of the Matrix**
  (*Ronen Schweitzer* / Elazar Zelzer / David Birk / Delphine Duprez / Audrey McAlinden)
- **Genetic Mechanisms of Disease**
  (*Leena Bruckner-Tuderman* / Cristina Has)
- **Collagen Regulation and Dysregulation**
  (*Sergey Leikin* / Peter Byers / Kazuhiro Nagata / Joan Marini / Giorgio Galli)
- **Stem Cells, Repair and Regenerative Medicine**
  (*Pamela Robey* / Fiona Watt)
- **Matrix Mechanobiology**
  (*Boris Hinz* / Janine Erler / Michael Kjaer / Dennis Discher)
- **Future Directions of Collagen Matrix Research**
  (*Collin Stultz* / Natalia Nieto / Markus Buehler)

Collagen
Jul 13-14, 2013
Chair: Lydia S. Murray
Associate Chair: Jorge A. Fallas

Daphnia pulex (commonly called waterflea). Courtesy of Jan Michels (Christian-Albrechts-Universität zu Kiel). Submitted by John Colbourne & Gretchen E. Hofmann, Chairs, Ecological & Evolutionary Genomics GRC.

COMPUTATIONAL ASPECTS - BIOMOLECULAR NMR
Jun 2-7, 2013
Mount Snow Resort, West Dover, VT
Chair: James H. Prestegard
Vice Chair: Alexandre Bonvin

- **Keynote Session: Meeting Challenges in Structural Biology with NMR and Computation**
  (*James Prestegard* / Hashim al-Hashimi / Jane Richardson)
- **Advances in Computer Aided Structure Determination**
  (*Antonio Rosato* / Peter Güntert / Oliver Lange / Thérèse Malliavin / Geerten Vuister)
- **Ensemble Representations and Conformational Sampling**
  (*Claudio Luchinat* / Malene Jensen / Gottfried Otting / Nikolai Skrynnikov)
- **Computer Simulations of Biomolecular Structure and Dynamics**
  (*Valerie Daggett* / Mikael Akke / Heather Carlson / Rebecca Wade / Willy Wriggers)
- **Optimizing Data Acquisition and Analysis**
  (*Arthur Edison* / Jeffrey Hoch / Tatyana Polenova / David Rovnyak)
- **Analyzing Metabolomic and Metabolism Data**
  (*David Wishart* / Silvia Mari / John Markley / Matthew Merritt / Göran Widmalm)
- **Complementing NOEs in Structure and Dynamics Determinations**
  (*David Case* / Gerhard Hummer / Ken Merz / Homayoun Valafar)
- **NMR Guided Ligand Docking and Functional Annotation**
  (*Alexandre Bonvin* / Teresa Carlomagno / Julie Mitchell / Robert Powers / Ichio Shimada)
- **Challenges in Structure Determination of Large Systems**
  (*David Cowburn* / Francesca Marassi / Jens Meiler / Gerhard Wagner)

Computational Aspects - Biomolecular NMR
Jun 1-2, 2013
Chair: Steven L. Robinette

COMPUTER AIDED DRUG DESIGN
Jul 21-26, 2013
Mount Snow Resort, West Dover, VT
Chair: Martin Stahl
Vice Chair: Anthony Nicholls

- **Practical Methods**
  (*Haihong Ni* / Pat Walters / Martha Head / Carleton Sage / Paul Czodrowski / Stephen Johnson / Istvan Enyedy / Derek Debe / Scott Brown / Peter Kenny)
- **Non-ideality of Data and Model Making**
  (*Anthony Nicholls* / Anna Linusson / Tom Darden)
- **Null Models in Modeling**
  (*Anna Linusson* / Woody Sherman / Tony Slater / Michael Bower / Marcel Verdonk)
- **The Perils of Parameters**
  (*Ajay Jain* / Vijay Pande / Kim Branson)
- **Incorporating Experimental Uncertainty in Models**
  (*Pat Walters* / John Chodera / Terry Stouch / Nathan Baker)
- **Industry-wide Issues**
  (*Glen Kellogg* / Ajay Jain / Greg Landrum / Alex Tropsha / Craig Bruce)
- **External Viewpoints**
  (*Rob Noyes-Smith* / Cosma Shalizi / Stephen Ziliak / George Wolford II / Carson Chow)
- **Practical Sessions**
  (*Ullrika Sahlin* / Ullrika Sahlin / Paul Czodrowski / Pat Walters / Tom Darden / Cosma Shalizi)

DEVELOPMENTAL BIOLOGY
Jun 30 - Jul 5, 2013
Renaissance Tuscany Il Ciocco Resort, Lucca (Barga), Italy
Chair: Kathryn V. Anderson
Vice Chair: Susan E. Mango

- **Organogenesis**
  (Brant Weinstein / Ottoline Leyser / Tania Attie-Bitach)
- **Cellular Mechanisms of Early Development**
  Angela Nieto / Laura Machesky / Bob Goldstein / Loydie Majeska)
- **Developmental Genetics**
  (Christiane Nüsslein-Volhard / Stefan Schulte-Merker / Anne Ephrussi)
- **Regulatory Networks of Gene Expression During Development**
  (Angela Stathopoulos / Chris Rushlow / Anne Brunet / Ueli Grossniklaus)
- **Evolution of Morphological Diversity**
  (Michalis Averof / Nipam Patel / Andrew Gillis / Erich D. Jarvis)
- **Modeling of Developmental Networks**
  (Naama Barkai / Ben Simons / Joanna Wysocka / Gerry Weinmaster)
- **Epithelial Patterning and Morphogenesis**
  (J.-P. Vincent / Yingzi Yang / Matthew Gibson)
- **Stem Cell Biology**
  (Yukiko Yamashita / Jason Rock / David Traver)
- **Patterning and Cell Fate**
  (David Kimelman / Kat Hadjantonakis / Nancy Papalopulu)

DRUG METABOLISM
The Many Faces of Drug Metabolism
Jul 7-12, 2013
Holderness School, Holderness, NH
Chair: James B. Mangold
Vice Chair: Kenneth R. Korzekwa

- **Keynote Presentation: Metabolism, DNA Adduct Formation, and Carcinogenicity of Tobacco-specific Nitrosamine Enantiomers**
  (Stephen Hecht)
- **Applications of TK-TD and PK-PD in Drug Discovery and Development**
  (*Wade Adams* / Frederick Oleson / Wade Adams / Harvey Wong / Wei-jian Pan)
- **Antibody-Drug Conjugates**
  (*Jae Lee* / Kedan Lin / Brooke VandenBrink / Steven Hansel)
- **Conjugation Enzymes and *In Vitro-In Vivo* Correlations**
  (*Rory Remmel* / Ida Owens / Moshe Finel / Charles Falany / Rory Remmel)
- **Carcinogen Metabolism and Bioactivation**
  (*Lisa Peterson* / Arthur Grollman / XinXin Ding / Lisa Peterson)
- **The Other Oxidases**
  (*Michael Zientek* / Matthew Hutzler / John Cashman / Dale Edmonson / Ronald Hines)
- **Graduate Student and Post-doc Presentations**
  (*Henry Strobel*)
- **Drug Transporters: In"sights" Into Predictive Endogenous and Inflammatory Biomarkers**
  (*Imad Hanna* / Manthena Varma / Daniel Bow / Lauren Aleksunes / Ryan Pelis)
- **New and Creative Applications of Technologies**
  (*Jimmy Flarakos* / Gary Van Berkel / Linda Griffith / Thomas Covey)

DYNAMICS AT SURFACES
Reaction Dynamics, Scattering Dynamics, and Molecular and Structural Dynamics at Surfaces and Interfaces
Aug 11-16, 2013
Salve Regina University, Newport, RI
Chair: Greg Sitz
Vice Chair: Alec Wodtke

- **Reactive Scattering at Surfaces**
  (*Rainer Beck* / Arthur Utz / Bret Jackson)
- **Electron Dynamics at Surfaces**
  (*Daniel Auerbach* / Hrvoje Petek / Anders Nilsson / Nicholas Camillone)
- **Dynamics at Water Surfaces**
  (*Gill Nathanson* / Veronica Vaida / Bruce Kay / Bernd Abel)
- **Dynamics at Novel Interfaces**
  (*John Tully* / Ludwig Bartels / Eckart Hasselbrink / Hannes Jonsson)
- **Connecting Surface Dynamics and Heterogeneous Catalysis**
  (*Michael White* / Karsten Reuter / Michael Henderson / Andrew Gellman / Emily Carter)

- **Quantum State Resolved Scattering at Surfaces**
  (*John Morris* / Timothy Minton / Ludo Juurlink / Geert-Jan Kroes)
- **Ultrafast Electron Dynamics**
  (*Martin Wolf* / Tony Heinz / Ulrich Hofer)
- **Young Investigator Presentations**
  (*Kurt Kolasinski*)

Dynamics at Surfaces
Aug 10-11, 2013
Chair: Christine Hahn
Associate Chair: Joerg Meyer

ECOLOGICAL & EVOLUTIONARY GENOMICS

Jul 14-19, 2013
University of New England, Biddeford, ME
Chairs: Gretchen E. Hofmann & John Colbourne
Vice Chairs: Michael A. Herman & John H. Werren

- **Keynote Presentation: Plant Evolutionary Genomics**
  (Loren Rieseberg)
- **Population Genomics**
  (*Victoria Sork* / Stephen R. Palumbi / Thomas Turner / Graham Coop / Paul Hohenlohe)
- **Biodiversity & Climate Change**
  (*Holly Blk* / Jessica Hellmann / Justin Borevitz / Sinead Collins)
- **Molecular Basis of Evolutionary Innovations**
  (*David Plachetzki* / Omer Gokcumen / Christina Richards)
- **EEG is 10 Years Old... What's Next?**
  (*Denis Tagu* / Paul Hebert / Michael Hansen)
- **Genomic Basis of Stress Tolerance**
  (*Anne Todgham* / Mikhail Matz / Maren Friesen / Karel De Schamphelaere)
- **Genome Biology of EEG Model Species**
  (*Michael Pfrender* / Andrew Whitehead / Felicity Jones / Mark Blaxter / Chris Jiggins / Ellen Ketterson)
- **Exploring Genomic Plasticity to Environmental Conditions**
  (Julien Ayroles / Emilie Snell-Rood / Bryan Turner / Ben Lehner)
- **Genomic Basis of Adaptation, Speciation and Species Interactions**
  (*Matt Arnegard* / Joy Bergelson / Diethard Tautz / Rowan Barrett)
- **Integration and Interpretation of Genomics Data**
  (*Monica C. Muñoz-Torres* / Gos Micklem / John Quackenbush)

ELASTIN, ELASTIC FIBERS & MICROFIBRILS

From Basic Concepts to Translational Applications
Jul 21-26, 2013
University of New England, Biddeford, ME
Chair: Dieter P. Reinhardt
Vice Chair: Zsolt Urban

- **Molecular Properties and Assembly of Elastin**
  (*Clair Baldock, Anthony Weiss* / Anthony Weiss / Clair Baldock / Markus Buehler)
- **Microfibrils, Fibrillins and Associated Proteins**
  (*Robert Mecham, Dirk Hubmacher* / Laetitia Sabatier)
- **Novel Approaches for Elastic System Analysis**
  (*Brenda Rongish, John Parkinson* / Peter Robinson / Christian Schmelzer)
- **Elastic Fiber-Related Cell Signaling in Health and Disease**
  (*Lynn Sakai, Bart Loeys* / Tim Springer / Bart Loeys / Boris Hinz / Lynn Sakai)
- **Functionalization of the Elastic Fiber / Microfibril System**
  (*Daniel Rifkin, Katri Koli* / Gerhard Sengle / Daniel Rifkin)
- **Elastic Fibers in Vascular and Lung Physiology and Remodeling**
  (*Beth Kozel, Richard Pierce* / Dianna Milewicz / Zsolt Urban / Enid Neptune / Beth Kozel / Yibing Qyang)
- **Elastic Fiber Diseases and Translational Aspects**
  (*Dianna Milewicz, Zsolt Urban*)
- **Biomedical Engineering and Stem Cells of Elastic Systems**
  (*Elliot Chaikof, Julia Bujan* / Elliot Chaikof)
- **Late-Breaking Topics Related to Elastic Fiber Research**
  (*Suneel Apte, Daniela Quaglino*)

Elastin, Elastic Fibers & Microfibrils
Jul 20-21, 2013
Chair: Katja Schenke-Layland
Associate Chair: Sandeep M. Khatri

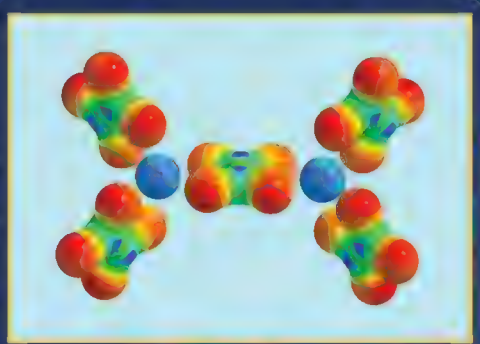

The electrostatic potential of $\{Zn_4(C_2O_4)_4\}^{8-}$ (a typical secondary building unit in Zn-oxalates metal organic frameworks). The potential is plotted on an isosurface of electron density. Red color highlights negatively charged regions, blue positively charged atoms. Submitted by Piero Macchi, Chair, Electron Distribution & Chemical Bonding GRC.

ELECTRON DISTRIBUTION & CHEMICAL BONDING

Pushing the Limits of Experimental and Theoretical Charge and Spin Density Studies
Jun 2-7, 2013
Les Diablerets Conference Center
Les Diablerets, Switzerland
Chair: Piero Macchi
Vice Chair: Wolfgang Scherer

- **Theory Assisted Charge Density Studies**
  (*Markus Reiher* / Carlo Gatti / Laura Gagliardi / Patrick Bultinck)
- **Subatomic Resolution and Non Covalent Interactions**
  (*Louis Farrugia* / Georg Eigerling / Julia Contreras Garcia)
- **Novel Concepts for Electron Density Reconstructions**
  (*Hans-Beat Bürgi* / Jean Michel Gillet / Dylan Jayatilaka)
- **Pushing the Experimental Limit**
  (*Bruce Patterson* / Dominik Schaniel / Phil Pattinson)
- **More than Single Crystal X-ray Diffraction**
  (*Alan Pinkerton* / Franz J. Giessibl)
- **Electron Density Studies for Drug Design**
  (*Paul L.A. Popelier* / Paulina Dominiak)
- **Modeling Electron Density and Interactions in Macromolecules**
  (*Claude Lecomte* / Benoit Guillot / Birger Dittrich / Dorothee Liebschner)
- **Electron Density Studies of Inorganic Materials**
  (*Bo B. Iversen* / Mette Schmekel / David Wolstenholme)
- **Material Properties from Electron Density Studies**
  (*Mark Spackman* / Jacqueline Cole)

ENVIRONMENTAL NANOTECHNOLOGY

NEW!
Novel Approaches to Meet Global Challenges
Jun 2-7, 2013
Stoweflake Resort and Conference Center, Stowe, VT
Chair: Nora Savage
Vice Chair: Paul Westerhoff

- **Evolution of Nanoscale Structures in the Environment**
  (*Kim Jones* / Mike Hochella)
- **Predicting Transport and Transformation Towards Sustainable Design**
  (Vicki Grassian / Howard Fairbrother)
- **Life Cycle Implications of Nanomaterials**
  (Arturo Keller)
- **Food Technologies and the Environment**
  (Jorge Gardea-Torresdey / Prabir Dutta)
- **Advancing Agricultural & Farming Breakthroughs with Nanotechnology**
  (Alistar Boxall / Carl Batt)
- **Tiny Solutions to Global Water Challenges**
  (Menachem Elimelec)
- **Ecological and Biological Responses: Nano Talks Back**
  (Cole Matson / Robert Tanguay)
- **Fantastic Voyage of Nanopharmaceuticals Within Biological Systems**
  (Kenneth Dawson)
- **Manufacturing the Future: Economy Versus Ecology**
  (*Rick Pleus*)

ENZYMES, COENZYMES & METABOLIC PATHWAYS

Jul 14-19, 2013
Waterville Valley Resort, Waterville Valley, NH
Chairs: Vahe Bandarian & Catherine L. Drennan
Vice Chairs: Paul R. Thompson & Walter L. Fast

- **Frontiers of Structure and Function - Tools for Studies of Complex Systems**
  (*Cathy Drennan* / Francisco Asturias / Vicki Wysocki / Donald Hamelberg)
- **Enzymology of Alternative Energy**
  (Rolf Thauer / Anne Jones / Markus Ribbe)
- **Flavoenzymes**
  (Giovanni Gadda / Amnon Kohen / Dewey McCafferty)
- **Molecular Mechanisms of Complex Biosynthetic Transformations**
  (Squire Booker / Chaitan Khosla / Ben Shen / Wendy Kelly)
- **Enzyme Mechanisms**
  (Tadhg Begley / Chris Whitman / Lana Saleh)
- **Catalysis and Regulation in Medicine**
  (Ruma Banerjee / Tom Meek / Stuart Licht)
- **Fundamentals of Enzyme Catalysis**
  (Richard Wolfenden / John Richard / Karen Allen)
- **Chemical Biology Tools: Development and Application**
  (Virginia Cornish / Minkui Luo / Pieter Dorrestein)
- **Amazing Enzymology**
  (*Vahe Bandarian* / JoAnne Stubbe / Chris Walsh)

EPIGENETICS

Mechanisms and Implications
Aug 4-9, 2013
Bryant University, Smithfield, RI
Chairs: Eric J. Richards & Emma Whitelaw
Vice Chairs: William G. Kelly & Ortrun Mittelsten Scheid

- **Overview of Epigenetic Mechanisms and Phenomena**
  (*Marjori Matzke*)
- **Deposition of Silencing Marks**
  (Steve Jacobsen)
- **Erasure of Silencing Marks**
  (Wolf Reik / Alexander Meissner)
- **Non-coding RNA & RNA Interference**
  (Rob Martienssen)
- **Nuclear Organization**
  (Edith Heard / Jason [illegible])
- **Epigenomics**
  (Joe Ecker)
- **Transgenerational Epigenetic Inheritance**
  (Bill Kelly / Vincent Colot)
- **Epigenetic / Environmental Interactions**
  (Ortrun Mittelsten Scheid / [illegible])

- Epigenetics & Disease / Synthesis
(Hera Vlamopoulou)

EXCITATORY SYNAPSES & BRAIN FUNCTION

Jun 9-14, 2013
Les Diablerets Conference Center
Les Diablerets, Switzerland
Chairs: Roger A. Nicoll & Gina G. Turrigiano
Vice Chairs: Suzanne Zukin & Daniel Choquet

- **Keynote Presentations: Visualizing Neural Circuits in the Brain / The Molecular Basis of Neurotransmitter Release**
(*Roger Nicoll* / Bert Sakmann / Thomas Sudhof)
- **Presynaptic Function**
(Pietro DeCamilli / Rob Edwards / Rolf Schneggenburger / Craig Jahr)
- **Glutamate Receptor Structure and Excitatory Synaptic Complexes**
(Mark Mayer / Yael Stern-Bach / Susumu Tomita)
- **Synaptic Plasticity**
(Rob Malenka / Rick Huganir / Juan Burrone)
- **Synapse Formation and Modulation**
(Anne Marie Craig / Graeme Davis / Kang Shen)
- **Dynamics of Receptor Signaling at Excitatory Synapses**
(Katherine Roche / Danielle Choquet / Peter Jonas / Villu Maricq / Michisuka Yuzaki / Susan Zukin)
- **Higher Order Signal Processing by Signaling Complexes and Networks**
(Dan Feldman / Bernardo Sabatini / Marla Feller)
- **Local Signaling and Plasticity**
(Yuki Goda / Ryohei Yasuda / Xiaowei Zhuang)

Excitatory Synapses & Brain Function
Jun 8-9, 2013
Chair: Veda Kumar Tatavarty

EYE MOVEMENTS

NEW!

The Motor System that Sees the World
Jul 7-12, 2013
Stonehill College, Easton, MA
Chairs: Brian D. Corneil & Michele A. Basso
Vice Chairs: Terrence Stanford & John Van Opstal

- **Keynote Presentations: Non-Visual Contributions to Eye Movements**
(*Jennifer Groh* / Kathleen Cullen / Eric Knudsen)
- **Intrinsic Oculomotor Circuits**
(*Paul May* / Martha Bickford / Carol Colby / Harvey Karten / Mayu Takahashi / Robert Wurtz)
- **Orienting in a Multisensory World**
(*Douglas Munoz* / Yoram Gutfreund / John McHaffie)
- **Rodent Models for Higher-Order Oculomotor Control**
(*Sascha du Lac* / Tansu Celikel / Yang Dan / Mark Segraves)
- **Beyond Black Boxes**
(*Henrietta Galiana* / Sophie Denève / Konrad Kording / Emilio Salinas)
- **More than Pretty Pictures: Imaging the Oculomotor System**
(*Paul Gamlin* / Pieter Medendorp / Katy Thakkar / Wim Vanduffel)
- **Diseases of the Oculomotor Brainstem**
(*David Zee* / Joseph Demer / Elizabeth Engle / Anja Horn)
- **Eye-Hand Coordination**
(*Douglas Crawford* / Mary Hayhoe / Bijan Pesaran / Larry Snyder / Melanie Wilke)
- **Where Does the Visual System End, and the Oculomotor System Begin?**
(*Jeffrey Schall* / Jude Mitchell / Christopher Pack / Martin Paré)

Eye Movements
Jul 6-7, 2013
Chair: Matthew H. Phillips
Associate Chair: Jaime Kaminer

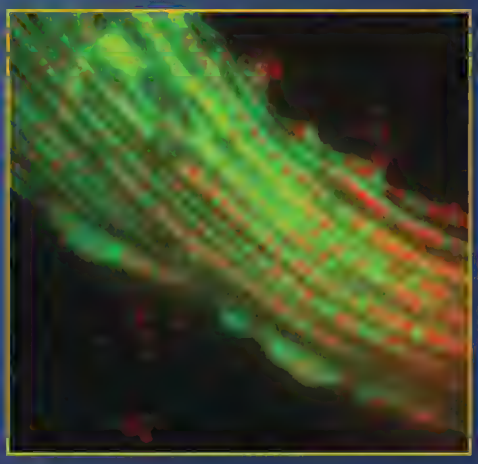

Perilipin 5 recruiting mitochondria to lipid droplets is revealed in this skeletal myocyte overexpressing perilipin 5. The mitochondria are stained green with a vital dye and lipid droplets are stained red with a lipophilic fluorochrome. Courtesy of: Nathan Wolins. (Washington University School of Medicine). Submitted by Rosalind Coleman, Chair, Molecular and Cellular Biology of Lipids GRC.

FERTILIZATION & ACTIVATION OF DEVELOPMENT

Jul 14-19, 2013
Holderness School, Holderness, NH
Chair: Pablo E. Visconti
Vice Chair: Gary Wessel

- **Epigenetics in Reproduction**
(*Jacquetta Trasler* / Brad Cairns / Alex Meissner / Oliver Rando)
- **Contribution of the Reproductive Tract to Fertilization**
(*Sylvie Breton* / Nicolas Da Silva / Mariana Wolfner / Robert Sullivan)
- **Molecular Mechanisms of Male Gamete Function**
(*Harvey Florman* / Alberto Darszon / Pascal Gagneux / Ravi Palanivelu)
- **Meiosis Resumption in the Oocyte**
(*Laurinda Jaffe* / Melina Schuh / Keith Jones / Evelyn Houliston)
- **Sperm Competition and Evolution**
(*Montserrat Gomendio* / Steve Ramm / Eduardo Roldan / Don Levitan)
- **Egg-to-Embryo Transition**
(*Janice Evans* / Karl Swann / Steve Ward / Frederic Berger / Coleen Murphy)
- **Late-Breaking Topics**
(*Gary Wessel*)
- **Ions in the Regulation of Sperm and Oocytes**
(*Gustavo Blanco* / Polina Lishko / Rafael Fissore / Jean Ju Chung)
- **Keynote Presentation: Mechanisms of Fertilization**
(*Patricia Cuasnicu* / Masaru Okabe)

Fertilization & Activation of Development
Jul 13-14, 2013
Chair: Matthew Marcello
Associate Chair: Adan Guerrero

GERMINAL STEM CELL BIOLOGY

NEW!

Jul 14-19, 2013
The Chinese University of Hong Kong, Hong Kong, China
Chair: Wai-Yee Chan
Vice Chair: Yun-Fai Chris Lau

- **Sex Determination and Germ Cell Differentiation**
(*Peter Koopman* / Blanche Capel / Josephine Bowles / Martin Matzuk)
- **Female Germinal Stem Cells**
(*David F. Albertini* / Ji Wu / Evelyn E. Telfer / Hiroo Ueno / Carlos Simon)
- **Male Germinal Stem Cells**
(*Martin Dym* / Marie Claude Hofmann / Kyle E. Orwig / Zuping He)
- **Epigenetic Programming**
(*Pei Duanqing* / Myriam Hemberger / Yi Zhang / Hiroyuki Sasaki / David Meissner)
- **Germline Stem Cells - Transdifferentiation**
(*Paul S. Cooke* / Mitinori Saitou / Pierre Fouchet)
- **Germ Cell Development**
(*Haifan Lin* / Teruhiko Wakayama / Paolo Sassone-Corsi / Tin-Lap Lee / Martine Culty)
- **Clinical Aspects - Diagnosis and Therapeutic Strategies for Germ Cell Diseases**
(*Csilla Krausz* / Douglas Carrell / Nancy Pitteloud / Manuela Simoni)
- **Germ Cell Tumors**
(*Peter Vogt* / Ewa Rajpert-De Meyst / Leendert Looijenga / Raju Chaganti / Hubert Schorle)
- **Application of Stem Cells in Animal Technology**
(*Le Ann Blomberg* / Ramiro Alberio / Fanyi Zeng / Budhan Pukazhenthi)

HETEROCYCLIC COMPOUNDS

Jun 16-21, 2013
Salve Regina University, Newport, RI
Chair: John L. Wood
Vice Chair: George S. Sheppard

- **Heterocyclic Compounds in Natural Products Synthesis I**
(*George Sheppard* / Amos B. Smith III / Glenn C. Micalizio)
- **Methods for the Synthesis of Heterocyclic Compounds I**
(*Robert M. Williams* / Jón T. Njardarson / Victor Snieckus / Seth Herzon / Karl J. Hale)
- **Heterocyclic Compounds of Pharmaceutical Relevance**
(*Sarah E. Reisman* / George A. Moniz / Prabhakar Jadhav)
- **Biological Applications of Heterocyclic Compounds**
(*Tatsuya Shirahata* / James R. Empfield / Carol M. Taylor / Ruth Wexler / David A. Spiegel)
- **Catalytic Methods for the Synthesis of Heterocyclic Compounds**
(*Frances R. Blase* / Joseph M. Ready / Elizabeth R. Jarvo)
- **Heterocyclic Compounds in Natural Products Synthesis II**
(*Graham C. Murphy* / Brian Lucas / Toshiaki Sunazuka / Ryan E. Looper)
- **Methods for the Synthesis of Heterocyclic Compounds II**
(*Eric M. Ferreira* / Javier Read de Alaniz / Gary A. Sulikowski)
- **The Evolution of a Research Program In Heterocyclic Chemistry**
(*Brian Love* / John Macor / Huw M. L. Davies / John Warner / Stephen F. Martin)
- **Perspective on Heterocyclic Chemistry**
(*John Lamattina* / Louis N. Jungheim / Edward C. Taylor)

HIGH TEMPERATURE CORROSION

Solution for Energy Issues and Future Role in High Temperature Processes
Jul 21-26, 2013
Colby-Sawyer College, New London, NH
Chair: Toshio Maruyama
Vice Chair: Gordon J. Tatlock

- **High Temperature Corrosion in Oxy-fuel Combustion** (*Gerald H. Meier* / Willem J. Quadakkers / Bruce A. Pint)
- **Role of Alloying Elements and Microstructure of Alloys in High Temperature Corrosion/Oxidation** (*Francisco J.P. Trujillo* / Brian Gleeson / John H. Perepezko)
- **Material Design for Advanced Energy Conversion** (*Elizabeth J. Opila* / Masao Takeyama / Clara Desgranges)
- **New Understanding in the Transport and Growth Mechanisms of Al2O3 Scales** (*Mike Graham* / Arthur H. Heuer / James L. Smialek)
- **Coating - Substrate Interactions and Its Effect on High Temperature Corrosion/Oxidation** (*Daniel Monceau* / John Nicholls / Hideyuki Murakami)
- **High Temperature Corrosion Process in Aggressive Environments** (*Peter F. Tortorelli* / Mathias Galetz / Joy Sumner)
- **Stress Development during Oxidation and Its Role in Scalel Properties** (*David Schiffer* / Hugh Evans / Micheal Schütze)
- **Novel Characterization / Application of Oxidation to Material Development** (*Sebastian Chevalier* / Isao Saeki / Makoto Nanko)
- **Internal Corrosion - Significance and Future Application** (*Toshio Narita* / David Young)

High Temperature Corrosion
Jul 20-21, 2013
Chair: Michael N. Task
Associate Chair: Thomas Gheno

HIGH THROUGHPUT CHEMISTRY & CHEMICAL BIOLOGY

Jun 2-7, 2013
Colby-Sawyer College, New London, NH
Chair: Lisa A. Marcaurelle
Vice Chair: Scott E. Wolkenberg

- **Frontiers in Chemical Biology** (*Paul Hanson* / Emily Balskus / Jennifer Prescher / Carolyn Bertozzi)
- **Chemical Methodology & Library Development** (*Aaron Beeler* / Thomas Nielsen / Adam Nelson / Jared Shaw / Andrei Yudin / Yujiro Hayashi / Stefan Gradl)
- **Synthetic Methodology** (*Corey Stephenson* / Tim Jamison / Sarah Reisman / Andy Phillips)
- **Cheminformatics & Chemical Biology** (*Donovan Chin, Jacqueline Wurst* / Jeremy Jenkins / Andrew Hopkins / Albert Bowers / M.G. Finn / Jiyong Hong / Ivan Cornella-Taracido)
- **Synthetic Chemistry & Chemical Biology** (*Michael Foley* / Derek Tan / Dale Boger / Herbert Waldmann)
- **Medicinal Chemistry & Drug Discovery** (*Ann Rowley* / Sam Gerritz / Rene Lemieux / Christopher Helal / Robert Nicewonger / Lyn Jones / Zhi-Cai Shi)
- **Catalysis & Reaction Discovery** (*Kevin Woller* / Abigail Doyle / Spencer Dreher / John Hartwig)
- **High-Throughput Screening & Fragment-Based Drug Discovery** (*Craig Thomas* / Matthew Boxer / David Maloney / James Bradner / Jeremy Duvall / Martin Drysdale / Richard Cummings)
- **Frontiers in Cancer Genomics & Drug Discovery** (*Peter Fekkes* / Markus Warmuth / Stuart Schreiber)

High Throughput Chemistry & Chemical Biology
Jun 1-2, 2013
Chair: Jacqueline Wurst
Associate Chair: Joanna Loh

HORMONE-DEPENDENT CANCERS

Development and Progression
Jul 28 - Aug 2, 2013
Bryant University, Smithfield, RI
Chair: Karen E. Knudsen
Vice Chair: Wayne Tilley

- **Hormone Action and Cancer Development** (*Karen Knudsen* / Charles Perou [*keynote*] / Gail Prins / Geoffrey Greene)
- **Chromatin Regulation in Cancer Development and Progression: Seq and You Will Find...** (*Vasan Yegnasubramanian, Geoffrey Greene* / Peter Jones / W. Lee Kraus / Carol Lange / Edwin Cheung)
- **Cross Talk of Hormone Receptor and DNA Damage Response Pathways** (*Edwin Cheung, Steve Balk* / Vasan Yegnasubramanian / Felix Feng / Helen Piwnica-Worms)
- **Stem Cells and Cancer Development** (*Gail Prins, Carol Lange* / Geoffrey Lindeman / Dean Tang / Michael Shen)
- **Microenvironment and Metastasis** (*Elahe Mostaghel* / Gail Risbridger / Kornelia Polyak / Nora Navone / Theresa Hickey)
- **Endocrine Therapy Resistance** (*Robert Clarke, Gail Risbridger* / Howard Scher / Joyce Slingerland / Leonie Young / Stephen Plymate)
- **Hormone Action in Cancers Beyond Breast and Prostate** (*Michael Shen, Joyce Slingerland* / Cheryl Walker / Jill Siegfried / Elahe Mostaghel)
- **Hormones in Translation** (*Wayne Tilley* / Johann deBono [keynote] / Jason Carroll / Cliff Hudis / Steve Balk)
- **The Future of Targeted Therapy** (*Felix Feng, Leonie Young* / Ganesh Raj / Robert Clarke / Charis Eng)

HUMAN GENETICS & GENOMICS

Jul 7-12, 2013
Bryant University, Smithfield, RI
Chair: David Goldstein
Vice Chair: Nancy Cox

- **Keynote Presentations: Integrating Human Genomics and Medical Genetics** (*David B. Goldstein* / Peter Donnelly / David Valle)
- **Genomic Data Analysis** (*Rick Myers* / Shaun Purcell / Carlos Bustamante / Aravinda Chakravarti)
- **Copy Number Variants** (*Nico Katsanis* / Heather Mefford / Evan Eichler / Jim Lupski)
- **Functional Genomics** (*George Church* / Barbara Stranger / David Page / Rick Myers)
- **Integrating Human and Functional Genomics** (*Les Biesecker* / Nico Katsanis / Greg Crawford / David B. Goldstein / Nancy Cox)
- **Interpreting Genome Sequences** (*Jim Lupski* / Les Biesecker / Jay Shendure / George Church)
- **Complex Trait Genetics** (*Jay Shendure* / David Altshuler / Anne Bowcock / Lynn Jorde / Mary Relling)
- **Genetics and Therapeutics** (*Aravinda Chakravarti* / Sue Slaugenhaupt / Joseph Gleeson / Helen Hobbs / Richard Lifton)
- **Keynote Presentations: Genetic Individuality in Health and Disease** (*Nancy Cox* / Daniel Geschwind / Maynard Olson)

Human Genetics & Genomics
Jul 6-7, 2013
Chair: Hinco J. Gierman
Associate Chair: Magdalena Harakalova

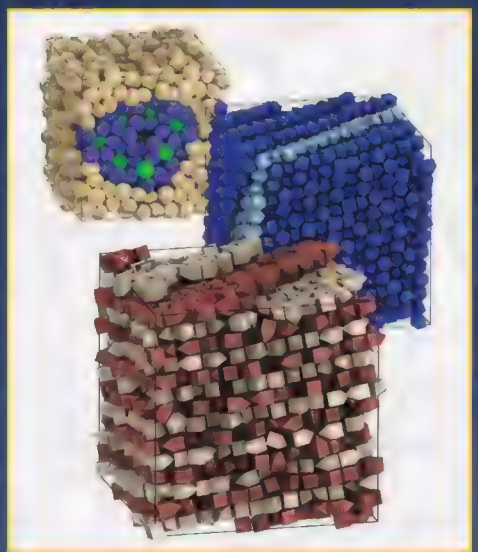

Predictive self-assembly of polyhedra into complex structures. The use of new geometries as building blocks for self-assembly is a route for creating more complex and useful structures in several scales. Courtesy of Pablo F. Damasceno, Michael Engel, and Sharon C. Glotzer (University of Michigan). Submitted by Randall D. Kamien, Chair, Liquid Crystals GRC.

HYDROGEN-METAL SYSTEMS

Hydrogen Interactions in Energy Storage
Jul 14-19, 2013
Renaissance Tuscany Il Ciocco Resort, Lucca (Barga), Italy
Chairs: Ewa C.E. Rönnebro & Maximilian Fichtner
Vice Chairs: Ragaiy Zidan & Bjørn C. Hauback

- **Hydrogen Interactions in Energy Storage**
- **Metal Hydrides for Battery Applications** (*Shin-Ichi Orimo* / Dag Noréus / Rana Mohtadi / Michel Latroche)
- **Hydrogen Storage Systems and Modeling** (*Donald Anton* / Bruce Hardy / Rajesh Ahluwalia)
- **Fundamentals and Nanoconfinement** (*Craig Jensen* / Elsa Callini / Daniele Colognesi / Christopher Wolverton)
- **Sensors** (*Bernard Dam* / Christoph Langhammer / Kazuki Yoshimura)
- **Physisorption** (*Michael Hirscher* / Anne Dailly / Myunghyun Paik Suh / Thomas Heine)
- **Advanced Characterization Methods** (*Sabrina Sartori* / Astrid Pundt / Stephen [illegible])
- **Progress on Interstitial Hydrides and Applications** (*Etsuo Akiba* / Volodymyr Yartys / Reinhard Juetz / Chaoling Wu)
- **Thermal Energy Storage Applications** (*Jacques Huot* / Craig [illegible])

[illegible]
Jul [illegible], 2013
Chair: [illegible]
Associate Chair: [illegible]

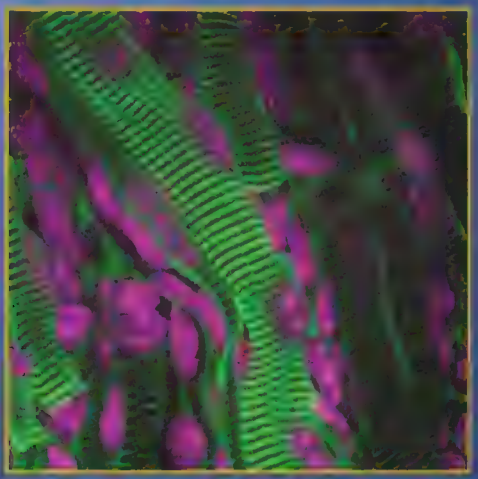

Fibers are stained for α-actinin (green) and nuclei are labeled with Hoechst 33342 (magenta). Skeletal muscle represents one of the best studied dynamic contractile systems. Courtesy of Meredith H. Wilson (University of Pennsylvania). Submitted by Erika L.F. Holzbaur, Chair, Motile & Contractile Systems GRC.

INFECTIONS OF THE NERVOUS SYSTEM — NEW!

Pathogenesis and Worldwide Impact
Jul 7-12, 2013
The Chinese University of Hong Kong, Hong Kong, China
Chair: Roberto Bruzzone
Vice Chair: Lisa F.P. Ng

- **Keynote Presentations: Challenges In Infections of the Nervous System** (*Diane Griffin* / Avindra Nath / Jun Wang)
- **Pathogen Discovery in Infections of the Nervous System** (*Christian Drosten* / Paul Newton / Antoine Gessain / Ian Lipkin)
- **Ways of Invading the Nervous System** (*Giampietro Schiavo* / Paul R. Gorry / Beate Sodeik)
- **Target Cells of the Nervous System and Host-pathogen Interactions** (*Marina Bentivoglio* / Christopher Broder / Alexander Khromykh / Chris Hunter / Chiara Zurzolo)
- **Immune Responses of the CNS to Invasion by Pathogens** (*Carol Reiss* / Roland Martin / Olaf Rotzschke)
- **Mechanisms of Pathogenesis: Clinical Features** (*Laurent Renia* / Tom Solomon / Charles Newton / Kum-Thong Wong / Robert Wilkinson)
- **Mechanisms of Pathogenesis: Cellular Features** (*Xavier Nassif* / Mark T. Heise / Dorian McGavern)
- **Experimental Models of Infections of the Nervous System** (*John Fazakerley* / Krister Kristensson / Elaine Tuomanen / Georges Grau)
- **New Diagnostic and Therapeutic Approaches** (*Ben Berkhout* / Tania Sorrell / Thiravat Hemachudha / Ronald J. Ellis)

INHIBITION IN THE CNS

Jun 16-21, 2013
Les Diablerets Conference Center
Les Diablerets, Switzerland
Chair: Zoltan Nusser
Vice Chair: Linda S. Overstreet Wadiche

- **Keynote Presentation: Familiar Receptors in Unexpected Places** (*Linda Overstreet-Wadiche* / Neil Harrison)
- **Structure and Function of $GABA_A$ Receptors** (*Istvan Mody* / Cynthia Czajkowski / Andrea Barberis / Matt Jones / Tim Hales / Raimund Dutzler)
- **Modulation of Inhibitory Synaptic Transmission** (*Jean-Marc Fritschy* / Jaideep Bains / Steve Mennerick / John Bekkers)
- **Inhibitory Synaptic Transmission** (*Jean-Marc Fritschy* / Henrique von Gersdorff / Lynn Dobrunz / Wade Regehr / Anatol Kreitzer)
- **Intrinsic Properties of GABAergic Interneurons** (*Chris McBain* / David DiGregorio / Angus Silver / Peter Jonas)
- **Interneurons in Dynamic Neuronal Networks** (*Chris McBain* / Peter Somogyi / Attila Losonczy / Pankaj Sah / Ivan Soltesz / Liset Menéndez de la Prida)
- **Talks Selected from Posters** (*Renata Batista-Brito*)
- **The Role of Inhibition in Behavior** (*Tamas Freund* / Gilles Laurent / Andreas Luthi / Jessica Cardin / Huibert Mansvelder / Massimo Scanziani)
- **Keynote Presentation: Tonic vs. Phasic Inhibition** (*Zoltan Nusser* / Mark Farrant)

Inhibition in the CNS
Jun 15-16, 2013
Chair: Renata Batista-Brito
Associate Chair: Scott F. Owen

INTERIOR OF THE EARTH

Jun 2-7, 2013
Mount Holyoke College, South Hadley, MA
Chair: Barbara Romanowicz
Vice Chair: Marc M. Hirschmann

- **Planetary Interiors** (*Lindy Elkins-Tanton* / Doris Breuer / Steve Hauck)
- **Core Structure and Composition** (*Arwen Deuss* / Satoru Tanaka / Renaud Deguen / James Badro)
- **Outer Core Processes and the Earth's Magnetic Field** (*Andy Jackson* / Chris Jones / Jonathan Aurnou)
- **The Structure, Origin and Role of LLSVPs** (*Jeroen Ritsema* / Vedran Lekic / Ed Garnero / Stéphane Labrosse)
- **Fine Scale Structure of the Deep Mantle** (*Christine Thomas* / Sebastian Rost / Jenny Jackson)
- **Rheology and Mineralogy of the Deep Mantle and Core-mantle Boundary Region** (*Shun-ichiro Karato* / San-Heong (Dan) Shim / David Dobson / Kenji Ohta)
- **Mantle Transition Zone and Interactions Between Reservoirs** (*David Stegman* / Yoshio Fukao / Saskia Goes / Steve Jacobsen)
- **Early Earth and Geochemical Reservoirs** (*Sujoy Mukhopadhyay* / Bernard Bourdon / Mark Harrison)
- **Unsolved Problems** (*David Stevenson* / David Gubbins / Rick Carlson)

Interior of the Earth
Jun 1-2, 2013
Chair: Maxim Ballmer

LASER DIAGNOSTICS IN COMBUSTION

Aug 11-16, 2013
Waterville Valley Resort, Waterville Valley, NH
Chair: Thomas B. Settersten
Vice Chair: Mark A. Linne

- **Keynote Presentation: X-Ray Lasers** (*Mark Linne* / John Bozek)
- **Diagnostics for Turbulent Combustion** (*Simone Hochgreb* / Andreas Dreizler / Jonathan Frank / ZS Li)
- **High-Repetition-Rate Diagnostics** (*Volker Sick* / Adam Steinberg / Waruna Kulatilaka)
- **Absorption-Based Techniques and Sources** (*Jay Jeffries* / Claire Gmachl / Aamir Farooq / Lin Ma)
- **Probing Soot Formation Chemistry** (*Katharina Kohse-Höinghaus* / Angela Violi / Arthur Suits)
- **Particle Diagnostics** (*Kevin Thomson* / Hope Michelsen / Stefan Will / Mike Bogan)
- **CARS Development and Application** (*James Gord* / Per-Erik Bengtsson / Paul Danehy)
- **IC Engine Diagnostics** (*Scott Parrish* / Öivind Andersson / Brian Petersen / Sebastian Kaiser)
- **Spray Diagnostics** (*Will Bachalo* / Lyle Pickett / Min Xu)

Laser Diagnostics in Combustion
Aug 10-11, 2013
Chair: Louise Lu
Associate Chair: Qing Nian (Shaun) Chan

LIPIDS, MOLECULAR & CELLULAR BIOLOGY OF

Jul 21-26, 2013
Waterville Valley Resort, Waterville Valley, NH
Chair: Rosalind A. Coleman
Vice Chair: Suzanne Jackowski

- **Keynote Presentations: The Molecular Mechanism of Membrane Fusion and Its Cellular Regulation / There are Many Ways to Get a Fatty Liver, or Not** (*Rosalind Coleman* / James Rothman / Henry Ginsberg)
- **Lipid Signals that Regulate Cell Metabolism** (*David Bernlohr* / Dagmar Kratky / James Ntambi / Douglas Mashek / Robert Murphy)
- **New Roles for Lipases and Acyltransferases** (*Hei Sook Sul* / Judy Storch / Richard Lehner / Daniel Nomura)
- **Membrane Lipids, Biogenesis and Turnover** (*Daniel Raben* / Melanie Ott / Russell DeBose-Boyd / Ana Maria Cuervo / Todd Graham)
- **Cellular Lipid Metabolism** (*Clay Semenkovich* / Tobias Walther / Sarah Spiegel / J. Mark Brown)
- **Fatty Acid Metabolism** (*William Dowhan* / Teresa Garrett / Charles Rock / Nada Abumrad / Gozoh Tsujimoto / David Cohen)
- **Transcriptional Control of Lipids** (*Steve Farber* / Rudolph Zechner / Fraydoon Rastinejad / Peter Espenshade / Amy Walker)
- **Spotlight on Phosphatidate** (*Miriam Greenberg* / George Carman / Brian Finck / Hongyuan Rob Yang / Susan Henry)
- **Genetic Regulation of Lipids** (*Carol Sztalryd* / Kathryn Moore / Tim Osborne / Kasey Vickers)

LIQUID CRYSTALS

Jun 16-21, 2013
University of New England, Biddeford, ME
Chair: Randall D. Kamien
Vice Chair: Nicholas L. Abbott

- **Defect Phases: The TGB Phase 25 Years Later** (*Miha Ravnik* / Gregory Grason / Michael Cates / Oleg Lavrentovich)
- **Substrates and Defects** (*David Walba* / Mohamed Gharbi / Juan de Pablo / Margarida Telo da Gama)
- **New Materials** (*Robert Lemieux* / Holger Eichhorn / Rudolf Zentel / Quan Li / Mark MacLachlan)
- **Theory** (*Robin Selinger* / Douglas Cleaver / Karl Saunders / Sharon Glotzer / Carl Modes / Rebecca Schulman)

- **Photons**
  (*Mohan Srinivasarao* / Alison Sweeney / Kristiaan Neyts / Bahman Taheri)
- **Young Investigator Presentations**
  (*Anne Pawsey*)
- **Biological Aspects of Liquid Crystals**
  (*Ka Yee Lee* / Jennifer Curtis / Laurence Navailles)
- **New Topics in Liquid Crystals**
  (*Kalman Migler, Mark Warner* / Pawel Pieranski / Françoise Brochard / Jacques Prost / Hiap Ong / Ronald Pindak)
- **The Future of Liquid Crystals**
  (*Seth Fraden* / Noel Clark / Tom Lubensky)

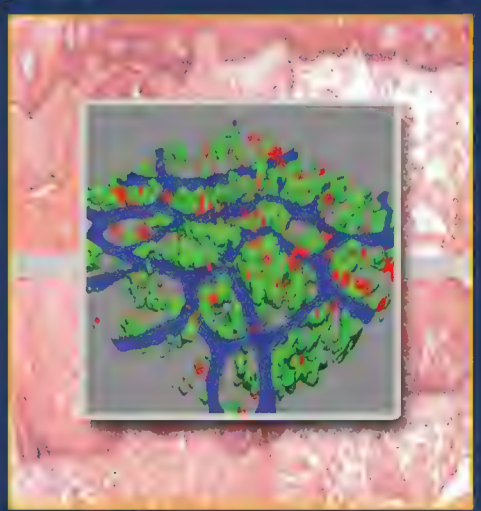

3D reconstruction of confocal microscopy images of the dome region of a murine Peyer's patch, demonstrating intestinal antigen sampling under homeostatic conditions (blood vessels [blue], CX3CR1+ dendritic cells [green] and orally administered labeled ovalbumine as antigen [red]). In contrast, dysfunction of mucosal homeostasis can lead to clinically significant disease such as oral mucositis caused by high-dose cancer therapy in oncology patients (histopathology, background). Images: Hans-Christian Reinecker, Harvard School of Medicine (3D reconstruction), Kevin Claffey and Douglas Peterson, University of Connecticut Health Center (histopathology), and Terrence Barrett, Feinberg School of Medicine, Northwestern University (contributed to conceptual design). Submitted by Douglas E. Peterson, Chair, Mucosal Health & Disease GRC

LIQUIDS, CHEMISTRY & PHYSICS OF

Aug 4-9, 2013
Holderness School, Holderness, NH
Chair: Mark D. Ediger
Vice Chair: Phillip L. Geissler

- **Hydrogen-Bonding at Interfaces**
  (*Branka Ladanyi* / Alex Benderskii / Juan Garrahan)
- **Crystallization and Nucleation**
  (*Baron Peters* / Thomas Koop / Christobal Viedma / Lian Yu)
- **Ionic Liquids**
  (*Ed Castner* / Jose Canongia Lopes / Mark Maroncelli)
- **Supercooled and Glassy Water**
  (*Valeria Molinero* / Pablo Debenedetti / David Chandler / Thomas Loerting)
- **Ions at Interfaces**
  (*Bruce Kay* / Heather Allen / Vincent Craig)
- **Self-Assembly**
  (*Michael Hagen* / Zvonimir Dogic / Tom Truskett / Rachel Segalman)
- **Competing Interactions in Nanodroplets**
  (*Ward Thompson* / Sylvie Roke / Juan de Pablo)
- **Biomolecular Dynamics**
  (*Mark Berg* / John Conboy / Jasna Brujic / Phill Geissler)
- **Young Investigator Presentations / Thin Liquid Films and Lubrication**
  (*John Fourkas* / Joanna Aizenberg)

LUNG DEVELOPMENT, INJURY & REPAIR NEW!

Aug 18-23, 2013
Proctor Academy, Andover, NH
Chair: Barry R. Stripp
Vice Chair: Thomas Mariani

- **A Foundation for Future Innovations in Lung Biology and Medicine**
  (*Barry Stripp* / Ed Morrisey / Serpil Erzurum)
- **Building the Lung**
  (*Wellington Cardoso* / Mark Krasnow / Xin Sun / Parviz Minoo)
- **Developmental Mechanisms in Lung Disease**
  (*Tom Mariani* / Jeff Whitsett / Maria Ramirez / Michael O'Reilly)
- **Epithelial Maintenance, Repair, and Regeneration**
  (*Susan Reynolds, Dan Weiss* / Brigid Hogan / Hal Chapman / Scott Randell)
- **Out of Control - Lung Cancer**
  (*Carla Kim* / John Minna / Brigitte Gomperts / Mark Onaitis)
- **Scarred for Life? Fibrosis and Matrix Remodeling**
  (*Bethany Moore, Andreas Gunter* / Naftali Kaminski / Lynn Schnapp / Patricia Sime)
- **Beyond the Genome - Epigenetics, Non-coding RNA's and Lung Disease**
  (*David Schwartz* / John Hollingsworth / Avi Spira)
- **Next Generation Approaches in Imaging and Disease Modeling**
  (*Jahar Bhattacharya* / Darrell Kotton / Luis Ortiz)
- **Breaking Down Barriers between Basic and Translational Research, Academia and Industry**
  (*Paul Noble* / Ric Boucher / Henry Danahay / Jay Kolls)

Lung Development, Injury & Repair
Aug 17-18, 2013
Chair: Lindsay M. Godin
Associate Chair: Craig Rackley

MAMMARY GLAND BIOLOGY

Jun 9-14, 2013
Stoweflake Resort and Conference Center, Stowe, VT
Chairs: John J. Wysolmerski & Terri L. Wood
Vice Chair: Mohamed Bentires-Alj

- **Keynote Presentation: Wnt Signaling and Regulation of Stem Cells**
  (*Terri Wood* / Roel Nusse)
- **Risk Factors in Breast Cancer**
  (*Victoria Seewaldt* / Derek LeRoith / Charlotte Kuperwasser / Thea Tisty)
- **Effects of Obesity and Diabetes on Lactation**
  (*Darryl Hadsell* / Steve Anderson / James McManaman)
- **Oncogenes & Hormone Signaling in Mammary Development and Cancer**
  (*Jeff Rosen* / Sarah Millar / Caroline Alexander / Dean Edwards)
- **IGFs/PI3K/Akt Signaling in Mammary Development and Cancer**
  (*Morno Bentires-Alj* / Adrian Lee / Lewis Chodosh)
- **Stem Cells and Luminal Progenitors in Mammary Development and Cancer**
  (*Mathew Smalley* / Cédric Blanpain / Jane Visvader / Sean Egan)
- **Genomics and Epigenetic Regulation of Mammary Development and Cancer**
  (*Steffi Oesterreich* / Monique Rijnkels / Kornelia Polyak)
- **Breast Cancer Progression and Metastases**
  (*Alana Welms* / Lance Liotta / Anthony Koleske / Theresa Guise)
- **Keynote Presentation: Mammary Gland Involution, Inflammation and Death Pathways**
  (*John Wysolmerski* / Christine Watson)

Mammary Gland Biology
Jun 8-9, 2013
Chair: Homer C. Adams
Associate Chair: Kelly C. Scribner

MALARIA

Molecular and Cell Biology of Malaria
Aug 4-9, 2013
Renaissance Tuscany Il Ciocco Resort, Lucca (Barga), Italy
Chair: Brendan Crabb
Vice Chair: Robert Sauerwein

- **Drugs and Drug Resistance**
  (*Xin-Zhuan Su* / Tim Anderson)
- **Liver Stage**
  (*Maria Mota* / Photini Sinnis)
- **Mosquito Stages**
  (*Marcelo Jacobs-Lorena* / George Dimopoulos)
- **Host Cell Invasion**
  (*Louis Miller* / Alan Cowman / Chetan Chitnis)
- **Virulence Mechanisms**
  (*Alexandra Rowe* / Hernando del Portillo)
- **Immunity**
  (*Jean Langhorne* / Kevin Marsh)
- **Malaria Vaccine Development**
  (*Robert Sauerwein* / Pedro Alonso)
- **Whole Genome Analyses**
  (*Jane Carlton* / Dyann Wirth / Dominic Kwiatkowski)
- **Physiology and Biochemistry of Malaria**
  (*Dan Goldberg* / Manuel Llinas / Mike Blackman)

Malaria
Aug 3-4, 2013
Chair: Wa-Hong Tham

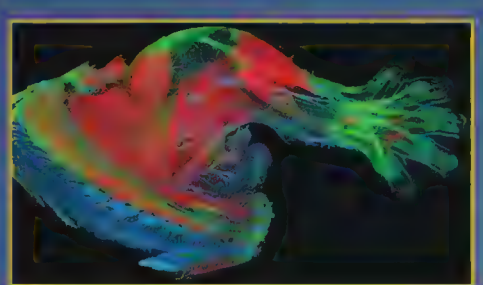

MARINE MOLECULAR ECOLOGY NEW!

Aug 11-16, 2013
Hong Kong University of Science and Technology, Hong Kong, China
Chairs: Pei-Yuan Qian & Roberto G. Kolter
Vice Chairs: Hongbin Liu & Stanley Lau

- **Deciphering Marine Ecology at the Molecular Level**
  (*Brian Palenik* / Peter Steinberg / Dan Distel / Sanjay Dechan)
- **Microbes-Invertebrates Interactions**
  (*Leo Nianzhi* / Tadashi Maruyama / Nicole Dubilier / Ute Hentschel Humeida)
- **Phylogeography and Population Connectivity**
  (Ka Hou Chu / Paul Bentzen)
- **Molecular Ecology of Marine Invertebrates and Vertebrates**
  (*Michael Gray* / Masumi Akihito / Brian Bowen / Allen Chen)

- **Molecular Ecology of Marine Microbes**
  (Markus Haunstetter / Steven J. Giovannoni)
- **New Tools for Studying Inter-species Interaction**
  (Huaiyang Wu / Pierre De Wit / Bradley Moore / Joern Piel)
- **Integrated Omics in Evolutional and Ecological Studies**
  (Noriyuki Satoh / Xaver Hoppert)
- **Energetics and Biogeochemical Cycling**
  (Kenji Kato / Jonathan P. Zehr / Sonya Dyhrman)
- **Marine Virus**
  (Dingru Zang / Curtis Suttle)

MECHANISMS OF MEMBRANE TRANSPORT

Jun 16-21, 2013
Mount Holyoke College, South Hadley, MA
Chair: Nancy Carrasco
Vice Chair: Lucy R. Forrest

- **Sugar Transport**
  (*Lucy Forrest* / Wolf Frommer / Lan Guan / Ron Kaback)
- **Thermodynamics, Kinetics, and Conformational States During Transport**
  (*Mario Amzel* / Lei Shi / Baron Chanda / Josè Faraldo-Gómez / Pancho Bezanilla / Mario Amzel)
- **ABC Transporters**
  (*Jue Chen* / Kasper Locher / Markus Seeger / Jue Chen)
- **Na+-driven transporters**
  (*Satinder Singh* / Ernie Wright / Christine Ziegler / Seok-Yong Lee / Joe Mindell)
- **Mechanisms of Iron Transport**
  (*Susan Buchanan* / Philip Klebba / Susan Buchanan)
- **Channels**
  (*Rachell Gaudet* / Rod MacKinnon / Eduardo Perozo / Nieng Yan / Rachell Gaudet)
- **Transporter Regulation and Disease**
  (*Geoffrey Abbott* / Sandra Gabelli / Poul Nissen / Geoffrey Abbott)
- **Unusual Membrane Proteins**
  (*Nancy Carrasco* / Filippo Mancia / Bruno Gasnier / Alessio Accardi / Chris Miller)
- **Late-Breaking Topics in Membrane Transport**
  (Stephen Long / Shimon Shuldiner)

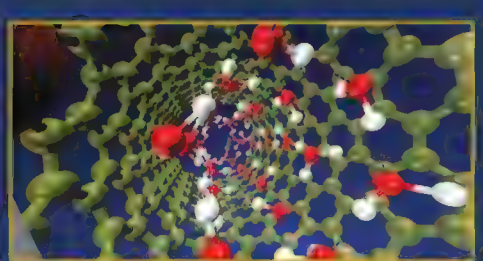

Water confined in carbon nanotubes. Courtesy of Narayan R. Aluru (University of Illinois at Urbana-Champaign). Submitted by Alfonso Ngan, Chair, Nano-Mechanical Interfaces GRC.

MEDICINAL CHEMISTRY

Aug 4-9, 2013
Colby-Sawyer College, New London, NH
Chair: Mark A. Murcko
Vice Chair: David P. Rotella

- **Phenotypic Screening**
  (*Bradley Tait* / Michelle Palmer / John Tellew / Paul Negulescu)
- **Antibody-Drug Conjugates**
  (*Christopher O'Donnell* / Peter Senter / Paul Polakis / Matt Francis / Pavel Strop)
- **Second Messenger Targets in Drug Discovery**
  (*James Barrow* / Jiang Lin / Craig Lindsley / Neil Press)
- **Advances in High Throughput Screening**
  (*Michael D. Wendt* / Andrew Pope / Philip Hajduk / John Mathias / Adam Hill)
- **Neuropathic Pain**
  (*Carolyn Dzierba* / Donna Hammond / Tom McCarthy / Sarah Skerratt)
- **Drug Delivery and Formulation: Pharmacological and Safety Benefits of Alternative Formulations and Routes of Administration**
  (*Laura C. Blumberg* / Anjali Kumar / Robert Clarke / Tamara Minko / Om Almarsson)
- **GPCR Structure and Function**
  (*Doris Riether* / Christofer Tautermann / Robert Leurs / Miles Congreve)
- **Late-Breaking Topics**
  (*Simon Haydar* / Alan Brown / Brad Savall / Michael Shultz / Richard Mackman)

Medicinal Chemistry
Aug 3-4, 2013
Chair: Mary M. Mader

MICROBIAL ADHESION & SIGNAL TRANSDUCTION

Jul 21-26, 2013
Salve Regina University, Newport, RI
Chairs: Craig R. Roy & Jean-Marc Ghigo
Vice Chairs: Matthew R. Parsek & Joerg Vogel

- **Probing the Function of Membrane-Bound Protein Secretion Machines**
  (John J. Mekalanos / Jorge E. Galan / Gabriel Waksman)
- **Social Interactions Between Bacteria**
  (Bonnie Bassler / Pradeep Singh / Regine Hengge)
- **Evolution of Signal Transduction Pathways**
  (Eduardo Groisman / Cynthia Sharma / Melanie Blokesch)
- **Adherence Factors and Surface Sensors**
  (Gerard Wong / Yves Brun / Shaynoor Dramsi / Guillaume Duménil)
- **New Approaches to Study Intracellular Pathogens**
  (Pascale Cossart / Michael Starnbach / Jost Enninga)
- **Bacterial Colonization and Survival in the Gut**
  (Paul O'Toole / Laurie Comstock / Manuela Raffatellu / Nina Salama)
- **Cross Kingdom Interactions**
  (Bruno Lemaitre / Heidi Goodrich Blair / Sheng Yang He)
- **Bacterial Cell Biology**
  (Petra Levin / William Margolin / David Rudner)
- **Post-Translational Modifications to Bacterial Structures**
  (M. Stephen Trent / Michael Koomey)

MICROBIAL POPULATION BIOLOGY

Jul 21-26, 2013
Proctor Academy, Andover, NH
Chair: Paul Turner
Vice Chair: Michael Travisano

- **Evolutionary Medicine**
  (*Paul Turner* / Angela McLean / Andrew Read)
- **Systems Biology**
  (Jesse Bloom / Rick Bushman / Roy Kishony)
- **CRISPRs**
  (Rodolphe Barrangou)
- **Microbial Population Biology Theory**
  (Lindi Wahl / Thierry Emonet / Claus Wilke)
- **Industry / Synthetic Biology**
  (*Jamie Bacher* / Timothy Lu)
- **Mutation and Mutation Rates**
  (Tim Cooper / Siobain Duffy / William Hanage)
- **Environmental Microbiology**
  (*Susanna Remold* / Susanna Remold / Elena Litchman / Martin Polz)
- **Interactions: From Genes to Communities**
  (*Zakee Sabree* / Joel Sachs / Zakee Sabree / Mark Siegal)
- **Microbes to the Extreme**
  (*Eric Gaucher* / Eric Gaucher / Rachel Whitaker / Victoria Orphan)

Microbial Population Biology
Jul 20-21, 2013
Chair: Betul K. Kacar
Associate Chair: Gabriel G. Perron

Australian Desert Ant Melophorous bagoti, having found food (a cookie crumb), scans the world for a familiar homeward direction. This behavior has inspired novel models of insect navigation. Courtesy of Paul Graham, Andy Philippides and Antoine Wystrach (University of Sussex). Submitted by Heather L. Eisthen & Hans A. Hofmann, Chairs, Neuroethology: Behavior, Evolution & Neurobiology GRC.

MICROFLUIDICS, PHYSICS & CHEMISTRY OF
Challenges, Advances and New Technologies for Diagnostics

Jun 9-14, 2013
Renaissance Tuscany Il Ciocco Resort, Lucca (Barga), Italy
Chairs: James P. Landers & Paul Yager
Vice Chairs: Shelley L. Anna & Jonathan D. Posner

- **Fluidic Control**
  (*Juan Santiago* / Stephen Quake / Matthew Begley)
- **Paper Microfluidics I**
  (*Charles Henry* / Barry Lutz / David Moore / Emanuel Carrilho)
- **Paper Microfluidics II**
  (*Marya Lieberman* / Charles Mace / David Juncker)
- **Microfluidic Acoustics**
  (*Joel Voldman* / Henrik Bruus / Steven Graves / Thomas Laurell)
- **Centrifugally-driven Microfluidics**
  (Yoon Cho / Marc Madou)
- **Diagnostics I**
  (*Amy Herr* / Rosanna Peeling / Bernhard Weigl / Sam Sia)
- **Diagnostics II**
  (*Abe Lee* / Carl Meinhart / David Erickson)
- **Commercialization of Microfluidic Technology**
  (Joan Bienvenue / Jason Hayes / Albert van den Berg)
- **Next Generation Sequencing**
  (*Jan Eijkel* / Michael Ramsey / Annelise Barron)

Microfluidics, Physics & Chemistry of
Jun 8-9, 2013
Chair: Dan Nelson
Associate Chair: Gina Fridley

MOLECULAR MEMBRANE BIOLOGY

Jul 14-19, 2013
Proctor Academy, Andover, NH
Chair: Francis Barr
Vice Chair: Frederick M. Hughson

- **Keynote Presentation: Pioneering the Frontiers of Membrane Biology**
  (*Francis Barr* / James Rothman)
- **Endoplasmic Reticulum Structure and Function**
  (*Sean Munro* / Tom Rappoport / Gia Voeltz / Susan Ferro-Novick / Tobias Walther)

- **Mechanisms of Protein Translocation and Biosynthesis**
  (*Karin Reinisch* / Rama Hegde / Irmi Sinning / Shu-ou Shan)
- **Vesicle Formation and Cargo Sorting**
  (*Anne Spang* / Randy Schekman / Elizabeth Miller / Felix Wieland / Charles Barlowe / Scott Emr)
- **Directed Vesicle Movement & Organelle Positioning**
  (*Suzanne Pfeffer* / Melina Schuh / Anna Ahkmanova / Adam Linstedt)
- **Structural Insights into Membrane Shaping and Bending**
  (*Fred Hughson* / James Hurley / Vincenz Unger / Patricia Bassereau / Mika Simons)
- **GTPases and the Coding of Membrane Identity**
  (*Gia Voeltz* / Sean Munro / Suzanne Pfeffer / Christian Ungermann / Karin Reinisch)
- **Golgi and post-Golgi Trafficking**
  (*James Rothman* / Vivek Malhotra / Catherine Rabouille / Ben Glick / Peter Novick)
- **Trafficking on Cell Polarization & Division**
  (*Anna Ahkmanova* / Anne Spang / Jon Audhya / Fernando Martin-Belmonte / Arnaud Echard)

Molecular Membrane Biology
Jul 13-14, 2013
Chair: Brooke M. Gardner
Associate Chair: Ashley A. Rowland

MOTILE & CONTRACTILE SYSTEMS

Cytoskeletal Dynamics from Single Molecules to Motile Organisms
Jul 28 - Aug 2, 2013
Colby-Sawyer College, New London, NH
Chair: Erika LF. Holzbaur
Vice Chair: Fred Chang

- **Keynote Presentations: Dynamic Approaches to the Cytoskeleton**
  (*Erika Holzbaur* / David Drubin / Tony Hyman)
- **Cytoskeletal Dynamics**
  (*Peter Rubenstein* / Tom Pollard / Margot Quinlan / Jenny Ross / Anna Akhmanova / Sophie Martin / Laurent Blanchoin)
- **Building Complex Structures and Long-Range Organization**
  (*John Cooper* / Tatyana Svitkina / Frank Bradke / Maxence Nachury / Grant Jensen)
- **Dividing a Cell**
  (*Patricia Wadsworth* / Jennifer Deluca / Helder Maiato / Charles Asbury / Michael Lampson / Buzz Baum)
- **Intracellular Dynamics: Movement of Motors, Organelles and Cargos**
  (*Vladimir Gelfand* / Susan Gilbert / Samara Reck-Peterson / Roop Mallik / Simon Bullock)
- **Cytoskeletal Dynamics: Insights from Bacteria, Parasites, Fungi, and Plants**
  (*Fred Chang* / Dyche Mullins / Joseph Pogliano / David Sept / Gero Steinberg / Magdalena Bezanilla / Ram Dixit)
- **Forces and Dynamics in Cell Biology**
  (*Michael Ostap* / Marileen Dogterom / Melissa Gardner / Yale Goldman / Sophie Dumont)
- **Cells in Context: Cytoskeletal-Matrix Connections**
  (*Alpha Yap* / Bill Brieher / Kris DeMali / Matt Tyska / Manuel Thery / John Condeelis)
- **Cells on the Move**
  (*Bill Bement* / Denis Wirtz / David Sharp / Matthieu Piel)

MUCOSAL HEALTH & DISEASE

NEW

Jun 9-14, 2013
Stonehill College, Easton, MA
Chair: Douglas E. Peterson
Vice Chair: Terrence A. Barrett

- **Keynote Presentations: The Convergence of Science - Mucosal Health and Disease**
  (Michael Clarke / Stephen Sonis)
- **Mucosal Biology: Mechanisms for Homeostasis and Repair**
  (*Mary Reyland* / Melissa Wong / Eva Helmerhorst)
- **The Microbome-Mucosal Interface**
  (*Hans-Christian Reinecker* / Curtis Huttenhower / Wendy Garrett)
- **Mucosal Injury Caused by Conventional and Molecularly Targeted Cancer Therapies**
  (*Siri Beier Jensen* / Xiao-Jing Wang / Dorothy Keefe / Courtney Houchen)
- **Immunologic Governance of Mucosal Health and Disease**
  (*Brian Kelsall* / Eran Elinav)
- **Mucosal Response to Stress**
  (*Ramnik Joseph Xavier* / Xiaoxia Li / Thirumala-Devi Kanneganti / Randal Kaufman / Andrew Neish / Charles Elson III)
- **Mucosal Drug Delivery Systems**
  (*Martin Thornhill* / Andy Wolff / Ana Cotrim)
- **The Mucosal-Dermatologic Interface**
  (*Stephen Challacombe* / Jane Setterfield)
- **Computational Biology: Cell and Tissue Analysis and Modeling**
  (*David Landsman* / Yosef Yarden / Julie Segre)

MYCOTOXINS & PHYCOTOXINS

Jun 16-21, 2013
Stonehill College, Easton, MA
Chairs: Stacey L. Degrasse & Gary A. Payne
Vice Chairs: Gregory L. Boyer & Genevieve Bondy

- **Keynote Session: Frontiers in Mycotoxin & Phycotoxin Research**
  (*Gary Payne, Stacey DeGrasse* / Corby Kistler / Kathi Lefebvre)
- **Novel and Emerging Toxins and Toxicities**
  (*James Pestka, Chris Miles* / Thomas Massey / James Metcalf / Jean-Denis Troadec / Michael Twiner)
- **Mechanisms of Action, Genomics, Proteomics, and the Phylogenetic Basis of Toxicity**
  (*Ronald Riley, Brett Neilan* / Charles Woloshuk / Ralf Kellmann / Paul Jennings)
- **Advances in Analytical Detection Methodologies: Analytical Recognition Elements**
  (*Betsy Yakes, David Miller* / Maria De Rosa / Jeffrey DeGrasse / Christopher Maragos)
- **Advances in Analytical Detection Methodologies: Direct Detection of Mycotoxins & Phycotoxins**
  (*Andrew Turner* / Rudolph Krska / Elizabeth Hamelin / Carmela Dell Aversano / Martino Forino / Monica Campas)
- **Outbreaks, Exposure, and Risk Assessment**
  (*Paul Turner, Emanuel Hignutt* / Vera Trainer / Manfred Metzler)
- **Evolution and Ecological Significance of Mycotoxins & Phycotoxins**
  (*Narash Megan, Sibel Bargu* / Chris Schardl / Hans Dam)
- **Strategies and Regulation for Prevention and Control**
  (*Deepak Bhatnagar, Quay Dortch* / Burton Bluhm / Kevin Sellner / Melissa Evans)
- **Keynote Presentation: Future Perspectives and Directions**
  (*Genevieve Bondy, Gregory Boyer* / Chris Elliott)

Mycotoxins & Phycotoxins
Jun 15-16, 2013
Chair: Emily A. Monroe
Associate Chair: Josephine M. Wee

MYOGENESIS

Mechanisms and Models
Jul 7-12, 2013
Renaissance Tuscany Il Ciocco Resort, Lucca (Barga), Italy
Chair: Peter D. Currie
Vice Chair: Gabrielle Kardon

- **Keynote Presentation: Development and Evolution of the Musculoskeletal System**
  (Cliff Tabin)
- **Early Muscle Development: Developmental and Evolutionary Origins of Muscle and Muscle Progenitor Migration**
  (*Margaret Buckingham, Peter Rigby* / Christophe Marcelle / Thomas Braun / Olivier Pourquie / Eldad Tzahor / Ullrich Technau)
- **Myofiber Formation: Role of Myoblast Fusion and Sarcomere Assembly in Forming Myofibers**
  (*Leslie Leinwand* / Susan Abmayr / Mary Baylies / Elizabeth Chen / Simon Hughes / Frank Schnorrer / Talila Volk)
- **Muscle Interactions with Connective Tissue, Tendon, Bone, Nerve: The Role of Tissue Interactions in Muscle Development and Regeneration**
  (*Fabio Rossi* / Pura Munoz Canoves / Krzysztof Jagla / Delphine Duprez / Eli Zelzer / Steve Burden / Tom Schilling)
- **Transcription, Epigenetics, MicroRNAs: Cell Autonomous Effectors of the Muscle Cell Phenotype**
  (*Rob Krauss* / Pascal Maire / Lorenzo Pun / Vittorio Sartorelli)
- **Muscle Stem Cells and Regeneration: The Role of Adult Muscle Stem Cells in Mediating Regeneration**
  (*Michael Rudnicki* / David Sassoon / Brad Olwin / D. Cornelison / Grace Pavlath / Shahraghim Tajbakhsh / Christophe Lepper)
- **Muscle Homeostasis and Aging: Molecular Mechanisms That Regulate Muscle and Muscle Stem Cells During Homeostasis and Aging**
  (*Tom Rando* / Helen Blau / Andrew Brack / Nadia Rosenthal / David Glass / Nobert Perrimon / Charlotte Peterson)
- **Muscle and Cancer: Rhabdomyosarcomas and Cachexia**
  (*Frederic Relaix* / Michael Dyer / Rene Galindo (JI) / Denis Guttridge / David Langenau)
- **Muscle Disease and Treatments: Dystrophies and Current Treatment Strategies**
  (*Giulio Cossu* / Graziella Messina / Steve Tapscott / Davide Gabellini)

Myogenesis
Jul 7, 2013
Chair: Nora D. Yucel
Associate Chair: David B. Gurevich

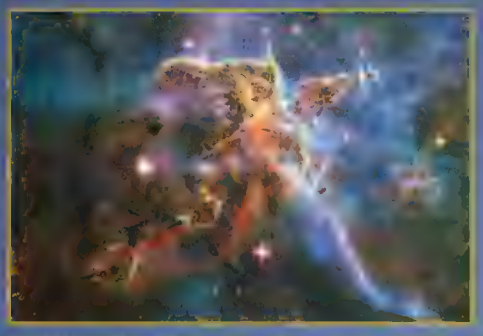

NANO-MECHANICAL INTERFACES
NEW!

Multiphysics Theory and Experiments
Aug 4-9, 2013
Hong Kong University of Science and Technology, Hong Kong, China
Chair: Alfonso Ngan
Vice Chair: Narayan R. Aluru

- **Nanomechanics**
  (W.D. Nix / Huajian Gao / Huajian Gao)
- **Mechanical-Electronic Interactions**
  (Yongyi Zhang / Yonggang Huang / Nicholas Fang / Min-Feng Yu)
- **Mechanical-Electrochemical Interactions**
  (Kwong Yu Chan / Yanchen Cheng / Katsuyo Thornton)
- **Biological Motors**
  (C.T. Lim / Jonathan Scholey / Daniel Fletcher / Krystyn J. Van Vliet)
- **Thermal-Mechanical Interactions**
  (Qingping Sun / Jose San Juan / Wenjing Ye)
- **Soft Materials**
  (Gang Li / David Weitz / Stephen Eichhorn / Christian Serre)
- **Nanoporous Actuator Materials**
  (Elias Aifantis / Jeff De Hosson)
- **Multiphysics Theory and Modeling I**
  (Guanhua Chen / Jacob K. White / Chung-ho Woo / Katerina Aifantis)
- **Multiphysics Theory and Modeling II**
  (Michel van Hove / Jayathi Murthy)

NANOPOROUS MATERIALS & THEIR APPLICATIONS
NEW!

Clean Energy
Aug 11-16, 2013
Holderness School, Holderness, NH
Chair: Yushan Yan
Vice Chair: David Sholl

- **Keynote Session: Zeolite Catalysis for Clean Energy**
  (Stacey Zones / Mark Davis / Ferdi Shuth)
- **Novel Synthesis**
  (Guang Gao / Russell Morris / Greg Lewis / Tatsuya Okubo / Svetlana Mintova)
- **Thin Films/Membranes and Separation**
  (K.B. Yoon / Jurgen Caro / Hae-Kwong Jeong / Zhengbao Wang / Krista Walton)
- **Catalysis**
  (Michael Tsapatsis / Aditya Bhan / Mark Snyder / Fengshou Xiao)
- **Characterization**
  (Lynne McCusker / Dan Xie / Xiaodong Zou)
- **Theory and Simulation**
  (Randy Snure / Krishna Rajamani)

GRS **Nanoporous Materials & Their Applications**
Aug 10-11, 2013
Chair: Christopher Lew

NATURAL PRODUCTS
Current State of the Art in Natural Product Synthesis, Isolation, Structure Elucidation, and Application in Drug Discovery
Jul 28 - Aug 2, 2013
Proctor Academy, Andover, NH
Chair: Rajinder Singh
Vice Chair: Michael Calter

- **Total Synthesis of Natural Products**
  (Gregory Dudley / Stephen Martin / Rick Danheiser)
- **Catalysis and Synthetic Methodology**
  (Ohyn Kwon / Alison Frontier / F. Dean Toste)
- **Synthesis of Heterocyclic Natural Products and Chemical Biology**
  (Uttam Tambar / Marco Ciufolini / Dirk Trauner)
- **New Methods and Biomimetic Synthesis of Biologically Active Natural Products**
  (Armen Zakarian / Jeremy Robertson / Matthew Shair)
- **Synthesis and Function of Bioactive Molecules**
  (Scott Snyder / Martin Burke / Viresh Rawal)
- **Developments in Technologies Towards Isolation, Chemistry and Biology of Natural Products**
  (Roger Linington / Hendrik Luesch / Kerry McPhail / William Fenical)
- **New Methods and Synthesis of Bioactive Molecules**
  (Gary Sulikowski / Amir Hoveyda)
- **New Reactions for Natural Product Synthesis and Diversity Oriented Synthesis**
  (Derek Tan / Jon Njardarson / Richard Hsung)
- **Total Synthesis of Bioactive Natural Products**
  (Robert Williams / Andrew Myers / Anthony Barrett)

Confocal microscopy image shows a neutrophil containing two yeast zymosan phagosomes. Submitted by Lee-Ann Allen, Chair, Phagocytes GRC

NEURAL CREST & CRANIAL PLACODES
NEW!

Concepts, Mechanisms and Models
Jul 21-26, 2013
Stonehill College, Easton, MA
Chair: David W. Raible
Vice Chair: Carole Labonne

- **Patterning the Neural Plate Border**
  (Jean-Pierre Saint-Jeannet / Gerhard Schlosser / Kristin Artinger)
- **Neural Crest Formation**
  (Chaya Kalcheim / Martin Garcia-Castro / Laura Gammill / Anne-Helene Monsuro-Burq)
- **Cell Lineage Determination**
  (Elizabeth Dupin / Andrew Groves / Jean-François Brunet)
- **Morphogenesis and Migration**
  (Carol Erickson / Richard Lang / Roberto Mayor / Paul Kulesa)
- **Gene Regulatory Networks**
  (Marianne Bronner / Anne Calof / Robert Kelsh)
- **Stem Cells and Regeneration**
  (Linda Barlow / Ruchi Bajpai / David Parichy / Neil Segil)
- **Focus on Disease: Melanoma**
  (Bill Pavan / Richard White / Lukas Sommer)
- **Cell Plasticity and Lineage Determination**
  (Raj Ladher / Ajay Chitnis / Melissa Harris / Patrik Ernfors)
- **Evolutionary Perspectives**
  (Brian Hall / Clare Baker / Daniel Meulemans Medeiros)

NEUROETHOLOGY: BEHAVIOR, EVOLUTION & NEUROBIOLOGY
Networks, Circuits, and Modules
Aug 18-23, 2013
Mount Snow Resort, West Dover, VT
Chairs: Heather L. Eisthen & Hans A. Hofmann
Vice Chairs: Karen A. Mesce & Eric Warrant

- **Evolution of Gene Networks in Neural Structures**
  (Lauren O'Connell / Seth Grant / Todd Oakley)
- **Social Networks, Cognition, and Health**
  (Melissa Coleman / Nicholas Christakis / Richard James / Michael Platt)
- **Echolocation in Mammals: Convergence and Plasticity**
  (Johannes Schul / Melvyn Goodale / Annemarie Surlykke)
- **Biomimetics: Natural and Artificial Neural Networks**
  (Masashi Kawasaki / Josh Bongard / Ansgar Büschges / Andrew Philippides)
- **Biogenic Amines and Neural Circuit Activity**
  (Paul Stevenson / Amir Ayali / Ana Silva)
- **Sources of Variability in Neural Circuits**
  (Jens Herberholz / David Bodznick / Paul Katz / Eve Marder)
- **Comparative Neurobiology of Language**
  (Ofer Tchernichovski / Tecumseh Fitch / Asif Ghazanfar)
- **Gene Networks Underlying Complex Behavior**
  (Karen Maruska / Ralph Greenspan / Kim Hoke / Amy Toth)
- **Sensorimotor Control of Reproduction**
  (Emma Coddington / Kathy French / Yoshitaka Oka)

GRS **Neuroethology: Behavior, Evolution & Neurobiology**
Aug 17-18, 2013
Chair: Brian G. Dias
Associate Chair: Paloma T. Gonzalez Bellido

NEUROTROPHIC FACTORS
Jun 2-7, 2013
Salve Regina University, Newport, RI
Chair: Rosalind A. Segal
Vice Chair: Freda Miller

- **Neurotrophic Factor Signaling**
  (Lloyd Greene, Columbia University / Carlos Ibanez / Barbara Hempstead / Azad Bonni / Philip Barker)
- **Peripheral Nervous System and Trophic Factors**
  (Lou Reichardt / Antonella Riccio / David Ginty / Rejji Kuruvilla / Susan Birren / Steve McMahon)
- **Trophic Factors in CNS Development and Disease**
  (Moses Chao / Kevin Jones / Francis Lee / Eric Nestler / Anne West)
- **Synaptic Regulation and Trophic Factor**
  (Mike Greenberg / Anirvan Ghosh / Peter Scheiffele / Corey Harwell)
- **Regulation of Morophology and Cytoskeleton**
  (Wilma Friedman / Mary Beth Hatten / Kim Tolias / Michael Sendtner)
- **Stem Cells**
  (Yves Barde / Alex Joyner / Gord Fishell / David Kaplan / Paola Arlotta)
- **Transport**
  (Mark Bothwell / Fred Saudou / Bill Mobley / Erika Holzbaur)
- **Local Translation**
  (Bai Lu / Jeffrey Twiss / Mollie Meffert / Kelsey Martin)
- **New Mechanisms, New Methods**
  (Bill Mobley / Rudiger Klein)

NUCLEAR CHEMISTRY
At the Intersection of Nuclear Structure and Reactions
Jun 9-14, 2013
Colby-Sawyer College, New London, NH
Chair: Alexandra Gade
Vice Chair: Umesh Garg

- **New Developments and Facility Updates** (*Ingo Wiedenhoever* / Georg Bollen / Hans Geissel / Robert Janssens)
- **Nuclei at the Extremes of Spin and Isospin and Confrontation with Theory** (*Michael P. Carpenter, Achim Schwenk* / Mark A. Riley)
- **Nuclear Collisions - From RIB Production to Multifragmentation** (*William G. Lynch* / Sherry J. Yennello)
- **Spin-isospin Response of Nuclei and Spectroscopy at the Extremes** (*Tom Aumann, Riturpana Kanungo* / Haik Simon / Kenishiro Yoneda / Rodi Herzberg / Dominic Rossi / Deniz Savran / Elena Litvinova)
- **Precision Measurements of Nuclear Properties** (*Andrew Stuchbery* / Sean N. Liddick / Mitch Allmond / Aaron Gallant)
- **The Nuclear Equation of State, Neutron Stars and Nuclear Astrophysics** (*Francesca Gulminelli, Daniel W. Bardayan* / Roy Lemmon / William Newton / Catherine Deibel / Rebecca Surman)
- **News on Nuclear Fusion and Fission** (*Walter Loveland* / Henning Esbensen / Karl-Heinz Schmidt)
- **Shell Evolution and Correlation Effects** (*Yang Sun, Augusto Macchiavelli* / Krzysztof Rykaczewski / Kathrin Wimmer / Marek Ploszajczak / Gregory Potel / Robert J. Charity)
- **Exploration and Discovery** (*Umesh Garg* / Sarah Milkovich / William Walters)

Nuclear Chemistry
Jun 8-9, 2013
Chair: Zachary Kohley
Associate Chair: Sherry J. Yennello

NUCLEIC ACIDS
Mechanistic Insights into DNA and RNA Metabolism throughout Biology
Jun 2-7, 2013
University of New England, Biddeford, ME
Chairs: Rachel Green & Karolin Luger
Vice Chairs: Wolf-Dietrich Heyer & Elena Conti

- **Recent Biochemical and Structural Approaches to Deciphering the Mechanisms of Protein Synthesis** (Harry Noller)
- **Genome Integrity and DNA Repair** (*Lorena Beese* / Sylvie Doublié / Wolf-Dietrich Heyer / Thomas Kunkel / Roland Kannaar)
- **Replication** (*James Berger* / Luca Pellegrini / Iestyn Whitehouse / Steven Bell)
- **Chromatin Structure and Dynamics** (*Geeta Narlikar* / Tom Owen-Hughes / Job Dekker / Yawen Bai / Craig Peterson)
- **Co- and Post- Transcriptional Regulation** (*David Bentley* / Elena Conti / Manny Ares / Chris Lima / Eric Phizicky)
- **Non-coding RNA** (*Brenda Bass* / John Rinn / Ian MacRae / Jon Staley)
- **RNA Processing, Export and Decay** (*Melissa Moore* / Tao Pan / Guillaume Chanfreau / Sean Ryder)
- **Ribosome Function and Regulation** (*Alan Hinnebusch* / Claes Gustafsson / Allen Buskirk / Kurt Fredrick)
- **Nucleic Acid Structure and Catalysis** (*Adrian Ferre D'Amare* / Ilya Finkelstein / Nils Walter / Christine Dunham)

NUCLEOSIDES, NUCLEOTIDES & OLIGONUCLEOTIDES
Jun 30 - Jul 5, 2013
Salve Regina University, Newport, RI
Chair: William B. Parker
Vice Chair: Vern L. Schramm

- **Keynote Presentation: Structure and Function of the Ribosome** (Thomas A. Steitz)
- **Nucleic Acid Chemistry and DNA Repair** (*Jennifer Heemstra* / Marc M. Greenberg / Cynthia J. Burrows / Zucai Suo)
- **Cancer - Small Molecule Approaches** (Varsha Gandhi)
- **Nucleic Acid Therapeutics** (*Muthiah Manoharan* / John J. Rossi / Punit Seth / John Maraganore / Neil Gibson)
- **Signaling Nucleotides** (*Steven M. Graham* / Scott A. Strobel / Barry Potter / Tom Ellenberger)
- **Antiviral Agents** (*Joy Feng* / Elijah Paintsil / Raymond F. Schinazi / Philip A. Furman / Jerome Deval)
- **RNA Metabolism** (*Eriks Rozners* / Robert A. Reenan / Barbara C. Nawrot)
- **Enzymology of Purine/Pyrimidine Metabolism** (*Stefan Lutz* / Stephen J. Benkovic / Karen S. Anderson / Staffan Eriksson / Albert Jeltsch)
- **Synthetic Biology** (*Zhen Huang* / Piet Herdewijn / John C. Chaput / Eric T. Kool)

ORGANIC REACTIONS & PROCESSES
Jul 14-19, 2013
Bryant University, Smithfield, RI
Chairs: Matthew M. Bio & Pascal Dube
Vice Chairs: Doug E. Frantz & Joseph M. Fox

- **New Methods in Catalysis** (Ruben Martin / Robert Bergman)
- **Transition Metal Catalysis** (Thomas Lectka / Mary Watson)
- **Complex Problems in Process Development** (Keith Frandrick / Martin Eastgate / Eric Ashley / Sheng Cui / Jared Piper / Eric Hansen / Remy Angelaud)
- **Exploring New Reaction Manifolds** (Guy Lloyd-Jones / Scott Miller)
- **New Strategies and Methods Applied to Natural Products and Protein Modification** (Sarah Reisman / Peter Senter)
- **New Frontiers in the Synthesis and Mechanism of Proteins and Peptides** (Jeff Bode / Tom Muir)
- **New Reactions of Nitrogen** (Ning Jiao / Armido Studer)
- **Efficient Strategies to Access Heterocycles and Complex Target Molecules** (Jimmy Wu / Francis Fang)
- **New Methods in Organic Synthesis, Quat-centers and Radicals** (Brian Stoltz / Armen Zakerian)
- **Cause and Effect in the Chemical Sciences** (*Doug Frantz* / Daniel Singleton / Daniel Nocera)

ORGANOMETALLIC CHEMISTRY
Jul 7-12, 2013
Salve Regina University, Newport, RI
Chair: James M. Boncella
Vice Chair: Bernadette T. Donovan-Merkert

- **Effects of Ligand Design on Reactivity** (*Bernadette Donovan-Merkert* / John Arnold / Mike Fryzuk)
- **Mechanisms** (*Alan Goldman* / Elon Ison / Liviu Mirica / Parisa Mehrkodavandi)
- **Electrocatalysis and Photocatalysis** (*Lisa McElwee-White* / Hansjorg Grutzmacher / Jim Mayer/ Etsuko Fujita)
- **Catalysis for Organic Synthesis** (*Keith Hollis* / Janis Louie / Dan Weix / Matt Tudge)
- **C-H Activation** (*Jerzy Klosin* / Miquel Costas / Theo Agapie)
- **Main Group Reactivity** (*John Walzer* / Louise Berben / Greg Robinson)
- **Early Transition Metal and f-Element Chemistry** (*Nora Radu* / Polly Arnold / Duncan Wass)
- **Transformations of Oxygenated Compounds** (*Adam Hock* / Dermot O'Hare / Susan Hanson)
- **Organometallic Chemistry and Energy Issues** (*Tom Baker* / Rich Eisenberg / Dan Nocera)

Organometallic Chemistry
Jul 6-7, 2013
Chair: Jonathan W. Napoline

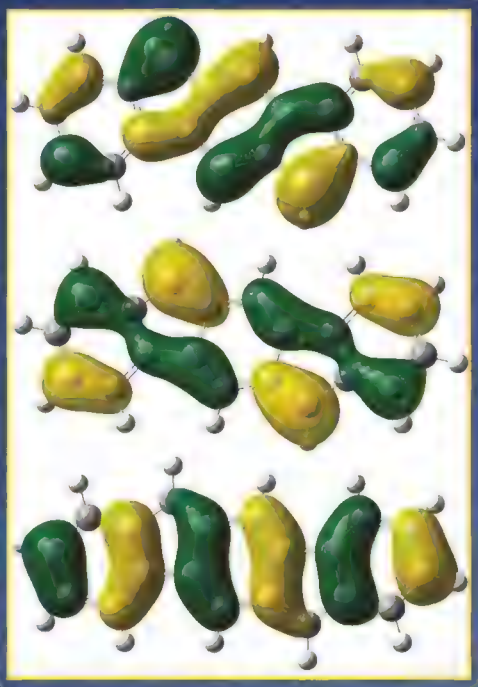

Kohn-Sham molecular orbitals of the HOMO-1, HOMO, and LUMO for [illegible] UB3LYP/6-31G(d) method. Image created in Gaussview 5.0.9 from Gaussian 09 Revision C.01 output. Courtesy of Michael M. Haley and Bradley Rose (University of Oregon). Submitted by Uta Wille, Chair, Physical Organic Chemistry GRC.

ORIGINS OF SOLAR SYSTEMS
Jun 23-28, 2013
Mount Holyoke College, South Hadley, MA
Chair: Edward D. Young
Vice Chair: Fred J. Ciesla

- **Birth Environments of Solar-like Stars and Implications for the Solar System** (*Jonathan Williams* / Roland Diehl / Paola Caselli)
- **Protoplanetary Disk Evolution** (*Lee Hartmann* / John Bally / Sean Andrews)
- **Chemistry of Protoplanetary Disks** (*Ted Bergin* / Karen Willacy / Karin Oberg)
- **Observational Records of Disk Chemical Evolution** [illegible] Wirstrom / Colette Salyk)
- **Building Blocks of Terrestrial Planets** (*Lindy Elkins-Tanton* / Ben Weiss / James [illegible])
- **Planetesimal Evolution** (*Ed Scott* / Erik Asphaug / Simone Marchi / Dav[illegible])

- **Planet Formation**
  (Hilke Schlichting / Ruth Murray-Clay)
- **Architectures of Planetary Systems**
  (Ivan Ramirez / Julia Fang)
- **Giant Impacts and Planet Formation**
  (David Stevenson / Francis Nimmo / Jay Melosh)

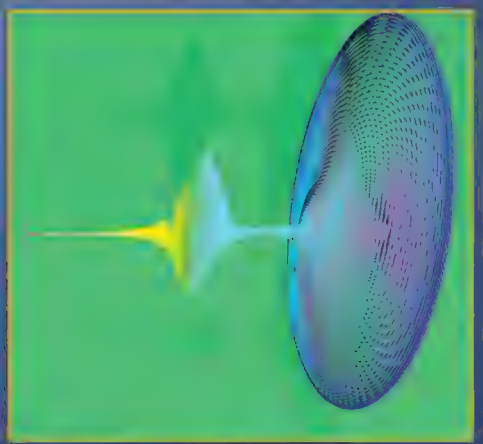

Example of a nearly circular attosecond pulse produced by applying two linearly polarized laser fields (two-color field) to the CO_2 molecule. The two laser fields i) produce High Harmonic Generation, and ii) will control the electron and hole dynamics in the molecule. Courtesy of Felipe Morales Moreno (Max-Born-Institut). Submitted by Thomas C. Weinacht & Misha Ivanov, Chairs, Quantum Control of Light & Matter GRC.

PANCREATIC DISEASES

NEW!

From Molecules to Patients
Jul 21-26, 2013
Mount Holyoke College, South Hadley, MA
Chair: Marco Falasca
Vice Chair: Michele Solimena

- **Keynote Presentation: Current Status of Pancreatic Diseases and Challenges**
  (*Claudio Bassi* / John Neoptolemos / Matthias Hebrok)
- **Pancreatic Models**
  (*Sunil Hingorani* / Owen Sansom / Piero Marchetti / Manuel Hidalgo)
- **Cell-Cell Interactions in Pancreas**
  (*Bernard Thorens* / Sarah Thayer / Dafna Bar-Sagi)
- **Molecular Mechanisms of Pancreatic Diseases**
  (*Maureen Gannon* / Donghui Li / Anil Bhushan / Gianfranco Delle Fave)
- **Novel Signaling Mechanisms in Pancreatic Diseases**
  (*Michael German* / Per Olof Berggren / Susumu Seino)
- **Signaling Pathways in Pancreatic Diseases**
  (*Rohit Kulkarni* / Guy Rutter / Ben Stanger / Howard Crawford)
- **Therapies and Clinical Aspects**
  (*Jens Siveke* / Nick Lemoine / Domenico Accili)
- **Pancreatic Stem Cells**
  (*Anne Grapain-Botton* / Helena Edlund / Christopher Wright / Diane Simeone)
- **Genetic and Epigenetic Aspects**
  (*Channing Der* / Mariano Barbacid / Jorge Ferrer)

PHAGOCYTES

Jun 9-14, 2013
Waterville Valley Resort, Waterville Valley, NH
Chair: Lee-Ann H. Allen
Vice Chair: Paul Kubes

- **Keynote Presentation: Macrophage Functional Genomics**
  (*David Mosser* / David Hume)
- **Inflammasomes**
  (*Lynda Stuart* / Maya Saleh / Fayyaz Sutterwala / John Kehrl / Jeffrey Cox)
- **Tumor Microenvironment**
  (*Dianne Cox* / Lissa Coussens / Mikael Pittet)
- **Bacterial Pathogens and the Host Response**
  (Frank DeLeo / Jason Carlyon / Alexander Hoffmann / Jeff Schorey)
- **Phagocytosis and Phagosomes**
  (Sergio Grinstein / Sergio Catz / Carmen Alvarez-Dominguez)
- **Cell Migration and Polarization**
  (*Paul Kubes* / Sussan Nourshargh / Anna Huttenlocher / Lani Wu / Minsoo Kim)
- **Effects of Phagocytes on Other Cell Types**
  (*Mary Dinauer* / Jessica Moreland / Leo Koenderman)
- **Altered states - Alzheimer's Disease, Arthritis & Smoking**
  (*William Nauseef* / V. Hugh Perry / Andrea Tenner / Andrew Luster / Martha Monick)
- **Talks Selected from Posters**
  (*Sergio Grinstein*)

Phagocytes
Jun 8-9, 2013
Chair: Juhi Bagaitkar
Associate Chair: Christine Becker

PHOTOCHEMISTRY

Jul 14-19, 2013
Stonehill College, Easton, MA
Chairs: Andrei G. Kutateladze & Bern Kohler
Vice Chairs: Malcolm D.E. Forbes & Anna D. Gudmundsdottir

- **Electron Transfer in Photochemistry**
  (*Claudia Turro* / Dirk Guldi / Frederick Lewis)
- **Photoassisted Synthetic Chemistry**
  (Thorsten Bach / Tehshik Yoon / Michael Oelgemöller)
- **Reaction Mechanisms**
  (*Axel Griesbeck* / John Toscano / Petr Klan)
- **Photobiology**
  (*Bruce Armitage* / Catherine Murphy / Vladimir Popik / Neil Branda)
- **Imaging: Molecules and Methods**
  (*Laren Tolbert* / Stefan Hell / Vladislav Verkusha)
- **Solar Energy Conversion**
  (*Ana Moore* / Gerald Meyer / Luping Yu / James Durrant)
- **Materials Photochemistry**
  (*Evgueni Nesterov* / Luisa De Cola / Seth Marder)
- **Spectroscopy and Dynamics**
  (*Ksenia Glusac* / Benjamin Schwartz / Tahei Tahara / Leticia Gonzalez)
- **Supramolecular Photochemistry**
  (*V. Ramamurthy* / Cornelia Bohne / Dario Bassani)

Photochemistry
Jul 13-14, 2013
Chair: Kevin Stamplecoskie
Associate Chair: Anoklase J. Ayitou

PHYSICAL METALLURGY

Materials at Extremes
Jul 28 - Aug 2, 2013
University of New England, Biddeford, ME
Chairs: Michael J. Mills & Easo George
Vice Chairs: Anthony D. Rollett & Roger C. Reed

- **High Temperature Materials**
  (Haruyuki Inui / Uwe Glatzel / Ron Noebe)
- **Radiation Effects**
  (*C.T. Liu* / Ian Robertson / Peter Hosemann)
- **High Strength / Ductility Materials**
  (Dierk Rabbe / Kaneaki Tzusaki / David Embury)
- **Behavior at Short Time-scales**
  (Ellen Cerreta / Glenn Daehn)
- **Behavior at Long Time-scales and Large Strains**
  (*Gunther Eggeler* / Antonin Dlouhy / Reiner Pippan)
- **Effects of Microstructure Extrema**
  (Tresa Pollock)
- **Behavior at Small Size-scale**
  (*William Nix* / George Pharr / Marc Legros)
- **Behavior Under Extreme Environments**
  (Neeraj Thirumalai)
- **Materials Far from Equilibrium**
  (Rajarshi Banerjee)

PHYSICAL ORGANIC CHEMISTRY

Understanding Chemical Reactivity - New Concepts and Applications
Jun 23-28, 2013
Holderness School, Holderness, NH
Chair: Uta Wille
Vice Chair: Michael M. Haley

- **Radicals in Biological Systems**
  (*John Murphy* / Bernd Giese / Joanne Stubbe / Derek Pratt)
- **New Insights into Catalysis**
  (*Gary Weisman* / Ruth Gschwind / Mark Taylor / Franziska Schönebeck / Richard Wong)
- **Developing Smart Polymers**
  (*Burkhard König* / Krystof Matyjaszewski / Malika Jeffries-EL)
- **Novel Functional Materials and Their Properties**
  (*Nancy Goroff* / Anke Krüger / Ivan Aprahamian / Miguel Garcia-Garibay / Rebecca Braslau)
- **Reactive Intermediates**
  (*Kathleen Kilway* / Malcolm Forbes / Bas de Bruin / Marc Robert)
- **Radicals and Radical Ions in Solution and Gas Phase**
  (*Carl Schiesser* / Robert Flowers / James Tanko / Stephen Blanskby / Richard O'Hair)
- **Conjugation - From Theory to Application**
  (*Luis Echegoyen* / William Karney / Andrew Holmes / Thoru Nishinaga)
- **Reaction Mechanisms - New Insights from Theory and Experiments**
  (*Kathleen Morgan* / Richard Johnson / Daniel Singleton / Nancy Mills / Peter Schreiner)
- **Talks Selected from Posters**
  (*Michael Haley*)

Physical Organic Chemistry
Jun 22-23, 2013
Chair: Lauren E. Jarocha
Associate Chair: Luke F. Gamon

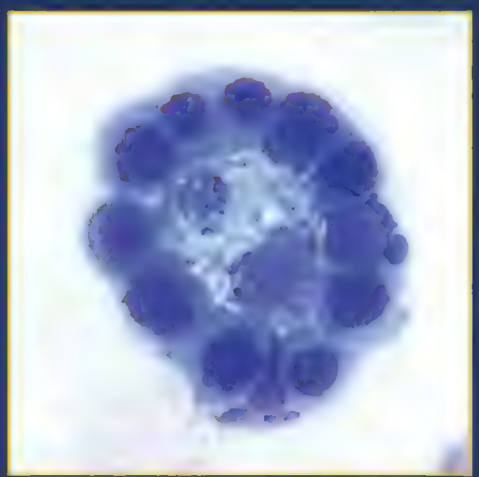

The niche for maturing erythroid precursors in the marrow are central macrophage cells that together constitute "erythroblastic islands". The functional role of macrophage cells during terminal erythropoiesis is recently receiving renewed scrutiny. Submitted by Jim Palis, Chair, Red Cells GRC.

PLANT METABOLIC ENGINEERING
The Interface of Plant Metabolism and Humanity
Jul 7-12, 2013
Waterville Valley Resort, Waterville Valley, NH
Chair: Dean Dellapenna
Vice Chairs: Richard A. Dixon & Sarah E. O'Connor

- **Keynote Presentations: Metabolic Engineering and Metabolism in Non Plant Systems**
  (*Natalia Dudareva* / Jim Liao / Matheos Koffas)
- **Using Quantitative Genetics and Genomics to Interrogate Plant Metabolism**
  (*Dean DellaPenna* / Dan Kliebenstein / Alisdair Fernie / Joost Keurentjes)
- **Using Genomics to Access Taxonomically Restricted Metabolism: Terpenoids**
  (*Joerg Bohlmann* / Robin Buell / Joe Chappell / Markus Lange)
- **Using Genomics to Access Taxonomically Restricted Metabolism: Alkaloids**
  (*Vince Deluca* / Peter Facchini / Sarah O'Connor / Ian Graham)
- **Transport Processes in Plant Metabolism**
  (*Andreas Weber* / Christoph Benning / Andreas Weber / Barbara Halkier)
- **Novel Approaches for Interrogating Plant Metabolism**
  (Dan Jones / Wolf Frommer / Valérie de Crécy-Lagard)
- **The Interface of Plant Metabolism and Human Health: Essential Nutrition**
  (*Barry Pogson* / Peter Beyer / Teresa B. Fitzpatrick)
- **The Interface of Plant Metabolism and Human Health: Non-essential Nutrients**
  (*Cathie Martin* / Anait S. Levenson / John Napier / Richard Mithen)
- **Phenylpropanoid Engineering and Metabolism**
  (*Rick Dixon* / Eric Grotewold / John Ralph / Vince Chang)

Plant Metabolic Engineering
Jul 6-7, 2013
Chair: Ruthie Angelovici
Associate Chair: Jing-Ke Weng

POLYAMINES
Regulation and Role of Polyamines in Biology and Disease
Jun 16-21, 2013
Waterville Valley Resort, Waterville Valley, NH
Chairs: John L. Cleveland & Chaim Kahana
Vice Chairs: Otto Phanstiel iv & Keiko Kashiwagi

- **Polyamines in New Arenas of Biology: Stem Cells, Aging and Autophagy**
  (*Leena Alhonen* / Leah Vardy / Guido Kroemer / Robert Casero)
- **Translational Control**
  (*Senya Matsufuji* / R. Jürgen Dohmen / Myung-Hee Park / Salim Merali / Jian-Ying Wang)
- **Roles of Polyamines in Metabolism and Disease**
  (*Bianca Verlinden* / Raghu Mirmira / Anne Uimari / Keith T. Wilson)
- **Polyamine Transport and Ion Channel Functions**
  (*Richard Poulin* / Kazuei Igarashi / Miki Fujita / Jacqui Gulbis / Pierre Paoletti)
- **Therapeutic Development and Applications**
  (*Alex Khomutov* / Patrick Woster / Margaret Phillips / Ilana Kolodkin-Gal)
- **Role of Polyamines in Cancer Development**
  (*David Feith* / Susan K. Gilmour / Jonas Nilsson / Lisa Shantz / Scott Lowe)
- **Cancer Chemoprevention Trials Targeting the Polyamine Pathway**
  (*Laurence J. Marton* / Frank L. Meyskens / Frank A. Sinicrope / Patrick Lynch)
- **Cancer Therapeutic Trials Targeting the Polyamine Pathway**
  (*André Bachman* / Michael D. Hogarty / Giselle Sholler / Eric S. Lightcap)
- **Keynote Presentation: How Do Polyamines Do It?**
  (Eugene Gerner)

Polyamines
Jun 15-16, 2013
Chair: Bianca BK. Verlinden
Associate Chair: Jenaro Garcia-Huidobro Prieto

POLYMERS
Jun 9-14, 2013
Mount Holyoke College, South Hadley, MA
Chair: Edward Bryan Coughlin
Vice Chair: Marc A. Hillmyer

- **New Trends in Polymer Synthesis**
  (*Rachel O'Reilly, Ian Stewart* / Todd Emrick / Geoff Coates)
- **Emerging Directions in Polymer Design**
  (*Ken Wagener, Tae Lim Choi* / Donghui Zhang / Harm-Anton Klok / Javid Rzayev)
- **Structures Derived From Polymers**
  (*Sheng Lin-Gibson, Frederick Beyer* / Mahesh Mahanthappa / Chinedum Osuji)
- **Biomimetic Polymers**
  (*Xinqiao Jia, Jerimiah Johnson* / Molly Schoichet / Matthew Becker / Theresa Reineke)
- **Controlled Radical Polymerization**
  (*Thomas McCarthy, Robert Mathers* / Krzysztof Matyjaszewski / Masami Kamigaito)
- **Polymers with Natural Components**
  (*Erik Berda, Malancha Gupta* / Stephen Miller / Rajeswari Kasi / Andrew Dove)
- **Conjugated Polymers**
  (*Daniel Knauss, Megan Robertson* / Christine Luscombe / Kenneth Carter)
- **Precision Polymers**
  (*Sam Thomas, Andrea Kasko* / Patrick Theato / Sebastian Perrier)
- **Self-Healing Materials**
  (*Melissa Grunlan, Derek Patton* / Zhibin Guan / Stuart Rowan)

Polymers
Jun 8-9, 2013
Chair: Ashlee A. Jahnke
Associate Chair: Elizabeth S. Sterner

POSTTRANSLATIONAL MODIFICATION NETWORKS
NEW!
Phosphosignaling
Jul 28 - Aug 2, 2013
Hong Kong University of Science and Technology, Hong Kong, China
Chair: Ning Li
Vice Chairs: Zhiyong Wang & Alma L. Burlingame

- **General Introduction to Posttranslational Modifications**
  (*Ning Li* / John Yates / Jian Kang Zhu / Donald Hunt / Al Burlingame)
- **Mass Spectrometry and Identification of PTM Sites**
  (*Al Burlingame* / Henry H.N. Lam / Josh Coon / Klaas Van Wijk / Ole N. Jensen)
- **Molecular and Cellular PTM Proteomics**
  (*Zhi Yong Wang* / Kazuo Shinozaki / Wilhelm Gruissem / Wendy Hsiao / Waltraud Schulze)
- **Cellular Phosphorylation**
  (*Josh Coon* / Blagoy Blagoev / Scott C. Peck / Hong Wei Xue / Jonathan Trinidad)
- **Quantitative and Functional Phosphoproteomics**
  (*Chentao Lin* / Jay J. Thelen / Rong Zeng / Frank L.H. Menke / Michael Sussman)
- **Kinase/Phosphatase-Mediated Cell Signaling Networks**
  (*Lan Huang* / Heribert Hirt / Sheng Luan / Martha Cyert / Jian-Min Zhou)
- **Kinase/Phosphatase and Phosphoprotein Interactomics**
  (*Pierre Thibault* / Zhi yong Wang / Chentao Lin / Marcus Smolka / Yasushi Ishihama)
- **Mass Spectrometry-Based Interactomics**
  (*Ole Jensen* / Steven Briggs / Thibault Pierre / Don Kirkpatrick)
- **PTM Networks and Systems Biology**
  (*Heribert Hirt* / Jesper Velgaard Olsen / Lan Huang / Ariel Bensimon / Tony Hunter)

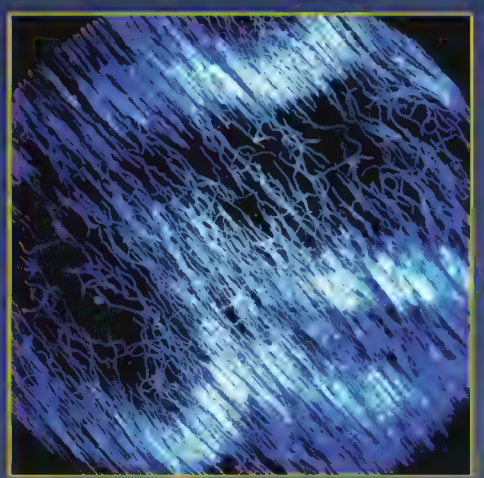

Self-organization of amphiphilic polymers in water: Small angle X-ray scattering study. Courtesy of Volker Abetz and Andreas H. Gröschel, Technische Universität München. Submitted by Andreas H. Gröschel & Axel H. Müller, Chair | Early Career Polymer Scientists Poster | GRC

PRECLINICAL FORM & FORMULATION FOR DRUG DISCOVERY
NEW!
Jun 2-7, 2013
Waterville Valley Resort, Waterville Valley, NH
Chairs: Brian T. Farrer & Raj Suryanarayanan
Vice Chairs: Michael Pikal & Robert Wenslow

- **Keynote Presentations: Form & Formulation**
  (*Raj Suryanarayanan* / Gordon Amidon / Christopher Sinko)
- **Solid Dispersions for Delivery**
  (*Nara Vaidyanathan* / Lynne Taylor / Robin Bogner / Lian Yu)
- **Ex Vivo Tools to Predict Bioperformance**
  (*Mike Bolger* / Hyun Jung Kim / Jianling Wang)
- **Cocrystals for Delivery**
  (*Mike Zaworotko* / Orn Almarsson / William Jones / Nair Rodriguez-Hornedo)
- **Nanoparticles for Delivery**
  (*Robert Lee* / Omid Farokhzad / Dennis Leung)
- **Beyond PO and IV: Alternate Delivery Routes and Dosing Paradigms**
  (*Ron Petts* / Cory Berkland / Sam Maynor / Audra Stinchcomb)
- **Breaching Delivery Obstacles in Preclinical Studies**
  (*Helen Burt* / Randy Wall / Avinash Thombre / Abu Serajuddin)
- **Assessing Developability from Preclinical Information**
  (*Vishal Saxena* / John Higgins / G. Richard Dickerson / Sudaker Gandi)
- **Analytical Tools to Probe Form & Formulation**
  (*Eric Munson* / Fred Wall / Dominic Pacitti / Marilyn Cicerone / Ken Clark)

PROTEINS
Jun 16-21, 2013
Holderness School, Holderness, NH
Chairs: Amy Keating & Bertrand Garcia-Moreno
Vice Chairs: Daniel Raleigh & Jane Clarke

- **Keynote Presentation: Visualizing the Molecular Machinery Controlling Human Gene Expression**
  (Eva Nogales)
- **Protein Interactions**
  (Jacob Corn / Barry Honig / [illegible])
- **Water and Pressure**
  (Catherine Royer / Woody Sherman / A. Joshua Wand)
- **Folding and Stability**
  (Susan Marqusee / Vijay Pande / Raghuveer Parthasarathy)
- **Mechanical Properties**
  (Frauke Gräter / Samara Reck-Peterson / Matthias Rief)
- **Protein Evolution**
  (Matthew Cordes / Michael Laub / David Liu / Joseph Thornton)
- **Assemblies and Large Complexes**
  (Grant Jensen / Klaus Schulten / Shu-ou Shan)
- **Membrane Proteins**
  (Olga Boudker / Ron Dror / Peter Hegemann)
- **Keynote Presentation: Anatomy of an ATP-fueled Molecular Machine**
  (Robert Sauer)

Multistage pathway of 2D crystallization by S-layer proteins on a lipid membrane. The monomeric proteins adsorb to the lipids in an extended conformation before condensing into initial liquid-like clusters. These clusters then reorganize into a crystalline array of tetramers, which expands through addition of new tetramers to edge sites. Analysis of the growth rate shows that the emergence of order in the clusters catalyzes S-layer folding and tetramer formation. The background was constructed from AFM images taken at different time points, while the foreground is based on cryo-electron tomography images. Experimental data from Sungwook Chung, Seong-Ho Shin and Luis Comolli (Lawrence Berkeley National Laboratory) and Jim De Yoreo (Pacific Northwest National Laboratory). Artwork by Kenneth X. Probst (Xavier Studio, San Francisco). Submitted by Joanna Millunchick, Chair, Thin Film & Crystal Growth Mechanisms GRC.

QUANTUM CONTROL OF LIGHT & MATTER
Jul 28 - Aug 2, 2013
Mount Holyoke College, South Hadley, MA
Chairs: Thomas C. Weinacht & Misha Ivanov
Vice Chairs: Thomas G. Baumert & Lorenza Viola

- **Keynote Presentation: Control Perspectives and Possibilities**
  (*David Tannor*)
- **Quantum Control in Open Systems**
  (*Paul Brumer* / Moshe Shapiro / Tommaso Calarco / Ronnie Kosloff)
- **Quantum Coherence in Meso-scopic and Biologically Relevant Systems**
  (*Jennifer Herek* / Jean-Pierre Wolf / Adam Cohen)
- **Ultrafast Spectroscopy and Control**
  (*Yaron Silberberg* / Tobias Brixner / Marcus Motzkus / Nirit Dudovich / Valery Milner)
- **Nonlinear Multi-Dimensional Spectroscopy**
  (*Shaul Mukamel* / Greg Scholes / Jurgen Hauer)
- **Quantum Information Applications of Quantum Control**
  (Misha Lukin / Klaus Molmer / Martin Plenio / Brian Neyenhuis)
- **Late-Breaking Topics**
  (*Philip Bucksbaum*)
- **Quantum Control of Chemical Reactions**
  (*Regina de Vivie Riedle* / Leticia Gonzalez / Herschel Rabitz / Kenji Ohmori / Robert Gordon)
- **Strong Field Control**
  (*Robert Levis* / Tamar Seideman / Andreas Baltuska)

RADIATION & CLIMATE
Observing the Interactions Among Radiation, Clouds, and the Climate System
Jul 7-12, 2013
Colby-Sawyer College, New London, NH
Chairs: Sally A. McFarlane & Robert Pincus
Vice Chairs: Bernhard Mayer & Eugene E. Clothiaux

- **Grand Challenges in Radiation and Climate**
  (*Stephen Klein* / Julia Slingo / Richard Allan)
- **Radiation and Cloud-Scale Dynamics**
  (*Brian Mapes* / Hirohiko Masunaga / Courtney Schumacher)
- **Radiation and Planetary-Scale Dynamics**
  (*David Randall* / Dargan Frierson / Qiang Fu)
- **Fast Forcing and Cloud Processes**
  (Sandrine Bony)
- **Radiation and the Earth's Surface**
  (Martin Wild / Anand Gnanadesikan / Paul Dirmeyer)
- **Novel Observations for Model Interpretation**
  (*David Turner* / Suzanne Crewell / Ann Fridlind / Elisabeth Moyer)
- **Ice Properties and Relevance for Climate**
  (*Jerry Harrington* / Ben Murray / Anthony Baran)
- **The Power of the Spectrum**
  (*Shaima Nasiri* / Peter Pilewskie / Stephen Leroy)
- **Challenges in Remote Sensing**
  (*Paquita Zuidema* / Larry Di Girolamo / Steven Platnick)

Radiation & Climate
Jul 6-7, 2013
Chair: Louise Nuijens
Associate Chair: Michael S. Pritchard

RED CELLS
Jul 7-12, 2013
Proctor Academy, Andover, NH
Chair: Jim Palis
Vice Chair: Luanne L. Peters

- **Developmental Biology of Hematopoiesis**
  (*Len Zon* / Len Zon / Nancy Speck / Elaine Dzierzak)
- **Epigenetics of Erythroid Cells**
  (*Emery Bresnick* / Emery Bresnick / Stuart Orkin / Guillaume Giraud / Laurie Steiner)
- **Red Cell Production**
  (*Lionel Blanc* / Luc Douay / Don Wojchowski / Saghi Ghaffari)
- **Terminal Erythroid Maturation**
  (*Merav Sokolovsky* / Theodosia Kalfa / Peng Ji / Merav Socolovsky / Yolanda Sanchez / Paul Frenette)
- **Transcriptional Regulation of Erythroid Gene Expression**
  (*Gerd Blobel* / Doug Higgs / Gerd Blobel / Andrew Perkins / Jim Bieker)
- **Membrane Protein Structures and Functions**
  (*Velia Fowler* / Velia Fowler / Athar Chishti / Lesley Bruce / Dennis Discher)
- **Iron, Heme and the Red Cell**
  (*Barry Paw* / Barry Paw / Tom Ganz / Iqbal Hamza / Jan Abkowitz)
- **Red Cell Disorders**
  (*Ben Ebert* / Stefano Rivella / Lily Huang / Ben Ebert / David Bodine / Vijay Sankaran)
- **Infections and the Red Cell**
  (*Mohan Narla* / Cheryl Lobo / Ian Lewis / Kastun Haldar / Lionel Blanc)

Red Cells
Jul 6-7, 2013
Chair: Lionel Blanc
Associate Chair: Katie M. Giger

SOFT CONDENSED MATTER PHYSICS
Bio-Soft Matter: Dynamical and Structural Complexity
Aug 18-23, 2013
Colby-Sawyer College, New London, NH
Chairs: Andreas R. Bausch & Robijn F. Bruinsma
Vice Chairs: Seth Fraden & Jean-Francois Joanny

- **Jamming in Flows**
  (*Claus Heussinger* / Heinrich Jäger / Matthieu Wyart)
- **Soft Materials**
  (Anthony Dinsmore / Dave Weitz / Itai Cohen)
- **Principles of Self Organziation**
  (*Erwin Frey* / Michael Brenner / Julia Yeomans)
- **Active Cytoskeletal Systems**
  (*Christina Marchetti* / Zvonimir Dogic / Margaret Gardel)
- **Living Soft Matter**
  (*Fred MacKintosh* / Stefan Grill / Cliff Brangwynne)
- **Complex Interfaces**
  (*Dave Pine* / Eric Dufresne / Kathleen Stebe / Clemens Bechinger)
- **Outreach**
  (*Alex Levine* / Gerard Wong / Dan Goldman)
- **Flow of Complex Fluids in Complex Geometries**
  (*Mireille Claessens* / Lyderic Bouquet / Howard Stone)
- **Tissue Dynamics**
  (*Dan Fletcher* / Francoise Brochard / Xavier Trepat)

Soft Condensed Matter Physics
Aug 17-18, 2013
Chair: Katharine E. Jensen
Associate Chair: Alexandre Franceschini

SPIN DYNAMICS IN NANOSTRUCTURES NEW!
Aug 18-23, 2013
Hong Kong University of Science and Technology, Hong Kong, China
Chair: Xiang Rong Wang
Vice Chair: Gerrit E. W. Bauer

- **Thermally Driven Spin Dynamics**
  (*Chia-Ling Chien* / Eiji Saitoh / Sebastian Gönnenwein / Stuart S.P. Parkin)
- **Spin Transfer Torques**
  (*Mark Stiles* / Ke Xia / Paul Kelly / Yoshishige Suzuki / Ulrich Nowak)
- **Spin Caloritronics**
  (*Jing Shi* / Joseph Heremans / Markus Münzenberg / Jiang Xiao)
- **Magnetization Dynamics: Experiment**
  (*Bernard Dieny* / John Xiao / Alina Deac / Theo Rasing / Bill Rippard)
- **Magnetization Dynamics: Theory**
  (*Sadamichi Maekawa* / Shufeng Zhang / Yaroslaw Bazaliy / Arne Brataas)
- **Magnetic Insulators**
  (*Jairo Sinova* / Bart van Wees / Burkard Hillebrands / Yaroslav Tserkovnyak / Rembert Duine)
- **Landau-Lifshitz-Gilbert Equation and Damping**
  (*Dan Wei* / Kyung J. Lee / Johan Akerman)

- **Spin Hall Dynamics**
  (*Allan H. MacDonald* / Daniel Ralph / Qian Niu / Yoshichika Otani / Gen Tatara)
- **Device and Materials**
  (*Bruce D. Terris* / Claudia Felser / Sara Majetich / Shinji Yuasa)

STAPHYLOCOCCAL DISEASES

Jul 28 - Aug 2, 2013
Waterville Valley Resort, Waterville Valley, NH
Chairs: Vance G. Fowler & Mark S. Smeltzer
Vice Chairs: Simon Foster & Jos Van Strijp

- **Staphylococcal Diseases GRC: Past And Present**
  (*Vance G. Fowler* / Richard Proctor / Michael Olson)
- **In the Center of It All: Metabolic Determinants of Virulence**
  (*Anthony Richardson* / Charles Rock / Neal Reiner / Linc Sonenshein)
- **The Flexible Genome and Its Impact on All Things Staphylococcal**
  (*Sharon Peacock* / Steven Tong / Anne Catrin Uhlemann / Matt Holden)
- **The Staphylococcal Circuit Board: Keeping The Virulence Flowing**
  (*Brice Felden* / Inigo Lasa / Svetlana Chabeskaya / Ambrose Cheung)
- **Alternative Lifestyles of the Staphylococci**
  (*Kelly Rice* / Bettina Loffler / Tammy Kielian)
- **Antibacterial Strategies**
  (*Michael Yeaman* / Victor Nizet / Paul Dunman / Chip Chambers)
- **The Animalistic Nature of The Beast: The Staphylococci as Zoonotic Pathogens**
  (*George Stewart* / Ross Fitzgerald / Robert Skov / Jose Penades)
- **The Other Side of the Equation: The Host Response to Staphylococcal Infection**
  (*Rachel McLoughlin* / Lloyd Miller / Eva Medina / Jovanka Voyich)
- **Late-Breaking Topics**
  (*Magnus Hook*)

Staphylococcal Diseases
Jul 27-28, 2013
Chair: Michael E. Olson
Associate Chair: Karen E. Beenken

STRESS PROTEINS IN GROWTH, DEVELOPMENT & DISEASE

Jul 7-12, 2013
Mount Snow Resort, West Dover, VT
Chair: Judith Frydman
Vice Chair: Ursula Jakob

- **Keynote Presentations: Protein Homeostasis and Stress Proteins in Aging and Disease**
  (*Ursula Jakob, Judith Frydman* / Kaz Nagata / Rick Morimoto)
- **Protective Mechanisms Against Protein Misfolding**
  (*Bernd Bukau* / Elizabeth Craig / Johannes Buchner / Jim Bardwell / Jonathan Weissman / Elke Deuerling)
- **Protein Aggregation: From Basic Mechanism to Disease**
  (*Lea Sistonen* / Harm Kampinga / Bernd Bukau / Helen Saibil / Ivor Benjamin)
- **Regulation of the Stress Response: Implications for Aging and Disease**
  (*Harm Kampinga* / Lea Sistonen / John Lis / Carol Gross / Roy Parker)
- **Detecting and Responding to Mitochondrial and Oxidative Stress**
  (*Ana Maria Cuervo* / Dirk Bohmann / Haynes CM / Wade Harper / Len Neckers)
- **Regulation of Protein Homeostasis in the Endoplasmic Reticulum**
  (*Andy Dillin* / Linda Hendershot / David Ron / Peter Walter / Ineke Braakman)
- **Protein Quality Control During Stress and Disease**
  (*Elke Deuerling* / Scott Emr / Anne Bertolotti / Jeff Brodsky / Ana Maria Cuervo)
- **Therapeutics Exploiting Stress Proteins to Ameliorate Disease**
  (*Jonathan Weissman* / Dennis Thiele / William Balch / Jeff Kelly / Jason Gestwicki)
- **Stress Responses as Regulators of Longevity and Aging**
  (*Peter Walter* / Keith Blackwell / Brian Kennedy / Andy Dillin / Allen Hsu)

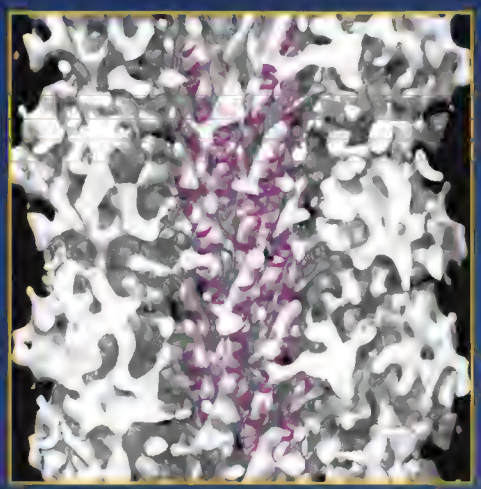

A cryo-EM reconstruction of an archaeal adhesion filament with alpha-helices built into the core. Submitted by Edward Egelman, Chair, Three-Dimensional Electron Microscopy GRC.

SYNTHETIC BIOLOGY

NEW!
(Re-)constructing and Re-programming Life
Jun 9-14, 2013
Mount Snow Resort, West Dover, VT
Chair: Vitor V. Martins Dos Santos
Vice Chair: Christopher Voigt

- **Living vs Non-living Matter**
  (*Steen Rasmussen* / Jack W. Szostak / Guenther von Kiedrowski)
- **Building Genomes**
  (*Luis Serrano* / Dan Gibson / Antoine Danchin / Mitshuiro Itaya)
- **Alternative Life**
  (*Phillipe Marliere* / Nejiko Budisa / Jason Chin)
- **Streamlining and Re-engineering Genomes**
  (*Victor de Lorenzo* / Gyorgy Posfai / Philippe Noirot / Jeff Boeke)
- **Enabling Technologies**
  (*Sven Panke* / George Church)
- **Applications of Synthetic Biology: Non-Medical**
  (*Drew Endy* / Jay Keasling / Pamela Silver / Christina Smolke)
- **Societal Aspects of Synthetic Biology**
  (*Joyce Tait* / Markus Schmidt / Ken Oye)
- **Applications of Synthetic Biology: Medical**
  (Martin Fussenegger / Ron Weiss / Hiroki Ueda)
- **Where Do (Can) We Go With Synthetic Biology?**
  (*Eric Lander* / Adam Arkin / J.J. Collins)

T FOLLICULAR HELPER CELLS

NEW!
Basic Discoveries and Clinical Applications
Jul 21-26, 2013
The Chinese University of Hong Kong, Hong Kong, China
Chair: Chen Dong
Vice Chairs: Carola Vinuesa & Sidonia Fagarasan

- **Keynote Presentations: Evolution and Interaction of Lymphocyte Subsets**
  (Max Cooper / Jason Cyster)
- **Genetic Program of Tfh Cells**
  (*Liwei Lu* / Chen Dong / Di Yu / Masato Kubo)
- **Imaging of Germinal Centers**
  (*Hai Qi* / Michel Nussenzweig / Takaharu Okada / David Tarlington)
- **Mucosal and Ectopic Germinal Centers**
  (*Wenjun Ouyang* / Sidonia Fagarasan / Troy Randall / Mi-Na Kwon)
- **Tfh Signaling and Homeostasis**
  (Joseph Craft / Roza Nurieva / Pam Schwartzberger)
- **Tfh in Infection**
  (Michael McHeyzer-William / Shane Crotty / Elina Zuniga)
- **Regulatory Mechanisms in GC Reaction**
  (Carola Vinuesa / Luis Graca / Harvey Cantor / Chris Goodnow)
- **Tfh Cells in Autoimmunity**
  (*Jingwu Zang* / Vijay Kuchroo / Mark Schlomchik / Robert Brink)
- **Human Tfh Cells**
  (*Ho-Youn Kim* / Steve Tangye / Hideki Oeno / Tak Mak / Zhigang Tian)

THIN FILM & CRYSTAL GROWTH MECHANISMS

Jul 7-12, 2013
University of New England, Biddeford, ME
Chair: Joanna Millunchick
Vice Chair: Lara A. Estroff

- **Crystallization Fundamentals**
  (*Seth Fraden* / Sharon Glotzer / Micheal Ward)
- **Crystal Growth at the Atomic Scale**
  (Kristen Fichthorn / Peter Smereka / Suzi Jarvis)
- **Biomineralization**
  (*Lia Addadi* / Julain Gale / Derk Joester / Nico Sommerdijk)
- **Nanowires**
  (Lincoln Lauhon / Stefano Sanguinetti / Henning Reichart)
- **Molecular Assembly**
  (*Jen Swift* / Jim DeYoreo / Elias Vlieg / Koji Harano)
- **Thin Films**
  (*Greg Salamo* / Kristin Volz / Darrell Schlom / Tom Tiedje)
- **Graphene**
  (Randy Feenstra / Ruud Tromp / Suneel Kodambaka)
- **Growth by Electrochemistry**
  (*Jonah Erlebacher* / Daniel [illegible] / [illegible])
- **Colloidal Crystallization**
  (*Chekesha Liddell Watson* / [illegible])

THREE DIMENSIONAL ELECTRON MICROSCOPY
Advancing the Cutting Edge
Jun 23-28, 2013
Colby-Sawyer College, New London, NH
Chair: Edward Egelman
Vice Chair: Henning Stahlberg

- **Keynote Presentations: From Cryo-EM Images to Atomic Models**
  (*Edward Egelman* / David Agard / Klaus Schulten)
- **Sample Preparation for Cryo-EM**
  (Bridget Carragher / Debbie Kelly / Montserrat Samso / Radosav Pantelic)
- **Conformational Heterogeneity**
  (Sjors Scheres / Hans Elmlund / Melanie Ohi)
- **Helical Assemblies at High Resolution**
  (Eva Nogales / Keiichi Namba / Z. Hong Zhou / Nigel Unwin)
- **Integral Membrane Proteins**
  (Karen Davies / Xiaodan Li)
- **The Challenges of Small Complexes**
  (*Wah Chiu* / Bruno Klaholz)
- **Different Approaches to Tomography**
  (Takashi Ishikawa / Michael Elbaum)
- **Talks Selected from Posters**
  (*Henning Stahlberg*)

TIME-DEPENDENT DENSITY-FUNCTIONAL THEORY NEW!
Aug 11-16, 2013
University of New England, Biddeford, ME
Chairs: Neepa T. Maitra & Eberhard K.U. Gross
Vice Chairs: Erin R. Johnson & Roi Baer

- **Functional Development**
  (*Carsten Ullrich* / Giovanni Vignale / Robert van Leeuwen)
- **Linear and Non-Linear Phenomena in Solids**
  (*Lucia Reining* / Sangeeta Sharma / Rex Godby / Kazuhiro Yabana)
- **Large Systems**
  (*John Dobson* / Alan Aspuru-Guzik / Adam Wasserman)
- **Electron Dynamics in Real-Time**
  (*George Bertsch* / Katsuyuki Nobusada / Alberto Castro / Andrea Marini)
- **Excitations in Molecules (TDDFT and Beyond)**
  (*Leeor Kronik* / Roi Baer / Anna Krylov)
- **Coupled Electron-Ion Dynamics**
  (*Tamar Seideman* / Joe Subotnik / Eric Suraud / Ivano Tavernelli)
- **Correlation Energies via TDDFT for Weak Interactions**
  (*Adrienn Ruzsinszky* / Filipp Furche / Erin Johnson)
- **Fundamentals of Functionals in DFT and TDDFT**
  (*Stephan Kuemmel, Stefan Kurth* / Kieron Burke / John Perdew / Walter Kohn)
- **Charge Transport**
  (*Barry Dunietz* / Eran Rabani / Troy van Voorhis)

Time-Dependent Density-Functional Theory
Aug 10-11, 2013
Chair: Florian G. Eich
Associate Chair: Stefano Pittalis

TISSUE REPAIR & REGENERATION
Jun 16-21, 2013
Colby-Sawyer College, New London, NH
Chair: Sabine A. Eming
Vice Chair: Enrique Amaya

- **Aging and Tissue Regeneration - The Enemy Within?**
  (*Sabine Eming* / Judith Campisi / Andrew Brack / Aleksandra Trifunovic)
- **Mechanotransduction and Cellular Responses**
  (*Thomas Krieg* / Reinhard Fässler / Sirio Dupont / Ellen Lumpkin / Catherine Nobes / Sara Wickström)
- **Barrier Homeostasis and Regeneration**
  (*Livingston Van De Water* / Dennis Roop / Angela Christiano / Michael Galko)
- **Whole Organ and Pattern Regeneration**
  (*Tanuja Harshani Peiris* / Philip Beachy / Phillip A. Newmark / Michael Brand / Enrique Amaya)
- **Parallels Between Wound Healing and Cancer**
  (*Alan Wells* / Sabine Werner / Paul Martin / Jeremy F. Reiter)
- **Myeloid Cells: Unique Sensors and Effectors of Tissue Damage and Repair**
  (*Luisa DiPietro* / F. Geissmann / Anna Huttenlocher / Judith Allen)
- **Epigenetic Control in Tissue Regeneration**
  (*Jeffrey Davidson* / Renato Paro / Lorenz Studer / Juan Carlos Izpisua Belmonte)
- **Signals in Growth Control and Metabolism**
  (*Enrique Amaya* / Nadia Rosenthal / Michael Hall / Alex P. Gould)
- **From Cells to Tissues: Tissue Engineering and Regenerative Medicine**
  (*Paul Martin* / Jeffrey Hubbell / Molly M. Stevens)
- **Panel Discussion: The Path to Translation - Cell Biology on to the Clinic**
  (*Duncan McGrouther, Paul Martin*)

Tissue Repair & Regeneration
Jun 15-16, 2013
Chair: Dunja Knapp
Associate Chair: Tanuja H. Peiris

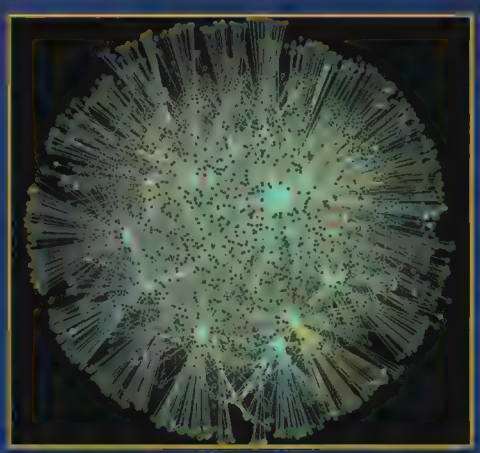

M. tuberculosis transcription factor binding network based on high throughput ChIP-seq helps identify novel, condition-specific drug targets. Courtesy of Kyle Minch (Seattle Biomedical Research Institute). Submitted by David R. Sherman & Veronique A. Dartois, Chairs, Tuberculosis Drug Development GRC.

TUBERCULOSIS DRUG DEVELOPMENT
Jul 21-26, 2013
Renaissance Tuscany Il Ciocco Resort, Lucca (Barga), Italy
Chairs: David R. Sherman & Veronique A. Dartois
Vice Chairs: Sabine Ehrt & David Barros

- **TB in 2050**
  (*David Sherman* / Barry Bloom)
- **Lessons from Microbes Other Than MTB**
  (*Eric Rubin* / Ruben Tommasi / Tim Wells / Kim Lewis)
- **Targets**
  (*Sabine Ehrt* / Luis Pedro de Carvalho / Christoph Grundner / Omonike Olaleye)
- **Screening Tools and Approaches**
  (*Thomas Dick* / Dirk Schnappinger / Tom Blundell / Brian VanderVen)
- **Target-based or Phenotypic Screening? You be the Judge**
  (*Ken Duncan* / Courtney Aldrich / David Olsen / Tanya Parish / Stewart Cole)
- **TB Medicinal Chemistry**
  (*David Barros* / Kelly Chibale / Michael Shultz / Giovanna Poce)
- **Cell and Tissue Issues**
  (*Gerry Davies* / Brendan Prideaux / Lalita Ramakrishnan)
- **EBA - What It Does and Doesn't Measure**
  (*Paul van Helden* / Carol Nacy)
- **Clinical Issues**
  (Clif Barry / Koen Andries)

Tuberculosis Drug Development
Jul 20-21, 2013
Chair: Anuradha Kumar

VISUALIZATION IN SCIENCE & EDUCATION
Jul 21-26, 2013
Bryant University, Smithfield, RI
Chairs: Brian E. Martin & Martin Storksdieck
Vice Chairs: Bob Kolvoord & Katharina Scheiter

- **Different Ways of Understanding Complexity in Visualization**
  (John Maeda / Mark Ballora)
- **Complexity in Visualization**
  (Sara Fabrikant / Stephan Schwan / Jeff Heer)
- **Augmented Reality and Other Modes of Visualization**
  (Susan Goldin-Meadow / John Bailey / Adam Jones)
- **The Evolving Role of Visualization in the Teaching of STEM**
  (Kathy Perkins / John Jungck / Eric Wiebe / Dan Schwartz)
- **Visualization in the Scientific Workplace**
  (Claude Lechene / Elizabeth Krupinski)
- **Role of Visualization in Communicating Complex Science to the Public**
  (Mike Stieff / David Uttal / Rachel Connolly / Ned Gardiner)
- **Visualizing Unseen Worlds**
  (Ralf Kaehler)
- **Visualization in Mobile Environments**
  (Gael McGill / Alex Clark)
- **Frontiers in Visualization**
  (*Peter Mahaffy*)

X-RAY SCIENCE
Aug 4-9, 2013
Stonehill College, Easton, MA
Chair: Harald Reichert
Vice Chair: Chi-Chang Kao

- **X-rays in the Quantum World**
  (Ralf Röhlsberger / Gema Martinez Criado)
- **Beyond the Obvious: Ultrafast Time Scales**
  (*E. Weckert* / R. Moshammer / E. Glover)
- **New Horizons for Storage Ring and Linac Based Sources**
  (*J. Hastings* / M. Borland / J. Wu / H. Graafsma)
- **X-rays in the Life Sciences**
  (*S. Wakatsuki* / J. Takagi / O. Paris)
- **X-rays Probing the Extreme**
  (*I. Silvera* / W. Mao / Leonid Dubrovinsky)
- **Caught in Action: *In-situ* Studies**
  (A.M. Beale / E. Lundgren / D. Fong)
- **Beyond the Simple: Complexity in Correlated Systems**
  (*J. Hill* / M. Le Tacon / T. Devereaux)
- **Excursions into the Nanoworld**
  (*G. Ice* / C. Schroer / R. Harder)
- **Late-Breaking Topics**
  (*C. Kao*)

X-Ray Science
Aug 3-4, 2013
Chair: Marco Moretti
Associate Chair: Leonard Mueller

Support the sciences. **Get rewarded.**

Show your AAAS pride and reward yourself with the new AAAS Platinum Advantage Rewards Card from NASA Federal Credit Union.

Apply now and get
10,000 bonus points!

Go to nasafcu.com/AAASpromo

Get **10,000 bonus points** if you sign up for a card and spend $3,000 within 90 days of account opening.

Learn more at
nasafcu.com/AAASpromo.

Subject to credit approval.
Membership in AAAS and NASA FCU is required.
NASA FCU is federally insured by NCUA.

The Clinical Aspirations of Microarrays

Although most microarray applications are currently research-use-only, this technology appears poised to move to the clinic for genomics-based applications. In fact, some products can already be used in medical diagnostics and many more are in development. For example, microarrays can be customized to detect small, specific genetic changes that indicate a particular disease. In the future, this technology will likely remain a useful tool for both research and clinical applications. **By Mike May**

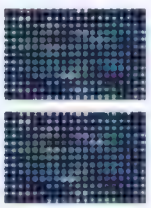

In today's translational genomics research, says Seth Crosby, alliance director of the Genome Technology Access Center at **Washington University School of Medicine in St. Louis,** "The biggest challenge is interpretation." Available technology makes it easy enough to collect information from someone's genome. The tricky part comes in interpreting the clinical relevance of that information. "Then, one can say a variation in a particular gene is known to have such and such impact on the patient's health or treatment options," Crosby explains.

As an example, Crosby describes a clinically certified next generation sequencing panel of 45 oncology genes offered by Genomics and Pathology Services, Washington University's clinical genomics laboratory. This panel is actively being used to profile tumors and guide the treatment of cancer patients. "We had to look at hundreds of papers," Crosby says, "to build a clinical-grade database of authoritative interpretations for each clinically relevant mutation found in these genes." He adds, "That took hundreds of Ph.D. and M.D. hours, reading through papers to identify the pertinent information."

Crosby notes that, over time, clinicians might come to understand which changes in the genome impact a patient's health and which are harmless. "Once the lists of relevant and irrelevant genes are narrowed down, and we have a sense of which polymorphisms are important, these could be used to create a very cheap array that would help detect diseases," he says. Beyond being economical, microarrays also deliver manageable amounts of data. As Crosby explains, "Much of the genome is invariant." So with microarrays, he says, "We collect only the data we need."

"Using microarrays as tools in cytogenetics is really accelerating."

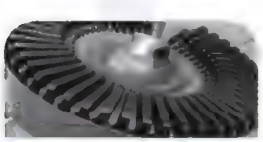

Developing Diagnostics

In some cases, clinicians can link specific chromosomal defects with particular diseases, and microarrays bring new capabilities to this karyotyping, or counting and assessing the appearance of chromosomes. Down syndrome is one of the best-known examples, in which the person has an extra copy of chromosome 21. Although additions or deletions of entire chromosomes, and even defects in parts of them, can be seen under a microscope, microarrays reveal fine-detail changes in chromosomes. "Using microarrays as tools in cytogenetics is really accelerating," says Andy Last, executive vice president of the genetic analysis business unit at **Affymetrix** in Santa Clara, California. When experts are asked in which areas microarrays are being used the most, many mention copy-number variation—the addition or deletion of specific regions of DNA, particularly those with clinical consequences.

"There are literally hundreds of syndromes [that have] chromosomal rearrangements associated with a particular phenotype," says James Clough, vice president, clinical and genomic solutions at **Oxford Gene Technology** (Oxfordshire, United Kingdom). "Depending on the population being tested, traditional karyotyping under a microscope provides a diagnosis about 5–8 percent of the time, and a microarray provides an 18–25 percent diagnostic yield. The resolution is far higher with an array." Still, he adds, "The challenge is determining if a small aberration is pathogenic or nonpathogenic, or a variance of unknown significance."

Upcoming Features

Proteomics—March 1
Fluorescence Multiplexing—April 12
Proteomics: Maldi Imaging—May 31

CREDIT: (FROM RIGHT) IMAGE COURTESY OF OXFORD GENE TECHNOLOGY; © ISTOCKPHOTO.COM/NANTELA

To help researchers make such distinctions, Oxford Gene Technology supplies a range of microarrays, such as the CytoSure ISCA Arrays, which look for genetic defects involved with known syndromes, such as Prader Willi and Williams-Beuren syndromes.

PerkinElmer (Waltham, Massachusetts) has also developed assays for detecting disease-related structural changes in chromosomes. For example, the company provides genomic testing of oncology samples with its OncoChip. "This is a high-density whole-genome array, targeting more than 1,800 cancer genes and clinically relevant balanced translocations," says Christopher Williams, market segment leader at PerkinElmer. The array can reveal copy-number variations as low as 10 kilobases in the targeted regions.

Additionally, the CytoScan HD Cytogenetics Solution, from Affymetrix, offers probes for both copy-number variation and single nucleotide polymorphisms (SNP). The probes for copy-number variation can reveal chromosomal changes that could cause clinical concerns, and the SNP probes help researchers assess more detail on the exact variation—specifically the changes in individual nucleotides. "This is the highest density microarray on the market," says Last. "It's being used in the classical sense of cytogenetics, [to detect] inherited disorders, and increasingly in oncology, especially [for] hematological malignancies." The array can reveal copy-number variations in chromosomal segments as small as 25,000 nucleotides. For the moment, this is a research-use-only tool, but Affymetrix is running clinical trials to test the use of this platform as an in vitro diagnostic.

Agilent (Santa Clara, California) also makes microarrays that detect copy-number variations, such as its CGH (comparative genomic hybridization) plus SNP microarrays. "These can be customized from more than 28 million probes in our library, and users can even upload their own probe sequences," says Patricia Barco, product manager for cytogenetics at Agilent. Within an exon, for example, these microarrays can detect copy-number variations in DNA segments as small as 100 base pairs. "These can be used in prenatal and postnatal research and cancer," Barco says. The most popular format, according to Anniek De Witte, product manager, clinical software at Agilent, includes 180,000 probes divided into four samples. "This is the best balance of the number of samples and resolution," she says. In addition, the Agilent CytoGenomics 2.5 software compares the results from these arrays with external and internal databases to distinguish between common variations and ones that could cause clinical problems.

Creating Custom Tools

To apply microarrays to clinical problems, physicians need approved tools. One FDA-cleared diagnostic tool, the Pathwork Tissue of Origin test from Pathwork Diagnostics in Redwood City, California, uses an Affymetrix microarray to determine the tissue type in which a patient's cancer started, such as breast or colon. Raji Pillai, senior director, product development and clinical affairs at **Pathwork Diagnostic** says, "This test uses formalin-fixed, paraffin-embedded [FFPE] tissue from a patient's tumor and 2,000 transcript markers to provide a readout of a tumor's gene-expression profile." Using several thousand different tumor specimens and proprietary computational algorithms, researchers at Pathwork Diagnostics have identified a set of 2,000 genes that can be used to distinguish 15 kinds of tumors.

When a pathologist receives a cancer sample that is difficult to identify visually, they can send it to Pathwork Diagnostics. "It takes four to five days to report out a result that's interpreted by a pathologist in our lab," says David Crawford, the company's chief commercial officer. A company pathologist reviews the results to ensure the most accurate interpretation of this diagnostic.

CREDIT: © ISTOCKPHOTO.COM/NANTELA

In the future, the company hopes to develop microarray tests that determine a tumor's tissue of origin and also distinguish between tumor subtypes. Such advanced tests might even "provide information on the [patient's] predicted response to a particular therapy," Crawford says.

> **"The resolution is far higher with an array. The challenge is determining if a small aberration is pathogenic or nonpathogenic, or a variance of unknown significance."**

In addition to being used for studying an individual's genetic profile, microarrays can be used to explore genetic variations across different populations and cultures. For example, Jennifer Stone, market development manager at **Illumina** in San Diego, California, says, "We developed our Infinium HumanCore BeadChip family of microarrays to provide a solution for population-level or biobank studies." Such research involves tens to hundreds of thousands of samples. "These genetic studies are on a scale above and beyond what's historically been done," says Stone. Because these microarrays accommodate a large number of samples, they provide an opportunity for researchers to perform robust statistical analyses which can reveal differences in the distribution of genetic variation between normal and diseased populations.

The HumanCore microarrays provide a standard set of over 300,000 SNP probes, which covers the entire genome and includes additional probes specifically focused on "variants that exist in the population and lead to the loss of function of genes," explains Stone. These new microarrays can also be customized, so researchers can study variants found from their own experiments or from public databases.

To explore genetic variations across entire populations, researchers need a family of flexible microarrays. Thus the second member of the HumanCore family, the Infinium HumanCoreExome BeadChip, includes the standard set of over 300,000 SNP probes plus 240,000 exome-focused markers. With this combination of markers, a scientist can compare single nucleotide variations between samples and potentially determine how they impact a protein's production, as indicated by the exome-based markers.

As companies begin to create increasingly customized continued>

Featured Participants

Affymetrix
www.affymetrix.com

Agilent
www.agilent.com

Ambry Genetics
www.ambrygen.com

Expression Analysis
www.expressionanalysis.com

Illumina
www.illumina.com

Life Technologies
www.lifetechnologies.com

Oxford Gene Technology
www.ogt.co.uk

Pathwork Diagnostics
www.pathworkdx.com

PerkinElmer
www.perkinelmer.com

Washington University School of Medicine in St. Louis
medschool.wustl.edu

tools, the concept of what makes a microarray has begun to evolve. Traditionally, microarrays consisted only of nucleotides attached to a solid surface, but variations on this theme also exist. For example, **Life Technologies** (Carlsbad, California) developed its TaqMan OpenArray Real-Time PCR plates, which include 3,072 wells. "The arrays can be formatted from our inventory of eight million TaqMan assays," says Jami Elliott, market development manager at Life Technologies. The real-time PCR assays, which use TaqMan probes (so named because these assays rely on the Taq polymerase), can be used to measure gene expression, identify biomarkers, and more.

If eight million choices aren't enough, Joshua Trotta, director, business development genetic analysis at Life Technologies, says, "We can custom design one."

Ongoing Data Dilemmas

Rather than making microarrays, **Expression Analysis,** a Quintiles company in Durham, North Carolina, uses arrays to conduct a wide range of studies for customers, such as gene-expression profiling. In doing so, Expression Analysis uses microarrays from several vendors, including Affymetrix, Illumina, and **Fluidigm** in South San Francisco, California. According to Pat Hurban, vice president of R&D at Expression Analysis, "Microarrays are very mature as a technology, but there are still a number of challenges in working with the data, especially when you want to drill down into the biology." He adds, "It's one thing to provide a statistical treatment of data, but another to understand the pathways involved and translate that into biology." This company uses a collection of proprietary tools in an effort to bridge that knowledge gap.

In fact, Hurban advises researchers to reassess the best technology to use as a project advances. "You must be mindful of the technical limitations of microarrays," he says. For example, he points out that microarrays provide excellent discovery tools. "It's not uncommon to identify specific genes of interest with microarrays," Hurban says. "When it comes to translational research, the question becomes: Is it advisable to continue on a microarray platform as you get closer to the clinic or transition to a more suitable and robust technology, such as [quantitative] PCR or sequencing."

In a recent project, Expression Analysis worked with a client who had what Hurban describes as "a preliminary gene-signature panel that was very useful as a diagnostic in a certain indication area." Researchers at Expression Analysis worked with patient samples from the sponsor to put that signature on microarrays. "We showed the validity of this panel," Hurban says. "Ultimately, the sponsor wanted to turn this signature into a diagnostic and became concerned with the microarray results because the precision was a bit of a challenge." Consequently, the client eventually turned to a PCR-based platform for the final diagnostic. As a result, Hurban says, "You might use a microarray to some point, and then go to another technology."

Tomorrow's Tools

The ongoing advances in sequencing technology have made more than a few experts predict the demise of microarrays. For example, Elizabeth Chao, director of translational medicine at **Ambry Genetics** in Aliso Viejo, California, says, "The expression arrays that I've been using for 14 years are incredible tools, but RNA sequencing is starting to replace microarrays in research and translation." She adds, "Sequencing is not replacing microarrays in the clinical setting yet, but it probably will soon."

The data generated by sequencing can be both beneficial and challenging. Sequencing provides a gigantic amount of data in a short period of time, but it can be difficult to interpret so much data. Chao is confident that interpreting sequencing data will improve rapidly. She says, "Bioinformatics has really come up, and new methods are making it possible to look at sequences across the entire genome."

To evolve with changes in technology, some companies provide services that teach researchers to use the growing amounts of data. For example, Todd Smith, senior leader, research and application at PerkinElmer, says, "We can help people as they go from microarrays to DNA sequencing." This can include analytical techniques for handling the higher volume of data. These technologies, though, will likely complement each other, according to Smith and his colleagues. "There are applications where microarrays work best, and others where sequencing works best," says Williams. "There are areas where sequencing won't work well, but microarrays can." As an example, Williams says they are about to start a study that involves 160 samples that must be processed in a matter of weeks. "There's no way we could go through that with sequencing and get it turned around in time to have meaningful data," he says. Moreover, Smith says microarrays are superior to sequencing when it comes to searching for structural variations in a genome.

Though some experts may have differing opinions, the general consensus predicts that microarrays will continue to benefit basic research and provide clinical tools related to genomics. In the end, microarrays will advance where they work the best.

Mike May is a publishing consultant for science and technology.

DOI: 10.1126/science.opms.p1300072

DNA ISOLATION WORKSTATION

Designed to meet the needs of biobanks and high throughput genomic laboratories, the Freedom EVO-HSM workstation provides reliable walkaway extraction of gDNA from large volume blood samples using Promega's proven ReliaPrep Large Volume HT gDNA Isolation System. The Freedom EVO-HSM workstation is designed to streamline biobanking workflows, offering intelligent one-tube gDNA extraction from up to 32 samples in less than four hours. The compact system is controlled by the intuitive TouchTools touchscreen interface and features preinstalled protocols. Using the platform's liquid level detection function, the system is able to automatically calculate the reagent volumes for each sample, ensuring efficient walkaway extraction of high-quality DNA from 1–10 mL of blood and meeting the specific requirements of next generation sequencing methods.

TECAN

For info: +41-(0)-44-922-81-11 | www.tecan.com/reliaprep

NUCLEIC ACID SIZE SELECTION

SPRIselect utilizes Solid Phase Reversible Immobilization (SPRI)-based chemistry to speed and simplify genomic DNA size selection for next generation sequencing fragment library preparation. Following shearing, the library construction process requires size selection to produce uniform distribution of fragments. SPRIselect allows size distribution to be adjusted between 150 and 800 base pairs to suit the application and sequencing platform. The process can be performed manually or automated for high throughput in 96-well plates. SPRIselect reagent kits are available in 5, 60, and 450 mL volumes, enable rapid and consistent size selection, and come with guidelines to assist users in customizing protocols. Gel cartridges, chips, and additional instruments are not needed. Samples should be fragmented, double-stranded DNA of 50 µL or greater and dissolved in molecular biology grade water, or such standard buffer solutions as Tris or TE. SPRIselect is ideal for use in most common next generation applications, including paired-end, single-end, targeted, ChiP, and RNA sequencing.

BECKMAN COULTER

For info: 800-742-2345 | www.spriselect.com

HIGH-CONTENT PEPTIDE MICROARRAYS

PEPperCHIP Peptide Microarrays are synthesized with a laser printer-based technology directly on the chip. The benefits of this approach are a unique flexibility in terms of custom peptide content, a high spot density, and reduced material consumption enabling very attractive chip prices. Microarrays are provided on conventional object slides (containing 9,000 individual peptides) and other glass slide formats with up to 275,000 peptide spots. Assays can be performed using fluorescently labeled proteins or sandwich immunoassays. The PEPperCHIP platform is suitable predominantly for antibody characterization by epitope mapping and epitope permutation scans. PEPperCHIP microarrays further allow the profiling of antibody immune responses in blood sera linked with infection, immunization, autoimmune diseases, or cancer. Besides antibody analysis, PEPperCHIP microarrays are also suitable for peptide drug development. The PEPperMAP services include microarray design and synthesis as well as immunoassays, read-out, data evaluation, and reporting.

PEPperPRINT

For info: +49-62-21726-4489 | www.pepperprint.com

SINGLE-CELL WHOLE-GENOME AMPLIFICATION

DNA sequence analysis and genotyping of biological samples using innovative instrumentation is often limited by the small amount of sample available. The new REPLI-g Single Cell Kit is specially designed to uniformly amplify genomic DNA (gDNA) from single cells (<1,000 cells to as little as one bacterial or tumor cell) or purified gDNA, with negligible sequence bias and maximized genome coverage. The kit uses innovative Multiple Displacement Amplification (MDA) technology to deliver high yields of DNA that is highly suited for use with, and delivers outstanding results on, new technologies such as next generation sequencing platforms. The REPLI-g Single Cell Kit can also be used for a broad range of sample types, including purified gDNA, fresh or dried blood, and fresh or frozen tissue. Innovative ultraviolet treatment eliminates any detectable trace of residual DNA in the kit components, ensuring highly reliable amplification.

QIAGEN

For info: 800-362-7737 | www.qiagen.com

LIGHT CYCLER SYSTEM

The new LightCycler 96 System offers highly accurate, reproducible, and fast data generation for researchers working in a wide range of fields such as gene expression and genetic variation research. The system permits flexible adaptation of workflows to specific assay formats and throughput needs. It also provides guided navigation and intuitive software for first-time users as well as a full set of analytical capabilities for experienced operators. The data generated by the system can be analyzed directly or remotely for translation to publication-ready results in line with MIQE guidelines. The instrument's new silver block ensures outstanding temperature homogeneity and therefore enables a maximum of data consistency and accuracy. In addition, the new Light Cycler 96 puts the user right at the center by providing highly intuitive, user-friendly software and interfaces. Thanks to its innovative glass fiber optics, the Light Cycler 96 System offers equal and simultaneous data capture from all 96 wells, while avoiding the signal variations commonly seen in systems that use optical scanning. It is also calibration-free as it does not require a passive reference dye.

ROCHE

For info: +49-88-56605-468 | www.roche.com

Science Careers Advertising

For full advertising details, go to ScienceCareers.org and click For Employers, or call one of our representatives.

Tracy Holmes
Worldwide Associate Director
Science Careers
Phone: +44 (0) 1223 326525

THE AMERICAS

E-mail: advertise@sciencecareers.org
Fax: 202-289-6742

Tina Burks
East Coast/West Coast/South America
Phone: 202-326-6577

Allyson Rosen
Midwest/Canada/Corporate
Phone: 202-326-6578

Marci Gallun
Sales Administrator
Phone: 202-326-6582

Online Job Posting Questions
Phone: 202-312-6375

EUROPE / INDIA / AUSTRALIA / NEW ZEALAND / REST OF WORLD

E-mail: ads@science-int.co.uk
Fax: +44 (0) 1223 326532

Lucy Nelson
Phone: +44 (0)1223 326527

Kelly Grace
Phone: +44 (0) 1223 326528

JAPAN

Yuri Kobayashi
Phone: +81-(0)90-9110-1719
E-mail: ykobayas@aaas.org

CHINA / KOREA / SINGAPORE / TAIWAN / THAILAND

Ruolei Wu
Phone: +86-1367-1015-294
E-mail: rwu@aaas.org

Science Careers
From the journal *Science* AAAS

ScienceCareers.org

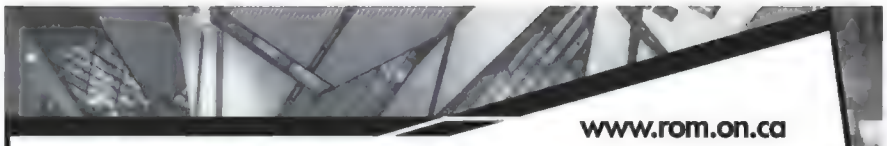

www.rom.on.ca

The Royal Ontario Museum (ROM) is Canada's pre-eminent international museum and houses some of Canada's most important collections in both Natural History and World Cultures. The Department houses Canada's largest mineral and gem collections, an important meteorite collection, and a comprehensive petrology collection.

Mineralogist
Natural History Department

The ROM invites applications from world-class scholars for the position of the Teck Chair in Mineralogy, to conduct field and collections-related research, and the strategic acquisition of new specimens, and to present these holdings through future exhibitions, gallery rotations and public programming. The Teck Endowed Chair in Mineralogy was established in 2007 thanks to the generous support of Teck Resources Limited. As a leading contributor to the new, public-facing Centre of Discovery for Earth and Space, the successful candidate will have demonstrated skills in transfer of scientific concepts and information in a manner that engages visitors to the museum and the general public, on site and on-line.

The successful applicant will be expected to: provide dynamic leadership for the Earth Sciences staff; develop a program of externally funded scholarly research and publications; curate and continue building the disciplinary collection of minerals; and have demonstrated ability and interest in the development and rotation of new permanent galleries and major exhibitions, traveling exhibits, science education, and public engagement.

Applicants must have a Ph.D. in mineralogy, and be well versed in the geological sciences; have a record of scholarly publication in peer-reviewed journals; be qualified for cross-appointment to the University of Toronto; and be eligible for NSERC funding in support of research (i.e., a proven record of successful grant applications). Experience in a museum or equivalent environment is preferable.

Salary and years in rank are commensurate with experience, as stipulated in the Collective Agreement between the ROM and ROM Curatorial Association.

Applications will be accepted until **5:00 p.m., March 29, 2013.** Applicants should provide a curriculum vitae, a summary of their research, and an outline of their proposed program of research, and arrange to have three confidential letters of recommendation sent on their behalf, to: **Mara Gunner, Human Resources Coordinator, Human Resources Department, Royal Ontario Museum, 100 Queen's Park, Toronto, Ontario, Canada, M5S 2C6. Fax: 416-586-5827.** All qualified candidates are encouraged to apply; however, Canadians and permanent residents will be given priority.

ROM Royal Ontario Museum

Are you currently registered to receive e-mails from AAAS and *Science*?

E-mail is the primary way that AAAS communicates with our members about AAAS programs, new member benefits, invitations to special events, and, of course, the latest news and research being published in *Science*.

Sign up today to receive e-mails from AAAS and ensure that you are getting the most out of your membership and *Science* subscription.*

To get started visit: **promo.aaas.org/stayconnected** You'll need your AAAS Member number. Find it above your name on your *Science* mailing label.

Don't miss a thing. Sign up for e-mail communications from AAAS today!

Science AAAS

*AAAS follows CAN-SPAM and European Safe Harbor guidelines for protecting your privacy. We will never sell your e-mail address and you can opt-out of receiving e-mails at any time.

Faculty Appointments for a New Initiative

The University of Chicago Institute for Molecular Engineering, with the Institute for Genomics and Systems Biology, invites applications for faculty positions at all ranks. Areas of interest include, but are not limited to

- synthetic and systems biology
- multi-scale modeling and prediction
- bioengineering
- bioinformatics
- imaging, genomics
- regenerative medicine
- medical diagnostics and therapeutics

While appointment at any level is possible, we particularly invite applications for tenure-track appointment at the Assistant and Associate Professor ranks. The appointment will be in the Institute for Molecular Engineering with membership in the Institute for Genomics and Systems Biology. Candidates must have a doctoral degree in a relevant field of study and have an outstanding research record. The successful candidate will be expected to establish and maintain a strong research program and to teach at the graduate level.

Interested applicants must apply online by uploading curriculum vitae, cover letter, research statement, and reference contact information to the University of Chicago Academic Career Opportunities website (**academiccareers.uchicago.edu**), posting number 01618. Applications will be reviewed until the position is filled.

The University of Chicago is an Affirmative Action/Equal Opportunity Employer

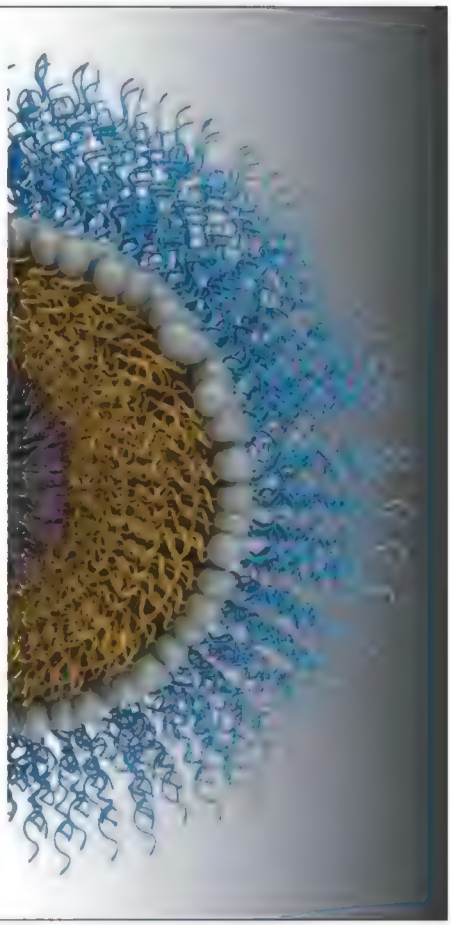

THE UNIVERSITY OF CHICAGO

Argonne NATIONAL LABORATORY

UHN Princess Margaret Cancer Centre

Scientists and Senior Scientists

Supported by a generous $50 million donation by Emmanuelle Gattusso, Allan Slaight and the Slaight family, the Ontario Cancer Institute at the Princess Margaret Cancer Centre in Toronto, Canada invites applications for multiple new faculty positions. These include: Directors of Cancer Genomics and/or Informatics, and outstanding candidates at the Scientist (Assistant Professor equivalent) or Senior Scientist (Associate/Full Professor equivalent) level in the areas of Computational Biology, Genomics/Clinical Genomics and Tumor Biology, including Stem Cell Biology.

The OCI/PMCC provides an extraordinarily rich scientific environment. It is the largest cancer research center in Canada and one of the largest in North America. The PMH treats approximately 18,000 patients per year, with 12,000 new cases. More than 20% of our patients participate in clinical trials, enabling patient-oriented research. With over 200 Scientists and Clinician-Scientists on staff, tightly integrated clinical and fundamental cancer research programs, and a top tier graduate teaching department, we have leading programs in the areas of stem cell biology, personal genomic medicine, epigenetics, signal transduction, immune therapy, radiation biology and medical imaging. Our downtown location is adjacent to other major Toronto hospitals and research institutes, and the University of Toronto, providing excellent opportunities for further collaborations.

These positions include full salary and benefits, as well as a very competitive startup package. We are affiliated with the University of Toronto, and successful candidates will be eligible for University appointments at the appropriate level.

Interested candidates should send their CV, list of three references, as well as a description of their research interests and future plans, highlighting their leadership experience or potential to:

Dr. Benjamin G. Neel
Director, Ontario Cancer Institute
7-504, 610 University Avenue, Toronto, Ontario M5G 2M9
oci@uhnresearch.ca

MRC | Toxicology Unit

Programme Leader

Starting salary will be in the range of £44,314 - £99,999

The MRC Toxicology Unit is an internationally renowned institution delivering field-changing mechanistic insights into toxicology and disease. Using an unbiased systems approach the Unit pursues an integrated scientific programme to examine the effects that occur following cellular exposure to chemicals, radiation and external biological agents. This research impacts directly on human health, with implications for reducing adverse drug reactions, drug attrition and bringing new insights leading to novel treatments for disease. The Unit has state of the art facilities with broad expertise in imaging, proteomics, genomics and deep sequencing.

Applicants will be highly motivated with an outstanding international research profile, a substantial record of high impact publications, a proven ability to attract research funding and experience in leading a research team. A proven track record of international excellence with a background in DNA damage, epigenetics or neural biology is required in order to develop and lead an independent programme of research within either of these areas that are pertinent to an understanding of fundamental toxicology.

The successful applicant will advance the discipline within the Unit and enhance its reputation both within the UK and internationally, provide leadership, demonstrate innovation and strategic vision in order to deliver a world-leading research agenda. In addition a contribution to the strategic management of the Unit and the successful implementation of its longer term vision for the Quinquennial Review (QQR) is expected. This is a tenured appointment with core funding including a number of research posts.

Informal enquiries can be made to Professor Anne Willis, Unit Director at: aew5@le.ac.uk

Applications should include a covering letter and full CV, an outline of current research interests (1 page) and a proposal for future research (up to 2 pages) together with the names and addresses of three professional referees who can be contacted prior to interview.

Applications are handled by the RCUK Shared Services Centre, to apply please visit our job board at: http://www.topcareer.jobs/ entering job reference IRC82929

Further information about the Toxicology Unit can be found at: http://www.mrctox.le.ac.uk/

Closing date: 28th March 2013

The MRC is an Equal Opportunities Employer

Unil

UNIL | Université de Lausanne

| le savoir vivant |

THE FACULTY OF BIOLOGY AND MEDICINE OF THE UNIVERSITY OF LAUSANNE, SWITZERLAND INVITES APPLICATIONS FOR THE FOLLOWING POSITION:

FULL PROFESSOR
DIRECTOR OF THE DEPARTMENT OF FUNDAMENTAL NEUROSCIENCE

The Department of Fundamental Neuroscience at the University of Lausanne (http://www.unil.ch/dbcm) has been inaugurated recently. It intends to strengthen its research programme and develop a new research focus in molecular and cell-biological aspects of neuroscience. We therefore seek an outstanding researcher (PhD, MD or MD/PhD) as full professor and new director of the Department. The position requires a record of scientific excellence and management experience, as well as vision and the motivation to lead and shape a Department.

The future Director of the Department is expected to lead a strong, internationally competitive research programme, attract external funding and promote an interactive and synergistic research environment. She/he is expected to provide leadership in order to develop the Department of Fundamental Neuroscience into a centre of excellence in molecular and cell-biological aspects of neuroscience.

The Department is embedded in a highly active and expanding research community in the Lake Geneva area, offering interactions with strong neurobiology programmes at the Federal Institute of Technology (EPFL) and the University Hospital (CHUV) in Lausanne, as well as at the University of Geneva. It also forms part of a programme of excellence in research by the Swiss National Science Foundation (NCCR Synapsy). Future developments in the Department will benefit from an excellent infrastructure in a new building on the main campus of the University.

Further information may be obtained from Prof. Tafti (Mehdi.Tafti@unil.ch), chair of the search committee.

The applications, in English, will include the curriculum vitae, the list of publications in which the five most significant ones are identified, a summary of the major discoveries (< 1 page), a short description of the present and future research programme (< 2 pages), and at least three names of referees. They should be sent via postal mail by March 15th, 2013 for the attention of Prof. Béatrice Desvergne, Dean of the Faculty of Biology and Medicine, rue du Bugnon 21, CH-1011 Lausanne, Switzerland.

Seeking to promote an equitable representation of men and women among its staff, the University encourages applications from women.

AAAS is here – promoting universal science literacy.

In 1985, AAAS founded Project 2061 with the goal of helping all Americans become literate in science, mathematics, and technology. With its landmark publications *Science for All Americans* and *Benchmarks for Science Literacy*, Project 2061 set out recommendations for what all students should know and be able to do in science, mathematics, and technology by the time they graduate from high school. Today, many of the state standards in the United States have drawn their content from Project 2061.

Every day Project 2061 staff use their expertise as teachers, researchers, and scientists to evaluate textbooks and assessments, create conceptual strand maps for educators, produce groundbreaking research and innovative books, CD-ROMs, and professional development workshops for educators, all in the service of achieving our goal of universal science literacy.

As a AAAS member, your dues help support Project 2061 as it works to improve science education. If you are not yet a AAAS member, join us. Together we can make a difference.

To learn more, visit **aaas.org/plusyou/project2061**

AAAS + U = Δ

AAAS is here – helping scientists achieve career success.

Every month, over 400,000 students and scientists visit ScienceCareers.org in search of the information, advice, and opportunities they need to take the next step in their careers.

A complete career resource, free to the public, *Science* Careers offers a suite of tools and services developed specifically for scientists. With hundreds of career development articles, webinars and downloadable booklets filled with practical advice, a community forum providing answers to career questions, and thousands of job listings in academia, government, and industry, *Science* Careers has helped countless individuals prepare themselves for successful careers.

As a AAAS member, your dues help AAAS make this service freely available to the scientific community. If you're not a member, join us. Together we can make a difference.

To learn more, visit **aaas.org/plusyou/sciencecareers**

AAAS + U = Δ

POSITIONS OPEN

AGROECOSYSTEM ECOLOGIST ASSISTANT PROFESSOR

The University of Nebraska-Lincoln (UNL) Institute of Agriculture and Natural Resources is inviting applications for a 12-month, tenure-leading Assistant Professor position with research and extension responsibilities in the Department of Entomology located at the University of Nebraska West Central Research and Extension Center in North Platte, Nebraska. Programming should address statewide resistance management issues and cropping systems work and contribute to Entomology efforts in managing arthropods and stress biology.

A Ph.D. degree or equivalent in entomology or related field is required. Degree must be completed before employment begins.

To view the complete position details and make application for this position, go to the UNL Employment **website: http://employment.unl.edu.** Search for **requisition number F_130050.** Complete the faculty academic administrative information form. Attach a letter of interest, curriculum vitae, and a personal statement describing your research and extension interests and experience. Candidates should also arrange for three letters of reference to be submitted to **e-mail: mweidner1@unl.edu.**

Review of applications will begin on March 15, 2013, and continue until the position is filled or the search is closed.

The University of Nebraska has an active National Science Foundation ADVANCE gender equity program, and is committed to a pluralistic campus community through Affirmative Action/Equal Opportunity, work-life balance, and dual careers.

OKLAHOMA STATE UNIVERSITY Stillwater, OK

ASSISTANT PROFESSOR, Animal Physiologist, Tenure-track. The Department of Zoology at Oklahoma State University (OSU, **website: http://zoology.okstate.edu**) is searching for a physiologist working within the context of behavior, ecology, environmental stress, or evolution. Examples of research focus could include aging, developmental biology, endocrinology, metabolic physiology, and neurophysiology. Applicants should have a Ph.D., postdoctoral experience, teaching experience, and success in obtaining extramural funding. Responsibilities include establishing an extramurally funded research program, mentoring M.S. and Ph.D. students, and teaching at the undergraduate and graduate levels. To apply please (1) send a single PDF file composed of a cover letter, curriculum vitae, and statements of research interests and teaching philosophy, and (2) have three letters of recommendation sent to the search committee chair, **Dr. Puni Jeyasingh,** at **e-mail: zoologysearch@okstate.edu.** Application review will begin March 29, 2013, with employment beginning August 15, 2013. Filling of this position is contingent upon availability of funding. *Oklahoma State University is an Affirmative Action/Equal Employment Opportunity/E-Verify Employer committed to diversity. OSU-Stillwater is a tobacco-free campus.*

FACULTY POSITIONS in Human Sociogenomics College of Liberal Arts and Sciences and Institute for Genomic Biology University of Illinois at Urbana-Champaign

The University of Illinois, Urbana-Champaign, seeks candidates who examine the interdependence of biology and social behavior, with a particular interest in human sociogenomics for full-time faculty positions. Scholars in various social science fields whose research agenda engages the biological sciences as well as scholars in the biological sciences whose research lies at the interface with the social sciences are invited to apply.

For complete details see **website: http://www.humansociogenomics.illinois.edu/.**

Illinois is an Affirmative Action/Equal Opportunity Employer **(website: http://www.inclusiveillinois.illinois.edu).**

POSITIONS OPEN

PLANT ARTHROPOD INTERACTIONS ASSISTANT PROFESSOR

The Department of Entomology at the University of Nebraska-Lincoln (UNL) Institute of Agriculture and Natural Resources is seeking applicants for the tenure-leading position of Plant Arthropod Interactions at the Assistant Professor rank with a focus on the molecular biology of plant defense to arthropods and in teaching. A joint appointment with another department such as Biochemistry is possible. Approaches could include molecular biology, plant physiology, functional genomics, or the analysis of large data sets.

A Ph.D. degree or equivalent in entomology or related field (degree must be completed before employment begins) with emphasis in molecular biology and research experience in arthropod interactions with plants.

To view the complete position details and make application for this position, go to the UNL Employment **website: http://employment.unl.edu.** Search for **requisition number F_130049.** Complete the faculty academic administrative information form. Attach a letter of interest, curriculum vitae, and a personal statement describing your research and teaching interests and experience. Candidates should also arrange for three letters of reference to be submitted to **e-mail: mweidner1@unl.edu.**

Review of applications will begin on March 15, 2013, and continue until the position is filled or the search is closed.

The University of Nebraska has an active National Science Foundation ADVANCE gender equity program, and is committed to a pluralistic campus community through Affirmative Action/Equal Opportunity, work-life balance, and dual careers.

VICE PRESIDENT FOR RESEARCH

Colorado State University (CSU), a Carnegie Research University (Very High Research Activity) in Fort Collins, Colorado, seeks an experienced, innovative research strategist to serve as Vice President for Research (VPR). CSU is one of the nation's premier land-grant universities, with current annual research expenditures in excess of $340 million and ranked 6th in federally funded expenditures among universities without medical schools in 2011. This position calls for an energetic, visionary individual, a creator of bold solutions setting the foundational environment for research and creative activities. The successful candidate must be a distinguished investigator/scholar with a demonstrated record of innovation in leadership and management at increasing levels of responsibility within academe and/or at the intersection of academic inquiry with private and governmental sectors.

Applications will be accepted until the position is filled; however, to be guaranteed full consideration, applications must be received by March 20, 2013, and include a single PDF document with the following information: (1) a letter of application stating applicant's qualifications, (2) a statement of vision and philosophy for this position, (3) curriculum vitae, and (4) names and contact information of three individuals who can comment on the applicant's abilities to assume this leadership role. The application should be uploaded as a single PDF at the following **website: http://cns.natsci.colostate.edu/employment/VPResearch/.**

A detailed description of this position can be accessed at, **website: http://www.provost.colostate.edu.**

CSU is an Equal Opportunity/Equal Access/Affirmative Action Employer. Colorado State University conducts background checks on all final candidates.

POSITIONS OPEN

VISITING ASSISTANT PROFESSOR BIOLOGY

The Biology Department at Denison University, a selective liberal arts college, invites applications for a one-year visiting **ASSISTANT PROFESSOR** position with emphasis in ecology, evolution, and organismal biology to begin August 2013. Teaching load for this position is two courses with laboratories each semester; all courses have enrollments of 24 or less. Anticipated teaching responsibilities include an upper-level majors course in organismal diversity/biology (such as plant diversity, ornithology, mycology), a sophomore-level majors course in Ecology and Evolution (BIOL 202), and the potential to teach a introductory majors or nonmajors course (visit **website: http://www.denison.edu/biology/** for a detailed description of the department and its curriculum). Demonstrated ability in undergraduate teaching is expected and a Ph.D. is preferred (ABD acceptable).

Please submit electronic application materials (a cover letter clearly indicating ability to teach an organismal biology course, Ecology & Evolution, and other teaching interests; curriculum vitae; statement of teaching philosophy; undergraduate and graduate transcripts; and three letters of recommendation) online at **website: https://employment.denison.edu.** Review of applications will begin February 26, 2013 and continue until the position is filled.

Denison University is an Affirmative Action/Equal Opportunity Employer. To achieve our mission as a liberal arts college, we continually strive to foster a diverse campus community, which recognizes the value of all persons regardless of religion, race, ethnicity, gender, sexual orientation, disability, or socio-economic background.

ASSISTANT PROFESSOR – SOLID EARTH Massachusetts Institute of Technology (MIT)

The Department of Earth, Atmospheric and Planetary Sciences at MIT seeks applications for multiple faculty positions in the broad fields of geology, geobiology, geochemistry, and geophysics, including but not limited to earth history, tectonics, earthquake source physics, surface processes, sedimentology, environmental science, deep earth properties and processes, and rock physics. Applicants who integrate across traditional boundaries are particularly encouraged to apply. The intention is to hire at the assistant professor level but more senior appointments can be considered.

Applicants should submit curriculum vitae, one- to two-page descriptions of research and teaching plans, and the names, e-mail addresses, and telephone numbers of three professional referees. Applicants should not ask their references to upload letters at the time of application; letters will be requested directly by MIT. Questions may be addressed to **Professor Samuel Bowring,** Search Committee Chair, at **e-mail: sbowring@mit.edu.** Applications are being accepted at Academic Jobs Online (**website: https://academicjobsonline.org/ajo**). To receive consideration, a complete application must be received by May 31, 2013.

Search Contact: **Mr. Michael Richard, Human Resources Administrator, EAPS, 54-912, Massachusetts Institute of Technology, 77 Massachusetts Avenue, Cambridge, MA 02139-4307; e-mail: mjr@mit.edu; telephone: 617-253-5184; fax: 617-253-8298.**

MIT is an Equal Opportunity/Affirmative Action Employer; applications from women and underrepresented minority candidates are encouraged. MIT is a nonsmoking environment.

POSTDOCTORAL POSITIONS

Postdoctoral positions are immediately available for the study of biomembranes and membrane-associated proteins. Our interdisciplinary research includes quantitative imaging of cellular lipids and genomic-scale analyis of membrane binding proteins with diverse cellular activities. This research group provides a highly challenging and supportive environment with state-of-the-art imaging and biophysical facilities. Motivated candidates with a strong background in cell biology, chemical biology, and microscopy are encouraged to apply. Please send curriculum vitae and names of three references to: **Wonhwa Cho, Department of Chemistry (M/C 111), University of Illinois at Chicago, 845 W. Taylor Street Chicago, IL 60607. E-mail: wcho@uic.edu. Website: http://brahms.chem.uic.edu.**

AAAS 2014 ANNUAL MEETING

13-17 FEB • CHICAGO

Call for Symposium Proposals

Symposium proposals for the 2014 AAAS Annual Meeting are now being solicited.
To submit a proposal, visit **www.aaas.org/meetings.** The deadline for submission is **23 April 2013.**

Meeting Global Challenges: Discovery and Innovation

Scientific discovery and innovation are helping to drive solutions to current and future global challenges. Economic progress in every community worldwide has meanwhile become increasingly interdependent with advances in science and technology. Challenges related to ensuring sufficient food for a growing population, quality healthcare, renewable fuels, and a sustainable and enriching environment demand innovation and international dialogue. Addressing these challenges depends upon discoveries emerging from the convergence of physical, life, engineering, and social sciences in innovative ways that are most useful to society.

In a weakened global economy, many countries have begun to limit their investments in the future. Yet, investments in innovations – including funding for education as well as basic and applied research – represent our best prospect for a sustainable environment and increased economic growth. Economists estimate, after all, that innovation in science and technology are the source of more than half of the economic growth in many countries. By increasing innovation in sustainable products and processes, world economies can continue to enhance human welfare across society.

Innovation springs from the translation, production, and distribution of discovery and invention to society. In the contemporary world, this is not a linear process, but rather, a matrix of interactions. Societies, with support from public and private sectors and institutions, struggle to integrate the necessary disciplines and interests into this matrix. Within the scientific and engineering community, we need to better integrate different disciplines and voices into a consensus supporting innovation. Developed and developing countries that accomplish this will become the economies of the future.

At the same time, it is imperative that we work in ways that are transparent and open to a diversity of contributors and ideas. Assessing risk versus benefit in adopting an innovation is complex and depends upon an open dialogue. Only then will we realize the promise of furthering scientific discovery and innovation to meet pressing global challenges and improve quality of life.

Call for Poster Submissions

Online entries will be accepted at **www.aaas.org/meetings** beginning **14 May 2013.**

AAAS
ADVANCING SCIENCE, SERVING SOCIETY

Illuminate Cancer Biology

The complexity of cancer systems biology requires innovative tools for interrogating the signaling pathways responsible for oncological transformation. Promega's integrated tools for reporter gene analysis assure biologically relevant results in cancer research.

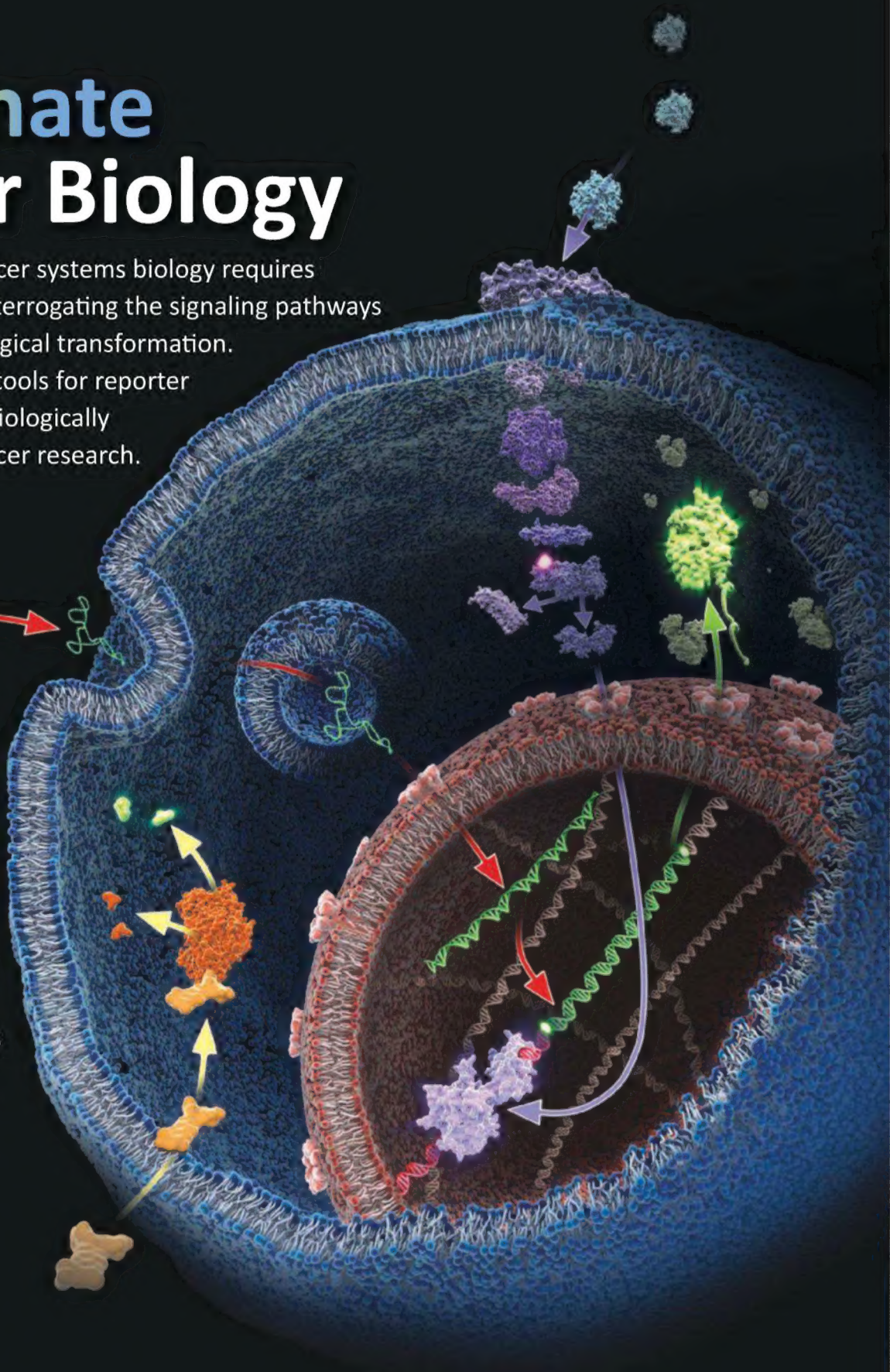

FuGENE® HD
The next generation transfection reagent, effective on almost every cell type with virtually no cell toxicity

ONE-Glo™ + Tox
Multiplexed reporter gene analysis with off-target toxicity detection in the same well

New! NanoLuc™ and pGL4 Tox Vectors
Introducing NanoLuc - the brightest, smallest, luciferase available - plus a new line of pGL4 response element vectors for mapping oncological pathways

Promega

To get a FREE sample of any one of these reagents, visit:

www.promega.com/pathwaybiology